

2016

Paper No	Paper Title	Author Details	Company	Page
1.1	Diagnosis and Mitigation of Contamination Build up in Multipath Liquid Ultrasonic Meters on the Danish Oil Pipe	Gregor Brown	Cameron	3
1.2	Using an Ultrasonic Flowmeter in the Transition Zone	David Mills	Oil & Gas Measurement Limited	28
1.3	Turbine Meters in Decline - Throwing the Baby Out with the Bathwater	Terry Cousins	CEESI	64
1.4	Proving Coriolis Meters with Small Volume Provers	Tim Patten	Emerson – Micro Motion Inc.	77
2.1	In-Situ Validation of ESMER MPFMs	Haluk Toral	Petroleum Software Ltd	86
2.2	Application of the Magnetic Resonance Multiphase Flowmeter to Heavy Oil	Mark van der Zande	KROHNE	106
2.3	Live Fluids or Controlled Fluids: How Should we Calibrate a Multiphase Flow Meter?	Norman Glen	NEL	115
3.1	Analysis of Field and Ownership Allocation Uncertainty in Complex Multi-Field Configurations	Ranveig Nygaard Bjørk	Christian Michelsen Research	128
3.2	When Allocation “Back Out” Agreements Can Become “Lose Out” Agreements	Phil Stockton	Accord Energy Solutions Limited	147
3.3	Application of Data Validation and Reconciliation to Production Allocation	Amin Amin	Letton Hall Group	170
4.1	Determination of Optimal Calibration Intervals – A Risk Based Approach	Nadezhda Pashnina	Emerson Process Management	197
4.2	Reynolds Number, the Correct Calibration, Characterization and Proving of Flow Meters	Terry Cousins	CEESI	217
5.1	Estimating Gas Ultrasonic Meter Field Error Using Diagnostics	John Lansing	CEESI	230
5.2	Clamp on Ultrasonic Flow Meters vs A Fiscal Orifice Station. How Accurate are Clamp On Meters out of the Box?	Andrew Runcie	PX Limited	253

2016

Paper No	Paper Title	Author Details	Company	Page
5.3	Diagnostics and Orifice Plates: Experimental Work	Michael Reader-Harris	NEL	266
5.4	Errors Due to Use of the AGA8 Equation of State Outside of Its Range of Validity	Norman Glen	NEL	294
5.5	Venturi vs. Ultrasonic Meter Comparisons – The Heretical Unauthorised Version	Richard Steven	CEESI	310
5.6	Performance of Coriolis Flowmeter for Metering of CO <sub>2</sub> with Impurities in CCS Applications	Mahmoud Nazeri	Heriot-Watt University	339
6.1	A New Approach to Measuring the Gas and Formation Water Flow Rates in Wet Gas	Andrew Charles Baker	OneSubsea (a Schlumberger Company)	341
6.2	Modeling of Wet Gas Flow in Venturi Meters to Predict the Differential Pressure	Hans R. E. van Maanen	Hint B.V.	356
6.3	Evaluation of the SONAR Meter in Wet Gas Flow for an Offshore Field Development	Siddesh Sridhar	Expro Meters	389
6.5	Wet Gas Flow Facility Inter-Comparison	Dennis van Putten	DNV GL	399
Poster 1	ISO/AWI 21354 Measurement of Multiphase Fluid Flow	Michael Reader-Harris	NEL	417
Poster 3	Investigation of Multiphase Flow-Regimes After a Blind-T Mixer and at the Throat of the Venturi – Using Gamma-Ray Tomography and CFD Modelling	Lars Anders Ruden	Roxar Emerson Process Management	421
Poster 5	Compressible Fluid Calibration of Coriolis Meters	Terry Cousins	CEESI	425
Poster 6	Are We Barking Up the Wrong Tree? Uncertainty vs Error and the Role of CBM to Measure Both	Anwar Sutan	i-Vigilant Technologies	437

**Technical Paper**

**Diagnosis and Mitigation of Contamination Build-up  
in Multipath Liquid Ultrasonic Meters  
on the Danish Oil Pipe**

**Dr Gregor J Brown, Cameron  
Lars Bach, DONG Oil Pipe A/S**

---

## **1 INTRODUCTION**

This paper describes an investigation and remedial work carried out on multipath liquid ultrasonic meters installed on the Danish Oil Pipe, owned by DONG Oil Pipe A/S (DOP). The meters in question were installed in an effort to improve the performance of the onshore metering system at the receiving end of the pipeline. When the second of two replacement meters was installed, 10 months after the first, and the two meters operated in series, it was discovered that the first replacement meter was not in good agreement with the second meter. Investigations revealed that the problem was the result of contamination build-up inside the first meter and work began to understand and to attempt to resolve the problem.

## **2 THE OIL PIPE METERING STATION**

The Danish Oil Pipe system includes the offshore tie-in platform Gorm "E" which feeds the 330 km pipeline. Seven export pumps on Gorm "E" pump the oil across the 220 km pipeline to the Filsø pumping station, seven kilometres from the west coast of Jutland. At Filsø the pressure is increased with the aid of five more export pumps so that the oil can be transported the final 110 km across the peninsula of Jutland to DOP's crude storage and export facilities adjacent to the Shell Refinery in Fredericia.

At the receiving end of the pipeline there is a metering system that is used primarily for leak detection. A photograph of the metering system (before upgrading) is shown in Figure 1 below. The system is configured for maximum flexibility and redundancy. Flow enters from one of the two headers on the right hand side and exits from the header on the left. The flow can be routed through only the first (top) metering stream to the downstream header, or it can enter on the other inlet header and flow through the second (bottom) metering stream, or it can flow through the first metering stream and then through the second meter stream by means of the cross-over line that is between the two streams. The metering streams can also be bypassed completely.

**Technical Paper**



Fig.1 - The DOP metering system at Fredericia

### **3 FLOW METER UPGRADING**

When originally commissioned the system used two 2-path process-grade liquid ultrasonic meters. Each meter employed a pair of direct diametrical paths in orthogonal planes at plus and minus 45 degrees to the horizontal.

The performance of these meters on site, evaluated by means of comparison with the custody transfer tank gauging downstream, did not meet expectations. Over the course of time efforts were made to improve performance, for example by calibrating the 2-path meters with their upstream pipework, but still performance on site did not improve.

Figure 2 shows a trend of the deviation of one of the 2-path meters relative to the flow rate computed using the tank gauging at the DOP storage and export facilities. Flow rate comparisons in this paper between the tanks and flow meters are presented as a 20-day average to reduce 'scatter' in the data that results from various factors including data archiving methods and tank switching operations.

# 34<sup>th</sup> International North Sea Flow Measurement Workshop 25-28 October 2016

## Technical Paper

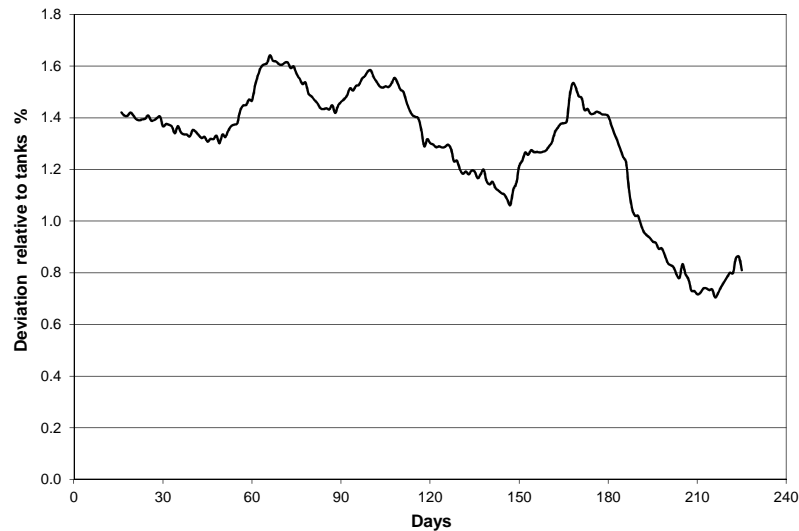


Fig. 2 - Typical performance of one of the 2-path meters

Following a visit to site by Cameron (Caldon) to review the installation, it was concluded that the upstream arrangement of bends in the metering system was non-ideal, as the arrangement of out-of-plane bends is well known to produce distortions of the axial profile and high levels of swirl. Therefore it was recommended that the 2-path meters be replaced by 4-path custody transfer grade meters, and that a flow conditioner be installed upstream to eliminate swirl. Nowadays, it would be usual to recommend an 8-path meter rather than a 4-path meter and conditioner, but at that particular point in time the Caldor 8-path meter for the petroleum industry had not yet been launched.

The upstream pipe section had an integral reducer to adapt the diameter from the 20-inch flange of the ball valve to the 16-inch diameter of the meter run. Although not ideal, the flow conditioner was installed between the ball valve and the reducer. This location was chosen for a number of reasons: (a) the primary purpose of the conditioner was swirl removal, and there was approaching 20 pipe diameters of separation between the conditioner and the meter (b) the location in the 20-inch section would result in lower pressure loss and (c) modifications to the existing system could be minimised, requiring only a short make-up spool downstream of the new meters.

The flow conditioner used was a Spearman type perforated plate conditioner, supplied by NEL. A drawing of the modified meter run is shown in Figure 3 below.

Technical Paper

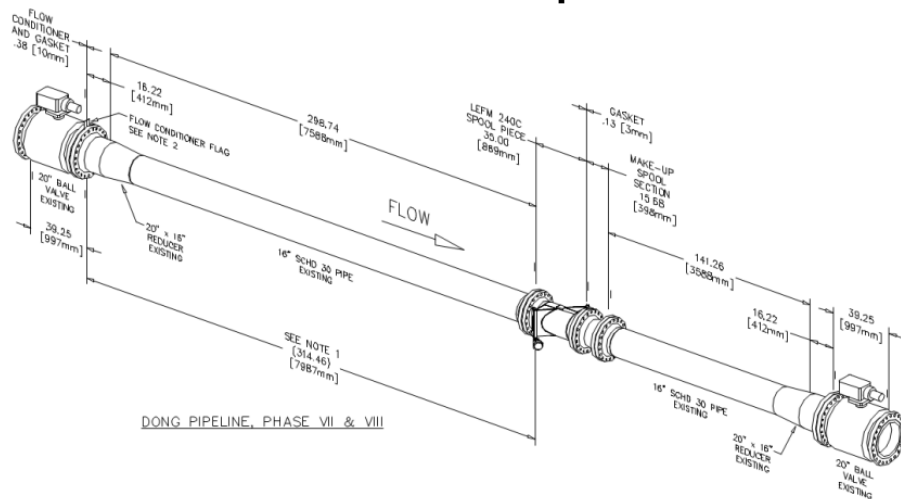


Fig 3. - The meter run layout following modification

#### 4 FLOW METER CALIBRATION

The two replacement 4-path meters were ordered, calibrated and installed separately, approximately 10 months apart, owing to budget considerations. The meters supplied were 4-path chordal meters of the Gaussian (Westinghouse) design, with stainless steel meter bodies and transducer housings. Both meters were calibrated at the COFRAC accredited Trapil calibration facility in France. For each calibration the flow conditioner and its respective upstream length from the site were used. The flow conditioner was installed upstream of the meter tube and the 20-inch reduced bore ball valve was simulated in the calibration by using an expansion from 16-inch to 20-inch situated upstream of the flow conditioner.

The first 4-path meter (Meter 1) was calibrated in February and installed a month later. The second meter (Meter 2) was calibrated in December of the same year and installed in January of the following year.

The meters were calibrated over a Reynolds number range of approximately 40,000 to 1,000,000. Only a single adjustment factor was used to bring the meters into agreement with the calibration lab and the resulting linearity was better than +/- 0.1 %, comfortably within specification the specification of +/- 0.15 % as shown in Figure 4 below for Meter 2.

# 34<sup>th</sup> International North Sea Flow Measurement Workshop 25-28 October 2016

## Technical Paper

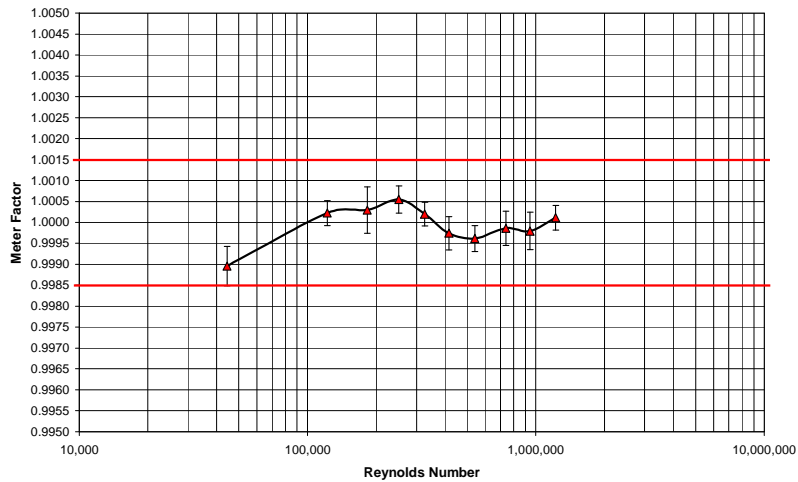


Fig. 4 - Trapil calibration result for a 4-path meter (Meter 2)

### 5 COMMISSIONING OF THE SECOND 4-PATH FLOW METER

By the time that the second 4-path meter was installed and commissioned, the first meter had been in service for 10 months. For commissioning the metering system the valves were configured to route flow through both meters in series. Once the second meter was commissioned it was immediately apparent that the two meters were reading differently, by approximately 1 %, with the newly installed meter reading higher than the first meter.

A diagnostic check had already been performed on the newly commissioned Meter 2 and had not highlighted any concerns. Therefore attention quickly turned to Meter 1 and a diagnostic log was taken from that meter for analysis. It was quickly determined, by analysis of various diagnostics, such as the velocity profile plot shown in Figure 5 below, that either the meter itself or the conditions of operation were different from what had been observed during commissioning.

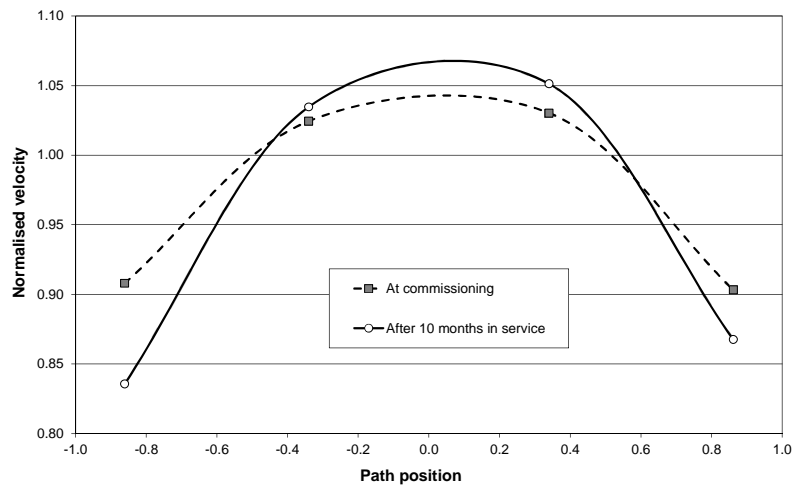


Fig. 5 - Comparison of velocity profiles at commissioning and after 10 months in service (Meter 1)

# 34<sup>th</sup> International North Sea Flow Measurement Workshop 25-28 October 2016

## Technical Paper

Of the various diagnostic parameters that were examined, it was noted in particular that the signal gain had reduced relative to commissioning. What drew attention to gain was that it had changed in a way that was not expected. As shown in Figure 6, the gain on the shorter, outside paths had reduced more than on the long paths. This was unexpected as the crude oil characteristics do not vary much and any change in absorption would be expected to affect the long paths more than the short paths. This led to a suggestion that perhaps the meter could be contaminated internally, as wax deposition could act like an acoustic matching layer on the stainless steel transducer housings of the meter. When this suggestion was made, the response from the technician on site was that, yes that could be the cause, as he had noticed that the decommissioned 2-path meters had been contaminated when they had been taken out of line.

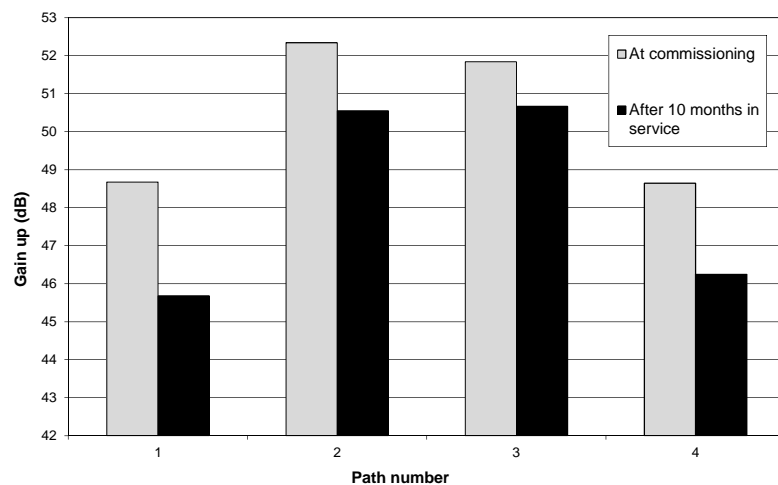


Fig. 6 - Comparison of applied gain at commissioning and after 10 months in service (Meter 1)

## 6 INSPECTION OF THE DECOMMISSIONED 2-PATH METERS

It transpired that the 2-path meters that had been decommissioned from the system were in storage not far from the metering station, and therefore it was decided that these should be inspected.

One of the two 2-path meters, the one removed from the line most recently, appeared to have been partly cleaned. The partly cleaned 2-path meter was corroded internally (being made of carbon steel) but was largely free of deposition in the bore. It did however have sticky deposits in the transducer housing cavities, partially covering the face of the transducer housings, as shown in the photograph of Figure 7.

**Technical Paper**



Fig. 7 - Deposition in the transducer cavity of a partially cleaned 2-path meter

The second 2-path meter had been removed from service some 10 months earlier and did not appear to have been cleaned at all. It was found in a more severe state of contamination. As well as having deposits in the transducer housing cavities, the internal surface of the meter was covered in a heavy, wavy deposition that had dried to a hard crust that was a few millimetres thick in places. Photographs of the interior of the second 2-path meter are shown in Figures 8, 9 and 10.



Fig. 8 - Interior of a contaminated 2-path meter (transducer housing in centre of photograph)

**Technical Paper**



Fig. 9 - Interior of a contaminated 2-path meter (close up of a transducer housing cavity)



Fig. 10 - Contaminated 2-path meter showing the thickness of the deposition (which had solidified/dried to a 'crust' during 10 months in storage)

**7 INSPECTION AND CLEANING OF METER 1**

Following the discovery of the condition of the decommissioned meters, it was agreed that Cameron would return to site at the earliest convenient time to participate in an internal inspection of the first 4-path meter that had been installed on site (Meter 1). The plan, agreed in advance, was that the meter, upstream pipe, and flow conditioner would each be inspected and cleaned if

# 34<sup>th</sup> International North Sea Flow Measurement Workshop 25-28 October 2016

## Technical Paper

necessary. The inspection of Meter 1 was carried out 1 month after the commissioning of Meter 2, i.e. 11 months after Meter 1 had been put into service.

Figure 11 shows the Spearman flow conditioner. The Spearman plate was found to be in good condition with no deposition on its surfaces and no upstream blockage or debris trapped in the holes.



Fig. 11 - Spearman conditioner after 11 months in service

Figure 12 shows the interior of the upstream pipe. It was observed that this carbon steel pipe had corrosion and deposition broadly similar to the 2-path meter body that had not been cleaned.



Fig. 12 - Photograph showing deposition in the upstream meter tube

**34<sup>th</sup> International North Sea Flow Measurement Workshop  
25-28 October 2016**

**Technical Paper**

When the bore of the 4-path stainless steel ultrasonic meter body was inspected it was found that it was not as badly contaminated as the bore of the carbon steel upstream pipe (or the bore of the carbon steel 2-path meter bodies), as shown in Figure 13.



Fig. 13 - Photograph showing the bore of the stainless steel 4-path meter after 11 months in service (Meter 1)

On closer inspection of the interior of the meter, there was clear evidence of deposition in the transducer housing cavities, particularly those that were facing downstream. This can be seen by comparing Figure 14 which shows two transducer cavities facing upstream and Figure 15 which shows a transducer cavity that is facing downstream. In every case, the deposition was worse in the cavities facing downstream than those facing upstream, suggesting that the flow was having a beneficial 'scouring' effect on the cavities that face into the flow.

**Technical Paper**



Fig. 14 - Photograph showing transducer housing cavities facing upstream



Fig. 15 - Photograph showing a transducer housing cavity facing downstream

Following the inspection, the upstream pipe was cleaned first and then the meter was returned to service. The cleaning of the upstream pipe altered the velocity profile and brought Meter 1 and Meter 2 into slightly better agreement but only by about 0.1%. In other words, although the actual velocity profile was altered, it did not have a very significant effect on the calibration of the meter. This finding is in line with expectations given knowledge of the robustness of the chordal integration technique used in these meters and corroborated by the linearity of the meters demonstrated at calibration.

# 34<sup>th</sup> International North Sea Flow Measurement Workshop 25-28 October 2016

## Technical Paper

The next step was to take Meter 1 out of service again and clean it. When this had been completed the diagnostic indicators such as normalised velocity of sound (VOS) and Gain came back into very close agreement with the commissioning data (see Figures 16 and 17). Cleaning Meter 1 had the effect of reducing the difference between the two meters from  $\sim 0.9\%$  to  $\sim 0.2\%$ .

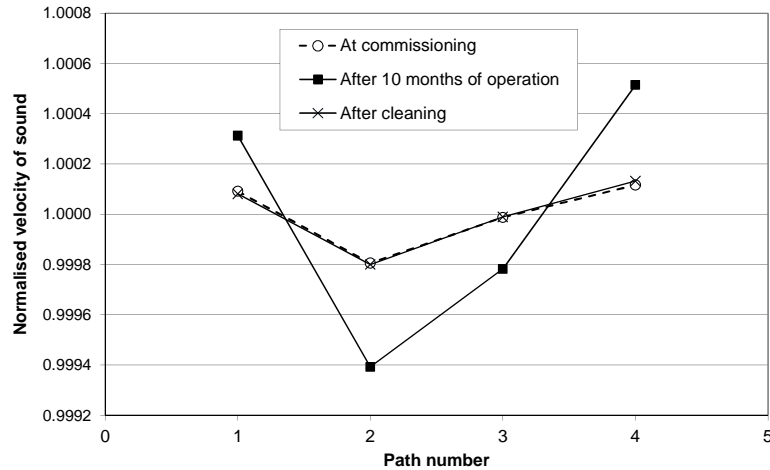


Fig. 16 - Velocity of sound comparison with commissioning baseline; after 10 months in service and following cleaning

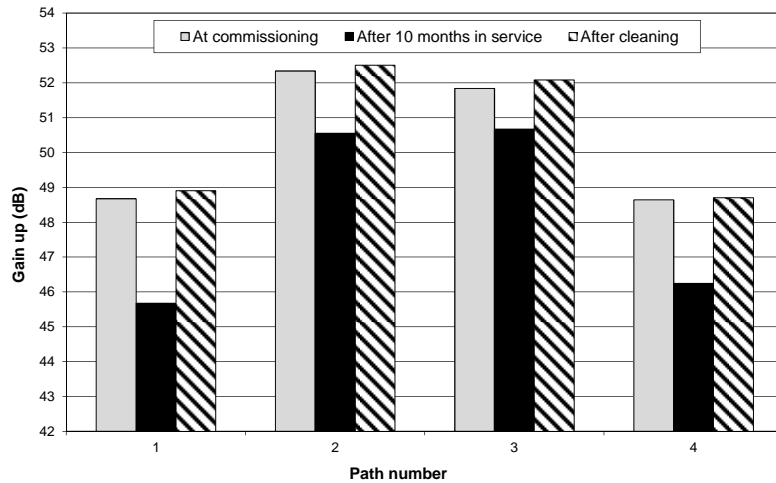


Fig. 17 - Gain comparison with commissioning baseline; after 10 months in service and following cleaning

# 34<sup>th</sup> International North Sea Flow Measurement Workshop 25-28 October 2016

## Technical Paper

### 8 ANALYSIS AND MITIGATION PLANNING

Once it had been confirmed that deposition was indeed the cause of the discrepancies observed, work began to obtain a better understanding of the problem and to develop mitigation plans.

Although some efforts were made to understand the nature of the deposition, the factors contributing to the deposition are still not very well understood. A sample taken from one of the meters was said to be mainly wax, with a high melting point of 76 degrees C, and approximately 2 % asphaltenes. Wax is present in the crude from Gorm and large amounts are regularly removed at the PIG receiver at Filsø. Drag reducing agent (DRA) is also used in the pipeline and it was often speculated that this might be contributing to the deposition problem. Some drag reducing agents exhibit some temperature dependent behaviour with a tendency to degrade at high temperatures and to clump or cluster at lower temperatures.

Diagnostic data logging was set up at site so that more information could be obtained while mitigation plans were discussed. It was also agreed that data from the tank gauging system downstream of the metering system would be examined so that the meters could be compared against an independent measurement. When this data was later analysed it was determined that the meters would be in good agreement with the tanks (and one another) when installed clean, and would stay that way for some time, which could be variable, but then they would begin to 'drift' relative to the tanks and then would settle at a fairly constant value somewhere between -0.5 % and -1.2 % relative to the tanks. Figure 18 below shows the deviation relative to the tanks, starting each time after a meter had been cleaned, and illustrates the variability of the deposition process and the resultant effect on the meters.

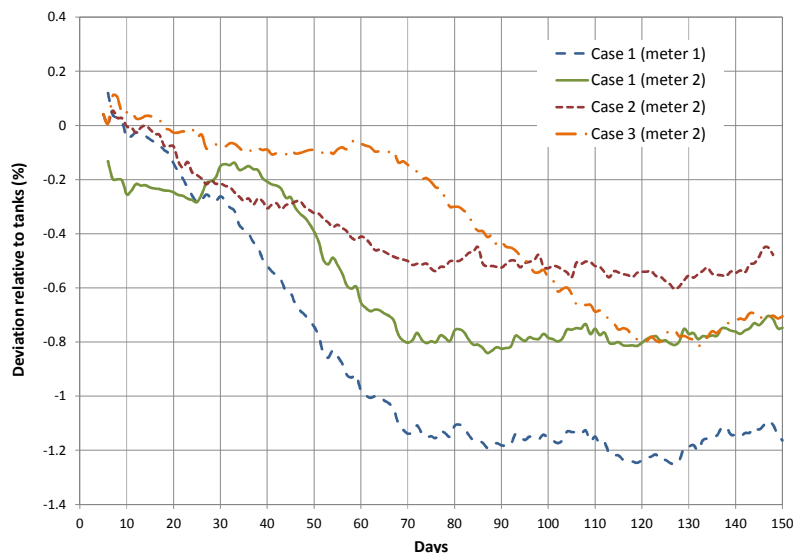


Fig. 18 - Flow rate deviation as a result of deposition, plotted versus time after cleaning, for three independent time periods

# 34<sup>th</sup> International North Sea Flow Measurement Workshop 25-28 October 2016

## Technical Paper

Diagnostic data was also analysed over these time periods. Of the various diagnostic available it was found that a carefully constructed Gain Diagnostic gave the most reliable correlation with the deviations due to contamination build up, though VOS monitoring was also found to be useful.

Figure 19 below show a gain diagnostic and a VOS diagnostic plotted versus the number of days since the meter was cleaned. This data corresponds with Case 1, Meter 1 in Figure 18 above. The Gain Diagnostic could easily be used to trigger an alarm in the first 10 to 15 days before the meter has shifted much, whereas the VOS Diagnostic does not give a clear indicate of a problem until around day 25, by which time the deviation was approximately 0.25 %.

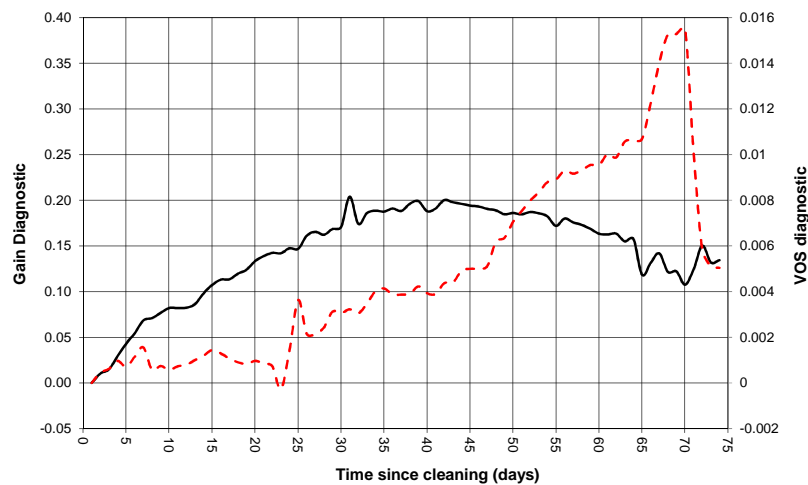


Fig. 19 - Gain and VOS diagnostic monitoring, Case 1, Meter 1

Analysing the data and considering the physics at work, it was concluded that the primary cause of the 'drift' was the deposition of material in the transducer housing cavities causing acoustic impedance changes and refraction effects and leading to a change in the path angle. This is illustrated in Figure 20. The angle between the path and the pipe axis increases, with the result that the measured transit time difference is reduced and the flow velocity is under-estimated.

**Technical Paper**

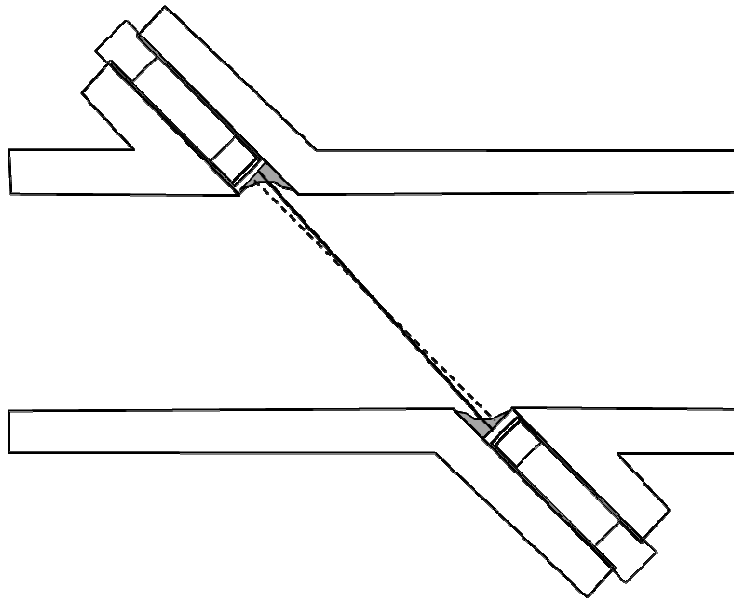


Fig. 20 - An illustration of path angle change resulting from deposits forming in the transducer housing cavities

Ideas that were then discussed in terms of mitigating the contamination build up were as follows:

- Filling the cavities in front of the housings with an acoustically conductive material of some sort
- Increasing the length of the transducer housings such that they would protrude into the flow and eliminate the cavity
- Applying an adhesion resistant coating to the wetted surfaces of the meter body and transducer housings

Filling the cavities with some other material was ruled out on the basis that it would just create a refraction issue of a different sort, causing the path angle to change with variations in the sound velocity of the fluid, e.g. due to temperature changes.

Intruding the transducers would be advantageous in terms of eliminating the problem area for deposition, but it was known from previous research and development work that this would make the uncalibrated (or 'dry' calibrated) meter much more non-linear than usual.

Coating the wetted surfaces was appealing as there was no potential downside, so long as the coating would be thin enough to be negligible in acoustic terms, and also assuming that it would continue to adhere to the surfaces in long term operation and would not peel or bubble.

Following a prolonged period of discussion and an investigation of various adhesion resistant coating processes, a decision was made to both intrude the transducers and coat the wetted surfaces of meter body and housings of Meter 1. The decision to intrude the housings was made on the assumption that the increased raw non-linearity could be corrected by calibration in the laboratory.

# 34<sup>th</sup> International North Sea Flow Measurement Workshop 25-28 October 2016

## Technical Paper

### 9 CALIBRATION OF METER 1 WITH MODIFICATION

Meter 1 was returned to Cameron for modification. First the transducer housings were removed and replaced with longer housings such that the face of the housing would protrude fully into the flow. Then the meter body was sent to be coated internally using a proprietary fluoropolymer coating formulation and application method.

Figure 21 shows a picture of the interior of the meter at the Trapil calibration lab, with the transducer housings protruding and the coating applied.



Fig. 21 - Meter 1 with protruding transducer housings and internal coating, photographed prior to calibration

When calibrated the meter had a 'raw' non-linearity of +/- 1% with an offset of -3.5 % relative to the calibration lab. This was more extreme than expected, but was corrected by adjusting the path velocity weighting factors. Following adjustment of the weighting factors, the calibration was repeated with two oils (kerosene and gas oil of approximately 2 and 5 cSt viscosity respectively) and the performance verified to be within +/- 0.15 % linearity over the meter's specified turndown, as shown in Figure 22 below.

# 34<sup>th</sup> International North Sea Flow Measurement Workshop 25-28 October 2016

## Technical Paper

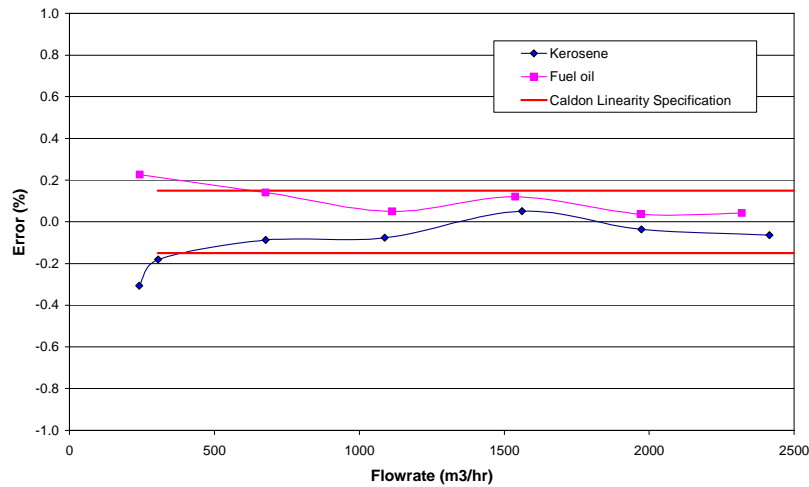


Fig. 22 - Calibration of Meter 1 post modification and weighting factor adjustment

### 10 COMMISSIONING AND MONITORING OF METER 1 AFTER MODIFICATION

When Meter 1 was re-commissioned, it was immediately checked against Meter 2, which had been left in service while Meter 1 was modified. Based on earlier comparisons of the contaminated meters with the tanks after some time in service, it was expected that Meter 1 in a clean and calibrated condition would register approximately 0.5 to 1 % higher than Meter 2 (i.e. it was expected that Meter 1 in a clean condition would be in close agreement with the tanks and that Meter 2 would be reading 0.5 to 1 % low). Contrary to expectations, it was found that the modified Meter 1 was reading approximately 2.9% higher than Meter 2, and about 2 % higher than the tanks.

Immediately an evaluation of diagnostic parameters was undertaken to determine the cause of this discrepancy. No fault could be found in the meter but when comparing diagnostic data from site against the calibration data it was noted that the flatness of the velocity profile at site was significantly higher than during calibration (0.815 flatness ratio in service versus a maximum of 0.775 at calibration). This was unexpected as the meter had been calibrated at Trapil using the upstream conditioner and pipework and the viscosity oils used had spanned the viscosity of the Danish crude oil.

Following some discussions with personnel at site, it was hypothesised that the drag reducing agent (DRA) that was in use might be affecting the flow velocity profile behaviour.

As the meter had been adjusted by means of the weighting factors, the effect on the meter behaviour is the same as applying a linear correction to the meter as a function of velocity profile flatness ratio. Figure 23 below shows the Trapil calibration data plotted in this way, with a point representing the operating condition at the time of commissioning. This shows that the operating condition at the time of commissioning was, in profile flatness terms, very far from the calibration conditions. Based on the comparison of Meter 1 with Meter 2 and with

# 34<sup>th</sup> International North Sea Flow Measurement Workshop 25-28 October 2016

## Technical Paper

the tank data it was clear that this linear extrapolation was not producing the desired measurement result at the field conditions.

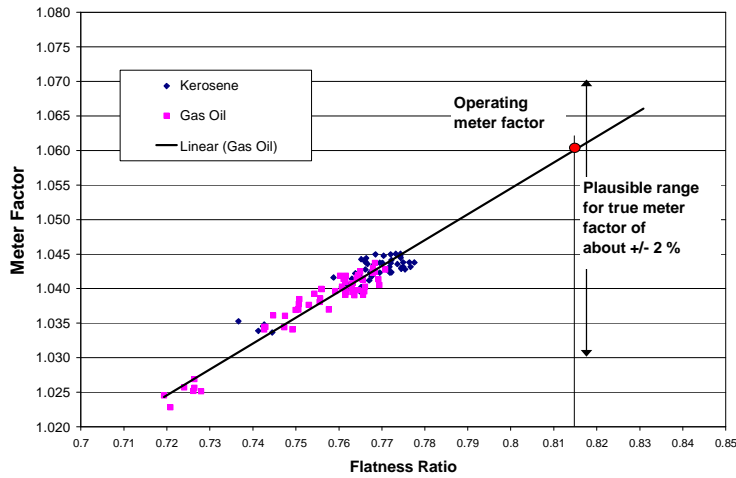


Fig. 23 - Calibration of Meter 1 post modification and weighting factor adjustment

In an effort to overcome this issue, and considering that the meter was not a custody transfer meter, the weighting factor adjustment that had been applied to the meter at the calibration was removed and the meter re-linearised using the computed Reynolds number as the calibration correlation parameter. This removed the influence of the unusually high flatness and brought the two meters into closer agreement, though it appeared that the modified meter was still reading approximately 0.6 % higher than expected.

The modified meter was then monitored for a period of some months and in this time it was easily determined that it was not performing as well as had been hoped. Figure 24 below shows the response of Meter 1 after modification, relative to the tank gauges.

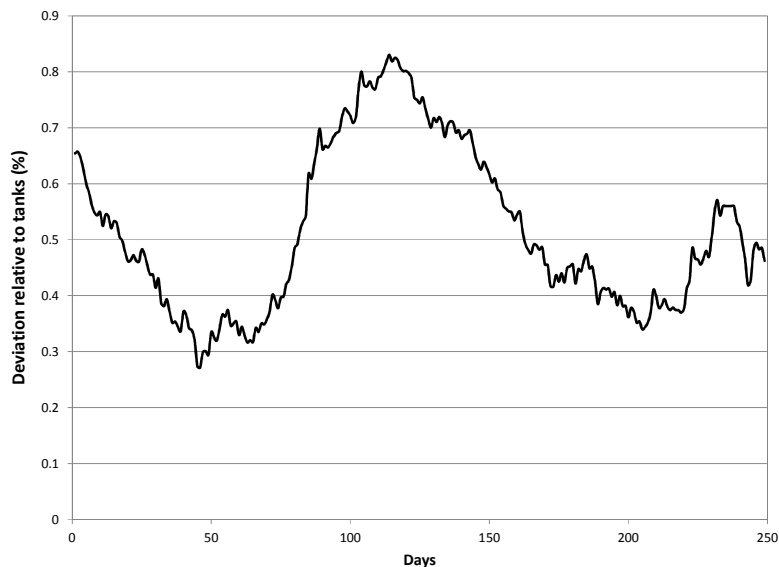


Fig. 24 - Comparison of Meter 1 (modified, with protruding transducer

# 34<sup>th</sup> International North Sea Flow Measurement Workshop 25-28 October 2016

## Technical Paper Housings) against the tanks

During the same time period, the influence and effectiveness of the drag reducing agent was discussed and it was noted that more DRA was used when the water content of the crude was high. Subsequent analysis showed that there was a degree of correlation between the water extraction flowrates and dewatering tank level indications at Fredericia and the indicated profile flatness, as shown in Figure 25 below. Given the suggestion that the DRA dose was increased when the water content of the crude is high, this was taken as corroboration that the profile flatness was varying in response to changes in the dosage of DRA.

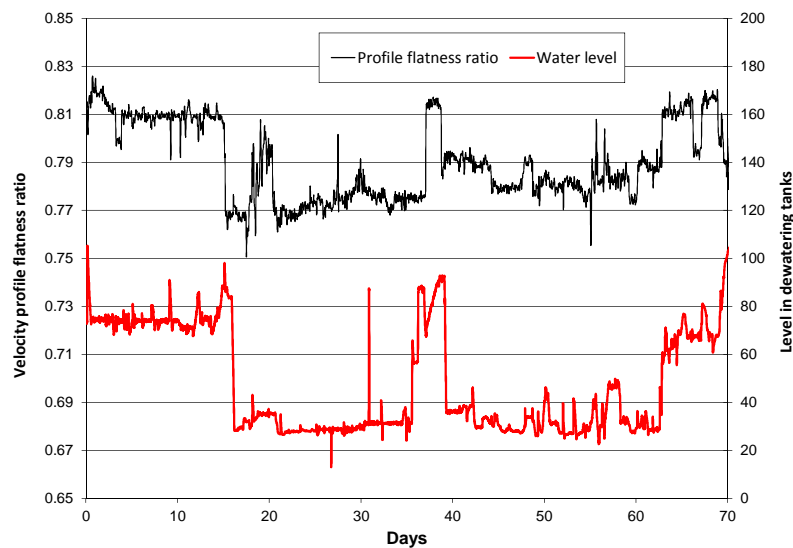


Fig. 25 - Water content and profile flatness correlation, linking DRA injection rates to profile flatness changes

Based on diagnostic analysis and an internal inspection of the meter after 9 months in service (see the photograph show in Figure 26), it was clear that the modified meter was no longer suffering from the problem of deposition in front of the transducer housings. However it was also clear that the decision to protrude the transducer housings had resulted in a different problem. As a result of protruding the transducer housings, the meter design did not respond appropriately to changes in the boundary layer of the flow. In other words, protruding the transducer housings had impaired the ability of the meter to properly integrate the velocity profile. This, in combination with the fact that DRA was being used, made it impossible for the meter to accommodate the changes in flow profile in the area close to the pipe wall, a problem that the standard, unmodified meter did not have.

**Technical Paper**



Fig. 26 - Inspection of the meter with protruding transducer housings and internal coating, after 9 months in service

Having discussed the conclusions above with the customer a decision was reached to return Meter 2 to Cameron and have it coated internally, but this time without also taking the step of protruding the transducers.

**11 CALIBRATION AND OPERATION OF METER 2 ONCE COATED**

The second meter was coated internally, with the transducer housings in their normal location and was then re-calibrated. When compared with the original calibration of Meter 2, meter factors obtained at similar Reynolds numbers agreed with the earlier calibration within the uncertainty of the results, as shown in Figure 27.

# 34<sup>th</sup> International North Sea Flow Measurement Workshop 25-28 October 2016

## Technical Paper

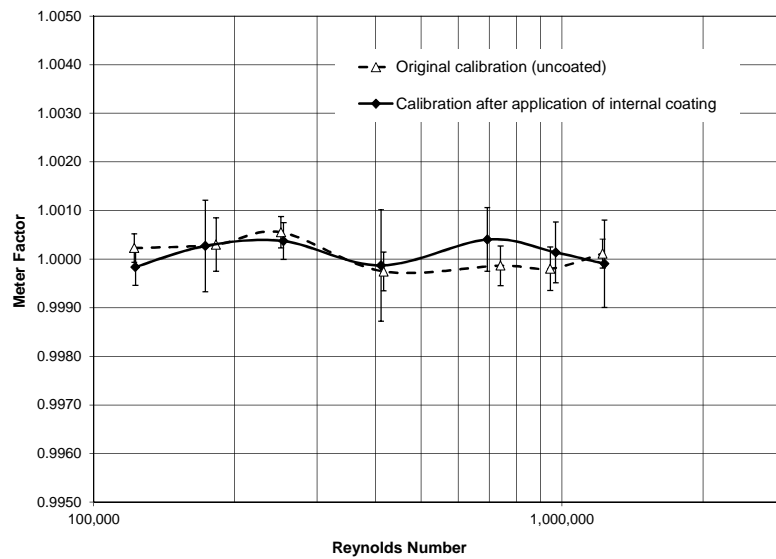


Fig. 27 - Comparison of calibration data for Meter 2; original calibration without internal coating, and after the coating was applied

After Meter 2 had been coated, calibrated and installed, it was monitored relative to the tanks. When the data was analysed it appeared that the meter was relatively stable at first, showing a slight downward trend, and then changed its behaviour after a couple of months in operation. It was feared that contamination problems had developed again, but analysis of the diagnostic data did not suggest that was the case. The tank comparison data for this period is shown in Figure 28 below. Initially this data was baffling, as the comparison with the tanks suggested that after about 75 days in service the meters started over-reading. The 4-path meters with transducer housings recessed had never shown over-reading behaviour prior to this point, even when contaminated. As a result of much discussion and speculation it was then discovered that the date of the change in meter behaviour coincided with the commissioning of a new de-gassing facility. The degassing facility is situated between the metering station and the tanks. As a result, the comparisons that were being carried out were no longer valid as they did not account for the inventory change in the degasser tanks, nor the change in volume due to extraction of gas and additional water from the degassing facility. Figure 28 shows that it is only after the point in time when the degasser unit was brought online, 56 days into the operation of the coated meter, that the deviation begins to trend upwards.

# 34<sup>th</sup> International North Sea Flow Measurement Workshop 25-28 October 2016

## Technical Paper

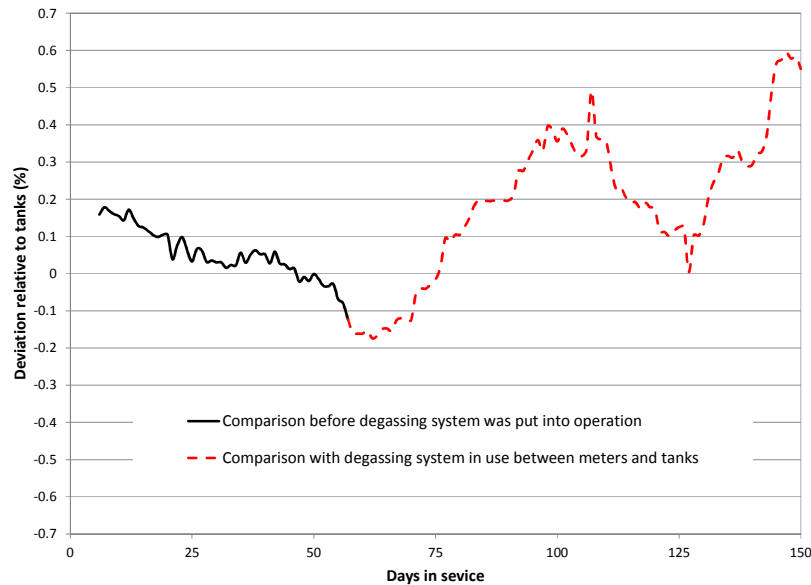


Fig. 28 - Comparison the coated meter with the tanks, not accounting for the operation of the degassing system

The next step was to try to account for the gas and water extracted from the crude oil in order that a comparison could be carried out over a longer time period. Efforts were made to improve the method of comparison, with corrections being made using data available from instrumentation on the degassing system. At first there were difficulties in obtaining good agreement. This was in part due to a defective temperature measurement on one of tanks. It was then discovered that the comparison should also account for recovered oil from the refinery could be added to the line between the meters and the tanks. Once the corrections had been made, a reasonable comparison could be obtained, albeit with greater uncertainty than before.

Figure 29 shows a longer-term comparison of the coated meter versus the tanks with corrections applied in an attempt to compensate for the volume changes owing to operation of the degassing system. It should be noted that this comparison is subject to significant uncertainty, as evidenced by the scatter in the daily comparison data. Given that uncertainty, it is difficult to ascertain if the fluctuations apparent in the 20-day average are influenced at all by contamination or if they are simply the result of the scatter in the daily comparisons. It is clear however, when compared with Figure 18, that there not the same systematic 'drift' due to contamination that was apparent with the uncoated meter.

# 34<sup>th</sup> International North Sea Flow Measurement Workshop 25-28 October 2016

## Technical Paper

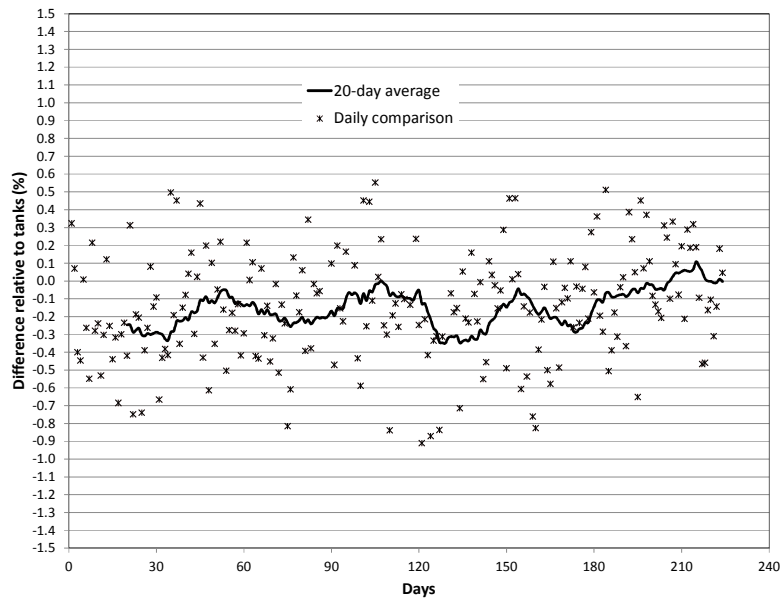


Fig. 29 - Comparison the coated meter with the tanks, including corrections for water and gas extracted, level changes, and recovered oil added

Following the evaluation Meter 2 after modification (coated and with transducer housings recessed as normal), Meter 1 was returned to the factory and made the same as Meter 2. Subsequent diagnostic checks and periodic inspections have shown that the meters are not completely free from the effects of contamination. However, the coating applied to the meters has substantially reduced the build-up problem. Figures 30 and 31 show photographs of the interior of Meter 2 after it had been coated and had been in service for approximately 10 months without cleaning. Although the interior surfaces are not free from contamination, it was observed that the contaminants have greater difficulty in adhering to the coated surface than they did with stainless steel, and in some places it appeared that the flow had stripped the contaminants off of the pipe wall, leaving the coated surface clean. Of particular importance it was observed that the problem of contamination build-up forming in the cavities of the upstream transducer housings was significantly reduced, as can be observed by comparing Figure 31 with that of Figure 15, which both show the deeper cavities of the outside paths. In the case of the uncoated meter the deposition covers the whole of the interior of the cavity and the face of the housing. With the coated meter there is much less deposition and it appears not to have consolidated in the same way as for the uncoated meter, suggesting the coating results in a 'self-cleaning' effect.

**34<sup>th</sup> International North Sea Flow Measurement Workshop  
25-28 October 2016**

**Technical Paper**



Fig. 30 - Photograph showing the coated meter with transducer housing cavities facing upstream



Fig. 31 - Photograph showing a the coated meter with a transducer housing cavity facing downstream

# 34<sup>th</sup> International North Sea Flow Measurement Workshop 25-28 October 2016

## Technical Paper

### 12 DISCUSSION AND CONCLUSIONS

Contamination build-up inside ultrasonic meters can affect performance. Often it is thought that the main error mechanism would be over-reading owing to a reduction in cross-sectional area. However, in this application the main effect of the contamination build-up was an alteration the effective path geometry relative to the conditions of calibration, causing the meter to under-read.

The precise mechanisms causing the contamination to build up in this case are not well understood, and although there is no evidence for or against the drag reducing agent (DRA) playing a part, there is a suspicion that the DRA may be contributing to the build-up. To date this is one of only two cases known to Cameron where contamination build up inside multipath meters on crude oil has been confirmed.

Contamination build-up can be detected and monitored by means of diagnostic information. For the 4-path meters in this case, a signal gain monitoring diagnostic was developed and could be shown to correlate well with the development of measurement deviations on the uncoated meters.

An initial attempt to resolve the problem by both coating the interior of the meter with fluoropolymer coating *and* protruding the transducer housings was effective as far as contamination build-up was concerned, but ultimately was unsuccessful as the protrusions prevented the meter from properly measuring changes in the boundary layer of the flow. Sensitivity to changes in the boundary layer of the flow was accentuated in this application owing to velocity profile variations being linked to the dosage of drag reducing agent.

Applying the fluoropolymer coating to the wetted surfaces (bore and transducer housings) of a standard meter with recessed transducer housings, did not alter its calibration performance and has been shown to be beneficial in terms of reducing the degree and effects of contamination build-up.

The meter with protruding transducer housings was modified a second time and both meters have now been in service for several years with their transducer housings recessed as normal with all wetted surfaces coated with the fluoropolymer coating. The meters are removed for calibration at annual intervals and are cleaned before they are sent to the laboratory. In the spring Meter 2 is also cleaned just before Meter 1 is removed and sent for calibration. In the fall Meter 1 is cleaned before Meter 2 is sent for calibration. This results in a maximum of 6 months operation in between each calibration and/or cleaning of a meter.

The internal coating has not shown any signs of deterioration in service, being described by the technician on site as being "in very good condition on both meters".

## Technical Paper

### Using an Ultrasonic Flowmeter in the Transition Zone

David Mills, Oil & Gas Measurement

Julien Porré, Oil & Gas Measurement

#### 1 INTRODUCTION

The abstract for this paper contained the following statement:-

*Liquid flow measurement is essential throughout the oil and gas industry. Ideally a flow measurement system would have high turndown and low measurement uncertainty, maintained over the complete flow range. Unfortunately velocity based meters such as turbine and ultrasonic meters can show significantly degraded linearity at low flows. Provided the measurements are repeatable this non-linearity can be defined and corrections applied in order to maintain a good turndown. If repeatability is not good, the overall uncertainty of measurement will be worse at the low flow end and may not be acceptable. This will result in much higher costs for metering as more meter tubes will be required to cover the overall flow range. These turndown effects become more and more significant as viscosity increases.*

*OIML R 117 for a class 0.3 meter requires the difference between the largest and smallest results of 3 successive (flow) measurements to be within 0.12% for flow greater than 5 times the minimum specified meter flow.*

*Flow below this point will typically be approaching the transition zone which is the flow region between turbulent flow (typically Reynold's Number (Re) >4,000 and laminar flow Re < 2,500). Flow in this transition zone is chaotic, where vortex sizes can vary from microscopic to a significant part of the pipe diameter. As they are chaotic in nature they are not evenly distributed across the pipe section and have rotational characteristics differing in magnitude and direction as well as linear velocities along the pipe axis. A turbine meter has mechanical inertia and as it occupies almost the complete cross section of the pipe can "smooth out" these effects, whereas a typical planar chordal liquid ultrasonic flow meter can suffer from degraded repeatability and thus worsened measurement performance. This effect can begin to be seen below Reynold's numbers as high as 10,000 for some USMs and the repeatability spread can be 10 times greater than the OIML requirement of 0.12% when in the transition zone.*

*The Nyquist sampling theorem states that a sampling rate of twice the highest frequency component enables a complete re-construction of the original signal. This suggests that a high sampling rate in the meter would overcome the problem; however, increasing the sampling rate in a planar chordal meter is likely to "over-sample" larger vortices and will not add extra linear velocity information above a certain sample rate as over-sampling in the time domain will not add extra linear velocity information.*

# 34<sup>th</sup> International North Sea Flow Measurement Workshop 25 – 28 October 2016

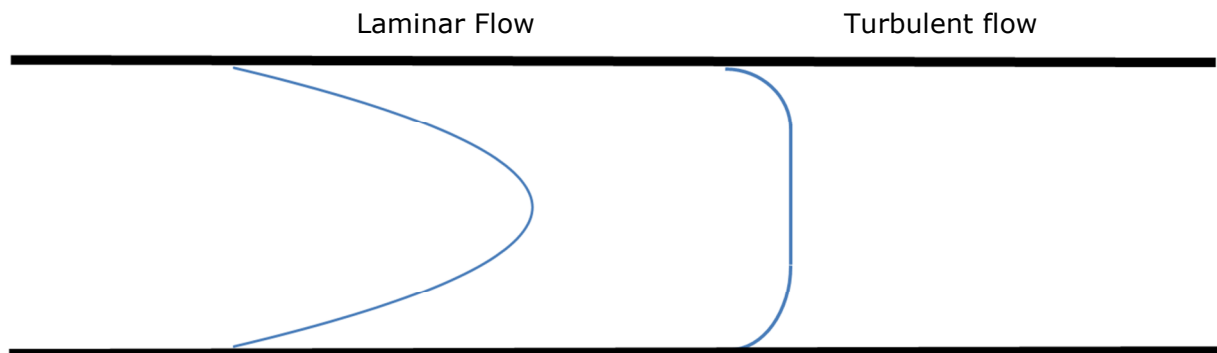
## Technical Paper

Reproducibility of measurement, not only short term repeatability - three consecutive measurements for example - but long term repeatability – do we achieve the same value the next day, or the next week, or even the next year, given at what we believe to be the same process conditions?

This is fundamental to high quality measurement.

Reynold's number is the dominant factor. As seen above, OIML R117 is effectively silent for low Reynold's number and typically liquid USMs are considered to have worsening repeatability as Re reduces below 10,000.

At very low flow rates flow is laminar with fluid motion being parallel to the pipe walls and with a parabolic flow profile, and at higher flow rates flow is turbulent and with a much flatter flow profile:-



The line drawings above represent ideal cases: in the real world the flow may include swirl or a profile which is not symmetrical about the pipe axis. Crossed, horizontal chordal beams can cope well with swirl, but clearly would not cope well, when for example, the profile "nose" is predominantly below the lowest beam path.

The laminar flow regime typically exists below  $Re < 2,000$

At higher flow rates, typically at  $Re > 4,000$  the profile becomes flatter as the flow becomes turbulent. In the region between laminar and turbulent flow the characteristics change rapidly and in a random manner where laminar flow dominates at low Reynold's numbers and turbulent flow dominates at higher Reynold's numbers. This is the transition zone.

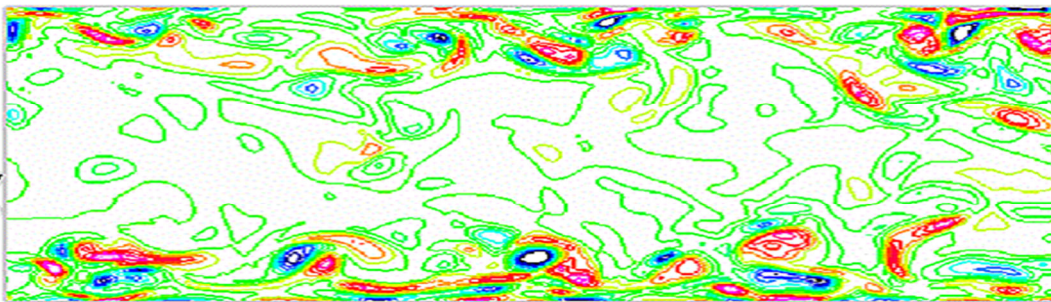
Flow in the transition zone was described as *chaotic*. In the English language this usually means *complete disorder and confusion* and in physics to be *the property of a complex system whose behaviour is so unpredictable as to appear random, owing to great sensitivity to small changes in conditions*. Again in the abstract, chaotic flow was described as *where vortex sizes can vary from microscopic to a significant part of the pipe diameter. As they are chaotic in nature they are not evenly distributed across the pipe section and have rotational characteristics differing in magnitude and direction as well as linear velocities along the pipe axis*.

# 34<sup>th</sup> International North Sea Flow Measurement Workshop 25 – 28 October 2016

## Technical Paper

A paper presented at the 6<sup>th</sup> Symposium. Smart Control of Turbulence, Tokyo March 6 to 9, 2005 <sup>[1]</sup> stated *The visualized flow field and the turbulent statistics suggest that the streaky structures..... exist only near the wall, while the large scale structures extend from the centre of the channel to the near wall region. Therefore, the near wall turbulence depends not only of the near wall fine scale structure, but also on the large scale structures.*

The image below shows a CFD model of such a flow, where the small structures near the pipe wall can be clearly seen, as can the large scale structures, which are predominantly visible within the central area of the pipe, but can also be seen extending near to the wall of the pipe. This image only shows a 2 dimensional "slice" cut through the centre line of the pipe, whereas the actual structure shapes in the 3 dimensional space would show random variability of cross section and shape in much the same way as those in the 2 dimensional slice. Velocities in those large scale structures will include both angular and axial velocities which will be constantly changing and thus changing the shape of the structure. Total flow momentum will be maintained, but will transfer from structure to structure as they change shape in this chaotic regime.



A transit time USM measures upstream and downstream transit times along the same path and calculates the axial fluid velocity:-

The diagram below shows a single beam. The velocity of fluid can be calculated from:-

$$V = ((t_2 - t_1)/(t_2 * t_1)) * (L / 2\cos\theta)$$

Where

V = fluid velocity

t<sub>2</sub> = transmission time upstream

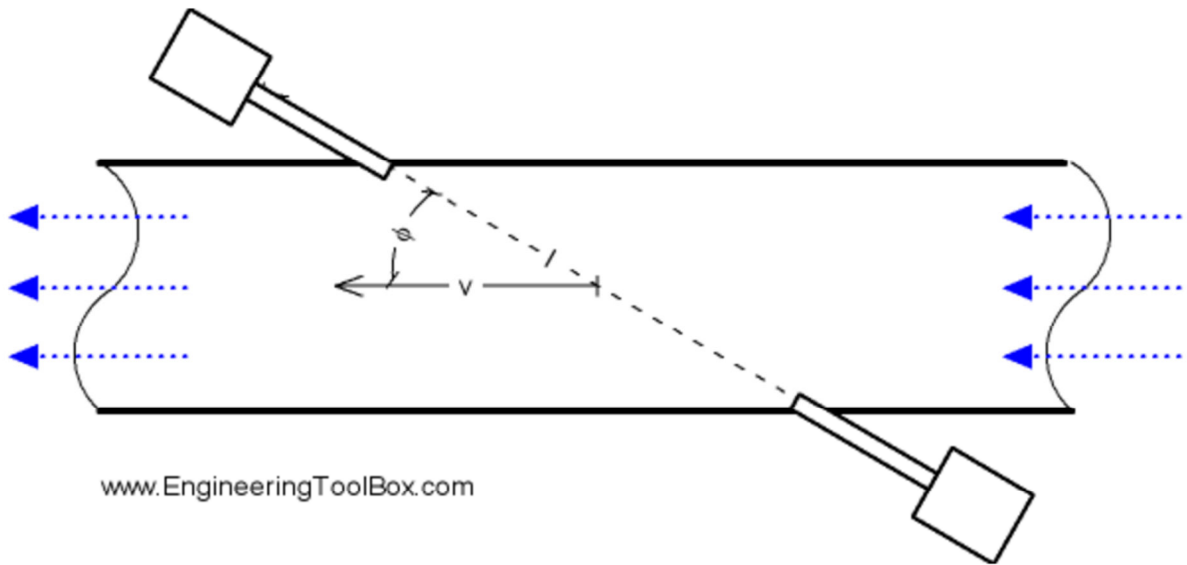
t<sub>1</sub> = transmission time downstream

L = distance between sensors

θ = angle between beam and pipe axis

**34<sup>th</sup> International North Sea Flow Measurement Workshop  
25 – 28 October 2016**

**Technical Paper**

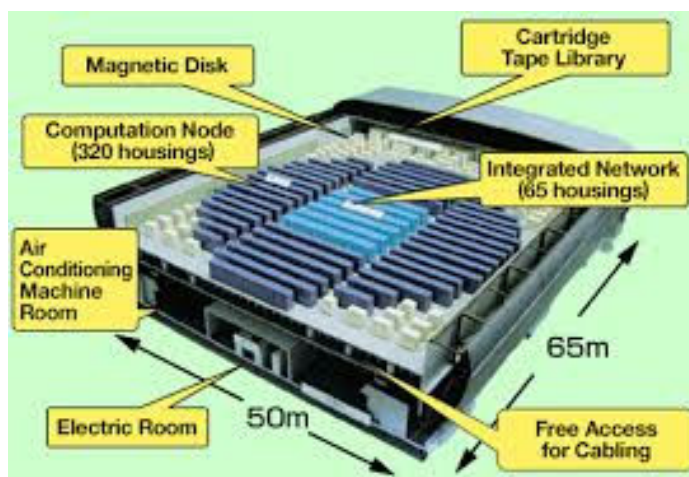


USMs used for custody transfer and other “high end” duties have more than one beam, arranged in a variety of different ways, with chordal beams arranged in horizontal planes being the most common. Some meters use dedicated beams arranged to obtain diagnostic data.

A single beam can only provide a *good* measurement when the flow profile is fully developed and there is no swirl at the measurement position.

How many beams, and how should they be arranged to obtain this *good* measurement?

Let us look at the question in a reverse and consider the computational fluid dynamics problem in reference [1]. This simulation used around 16 billion grid points with calculations being performed using 2048 CPUs with 4TB of memory – and even with all this computing power it did not work in “real time”!



The Earth Simulator computer used for the CFD modelling in reference [1]

This is not a good solution – a flowmeter electronics housing 65m x 50m and occupying 2 floors is definitely not practical!

# 34<sup>th</sup> International North Sea Flow Measurement Workshop 25 – 28 October 2016

## Technical Paper

This is not a reasonable comparison as the problem is different; the CFD simulation is looking at the properties of the individual cells defined by the matrix of those 16 billion grid points and determining the effect of one cell on the adjoining cells whilst maintaining overall momentum of the flowing fluid; the USM is **measuring** time of flight (TOF) along a small number of fixed paths, and is then using these TOF values as the basis for calculating, or rather *estimating*, the flow rate.

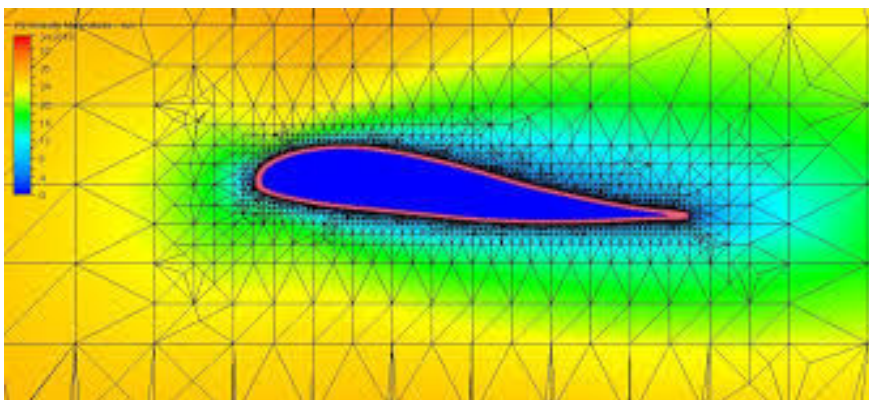
The processing power required to simulate flow in this regime is clearly very high indeed, so can we hope to achieve acceptable results by just measuring TOF along these few paths?

What is the optimum arrangement of these beams in order that sufficient information is provided to enable the mean axial velocity,  $V$  along the pipe to be determined? Provided  $V$  is known, then flowrate is simply:

$$V \times A \text{ m}^3/\text{h}$$

Where  $V$  is in  $\text{m/s}$  and  $A$ , *the cross sectional area of the pipe*, is in  $\text{m}^2$

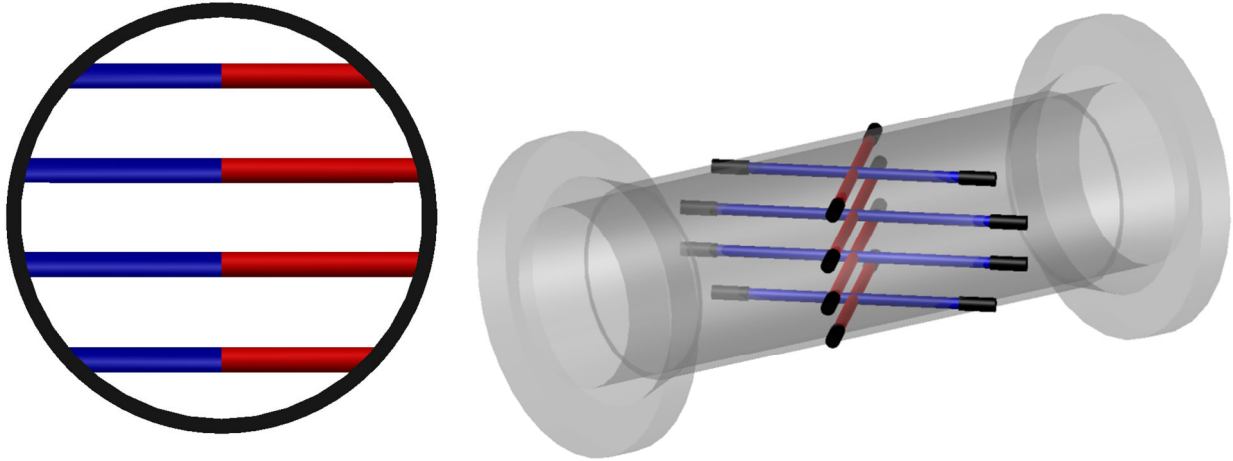
The CFD simulation does provide useful indicators for the USM; the simulation uses very small grid matrix sizes where flow patterns are complex; the flow simulation in reference [1] is a good example, where a very small mesh size was used close to the wall, and a larger size in the centre of the pipe; around the surface of an aircraft wing is a common example where grid matrices are very detailed around the wing surface, and particularly where flow directions change rapidly and larger, simpler grid matrices where flow patterns are simpler at greater distances from the wing surface – in other words more information equates to a “tighter” matrix.



# 34<sup>th</sup> International North Sea Flow Measurement Workshop 25 – 28 October 2016

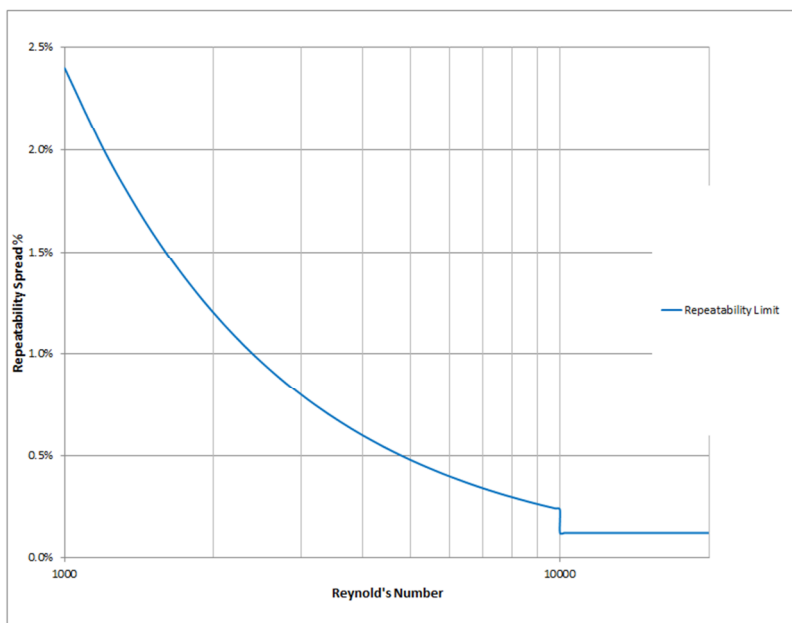
## Technical Paper

A typical 8 beam chordal meter path layout is shown below:



Reference [2] explains clearly that changes between laminar like and turbulent like flow regimes in the transition zone causes non-axial flow components to be developed. The velocity profile thus changes rapidly and prevents good repeatability being achieved. This referenced paper was based on chordal meter designs and notes that “a lower Reynold’s number limit of 10,000” is recommended. Although not referenced in [2], but elsewhere in the same manufacturer’s literature it is also stated that for the 8 chordal path meter the maximum spread in three repeats below  $Re = 10,000$  is  $\neq 20,000 \times 0.12/Re$ .

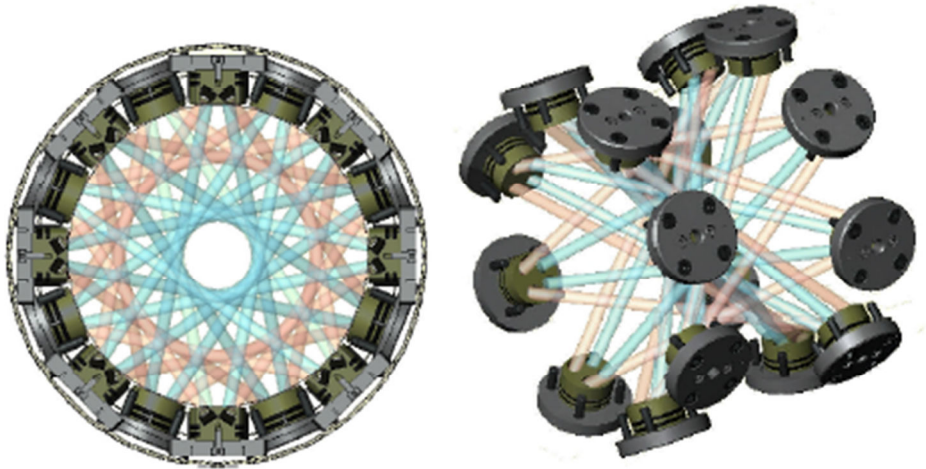
This is graphically represented below. It should be noted that it shows the repeatability spread acceptance limits, and does not necessarily represent the results which would be obtained in practice.



# 34<sup>th</sup> International North Sea Flow Measurement Workshop 25 – 28 October 2016

## Technical Paper

The 32 beam layout for DFX meter used for the tests in this paper is shown below:



The 32 beam design gives an axially symmetric layout. This ensures that the meter is installation insensitive to the plane of an upstream bend and the beam coverage provides much enhanced information on the flow profile. See reference [3] for examples.

Given this “enhanced information” can we expect to achieve a high order of repeatability, or will it still require “averaging” over a longer period of time? [cf. turbine meter which “averages” thanks to mechanical inertia and almost full coverage of the pipe cross section]

The tests carried out concentrated on low Reynold’s numbers (<10,000). Results have been included for Reynold’s numbers >20,000 for comparison purposes when the meter(s) are used well above the transition zone and where flow can be assumed to be well developed turbulent flow.

## 2 DESCRIPTION OF TESTING CARRIED OUT

Three main groups of test results are included in Appendix A.

Tests 1 and 2 were carried out using M&T DFX liquid USMs. As described above, these meters have 32 beams arranged in an axially symmetric design. Each of the 16 transducer assemblies contains four separate transducers with 2 of the transducers handling the outer ring of 16 beams (shown in red above) and the other 2 transducers handling the inner ring of 16 beams (shown in blue above).

Test 1            4 inch DFX calibration, NEL, East Kilbride - UKAS 0009

Test 1.1        Velocite with a viscosity of ~45 cSt at ~12°C . Reynold’s number from ~1,600 to 22,000

Test 1.2        Gas oil with a viscosity of 6cSt at 44°C. Reynold’s number ~10,000 to 163,000

# 34<sup>th</sup> International North Sea Flow Measurement Workshop 25 – 28 October 2016

## Technical Paper

Test 2            8 inch DFX calibration, IMS Calibration Facility, Belgorod - VSL CMC Certification LF2015.04.0012

These tests were carried out specifically for this presentation using oil with a viscosity of ~26 cSt at ~25°C. Reynold's number from ~2,900 to 26,300

Test 3            16 inch USM (3 off) from A.Nother Company

These calibrations were carried out by ANO Company, using their accredited flow calibration laboratory as part of their "contract to supply and calibrate" 3 off liquid ultrasonic meters to Oil & Gas Systems. The calibration fluid was Drakeol 32 with a viscosity of ~80 cSt at ~20°C. Reynold's numbers for ~1,700 to 37,000.

The meters have been installed offshore as 2 off 100% meter tubes, with a "spare" meter on hand to be used when either of the two working meters are sent on-shore for re-calibration. Due to the size of the assembled meter/meter run assembly, it was proposed that only the meter should be sent on-shore. Although these meters are described as being very tolerant of upstream flow conditions, bored and axially aligned upstream meter tubes were required by the end customer to confirm that measurement results would be acceptable if only the meter body itself were to be re-calibrated without its installed meter tubes. A pair of upstream and downstream meter tubes manufactured in the same way as the installed meter tubes were retained at the USM suppliers and have been used for all subsequent calibrations.

Test 3 results were extracted from calibration data for 3 off 16 inch liquid USMs supplied to Oil & Gas Systems for a customer contract. Details are given in the test results.

### 3 DISCUSSION OF TEST RESULTS

Test result data is given in Appendix 1 for reference purposes. All data shown in the figures is taken directly from the calibration results.

Repeatability spread in all cases is simply calculated as:-

$$\frac{(Kfactor\ max - Kfactor\ min) \times 100\%}{Kfactor\ min}$$

4 inch 32 beam USM

The volumes used for the 4 inch 32 beam meter were dependent on flow rate and varied from nominally 1.48 m<sup>3</sup> to 12.2 m<sup>3</sup>. These volumes were measured using PD meters as master meters.

8 inch 32 beam USM

As can be seen from the detailed results in Appendix A the bi-directional prover volumes were nominally 3.18m<sup>3</sup> for the 8 inch 32 beam meter. This was the complete swept volume for the combined forward and reverse passes of the sphere.

All test sequences were of 4 runs only.

**34<sup>th</sup> International North Sea Flow Measurement Workshop  
25 – 28 October 2016**

**Technical Paper**

16 inch 8 beam meters

The low flow tests ( $\sim 150 \text{ m}^3/\text{h}$  and  $450 \text{ m}^3/\text{h}$ ) were run with a nominal  $10.06 \text{ m}^3$  uni-directional prover.

Test sequence run lengths were not consistent, with 20 at 3 runs, 2 at 4 runs, 6 at 5 runs and 1 at 9 runs. It is understood that extra runs were made when the repeatability required by the formal test procedure could not be reached with 3 runs.

All higher flow rate tests used a USM master meter system with measured volumes varying from  $\sim 21 \text{ m}^3$  to  $\sim 38 \text{ m}^3$ .

Pulses counted by the master meter obviously corresponded to these volumes and varied from 20,000 to 57,000.

# 34<sup>th</sup> International North Sea Flow Measurement Workshop 25 – 28 October 2016

## Technical Paper

### 3.1 Test 1

This 4 inch meter was calibrated on 2 products with different viscosities for use in metering oil flow from an offshore separator where both varying amounts of water and gas slugs occur in practice. This application has previously been discussed in references [3] [4]

Figure 1 shows the repeatability spread for each point in the calibrated flow range.

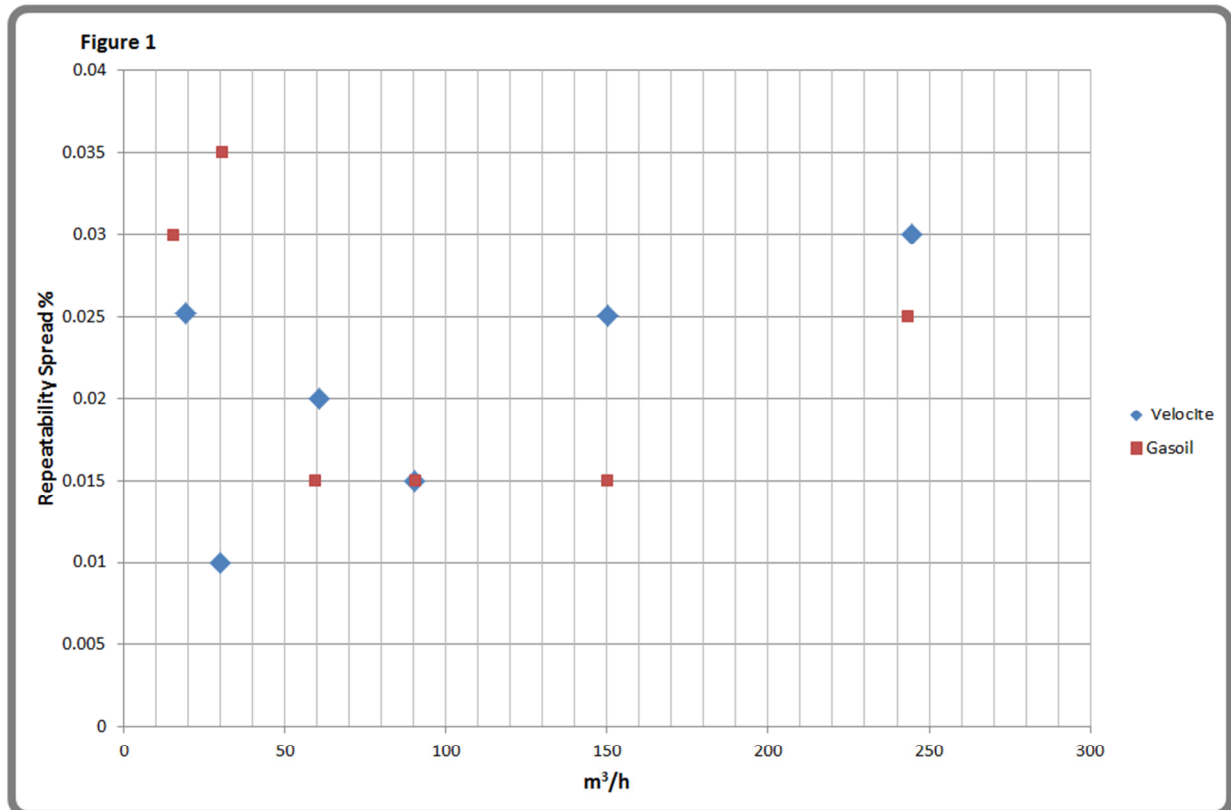


Figure 1

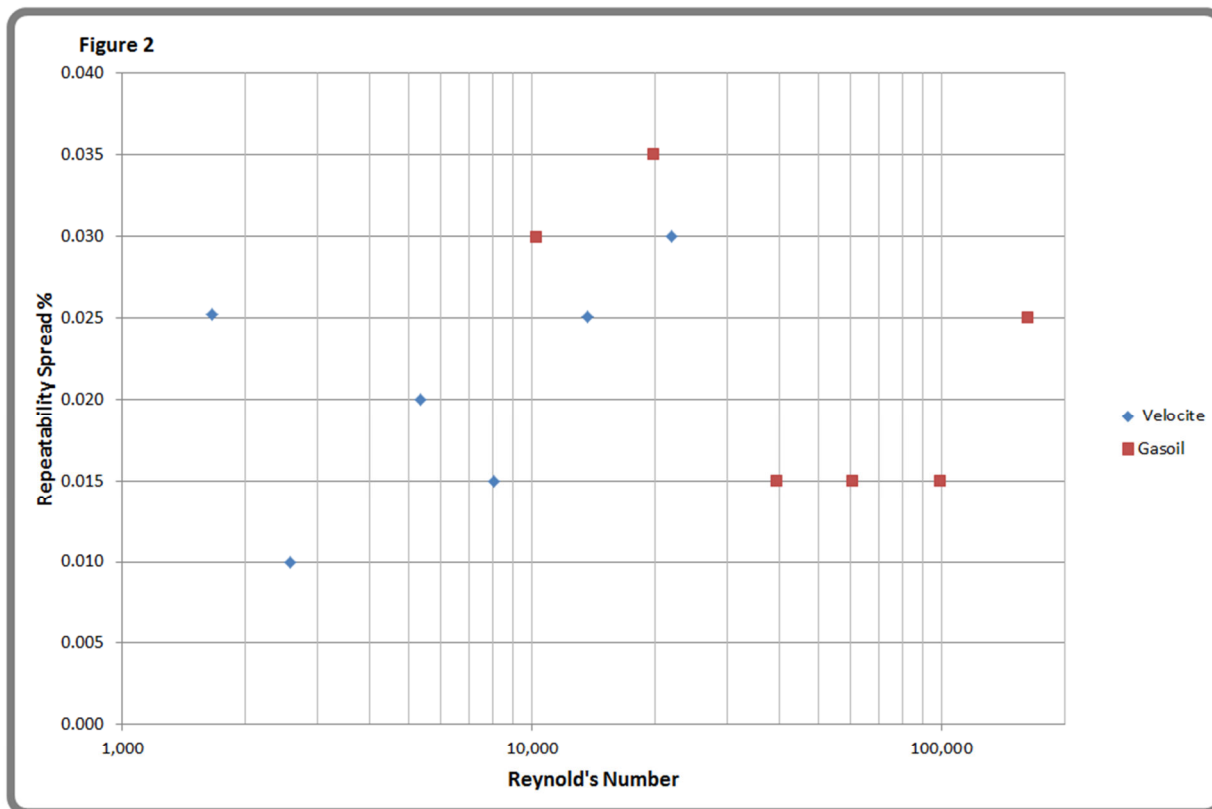
The volumetric flow rate measurement points go from the laminar flow region, through the transition zone and extend up well into the turbulent flow region. As has been discussed at many conferences, Reynold's number is the key factor in the characterisation of all velocity meters, such as USMs and turbines. In the case of the USM the flow profile, described in various ways including *profile number* and *flatness ratio*, for example, is often used as part of the initial characterisation of a USM before final calibration and this value can be derived from the initial characterisation results.

When examined in volumetric terms, the results for the two products show good correlation, with worst case occurring at  $\sim 30\text{m}^3/\text{h}$ , and even there the difference in repeatability spread is only 0.025%.

# 34<sup>th</sup> International North Sea Flow Measurement Workshop 25 – 28 October 2016

## Technical Paper

Figure 2 shows the repeatability spread when plotted against Reynold's number, plotted here, conventionally, on a logarithmic scale.



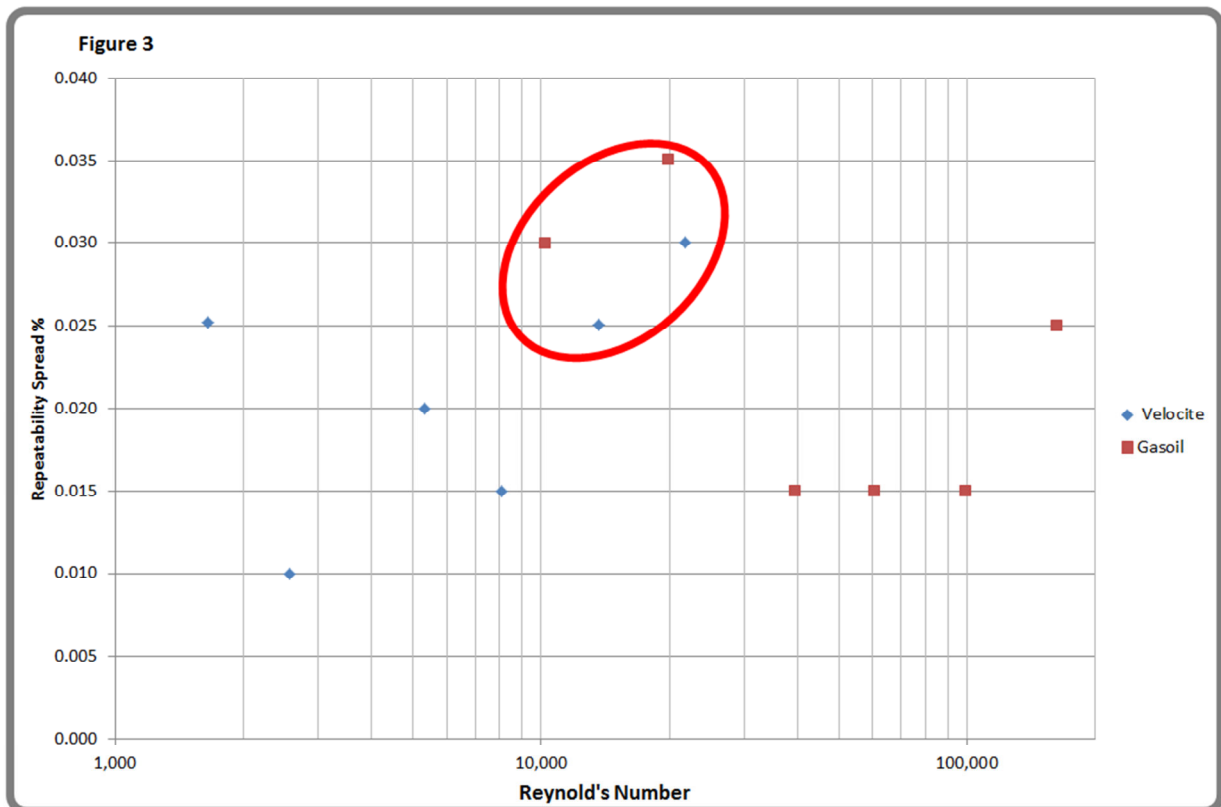
As mentioned above, since Reynold's number is a key parameter in USM characterisation, the use of 2 calibration fluids of different viscosities is accepted for calibration purposes where the calibration laboratory cannot achieve a high enough volume flow rate on a high viscosity fluid, but can achieve a high enough Reynold's number flow rate by using a lower viscosity fluid. In the case of this testing the two viscosities were used in order that the meter could be used on crude oil and also crude oil with high water content, where the apparent viscosity can rise rapidly as water content rises.

# 34<sup>th</sup> International North Sea Flow Measurement Workshop 25 – 28 October 2016

## Technical Paper

Figure 3 shows the four calibration points highlighted where the Reynold's numbers overlap.

These points correspond to about 150 m<sup>3</sup>/h and 250 m<sup>3</sup>/h for the velocite calibration and 15 m<sup>3</sup>/h and 30 m<sup>3</sup>/h for the gasoil calibration. Although outside the main transition zone area of interest for this paper it is a good demonstration that repeatability for this meter was largely independent of viscosity. In practice, good profile number characterisation and modelling would also be required to ensure that volumetric flow calibration linearity could be obtained, although neither can be obtained without good repeatability.



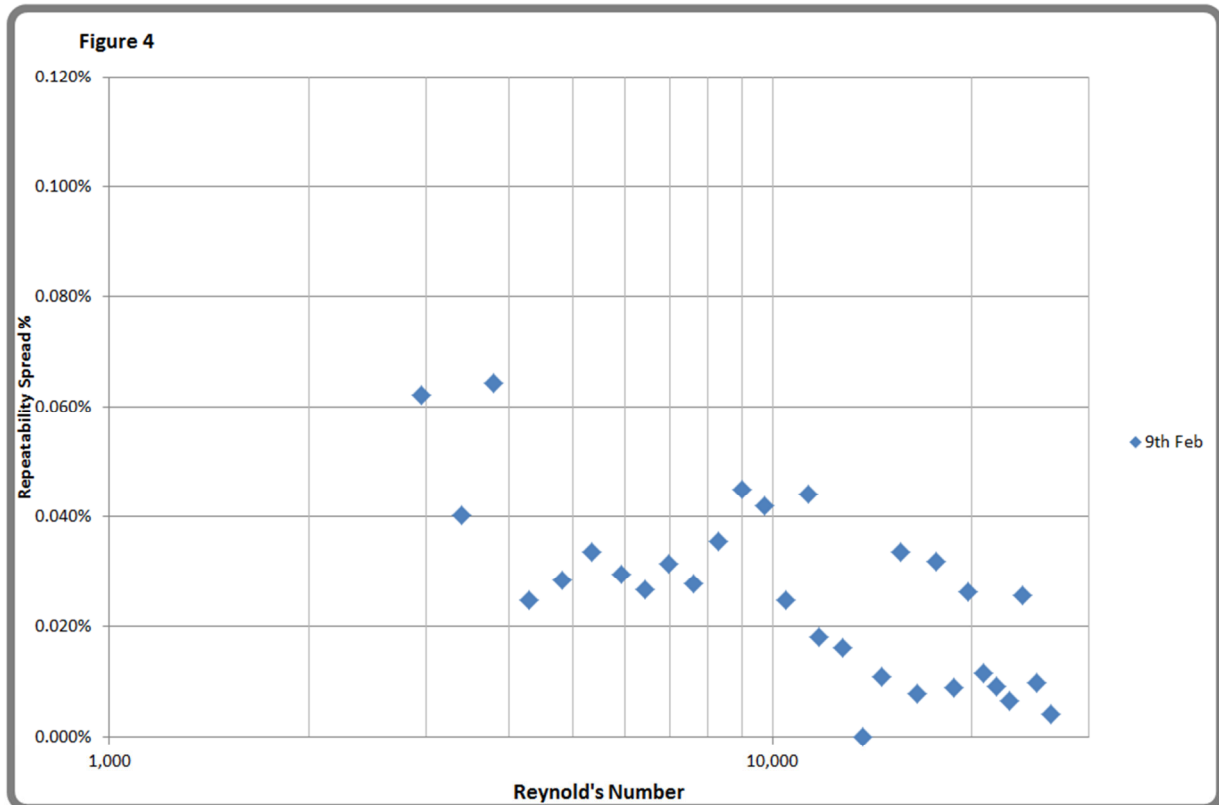
# 34<sup>th</sup> International North Sea Flow Measurement Workshop 25 – 28 October 2016

## Technical Paper

### 3.2 Test 2

These tests were carried out using an 8 inch DFX 32 beam meter specifically for this presentation using oil with a viscosity of  $\sim 26$  cSt at  $\sim 25^\circ\text{C}$ . The tests were repeated 3 days later for comparison purposes.

Figure 4 shows repeatability spread for all test carried out on February 9th

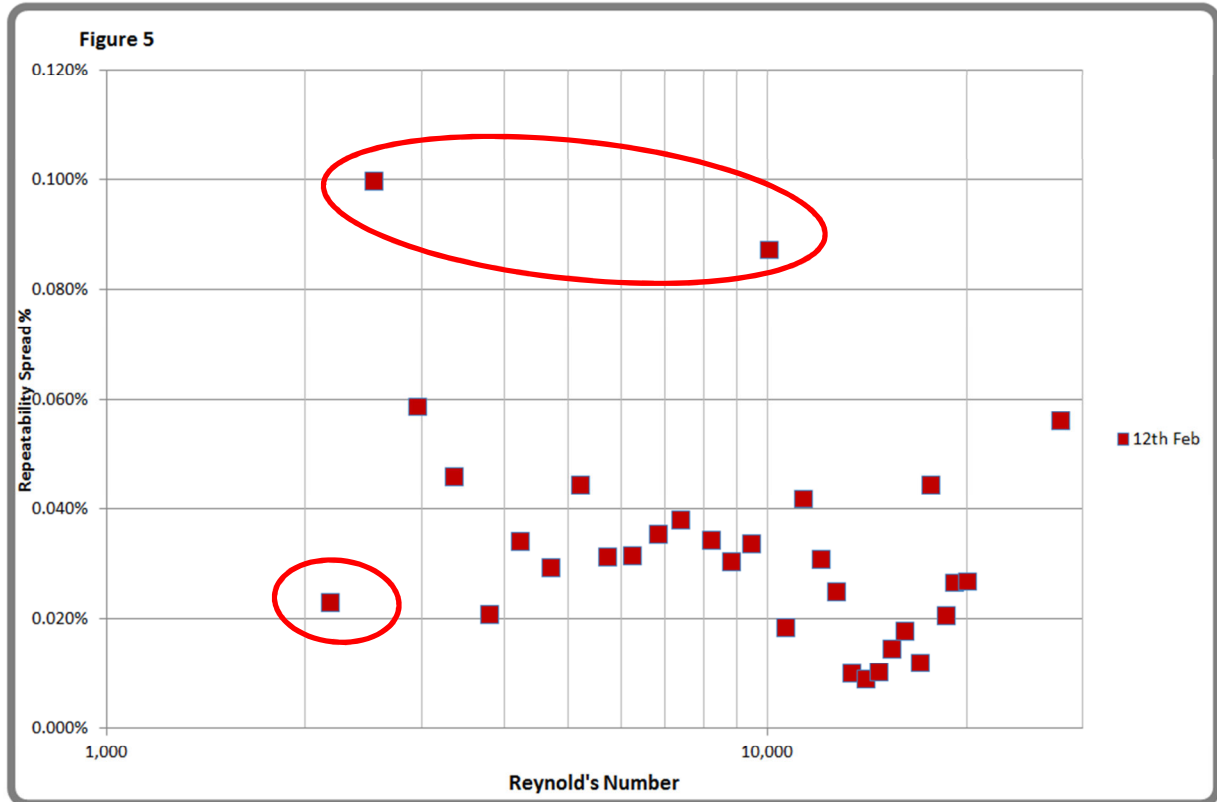


# 34<sup>th</sup> International North Sea Flow Measurement Workshop 25 – 28 October 2016

## Technical Paper

Figure 5 shows uncertainty spread for all test carried out on February 12<sup>th</sup>

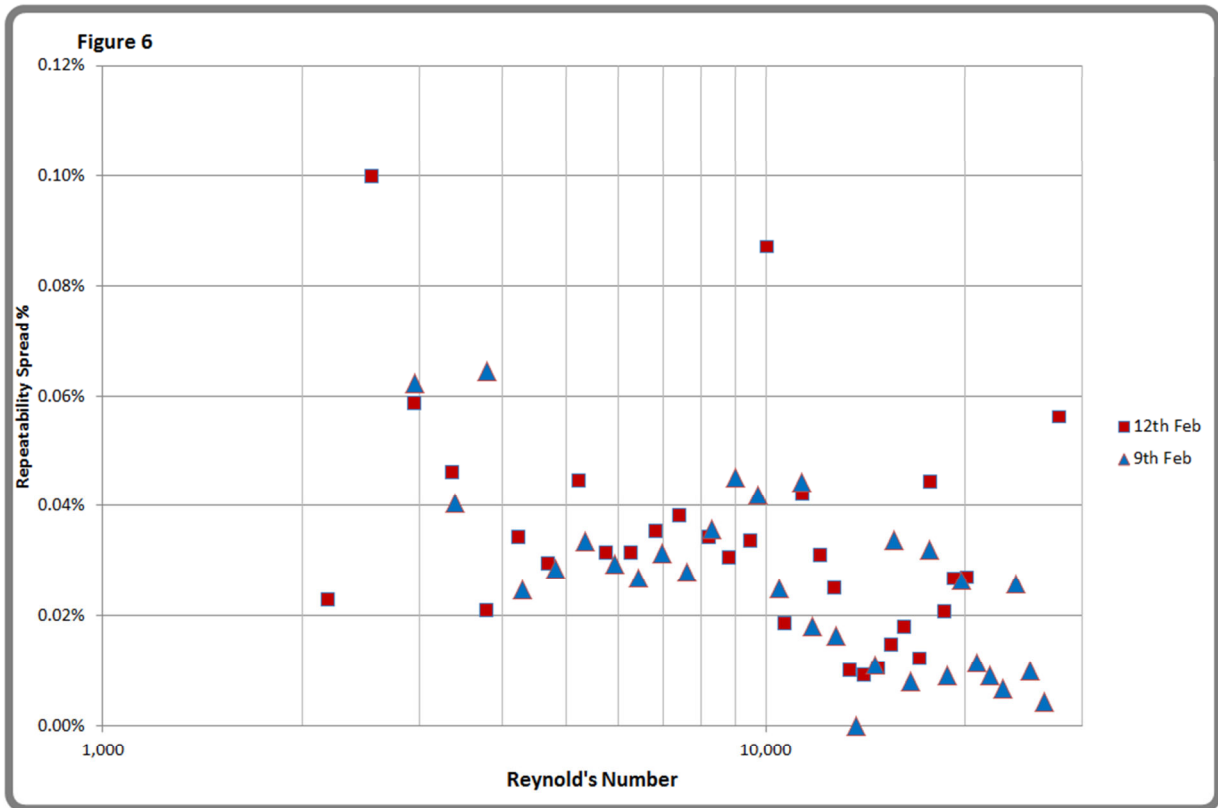
The results show a similar pattern to those in figure 4, with the exception of the three ringed results, although even the 2 higher values are within the OIML requirements for a 0.3 class meter when being used at  $>5$  times  $Q_{min}$ .



# 34<sup>th</sup> International North Sea Flow Measurement Workshop 25 – 28 October 2016

## Technical Paper

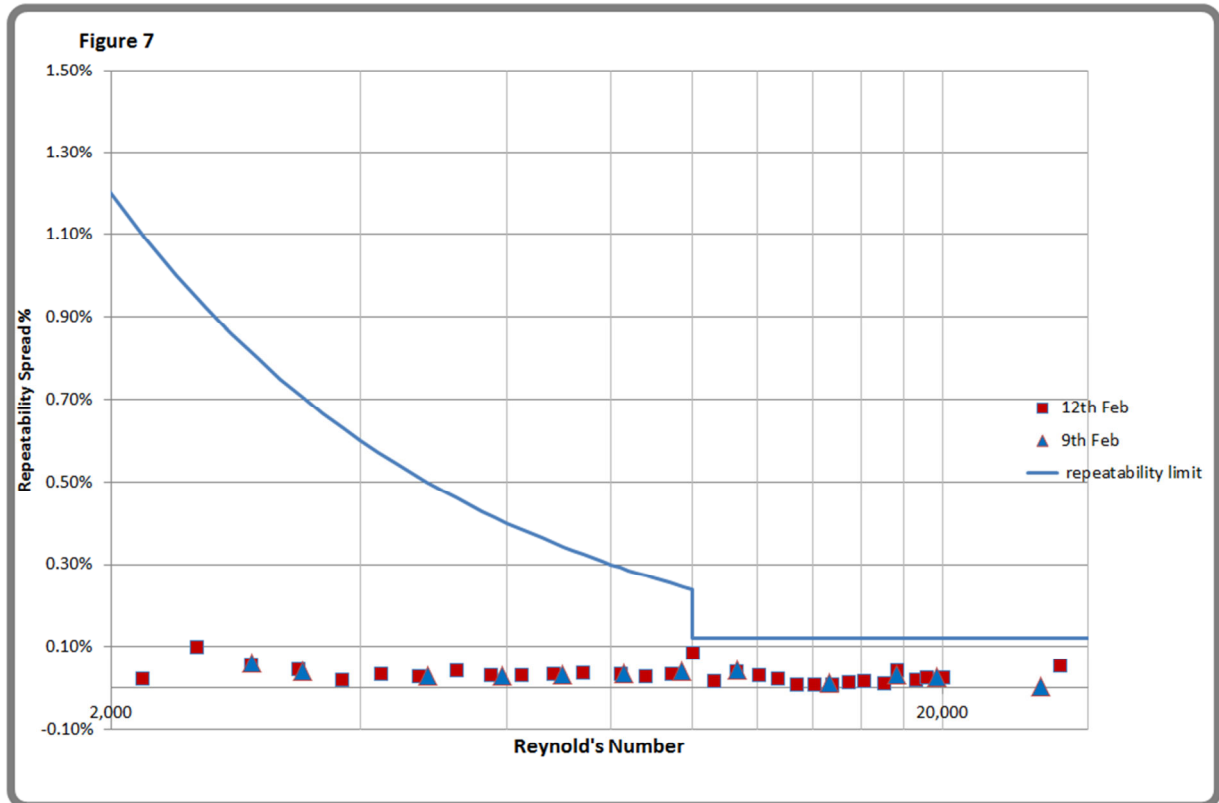
Figure 6 shows uncertainty spread for both sets of tests.



# 34<sup>th</sup> International North Sea Flow Measurement Workshop 25 – 28 October 2016

## Technical Paper

Figure 7 shows both the February 9<sup>th</sup> and 12<sup>th</sup> results plotted along with the “allowable repeatability spread” curve discussed earlier. It can be seen that all results, including those in the transition zone fall within the 0.12% band, with no significant degradation in repeatability performance for  $R_e < 10,000$ .



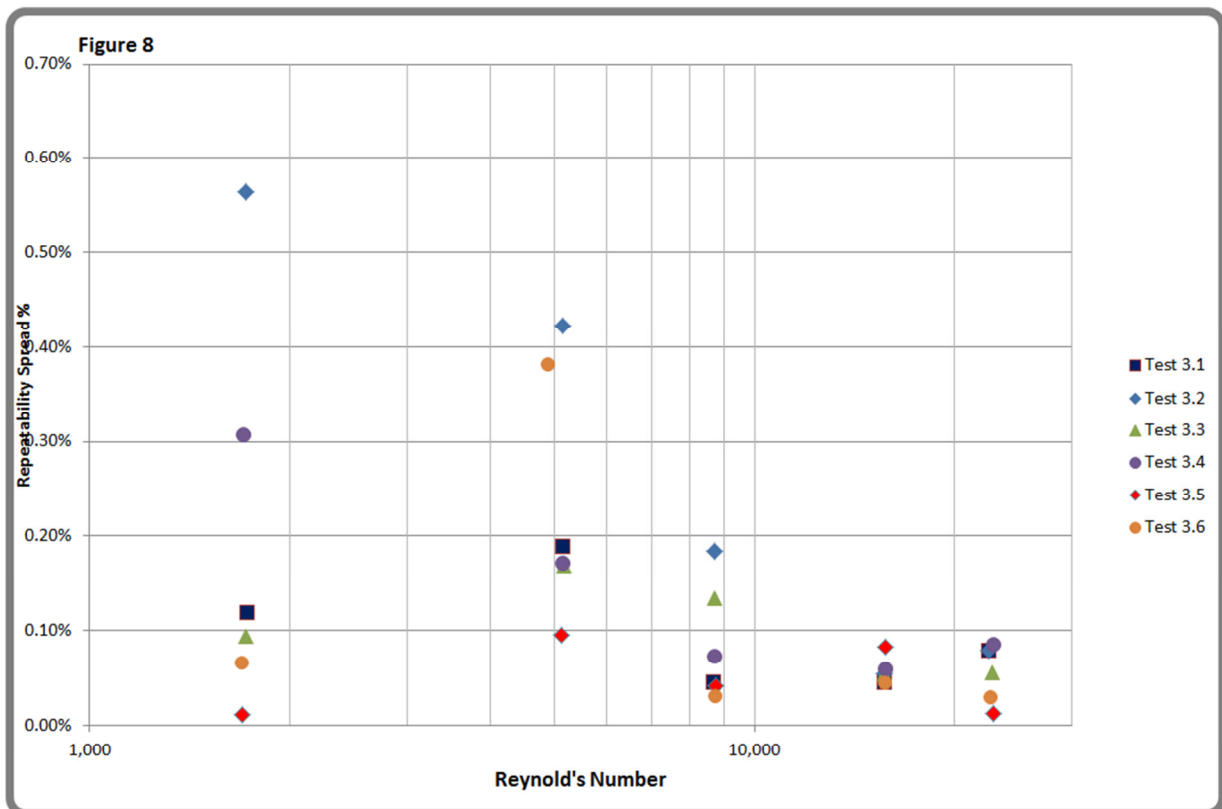
# 34<sup>th</sup> International North Sea Flow Measurement Workshop 25 – 28 October 2016

## Technical Paper

### 3.3 Test 3

As discussed earlier, this data is from calibration testing of 3 USMs with different upstream and downstream piping configurations, to confirm that any of the 3 meters could be calibrated when using the upstream and downstream meter spools held at the calibration laboratory. These spools were all bored through to within  $\pm 1$  mm and were axially located to the meter(s) using shoulder bolts. The manufacturer, our Company and the end user all believed that this "interchangeability" would be demonstrated during calibration and that the planned routine "in service" procedure referred to in **DESCRIPTION OF TESTING CARRIED OUT** would be achievable.

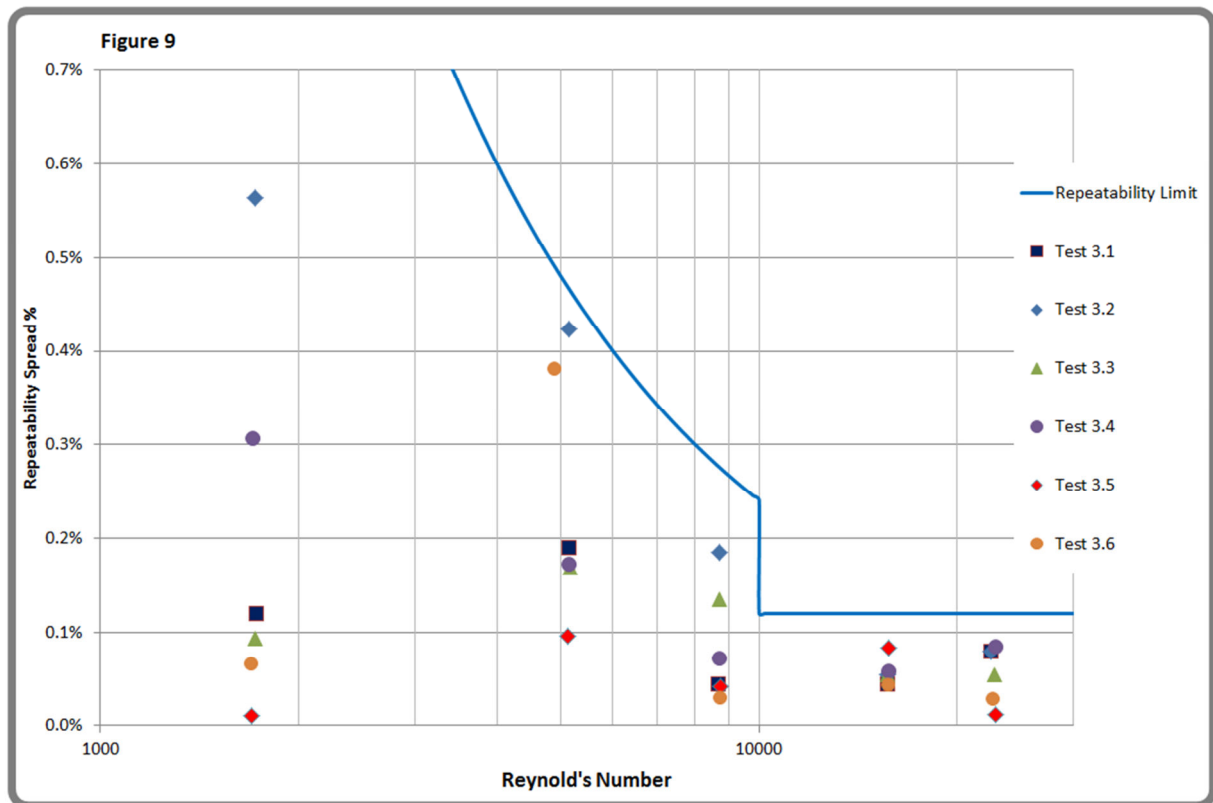
Figure 8 shows the repeatability spread for the data points for each test. All results are within the acceptance limits as described for figure 7. However, for those results in the previous Figure 7, the repeatability spreads were all within the 0.12% band required for and OIML 0.3 meter even at flow rates (Reynold's numbers) below that required by that standard.



# 34<sup>th</sup> International North Sea Flow Measurement Workshop 25 – 28 October 2016

## Technical Paper

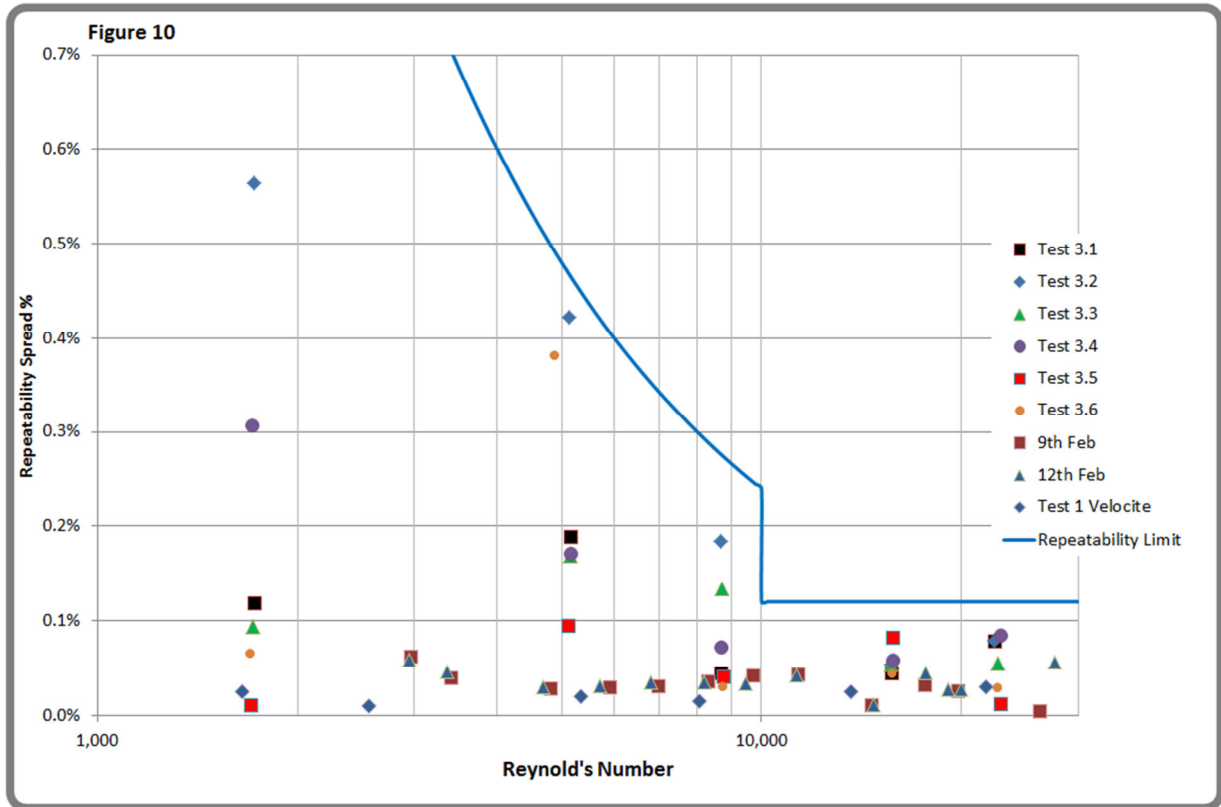
Figure 9 shows the same results when plotted along with the Repeatability Limit curve. Although the tests were carried out on 3 meters, with varying upstream and downstream spools, these spools were manufactured to close tolerances and were expected by the meter manufacturer to not cause significant “shifts” in the meter calibrations. In the context of the intended use of those meters, the final calibration results were all acceptable. However when analysed as has been done here, it is evident that the repeatability at low Reynold’s numbers – in fact at Reynold’s numbers below 10,000, is not good.



# 34<sup>th</sup> International North Sea Flow Measurement Workshop 25 – 28 October 2016

## Technical Paper

Figure 10 shows the repeatability spreads for all results for all 3 sets of tests and includes the repeatability limit curve.

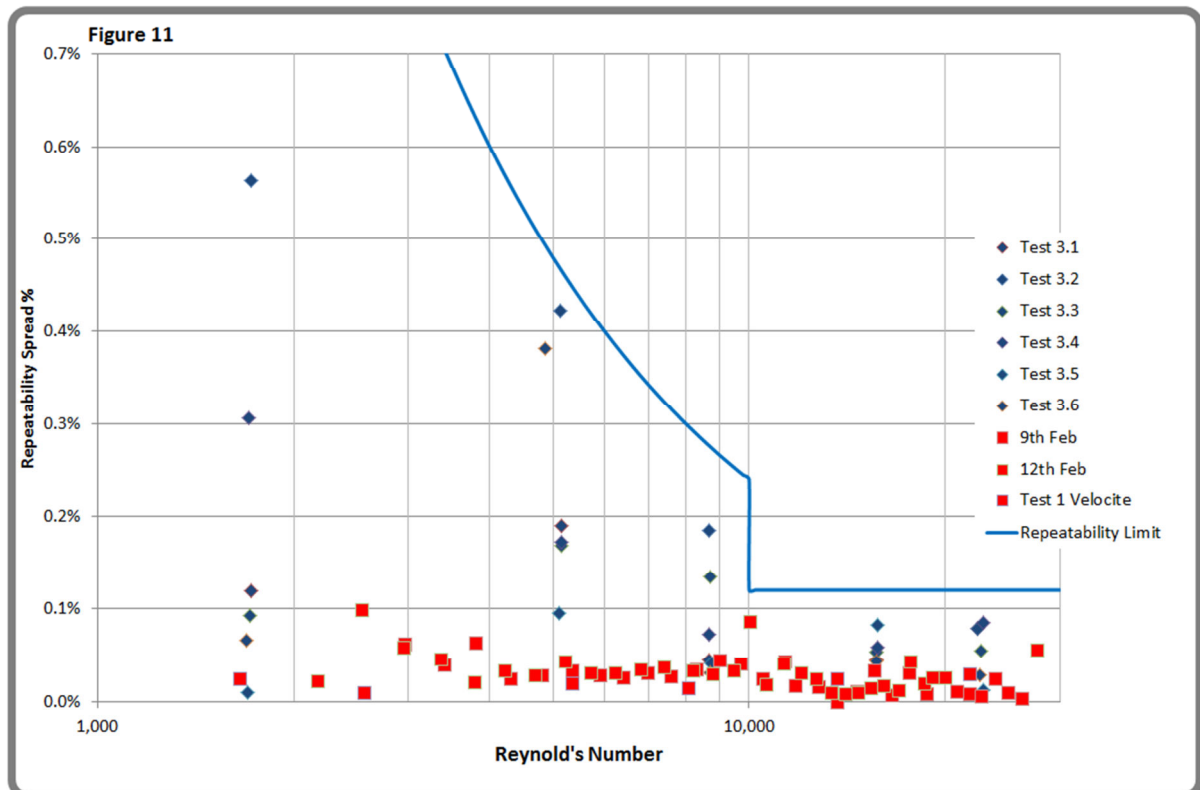


# 34<sup>th</sup> International North Sea Flow Measurement Workshop 25 – 28 October 2016

## Technical Paper

Figure 11 shows the repeatability spreads for all tests, including the repeatability limit curve. All 32 beam results have been shown in red ■ and all 8 beam chordal meter results have been shown in blue ◆

The figure shows clearly that the 32 beam meter has a consistently better performance in terms of repeatability spread both above and below  $Re = 10,000$  and in fact shows very little loss of repeatability throughout the whole transition zone.



## 4 CONCLUSIONS

These results show that the 32 beam, axially symmetric USM has a repeatability performance which is largely unaffected by Reynold's number and can be used at flow rates which correspond to Reynold's number from below the transition zone, through the transition zone and up into the turbulent flow region. The OIML requirement for a class 0.3 meter requires *3 consecutive runs*; these tests were carried out with 4 consecutive runs; however when the repeatability spread for the first three runs is calculated no repeatability spreads are greater than for 4 runs.

In these tests the 8 chordal beam meter demonstrated repeatability within the defined repeatability limits, but showed large spreads in repeatability within these limits.

It can be concluded from these results that the 32 beam axially symmetric USM has a superior repeatability performance which allows it to be used at low Reynold's numbers, and in particular, through the transition zone, where repeatability performance hardly varies from that in the turbulent flow region

# 34<sup>th</sup> International North Sea Flow Measurement Workshop 25 – 28 October 2016

## Technical Paper

The test results provide the data, but how can the reasons behind the results be explained?

Good Repeatability of a measurement is obviously a combination of stable conditions of the measured quantity (measurand as per VIM version 3) and the intrinsic meter stability. In our application, the measurand is a derived quantity and is not directly measured, which adds complexity.

Flow stability as volume over time (for volumetric meters), requires stability of product characteristics such as viscosity, density and composition and also process conditions including flow and turbulence intensity as well as environmental conditions. This control is effected by pressure, temperature and flow regulation during each calibration point measurement.

From the meter point of view repeatability would be directly linked to the meter sensitivity to small differences in the measurand, process and environmental conditions.

Each meter technology will react differently to those differences.

In the case of a USM, as it is a time measurement machine, everything is down to the time measurement stability.

This time measurement is directly proportional to the average flow velocities along the ultrasonic path and therefore is constantly changing through turbulent flow.

The integration methods used to locate the path of standard USM assume averaged flow profile. Even when they are based on CFD modelling it is likely to be based on a RANS model producing an averaged flow profile.

The less you measure, the more you have to rely on the average converging to a non-biased value. In other words, longer times for the measurement of the point requires bigger volumes, which creates more difficulties in keeping stable conditions during proves. It can be noted here that the 8 inch 32 beam results were all obtained using a nominal 3.18 m<sup>3</sup> prove volume and that the 16 inch 8 beam results used volumes from a nominal 10.06 m<sup>3</sup> to over 38 m<sup>3</sup>.

The ways to improve the time measurement in a USM are well known:

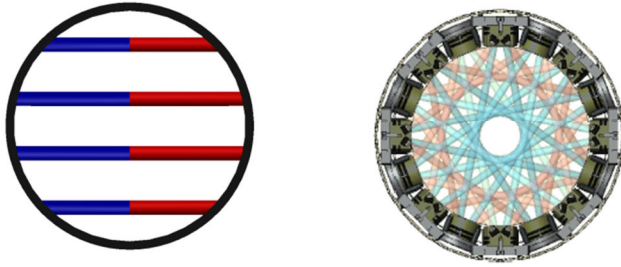
- Stability of the electronics ( clock, signal to noise ratio, pulse output)
- Signal processing ( the way we perform the time measurement on the ultrasonic pulse)
- The transducer quality ( stability and repeatability of the signal rising edge, amplitude, temperature stability of the electronics)

We believe that, the number of beams and their location should be added to the list.

We return to the comparison of the chordal meter and the 32 beam meter:-

# 34<sup>th</sup> International North Sea Flow Measurement Workshop 25 – 28 October 2016

## Technical Paper



The more you cover the pipe cross section, the less you need to average spatially. This is particularly important in the transition zone where turbulence can occur at any moment anywhere in the cross section.

The Results presented in this paper showed that the combination of high end electronic, signal processing and transducers with an innovative 32 beam design covering the pipe cross section, brings a significant improvement to the repeatability of USMs especially for Reynolds numbers below 10 000 and through the transition zone.

This combination of features is essential to be able to prove and use this technology efficiently and effectively in this flow regime region.

# 34<sup>th</sup> International North Sea Flow Measurement Workshop 25 – 28 October 2016

## Technical Paper

### 5 REFERENCES

- [1] Direct Numerical Simulation of Turbulent Channel Flow at  $Re_{\tau} = 2320$ , Kaoru Iwamoto, Nobuhide Kasagi and Yuji Suzuki Department of Mechanical Engineering, the University of Tokyo, 6<sup>th</sup> Symp. Smart Control of Turbulence, Tokyo March 6 – 9, 2005
- [2] A Multipath Ultrasonic Meter with Reducing Nozzle for improved performance in the laminar/turbulent flow region, Gregor J Brown, et al, Cameron, 27<sup>th</sup> International North Sea Flow Measurement Workshop October 20 – 23, 2009
- [3] Use of a Liquid Ultrasonic Flow Meter in Mixed Phase Flow, David Mills, Julien Porré, Advances and Developments in Industrial Flow Measurement , University of Warwick July 1-2 2015
- [4] Separator Oil Metering Using 32 Beam USM, Julien Porré, 2016 European Flow Measurement Workshop, Netherlands
- [5] 32 Beam Ultrasonic Technology for Multi Viscosity Custody Transfer Applications, Special Case Applications, Julien Porré, 2016 CEESI North American Custody Transfer Measurement

# 34<sup>th</sup> International North Sea Flow Measurement Workshop 25 – 28 October 2016

## Technical Paper

### Appendix A - Test Results

#### Test 1

4 inch DFX calibration at NEL, East Kilbride UKAS 0009

These results were obtained as part of normal calibration on two different viscosity products (Velocite with a viscosity of ~45 cSt at ~12°C and Gasoil with a viscosity of ~6 cSt at ~44°C)

#### 1. 1 Velocite

	T°C	cSt	m <sup>3</sup> /h	V m/s	Re	pulses/m <sup>3</sup>	%spread	proved vol m <sup>3</sup>
1	12.61	46.50	19.008	0.882	1,656	19.844	0.025	1.48
2	12.57	46.59	19.044	0.883	1,656	19.844		PD meter
3	12.53	46.69	19.044	0.883	1,652	19.839		
4	12.21	47.45	29.736	1.379	2,538	20.043	0.010	2.32
5	12.34	47.14	29.772	1.381	2,558	20.044		PD meter
6	12.59	46.56	29.808	1.383	2,593	20.042		
7	12.72	46.25	60.660	2.814	5,312	19.983	0.020	3.04
8	12.83	46.00	60.732	2.817	5,348	19.982		PD meter
9	12.96	45.72	60.696	2.815	5,377	19.979		
10	13.08	45.44	90.108	4.180	8,032	20.011	0.015	4.50
11	13.18	45.23	90.072	4.178	8,066	20.013		PD meter
12	13.28	45.00	90.072	4.178	8,107	20.014		
13	13.36	44.82	150.336	6.973	13,586	19.957	0.025	7.52
14	13.40	44.73	150.336	6.973	13,613	19.952		PD meter
15	13.47	44.58	150.336	6.973	13,659	19.954		
16	13.36	44.82	244.692	11.350	22,113	19.998	0.030	12.24
17	13.12	45.43	244.728	11.352	21,819	19.997		PD meter
18	12.83	46.00	244.728	11.352	21,549	19.992		

#### 1.2 Gasoil

	T°C	cSt	m <sup>3</sup> /h	V m/s	Re	pulses/m <sup>3</sup>	%spread	proved vol m <sup>3</sup>
1	44.73	6.09	15.516	0.720	10,319	20,031	0.030	2.16
2	44.32	6.15	15.516	0.720	10,219	20,025		PD meter
3	43.95	6.21	15.552	0.721	10,144	20,025		
4	43.53	6.28	30.528	1.416	19,689	19,993	0.035	2.32
5	43.48	6.28	30.744	1.426	19,829	19,987		PD meter
6	43.86	6.22	30.888	1.433	20,114	19,986		
7	44.37	6.15	59.364	2.754	39,097	19,997	0.015	2.97
8	44.71	6.09	59.364	2.754	39,482	20,000		PD meter
9	45.04	6.04	59.364	2.754	39,809	19,999		

**34<sup>th</sup> International North Sea Flow Measurement Workshop  
25 – 28 October 2016**

**Technical Paper**

10	45.25	6.01	90.684	4.206	61,115	20,004	0.015	4.54
11	45.01	6.05	90.720	4.208	60,735	20,001		PD meter
12	44.72	6.09	90.792	4.211	60,384	20,002		
13	44.45	6.13	150.228	6.968	99,262	19,994	0.015	7.52
14	44.35	6.15	150.264	6.970	98,963	19,997		PD meter
15	44.50	6.12	150.300	6.972	99,472	19,996		
16	44.78	6.08	242.172	11.233	161,330	19,989	0.025	12.26
17	44.87	6.07	243.900	11.313	162,749	19,994		PD meter
18	44.97	6.05	244.584	11.345	163,744	19,991		

# 34<sup>th</sup> International North Sea Flow Measurement Workshop 25 – 28 October 2016

## Technical Paper

Test 2

8 inch DFX Calibration at Belgorod, VSL CMC Certification LF2015.04.0012

2.1 These tests were carried out using oil with a viscosity of ~26 cSt at ~25°C. Test date 9<sup>th</sup>

	T°C	cSt	m <sup>3</sup> /h	V m/s	Re	pulses/m3	%spread	proved vol m <sup>3</sup>
1	11.27	43.80	63.35	0.748	2,956	9,810.392	0.062%	3.18
2	11.27	43.80	63.35	0.748	2,956	9,814.206		bi-di
3	11.29	43.80	63.35	0.748	2,956	9,808.094		
4	11.29	43.80	63.35	0.748	2,956	9,811.543		
5	11.36	43.60	72.64	0.858	3,404	9,837.319	0.040%	3.18
6	11.36	43.60	72.63	0.857	3,404	9,841.282		bi-di
7	11.37	43.60	72.62	0.857	3,404	9,837.600		
8	11.37	43.60	72.64	0.858	3,404	9,839.139		
9	11.46	43.4	80.69	0.953	3,799	9,868.948	0.064%	3.18
10	11.46	43.4	80.69	0.953	3,799	9,872.275		bi-di
11	11.48	43.3	80.70	0.953	3,808	9,865.926		
12	11.48	43.3	80.70	0.953	3,808	9,869.808		
13	11.59	43.1	90.68	1.071	4,299	9,903.524	0.025%	3.18
14	11.59	43.1	90.68	1.071	4,299	9,905.978		bi-di
15	11.63	43.1	90.69	1.071	4,300	9,903.543		
16	11.63	43.1	90.70	1.071	4,300	9,905.534		
17	11.76	42.7	100.42	1.186	4,806	9,930.529	0.028%	3.18
18	11.76	42.7	100.41	1.185	4,805	9,933.173		bi-di
19	11.81	42.6	100.42	1.186	4,817	9,930.904		
20	11.81	42.6	100.41	1.185	4,816	9,933.355		
21	11.95	42.2	110.09	1.300	5,331	9,950.931	0.034%	3.18
22	11.95	42.2	110.09	1.300	5,331	9,953.717		bi-di
23	12.00	42.1	110.20	1.301	5,349	9,951.161		
24	12.00	42.1	110.19	1.301	5,348	9,954.269		
25	12.22	41.6	120.10	1.418	5,899	9,966.848	0.030%	3.18
26	12.22	41.6	120.08	1.418	5,898	9,969.790		bi-di
27	12.27	41.5	120.15	1.419	5,916	9,968.779		
28	12.27	41.5	120.16	1.419	5,917	9,969.652		
29	12.44	41.5	129.89	1.534	6,396	9,980.315	0.027%	3.18
30	12.44	41.5	129.89	1.534	6,396	9,981.640		bi-di
31	12.50	41.3	129.92	1.534	6,428	9,978.966		
32	12.50	41.3	129.91	1.534	6,428	9,980.585		
33	12.68	40.8	140.27	1.656	7,025	9,989.523	0.031%	3.18
34	12.68	40.8	140.27	1.656	7,025	9,991.062		bi-di
35	12.76	41.3	140.33	1.657	6,943	9,987.923		
36	12.76	41.3	140.31	1.657	6,942	9,989.925		
37	12.99	40.5	149.67	1.767	7,552	9,992.912	0.028%	3.18
38	12.99	40.5	149.66	1.767	7,551	9,994.567		bi-di
39	13.07	40.3	150.48	1.777	7,630	9,994.037		
40	13.07	40.3	150.46	1.776	7,629	9,995.692		
41	13.30	39.7	160.70	1.897	8,272	9,998.309	0.036%	3.18
42	13.30	39.7	160.68	1.897	8,270	10,000.339		bi-di
43	13.40	39.5	160.75	1.898	8,316	9,996.780		
44	13.40	39.5	160.74	1.898	8,315	9,998.595		

**34<sup>th</sup> International North Sea Flow Measurement Workshop  
25 – 28 October 2016**

**Technical Paper**

45	13.67	38.9	170.87	2.017	8,976	10,002.491	0.045%	3.18
46	13.67	38.9	170.83	2.017	8,974	10,005.095		bi-di
47	13.77	38.7	170.94	2.018	9,026	10,000.584		
48	13.77	38.7	170.90	2.018	9,024	10,002.930		
49	14.12	38.1	180.49	2.131	9,680	10,000.379	0.042%	3.18
50	14.12	38.1	180.45	2.130	9,678	10,003.036		bi-di
51	14.24	37.8	180.45	2.130	9,755	10,003.455		
52	14.24	37.8	180.44	2.130	9,754	10,004.575		
53	14.58	37.3	190.78	2.252	10,452	10,002.229	0.025%	3.18
54	14.58	37.3	190.77	2.252	10,451	10,003.350		bi-di
55	14.71	37.1	190.82	2.253	10,510	10,001.075		
56	14.71	37.1	190.78	2.252	10,508	10,003.557		
57	15.12	36.4	201.20	2.375	11,295	10,002.666	0.044%	3.18
58	15.12	36.4	201.19	2.375	11,294	10,003.210		bi-di
59	15.25	36.2	201.37	2.377	11,367	9,998.796		
60	15.25	36.2	201.32	2.377	11,364	10,001.300		
61	15.42	35.9	206.15	2.434	11,734	9,990.539	0.018%	3.18
62	15.42	35.9	206.14	2.434	11,733	9,991.642		bi-di
63	15.51	35.8	205.97	2.432	11,757	9,989.834		
64	15.51	35.8	205.96	2.432	11,756	9,990.817		
65	15.86	35.3	220.43	2.602	12,760	9,994.776	0.016%	3.18
66	15.86	35.3	220.43	2.602	12,760	9,995.756		bi-di
67	15.96	35.2	220.38	2.602	12,793	9,994.808		
68	15.96	35.2	220.41	2.602	12,795	9,994.127		
69	16.36	34.5	230.00	2.715	13,623	9,995.698	0.045%	3.18
70	16.36	34.5	230.00	2.715	13,623	9,995.992		bi-di
71	16.47	34.3	230.03	2.716	13,704	9,998.248		
72	16.47	34.3	230.00	2.715	13,702	10,000.209		
73	16.88	33.7	240.32	2.837	14,572	9,998.037	0.011%	3.18
74	16.88	33.7	240.32	2.837	14,572	9,998.735		bi-di
75	17.01	33.5	240.27	2.837	14,656	9,997.641		
76	17.01	33.5	240.26	2.837	14,655	9,998.700		
77	17.36	33.0	250.36	2.956	15,503	9,999.037	0.034%	3.18
78	17.36	33.0	250.39	2.956	15,505	9,998.355		bi-di
79	17.49	32.7	250.53	2.958	15,656	9,996.496		
80	17.49	32.7	250.55	2.958	15,657	9,995.670		
81	17.86	32.3	260.75	3.078	16,496	9,999.438	0.008%	3.18
82	17.86	32.3	260.74	3.078	16,495	9,999.766		bi-di
83	18.00	32.1	260.76	3.079	16,600	9,999.324		
84	18.00	32.1	260.78	3.079	16,601	9,998.975		
85	18.45	31.5	270.66	3.195	17,558	9,997.763	0.032%	3.18
86	18.45	31.5	270.64	3.195	17,557	9,998.606		bi-di
87	18.60	31.3	270.92	3.199	17,687	9,995.410		
88	18.60	31.3	270.85	3.198	17,683	9,998.082		
89	19.04	30.7	280.76	3.315	18,688	9,996.298	0.009%	3.18
90	19.04	30.7	280.76	3.315	18,688	9,996.692		bi-di
91	19.21	30.5	280.70	3.314	18,806	9,996.705		
92	19.21	30.5	280.69	3.314	18,806	9,997.196		

## 34<sup>th</sup> International North Sea Flow Measurement Workshop 25 – 28 October 2016

### Technical Paper

93	19.54	30.1	290.24	3.427	19,704	9,991.106	0.026%	3.18
94	19.54	30.1	290.23	3.427	19,703	9,991.685		bi-di
95	19.61	30.0	290.10	3.425	19,760	9,993.168		
96	19.61	30.0	290.09	3.425	19,759	9,993.739		
97	19.93	29.6	300.94	3.553	20,775	9,993.507	0.011%	3.18
98	19.93	29.6	300.91	3.553	20,773	9,994.402		bi-di
99	20.01	29.5	300.77	3.551	20,834	9,993.461		
100	20.01	29.5	300.78	3.551	20,835	9,993.259		
101	20.21	29.3	311.65	3.679	21,735	9,995.875	0.009%	3.18
102	20.21	29.3	311.66	3.680	21,736	9,995.730		bi-di
103	20.29	29.2	311.53	3.678	21,801	9,994.969		
104	20.29	29.2	311.53	3.678	21,801	9,995.090		
105	20.52	28.9	321.60	3.797	22,739	9,996.180	0.007%	3.18
106	20.52	28.9	321.59	3.797	22,739	9,996.814		bi-di
107	20.62	28.9	321.56	3.796	22,736	9,996.833		
108	20.62	28.9	321.57	3.797	22,737	9,996.696		
109	20.94	28.4	330.95	3.907	23,812	9,997.058	0.026%	3.18
110	20.94	28.4	330.94	3.907	23,812	9,997.775		bi-di
111	21.06	28.3	330.94	3.907	23,896	9,995.204		
112	21.06	28.3	330.93	3.907	23,895	9,995.582		
113	21.42	27.9	340.63	4.022	24,948	9,995.649	0.010%	3.18
114	21.42	27.9	340.61	4.021	24,947	9,996.262		bi-di
115	21.55	27.8	340.60	4.021	25,036	9,995.554		
116	21.55	27.8	340.62	4.021	25,037	9,995.286		
117	21.92	27.4	351.04	4.144	26,180	9,998.182	0.004%	3.18
118	21.92	27.4	351.04	4.144	26,180	9,998.329		bi-di
119	22.05	27.2	350.76	4.141	26,351	9,997.900		
120	22.05	27.2	350.76	4.141	26,351	9,998.109		

2.2 A repeat of the test 3 days earlier to check on repeatability when compared with the earlier tests.

	T°C	cSt	m <sup>3</sup> /h	V m/s	Re	pulses/m <sup>3</sup>	%spread	proved vol m <sup>3</sup>
1	6.80	57.6	61.31	0.724	2,175	9,876.008	0.023%	3.18
2	6.80	57.6	61.33	0.724	2,176	9,878.059		bi-di
3	6.84	57.4	61.27	0.723	2,181	9,875.829		
4	6.84	57.4	61.29	0.724	2,182	9,877.719		
5	6.93	57.1	70.83	0.836	2,535	9,934.091	0.100%	3.18
6	6.93	57.1	70.83	0.836	2,535	9,937.001		bi-di
7	7.03	56.8	70.65	0.834	2,542	9,927.091		
8	7.03	56.8	70.67	0.834	2,542	9,928.826		
9	7.24	56.2	81.06	0.957	2,947	9,947.059	0.059%	3.18
10	7.24	56.2	81.07	0.957	2,948	9,948.820		bi-di
11	7.32	55.9	80.70	0.953	2,950	9,942.965		
12	7.32	55.9	80.72	0.953	2,951	9,943.926		
13	7.43	55.5	90.89	1.073	3,346	9,951.624	0.046%	3.18
14	7.43	55.5	90.89	1.073	3,346	9,953.621		bi-di
15	7.55	55.2	90.90	1.073	3,365	9,949.029		
16	7.55	55.2	90.90	1.073	3,365	9,950.168		

# 34<sup>th</sup> International North Sea Flow Measurement Workshop 25 – 28 October 2016

## Technical Paper

17	7.76	54.5	100.74	1.189	3.777	9967.784	0.021%	3.18
18	7.76	54.5	100.74	1.189	3,777	9,969.150		bi-di
19	7.85	54.2	100.77	1.190	3,799	9,968.330		
20	7.85	54.2	100.78	1.190	3,800	9,969.879		
21	8.09	53.5	110.13	1.300	4.206	9984.516	0.034	3.18
22	8.09	53.5	110.13	1.300	4,206	9,985.990		bi-di
23	8.18	53.2	110.15	1.300	4,231	9,982.562		
24	8.18	53.2	110.16	1.301	4,231	9,983.538		
25	8.44	52.5	119.95	1.416	4,669	9,998.267	0.030%	3.18
26	8.44	52.5	119.95	1.416	4,669	9,999.904		bi-di
27	8.54	52.1	119.99	1.417	4,706	9,996.939		
28	8.54	52.1	119.99	1.417	4,706	9,998.500		
29	8.78	51.5	130.91	1.546	5,194	10,011.117	0.045%	3.18
30	8.78	51.5	130.88	1.545	5,193	10,014.489		bi-di
31	8.89	51.1	130.88	1.545	5,234	10,010.018		
32	8.89	51.1	130.86	1.545	5,233	10,013.088		
33	9.28	50.2	139.97	1.653	5,698	10,017.235	0.032%	3.18
34	9.28	50.2	139.94	1.652	5,696	10,020.398		bi-di
35	9.38	49.9	140.00	1.653	5,733	10,018.019		
36	9.38	49.9	140.00	1.653	5,733	10,019.699		
37	9.59	49.3	149.97	1.771	6,216	10,023.196	0.032%	3.18
38	9.59	49.3	149.94	1.770	6,215	10,025.977		bi-di
39	9.72	49.0	150.01	1.771	6,256	10,022.808		
40	9.72	49.0	150.01	1.771	6,256	10,023.969		
41	9.98	48.3	160.28	1.892	6,781	10,025.759	0.035%	3.18
42	9.98	48.3	160.26	1.892	6,780	10,027.719		bi-di
43	10.10	47.9	160.32	1.893	6,839	10,025.146		
44	10.10	47.9	160.28	1.892	6,838	10,028.702		
45	10.38	47.3	170.40	2.012	7,362	10,030.067	0.038%	3.18
46	10.38	47.3	170.40	2.012	7,362	10,030.828		bi-di
47	10.52	46.9	170.34	2.011	7,422	10,026.996		
48	10.52	46.9	170.33	2.011	7,421	10,028.319		
49	11.00	45.7	182.85	2.159	8,176	10,030.206	0.034%	3.18
50	11.00	45.7	182.83	2.159	8,175	10,031.602		bi-di
51	11.15	45.3	182.05	2.149	8,212	10,028.146		
52	11.15	45.3	182.03	2.149	8,211	10,029.272		
53	11.43	44.7	191.50	2.261	8,754	10,023.847	0.031%	3.18
54	11.43	44.7	191.46	2.260	8,752	10,026.242		bi-di
55	11.59	44.3	191.50	2.261	8,833	10,025.065		
56	11.59	44.3	191.47	2.261	8,832	10,026.926		
57	11.95	43.5	200.29	2.365	9,409	10,026.145	0.034%	3.18
58	11.95	43.5	200.28	2.365	9,408	10,027.519		bi-di
59	12.12	43.1	200.37	2.366	9,500	10,024.136		
60	12.12	43.1	200.36	2.366	9,499	10,024.960		
61	12.18	43.0	210.32	2.483	9,995	10,027.015	0.087%	3.18
62	12.18	43.0	210.33	2.483	9,995	10,026.925		bi-di
63	12.28	42.7	210.06	2.480	10,053	10,018.271		
64	12.28	42.7	210.02	2.480	10,051	10,020.768		
65	12.52	42.3	219.74	2.594	10,615	10,017.629	0.019%	3.18
66	12.52	42.3	219.74	2.594	10,615	10,018.260		bi-di
67	12.61	42.1	219.63	2.593	10,660	10,018.892		
68	12.61	42.1	219.63	2.593	10,660	10,019.501		

## 34<sup>th</sup> International North Sea Flow Measurement Workshop 25 – 28 October 2016

### Technical Paper

69	12.82	41.8	230.74	2.724	11,280	10,017.579	0.042%	3.18
70	12.82	41.8	230.74	2.724	11,280	10,018.292		bi-di
71	12.92	41.6	230.58	2.722	11,326	10,021.218		
72	12.92	41.6	230.57	2.722	11,326	10,021.786		
73	13.17	41.1	241.25	2.848	11,995	10,020.943	0.031%	3.18
74	13.17	41.1	241.30	2.849	11,997	10,019.372		bi-di
75	13.26	40.9	241.38	2.850	12,060	10,018.156		
76	13.26	40.9	241.39	2.850	12,060	10,017.831		
77	13.42	40.6	250.99	2.963	12,633	10,020.639	0.025%	3.18
78	13.42	40.6	251.01	2.963	12,634	10,020.380		bi-di
79	13.51	40.4	251.23	2.966	12,707	10,018.130		
80	13.51	40.4	251.21	2.966	12,706	10,019.034		
81	13.72	40.0	260.99	3.081	13,333	10,023.047	0.010%	3.18
82	13.72	40.0	260.99	3.081	13,333	10,023.188		bi-di
83	13.80	39.8	260.78	3.079	13,389	10,023.630		
84	13.80	39.8	260.78	3.079	13,389	10,024.063		
85	13.99	39.5	270.82	3.197	14,010	10,021.274	0.009%	3.18
86	13.99	39.5	270.83	3.198	14,011	10,021.246		bi-di
87	14.07	39.3	270.65	3.195	14,073	10,022.159		
88	14.07	39.3	270.67	3.196	14,074	10,021.421		
89	14.21	39.1	281.37	3.322	14,705	10,026.104	0.011%	3.18
90	14.21	39.1	281.4	3.322	14,706	10,025.397		bi-di
91	14.3	39.0	281.17	3.320	14,732	10,025.298		
92	14.3	39.0	281.18	3.320	14,733	10,025.049		
93	14.44	38.6	290.78	3.433	15,394	10,025.117	0.015%	3.18
94	14.44	38.6	290.82	3.434	15,396	10,024.229		bi-di
95	14.54	38.6	290.91	3.435	15,400	10,024.030		
96	14.54	38.6	290.93	3.435	15,401	10,023.642		
97	14.83	38.0	298.44	3.523	16,048	10,023.698	0.018%	3.18
98	14.83	38.0	298.45	3.524	16,049	10,023.384		bi-di
99	14.93	37.7	298.34	3.522	16,171	10,025.187		
100	14.93	37.7	298.38	3.523	16,173	10,023.957		
101	15.26	37.5	311.79	3.681	16,990	10,026.508	0.012%	3.18
102	15.26	37.5	311.82	3.681	16,992	10,025.290		bi-di
103	15.37	37.3	309.87	3.658	16,976	10,025.663		
104	15.37	37.3	309.87	3.658	16,976	10,025.314		
105	15.68	37.2	320.44	3.783	17,602	10,025.375	0.045%	3.18
106	15.68	37.2	320.47	3.784	17,604	10,024.649		bi-di
107	15.8	37.0	320.31	3.782	17,690	10,021.297		
108	15.8	37.0	320.33	3.782	17,691	10,020.910		
109	16.04	36.2	329.70	3.893	18,611	10,024.478	0.021%	3.18
110	16.04	36.2	329.72	3.893	18,612	10,023.984		bi-di
111	16.15	36.4	329.95	3.895	18,523	10,022.565		
112	16.15	36.4	329.95	3.895	18,523	10,022.389		
113	16.35	36.6	339.34	4.006	18,946	10,019.935	0.027%	3.18
114	16.35	36.6	339.38	4.007	18,948	10,019.200		bi-di
115	16.48	35.9	339.25	4.005	19,310	10,021.882		
116	16.48	35.9	339.27	4.006	19,311	10,021.649		
117	16.71	35.9	349.03	4.121	19,867	10,021.845	0.027%	3.18
118	16.71	35.9	349.05	4.121	19,868	10,021.589		bi-di
119	16.85	35.4	349.14	4.122	20,154	10,019.134		
120	16.85	35.4	349.15	4.122	20,154	10,019.231		

**34<sup>th</sup> International North Sea Flow Measurement Workshop  
25 – 28 October 2016**

**Technical Paper**

121	6.17	59.8	805.13	9.506	27,512	10,038.174	0.056%	3.18
122	6.17	59.8	805.05	9.505	27,509	10,039.311		bi-di
123	6.38	59.2	805.96	9.515	27,820	10,033.666		
124	6.38	59.2	805.83	9.514	27,815	10,035.177		

# 34<sup>th</sup> International North Sea Flow Measurement Workshop 25 – 28 October 2016

## Technical Paper

Test 3

Three off 16 inch USM calibrated using Drakeol 32 using three sets of upstream and downstream spools.

The meters have been designated Meter A, Meter B and Meter C

The spools have been designated Upstream 1, Upstream 2, Upstream Spare, Downstream 1, Downstream 2 and Downstream Spare

The following tests were carried out:

Test	Upstream Spool	Meter	Downstream Spool
3.1	Spare	A	Spare
3.2	Spare	A	1
3.3	1	A	1
3.4	Spare	B	Spare
3.5	2	B	2
3.6	Spare	C	Spare

Test 3.1      Test setup Upstream Spare/ Meter A/ Downstream Spare

	T°C	cSt	m <sup>3</sup> /h	V m/s	Re	pulses/m3	%spread	proved vol m <sup>3</sup>
1	19.95	79.21	149.500	0.217	1,722	940.462	0.119	10.06
2	19.92	79.36	149.600	0.218	1,721	940.053		Uni
3	19.96	79.20	149.500	0.217	1,724	939.341		

	T°C	cSt	m <sup>3</sup> /h	V m/s	Re	pulses/m3	%spread	proved vol m <sup>3</sup>
1	19.98	79.10	447.000	0.650	5,156	940.738	0.190	10.06
2	19.93	79.30	446.100	0.649	5,136	940.054		Uni
3	19.93	79.31	447.300	0.650	5,151	939.637		
4	19.94	79.24	446.900	0.650	5,142	941.418		

	T°C	cSt	m <sup>3</sup> /h	V m/s	Re	pulses/m3	%spread	proved vol m <sup>3</sup>
1	20.00	78.98	751.500	1.093	8,682	940.543	0.045	21.26
2	20.00	78.98	750.700	1.092	8,672	940.754		USM master meter
3	19.99	79.05	750.500	1.091	8,660	940.964		

	T°C	cSt	m <sup>3</sup> /h	V m/s	Re	pulses/m3	%spread	proved vol m <sup>3</sup>
1	20.08	78.65	1356.500	1.972	15,737	940.543	0.045	21.26
2	20.06	78.73	1356.300	1.972	15,716	940.754		USM master meter
3	20.02	78.89	1355.600	1.971	15,680	940.964		
4	19.97	79.13	1353.100	1.967	15,608	940.754		
5	19.91	79.39	1353.100	1.967	15,558	940.964		

# 34<sup>th</sup> International North Sea Flow Measurement Workshop 25 – 28 October 2016

## Technical Paper

	T°C	cSt	m <sup>3</sup> /h	Re	pulses/m3	%spread	proved vol m <sup>3</sup>
1	19.99	79.06	1950.300	22,517	940.342	0.079	38.28
2	19.90	79.43	1954.700	22,450	940.761		USM master
3	19.91	79.41	1952.600	22,449	940.017		

### Test 3.2 Test setup Upstream Spare/ Meter A/ Downstream 1

	T°C	cSt	m <sup>3</sup> /h	V m/s	Re	pulses/m3	%spread	proved vol m <sup>3</sup>
1	20.11	78.52	148.600	0.216	1,728	940.022	0.564	10.06
2	19.92	79.37	148.900	0.217	1,709	941.987		Uni
3	20.03	78.88	148.900	0.217	1,721	941.594		
4	20.11	78.51	148.800	0.216	1,729	941.084		
5	19.88	79.55	149.300	0.217	1,704	945.320		

	T°C	cSt	m <sup>3</sup> /h	V m/s	Re	pulses/m3	%spread	proved vol m <sup>3</sup>
1	19.86	79.62	446.500	0.649	5,110	942.033	0.423	10.06
2	19.92	79.37	447.000	0.650	5,129	942.585		Uni
3	19.93	79.30	445.400	0.648	5,132	939.313		
4	20.00	78.99	446.400	0.649	5,159	940.110		
5	19.88	78.81	445.300	0.647	5,167	938.616		

	T°C	cSt	m <sup>3</sup> /h	V m/s	Re	pulses/m3	%spread	proved vol m <sup>3</sup>
1	20.02	78.92	754.700	1.097	8,711	942.174	0.185	31.86
2	19.95	79.22	753.900	1.096	8,685	940.437		USM master meter
3	19.93	79.32	754.700	1.097	8,678	940.991		
4	19.93	79.28	755.800	1.099	8,693	941.297		
5	19.97	79.12	756.300	1.100	8,715	941.456		

	T°C	cSt	m <sup>3</sup> /h	Re	pulses/m3	%spread	proved vol m <sup>3</sup>
1	20.08	78.65	1356.500	15,737	940.664	0.054	26.60
2	20.06	78.73	1356.300	15,716	940.752		USM master meter
3	20.02	78.89	1355.600	15,680	940.631		
4	19.97	79.13	1353.100	15,608	940.377		
5	19.91	79.39	1353.100	15,558	940.242		

	T°C	cSt	m <sup>3</sup> /h	Re	pulses/m3	%spread	proved vol m <sup>3</sup>
1	19.99	79.06	1950.300	22,517	940.342	0.079	38.28
2	19.90	79.43	1954.700	22,450	940.761		USM master meter
3	19.91	79.41	1952.600	22,449	940.017		

# 34<sup>th</sup> International North Sea Flow Measurement Workshop 25 – 28 October 2016

## Technical Paper

### Test 3.3      Test setup Upstream 1/ Meter A / Downstream 1

	T°C	cSt	m <sup>3</sup> /h	Re	pulses/m3	%spread	proved vol m <sup>3</sup>
1	19.88	1709.00	148.900	1,709	941.576	0.094	10.06
2	16.96	1718.00	149.000	1,718	940.797		uni
3	20.03	1724.00	149.000	1,724	940.696		

	T°C	cSt	m <sup>3</sup> /h	Re	pulses/m3	%spread	proved vol m <sup>3</sup>
1	20.06	78.70	447.300	5,182	941.420	0.169	10.06
2	19.96	79.15	446.900	5,156	939.851		uni
3	19.92	79.37	446.700	5,141	939.836		

	T°C	cSt	m <sup>3</sup> /h	Re	pulses/m3	%spread	proved vol m <sup>3</sup>
1	19.92	79.34	754.300	8,672	940.922	0.135	10.06
2	19.92	79.35	754.500	8,676	940.559		uni
3	19.93	79.28	756.200	8,692	941.825		
4	19.98	79.10	755.900	8,718	940.810		
5	20.02	78.90	756.600	8,750	940.641		

	T°C	cSt	m <sup>3</sup> /h	Re	pulses/m3	%spread	proved vol m <sup>3</sup>
1	20.13	78.43	1361.600	15,848	940.295	0.051	37.20
2	20.10	78.52	1358.800	15,787	940.771		USM master
3	20.05	78.79	1358.600	15,737	940.413		

	T°C	cSt	m <sup>3</sup> /h	Re	pulses/m3	%spread	proved vol m <sup>3</sup>
1	19.93	79.31	1967.900	22,654	940.010	0.055	38.20
2	19.94	79.25	1970.500	22,705	939.838		USM master
3	20.00	79.00	1974.100	22,809	940.353		

### Test 3.4      Test setup Upstream Spare/ Meter B/ Downstream Spare

	T°C	cSt	m <sup>3</sup> /h	Re	pulses/m3	%spread	proved vol m <sup>3</sup>
1	19.93	79.31	147.900	1,703	940.319	0.307	10.06
2	19.98	79.08	147.800	1,708	939.321		Uni
3	19.97	79.14	148.300	1,706	942.201		

	T°C	cSt	m <sup>3</sup> /h	Re	pulses/m3	%spread	proved vol m <sup>3</sup>
1	20.03	78.85	447.200	5,176	940.404	0.172	10.06
2	19.93	79.20	446.900	5,142	940.860		Uni
3	19.98	79.50	446.800	5,136	939.243		

	T°C	cSt	m <sup>3</sup> /h	Re	pulses/m3	%spread	proved vol m <sup>3</sup>
1	19.91	79.41	754.700	8,671	940.636	0.072	31.88
2	19.93	79.32	755.700	8,690	941.078		USM master

# 34<sup>th</sup> International North Sea Flow Measurement Workshop 25 – 28 October 2016

## Technical Paper

	ToC	cSt	m <sup>3</sup> /h	Re	pulses/m <sup>3</sup>	%spread	proved vol m <sup>3</sup>
3	19.96	79.16	755.600	8,712	940.397		
1	19.99	79.03	1358.200	15,689	940.157	0.059	37.20
2	20.02	78.92	1360.800	15,735	940.621		USM master
3	20.06	78.73	1358.700	15,757	940.067		
	ToC	cSt	m <sup>3</sup> /h	Re	pulses/m <sup>3</sup>	%spread	proved vol m <sup>3</sup>
1	20.06	79.03	1358.200	22,845	938.883	0.085	38.30
2	20.04	78.92	1360.800	22,832	939.404		USM master
3	20.07	78.73	1358.700	22,909	939.680		

### Test 3.5 Test Setup Upstream 2/ Meter B / Downstream 2

	T°C	cSt	m <sup>3</sup> /h	Re	pulses/m <sup>3</sup>	%spread	proved vol m <sup>3</sup>
1	20.17	78.22	146.300	1,694	939.801	0.011	10.06
2	20.11	78.50	146.100	1,699	939.902		Uni
3	20.04	78.79	146.200	1,708	939.834		

	T°C	cSt	m <sup>3</sup> /h	Re	pulses/m <sup>3</sup>	%spread	proved vol m <sup>3</sup>
1	20.05	78.76	441.200	5,122	938.626	0.095	10.06
2	20.05	78.77	441.900	5,124	939.521		Uni
3	20.04	78.80	441.200	5,117	939.124		

	T°C	cSt	m <sup>3</sup> /h	Re	pulses/m <sup>3</sup>	%spread	proved vol m <sup>3</sup>
1	20.04	78.81	756.300	8,756	940.699	0.042	31.88
2	20.04	78.80	756.000	8,752	940.820		USM master
3	20.05	78.78	756.200	8,754	941.091		

	T°C	cSt	m <sup>3</sup> /h	Re	pulses/m <sup>3</sup>	%spread	proved vol m <sup>3</sup>
1	20.02	78.91	1358.600	15,717	940.174	0.083	37.20
2	20.03	78.85	1357.600	15,731	939.454		USM master
3	20.07	78.68	1359.900	15,778	940.232		

	T°C	cSt	m <sup>3</sup> /h	Re	pulses/m <sup>3</sup>	%spread	proved vol m <sup>3</sup>
1	20.11	78.51	1968.600	22,902	939.712	0.013	38.30
2	20.08	78.66	1969.000	22,861	939.798		USM master
3	20.07	78.70	1970.200	22,866	939.680		

### Test 3.6 Test Setup Upstream Spare/ Meter C/ Downstream Spare

	T°C	cSt	m <sup>3</sup> /h	Re	pulses/m <sup>3</sup>	%spread	proved vol m <sup>3</sup>
1	19.95	79.22	146.700	1,690	940.657	0.067	10.06
2	20.00	79.00	146.700	1,695	940.031		Uni
3	20.01	78.95	146.400	1,693	940.128		
4	19.95	79.19	146.600	1,690	940.541		

**34<sup>th</sup> International North Sea Flow Measurement Workshop  
25 – 28 October 2016**

**Technical Paper**

	T°C	cSt	m <sup>3</sup> /h	Re	pulses/m3	%spread	proved vol m <sup>3</sup>
1	20.02	78.88	421.500	4,871	939.733	0.382	10.06
2	19.99	79.04	420.800	4,861	940.117		Uni
3	19.98	79.06	420.700	4,856	940.531		
4	20.02	78.91	421.700	4,866	942.412		
5	20.04	78.84	421.700	4,971	942.498		
6	19.97	79.11	421.900	4,855	942.703		
7	19.98	79.09	421.300	4,856	941.414		
8	19.99	79.03	421.700	4,858	942.701		
9	19.98	79.11	421.700	4,850	943.322		

	T°C	cSt	m <sup>3</sup> /h	Re	pulses/m3	%spread	proved vol m <sup>3</sup>
1	19.98	79.07	756.300	8,729	940.168	0.031	31.90
2	91.94	79.26	756.000	8,703	940.223		USM master
3	19.91	79.37	756.200	8,681	939.932		

	T°C	cSt	m <sup>3</sup> /h	Re	pulses/m3	%spread	proved vol m <sup>3</sup>
1	19.98	79.07	756.300	8,729	940.168	0.031	31.90
2	91.94	7926.00	756.000	8,703	940.223		USM master
3	19.91	79.37	756.200	8,681	939.932		

	T°C	cSt	m <sup>3</sup> /h	Re	pulses/m3	%spread	proved vol m <sup>3</sup>
1	19.95	79.23	1358.800	15,652	940.451	0.044	37.20
2	19.98	79.07	1357.100	15,671	940.034		USM master
3	19.99	79.03	1357.600	15,684	940.113		

	T°C	cSt	m <sup>3</sup> /h	Re	pulses/m3	%spread	proved vol m <sup>3</sup>
1	19.94	79.26	1960.800	22,582	940.293	0.029	38.30
2	19.97	79.11	1960.000	22,611	940.457		USM master
3	19.97	79.14	1958.400	22,591	940.180		

## Technical Paper

# Turbine Meters in Decline - Throwing the Baby Out with the Bathwater

Terry Cousins, CEESI - USA

### ABSTRACT

While there is no doubt that the new meters, Coriolis and USMs, have some great advantages, the fact that no single flowmeter is best for all applications is being lost in the almost born again Apple like fervor to promote them. This results in missing the true advantages of older meter designs such as the turbine meter.

The paper describes the design and operation of turbine meters, concentrating, unlike past papers, on the methods used for linearizing them by modifying the basic physics by changing the rotor aerodynamics. Thus unlike the Coriolis and USM their base performance does not require a base viscosity to be determined to correct them. Once linearised they find their own Reynolds number correction by virtue of the fluid dynamics.

The paper presents large amounts of data showing the effect and methods of linearisation, the Reynolds number performance of turbine meters and discusses some of the installation effects

### 1 INTRODUCTION

"We humans have a talent for deceiving ourselves. Skepticism must be a component of the explorer's toolkit, or we will lose our way. There are wonders enough out there without us inventing any" Carl Sagan.

We see this continuously now in the area of flow measurement, the new is automatically better in every way compared to the old. The result is that we throw away or dismiss experience, quality and competent meters. Further we are prepared to bend practices that have served well to make the new meters acceptable. Is this the whining of an old man, for whom technology has passed him by? Unfortunately this old man loves the new technology, Ultrasonic flow meters have provided him the most interesting years in flow measurement, but this should not obscure their faults, **the talent for deceiving ourselves**, and we should be aware that there is no one flowmeter that solves every flow problem. The variations in required performance, the fluid conditions, the ambient conditions, the flowrates etc. all make it fundamentally impossible for one technology to solve every measurement problem, even though marketing would have it so.

This brings us therefore to the subject of the paper, turbine meters. When I first worked in flow measurement they were the de-facto standard for measuring low uncertainty fluids. They had their faults, and of course we used them for measurement applications where they were inappropriate, and like all meters they had at times reliability problems. However, within the grand scheme of things they produced generally good results, which even in hindsight still stand. However, talk to most new young engineers and technicians and if they even consider them they are immediately dismissed, old technology, moving parts, totally unreliable and so Coriolis and USMs are taking over rapidly within such an environment.

# 34<sup>th</sup> International North Sea Flow Measurement Workshop 25-28 October 2016

## Technical Paper

With the development of the new CEESI oil calibration facility my first reaction was to use USMs for master meters. My experience had however counselled me to look around, I knew that I would have problems with proving them, in fact I knew that I would need to use a master meter system to calibrate USMs successfully. So I decided to look again after many years away at turbine meters, and realized that I was probably also guilty of deceiving myself! This has made me look again at turbine meters and to realize that they still have a place in low uncertainty flow measurement.

The paper sets out to at least give an insight for those new to turbines, and for those who have forgotten about them jolt their memories about the qualities they possess and hopefully give a balanced assessment as to their value in the flow measurement world.

## 2 METHOD OF OPERATION

The paper is not intended to have a detailed discussion of the design, there are plenty of references for this, but to point out the salient features so that the data and calibrations can be explained. The turbine meter is simply a set of blades set at an angle to the fluid mounted around a hub on an axle, figure 1.



**Figure 1 Turbine Meter Rotor Assembly**

The fluid across the blades produces a lift force which, because the axle constrains the movement to an axial motion, causes the assembly to rotate. This imparts an angular velocity (RPM) to the turbine rotor which is proportional under ideal conditions to the linear velocity of the fluid.

Many turbine meters use a set of blades set at an angle to the oncoming flow to produce lift, figure 2.

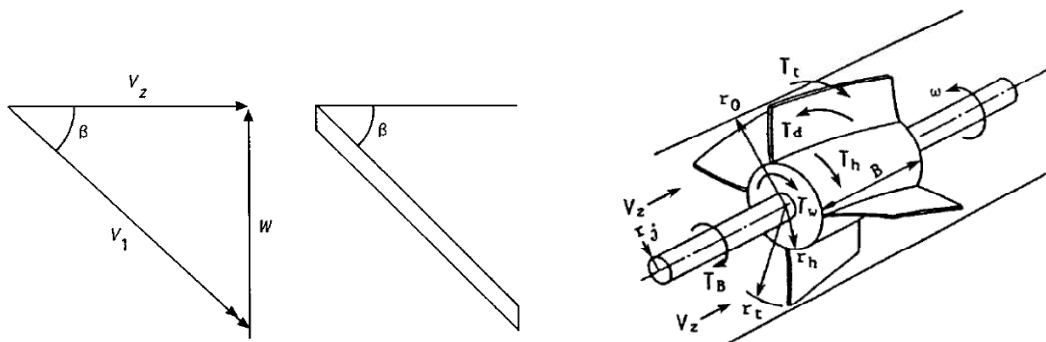


**Figure 2 Forces and Flow on a Turbine Meter Rotor [1]**

# 34<sup>th</sup> International North Sea Flow Measurement Workshop 25-28 October 2016

## Technical Paper

Under ideal conditions these will cut through the fluid to form a perfect helix. Using this basic concept the value of the oncoming flow velocity can be obtained by determining the frequency,  $f$ , of the blades passing a fixed position.

$$V_z = w / \tan \beta \dots\dots\dots [1]$$

And  $f = N \tan \beta V / 2 \pi r \dots\dots\dots [2]$

Where  $N$  is the number of blades,  $\beta$  the blade angle,  $V$  the oncoming fluid velocity and  $r$  the point of measurement along the blades.

The rotor accelerates until the driving torque on the blades balances the sum of the resisting torques. The resisting torques are the hydraulic drag of blades, bearing friction, both from the axial and the end thrust bearings and viscosity. For the steady state condition the following relationship is obtained for the torque produced by the lift and the various drag components:

$$T_d = T_B + T_t + T_w + T_h \dots\dots\dots [3]$$

Where:  $T_d$  is the torque produced by lift on the blades, which by virtue of being a lift component is Reynolds number sensitive.  
 $T_B$  is due to the rotational bearing friction  
 $T_w$  is due to the end thrust bearing friction, sometimes alleviated by floating rotor designs.  
 $T_t$  is the tip blade clearance drag, which can have a significant impact on the shape of the calibration curve, and the Reynolds number performance.  
 $T_h$  is the fluid dynamic drag on the rotor, which again because it is a function of the drag will be Reynolds number sensitive.

When the meter is running at the point where the meter is linear it is assumed that the bearing and tip blade drags are so small compared to the lift and fluid dynamic drags that they are zero. At this point the equation becomes:

$$T_h = T_d \dots\dots\dots [4]$$

$$T_h - T_d = 0 \dots\dots\dots [6]$$

There are a number of different equations for torques<sup>1</sup>, but essentially they end up with an equation similar to:

$$\int_{r_h}^{r_t} \frac{r V_z^2 c}{\cos \beta_m} (K C_L - C'_D \tan \beta_m) dr = 0 \dots\dots\dots [7]$$

Where  $r_t$  and  $r_h$  are the radius at the hub and tip of the blades respectively.  $C_L$  and  $C'_D$  are the corresponding lift and drag coefficients for the blades.  $K$  is the correction from a single blade to a cascade and  $c$  is blade width.

Equations in themselves are interesting but they do also hopefully tell us the potential issues we will see in using the meter. The above tell us:

- Bearing friction is going to be an issue if the fluid forces are not sufficient to overcome them. Further if they are a big contribution then as the bearings change their characteristics the calibration is likely to change.

# 34<sup>th</sup> International North Sea Flow Measurement Workshop

## 25-28 October 2016

### Technical Paper

- Lesson: do not use the meter at low flows where the bearings will affect the performance.
- It tells us the performance will be subject to tip blade clearance.
  - Lessons: The design will be influence the performance, a shroud for example will have a significant effect. Also it tells us the Reynolds number will play a part. Also any build up on the walls or shroud will affect the performance.[2]
- Equation 7 shows that variation in velocity profile along the blades will change the calibration.
  - Lesson: upstream flow profile is likely to affect the performance.
- Equation 7 includes a lift and drag coefficient.
  - Lessons: both are well known to be sensitive to Reynolds number, further the shape of the blades will influence the meter performance.

#### 2.1 Performance

The performance of the turbine meter is encapsulated in several issues:

- Reynolds Number
- Calibration.
- Design, particularly the blade design.
- Installation and Proving.

The paper does not discuss pick up design etc. reference [1], describes the operation. It should be noted that some inductive pickups do give a drag to the rotor, but this is generally only an issue on very small meters.

The classic curve shown in most literature for a turbine meter is shown in figure 3. At the lowest flow there is no rotation as bearing friction is too great compared to the lift available. Finally the lift is sufficient to turn the rotor, but going to equation 3 it still provides a large retarding force. During this section the rotation is not directly proportional to the flow velocity. Classically there is then a hump as the meter becomes linear. This is largely controlled by the tip blade clearance. Finally the meter reaches the point where there is a solid linear relationship between velocity and rotation. It is generally accepted that the sweet spot for the turbine is to operate at around 75% of the rated full scale flow.

Technical Paper

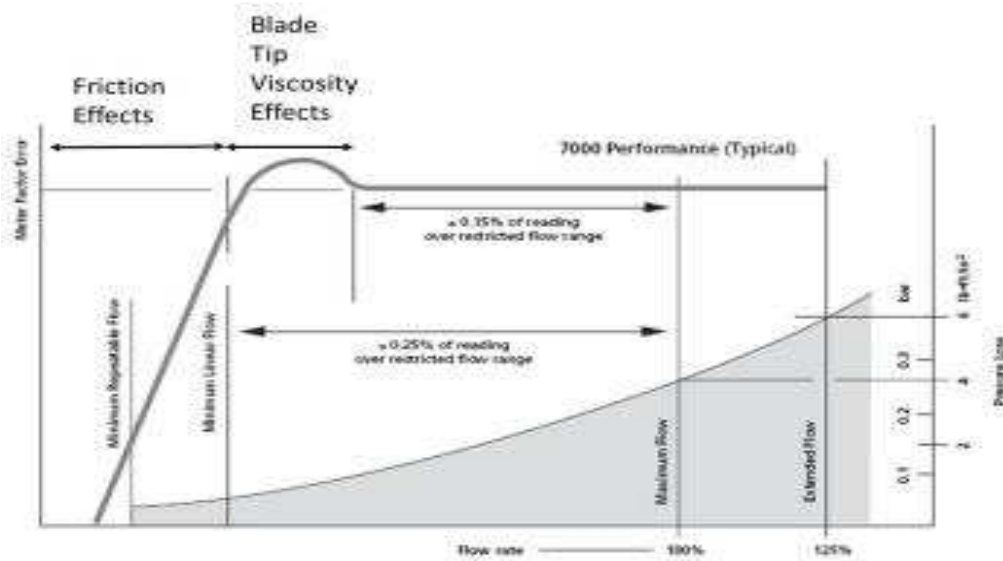


Figure 3 Classical Turbine Calibration Curve [1]

This curve would be typical for a low viscosity fluid such as water.

2.2 Reynolds Number

Unfortunately, as with all meters, we come back to Reynolds number. Turbine meters when away from the effect of bearing friction are subject to Reynolds number. The classical set of curves for a flat bladed meter are shown in figure 4. When plotted against Reynolds number it can be seen that away from the bearing friction effects there is a good agreement of the curve with Reynolds number.

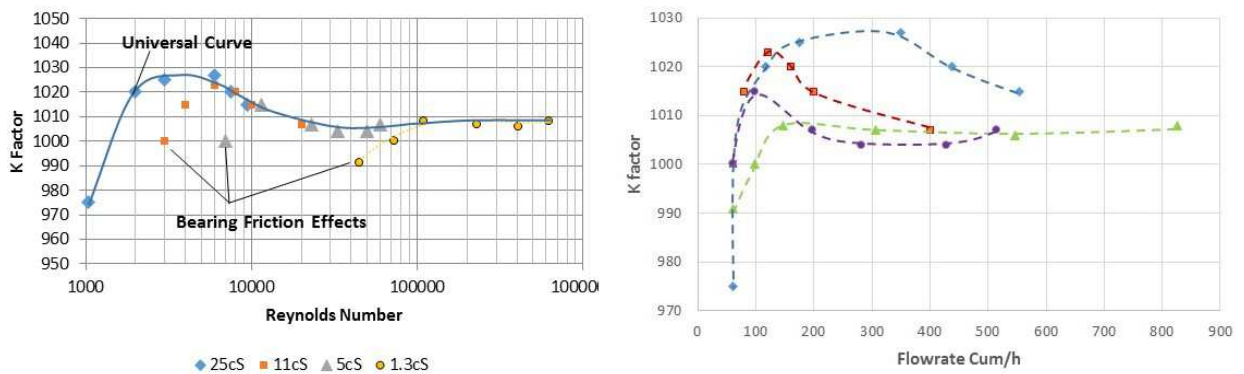


Figure 4 Calibration of a Flat Bladed Turbine Meter [2]

It can be seen clearly that the flat bladed meter suffers from changing calibration with a relatively small change in viscosity, evidenced by the hump produced at low Reynolds numbers. It should be noted however the effect varies significantly with meter size, the larger the meter the less the effect. Blade configuration effects the performance, as we will see with helical blades have a more stable performance with Reynolds number than than flat blades. Tip blade clearance and mechanical design will affect the performance.

## Technical Paper

### 2.3 Calibration

To an extent the meter linearity can be improved for a given viscosity, Reynolds number, by modifying the blades. Very few outside of the manufacturers understand how turbine meters are linearised. The meter is calibrated initially and a calibration curve ascertained. Once this curve is determined a technician will either file or bend the blades to make the calibration curve the required shape. The usual practice is to perform a calibration using the calibration fluid. If this curve is not within the specification of the meter, it is removed and the blades modified. Figure 5 shows a set of experimental data<sup>1</sup> for the effect of changing the downstream of a flat bladed turbine meter. A similar set of curves can be obtained for the upstream of the blades. In practice the most common method of modification is to use a file on the blades, usually done by a technician "who knows how to do these things!!" There is generally not a procedure that specifies in detail how exactly to modify the blades.

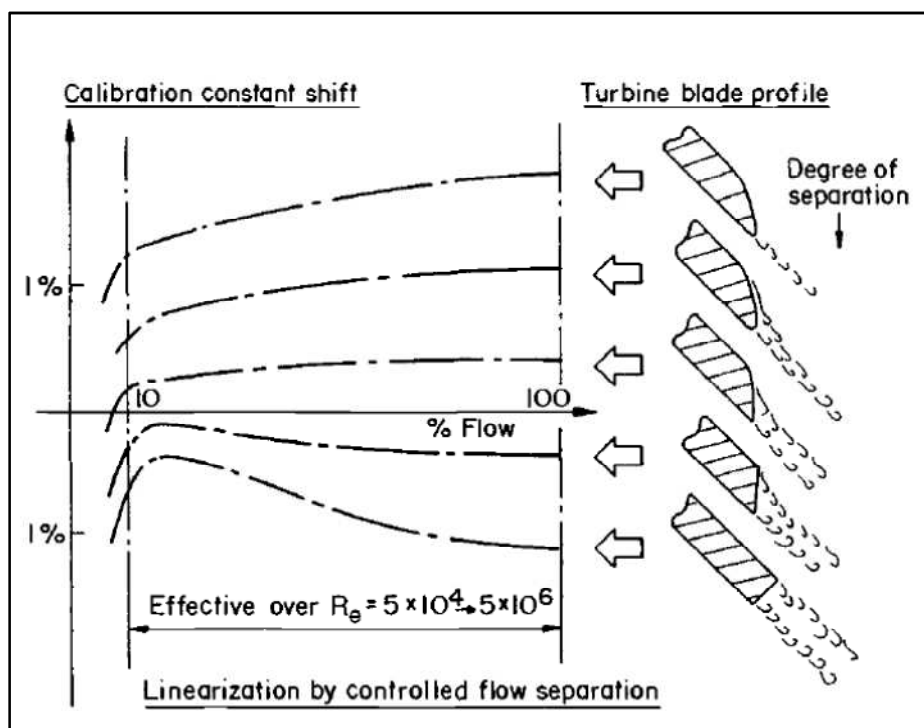


Figure 5 Effect of Blade Modification on the Calibration [1]

The effect of modifying a production 6" turbine is shown in figure 6 [3]. The meter is shifted in terms of K factor and it is linearized.

## Technical Paper

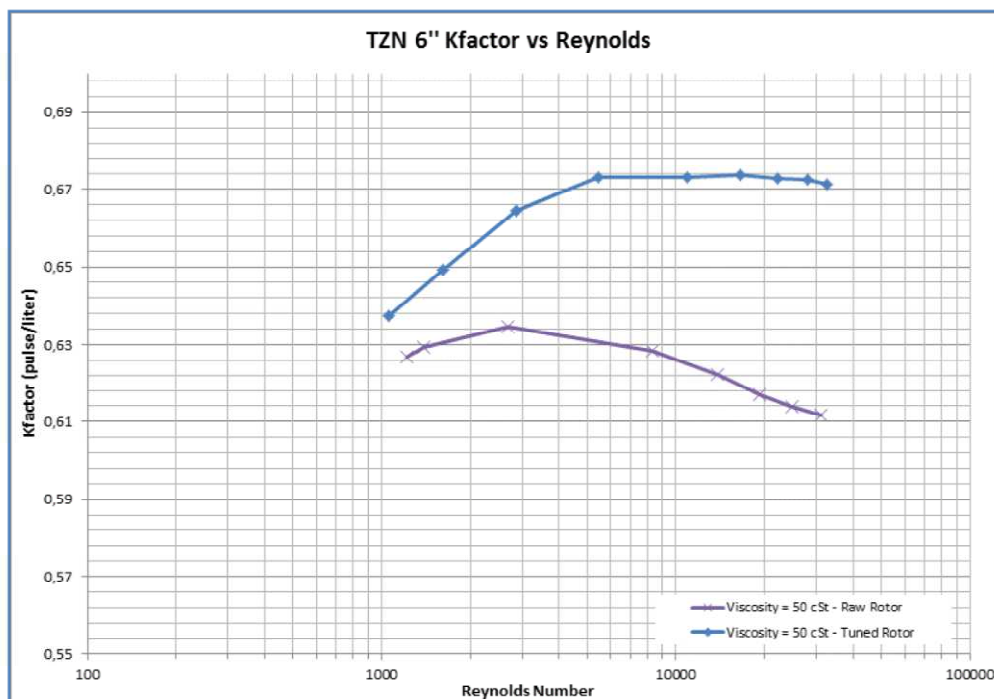


Figure 6 Modification of Meter Calibration

The essential points to make about this method are:

- It implies that unless the meter is calibrated over the range of operation, in terms of Reynolds number the meter will be non-linear when in operation.
- The method of linearization, unlike that for Coriolis and USMs is by modification of the physics of the meter, rather than by software correction. This implies that the meter essentially when modified for a given Reynolds number will be self-correcting, and does not require the exact knowledge of the fluid viscosity. The only way in which the meter will differ on site from the calibration will be due to installation effects.

### 2.4 Design, Blade Configuration

The major difference in designs revolves around the blade configuration. The "standard" design is based on flat blades forming the rotor. This is simple and robust to construct. Fluid dynamically it does give issues as the flow "separates" across the blades resulting in it being very susceptible to Reynolds number variations, figure 7. To improve this performance the helical bladed meter was developed, figure 7. The design is such that across the rotor the boundary layer of the fluid does not separate, resulting in a more consistent operation with Reynolds number. This does not mean that without modification the meter is linear. It still has to be modified in a similar way to the flat bladed meter, it is just that the modification is less and the consistency over the range is better.

Technical Paper

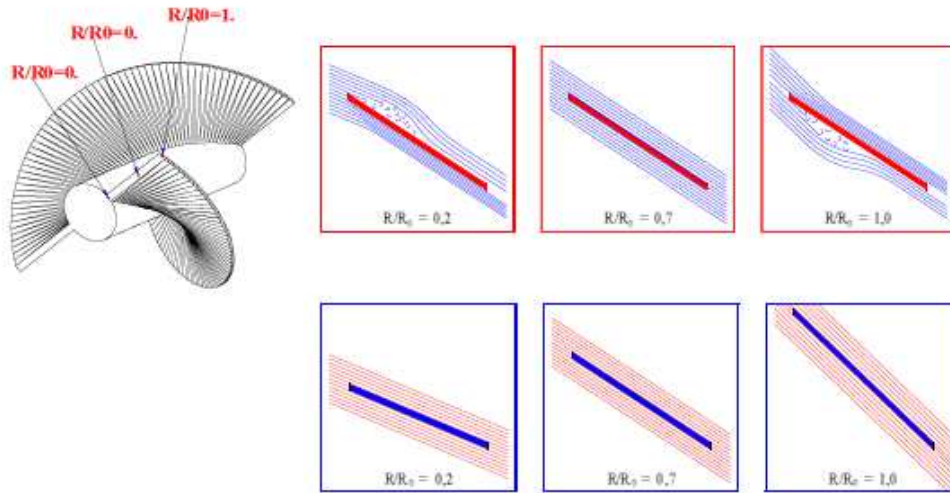


Figure 7 Flow Across a Flat and Helical Bladed Rotor [2]

Figure 8 shows an 8" helical bladed meter that has been modified over a 2000:1 Reynolds number range. Over 230:1 the linearity is +/- 0.3%. The dotted line is the shape of the curve before modification.

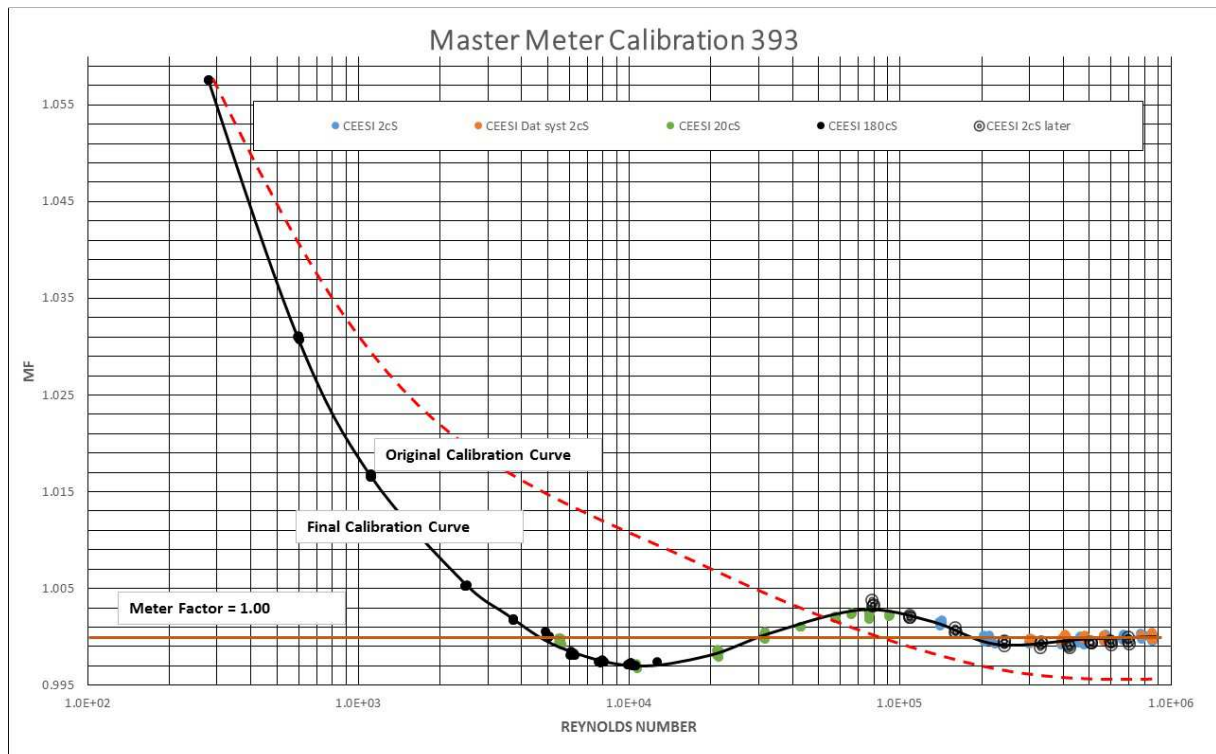


Figure 8 Calibration of an 8" Helical Bladed Turbine Meter

# 34<sup>th</sup> International North Sea Flow Measurement Workshop 25-28 October 2016

## Technical Paper

It should be noted that this meter was modified over such a large range for the CEESI calibration facility, two other meters have very similar curves. Normally the meter would be "corrected" over a smaller range and would have a much tighter linearity.

### 2.5 Installation and Proving

One of the major criticisms of turbine meters is their susceptibility to flow induced installation effects, such as profile distortion and swirl. There is no doubt that the meter is particularly prone to calibration change due to swirl, and that generally speaking they should be protected by some form of flow conditioner. The de-facto standard is the tube bundle, not the world's greatest and most consistent conditioner, but generally good at reducing the effect of swirl. Certainly it would not be sensible to install a turbine meter in operation without a conditioner and expect a good installed uncertainty without proving. Equally they may not be as bad as the conventional wisdom predicts. Figure 9 shows the calibration of an 8" Helical meter installed at CEESI compared to the manufacturer's calibration. The Manufacturer used a CPA flow conditioner, the meter at CEESI, had no conditioner and is 10 diameters downstream of a large header. Over the range, where the meter is not affected by bearing drag, the two agree within 0.03%. The combined uncertainty of the two facilities is 0.08%, excluding the uncertainty of the meter. The same effect was seen with the other two meters.

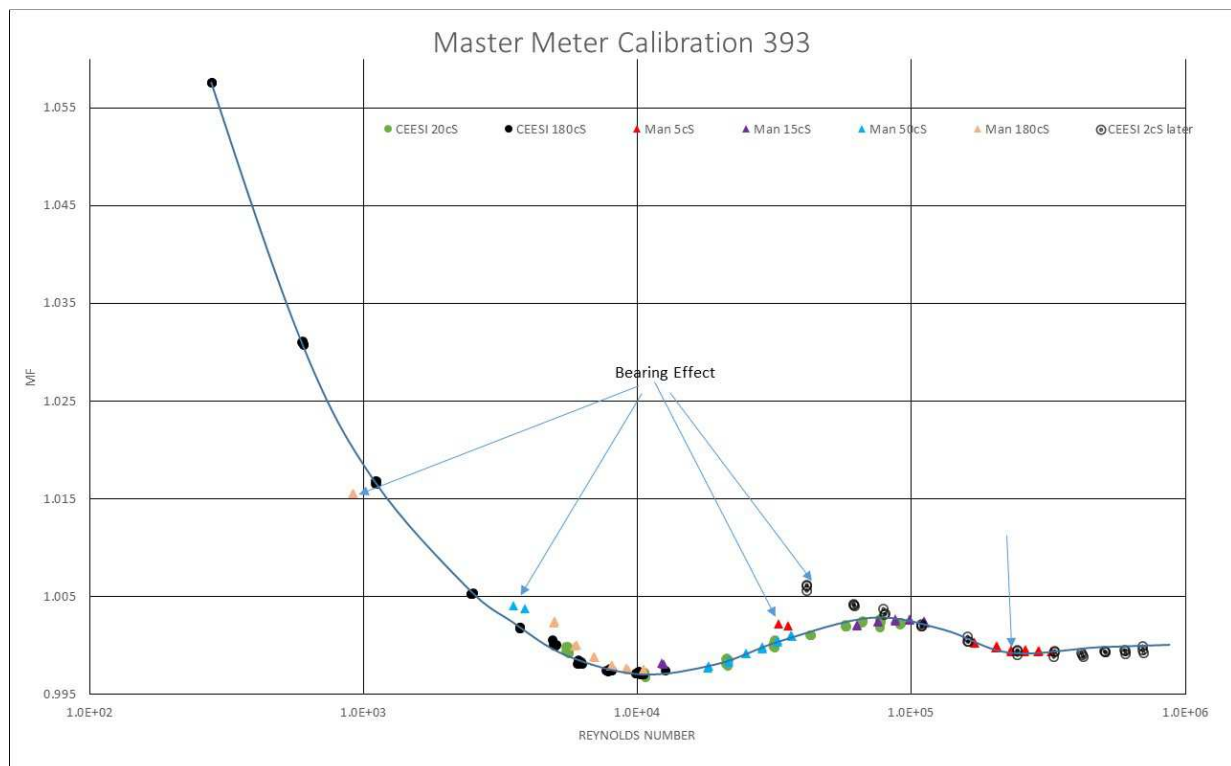


**Figure 9 Comparison of CEESI Calibration with Manufacturer**

This should not however be taken as an absolute that this will happen, there is plenty of data to show that the calibration can shift with installation, and it is better to safe than sorry and use a flow conditioner.

Equally for the best performance a prover should be used, in the end it removes the concerns with installation, and when we are looking for 0.1% then that confidence is needed with flow measurement.

# 34<sup>th</sup> International North Sea Flow Measurement Workshop 25-28 October 2016

## Technical Paper

It is with proving that the turbine truly comes into its own, because essentially the prover was designed for turbine meters, and as such is at its most effective. Much has been said of the lack of diagnostics available for turbines when compared to Coriolis and USMs, but the prover is truly effective as a diagnostic for a turbine meter. It is not just the variation in the prove meter or K factor that tells the tale, it is the general rule of repeatability of turbine meters. If the repeatability of the turbine meter is worse than 0.05% in 5 runs then something is wrong. There could be a flow problem, the meter could be failing, there could be leaks, or the prover could have issues. The point is that if it does not meet this criteria there is almost certainly a problem. With the Coriolis and USM, if proving does not meet this criteria or any consistent criteria of repeating it probably means that the meter is just not proving well [4], it does not necessarily mean there is a problem.

### 3 RELIABILITY

Perhaps the biggest complaint against the turbine is the fact that it has bearings, and hence moving parts. The result is thus failure over time by bearings wearing out and also being prone to failure due to bearings becoming blocked. There is a truth in both of these views, but equally the long term reliability issue can be addressed by the right application. It is obvious that the meter should not be used where the fluid has poor lubricity, this will certainly reduce the life of the meter and result in the early demise of bearings. It should be noted that Gas turbine meters have a lubricant injected into the bearings, this is not feasible on liquids. Any fluid, particularly cleaning fluids that attack the bearing material, generally tungsten carbide for liquid meters will reduce the life expectancy. A common cause of damage is over speeding, many times I have come across meters that have been "steam cleaned", subjecting the meter to a quick burst of high pressure, high velocity steam. A combination of temperature and velocity will be sufficient to ensure internals of the meter will be found downstream of the meter section. Under good conditions however the expectation of meter life can be several decades. In 2000 I audited turbine meters measuring crude coming from the gulf of Arabia to Alexandria in Egypt. At the time these had been in operation for nearly 30 years, with only two of the 25 meters having any repair over that period of time. Their calibrations did not change outside of the uncertainty limits, and to my knowledge they are still in operation.

The buildup of material in the bearings is not as straight forward. There should always be some filter or strainer upstream to protect the meter, but this is also true of all meters with the possibility of buildup. Both USMs and Coriolis will have their performance affected with the buildup of material, USMs are likely to get it in the ports and Coriolis will see a calibration shift with buildup of material trapped in the tubes. Perhaps the big difference is that the Turbine is likely to stop working! A nuisance but at least it makes one think about the issue. Having a meter operate but giving the wrong answer is not a great solution. Wax buildup is a typical issue, times there are complaints that a turbine will stop working with wax in the meter. The fact is there should be no measurement using any meter with wax build up, the problem needs to be resolved.

# 34<sup>th</sup> International North Sea Flow Measurement Workshop 25-28 October 2016

## Technical Paper

### 4 DRIFT

One area that is difficult to understand and quantify is the long and medium term drift of a turbine meter. In the US it is generally accepted that the proving reproducibility should keep the meter within 0.2-0.25%. This comes largely from the history with turbine meters. A control chart of a turbine meter will often show that the proves drift over time to this span. The reasons for this are not clear, but possibly it is the mechanical movement that causes the meter to locate into different positions.

### 5 MIXTURES

Like all single phase meters they have issues with multi-phase flow measurement. Turbine meters seem to work in the same way as all meters with water in oil mixtures. As can be seen from the calibration shown in figure 10 [5], above the point where the water and oil mix then the meter does a good job of measuring the combined water and oil volume, the data is not clear as to whether they retain the same level of uncertainty, but there is good agreement. Once the water separates out at the lower velocities the meter uncertainty increases significantly.

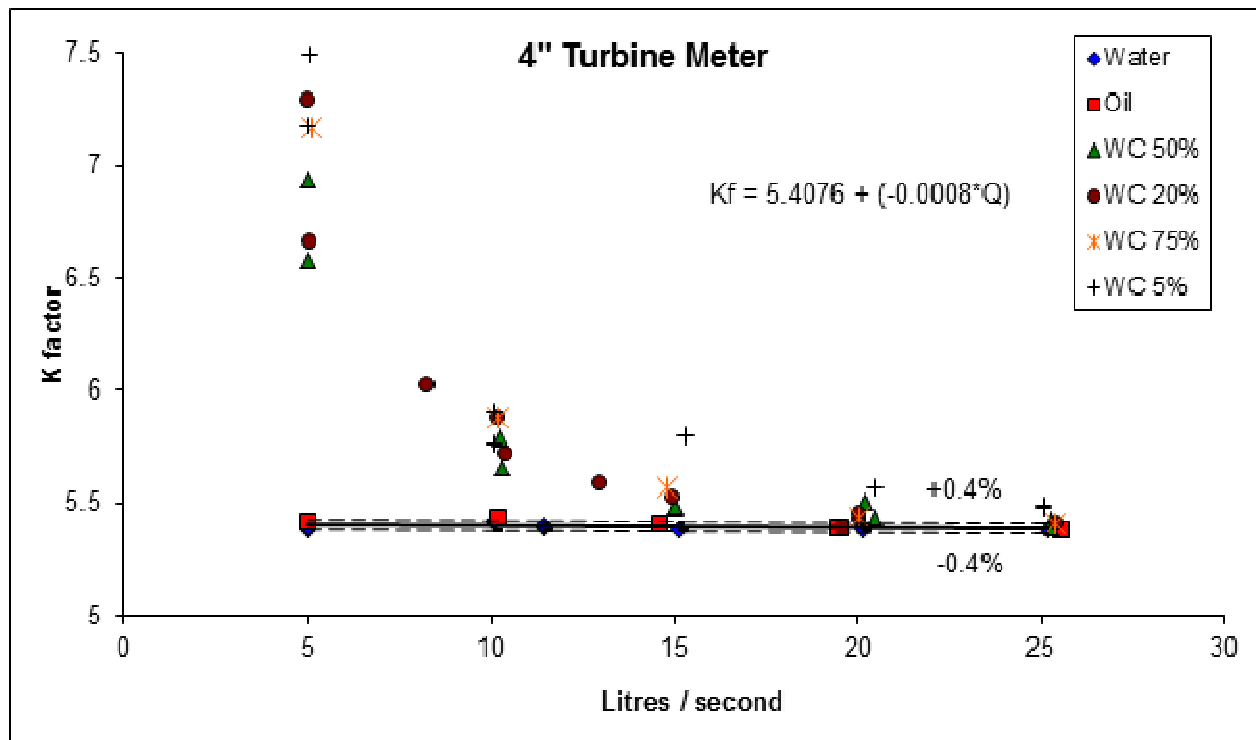


Figure 10 Calibration of a Turbine Meter with High water Oil Mixing

"Fiscal measurement of oil with high water fraction" [6] gives a very good account of the issues relating to measurement of oil in water mixtures, including the effect on such issues as the corrections Ctl etc.

Less data is available on the performance of a turbine meter measuring a gas in oil mixture. The only circumstantial evidence I have, comes from the replacement of turbines by USMs in a leak detection system. Unfortunately gas would be mixed in the oil towards the end of each tank in the application. The customer was disappointed that the USM would essentially stop reading because of the gas interference with the signals, or

# 34<sup>th</sup> International North Sea Flow Measurement Workshop 25-28 October 2016

## Technical Paper

became very noisy, when his old turbines kept running. This would result in leak detection alarms from the USM system. However, what answer was given by the turbines is a matter of conjecture. Again it would be expected that if fluids mixed the turbine would measure the combined volume.

### 6 CRYOGENIC METER

With the metering world looking at measuring LNG, interest in cryogenic metering is increasing. This is concentrated on Coriolis and USMs, and we have forgotten the turbine meter. They have however been used successfully in this application for many years. Figure 11 shows the calibration of a 2" IDEX turbine meter on water and the NIST liquid nitrogen facility, now in operation at CEESI. Against Reynolds number it can be seen that the curves are joining together at the high end of the water and low end of the liquid nitrogen curves. There is a shift between the two calibrations but the actual scatter of the low end results on the liquid nitrogen includes the water calibration.

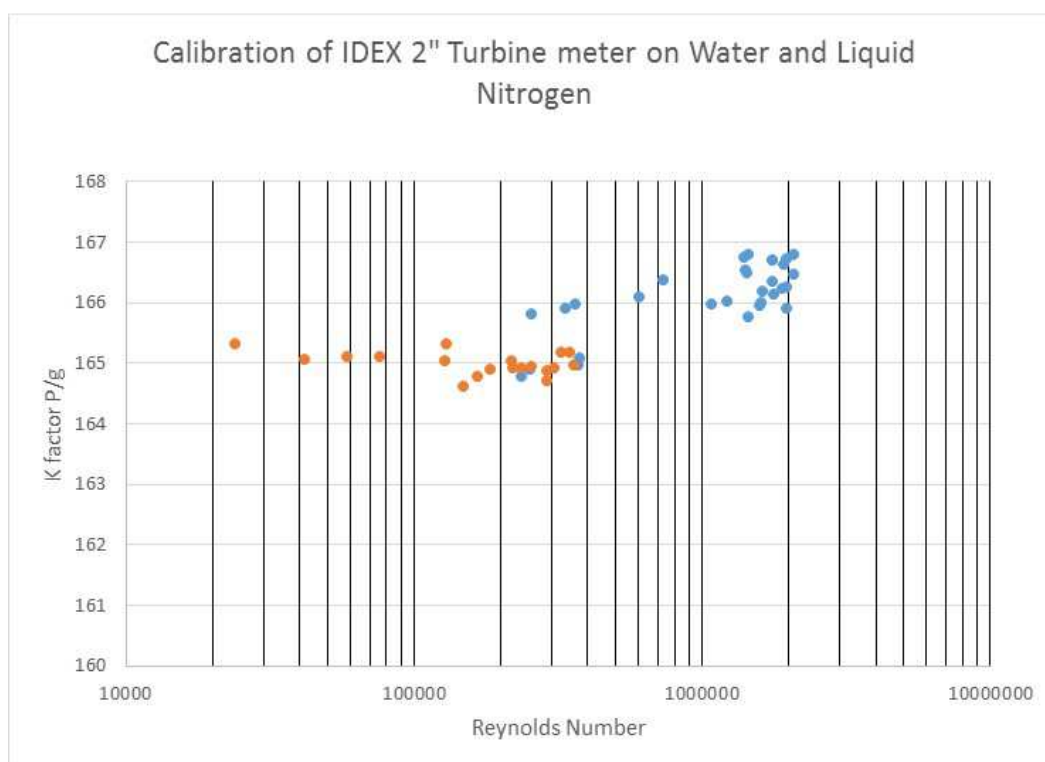


**Figure 11 Calibration of 2" Turbine Meter on Water and Liquid Nitrogen**

# 34<sup>th</sup> International North Sea Flow Measurement Workshop 25-28 October 2016

## Technical Paper

### 7 CONCLUSIONS

The paper put forward the concept that with turbine meters we should not “throw the baby out with the bathwater” because it is old technology. That the meter still has some very good attributes and that when looking at flow meter applications it should always be considered. The paper went through the theory and some of the operational aspects to explain again the possible value and also the downsides of the meter. From it the following conclusions can be drawn:

- Under good flow conditions, lower viscosities, say below 50-100cS the performance can be as good as any meter.
- The repeatability, particularly in combination with a prover is probably better than any other meter, and gives the opportunity to use the prover as a method not only of calibration but a diagnostic tool.
- The method of linearization is very strong compared to other meters, especially if calibrated correctly under similar conditions to the operation.
- They are probably as good as other single phase meters at dealing with water and gas in oil.
- They have a good history with cryogenic operation.
- Care must be taken to avoid build up in the meter and contamination of the bearings.
- There is an issue with long term stability in some meters.
- Care must be taken with installation, and it is advisable to include a flow conditioner.

Overall the meter should still take its place in consideration when reviewing meters particularly for use in Fiscal/Custody transfer of clean hydrocarbon liquids.

So to end with an appropriate quote by the physicist Richard P Feynman that can be applied to reviewing the use of flow meters “For a successful technology, reality must take precedence over public relations, for nature cannot be fooled.”

### 8 REFERENCES

1. Baker R.C , “Flow Measurement Handbook” Cambridge University Press 2000
2. Cousins T. “GUIDE TO LIQUID METER CUSTODY TRANSFER METERING” CEESI 2013
3. Dupuis D. Private communication. March 2016
4. Augenstein D “Proving Ultrasonic Meters” ISHM 2005
5. Cousins T & Stevens R “The Emperor’s New Clothes? - Oil with Water Flow Metering” NSFMS 2014
6. Hallanger A, Kjell-Eivind Frøysa & Per Lunde “ Fiscal measurement of oil with high water fraction” CMR-07-A10050-RA-01 2007
7. Hutton, S. P. (1974), “The effect of inlet flow conditions on the accuracy of flowmeters”. *Int. Mech.E Conf. Publ*, 4:1-8.(1986)
8. Hutton, S. P, “ The effects of fluid viscosity on turbine meter calibration.” *Flow Measurement in the Mid 80s*, East Kilbride, Scotland: National Engineering Laboratory, Paper 1.1.

## **Technical Paper**

# **Proving Coriolis Meters with Small Volume Provers**

**Tim Patten, Emerson**

---

## **1 INTRODUCTION**

Coriolis meters have many advantages for mass flow and volumetric measurement in a wide variety of applications. Inherent reliability, linearity and stable meter factor (MF) on a wide variety of products make them an ideal choice for pipeline transfer. With the recent introduction of high flow rate meters, Coriolis technology can now be used in line sizes up to 16". Custody transfer of products is very common in these large pipelines; in many applications contractual requirements dictate that meters be proved in situ periodically to ensure accurate measurement over time and/or product changes.

Traditionally, large stationary pipe provers have been employed at metering stations. These provers are large, expensive and take up valuable real estate. Maintenance costs of the complex four-way valve can also be a concern. Small volume "ballistic" or "piston-type" provers are becoming more common because they have a much smaller foot-print and reduced maintenance costs. Even the largest small volume provers are small compared to pipe provers; a large small volume prover has a measuring volume that is as much as 10 times smaller than an equivalent pipe prover. Additionally, small volume provers disturb the flow slightly when the piston launches. Because the measuring volume is small, the rate change created by the prover becomes an integral part of the proving cycle and is measured by the metering device.

Coriolis meters are "manufactured pulse" devices. Sophisticated signal processing resolves the vibrating characteristics of the meter, namely phase and frequency, to calculate mass or volume flow rate. The pulse output is generated from the calculated flow rate within the transmitter. The signal processing to calculate the flow measurement, then translate that measurement into a pulse output, takes a finite amount of time. The delay associated with the signal processing must be fast enough such that it properly measures the change in flow created by the small volume prover. The signal processing must also filter the signal noise properly to achieve adequate repeatability (typical API requirement is five consecutive runs within 0.05%).

Data will be presented that illustrates the overall performance of Coriolis meters when proved with a small volume prover. Average MF and repeatability results will be presented for a range of flow rates and (small) prover sizes. Recommendations are made to optimize the response time of meters to accommodate the small size of the provers and also how to utilize averaging techniques to achieve acceptable repeatability.

# 34<sup>th</sup> International North Sea Flow Measurement Workshop 25-28 October 2016

## Technical Paper

### 2 CORIOLIS METER PERFORMANCE

Coriolis meters are largely unaffected by process conditions including temperature, pressure, density and viscosity. An illustration of performance is shown in Figure 1.

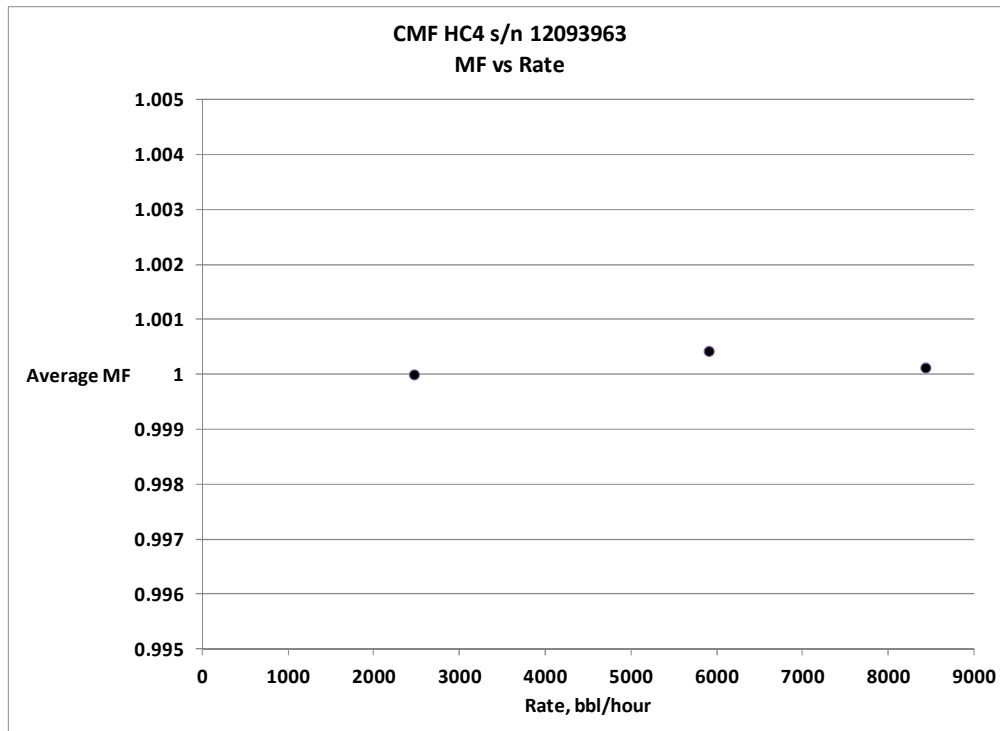


Figure 1 – Micro Motion CMF HC4 Flow Test

Conditions during the test were as follows:

Table 1 – Operating Conditions during Flow Test of Fig. 1

Rate, bbl/h	Re	Avg Volumetric MF	Avg Temp, °C	Avg Pressure, barg	Viscosity, cSt
2469	8,000	1.0000	25.2	2.9	75
5906	20,000	1.0004	24.5	3.4	75
8432	40,000	1.0001	33.4	4.3	45

The test was performed on a Micro Motion CMFHC4 which has a nominal flow rate of 13,000 bbl/hour. A 24" Daniel Compact Prover at Emerson's Micro Motion facility in Boulder, Colorado serves as the reference. Test fluid was mineral oil; notice that temperature and pressure rise considerably as the flow rate increases. This is because the facility is closed-loop and the heat exchanger doesn't reject 100% of the heat generated by the pump, especially at the highest rates. The

# 34<sup>th</sup> International North Sea Flow Measurement Workshop 25-28 October 2016

## Technical Paper

maximum system rate is limited to 8400 bbl/hour due to pump capacity. No changes to meter parameters (e.g. meter zero or MF) were made during the test and the calibration constants were established on water. The prover's measuring volume is traceable to the Daniel factory water draw. Linearity errors of less than 0.05% as shown here are typical.

### 3 SMALL VOLUME PROVERS

Small volume provers have been in the marketplace for at least 30 years and have steadily gained acceptance as a viable reference standard for custody transfer, refer to Figure 2. The use of small provers coinciding with the release of high flow Coriolis meters larger than 8" has created a need for a better understanding of the interaction between the two technologies.

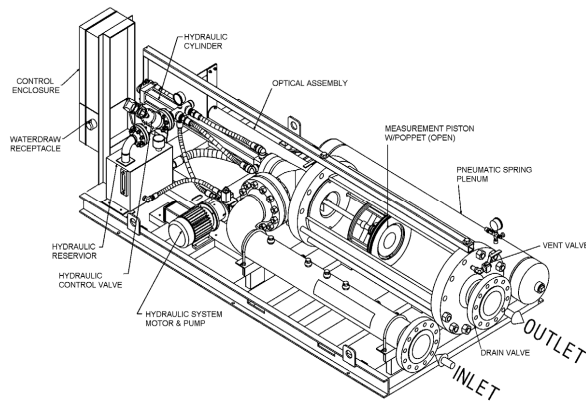


Figure 2 – Daniel Compact Prover

Figure 3 is an example of the changing flow rate as the piston launches. Four complete prover cycles are shown. Each time the piston launches the rate increases by 500 bbl/hour. Rate increases because the overall pressure loss of the system is lower when the piston is moving and the plenum pressure had not been optimized. In some instances the rate will decrease, such as a

The flight time of the piston in a small volume prover can be as short as 0.5 seconds. Additionally, the time between when the piston launches and the first detector (pre run time) can be as short as 0.25 seconds. The very short times, coupled with the fact that the flow is disturbed by the piston when it launches creates challenges for Coriolis meters.

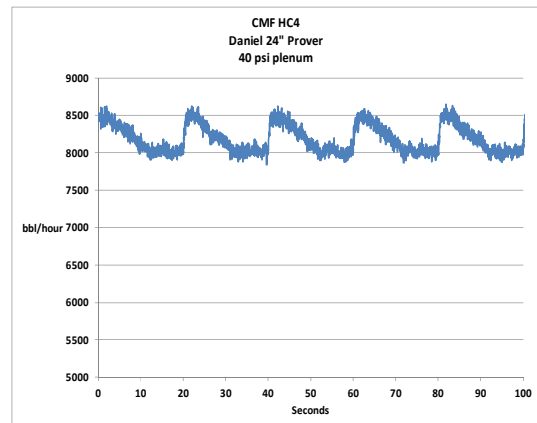


Figure 3 – Example of Changing Rate during Prover Piston Launch

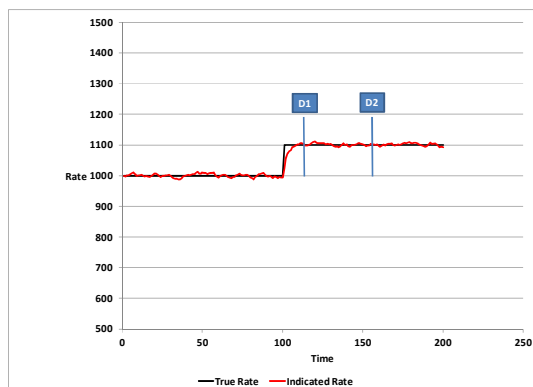


Figure 4 – Example of Adequate Meter Response Time

pipe prover because the ball adds resistance to the flow. Regardless of an increase or decrease in flow, the meter response time must be fast enough to have fully responded to the change imparted by the prover. For example, if the pre-run time is 0.25 seconds the meter has 0.25 seconds to fully respond to the flow change

# 34<sup>th</sup> International North Sea Flow Measurement Workshop 25-28 October 2016

## Technical Paper

before the first detector is encountered. An example of good response time is shown in Figure 4, and results in an accurate MF.

Notice that meter flow indication (red) is equal to the true flow when the piston passes the first detector (D1). Figure 5 shows what happens when meter response time is too slow. The small area between the true rate and indicated rate is not "seen" by the meter and is therefore not totalized correctly. This phenomenon artificially creates a MF > 1.000 (note that MF will be less than 1.000 if the rate change is negative). Adequate response time is critical to accurate proving.

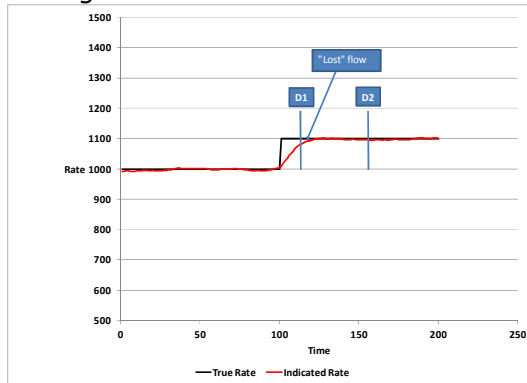


Figure 5 – Example of Inadequate (slow) Meter Response Time

Because a prover is a fixed volume device, the pre-run time and pass time between detectors changes with rate. For instance, a 2 barrel prover at 5,000 bbl/hour has a pass time of  $\frac{2}{\left(\frac{5,000}{3600}\right)} = 1.4$  seconds. At 10,000 bbl/hour the pass time is 0.72 seconds. Likewise, the pre-run time is half when the pass time is half.

An example of changing pass time vs. Rate for the Daniel 24" prover is shown in Figure 6. The importance of understanding the pass time vs. rate

dependence will be discussed in the section "Coriolis Meter Repeatability and Uncertainty".

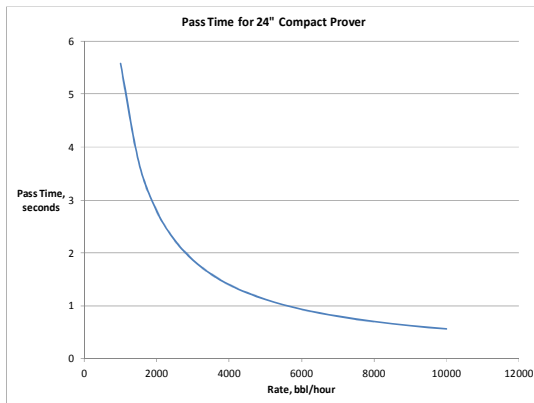


Figure 6 – Pass Time vs. Rate for the Daniel 24" Compact Prover

## 4 CORIOLIS METER RESPONSE TIME REQUIREMENTS

A meter must have adequate response time to avoid bias errors associated with the short pre run time of a small volume prover. The pass time and pre run time of the prover during the test of Figure 1 are shown in Table 2.

# 34<sup>th</sup> International North Sea Flow Measurement Workshop 25-28 October 2016

## Technical Paper

Table 2 – Pass Time and Pre Run Times for Test Shown in Figure 1

Rate, bbl/h	Re	Avg Volumetric MF	Pass time, seconds	Pre Run Time, seconds
2469	8,000	1.0000	2.19	1.09
5906	20,000	1.0004	0.91	0.46
8432	40,000	1.0001	0.64	0.32

The good linearity and lack of any MF trend substantiates that for pre run time of 0.32 seconds the response time is adequate. If a trend in MF had been observed it would have been indicative of response time that was too slow.

The Micro Motion CMFHC4 (and all smaller meters, too) have a stated 99% response time of better than 0.05 seconds. A meter response time of 0.05 seconds allows for pre run times as short as 0.1 seconds, although most small volume provers are limited to a minimum pre run of approximate 0.25 seconds. When configured for the fastest response time and no damping, Micro Motion meters have no issues with the short pre run time of small provers.

## 5 SIGNAL TO NOISE IN CORIOLIS METERS

Coriolis meters measure two dynamic signals – phase (or delta T) and frequency. The signals are sampled at a very high rate (up to 48 kHz) then filtered using sophisticated DSP techniques to improve the signal-to-noise ratio as much as possible. In a system where fast response time is important (e.g. proving) any time-based averaging (damping) is not recommended.

System noise can originate from many sources: cavitating valves and strainers, pumps, mixers and even the flow turbulent velocity itself. Each of these noise sources can influence the signal stability of a Coriolis meter, especially as the velocity gets high (greater than 10 m/s). Figure 7 shows typical signal noise response of Coriolis meter at two flow rates.

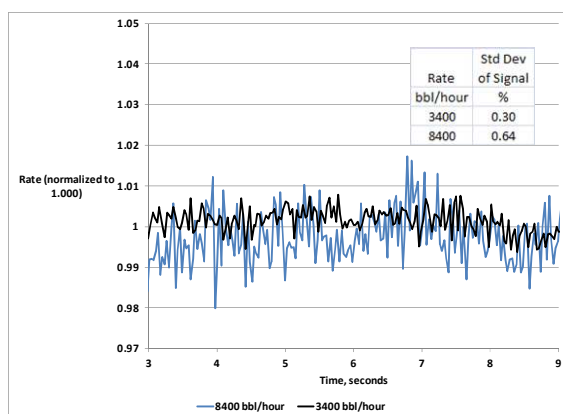


Figure 7 - Signal Noise at 3400 & 8400 bbl/hour

The signal noise at 8400 bbl/hour is approximately twice the noise at 3400 bbl/hour. The relationship between noise and rate is complex, but it is directionally correct to say that noise increases with rate. The implication is that as rate increases signal noise will impact proving repeatability. Concurrently, as rate increases the prover pass time

decreases. The two effects on repeatability are normally convolved together and it is difficult to separate them. The next section describes modifications made to the prover at Emerson to study the impacts of rate change and prover pass time separately.

# 34<sup>th</sup> International North Sea Flow Measurement Workshop 25-28 October 2016

## Technical Paper

### 6 PROVER MODIFICATIONS AT EMERSON

In all commercially available provers there is at least one set of photo detector switches (in some models there are two). Referring to Figure 6, as rate increase the pass time decreases. Since the meter signal noise changes as rate increases at the same time, we needed a way to study the effects of changing rate independently of pass time (prover size). The solution was to add adjustable detectors to the optical assembly, which made the measuring volume of the prover adjustable. The modifications allowed us to study the affect of different size provers simply by changing the location of the detectors. Specifically, the modifications were made to study the affect of different pass times on repeatability while holding flow rate constant. Conversely, we can study the affect of different rates for the same pass time. Figure 8 is a photograph of the modifications.

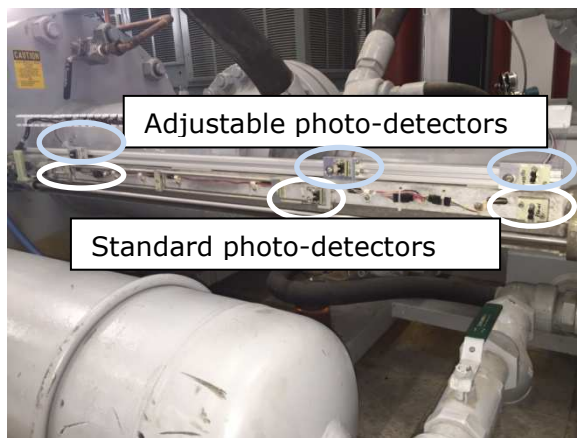


Figure 8 – 24” Prover with Adjustable Photo Detectors

A very important caveat – by using adjustable photo detectors there is no water draw calibration reference. The study using the adjustable detectors was intended to only quantify the affect of rate and pass time on repeatability.

For definition purposes, a pass is the time between detectors (sometimes referred to as flight time). A run is one or more passes averaged together.

### 7 CORIOLIS METER REPEATABILITY AND UNCERTAINTY RESULTS

The Coriolis measurement is a dynamic, time-based measurement and requires some amount of averaging to determine the correct MF. A large part of the challenge in proving is to minimize the uncertainty (API suggests less than  $\pm 0.027\%$ , which is derived from 0.05% repeatability of 5-in-a-row). The uncertainty calculation is simple:

$$MF \text{ Uncertainty} = \pm \frac{2\sigma}{\sqrt{n}} \quad (1)$$

Where  $\sigma$  is the population standard deviation of the meter signal variation and “2” is the coverage factor for 95% confidence. Normally, “n” is considered to be the number of passes (or runs); however, each pass is itself an average of a number of samples internal to the meter. If the pass time is too short there are not enough samples to drive the uncertainty to an acceptable level. The number of internal samples and the sample rate is not of much value to the user but since the sample rate is fixed, the number of samples is directly proportional to time, which is a more useful quantity. When proving, pass time (in seconds) and total run time (passes averaged together) are the relevant quantities.

# 34<sup>th</sup> International North Sea Flow Measurement Workshop 25-28 October 2016

## Technical Paper

A large test plan using a Micro Motion CMFHC4 was conducted to quantify how flow rate and pass time impact meter repeatability. The HC4 was chosen because its low pressure drop allowed testing up to the maximum rate of 8400 bbl/hour. The test plan and results are shown in Table 3.

Table 3 – Test Plan and Results of Pass Time Study

Test No.	Rate, bbl/hour	Pass Time, seconds	Pre Run Time, seconds	No. of Passes	Std Dev of MF, %
1	3000	1.43	0.50	100	0.024
2	3000	1.19	0.50	100	0.030
3	3000	0.95	0.50	100	0.032
4	3000	0.72	0.50	100	0.041
5	3000	0.48	0.50	100	0.044
6	3000	0.24	0.50	100	0.070
7	3000	0.13	0.50	100	0.102
8	5000	1.01	0.50	100	0.043
9	5000	0.85	0.50	100	0.041
10	5000	0.67	0.50	100	0.042
11	5000	0.46	0.50	100	0.062
12	5000	0.34	0.50	100	0.068
13	5000	0.17	0.50	100	0.120
14	5000	0.08	0.50	100	0.177
15	8400	0.24	0.50	50	0.211
16	8400	0.35	0.50	50	0.162
17	8400	0.59	0.50	50	0.109
18	8400	0.65	0.50	50	0.117

The number of passes was limited to 50 at 8400 bbl/hour due to temperature rise considerations. Given the large number of samples for each test, the sample standard deviation will be assumed to be the population standard deviation. For brevity, the data isn't shown but each population of data in Table 3 is normally distributed.

For a given flow rate, Equation 1 predicts that the MF repeatability ( $2 \times \text{Std Dev}$ ) is related to  $\frac{1}{\sqrt{\text{pass time}}}$ , recalling that each pass is an average and subject to the integration time. This is illustrated graphically in Figure 9 using the data collected at 3000 bbl/hour.

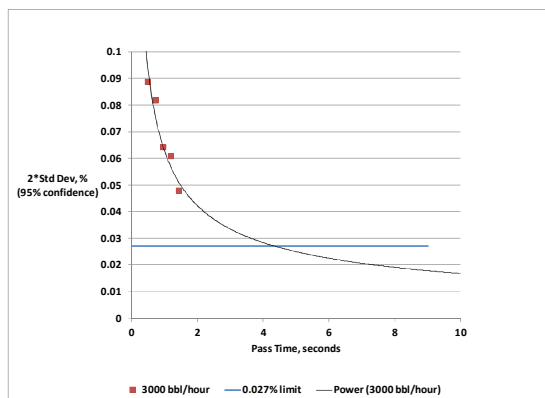


Figure 9 – Repeatability vs. Pass Time at 3000 bbl/hour (95% confidence limit)

The interpretation of Figure 9 is: a pass time of 4.5 seconds is required to make  $2 \times (\text{std dev})$  equal to  $\pm 0.027\%$ . In other words, if the pass time is 4.5 seconds, the uncertainty of the measurement will be  $\pm 0.027\%$  with a confidence limit of 95%. Equivalently, ten 0.45 seconds passes averaged together for one run will give exactly the same uncertainty. A 95% level of confidence assures that the meter will pass 5-in-a-row repeatability nearly every time it is proved. Although 95% confidence is the normal industry

# 34<sup>th</sup> International North Sea Flow Measurement Workshop 25-28 October 2016

## Technical Paper

standard, adhering strictly to a high confidence limit has the potential to result in many passes per run. For instance, if our prover was ½ the size (32 gallons instead of 65), then ten passes per run would have been required to achieve 5-in-a-row repeatability within 0.05%.

Figure 10 represents the same data as shown in Figure 9 but at a confidence limit of 68% (1\*std dev). Relaxing the confidence limit does not mean less uncertainty, rather it means that 68% (instead of 95%) of the time the expected uncertainty will be within ±0.027%. Another way to say this: if the prove requirement is 5-in-a-row at 0.05%, approximately 2/3 of the proves will pass with single pass runs (no averaging is required).

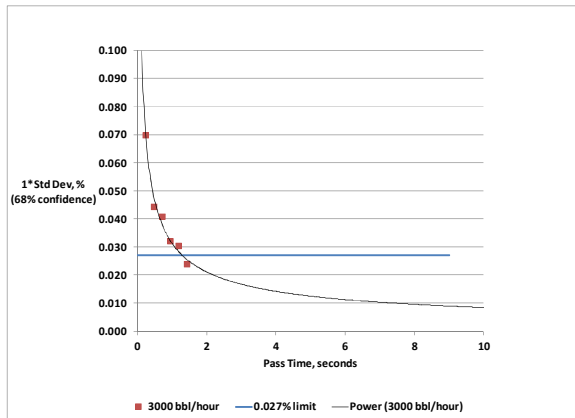


Figure 10 - Repeatability vs. Pass Time at 3000 bbl/hour (68% confidence limit)

Using the 68% confidence data of Figure 10, pass time should be at least 1.4 seconds. This says that the 24" Compact Prover is large enough to give good repeatability results at 3000 bbl/hour with no averaging.

Point no. 1 from Table 3 was analysed by grouping the 100 data points into 20 groups of five. Each group of five was evaluated for repeatability, requiring the range to be better than 0.05%. Of the 20 groups, 10 passed 0.05% repeatability, which is in-line with statistical theory. While not strictly in-line with API guidelines, analysing

to 68% confidence strikes a reasonable balance that minimizes the number of required passes while maintaining required uncertainty.

Figure 11 shows all of the data for all rates that are summarized in Table 3.

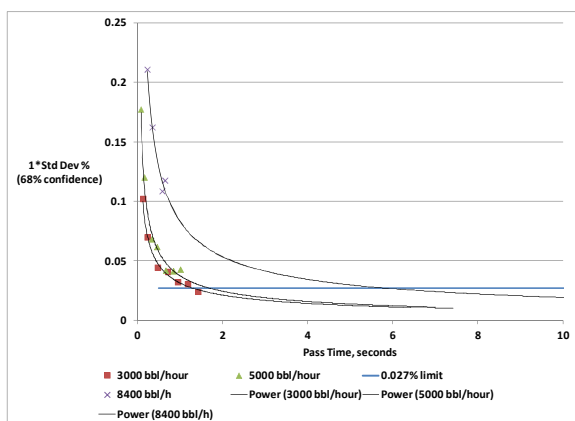


Figure 11 - Repeatability vs. Pass Time for all Rates (68% confidence limit)

At the highest rate of 8400 bbl/hour a total pass time of 6 seconds is necessary to achieve ±0.027% uncertainty. For example, a prover that has a 1 second pass time at 8400 bbl/hour will require six passes to be averaged together for a single run. Approximately 2/3 of the time the meter will prove with 5-in-a-row within 0.05%. The total number of passes required is 30 (six passes per run and five runs).

# 34<sup>th</sup> International North Sea Flow Measurement Workshop 25-28 October 2016

## Technical Paper

### 8 SUMMARY OF REPEATABILITY AND UNCERTAINTY STUDY

By evaluating the intersection point between the data in Figures 9, 10 & 11 and 0.027%, a relationship is drawn between total pass time and flow rate. Figure 12 provides a guideline for estimating the required number of passes per run and ultimately guidance for sizing small volume provers.

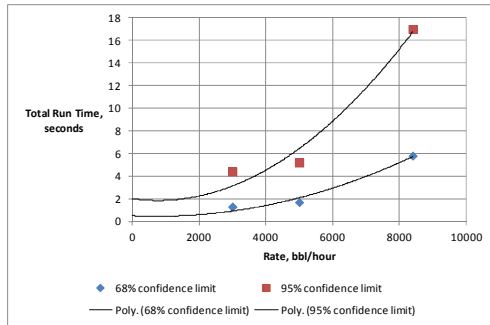


Figure 12 – Run Time Estimates for CMF HC4 vs. Flow Rate

The case for using a 68% confidence limit also is apparent. Especially at high flow rates the total run time is significantly less at 68% confidence vs. 95%.

The data presented in this paper was collected on the laboratory at Emerson in Boulder, Colorado. Although representative of CMFHC4 performance, field performance may vary.

### 9 SUMMARY AND RECOMMENDATIONS

Coriolis meters are an excellent choice for custody transfer applications that are proven in-situ. When using a small prover it is important to understand the fundamentals of Coriolis meter performance to get optimum performance:

- Minimize noise sources. This is especially important at flow rates above 10 m/s where cavitation from strainers, valves, etc. and other high velocity noise sources can influence repeatability.
- Configure the meter for its fastest response time.
- Minimize time-based damping.
- The number of passes per run will depend on the prover volume and the flow rate. Use Figure 12 to help make averaging and prover sizing decisions.
- When evaluating repeatability, use a confidence limit of 68% (1 standard deviation). This minimizes the number of passes required while maintaining required uncertainty of  $\pm 0.027\%$ .
- Data presented in this paper is specific to the Micro Motion CMFHC4. Further testing is planned for additional sizes.

## **Technical Paper**

### **In-Situ Validation of ESMER MPFMs**

**Haluk Toral, Shiqian Cai and Bahar Hosgor, Petroleum Software Ltd**

---

#### **1 INTRODUCTION**

This paper describes a project for the implementation of ESMER multiphase meters [1,2] for an entire oil field including the wellhead (one for each one of the 17 wells in the field) and the production lines (one for each one of the three production lines).

Badra oil field situated in the Wasit Province in Eastern Iraq and operated by Gazprom is estimated to hold reserves of over 3 billion barrels. Current production rate stands at 64,000 bpd from 9 wells. Gazprom aims to raise the production capacity to 170,000 bpd by the end of 2017 when all 17 wells will be producing.

Petroleum Software Ltd has designed manufactured and supplied twenty multiphase meters for the project comprising 17 off 6" well head MPFMs and 3 off 14" production line MPFMs.

The paper chronicles the highlights of the various stages of the full project cycle starting with the customer requirements and culminating with the field validation of the meters. We recount the comparison between competing technologies, an alliance with a potential competitor; recall the challenges in selection and procurement of materials and manufacturing against tight deadlines; narrate the testing, calibration, field validation of the MPFMs set against the background of customer expectations, industry guidelines and what's been found to be practical and possible.

#### **2 ESMER MPFM FIELD IMPLEMENTATION PROJECT**

##### **2.1 Technical Specification**

What was particularly noteworthy in the technical specification was the corrosive nature of the fluids (high H<sub>2</sub>S and chlorides). Strict requirements were imposed for the selection and testing of the materials for pipes, flanges and transmitters. Otherwise, there was only one restriction about the MPFM technology itself; radioactive sensors were not permitted.

Of the many issues facing multiphase metering that of validation of its field performance ("accuracy") is the most challenging. In this instance, the requirement was stated as "matching 5% of true liquid flow rate, 10% of true gas flow rate within 95% confidence level". During many years of experience in the multiphase metering industry, we've found that accuracy is intensely debated prior to selection, rigorously treated during the flow loop test, and then finally abandoned to oblivion in the field. In this instance we took a bold step and raised the issue in the early stages of the bidding process. We asked our prospective customer: "How will you know that the MPFM you've selected will meet the accuracy targets in the field"? The question of course implicitly makes the point that an MPFM that works in the flow loop may not work (as well) in the field. We made the answer to this question the lynchpin of our technical proposal.

# 34<sup>th</sup> International North Sea Flow Measurement Workshop 25-28 October 2016

## Technical Paper

Another argument which we put forward to the tender committee was that the effectiveness of each MPFM technology should be evaluated against specific fluid and process conditions and that it would be complacent to accept claims of “universally applicable plug-play devices” that would work equally well under all conditions. We’ve also pointed out that in some cases design features (such as dead T mixing) would give rise to serious side effects (large pressure loss) and/or cannot be maintained effectively (eg due to sand accumulation) even in the short term.

In the present project we were confident that esmerMPFM would satisfy the “performance requirement” because of two pre-requisites being in place; availability of PVT data (more of this later) and test separator for validation / recalibration (which was proposed as a part of our own scope of supply – more of this later also).

The corrosive nature of the fluids, maintenance and accessibility issues also favoured esmerMPFM’s robust industry standard skid.

### 2.2 ESMER Technology

**ESMER MPFM** comprises a mechanical skid (field unit) on which a set of transmitters are mounted specially selected as per process requirements. Measurements are processed in a flow computer which takes the form of a microprocessor inside an ExD enclosure or a rack mounted industrial PC for use from the safe area. Measurements can be displayed /stored on the flow computer or transmitted via serial / Ethernet ports.

Simplicity and technology leverage are the governing design principles of ESMER MPFMs. The ground rules of ESMER MPFM technology and its implementation can be expounded as follows:

- **ONE SIZE DOES NOT FIT ALL:** The solution of the multiphase metering problem requires multi-disciplinary collaboration between the instrumentation engineer, the petroleum engineer, the supplier and the end user. Present and future process conditions should be evaluated carefully together with the end users to provide the best fit solution
- **NOT A WIDGET:** An MPFM skid should comprise a selection of sensors ideally suited to given process conditions. It is not possible to develop a single device which can provide a shrink wrapped solution to all multiphase metering problems eg consider the fact that the physics of heavy oil and wet gas systems are incompatible
- **EXTRACTING MAXIMUM OUT OF INDUSTRY STANDARD SENSORS:** Sensors which respond to multiphase flow characteristics are commonly available already; they just need to be applied better to provide a multiphase metering solution eg ESMER MPMFs take advantage of high frequency components of commonly available pressure transmitters.
- **OVERCOMING THE NOT INVENTED HERE SYNDROME:** It helps to collaborate with the competitors where synergies can be identified. For example, in this instance we have included the Weatherford Red Eye sensors on the esmerMPFM skid in addition to our own impedance technology for water cut measurement.

# 34<sup>th</sup> International North Sea Flow Measurement Workshop 25-28 October 2016

## Technical Paper

- NEURAL NETS CAN WORK UNDER THE RIGHT CONDITIONS: Digital signal processing techniques / algorithms will enhance the performance of MPFMs eg ESMER MPFMs' conventional fluid models are enhanced by neural net algorithms
- CLASSICAL FLUID / THERMO DYNAMIC MODELS CAN WORK UNDER THE RIGHT CONDITIONS- Thermodynamic (EOS) models will enhance the performance of MPFMs. ESMER MPFMs implement EOS models which take real time P,T inputs in order to predict GVF at actual pipeline conditions.
- NOT FIT AND FORGET. NOT OUT OF THE BOX: It is not possible to design / supply an out-of-the-box-fit-forget MPFM. An in-line MPFM has to be recalibrated/validated in the field against physical separation systems as per API recommendations. Petroleum Software Ltd will provide in-field calibration / validation services as an integral part of every project.

For the current project we considered that the following compliment of transmitters were the best match to customer / process / fluid requirements:

- Cone with AP, DP, Recovery DP and RTD transmitters
- Capacitance transmitter (embedded in the cone)
- Weatherford Red Eye

The above set of transmitters provided the required inputs into the hydrodynamic model described in Appendix A. In addition, pressure and temperature measurements were input into a thermodynamic model (founded on an EOS software package provided by Calsep of Denmark) for prediction of phase densities and gas volume fraction in real time. The TD model was fine tuned against PVT data provided by the customer in accordance with the procedure described in Appendix A. The output from the thermodynamic model was input directly into the hydrodynamic model. The data acquisition system, the flow models and the output (comprising a database on the local disk and MODBUS output to SCADA)

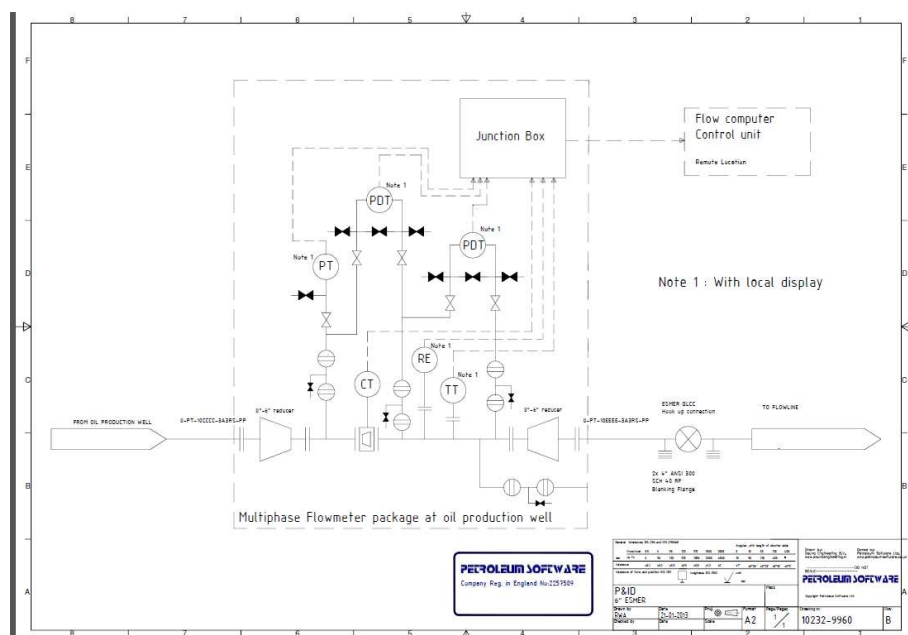


Fig.1 - ESMER C6+ PID

34<sup>th</sup> International North Sea Flow Measurement Workshop  
25-28 October 2016

Technical Paper

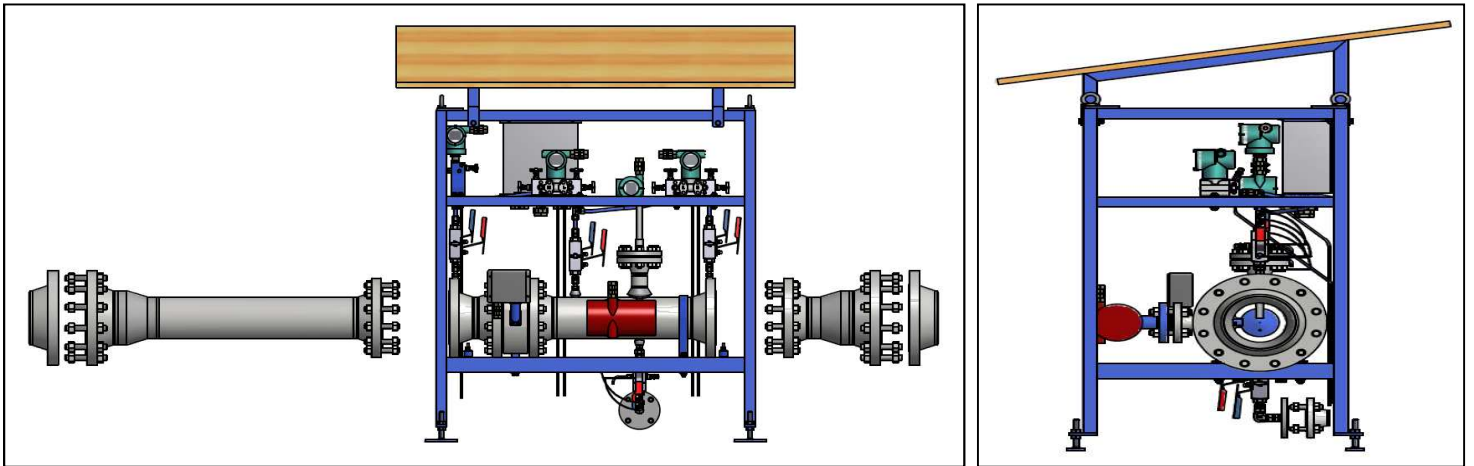


Fig.2 - ESMER C6+ General Arrangement Drawing



esmerMPFM C6+ at the Wellhead Badra Gazprom



esmerMPFM C14+ Installed at the Production Line Badra Gazprom

Fig.3 - ESMER C6+ at the Well Head and ESMER C14+ at the Production Line

# 34<sup>th</sup> International North Sea Flow Measurement Workshop 25-28 October 2016

## Technical Paper

### 2.3 Project Chronicle

#### Competing Technologies

Several technical presentations were made to the tender technical committee during which we had a chance to express our opinion on competing technologies. For example, we expressed the opinion that it would be prudent to avoid:

- "Plug-and-play systems" based on mechanistic flow modelling and those based on empirical models calibrated in the flow loop
- Systems based on vertical flow, because they would
  - o Choke due to elbows
  - o Result in extra pressure drop of about 2 bar due to 4 elbows
  - o Be prone to strong flow induced vibrations, which would be especially risky for the larger production line MPFM
- Complex field electronics, because they are sensitive to harsh environmental conditions such as those which exist in hot/cold desert climate.

#### Some of the Issues Encountered

In the early days of our interaction with the customer, we spent a good deal of time on issues which turned out to be trivialities later on (such as the material for the sun shade, the drains and height of unit from the base).

Serious discussion started upon realisation that the length of upstream and downstream adaptors required (8 D and 3 D respectively) were not taken into account by the pipeline engineers and the fact that the diameter of the by-pass for the test separator could have been a bit larger than proposed.

Things got worse with the realisation that it was going to take much longer than initially anticipated to procure the pipes and flanges of special composition required for the highly corrosive process conditions. Materials tests required (HIC, SSC) would also add further two months before machining and assembly can start. This was a long time in view of the stringent delivery date of six months (first batch of six units) and nine months for another batch of fourteen units.

At the same time, the customer brought up another issue for discussion. How would we calibrate / flow loop test the production MPFMs (14")? Problem was a difficult one as no such flow loop exist to create the flow conditions mildly approaching those in the pipeline.

#### Flow Loop Selection

The prerequisites of the flow loop test, expected benefits and fine tuning of the "factory" calibration in the field were discussed within the framework of API 2566 State of the Art Multiphase Metering as per tender requirement [4]. API 2566 highlights regarding flow loop testing are quoted in Appendix B.

A multiphase flow loop which could simulate the process conditions for the 14" production line MPFMS could not be found. A decision was then made to test the 14" MPFMs in the single phase oil flow loop at NEL. This was not a wholly satisfactory match with the requirements of API 2566 but at least the exercise provided an opportunity to verify that the transmitters were in good working order prior to delivery to the field and

# 34<sup>th</sup> International North Sea Flow Measurement Workshop 25-28 October 2016

## Technical Paper

allowed full characterisation of the coefficient of discharge of the cone under single phase conditions.

NEL multiphase loop also fell short of the required flow rates for testing 6" wellhead MPFMs (Fig. 4) but the wet gas loop offered a reasonable match for both the flow rates and pressure (but not temperature) Fig.5. However, the flow loop fluids were of course different to field and besides, no water/oil mixture can be employed in the wet gas loop. It was finally agreed to test the 6" wellhead MPFMs at the NEL Wet Gas Loop which showed reasonable overlap with the present flow conditions as shown in the operating envelope diagram below (Fig.5).

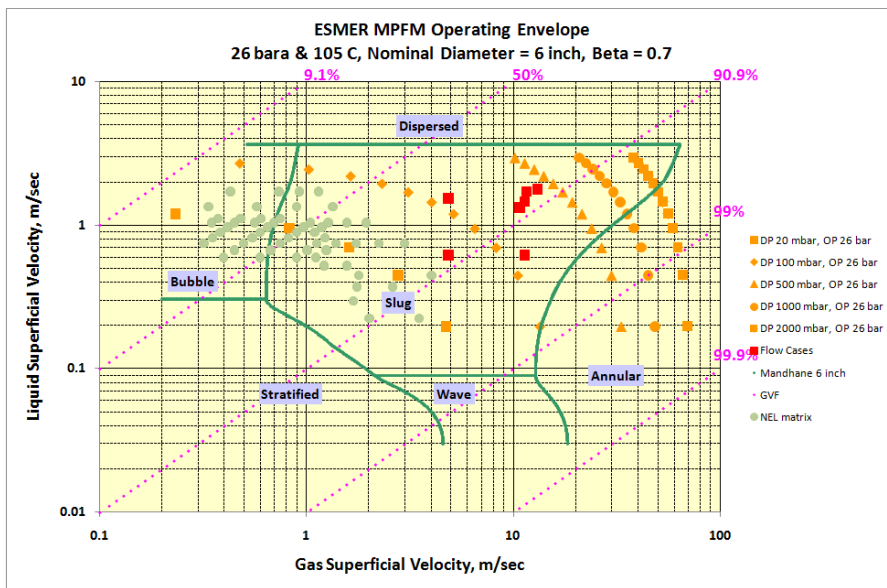


Fig.4 - NEL Multiphase Loop vs 6" Well Head MPFM

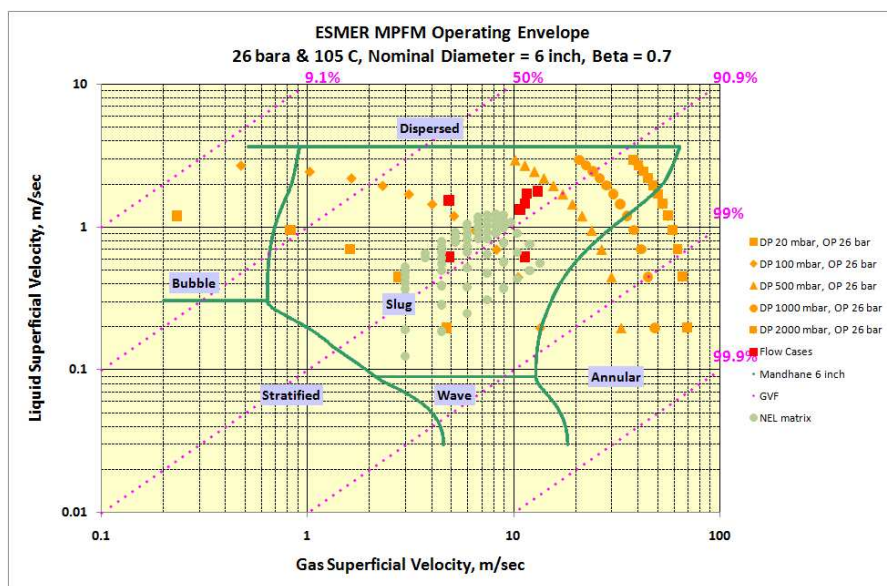


Fig.5 - NEL Wet Gas Loop vs 6" Well Head MPFM

# 34<sup>th</sup> International North Sea Flow Measurement Workshop 25-28 October 2016

## Technical Paper

### Flow Loop Test Results

Results of the NEL flow loop test are shown in the figures below giving a comparison of MPFM measurements against reference flow rates. The accuracy of the MPFM was demonstrated to be within the customer requirements of  $\pm 10\%$  at 95% confidence level.

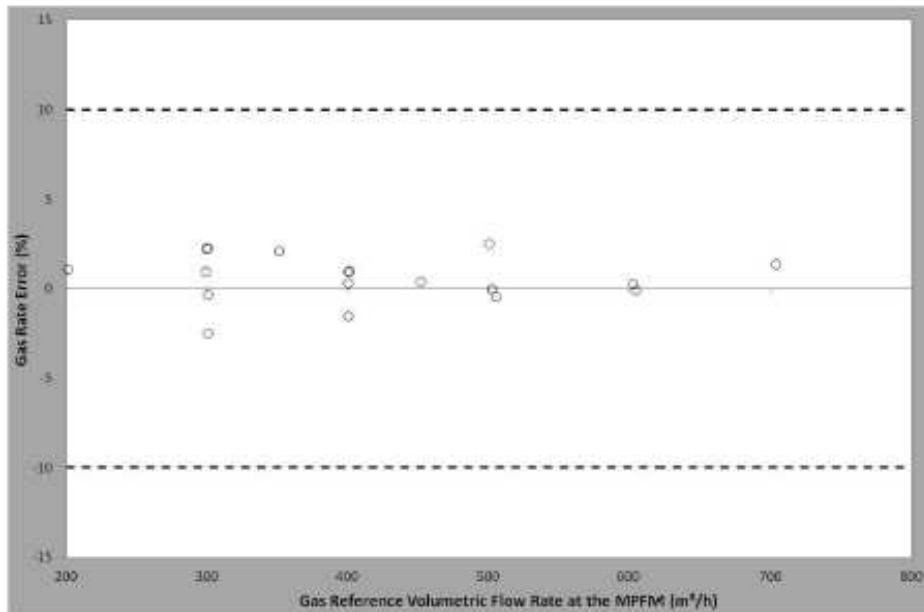


Figure A1.1 Gas Volumetric Flow Rate Error vs the Reference Gas Volumetric Flow Rate at the MPFM

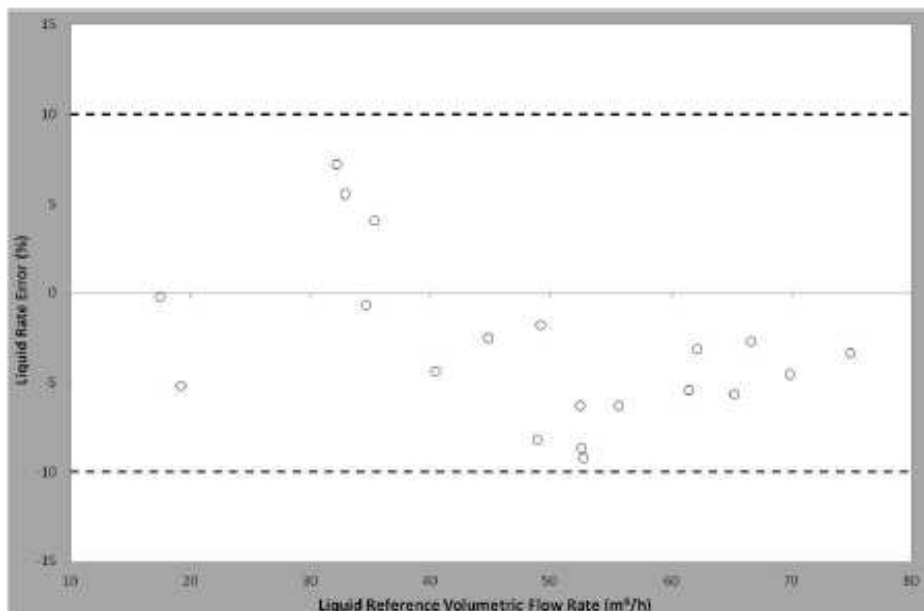


Figure A1.2 Liquid Volumetric Flow Rate Error vs the Reference Liquid Volumetric Flow Rate

Fig.6 - Flow loop test Results

**Technical Paper**

**2.4 Field Implementation / Validation / Calibration**

Installation and commissioning of first five units (3 off wellhead and 2 off production line MPFMs) took place in August 2014. Since then we have installed seven more systems as drilling progressed and more wells were brought online. Five further MPFMs are due to be installed by the end this year to complete the project.

**Vertical Cyclonic Test Separator**

As part of the project scope we had offered the customer a mobile test separator for validation and field calibration of the wellhead MPFMs. Initially seen as an optional tool, the importance of the test separator grew in time and became an indispensable tool.

We started by investigating the suitability of the GLCC technology (gas-liquid-compact-cyclone) as a test separator, an area subject to much research in recent years, considered by some to be an alternative to in-line multiphase metering. We had a choice of active and passive controlled systems. The latter sounded promising due to its simplicity. The passive controlled GLCC which we commissioned turned out to be 5 m tall column supported on a base of 4mx2m weighing and comprises a toroidal chamber of 40 cm diameter, as compact as it got.



We could have lived with the size but unfortunately the GLCC did not work as well as hoped! Experiments at the well head demonstrated that the separation efficiency was poor; too much liquid carried over with the gas and too much gas carried under with the liquid. Basically, the GLCC did not like the prevailing high GVF conditions and with hindsight its operating envelope turned out to favour a GVF range from 20% to 70% below.

Is it possible to extend the operating envelope to higher GVF by means of active controls? Worth an experiment another time, but on this occasion we thought it would be more prudent to go for a conventional horizontal separator described next.

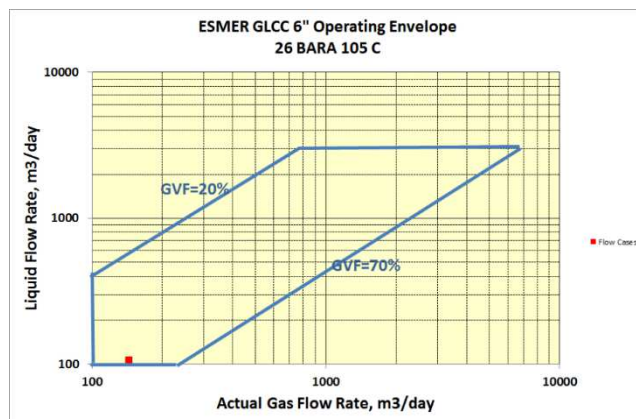
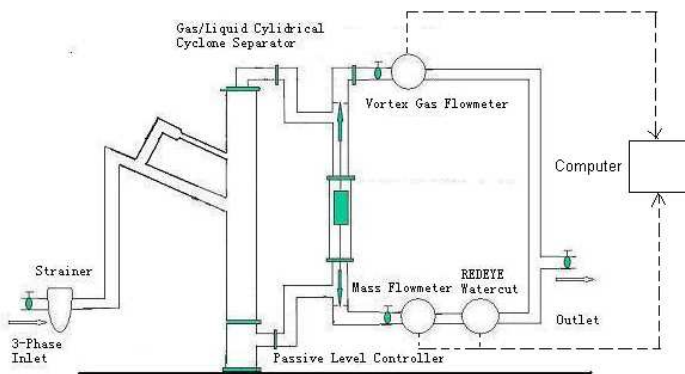


Fig 7. - Photo, Block Diagram and Operating Envelope of ESMER Passive GLCC

# 34<sup>th</sup> International North Sea Flow Measurement Workshop 25-28 October 2016

## Technical Paper

### Horizontal Conventional Separator

The horizontal separator turned out to be not as large as feared and could be transported “easily” between wells on the back of a trailer as shown on the photo below.



Fig.8 - MPFM and Test Separator Side by Side

	MPFM	GLCC	Horizontal Separator
Footprint LxWxH (m)	1.3 x 0.8 x 1.3	4.0 x 2.0 x 5.3	12.5 x 3.6 x 6
Empty Weight (kg)	273	7,500	38085
Full Weight (kg)	291	10,000	57419

**Table 1 Dimensions and Weight of MPFM vs GLCC vs Horizontal Separator (For Same Duty of handling flow through a 6” pipeline – Appendix C)**

### Separator Operation

#### Installation Effects

The test separator was connected in series and downstream of the MPFM. We had two concerns about the expected performance of the separator. Naturally the separation efficiency was foremost in our minds but we also worried about its back effect on the MPFM, ie whether the separator would contaminate the “normal” conditions in the MPFM.

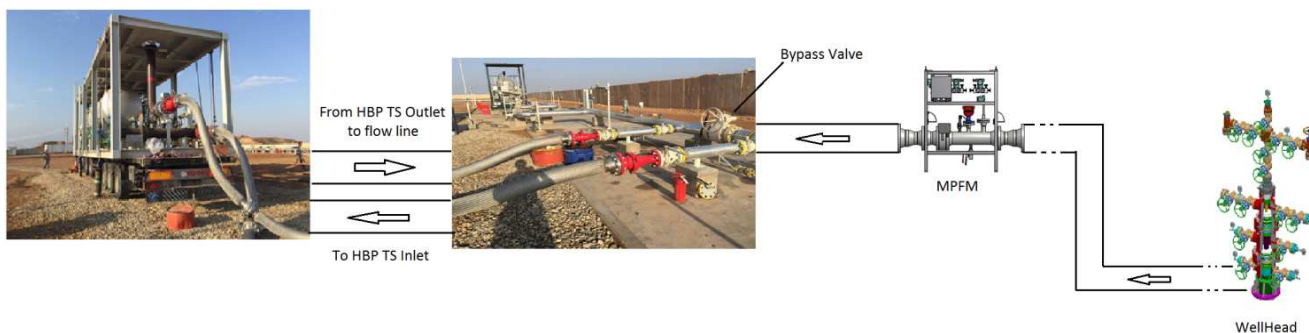


Fig.9 - Test Separator and MPFM in Series

**Technical Paper**

The pressure loss (ie increase in back pressure at the MPFM) was 5 bar at maximum flow rate. It was estimated that more than half this loss was caused by the reduction in the bypass pipe line diameter from 8" to 4". The effect of the pressure change on fluid properties and gas volume fraction was taken into account automatically by the MPFM via the thermodynamic model. The back effect of the separator on the MPFM is shown below. The back effect of the separator on pressure, temperature, DP and GVF change was in line with expectations.

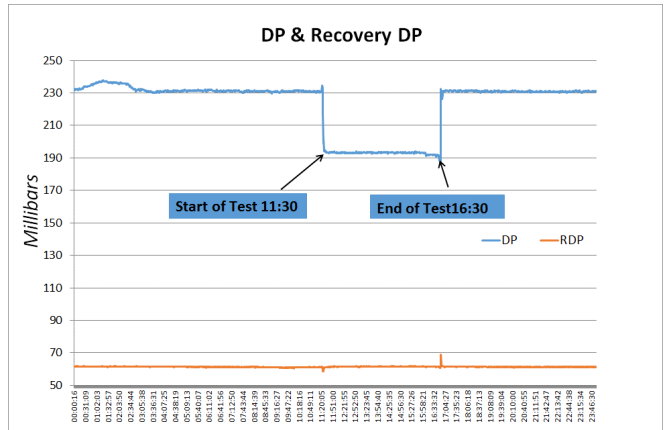
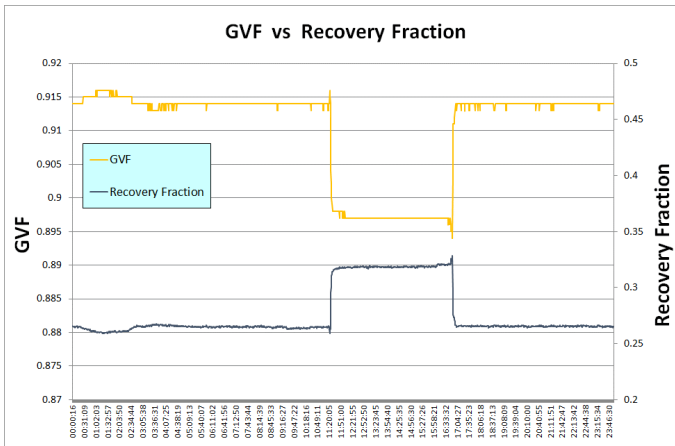
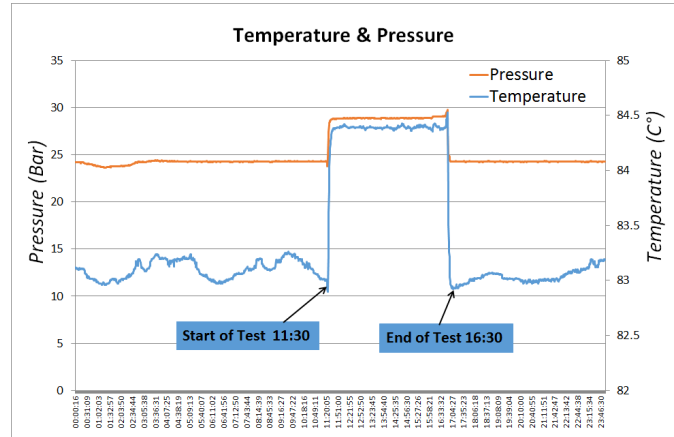


Fig.10 - Effect of the Test Separator on the MPFM

**Separation Efficiency**

Stable operation conditions could be reached within half an hour. It was not possible to quantify the separation efficiency but the stable operation of the system was encouraging and we believe that the design target efficiency (1% by mass liquid carry over in the gas leg and 1% gas carry under by volume in the liquid leg ) was met. The trend of the influences can be reviewed as:

1. Gas carry under → underestimation of true gas
2. Gas carry under → turbine meter instrument error resulting in overestimation of oil
3. Liquid carry over → underestimation of true oil
4. Liquid carry over → orifice instrument error resulting in overestimation of gas

It appears that separation inefficiency results in two overestimations and two underestimations per phase. Hence, at least, the effects were counterbalancing.

# 34<sup>th</sup> International North Sea Flow Measurement Workshop 25-28 October 2016

## Technical Paper

### Validation & Calibration Results

Well Id	Start Time	Test Duration (hour)	Well Head			MPFM								HBP				Performance		
			WHP (Well head Pressure)	Well Head Temperature C	Choke Valve position (%)	Pressure At Flowline	Temperature at Flowline	Oil m3/h	Gas m3/h	GVF %	GOR Sm3/Sm3	Oil at Standard Sm3/h	Gas at Standard Sm3/h	Oil at Actual (m3/h)	Oil at Standard Condition	Total Gas at Standard Condition	GOR (Sm3/Sm3)	Oil (%)	Gas (%)	GOR (%)
P13	08/02/2016 12:00	4:00	50.0	84.4	53.7	28.9	84.4	79.1	693.9	89.7	223.9	70.4	15758.5	78.1	71.2	16065.3	225.6	-1.2	-1.9	-0.8
BD5	12/02/2016 10:30	4:30	52.0	81.9	52.2	26.6	82.3	74.2	703.5	90.5	221.8	66.5	14742.3	69.6	64.2	15203.5	236.8	3.5	-3.0	-6.3
P05	16/02/2016 11:30	4:00	54.6	85.4	51.2	30.2	86.0	81.3	679.9	89.3	224.2	72.1	16154.5	82.2	72.8	14872.3	204.2	-1.1	8.6	9.8
P04	18/02/2016 12:00	4:30	57.6	83.0	35.5	29.5	82.9	47.7	402.8	89.4	221.1	42.4	9369.1	56.7	50.4	10021.6	198.8	-16.0	-6.5	11.2

Table 2 Well Test Result with Test Separator (HBP) and MPFM Connected Inline

Table above summarises typical in-line test results comparing cumulative MPFM measurements versus the test separator over a four hour well test. Charts below show typical measurements on a minute by minute basis. The large fluctuation in the separator is due to the effect of the level controller.

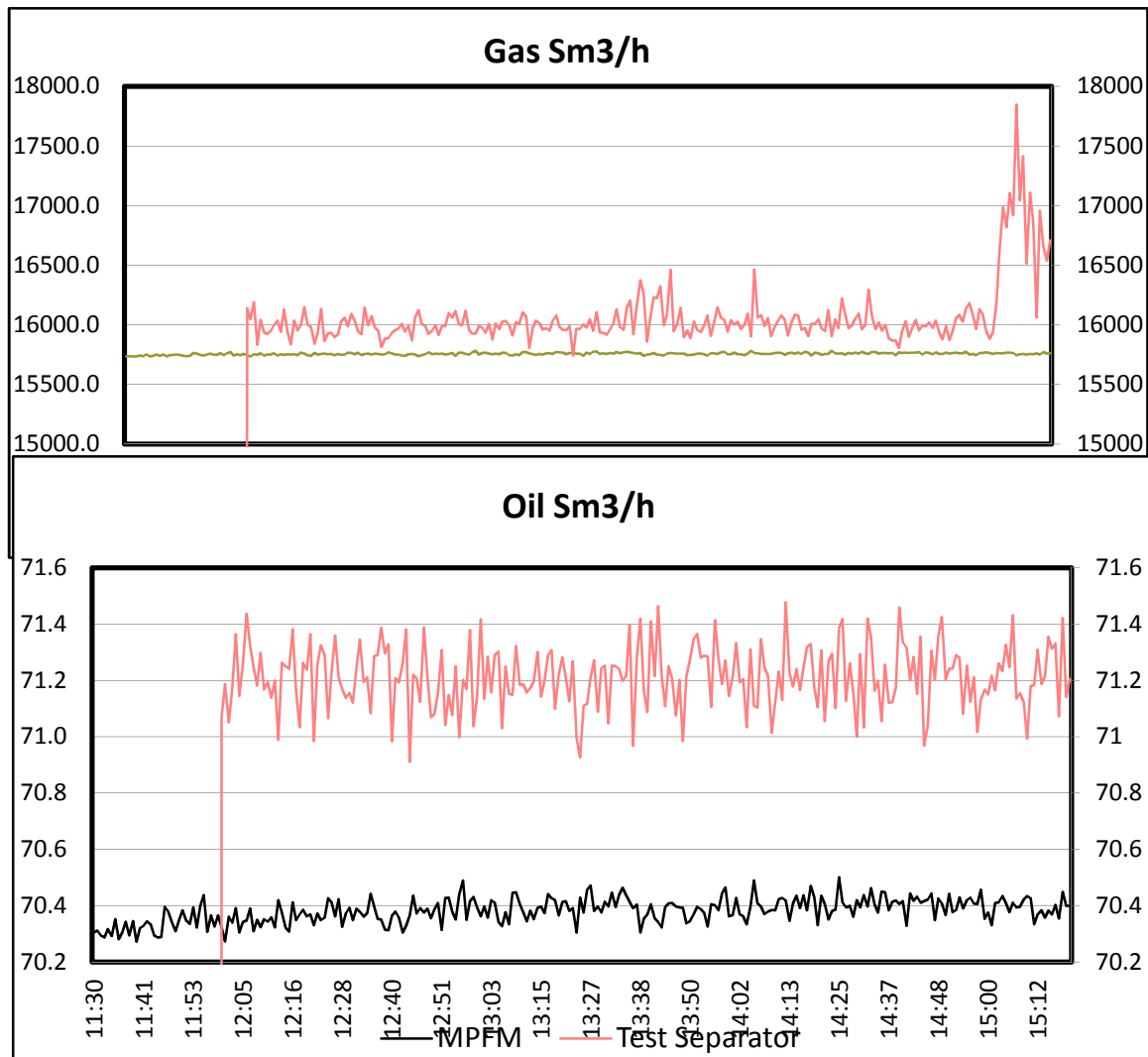


Fig.11 Typical Calibration Test Run – MPFM and Test Separator are Inline. Measurements are made on a minute-by-minute basis.

# 34<sup>th</sup> International North Sea Flow Measurement Workshop 25-28 October 2016

## Technical Paper

### Repeatability & Uncertainty

In order to qualify the uncertainty of the measurements, we've calculated the standard deviation of oil and gas flow rates at the test separator and the MPFM based on measurements averaged over a minute. The results are shown in the table below.

Well Test Information			MPFM						Test Separator					
Well_ID	Date	Test Time	Oil			Gas			Oil			Gas		
			Sd	avg	sd/avg(%)	Sd	avg	sd/avg(%)	Sd	avg	sd/avg(%)	Sd	avg	sd/avg(%)
P13	08.02.2016	12:00-16:30	0.04	70.39	0.06	8.93	15758.51	0.06	0.11	71.21	0.16	261.54	16065.32	1.63
BD4_1st	10.02.2016	10:00-14:30	0.18	14.90	1.24	37.56	3083.35	1.22	1.55	17.02	9.12	108.60	2674.75	4.06
BD5	12.02.2016	10:30-15:00	0.06	66.46	0.09	13.29	14742.34	0.09	0.66	64.22	1.03	24.21	15203.54	0.16
P08	14.02.2016	11:00-15:30	0.16	10.06	1.56	30.65	1996.20	1.54	0.65	11.62	5.64	6.67	2390.05	0.28
P05	16.02.2016	11:30-15:30	0.03	72.05	0.04	5.69	16154.51	0.04	0.16	72.85	0.22	16.29	14872.28	0.11
P04_1st	18.02.2016	12:00-16:30	0.09	42.37	0.21	19.84	9369.15	0.21	0.88	50.43	1.74	27.98	10021.64	0.28
P04_2nd	19.02.2016	09:00-13:00	0.07	45.81	0.16	18.50	10125.40	0.18	0.87	50.29	1.73	24.75	10040.67	0.25
BD4_2nd	20.02.2016	10:30-15:00	0.19	17.25	1.10	44.16	3564.66	1.24	2.03	16.99	11.92	75.25	3557.77	2.12
<b>Average</b>					<b>0.56</b>			<b>0.57</b>			<b>3.94</b>			<b>1.11</b>

**Table 3. Typical Calibration Test Run – Standard Deviation of MPFM vs Separator Measurements Averaged over Each Minute**

It is seen that the **experimental standard deviation** of the minute by minute measurements made by the test separator range from 11.9% (BD4) for the oil flow rate at low producing wells to 0.16% (P13) at high producing wells. The high value of the fluctuation is attributed to the activation of the level control mechanism of the separator. Repeatability of the measurements for the MPFM is better, ranging from 0.06% to 1.1%.

Experimental standard deviation was also repeated based on hourly averages. The results shown below are more representative of the "true" repeatability of the measurements (ie removal of the minute by minute influence of the level controller action). Maximum standard deviation encountered on an hourly basis was reduced to 2.73% (Well BD4).

Well Test Information			MPFM						Test Separator					
Well_ID	Date	Test Time	Oil			Gas			Oil			Gas		
			Sd	avg	sd/avg(%)	Sd	avg	sd/avg(%)	Sd	avg	sd/avg(%)	Sd	avg	sd/avg(%)
P13	08.02.2016	12:00-16:30	0.02	70.39	0.02	3.25	15758.51	0.02	0.02	71.21	0.03	109.74	16065.32	0.68
BD4_1st	10.02.2016	10:00-14:30	0.12	14.90	0.81	23.69	3083.35	0.77	0.46	17.02	2.73	119.30	2674.75	4.46
BD5	12.02.2016	10:30-15:00	0.05	66.46	0.07	11.52	14742.34	0.08	0.07	64.22	0.11	4.98	15203.54	0.03
P08	14.02.2016	11:00-15:30	0.16	10.06	1.60	31.13	1996.20	1.56	0.02	11.62	0.20	1.97	2390.05	0.08
P05	16.02.2016	11:30-15:30	0.01	72.05	0.01	2.58	16154.51	0.02	0.02	72.85	0.03	0.55	14872.28	0.00
P04_1st	18.02.2016	12:00-16:30	0.04	42.37	0.10	8.69	9369.15	0.09	0.14	50.43	0.29	17.36	10021.64	0.17
P04_2nd	19.02.2016	09:00-13:00	0.02	45.81	0.04	7.52	10125.40	0.07	0.07	50.29	0.13	3.92	10040.67	0.04
BD4_2nd	20.02.2016	10:30-15:00	0.15	17.25	0.88	37.80	3564.66	1.06	0.19	16.99	1.12	69.11	3557.77	1.94
<b>Average</b>					<b>0.44</b>			<b>0.46</b>			<b>0.58</b>			<b>0.93</b>

**Table 3. Typical Calibration Test Run – Standard Deviation of MPFM vs Separator Measurements Averaged Hourly.**

### 2.5 Routine Use

Measurements are transmitted directly to the SCADA at the central processing facility by MODBUS (averaged over a minute). The operators only need to visit the wellhead for special verification and maintenance actions. Downtime has been negligible (only one

# 34<sup>th</sup> International North Sea Flow Measurement Workshop 25-28 October 2016

## Technical Paper

incident of shut down due to debris washed into the production line MPFM after pigging during two years of operation)

A number of checks (comparisons) are carried out daily for validating the measurements:

- Cumulative daily average of wellhead MPFMs (of which there are 17) vs Production Separator at the Central Processing Facility (CPF)
- Production line daily average MPFM measurement (for each one of the three production trains) vs CPF
- Cumulative of wellhead MPFMs vs production line MPFMs

Typically oil and gas rates agree to within 5% as shown in the sample charts from 20<sup>th</sup> March to 20<sup>th</sup> April 2016. We see that the daily average cumulative MPFM measurements over-state the production separator oil and gas flow rates (Fig 12) whereas production line MPFM under-state the production separator (Fig 13).

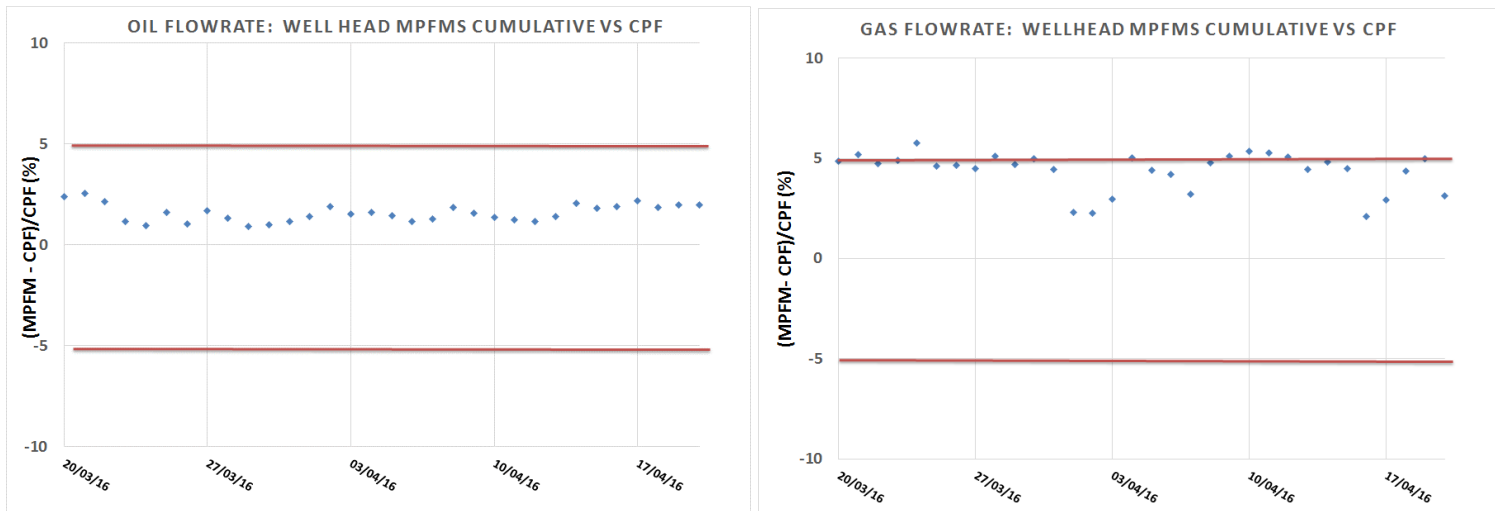


Fig.12 - Daily average cumulative measurement by Well Head MPFMs (6" MPFMs) compared against Central Processing Facility Separator Measurement 20.3.16 – 20.4.16

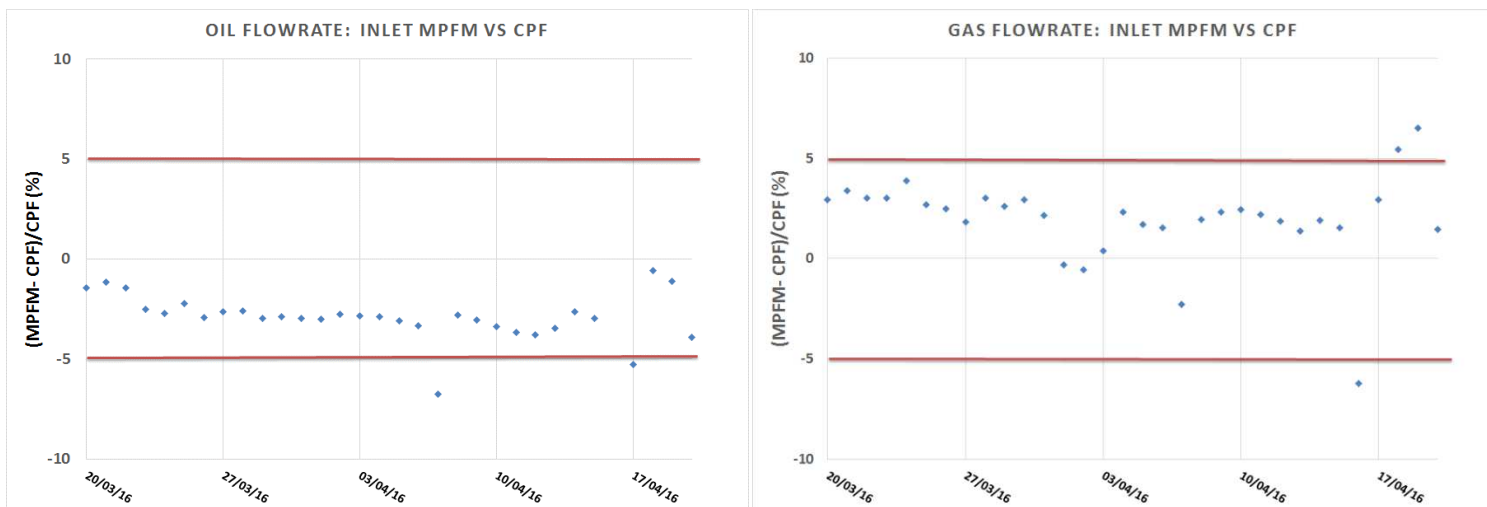


Fig.13 - Daily average Production Line MPFM (14" MPFM) compared against Central Processing Facility Separator Measurement 20.3.16 – 20.4.16

# 34<sup>th</sup> International North Sea Flow Measurement Workshop 25-28 October 2016

## Technical Paper

### 3 CONCLUSIONS

- Project experience shows that fit-for-purpose multiphase meters deploying conventional transmitters and flow models can deliver a robust performance and a satisfactory level of accuracy /repeatability for wellhead and production line metering.
- Thermodynamic (phase equilibrium) model can provide an effective means of predicting / validating the gas volume fraction and physical properties of the phases in line.
- MPFMs can be effectively validated in-field and their calibration tuned up by means of a test separator
- A conventional horizontal separator is recommended in place of "compact cyclonic separators" under high GVF / high flow rate conditions.

### 4 REFERENCES

- [1] T. Darwich, H. Toral and J. Archer, A stochastic study of horizontal two-phase flow, SPE paper 19511, 1989.
- [2] H. Toral, S. Cai, E. Akartuna, K. Stothard and A. Jamieson, Field tests of the Esmer multiphase flowmeter, The North Sea Flow Measurement Workshop, 26-29 October 1998, Perthshire, Scotland.
- [3] RICHARD HONE Evaluation of an ESMER C6+ MPFM in Wet Gas NEL Report No 2013/432 August 2013
- [4] Standard: API PUBL 2566 STATE OF THE ART MULTIPHASE FLOW METERING American Petroleum Institute 2004-05-01

# 34<sup>th</sup> International North Sea Flow Measurement Workshop 25-28 October 2016

## Technical Paper

### Appendix A ESMER MPFM Theoretical Model

Like all flow meters, whether designed for single or multiphase measurement applications, ESMER MPM requires three stages of calibration:

1. Theoretical calibration
2. Flow loop calibration
3. Field adjustment

To understand the methodology of flow loop calibration and field adjustments we first need to understand the theoretical model underlying the ESMER MPM. The main parameters measured by ESMER MPM are the total flow rate and phase fractions (gas / liquid and water/liquid). The measurement is founded on **hydrodynamic\_and thermodynamic models** as described below.

#### Overview

Thermodynamic Model is used to predict the GVF ( a key parameter for the MPFM), density of phases at actual and standard conditions and shrinkage. The model is created by means of an EOS package provided by Calsep of Denmark named PVTsim.

The package takes the usual inputs such as feed composition (PVT lab), binary interaction coefficients (library), critical temperatures and pressure of components (library). Heavy end is characterised by means of proprietary models of Calsep. We use PVT data from the field (eg reservoir saturation pressure, multistage flash PVT) to tune up multi-stage flash model by iterative or regression methods for matching targets. The end result is a synthetic fluid composition. Using the synthetic fluid composition we perform multi-stage flash across a range of P,T and save the output (P,T,GVF, density of phases). We then train a neural net to create an algorithm which can be executed locally on-line on the MPFM flow computers.

What's described up to this point is the initial tune up of the Thermodynamic Model which takes place before installation. For field tune up the procedure is to be repeated against measurements obtained from the test separator after installation of the MPFMs. It should be noted that liquid / gas phase compositions, not measured at present, would be of additional value for field tune up.

The construction of the Hydrodynamic Model starts at the flow loop. This is an empirical exercise and involves essentially the characterisation of the *Discharge Coefficient* (Cd) which depends on flow regime, GVF, superficial velocities and densities of the phases (all inputs into the model are measured at the flow loop). The relationship between Cd and the parameters are non-linear and a neural network is used for implementation of the Hydrodynamic Model (as per Thermodynamic Model). The flow loop test was carried out at NEL for a range of flow rates and a test report was provided. The discharge coefficient model obtained from NEL measurements ("factory setting") will be tuned up empirically by comparing MPFM measurements against separator measurements. However, it is important to stress that the Hydrodynamic Model cannot be tuned up in isolation and must be tuned up in tandem with the Thermodynamic Model (eg Cd depends strongly on GVF which in turn depends on the Thermodynamic Model)

# 34<sup>th</sup> International North Sea Flow Measurement Workshop 25-28 October 2016

## Technical Paper

### ESMER HYDRODYNAMIC MODEL

The calculation starts with the conventional differential pressure equation (Bernoulli equation)

$$m_f = \frac{C_d \varepsilon_1 \beta^2 \sqrt{2}}{\sqrt{1 - \beta^4}} * A * \sqrt{\Delta p * \rho_m} \quad (1a)$$

Or

$$Q_f = \frac{C_d \varepsilon_1 \beta^2 \sqrt{2}}{\sqrt{1 - \beta^4}} * A * \sqrt{\Delta p / \rho_m} \quad (1b)$$

where:

$m_f$  mass flow rate kg/sec

$Q_f$  volume flow rate m<sup>3</sup>/sec

$\Delta p$  DP across cone N/m<sup>2</sup> (Pa)

$\rho_m$  fluid density (Kg/m<sup>3</sup>)

$C_d$  discharge coefficient (including multiphase effect; ie function of gvf

$\varepsilon_1$  expansion factor

$A$  flow area through full bore (m<sup>2</sup>)

$\beta$  beta ratio where for a cone  $\beta = \frac{\sqrt{(D^2 - d^2)}}{D}$

The Bernoulli equation presents a number of challenges in multiphase flow.

$$C_d = \text{fn}(\text{“Effective” Reynolds Number}). \quad (2)$$

Note: We propose the term “Effective Reynolds Number” in recognition of conventional fluid mechanics (the ratio of inertia and viscous forces). We do not profess to know / propose a deterministic equation here. The term can only be quantified empirically. For the sake of recognition of the influence parameters, we can propose the following “pseudo equation”:

$$\text{EffectiveReynoldsNo} = \text{fn}(m_f, \text{GVF}, \text{WaterCut}, \text{flow regime}, \text{physical properties}) \quad (3)$$

Note: physical properties include density, viscosity, salinity under actual conditions. Hence P,T effects are implicitly taken into account in this term

Next, we look at the water composition model. The principal input into the water composition model comes from one of the following sensors (signals):

- Capacitance
- Conductance
- Infra-red absorption spectroscopy
- Gamma ray absorption spectroscopy

The following general equation applies to any of the foregoing sensors.

$$\text{Output Signal (of Sensor)} = \Phi (\text{flow regime}, \text{GVF}, \text{Watercut}, \text{physical properties})$$

Hence inverting this equation, GVF and watercut can be (theoretically) obtained from:

# 34<sup>th</sup> International North Sea Flow Measurement Workshop 25-28 October 2016

## Technical Paper

$$\text{GVF, WaterCut} = \Phi (\text{Signals, flow regime, physical properties}) \quad (4)$$

Where "Signals" stand for outputs of various transmitters on the MPFM skid; in this instance: impedance, DP, RecoveryDP, P, T

We now have four equations and four unknowns, mf, GVF, water composition, flow regime. A theoretical solution is possible but not probable !

Furthemore;

$$\text{Flow regime} = \Phi (\text{DP, RecoveryDP}) \quad (5)$$

Substituting 5 into 4 we get:

$$\{\text{GVF, WaterCut}\} = \Phi (\text{impedance, DP, RecoveryDP, P, T, salinity}) \quad (6)$$

The last relationship means that it is the combination of GVF and water cut that is correlated with the parameters on the right hand side. This relation cannot be expressed in the form of a linear mathematical correlation and an analytical solution is not possible.

**However, neural nets can establish this relationship with relative ease given sufficient data.** In neural networking terminology, the terms on the left hand side of relationship 6 represent the *joint targets* of a supervised network and those on the right hand side represent *the training inputs*.

Similarly, a separate neural net is trained with same inputs to predict the coefficient of discharge.

Substituting 5 into 3 and then into 2 we get:

$$\text{Cd} = \Phi (\text{impedance, DP, RecoveryDP, P, T, salinity}) \quad (7)$$

Once the mass flow rate is determined from equation 1 & 7 (Cd neural net); oil, water and gas flow rates can then be derived from GVF and Water cut given by 6 (GVF-Wcut neural net)

### ESMER THERMODYNAMIC MODEL

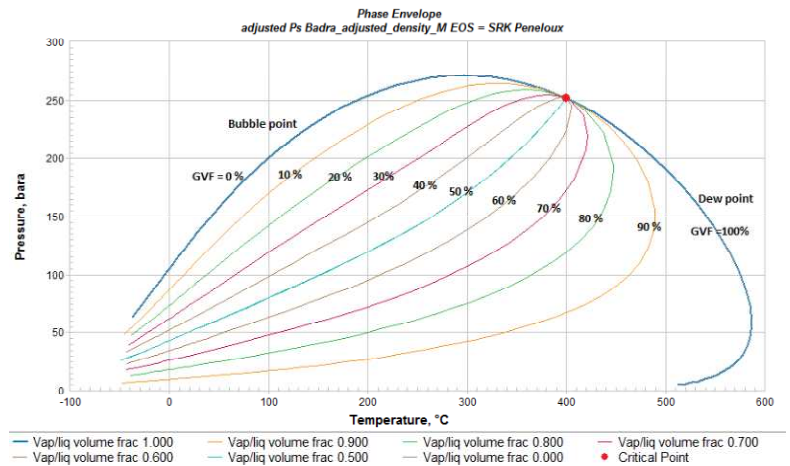
ESMER theoretical model also comprises a thermodynamic (PVT) mathematical model which supplements the hydrodynamic core system described above. The PVT model, which runs on the flow computer in real time, permits the calculation of GOR from fluid composition and in-situ P,T measurement by flash calculation assuming equilibrium conditions. ESMER PVT model is based on the Soave Redlich Kwong Equation with Peneloux Correction. The EOS model is represented in the equations below. The model is tuned to field-fluid conditions by regression against GOR measurements made in the production separator train (multistage separation)

An example application of the thermodynamic model will be illustrated next. The phase envelope predicted by the thermodynamic model (based on fluid composition provided by the customer shown in table below) is shown below.

# 34<sup>th</sup> International North Sea Flow Measurement Workshop 25-28 October 2016

## Technical Paper

Gazprom		Doc. No. GB164-BD01-100-PR-DS-002 PROCESS DATA SHEET FOR MPFM (OIL PRODUCTION WELLS AND CPF INLET MANIFOLD)	Rev.: 0 Date: 19.12.12 Page: 8 / 10	CPP
Annex-3: Fluid Composition and Properties				
Component	% mole			
N <sub>2</sub>	0.28			
CO <sub>2</sub>	3.5			
H <sub>2</sub> S	3.07			
C <sub>1</sub>	35.17			
C <sub>2</sub>	9.36			
C <sub>3</sub>	6.11			
iC <sub>4</sub>	1.06			
nC <sub>4</sub>	3.32			
iC <sub>5</sub>	1.49			
nC <sub>5</sub>	2.07			
C <sub>6</sub>	3.19			
C <sub>7</sub>	3.1			
C <sub>8</sub>	3.25			
C <sub>9</sub>	2.93			
C <sub>10</sub>	2.56			
C <sub>11</sub>	2.02			
C <sub>12</sub>	17.54			
Sum	100			
Molar mass reservoir oil, [g/mol]	93.87			
Reservoir pressure, [bara]	455.88			
Reservoir temperature, [°C]	118.96			
Saturation Pressure @ iPres, bar	214			
Dynamic Viscosity, [cP]				
at Pres	0.43			
at Ps	0.32			
Results of Multistage Separation:				
Formation Volume Factor (FVF), [m <sup>3</sup> /st m <sup>3</sup> ]	1.500855			
solution gas-oil ratio, [Sm <sup>3</sup> /Sm <sup>3</sup> ]	162.995			
solution gas-oil ratio, [Sm <sup>3</sup> /ton]	190.145			
stock-tank oil density, [kg/m <sup>3</sup> ]	854.5			
Note: 1. Maximum H <sub>2</sub> S Content: 3.8 mol %; Maximum CO <sub>2</sub> Content: 3.7 mol %; Water content up to 25% should be considered.				
2. For sour service conditions, the materials shall comply with NACE MR0175 / ISO 15156.				



The table shows the result of single stage flash calculation at 26bara and 105 C (upstream conditions where the 6" MPM will be installed). The GOR predicted under these conditions is 86.7% which ties up with the process data provided by the customer under these conditions.

The flash calculation was repeated at 16bara and 62C (downstream conditions where the 14" MPMs will be installed). The GOR predicted under these conditions is 90.3% which ties up with the process data provided by the customer under these conditions.

The predictions of the PVT model will be improved by tuning up against production separator GOR. The three steps of the tune up procedure are described next.

### Step 1 Recombination

Recombination of the separator gas and separator liquid to one reported separator GOR will be initially conducted assuming a single stage separation (multi-stage separation is also possible).

### Step 2 Fine Tuning of Fluid Composition

The recombined fluid from (1) will be flashed at separator conditions to check if the measured separator GOR is replicated by the simulation models. Only in the case of perfect separation and equilibration in the separator, perfect sampling, perfect fluid analysis and perfect modeling frame-work the measured and simulated separator GOR's will match perfectly. After this check the recombined fluid from (1) will be fine tuned so that the simulated separator GOR matches the measured separator GOR.

### Step 3 Flash Calculation

The recombined fluid from (1) will be flashed at the pressure and temperature conditions of the MPM. The flash simulation provides the relative volume rates of gas and liquid at MPM conditions. The required information is: Pressure and temperature conditions of the MPM.

# 34<sup>th</sup> International North Sea Flow Measurement Workshop 25-28 October 2016

## Technical Paper

### Appendix B API 2566

#### **"Section 19 TESTING GUIDELINES (factory acceptance – flow loop tests)**

*Section 19.1.8 pg 44: It should be pointed out that one cannot extrapolate performance between (flow loop) test points, mainly because the flow models are not linear solutions. These tests are not the final system calibration. For all multiphase measurement systems including Types II and III, the final calibration of the system is part of the field commissioning activity.*

#### **Section 20- FIELD TESTING GUIDELINES**

*Field tests may be conducted to qualify the meter performance under operating conditions, either as a precondition to the purchase or subsequent to the field installation, to verify the meter performance. The two types of field tests have to address a common problem – i.e. knowing the exact amount of multiphase fluid that flows through the meter.*

*There are three options for establishing the correct amount of fluid:*

- Capturing fluids that flow through the system during the test and measuring them with secondary equipment except for the gas. This option requires extra equipment that must be calibrated and certified.*
- Proving all system components including the model, and then calculating an implied accuracy by inference. This option requires calibration of end devices under similar conditions of fluid properties, pressure, and temperature as well as flow modelling. These requirements make this option impractical.*
- Indexing the performance of the new system against an established multiphase measurement system such as a Type I gravity based test separator."*

*Not surprisingly, the third option is the most common method employed in the field tests.*

**34<sup>th</sup> International North Sea Flow Measurement Workshop  
25-28 October 2016**

**Technical Paper**

**Appendix C Process Data Sheet Well Head Production Lines Badra Oil Field**

<b>Flow rate range</b>	<b>Min</b>	<b>Normal</b>	<b>Max</b>
<b>Gas flow rate ( Sm<sup>3</sup>/d)</b>	2688	360000	432000
<b>Gas flow rate ( Am<sup>3</sup>/d)</b>	151	20170	24205
<b>Liquid flow rate (m<sup>3</sup>/d)</b>	96	2400	2880
<b>Water Cut (%)</b>	0	25	100
<b>Operating Pressure ( barg)</b>	15	22	35
<b>Operating Temperature ( C)</b>	50	80	105
<b>Design Pressure ( barg)</b>		43	
<b>Design Temperature ( C )</b>		120	
<b>Density at Standard conditions</b>			
<b>Oil density (kg/m<sup>3</sup>)</b>	840	850	860
<b>water density (kg/m<sup>3</sup>)</b>	1001		1134
<b>Gas ( A Kg/m<sup>3</sup>)</b>		24	
<b>Viscosity at Actual conditions</b>			
<b>Oil viscosity (cP)</b>		0.53	
<b>Gas Viscosity (cP)</b>		0.015	

## **Extended Abstract**

# **Application of the Magnetic Resonance Multiphase Flowmeter to Heavy Oil**

**Jankees Hogendoorn, Mark van der Zande, André Boer, Lucas Cerioni,  
Stephanie Luik, KROHNE**

---

## **1 INTRODUCTION**

In the upstream oil and gas industry, mixtures of oil, gas and water are produced. To measure these fluids simultaneously inline, KROHNE has developed and manufactured a multiphase flowmeter based on Magnetic Resonance (MR). This measurement principle allows for a very direct measurement of the hydrogen atoms present in the oil, gas and water, resulting in accurate values for the flowrates as well as in information on the flow regime and velocity profiles [1] [2] [3]. The Magnetic Resonance multiphase flowmeter has been extensively tested at international multiphase flow laboratories [3] and in applications in the field, as presented e.g. at last year's North Sea Flow Measurement workshop [4].



Fig 1 - The magnetic resonance multiphase flowmeter (M-PHASE 5000)

In this year's presentation, we will focus on applications concerning high viscous oil, also known as heavy and extra heavy oil. It is well known that not only the production, transport and processing of heavy oil is challenging, but also metering of such high viscous oils using conventional technologies has its limitations. We will present results obtained with our MR based multiphase flowmeter on mixtures of viscous oils, in which the oil viscosity ranged between 190 cSt and 2200 cSt, the WLR ranged between 0% and 40% and the GVF ranged between 23% and 90%. Based on these results we will show the suitability of the MR measurement principle to heavy and extra heavy oil applications.

## **2 HEAVY OIL AND EXTRA HEAVY OIL**

In the oil industry, viscous oils are often referred to as heavy oil and extra heavy oil and they can be characterised amongst others by their asphaltenic content, their API gravity (below 22 API for heavy oil and below 10 API for extra heavy oil) and their viscosity, which ranges typically between 100 cP and 10000 cP.

Whereas in the early years of the oil industry, mainly the conventional and easy to produce resources have been produced, it can be observed that in the past decades production has shifted to unconventional resources such as (extra) heavy

# 34<sup>th</sup> International North Sea Flow Measurement Workshop 25-28 October 2016

## Extended Abstract

oil<sup>1</sup>. The world reserve of unconventional resources is about equal to that of conventional resources [5].

As the cost of production for heavy oils is higher than for conventional oil, the need for accurate multiphase flow measurements to optimize the well and reservoir management is even more apparent for these demanding applications. There are, however, quite some challenges in the measurement of multiphase flows of heavy oil. The challenges are related amongst others to differential pressure measurements, the tendency to form emulsion and the complex composition of heavy oil. However, the M-PHASE 5000 makes use of a fundamentally different measurement principle (MR) and does not rely on differential pressure measurements. Therefore, we will focus in this paper on the performance of the magnetic resonance multiphase flowmeter on multiphase mixtures containing viscous oil, to share our observations and to demonstrate its suitability for heavy oil applications.

### 3 EXPERIMENTAL SET-UP

In the KROHNE Research and Development laboratory, a compact multiphase flow loop has been built. In Figure 2 a schematic representation of the flow loop is shown and in Figure 3 a picture of the loop is shown.

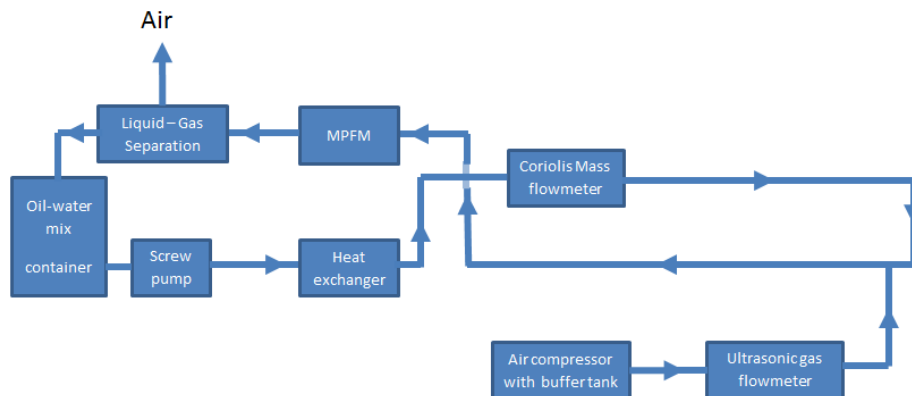


Fig 2 - Schematic representation of the multiphase flow loop at the KROHNE Research and Development laboratory.



Fig 3 - Picture of the upstream part of the multiphase flow loop, including the transparent section for flow visualization.

<sup>1</sup> In the remainder of the paper, when mentioning 'heavy oil' we actually refer to heavy oil as well as extra heavy.

# 34<sup>th</sup> International North Sea Flow Measurement Workshop 25-28 October 2016

## Extended Abstract

In the multiphase flow loop a two-phase mixture of oil and water is pumped via screw pumps through 4" lines. By means of a heat exchanger the temperature of the mixture is controlled. As reference the oil-water mixture is measured by a Coriolis mass flowmeter. The uncertainty on the liquid flow rate is 2% of the measured value (MV). Furthermore, the WLR is determined on basis of the density measurement of the Coriolis mass flowmeter using the density of pure water and of oil as reference values. This yields an uncertainty on the reference WLR of 1% absolute error. Compressed air is injected downstream of the Coriolis mass meter. The compressed air represents the gas phase and the flow is measured by means of an Ultrasonic flowmeter, which results in an uncertainty of 2% of the MV. In the flow loop a transparent pipe section of several meters length is installed to allow visualisation of the various flow regimes that occur in the flow loop. The three phase mixture flows through the MR multiphase flowmeter (3" internal diameter) after which the air is separated from the oil-water mixture. In Table 1 some specifications of the multiphase flow loop are listed.

**Table 1 - specification of the multiphase flow loop**

Parameter	Range	Unit
Line pressure	0 - 3	barg
Line temperature	20 - 35	°C
Flow range gas	0 - 50	am <sup>3</sup> /h
Flow range liquid	2 - 20	m <sup>3</sup> /h
Viscosity range	1 - 2200	cSt

## 4 FLOW REGIME

A very convenient part of the multiphase flow loop is the long transparent pipe in which the multiphase flow regime can be observed. In the tests described in this paper, we have worked with mixtures of viscous oil (190 cSt to 2200 cSt) in the range of conditions as described in Table 2. For all these conditions it was observed that the flow regime developed into a slug flow or plug flow. This can be understood by considering that the viscous forces in the liquid phase are such high, that the gas phase cannot drag the liquid along to establish a stratified, or stratified wavy flow. Consequently, the main transport mechanism of the fluids is slug flow and plug flow.

In field applications of heavy oil flowing through horizontal production lines, the prevailing flow regime is also expected to be slug flow and plug flow. On one hand this is related to the remark made above, explaining why stratified flow is not possible and on the other hand this is caused by the fact that in typical heavy oil applications the characteristic GVF and liquid flowrates are relatively low, and as such, not enabling mist flow.

### 4.1 Slug Velocity

As described in the previous section the dominant flow regime in heavy oil applications is expected to be slug flow. Therefore in this section we will focus on the slug flow regime and try to understand the flow dynamics of this flow regime. The slug flow regime has been the focus of many research studies and some practical relations have been derived to describe slug flow. For example one of the relations found in literature [6] describes the velocity of the liquid inside a slug,  $v_{LS}$ , as function of several parameters:

# 34<sup>th</sup> International North Sea Flow Measurement Workshop 25-28 October 2016

## Extended Abstract

$$v_{LS} = \frac{\alpha_G v_G + \alpha_L v_L - (1 - \alpha_{LS}) v_{GS}}{\alpha_{LS}} \quad (1)$$

Where  $\alpha_G$  and  $\alpha_L$  are the gas fraction and the liquid fraction, respectively, and  $\alpha_{LS}$  is the liquid fraction inside the slug;  $v_G$  and  $v_L$  is the actual velocity of gas and liquid respectively, and  $v_{GS}$  is the velocity of the gas inside the slug. Note that  $(\alpha_G v_G)$  is the average superficial velocity for the gas and  $(\alpha_L v_L)$  is the average superficial velocity for the liquid.

Under the assumption that the velocity of the gas inside the slug is equal to the velocity of the liquid in the slug, equation 1 simplifies to:

$$v_{LS} = \alpha_G v_G + \alpha_L v_L \quad (2)$$

which is equal to

$$v_{LS} = (Q_{v,G} + Q_{v,L}) / A \quad (3)$$

where  $Q_{v,G}$  and  $Q_{v,L}$  are the volumetric flowrate of gas and oil respectively, and  $A$  is the cross-sectional area of the pipe. Equation 3 can be a very powerful relation when designing flowlines that have to handle slug flow.

Some remarks can be made with regard to equation 3:

- For the derivation of equation 3 it is assumed that the velocity of the gas inside the slug is equal to the velocity of the liquid in the slug. A sensitivity analysis shows that in case there is a small difference in these velocities (slip) this only has a small effect on the correlation in equation 3.
- It is important to note that the velocity of the liquid in the slug ( $v_{LS}$ ) is not equal to the velocity of the slug. When visualising slug flow, it can be observed that the slugs move like a wave pattern through the pipe with a certain (phase) velocity. The liquid inside the slug, however, moves at a lower velocity than this phase velocity. This can be understood as liquid is constantly fed into the slug at its front and drained from it at its tail.
- It can be found in literature [6] that the ratio between the phase velocity of the slug and the velocity of the liquid in the slug depends on the flow regime; for laminar flow the ratio is approximately 2, and for turbulent flow it is approximately 1.2.

Given the remarks made above it is interesting to check whether the simple relation for the velocity of the liquid in the slug (equation 3) is valid for both laminar and turbulent slug flow.

## 4.2 SLUG VELOCITY MEASUREMENT

To validate the applicability of equation 3 to slug flow of viscous oil, tests have been performed on the multiphase flow loop at the KROHNE laboratory. The focus of the study is to see whether indeed equation 3 is applicable, both to laminar flow and to turbulent flow.

The MR multiphase flowmeter is applied to measure the velocity of fluids inside the pipe. For this purpose the so-called convective decay method is applied [2], in which the decay of the magnetic resonance signal is measured as function of

# 34<sup>th</sup> International North Sea Flow Measurement Workshop 25-28 October 2016

## Extended Abstract

time, and from this decay the liquid velocity is derived. In case of slug flow, this automatically yields the velocity of the liquid inside the slug. The reference flowmeters of the multiphase flow loop are applied to determine the total volumetric flowrate of the liquid and the gas.

For the tests, several batches of oil-water mixtures have been made with oil viscosity of 190 cSt and WLR ranging between 0 to 40%. Further details on the tested conditions can be found in Table 2. Due to the screw pumps immediately oil-water emulsions are formed. For low WLR the emulsions are oil continuous, resulting in a high effective viscosity and laminar flow inside the slug, with a maximum Reynolds number of approximately 1000. For WLR approaching 40% the emulsion changed to water continuous resulting in a low effective viscosity and turbulent flow inside the slug with a minimum Reynolds number of approximately 35000. From the Reynolds numbers it can be derived that indeed the flow is either laminar ( $Re < 1000$ ) or turbulent ( $Re > 35000$ ), and flow conditions in the transition between laminar to turbulent are not to be expected.

**Table 2 - Summary of the test conditions**

Parameter	Min. Value	Max. Value	Unit
Line pressure	~ 0		barg
Line temperature	~ 25		°C
Oil viscosity	190		cSt
Fresh water viscosity	1		cSt
Flow range gas (air)	5.0	35.6	am <sup>3</sup> /h
Flow range liquid	4.0	19.0	m <sup>3</sup> /h
GVF	23	90	%
WLR	0.0	40	%

In figure 4 the results of the slug velocity measurements are shown. It can be observed that the measured liquid velocity in the slug can be described using the theoretical prediction (eq. 3). The measured data points follow equation 3 closely. For laminar flow conditions the match is better than for turbulent flow conditions for which the deviation is in the range of 10%. However, it should be noted that equation 3 still describes the trend observed in the experiments. We have not investigated why the match for the laminar flow data is better than for the turbulent flow data, but perhaps it is related to the assumption made to derive equation 2 from equation 1; it is assumed that the gas velocity in the slug is equal to the liquid velocity in the slug. This is an interesting topic for further research; however it is not in scope of the current paper.

The experimental results lead to the conclusion that despite the difference for laminar and turbulent slug flow regarding the ratio between the phase velocity of the slug and the actual liquid velocity in the slug (1.2 for turbulent flow and 2 for laminar flow), it is possible to describe the liquid velocity in the slug with a single relation (equation 3) for both conditions.

## Extended Abstract

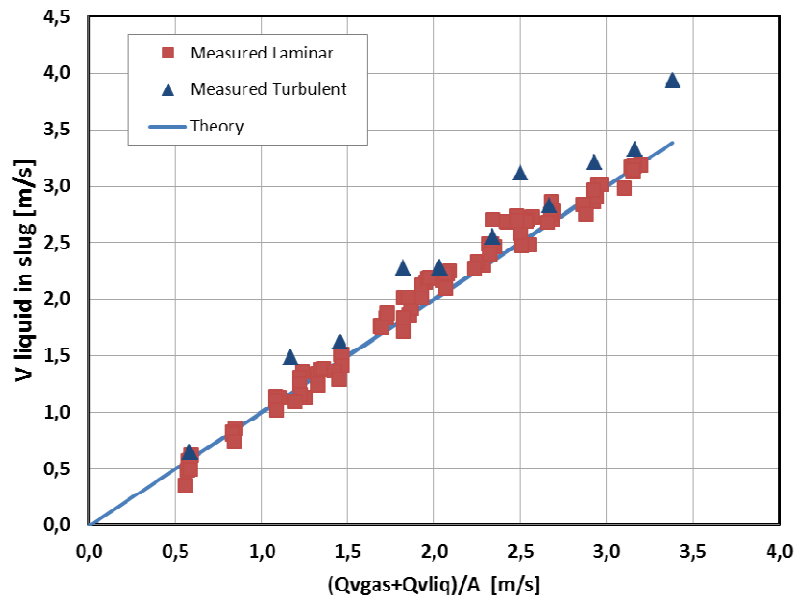


Fig4 - Results of the measured liquid velocity in a slug as function of the total volumetric fluid flow rate divided by the cross-sectional area. The liquid velocity has been measured using the magnetic resonance multiphase flowmeter. The line denotes the theoretical prediction according to equation 3. The red squares represent the measured values for oil continuous emulsion (laminar flow), and the blue triangles represent the water continuous emulsion (turbulent flow).  $Q_{v\text{gas}}$  and  $Q_{v\text{liq}}$  denote the volumetric flow rate of gas and liquid, respectively, and  $A$  denotes the cross-sectional area.

## 5 MEASURED FLOWRATES

In the previous section we have demonstrated that the MR measurement principle is suitable to measure liquid velocity in the slug flow regime. As presented in previous papers [2], [3], [4] not only the fluid velocity can be measured, but also the volumetric flowrate of liquid and gas and the water to liquid ratio can be measured using MR. For the conditions as described in Table 2 the volumetric flowrates have been measured. In figures 5 to 7 the results are plotted.

It can be observed in figures 5 to 7 that over the entire range of the tested conditions good accuracy is achieved for the volumetric flowrate for liquid and gas as well as for the WLR. For the volumetric liquid flow rate the accuracy was better than 5% of the MV, for the measured volumetric gas flow rate the accuracy was better than 10% of the MV and for the measured WLR the accuracy was better than 1% absolute.

Visual inspection of the flow regime, showed that for all test points the flow regime corresponded to slug or plug flow. The WLR was varied in the experiments in discrete steps (0%, 2%, 6%, 12%, 20% and 40%). For all tested WLR values similar accuracy has been achieved for the volumetric flowrates of liquid and gas. As discussed in §4.2, for WLR below 20% the slug flow was laminar and for the condition with WLR of 40% the slug flow was turbulent. The accuracy on the measured volumetric flowrate for liquid and gas was achieved for both the laminar and the turbulent slug flow.

# 34<sup>th</sup> International North Sea Flow Measurement Workshop 25-28 October 2016

## Extended Abstract

The data plotted in figures 5 to 7 is measured for oil viscosity of 190 cSt, however similar performance has been obtained for higher oil viscosity (700 cSt, 1100 cSt and 2200 cSt).

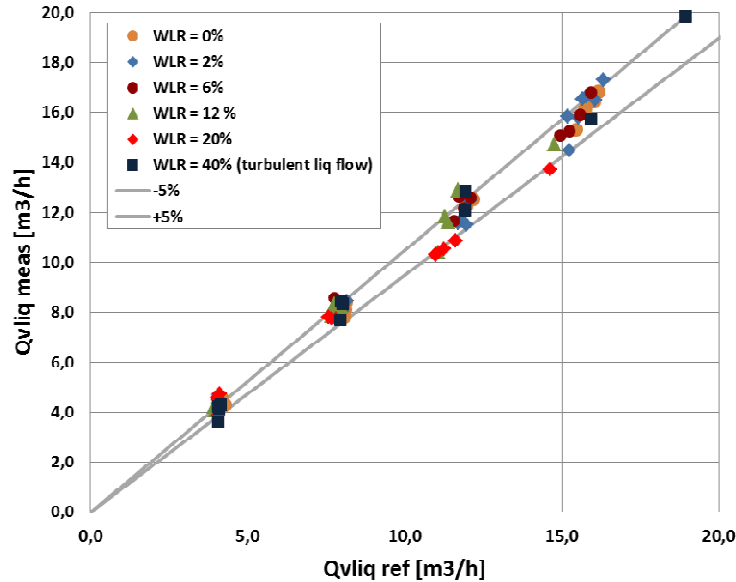


Fig5 - The measured volumetric flowrate of liquid as function of the reference values for the volumetric liquid flowrate. All measurements have been performed with oil viscosity of 190 cSt. The WLR has been varied in discrete steps as denoted in the legend of the graph. The GVF has been varied from 23%-90% for each WLR. The standard deviation in the measurement is less than 5% of the MV.

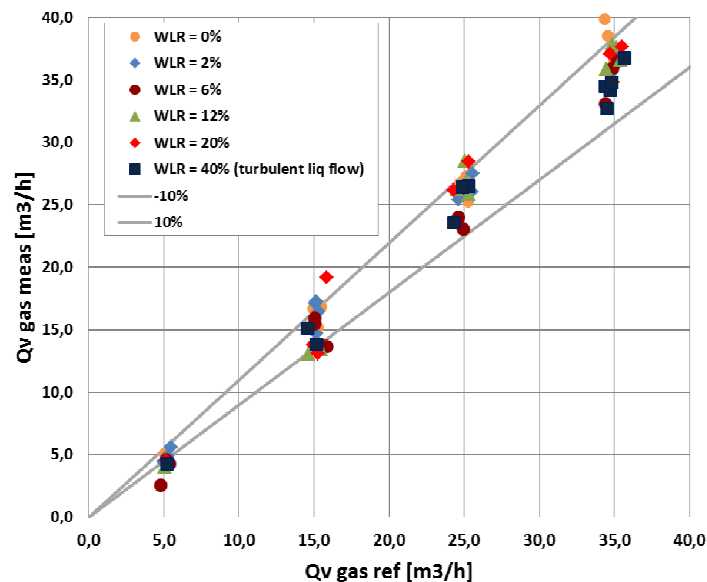


Fig 6 - The measured volumetric flowrate of gas as function of the reference values for the volumetric gas flowrate. All measurements have been performed with oil viscosity of 190 cSt. The WLR has been varied in discrete steps as denoted in the legend of the graph. For each gas flowrate the liquid flowrate has been varied between 4 to 19  $m^3/hr$ . The standard deviation in the measurement is less than 10% of the MV.

**Extended Abstract**

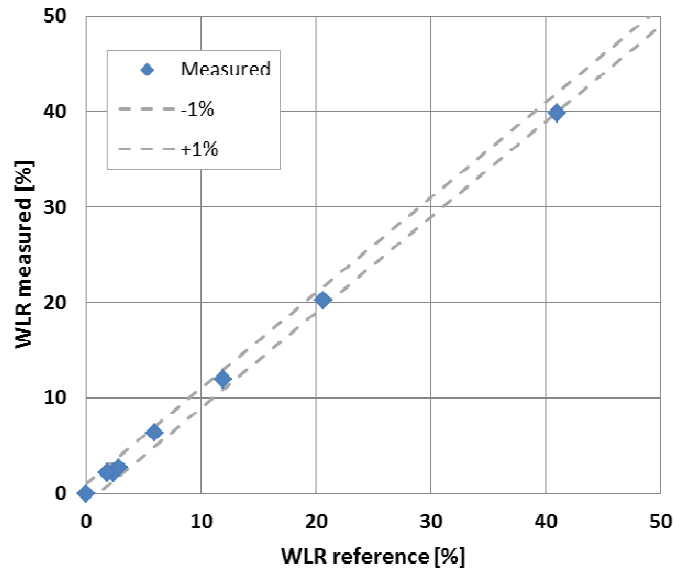


Fig 7 - The measured water-liquid ratio (WLR) as function of the reference values as measured by the Coriolis mass flowmeter. The dotted lines denote a deviation of  $\pm 1\%$  absolute of the WLR value.

## **6 SUMMARY AND CONCLUSIONS**

In the oil and gas industry a shift can be observed from production of conventional resources to the production of unconventional resources. One of these unconventional resources is heavy oil. As the production cost of heavy oil is typically higher than for lighter oils, a clear need is present for optimal well and reservoir management in order to make production of heavy oil economically feasible. One aspect of good well and reservoir management is accurate multiphase flow measurement and for heavy oil applications this can be quite challenging. Therefore, in this paper we have focussed on multiphase flow measurement of mixtures of high viscosity oil, gas and water.

In the multiphase flow loop at the KROHNE Research and Development Laboratory, multiphase flow measurements have been performed using the magnetic resonance multiphase flowmeter. In the experiments the focus was on high viscosity oil. From observation of the flow patterns it is concluded that slug flow is the dominant flow regime for multiphase flow of high viscosity oil.

From literature, relations are available that describe the correlation between the velocity of liquid in a slug as function of the total volumetric liquid and gas flow rate (equation 3). By means of liquid velocity measurements based on magnetic resonance it has been shown that for a wide range of conditions equation 3 can be used to estimate the velocity of liquids in slug flow. The relation is applicable to varying WLR, even when the flow changes from laminar slug flow to turbulent slug flow.

The magnetic resonance measurement principle is not only suitable to measure fluid velocity; it also enables accurate volumetric flowrate measurements. In the multiphase flow loop, measurements have been performed to demonstrate the performance of the multiphase flowmeter for high viscosity oil. For oil/water/gas

# 34<sup>th</sup> International North Sea Flow Measurement Workshop 25-28 October 2016

## Extended Abstract

mixtures with oil viscosity between 190 cSt and 2200 cSt, the WLR has been varied between 0% to 40% and the GVF has been varied between 23% and 90%. The accuracy achieved in the volumetric flowrate was better than 5% of the MV for the liquid flowrates, better than 10% of the MV for the gas flowrates and better than 1% absolute for the WLR.

A final conclusion that can be drawn is that magnetic resonance is indeed a suitable measurement principle to measure multiphase flow of high viscosity oil.

### 7 NOTATION

$\alpha$	fraction	$Q_v$	volumetric flowrate
A	cross-sectional area	GVF	gas volume fraction
G	gas	MPFM	multiphase flowmeter
GS	gas in slug	MR	magnetic resonance
L	liquid	MV	measured value
LS	liquid in slug	WLR	water liquid ratio
v	actual velocity		

### 8 ACKNOWLEDGEMENTS.

The authors of this paper like to express their appreciation to the entire KROHNE development team of the magnetic resonance multiphase flowmeter for their continuous effort to develop and improve the multiphase flowmeter.

### 9 REFERENCES

- [1] M. Appel, et al., *Robust Multi-Phase Flow Measurement Using Magnetic Resonance Technology*, Society of Petroleum Engineers, MEOS, Manama, Bahrain, 6-9 March, 2011.
- [2] Jankees Hogendoorn, et al., *Magnetic Resonance Technology, A New Concept for Multiphase Flow Measurement*, 31<sup>st</sup> International North Sea Flow Measurement Workshop, Tønsberg, Norway, 22-25 Oct., 2013.
- [3] Jankees Hogendoorn, et al., *Magnetic Resonance Multiphase Flowmeter: Gas Flow Measurement Principle and Wide Range Testing Results*, 32<sup>nd</sup> International North Sea Flow Measurement Workshop, St. Andrews, Scotland, 21-24 Oct., 2014.
- [4] Jankees Hogendoorn, et al. *Practical Experiences obtained with the Magnetic Resonance Multiphase Flowmeter*, 33<sup>rd</sup> International North Sea Flow Measurement Workshop, Tønsberg, Norway, 20-23 Oct., 2015.
- [5] Publication from International Energy Agency, *Resources to Reserves 2013; Oil, Gas and Coal Technologies, for the Energy Markets of the Future*.
- [6] Ove Bratland, *'Pipe Flow 2, Multi-phase Flow Assurance'*, 2010, ISBN 978-616-335-926-1.

## **Technical Paper**

# **Live Fluids or Controlled Fluids: How Should we Calibrate a Multiphase Flow Meter?**

**Norman Glen and David Millington, NEL**

---

## **1 ABSTRACT**

This paper presents findings on mass transfer-related fluid properties errors that can occur during multiphase flow meter factory acceptance testing (FAT). A dynamic FAT determines the optimum performance of an MPFM before service in the field. Substantial uncertainties in this process can result in poor device qualification that consequently impacts their quality in the field.

Two multiphase flow facility configurations, live hydrocarbon fluids and controlled (inert) fluids, have been assessed using the PPDS thermophysical properties software package. A test programme was constructed to determine fluid properties errors that occur due to component mass transfer between the gas and liquid hydrocarbon phases, thus causing a difference in measured fluid volumes between the reference measurement section and the location of the device under test.

The results show that the effect of component mass transfer for controlled fluids can be considered negligible. However, the live hydrocarbon tests showed significant mass transfer between the liquid and gaseous phases, therefore, potentially impacting the quality and stability of the reference system or possibly corrupting the calibration process if unaccounted for.

## **2 INTRODUCTION**

For over 20 years, multiphase flow meters (MPFM's) have been employed as complex measurement systems for the upstream oil and gas sector, delivering real-time well performance data that allows operators to maximise production and increase field recovery factors.

Although MPFM's are now widely regarded as reliable measurement tools, their claimed theoretical uncertainty will often not meet that of a conventional test separator setup, where the flow is split into its respective phases and each metered as a single phase. Therefore, the accuracy of an MPFM is regularly subject to scrutiny. Although the measurement stability of multiphase metering systems does not yet emulate that of a test separation system in most environments, there is a major industry push towards replacing the test separation procedure with the modernised multiphase flow measurement alternative [1]. This solution is attractive in many respects; enabling production monitoring, minimising cost (both capital and operational), minimising required human resources and also increasing available platform space. Clauses have already been implemented that permit the use of MPFM's for fiscal metering applications of mature fields [2], where the capital and operating expenditure associated with installing test separation equipment is not financially viable. However, it is worth reiterating that questions still remain about accuracy in service, hence employing MPFM's as fiscal meters remains a controversial

# **34<sup>th</sup> International North Sea Flow Measurement Workshop 25-28 October 2016**

## **Technical Paper**

approach that has only been adopted in a small number of locations. Generally, MPFM's will not provide the confidence, reliability or combined measurement uncertainty of a conventional fiscal metering assembly [3].

With financial factors driving the implementation of MPFM's into fiscal applications - even though their accuracy may be viewed as undesirable - a potential development could be to improve the baseline uncertainty of the device itself. This may seem perfectly feasible, but could be considered untimely, relying upon heavy research investment during a period of economic uncertainty in the oil and gas industry. Conversely, additional uncertainties that arise from calibration effects could be explored. Calibration effects influence the uncertainty of all metering systems and include geometrical factors, line condition-based errors as well as flow patterns influences to name a few. Understanding these effects is critical to translating between laboratory validation and field validation, therefore bridging the gap associated with the leap from lab to field.

The guidelines directing the validation procedure of a MPFM are open to individual interpretation. Standards state that the dynamic testing of a multiphase meter in a third-party flow facility is at the discretion of the end user [4]. Currently, no standards exist that advise on the pre-requisites of a flow loop trial. Ultimately, this means the meter may be tested in a facility operating at low pressure or high pressure, using live fluids or controlled fluids, or with different operating principles, such as single phase or multiphase fluid transport.

The factory acceptance test (FAT) of the multiphase meter is designed to test the optimum performance of the device and ensure that measurements are within the quoted ranges. This paper will investigate the fluid properties errors that can occur when using live hydrocarbons instead of controlled fluids for a MPFM FAT and how this reflects the qualification of meter performance.

### **3 CALIBRATION BEST PRACTICE**

#### **3.1 A Brief Reminder**

Calibration is an essential step for all measurement systems and has been scientifically practiced for thousands of years. The term 'calibration' refers to the process in which a device is compared, and assessed, against a reference transfer standard with good temporal stability [5]. For example, prior to the introduction of a non-physical, coefficient-based reference system, the primary physical reference for a unit of length was contained in a controlled environment. This ensured no expansion/contraction due to changes in critical parameters such as temperature or humidity. Hence, the reference must show a degree of resilience to changes in its physical properties under changing conditions.

The primary reference standard tops the calibration hierarchy. The quality of all subsequent references are defined in terms of their position in the calibration pyramid and consequent reference uncertainty. Further down the pyramid, the reference uncertainty increases. An illustration of the calibration pyramid for the unit of mass is shown in Figure 1.

The uncertainty obtained from calibration will be a combination of practicality and operational requirements. For high precision applications, the reference standard should be as high up the calibration pyramid as possible. On the other hand, it is

# 34<sup>th</sup> International North Sea Flow Measurement Workshop 25-28 October 2016

## Technical Paper

more practical (and cost effective) to calibrate low precision devices nearer the base of the pyramid.

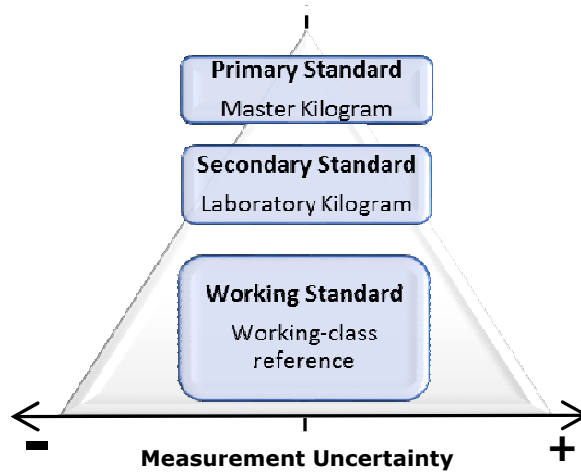


Fig 1 - Calibration Pyramid

### 3.2 So, How Accurate Should a Multiphase Flow Meter Be?

If this question was asked twenty years ago, then it is likely the answer would be 'not very' - mainly due to a lack of research, knowledge and expectation. However, now that MPFM's have gained industry acceptance as high performance measurement systems, complimented by a few hardware and software upgrades along the way, these initially restricting factors have decayed. This has induced a knock-on effect in the standard of MPFM application, going from delivering low accuracy measurement approximations to now being employed as high accuracy fiscal and allocation flow meters. This step change in performance must be harmonised with a step change in calibration. For multiphase flow meters, the term 'calibration' is rarely used, as the device generally undergoes 'qualification' and is not adjusted to conform with the reference system.

By analogy, if a balance that was used to weigh vegetables is now being used to weigh gold, the application and requirements have changed, hence the quality of calibration and subsequent quality of the device must change to reflect this. Therefore high accuracy reference calibrations are essential for MPFM's progression for use into high accuracy applications.

As discussed, calibration best practice fundamentally relies upon stable conditions (regardless of the system under test) to obtain reliable results with minimum uncertainty. Translating this into multiphase flow measurement terms, the flowing medium acts as the transfer standard, essentially calibrating the MPFM against a multi-component, multiphase mixture. Therefore, a critical aspect of MPFM calibration is the uncertainty that arises from transport of multiphase fluids from the single phase reference measurement section to the device under test. Multiphase test loops do not measure complex phase interaction effects, such as mass transfer, that may occur during component mixing. Therefore, additional uncertainties arise from the fluid properties themselves. This phenomenon introduces the key question - should one use live fluids or controlled fluids in a multiphase flow loop?

# 34<sup>th</sup> International North Sea Flow Measurement Workshop 25-28 October 2016

## Technical Paper

### 3.3 Live Fluids and Controlled Fluids

The advantages of testing in live fluids are easily understood. The meter will undergo service in live fluids, so it seems logical to perform the meter's FAT in a fluid that reflects service conditions.

A MPFM will go through the process of several qualification stages before being considered a competent measurement system; see Table 1 for details. These stages will not be followed for every meter, possibly due to financial or field constraints, but are used as a general qualification guide.

**Table 1 - MPFM Qualification Stages and API 20.3 Narrative [4]**

Qualification Stage	Description	API 20.3 Extract
Static Testing	Calibration of all measurement devices such as pressure and temperature sensors, gamma-ray densitometers etc.  This calibration ensures the functionality of the meter components.	<i>"The individual calibration of the individual sensors and the primary devices is of prime importance in maintaining the performance of the MPFM."</i>
Dynamic (Flow Loop) Testing	The user must test the meter in flow conditions that are the same as field application –multiphase, wet-gas, heavy oil etc.  Choice of dynamic FAT fluid types, either controlled or live, are at the discretion of the end user. However, it is advised that inert fluids may provide a better test of the actual performance of the meter.	<i>"Meter flow loop verification often may also involve testing on 'inert' fluids – stabilized crudes, kerosene, nitrogen, etc. – which may provide a better test of the meter's basic flow dynamics and sensor responses than can be guaranteed with 'live' fluids."</i>  <i>"The objective of testing in a reference facility is verification to an agreed level of the manufacturers claimed performance specification for the instrument"</i>
Field Trial/ Site Acceptance Test (SAT)	A field trial tests the device in actual operating conditions. This gives a good indication of in-service performance, however is unlikely to determine the critical baseline performance of the device upon which it demonstrates minimal measurement uncertainty.	<i>"Though the meter may have performed well in prior tests, there will likely be sufficient difference between test and field conditions that having the additional data provided at site may prove extremely important"</i>

As can be observed from the API 20.3 extract in Table 1, the recommended practice for the dynamic qualification (flow loop FAT) of a MPFM is to verify the meters optimum performance and confirm stated uncertainties. The benefits of this approach are also recognised within the UK Oil and Gas Authority Guidance Notes for Petroleum Measurement [2]:

*"Where the comparison is on a volume basis, it should be referred to a common set of conditions (e.g. standard conditions) and must take account of possible transfer between phases."*

# 34<sup>th</sup> International North Sea Flow Measurement Workshop 25-28 October 2016

## Technical Paper

*The calibration fluids may be either 'process' (live crude, hydrocarbon gas, formation water) or 'model' (e.g. oil, water, nitrogen). The latter set-up is by far the most common; not only is it far less hazardous to operate but the PVT characteristics of the fluids are likely to be relatively well understood, so that it becomes possible to compare the reference measurements with those of the MPFM with minimal additional uncertainty."*

Generally, good device calibration requires reference accuracy of at least 5-10 times greater than the device under test. This means for a test condition by which a 5% measurement uncertainty would be expected from the MPFM, a 0.5-1% uncertainty should be attained from the reference flow facility.

Following FAT, the MPFM will then undergo testing in live hydrocarbon fluids during a field trial, which acts to assess the performance in real service conditions. It should be noted that live hydrocarbon flow loop testing does not emulate testing of field conditions.

Ultimately, the responsibility of a MPFM is to calculate the flow rates of each phase within a multiphase flow, irrespective of the process fluids. A calibration is input into the meter using the individual phases that comprise the multiphase flow, providing the basis of its operational envelope. This envelope is sensitive to variations in fluid properties, in theory, as long as the fluid properties do not change over time, then the meter should stay within the operating envelope and maintain its accuracy.

### 4 NEL MULTIPHASE FLOW LOOP

The NEL multiphase flow loop is a three phase (gas-oil-water) facility. The facility features a three phase separation vessel, with the liquid phases re-circulated and metered as single phases. The gas phase is injected externally and also metered as a single phase prior to mixing with liquid phases in the test section. An illustration of this configuration is displayed in Figure 2. The oil, Paraflex HT9, is a controlled reference fluid, pure nitrogen is used for the gaseous phase and the water phase is a synthetic brine to reflect standard operating environments.

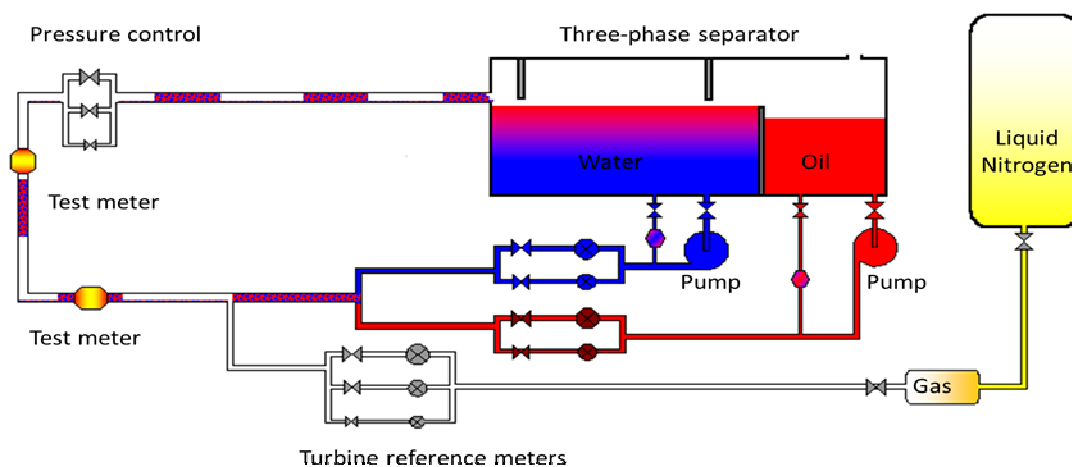


Fig 2 - NEL Multiphase Flow Loop Diagram

Technical Paper

The NEL facility is optimised to provide accurate and stable reference measurements:

1. Pure nitrogen is used as the gas phase. This has minimal mass transfer with the liquid phases and its PVT behaviour is well defined. Single pass gas injection means no possibility of separator liquid carry-over into gas outlet stream, improving measurement uncertainty.
2. The oil fluid properties represent that of a standard light crude, however its separation qualities have been improved ensuring reduced residence time and minimal oil carry-under in the outlet water stream. Both oil and water outlet streams are closely monitored in real-time to assess phase contamination levels.

5 MASS TRANSFER OF MULTIPHASE COMPONENTS

When dealing with a multi-component mixture, the fundamental questions that need to be answered are:

- How much of a phase is present? (Phase fraction or quality)
- What are the compositions of the components in a phase?
- Is the phase stable?

A common stumbling point in the understanding of mixture behaviour is the differentiation between how much of a phase is present and the compositions of a phase. Figure 3 illustrates the key definitions for a two phase binary mixture.

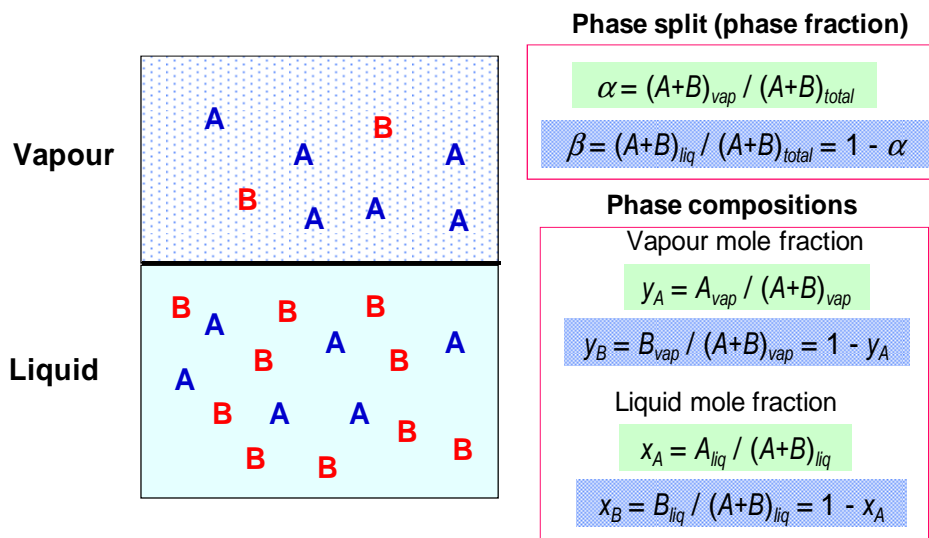


Fig 3 - Phase split and phase composition definitions

The key fact is that the compositions of phases in equilibrium are not, in general, equal. This is completely opposite to the pure component case, where the compositions must be equal because there is only one component! This inequality of compositions in phases that are in equilibrium is the reason why a component can be separated from a mixture by distillation or extraction and also

# **34<sup>th</sup> International North Sea Flow Measurement Workshop 25-28 October 2016**

## **Technical Paper**

why the composition of the phases in a multi-component mixture can vary as the temperature and pressure changes.

Numerous equations of state (EoSs) have been developed to enable the calculation of phase fractions and phase compositions for multi-component mixtures, allowing the calculation of phase properties such as density. However, in a multiphase flow facility, in addition to the transfer of components between phases due to chemical thermodynamics, additional mass transfers can occur, due to liquid pick-up into the gas phase and solubility of the gas in the liquid phases.

Mass transfer that occurs within a multiphase environment is thus influenced by many factors including temperature and pressure dependent chemical thermodynamics, flow dynamics effects, multiphase flow patterns and phase area distributions. Not only that, mass transfer may be a time-dependant process – just because it happened before, does not mean it will happen again!. For example, although water is generally not considered a primary contributor in the mass transfer equation, it may contain partially dissolved gas with later potential to contribute to the hydrocarbon phase exchange process.

Good reference systems entail tightly controlled operating conditions, excellent condition understanding and very high levels of stability. Having a difficult to characterise, highly complex phenomena within a reference measurement standard is regarded as poor metrology practice, especially if the reference standard is to be considered for high accuracy multiphase flow devices. Good design and operation can reduce or eliminate many of the physical influence factors causing mass transfer between phases. The use of stable reference fluids is the most obvious way to reduce the effects of chemical thermodynamically driven mass transfer between phases.

In order to test the magnitude of this mass transfer effect, a dedicated physical properties test programme was constructed. This programme featured a selection of multiphase and wet-gas test cases to determine how changing operating conditions influenced the phase transfer for both live hydrocarbon and controlled fluid flows. The test cases were performed using the PPDS thermophysical properties software package.

PPDS [6] is a physical properties data bank containing over 1400 pure components and many pseudo-components, such as light crude, that can be analysed as if it were pure. The software package features many equations of state that enable the calculation of thermophysical properties of multi-component mixtures. In addition, it allows user-defined binary interaction parameters (BIP's) to optimise the calculation depending on the mixture components.

## **6 PHASE INTERACTION ANALYSIS AND TEST PROGRAMME**

Exploring the mass transfer phenomenon in greater detail, the PPDS package was used to perform three phase vapour-liquid-liquid flash calculations. This uses the Peng-Robinson (PR) equation of state to perform an initial vapour-liquid flash calculation followed by use of Henry's Law to split the liquid into two liquid phases. The analysis featured two key stages for a given test point. First, a superficial single phase gas mixture was calculated to determine baseline fluid properties at chosen conditions. Second, this test was repeated including specified quantities of oil and water components. The variation in gas density between both

# 34<sup>th</sup> International North Sea Flow Measurement Workshop 25-28 October 2016

## Technical Paper

calculations therefore describes the levels of mass transfer that has occurred. The test calculation programme is described in Table 2.

$$\text{Gas Density Difference (\%)} = \frac{(\text{Mixture Density} - \text{Superficial Density})}{\text{Superficial Density}} \times 100 \quad (1)$$

**Table 2 - Test Programme Parameters**

CASE	TEST TYPE	FLUID TYPE	OIL COMPONENT (PPDS)	GAS COMPONENT (PPDS)	TEMP.	PRESSURE	GVF
1A	Multiphase	Live Hydrocarbon	M1	AGA-8	25	10 bar	30%
2A	"	"	"	"	25	80 bar	30%
3A	"	"	"	"	25	10 bar	50%
4A	"	"	"	"	60	10 bar	50%
5A	"	"	"	"	25	80 bar	50%
6A	"	"	"	"	60	80 bar	50%
7A	Wet-gas	Live Hydrocarbon	M1	AGA-8	25	10 bar	90%
8A	"	"	"	"	60	10 bar	90%
1B	Multiphase	Controlled	Kerosene	Nitrogen	25	10 bar	30%
2B	"	"	"	"	25	80 bar	30%
3B	"	"	"	"	25	10 bar	50%
4B	"	"	"	"	60	10 bar	50%
5B	"	"	"	"	25	80 bar	50%
6B	"	"	"	"	60	80 bar	50%
7B	Wet-gas	Controlled	Kerosene	Nitrogen	25	10 bar	90%
8B	"	"	"	"	60	10 bar	90%

\*M1 = Hexane, Dodecane, Hexadecane and n-Eicosane

For this test programme, the effect of water cut was not explored and was held constant at WC=20%. As can be seen in Table 2, the first set of eight test cases, 1A-8A, were in a live hydrocarbon environment for both multiphase and wet-gas flows. Test points 1B-8B were repeats of the first eight cases only replacing the live hydrocarbons with controlled fluids.

# 34<sup>th</sup> International North Sea Flow Measurement Workshop 25-28 October 2016

## Technical Paper

A liquid hydrocarbon combination of Hexane, Dodecane, Hexadecane and n-Eicosane was chosen to reflect the liquid phase, defined as M1 in Table 2. A representative natural gas mixture was also used (AGA-8, Gas 3, Table C.1 [7]).

For the controlled fluid calculation, kerosene was used as the oil and nitrogen was used for the gas. A standard pure water was used for both hydrocarbon and controlled fluid test cases.

### 7 PPDS RESULTS

To illustrate the basic calculation objectives, a summarised calculation process is displayed in Figure 4. This example shows the calculation of live hydrocarbon test case 1A.

**Table 3 - Test Case 1A**

Fluid	Oil	Gas	Temp.	Press.	Water Cut	GVF
Live Hydrocarbon	M1	AGA-8	25°C	10 bar	20%	30%

Input Stream Composition	Mol Fraction	Mol Weight (g mol <sup>-1</sup> )	Mass (g)	Volume (m <sup>3</sup> )	Density (kg/m <sup>3</sup> )	GVF (%)
CARBON DIOXIDE	0.015	44.00999832	0.660149975	2.194	<b>8.554</b>	30
NITROGEN	0.01	28.01300049	0.280130005			
METHANE	0.859	16.04299927	13.78093637			
ETHANE	0.085	30.06999969	2.555949974			
PROPANE	0.023	44.09700012	1.014231003			
ISOBUTANE	0.0035	58.12400055	0.203434002			
BUTANE	0.0035	58.12400055	0.203434002			
ISOPENTANE	0.0005	72.15100098	0.0360755			
PENTANE	0.0005	72.15100098	0.0360755			
HEXANE	1.5132355	86.1780014	130.4076111	4.096	793.995	
DODECANE	4.5397065	170.3399963	773.2935887			
HEXADECANE	6.052942001	226.447998	1370.676598			
n-EICOSANE	3.026471	282.5559998	855.1475392			
WATER	56.71408895	18.01499939	1021.704278	1.024	997.694	

Output Stream Composition	Volume (m <sup>3</sup> )	Density (kg/m <sup>3</sup> )	GVF (%)
GAS	2.436	<b>7.704</b>	31.95
HYDROCARBON LIQUID	4.165	751.421	
WATER	1.025	996.757	

$$\text{Gas Density Difference (\%)} = \frac{(\text{Mixture Density} - \text{Superficial Density})}{\text{Superficial Density}} \times 100 \quad (1)$$

$$\text{Gas Density Difference (\%)} = -9.94\%$$

# 34<sup>th</sup> International North Sea Flow Measurement Workshop 25-28 October 2016

## Technical Paper

The calculation process illustrated in Table 3 was repeated for all 16 test cases. The resultant mass transfer, in terms of gas density difference, for each test case is provided in Table 4.

**Table 4 - PPDS Results for all 16 Test Cases**

<b>LIVE HYDROCARBON FLUIDS</b>					DIFFERENCE FROM SUPERFICIAL GAS FLOW
CASE	TEST TYPE	TEMP	PRESS.	GVF	DENSITY (%)
1A	Multiphase	25	10 bar	30%	<b>-9.93</b>
2A	"	25	80 bar	30%	<b>-13.54</b>
3A	"	25	10 bar	50%	<b>-8.57</b>
4A	"	60	10 bar	50%	<b>-4.46</b>
5A	"	25	80 bar	50%	<b>-10.68</b>
6A	"	60	80 bar	50%	<b>-7.01</b>
7A	Wet-gas	25	10 bar	90%	<b>-2.75</b>
8A	"	60	10 bar	90%	<b>0.71</b>

<b>CONTROLLED FLUIDS</b>					DIFFERENCE FROM SUPERFICIAL GAS FLOW
CASE	TEST TYPE	TEMP	PRESS.	GVF	DENSITY (%)
1B	Multiphase	25	10 bar	30%	<b>-0.04</b>
2B	"	25	80 bar	30%	<b>0.05</b>
3B	"	25	10 bar	50%	<b>-0.04</b>
4B	"	60	10 bar	50%	<b>-0.17</b>
5B	"	25	80 bar	50%	<b>0.05</b>
6B	"	60	80 bar	50%	<b>0.22</b>
7B	Wet-gas	25	10 bar	90%	<b>-0.04</b>
8B	"	60	10 bar	90%	<b>-0.17</b>

The results described in Table 4 are also portrayed graphically in Figure 4 below.

Technical Paper

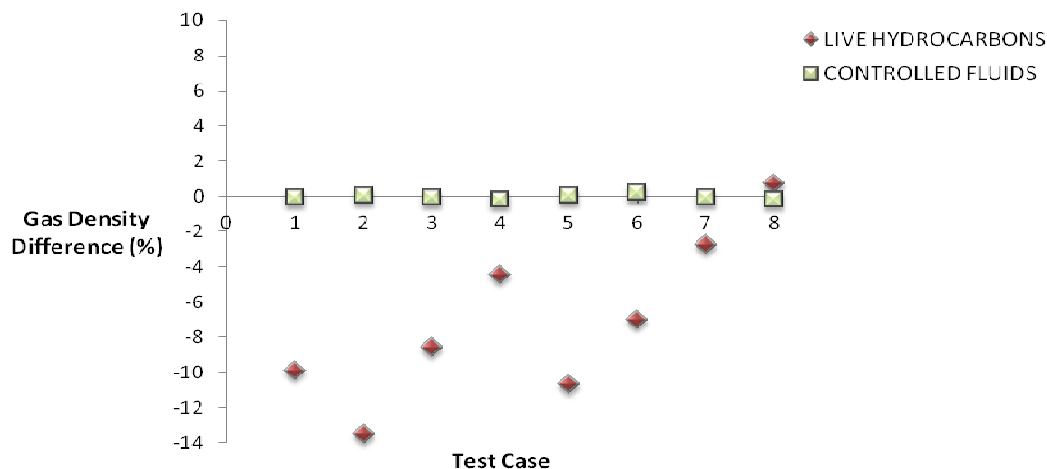


Fig 4 - Gas density difference for hydrocarbon and controlled fluids

## 8 RESULTS DISCUSSION

From initial observation of each test case, it is clear that the stability of controlled fluids far outweighs the stability of the live hydrocarbon fluids for all test cases. The live hydrocarbon test points improve as the conditions transition into the wet-gas regime. However, it should be noted that the PPDS solver will not account for flow pattern-based interaction effects that may also influence the mass transfer process.

The minimum gas density difference for controlled fluids was -0.04% for Test Cases 1B, 3B, 7B and maximum 0.22% in Test Case 6B. In comparison to the live hydrocarbons where the minimum deviation was 0.71% in Test Case 8A and maximum deviation of 13.54% in Test case 2A. As expected, increasing pressure increased the mass transfer of gas into liquid phase. Increasing temperature had the reverse effect, encouraging the flashing of gas from the liquid phase.

The PPDS results for the controlled fluids are in good agreement with the expected physical behaviour of these fluids, i.e. they are essentially immiscible, thus minimising errors due to mass transfer of components between phases. Using this approach largely eliminates the need to use EoSs to correct for any changes in fluid properties due to component mass transfers.

Whilst it is possible to account for the effects of component mass transfers between phases for a multiphase loop using live fluids by using EoSs, it should be noted that all EoSs will introduce their own errors. The magnitude of these errors will be a function of the combination of EoSs chosen, the test point conditions and the compositions of the hydrocarbon gas and liquid phases and the availability, if required, of binary interaction parameters for all the components.

As noted above, the PPDS package uses a combination of the Peng-Robinson (PR) EoS and Henry's Law to perform vapour-liquid-liquid equilibrium (VLE) calculations. The Peng-Robinson EoS generally performs well for mixtures containing relatively short chain hydrocarbon molecules and the use of Henry's Law is a reasonable approximation since the two liquid components will consist of

# **34<sup>th</sup> International North Sea Flow Measurement Workshop 25-28 October 2016**

## **Technical Paper**

a hydrocarbon-rich mixture with very little water and an aqueous phase with very little hydrocarbons.

Although the VLE calculations in PPDS can only use the PR/Henry's Law combination of models, it is possible to attempt to perform VLE calculations in two stages: the output liquid phase compositions from an initial VLE calculation are used as the inputs for a subsequent liquid-liquid equilibrium (LLE) calculation. Case 1A was examined in this manner, to assess the potential differences in calculated gas densities due to varying the EoSs used.

Applying the PR EoS to the input compositions at the specified temperature and pressure indicated that the system would be a single phase liquid only! Applying the Lee-Kesler-Plocker (LKP) EoS did predict a two phase, vapour + liquid system. For this calculation the difference in density of the gas phase from the superficial gas density was -4.83% but although this value is smaller than that from the full VLE calculation, it may have a larger uncertainty, as this VLE calculation does not properly account for the formation of three phases.

In the absence of measured data, it is therefore very difficult to assign realistic uncertainty estimates to the calculated fluid properties and hence it is better metrology practice to use a reference system that avoids this problem.

## **9 CONCLUSION**

It has been found that live fluids create significant additional uncertainties in fluid properties through phase interaction effects that could otherwise be assumed negligible when using controlled fluids. The significance of these effects can be subject to flowing conditions, where additional uncertainties may also arise in the choice of EoS. Ultimately, these effects alter the volume of each phase that has been assessed during single phase reference measurement and also changes fluid properties. The outright impact that unstable fluid properties and volume flow rate measurements may cause on a MPFM has yet to be explored, however, it can be expected that a significant change in phase concentration and fluid properties will have a significant effect on the quality of an MPFM dynamic test.

Controlled fluids showed much less sensitivity to changing conditions and align to the objectives of calibration best practice, ensuring stability of the transfer fluid across the full range of test cases and a resilience to changing properties across all test conditions. Without accurate qualification, the optimal baseline performance of MPFM's will be unknown. With the multiphase flow measurement sector looking towards high accuracy allocation and fiscal measurements, high accuracy meter qualification must be performed. This means ensuring that you can accurately determine the characteristics of the transfer fluid, as changes from its state following reference metering could result in substantial errors and the incorrect assessment of the MPFM in question.

**34<sup>th</sup> International North Sea Flow Measurement Workshop  
25-28 October 2016**

**Technical Paper**

**10 REFERENCES**

- [1] NFOGM. 2005. *Handbook of Multiphase Flow Metering*.
- [2] Guidance Notes for Petroleum Measurement, Issue 9.2. Oil and Gas Authority, Aberdeen, October 2015.
- [3] K Folgerø, et al.,. *Uncertainty analysis of multiphase flow meters used for allocation measurements: Field experiences and future challenges*. 31st International North Sea Flow Measurement Workshop. 22–25 October 2013
- [4] API Committee on Petroleum Measurement and Allocation. 2013. *Chapter 20.3 Measurement of Multiphase Flow*
- [5] ISO/IEC Guide 98-3:2008. *Uncertainty of measurement. Part 3: Guide to the expression of uncertainty in measurement (GUM:1995)*
- [6] NEL PPDS. Thermodynamic properties software packages and databases. [www.ppds.co.uk](http://www.ppds.co.uk).
- [7] ISO 12213-2, *Natural Gas Calculation of Compression Factor: Part 2 Molar Calculation (AGA8)*.

## Technical Paper

### **Analysis of field and ownership allocation uncertainty in complex multi-field configurations**

**Ranveig Nygaard Bjørk<sup>1</sup>**  
**Astrid Marie Skålvik<sup>1</sup>**  
**Armin Pobitzer<sup>1</sup>**  
**Eivind Nag Mosland<sup>1</sup>**  
**Camilla Sætre<sup>1</sup>**  
**Kjell-Eivind Frøysa<sup>1,2</sup>**

<sup>1</sup>Christian Michelsen Research, Norway  
<sup>2</sup>Bergen University College, Norway

---

#### **ABSTRACT**

Current focus on cost-effective developments of new hydrocarbon fields aims at exploiting the capacity of existing production units to the maximum using a number of tie-ins to subsea developments. This results in increasingly complicated process flows, where individual multiphase streams may or may not be measured. This increased complexity makes design and analysis of allocation systems a challenging task.

Allocation principles, metering system setup, use of test separator time, ownership structure, flow rates and life time profiles are all factors which affect the field and ownership allocation uncertainty. In order to find how each field or each owner is exposed to economic risk associated with measurement and allocation uncertainty, an uncertainty analysis combined with a risk-cost-benefit analysis should be carried out. Traditionally, the analysis of such allocation systems is based on analytic calculations. These calculations increase rapidly in complexity as the process flow becomes more complicated. For systems with several tie-ins and satellites, and with a fragmented ownership, powerful numerical methods are required to perform this analysis.

This paper demonstrates the **calculation of field and ownership allocation uncertainty** for realistic measurement setups and allocation scenarios in a multi-field setting based on industrial projects. A flexible framework for analysis of complex multi-field configurations is used in these numerical calculations, which are based on an ISO GUM (ISO/IEC, 2008) compliant Monte Carlo technique.

# 34<sup>th</sup> International North Sea Flow Measurement Workshop 25-28 October 2016

## Technical Paper

Further on, **it is demonstrated how different field configurations, ownership structures, allocation principles, meter uncertainties and flow rates affect the total cost and risk for each owner.** This investigation includes the exposure to **economic risk associated with measurement uncertainty** associated with the different alternatives. We also give examples of how the **lifetime cost** of the metering system may vary depending on choices in **allocation principle, flow rate profiles, as well as placement and calibration** scheme of the individual meters. A particular focus of our work is how each owner is exposed to misallocation risk. In this context it is mandatory to take into account the **correlation** between the uncertainties in the field-allocated streams. Failure to include these correlations may result in erroneous estimations of each owner's economic exposure due to misallocation, and may thus potentially result in sub-optimal field developments.

Through **realistic example systems based on industry projects**, it is shown how an **uncertainty analysis** combined with a **risk** analysis may provide valuable insight into the exposed economic risk for each owner due to misallocation. It is demonstrated how thorough knowledge and understanding of the allocation uncertainty is essential in order to minimize each parties' economic exposure, especially in real-life complex allocation systems.

## 1 INTRODUCTION

The aim of this paper is to demonstrate the calculation of field and ownership allocation uncertainty for realistic measurement setups and allocation scenarios in a multi-field setting based on industrial projects. Allocation uncertainty entails a financial risk in the form of an exposure to losses due to misallocation as discussed in Section 2.

In order to estimate these allocation uncertainties correctly, thorough knowledge and understanding of the allocation uncertainty is essential. The field allocation uncertainty is influenced by a number of parameters: Metering station uncertainties (or uncertainty related to performance curves in the cases where no metering station is installed), use of test separator time, production profile, fluid composition, uncertainty in process parameters, system topology and the allocation principles agreed upon among other things.

Recognising that the field allocation uncertainty may differ significantly from the individual metering station uncertainties, it is essential to have correct and effective methods for estimating this uncertainty. As there are many influencing parameters as exemplified above, these calculations increase rapidly in complexity and powerful numerical methods are required to perform this analysis. In this paper

# **34<sup>th</sup> International North Sea Flow Measurement Workshop 25-28 October 2016**

## **Technical Paper**

we present a flexible framework for such an analysis based on an ISO GUM [1] compliant Monte Carlo technique as shown in Section 3.

For many companies dealing with fiscal measurements of hydrocarbons, the overall question is what economic risk their company is exposed to. In order to answer this question, the ownership uncertainty must be estimated and based on this, the risk each owner is exposed to may be evaluated. When estimating the ownership uncertainty, it is mandatory to take into account the correlations between the field allocated quantities. These correlations stem from the chosen allocation setup itself and may significantly influence the ownership uncertainty. This topic is further discussed in Section 4.

In Section 5 we show a number of examples illustrating the financial risk in the form of an exposure to losses due to misallocation as a direct consequence of metering uncertainty, flow rates and allocation principles. We illustrate important concepts in small, constructed systems before analysing a real-life complex allocation system.

Regarding the notation applied throughout this paper, we refer the reader to section 7.

Beyond illustrating exposed economic risk for each owner due to misallocation through realistic example systems based on industry projects, this paper has three main messages:

- The field allocation uncertainty will in many cases differ significantly from the individual metering station uncertainties (dependent on the system setup).
- In most real life setups, it is not intuitive to decide which owner(s) that are most exposed to economic loss due to misallocation.
- It is mandatory to take into account the correlation between the uncertainties in the field-allocated streams in order to estimate the owner allocation uncertainty correctly.

## **2 ECONOMIC RISK DUE TO ALLOCATION UNCERTAINTY**

In estimating the allocation uncertainty of a system, several metering station uncertainties are included. Typically, one of them is an export measurement with low uncertainty, while others may be multiphase measurements with higher uncertainties or stem from performance curves with even higher uncertainties.

If a fiscal measurement result is different from the "true" value, then erroneous numbers are used in the allocation calculations, and the allocated quantities to each well or each field will thus also be erroneous. One possible consequence of this may be that decisions regarding field development are taken based on flawed information, which in the end may result in a less optimal field exploitation.

Another possible consequence, which we discuss in this paper, is the possibility of inaccurate allocation of revenue between the various owners. Thus each owner is exposed to an economic risk associated with measurement and allocation uncertainty, also referred to as potential loss due to misallocation.

# 34<sup>th</sup> International North Sea Flow Measurement Workshop 25-28 October 2016

## Technical Paper

The risk of an undesirable event is commonly quantified by the loss associated to the event multiplied by its probability [2]. The key undesirable event in allocation systems is misallocation, or perhaps more precisely under-allocation, due to allocation uncertainty.

In [3], Philip Stockton demonstrates one way of quantifying the economic risk associated with allocation uncertainty. The definition of economic risk in equation (1) is based on [3], given here with slightly modified notation:

$$R = \frac{U \cdot V}{k \cdot \sqrt{2\pi}} \quad (1)$$

In Equation (1),  $R$  represents the exposure to lost revenue of a quantity with an associated uncertainty, illustrated by the yellow part of Figure 1.  $U$  is the absolute expanded uncertainty of the quantity,  $k$  the coverage factor for the given confidence level, and  $V$  is the value per unit of the quantity. For oil volume allocation,  $U$  could be the absolute expanded uncertainty of oil volume in barrels, and  $V$  the oil price per barrel. Simply explained, this equation comes from assuming that the allocated quantity has a normal distribution, and then integrating this distribution from the mean allocated value to minus infinity. This is illustrated in Figure 1.

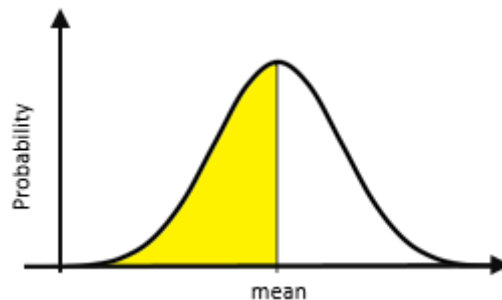


Figure 1: Illustration of principle for calculating economic risk associated with allocation uncertainty.

A common misconception is that “you lose some, you win some”, i.e. that misallocation related to allocation uncertainty will “even out” after a while. Stockton [3, pp. 3-5] explains thoroughly how the assumption that uncertainty “even out” over time is erroneous in most cases and the examples below are based on the same paper.

**Masking of systematic errors/meter bias:** One reason why the uncertainty may not “even out” after a while is that a high uncertainty may mask a systematic error. If the uncertainty of a metering station for instance is 10 %, it may be difficult to detect a systematic error of for instance 2 %. If the value of the product flowing through this metering station is for example 100 000 USD/day, this masked, uncorrected systematic error would result in a daily economic loss of 2 000 USD/day.

**Allocation bias:** Let A and B be two fields producing 100 units each per day. Allocation follows the pro rata principle. Field A’s production and the export measurement have a negligible uncertainty and Field B has an uncertainty of 10 %.

# 34<sup>th</sup> International North Sea Flow Measurement Workshop 25-28 October 2016

## Technical Paper

The first day 110 units are measured from Field B, and  $\frac{110}{100+110} \cdot 200 = 104.8$  units are allocated to Field B. The next day 90 units are measured, and only  $\frac{90}{100+90} \cdot 200 = 94.7$  units are allocated to Field B. Even though the sum measured at Field B the two days equals 200, only  $104.8 + 94.7 = 199.5$  units are allocated to Field B. This equals a systematic under-allocation of 0.25 %. Note that this under-allocation is systematic, meaning that statistically 0.25 % of Field B's allocation is allocated to Field A instead, and the owner of field B will not be paid for 0.25 % of the fields production.

### 3 CALCULATION OF FIELD ALLOCATION UNCERTAINTY

As explained in section 2, the potential loss due to misallocation is a direct consequence of allocation uncertainty which in turn is dependent on uncertainties of measurements and/or flow estimation. It is thus essential to estimate the allocation uncertainty in a proper manner. Note that the allocation uncertainty for a field or tie-in is often different from the field metering station uncertainty, as illustrated in Figure 2. The reason for this is that the other uncertainties in the system affect the allocation uncertainty of each field, through the allocation calculations. An exception to this is the case of by-difference allocation, here all fields with measurements have an allocation uncertainty equal to their measurement uncertainty.

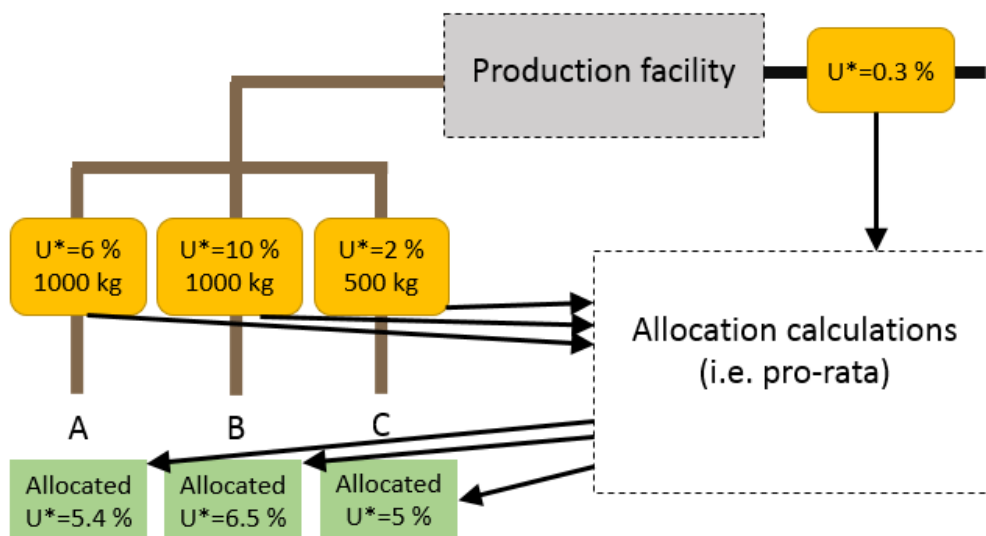


Figure 2: Illustration showing that field allocated uncertainty is in most cases not identical to the field measurement uncertainty. The allocation uncertainty depends on the other uncertainties in the allocation system, the flow rates and the allocation principle. In the figure  $U^*$  denotes the relative expanded uncertainty of the measured and allocated quantities.

The uncertainty in field allocated quantities can be calculated using analytical or numerical methods. For straightforward allocation systems with few tie-ins and a limited number of gas lifts as well as water or gas injections, it is possible to calculate the allocation uncertainties using an analytic approach. This is done by writing down all allocation calculations, performing partial derivatives of all input

**Technical Paper**

parameters and then calculating the combined uncertainty according to the method described in ISO GUM [4].

However, as the process flow becomes more complicated, these calculations increase rapidly in complexity. For systems with several tie-ins and satellites, as well as several gas lifts or water or gas injections, the analytic approach may be time-consuming and difficult to achieve. It is therefore advantageous to apply more powerful numerical methods to calculate the allocation uncertainties. Supplement 1 to ISO GUM [1], describes how the propagation of uncertainties through a system may be calculated using a Monte Carlo method.

In this section, we show how an **ISO GUM-compliant Monte Carlo method** may be used to calculate allocation uncertainties. Easily explained, we model each input parameter by a probability distribution instead of only one value. The standard deviations of these distributions are set based on the uncertainty of each of the parameters. The distributions are then combined and commingled according to the allocation calculations, and the standard deviations of the resulting distributions indicate the uncertainty of the allocated quantities. Figure 3 illustrates this method.

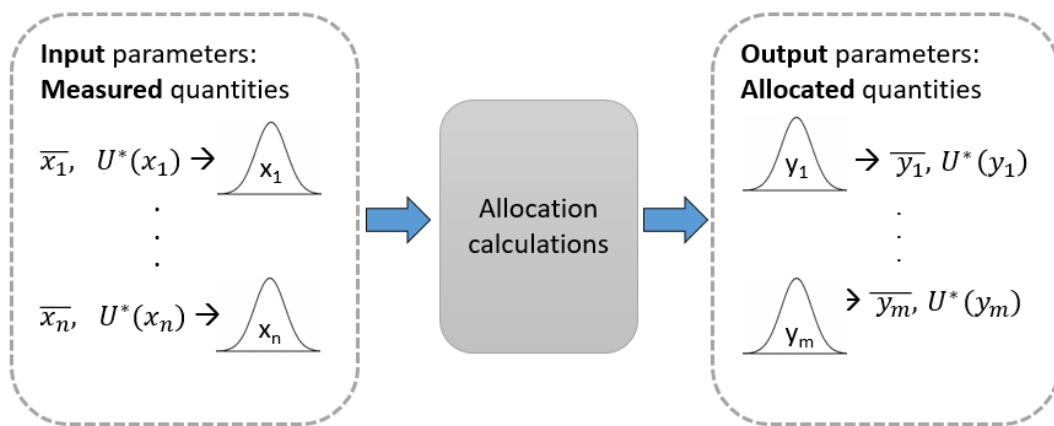


*Figure 3: Illustration of a Monte Carlo based method for calculating allocation uncertainties. Whereas the input distributions are depicted as normal distributions in the figure, this is not a requirement for using the Monte Carlo method. In the figure  $U^*(x_i)$  symbolizes the relative expanded uncertainty of a quantity  $x_i$ , and  $\bar{x}_i$  its average value. Similar symbolism applies to  $y_i$ .*

The **major advantages** of using a numerical Monte Carlo (MC) approach, as compared to the analytical calculations, are the following:

- More complex allocation systems can be analysed using the MC approach, while the analytical approach is laborious and cumbersome for complex systems.
- The analytical approach is based on the assumption that the input parameters follow normal distributions, which are linearly combined in order to produce the output distributions. Using the MC approach, none of these assumptions are required.
- Any correlations between input parameters are easily taken into account by generating correlated input distributions.

The field allocation uncertainty gives valuable information regarding how each *field* is exposed to economic risk. In our context, each field may consist of several

# 34<sup>th</sup> International North Sea Flow Measurement Workshop 25-28 October 2016

## Technical Paper

satellites and tie-ins which in turn may have a number of owners. For each of these owners, the most interesting question to highlight is the economic risk to *their* particular company in the overall picture. In order to examine this question, we need to estimate the ownership allocation uncertainty. This is the topic of section 4.

### 4 OWNERSHIP ALLOCATION UNCERTAINTY

In order to evaluate the risk each owner is exposed to, it is necessary to find the ownership allocation uncertainties. In cases with only one single owner of each field, the ownership allocation uncertainty coincides with the field allocation uncertainty. In reality, a more fragmented ownership structure is often the case, due to more complex field development with several tie-ins and satellites.

#### 1.1 The intuitive method is often incorrect

When allocating the total exported production between the various owners, the various field production streams are multiplied with the ownership matrix. A common misconception is that the same can be done with the field allocation uncertainties in order to find the ownership allocation uncertainties. However, if one simply multiplies the field allocation uncertainties with the corresponding ownership fractions, and add the resulting uncertainties together for each owner, there is an indirect, often incorrect, assumption that all field allocated uncertainties are correlated with a correlation coefficient of +1. Following the method for combining correlated uncertainties as described in ISO GUM [4], this intuitive but erroneous method can be written as:

$$U_{owner\ 1} = F_{field\ A}^{owner\ 1} \cdot U_{field\ A} + F_{field\ B}^{owner\ 1} \cdot U_{field\ B} \quad \leftarrow \text{assumes } r_{A,B} = +1 \quad (2)$$

Here  $F_{field\ y}^{owner\ x}$  is the ownership fraction for owner  $x$  in field  $y$ .  $U^*$  symbolizes relative expanded uncertainty of the quantity allocated to a field or to an owner and  $Q_A$  and  $Q_B$  are the measured productions of Field A and B respectively.

Another possible way of estimating the ownership uncertainty which might seem intuitive at first glance is to compute the sum of squares of the allocated quantities:

$$U_{owner\ 1} = \sqrt{(F_{field\ A}^{owner\ 1} \cdot U_{field\ A})^2 + (F_{field\ B}^{owner\ 1} \cdot U_{field\ B})^2} \quad \leftarrow \text{assumes } r_{A,B} = 0 \quad (3)$$

However, this approach is based upon the assumption that all field allocated uncertainties are uncorrelated which is often not the case.

#### 1.2 Correlation between field allocated streams due to allocation equations

In real-life systems, the correlation coefficients between the various fields are seldom +1 or zero, and can even be negative in many cases. The correlation comes from the allocation principle itself; the sum of the production allocated to each field must equal the exported production. In most cases, the export metering station from the cluster of fields has a lower metering uncertainty than the meters

# 34<sup>th</sup> International North Sea Flow Measurement Workshop 25-28 October 2016

## Technical Paper

measuring the production from the individual satellite fields to the mother field. This is due to the fact that while the export production is separated and then measured using single phase meters, the different field streams are often measured using multiphase meters, or single phase meters after 1<sup>st</sup> stage separators with more or less incomplete separation. The production from a field may also just be estimated based on individual well measurements and performance curves, which may result in an even higher uncertainty.

Consider a simplified allocation system with two fields A and B. If too much production is allocated to Field A, then it logically follows that too little is allocated to Field B, as the sum of the two field allocated streams must equal the measured export production. In other words, the allocated production between fields A and B have negative correlation.

### 1.3 Correlation between streams due to correlation in input parameters

The field allocated streams may also be correlated due to correlation in the measurement instrumentation or in the performance curves used to estimate field production. Flow meters used at different points in the measurement system that have been calibrated at the same flow laboratory or with the same prover may have correlated measurement uncertainties.

Another example is that flow meters based on the same measurement technology may have the same deviations due to changes in flow profile, scale build-up etc. For these cases, if one meter is under- or overestimating the flow, then a meter with similar technology or shared calibration facilities, in general may be expected to deviate in the same direction. A similar behaviour may be expected for performance curves based on the same model. The correlation coefficients between different meters and modelling uncertainties are therefore often positive.

Using the proposed numerical Monte Carlo-framework, it is straightforward to generate correlated input distributions.

### 1.4 Different methods for including correlations in the ownership allocation calculations

The correlations between the various field allocated streams must be taken into consideration in order to obtain a proper estimate of the ownership allocation uncertainty. This can be done using different methods:

- Analytically: Write down the ownership allocation equations so that the production allocated to each owner is expressed directly from the input parameters and measurements together with the ownership matrix.

$$U_{owner\ 1}^* = f(\text{input measurements, ownership fractions}) \quad (4)$$

This method gives valuable insight into what drives the allocation uncertainty for each owner, but the analytical calculations are intricate and time-consuming.

# 34<sup>th</sup> International North Sea Flow Measurement Workshop 25-28 October 2016

## Technical Paper

- Calculate the correlation coefficients between the various field allocated streams either analytically or numerically, and then calculate the ownership allocated production using the method described in ISO GUM [4] :

$$(U_{owner\ 1}^*)^2 = (F_{field\ A}^{owner\ 1} \cdot U_{field\ A}^*)^2 + (F_{field\ B}^{owner\ 1} \cdot U_{field\ B}^*)^2 + 2r_{A,B} \cdot F_{field\ A}^{owner\ 1} \cdot U_{field\ A}^* \cdot F_{field\ B}^{owner\ 1} \cdot U_{field\ B}^* \quad (5)$$

- Multiply the field allocated distributions with the ownership matrix, and find the ownership allocation uncertainties from the resulting distributions as in a Monte Carlo approach:

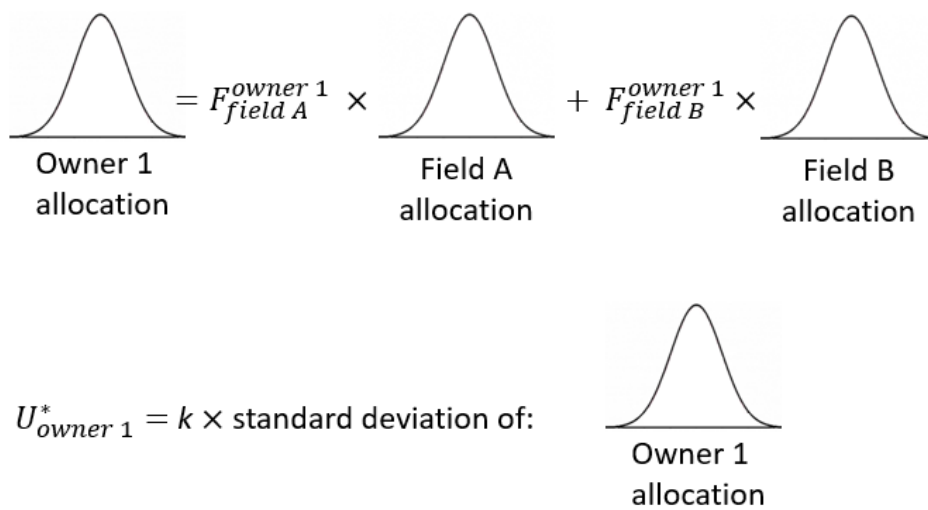


Figure 4: Illustration of how the correlation between field allocated quantities can be taken into account by multiplying the ownership fractions with the allocated field distributions. In the figure,  $U^*$  symbolizes relative expanded uncertainty of a quantity,  $F$  symbolizes ownership fraction and  $k$  is the coverage factor applied to estimate the expanded uncertainty. For the standard normal distribution at 95 % confidence interval this factor equals 1.96.

As described in chapter 3, the field allocated distributions are output from the numerical allocation calculations we use in this paper. In the examples presented in this paper, we have therefore applied the third method where the field allocated distributions are directly multiplied with the ownership fractions. Note however that if the calculations are carried out correctly, all the three different methods above are expected to produce the same results<sup>1</sup>.

## 5 ANALYSIS OF COMPLEX MULTI-FIELD CONFIGURATIONS BASED ON REAL LIFE SYSTEM

In order to illustrate the principal effects related to how different field configurations, ownership structures, allocation principles, meter uncertainties and flow rates affect the total cost and risk for each owner we start out by a small, simplified example. This is done for educational purposes in order to highlight the

<sup>1</sup> This is true for a linear system with normal distributions.

**Technical Paper**

effect of specific parameters. We then proceed to a larger real-life system illustrating the real usefulness of such an analysis framework in situations where a manual cost-benefit analysis becomes tedious. The numerical Monte Carlo based framework applied for analysis of these multi-field configurations is shown in Figure 5. In this illustration there are three hydrocarbon streams, one multiphase metering station (MPFM), one virtual flow metering station (VFM) in addition to export oil and gas metering stations and a production facility. The figure illustrates the process of performing allocation calculations including allocation uncertainty and the transition to ownership allocation.

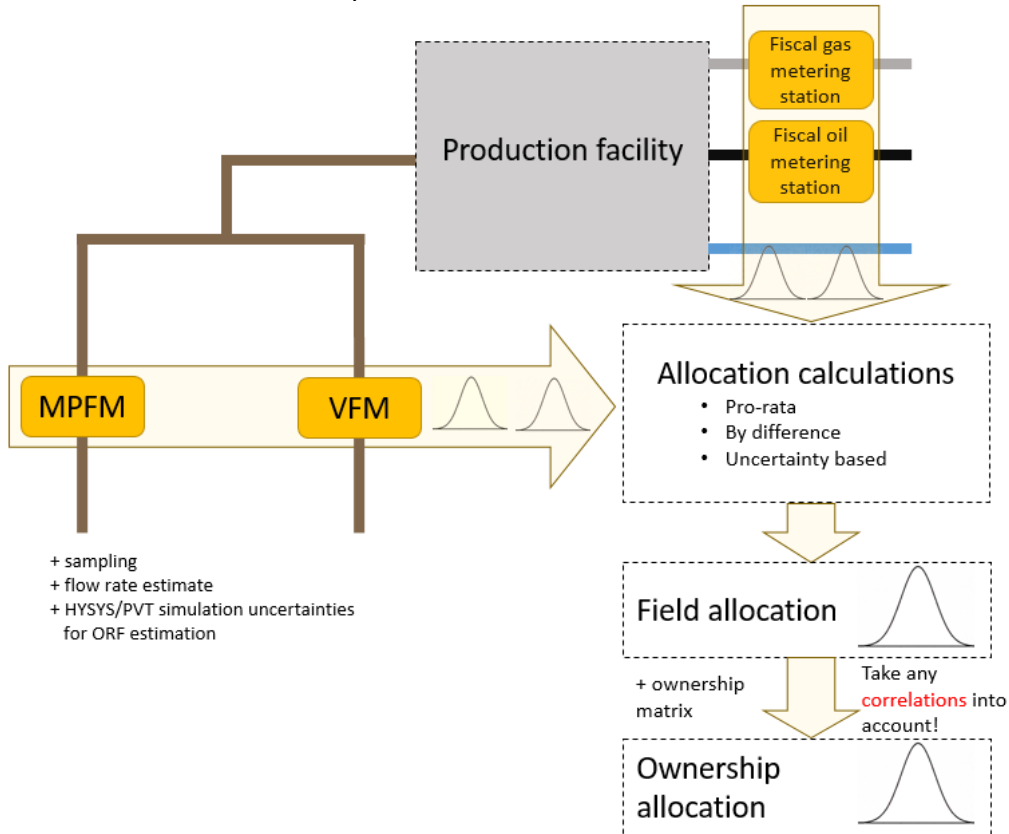


Figure 5: Illustration of the numerical Monte Carlo based framework applied for analysis of multi-field configurations in this paper. This simple setup includes one multiphase metering station (MPFM), one virtual flow metering station (VFM) in addition to export oil and gas metering stations and a production facility. ORF is short for Oil Recovery Factor and specifies expected oil fraction of the total hydrocarbon mass at the output of the production facility. The measurement setup is chosen for illustration purposes only.

**2.1 Simple case**

Our first example is a simple allocation system that originally consists of two hydrocarbon sources, Field A and Field B, that are commingled before processing. Field A has metering station with the specified relative uncertainty  $U_A^*$ . Field B is not measured separately. The commingled stream is processed and separated in a production facility before the separated oil and gas streams are measured by single-phase export meters. The amount of hydrocarbons measured by the export meters is allocated by difference to the individual fields and owners.

# 34<sup>th</sup> International North Sea Flow Measurement Workshop 25-28 October 2016

## Technical Paper

A new tie-in, Field C, is planned to connect and share the production facility. The new tie-in will have a separate metering station with a specified relative metering uncertainty  $U_C^*$ .

As Field C is connected, the exposure to economic risk will change for the fields A and B and thus for the owners of Field A and B. Two options are considered for Field B after Field C is connected as illustrated in Figure 6:

- Continue with the same metering setup and apply by-difference allocation
- Install a new metering station at Field B and convert to pro rata allocation

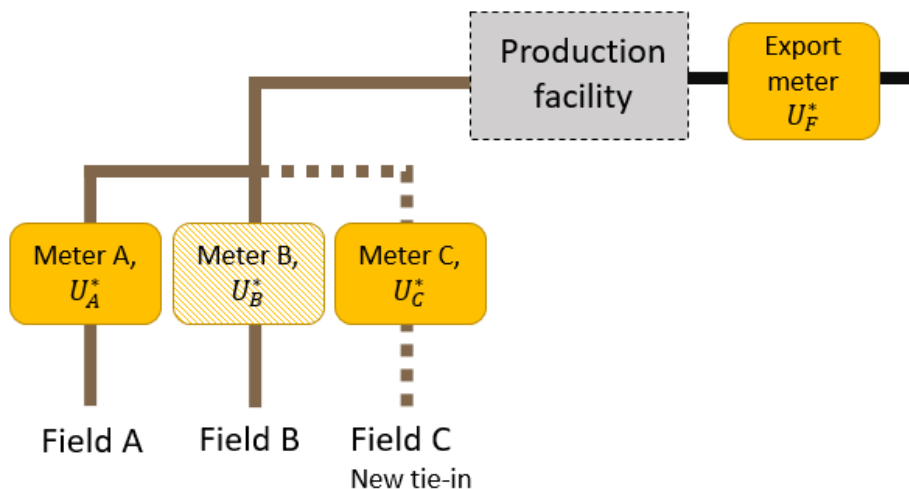


Figure 6: Illustration of simple case setup with fields A and B and the new tie-in, Field C. After the new tie-in two options are considered for Field B: 1) Continue with the same metering setup and apply by-difference allocation or 2) Install a new metering station and convert to pro rata allocation.

In order to make the decision as to whether or not a metering station should be installed at Field B, it is useful to investigate how the economic risk changes for Field A and B and the owners of these fields as a consequence of the new tie-in. It is important to do so in a proper manner in order to have solid decision support in evaluating the options for Field B. Here it is worth mentioning that the decisions made for Field B regarding metering setup will most likely affect all the owners of Field A, B and C regardless of whether they are shareholders in fields B or not.

The production profile for each field is modelled according to [5] and are shown in Figure 7 for the fields A, B and C. The two original fields have a production profile such that peak production is 20 million and 360 million tons/year for fields A and B, respectively. The tie-in ratio (Field C) is based on an estimate of total exploitable resources amounting to 50 billion tons. It is drilled a total of 15 wells with a capacity of 50 million tons each, and the field is put in production when eight of them is completed. The remaining wells are completed within three years.

## Technical Paper

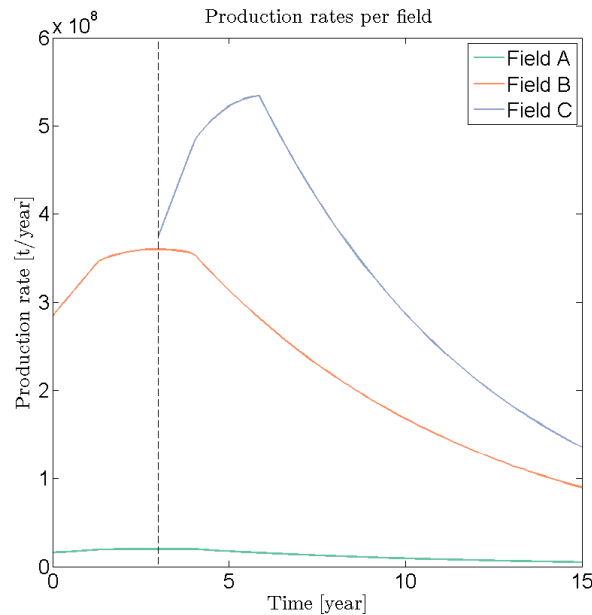


Figure 7: Production rates of the fields A and B and the new tie-in, Field C, used in this example. The dashed vertical line indicates the start-up time for Field C.

We consider five different scenarios. In the first scenario no metering station is installed at Field B and the allocation is performed by difference. In the remaining scenarios, a metering station is installed at Field B and allocation is performed using the pro rata allocation principle. The relative expanded uncertainties of the metering station installed on stream B for the different scenarios are 1%, 5%, 10% and 15% percent. The relative expanded uncertainty of the export station is set to 0.25% while the metering stations at A and C have a 5% relative expanded uncertainty. The metering station uncertainties will be dependent on both the specified uncertainty of the specific meter as well as the chosen calibration and maintenance scheme.

Uncertainty and risk are calculated over a 15 years period using the framework described in [6], based on the production profiles for the three fields shown in Figure 7.

### 2.1.1 Uncertainty in field allocation

The results of the calculations reported as relative expanded uncertainty per field are shown in **Error! Reference source not found.** We observe that the transition from the by difference to the pro rata allocation principle proves disadvantageous for the allocation uncertainty of Field A, regardless of the quality of the metering station installed to measure stream B. The allocation uncertainty of Field B, on the other hand, clearly benefits from the transition in all cases but case 5 (i.e. 15 % uncertainty). As a matter of fact, in this particular example the allocation uncertainty for Field B is worse than if using by difference allocation. This illustrates that installing additional metering stations does not necessarily improve the allocation uncertainty, neither for the measured stream, nor for others. Like Field A, the allocation uncertainty in Field C, i.e. the tie in, is also effected by the choice of metering station on stream B, but unlike for Field A, the effect may be beneficial compared with a by difference approach (1 % and 5 % cases) partly

Technical Paper

beneficial (10 %) or disadvantageous (and 15 % cases), depending on the quality of the installed meter.

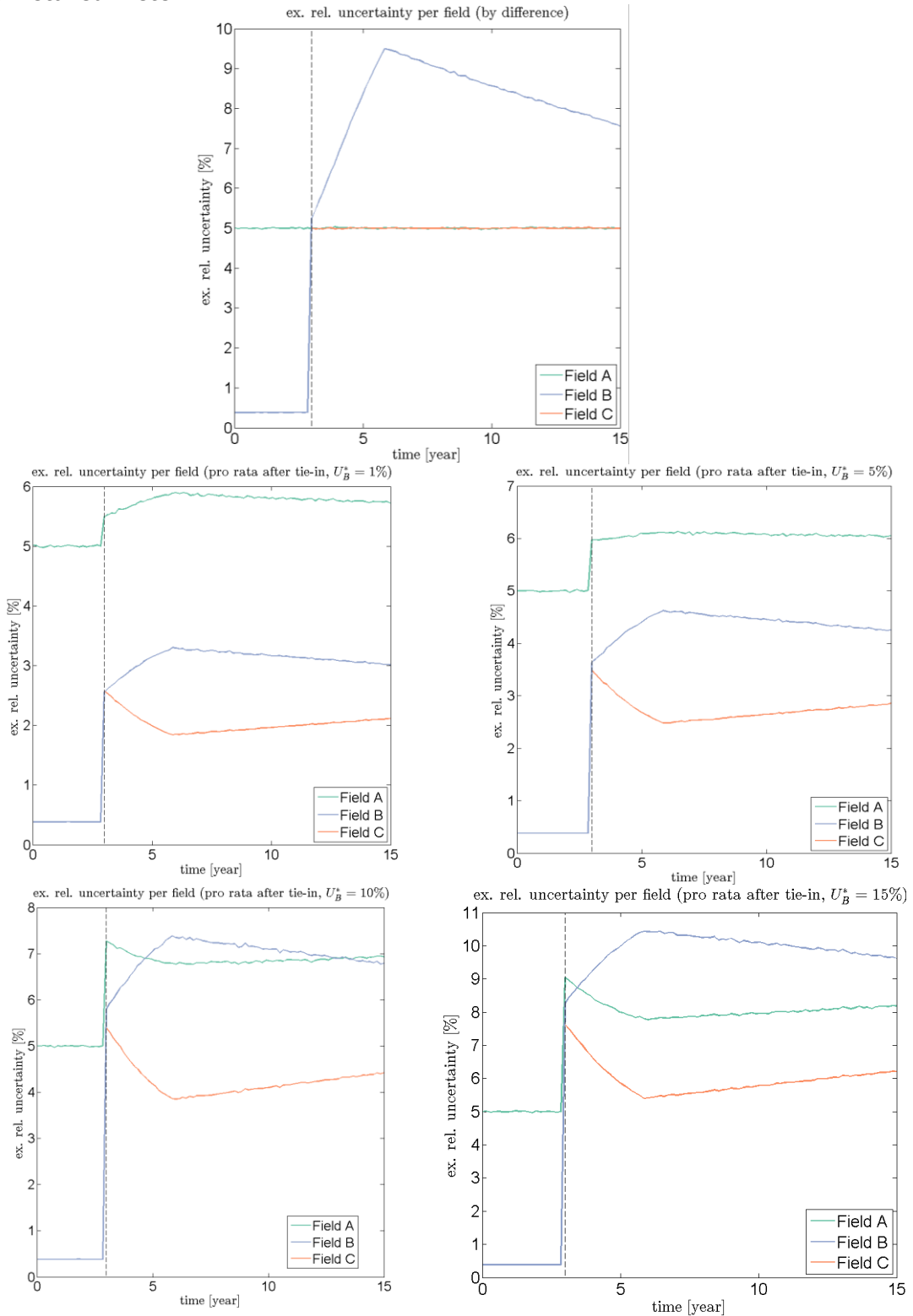


Figure 8: Development of relative expanded uncertainty per field over life time. The top panel gives the uncertainty using by difference allocation after the tie in, while the remaining four describe the uncertainty using pro rata allocation with different uncertainties of the meter installed on stream B.

**Technical Paper**

**2.1.2 Uncertainty in ownership allocation**

As outlined in the introduction to this example, the underlying business case is the need to decide whether or not to install a metering station on stream B, and, if yes, which uncertainty this metering station ought to have. The installation of a metering station entails an upfront investment (CAPEX) and running cost (OPEX) to which one or several owners of the involved fields need to commit. We assume a fragmented ownership for the fields A, B and C as shown in Table 1 and shall investigate the case from the different owners' point of view. Note that for Field B there are additional owners, that are not included in this discussion. Owner 1 owns the majority of a marginally contributing source (Field A) while Owner 2 holds larger shares in the main source of the original fields (Field B), while Owner 3 controls the tie in, estimated to produce more than the other two fields.

**Table 1: Ownership matrix illustrating the ownership for Owner 1, Owner 2 and Owner 3 in the fields A, B and C.**

	Field A	Field B	Field C
<b>Owner 1</b>	75 %		
<b>Owner 2</b>	25 %	50 %	
<b>Owner 3</b>			100 %

We recall from the plots in the previous section that Field B experiences a quite dramatic increase in allocation uncertainty due to the tie in. Hence, it may seem reasonable to assume that Owner 2 is the party that would benefit the most from the installation of an additional metering station. Converting the relative uncertainty to economic risk using Equation (1) shows, however, that Owner 3 is most exposed to risk and would have the largest risk reduction (cf. Figure 9 for a comparison of by difference and pro rata with  $U_B^* = 10\%$ ) if a metering station is to be installed. Hence, Owner 3 may be interested in contributing to the investment.

Owner 1, on the other hand, will experience an increased risk if a metering station is installed and may therefore be reluctant to accept such a modification. The total value of this risk is, however, so small compared to the possible benefits of the other owners that compensating Owner 1 may be a reasonable option.

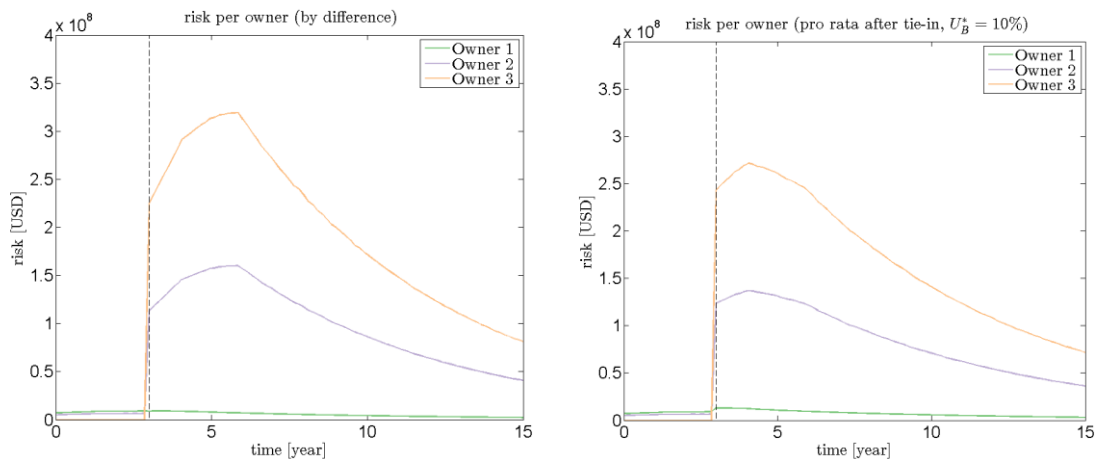


*Figure 9: Development of risk over time per owner in USD. The relative expanded*

# 34<sup>th</sup> International North Sea Flow Measurement Workshop 25-28 October 2016

## Technical Paper

uncertainty of metering station B is set to 10% in the left plot. An oil price of 60 USD is assumed.

From Figure 9 it becomes apparent that also the temporal evolution of the risk ("peak risk" in year 7 with by difference allocation vs. "peak risk" in year 4 with pro rata, and similar risk values for the three owners in year 15) changes depending on the chosen solution and the metering solutions need to be assessed from a lifetime perspective. Figure 10 shows the accumulated risk for each owner after 15 years,. The difference in risk between different metering solutions is a quantifiable benefit of one solution over the other and may as such be used in the decision making process. In order to make a fair assessment it is important to keep in mind at this point that the CAPEX and OPEX of different metering stations will vary depending on the specifications of the metering station and the maintenance and calibration scheme chosen. This risk calculation also prepares the foundation for full cost-benefit analysis including CAPEX and OPEX as described in [6] and can be extended to include other types of risk as in [7].

We have chosen not to include the full cost-benefit analysis in this paper as the CAPEX and OPEX may vary significantly from one setup to another, nor is it essential for the main results of this paper.

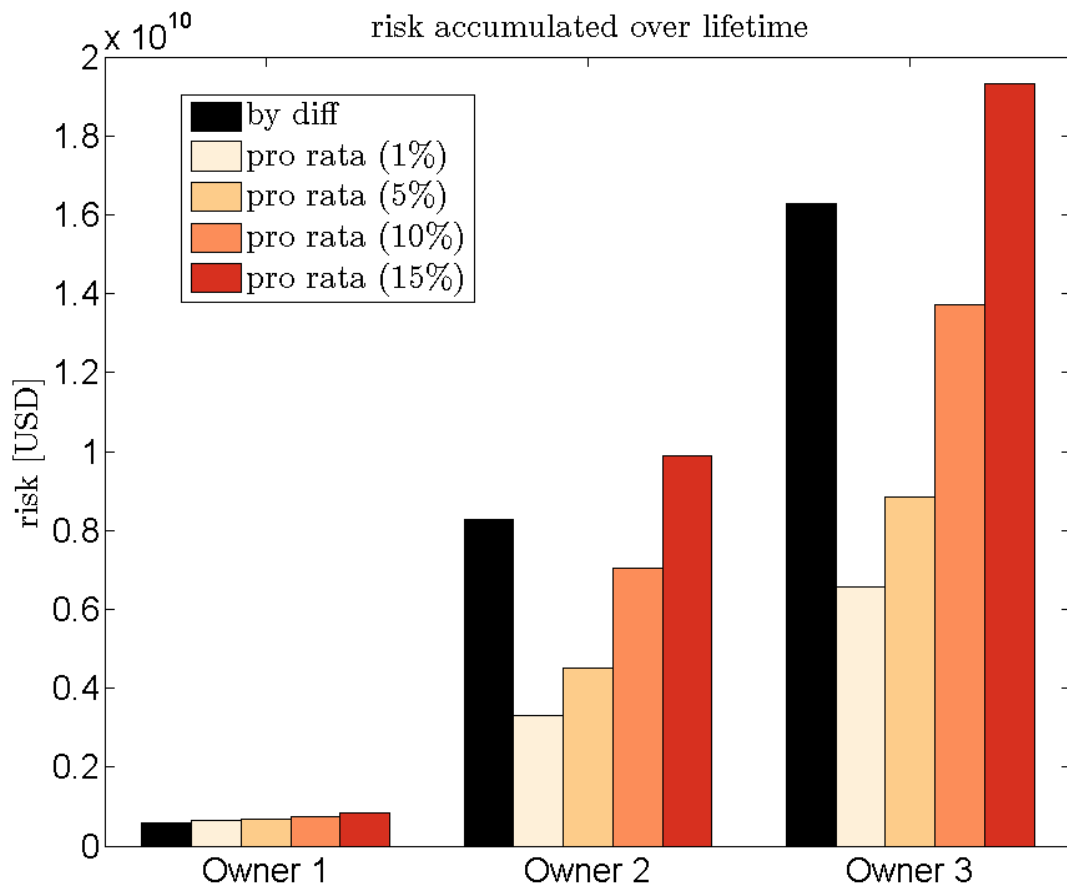


Figure 10: Risk associated with allocation uncertainty per owner accumulated over lifetime with different metering setups. The relative expanded uncertainty for the export metering station is set to 0.25 % (95 % confidence interval) in all cases. An oil price of 60 USD per barrel is assumed. The uncertainty numbers and oil price used in the different scenarios are chosen for illustration purposes only.

# 34<sup>th</sup> International North Sea Flow Measurement Workshop 25-28 October 2016

## Technical Paper

### 2.2 Realistic example system based on industry projects

In order to illustrate the real usefulness of our analysis framework we present results from a realistic example system based on industry projects. We show how an uncertainty analysis combined with a risk analysis may provide valuable insight into the exposed economic risk for each owner due to misallocation. Note that the example setup presented in this section is modified from the real industry setup and that all numbers are example numbers in order to anonymize the data.

A simplified sketch of the example setup is shown in Figure 11. There are two existing fields: Field A is processed through a 1<sup>st</sup> stage separator before the oil and gas streams are measured by single phase meters and then passed on to a production facility. Field B is not measured separately before being processed in the production facility. At the output of the production facility the separated streams of oil and gas are measured by export meters. The oil and gas measured by this export meter is allocated by difference to the individual fields A and B, and the respective owners. Samples are taken regularly at the inlet of each field, as well as at the export station. The allocation is performed on component level and HYSYS simulations are performed in order to estimate the component oil recovery factors, including their uncertainty. There are also facilities for gas lift and water injection not shown in this simplified setup.

The new tie in, Field C, is planned to connect and share the production facility. The new tie-in is planned to have a dedicated metering station based on a multiphase meter and sampling.

The shareholders in the system are concerned about how this new tie-in will affect their exposure to economic loss. Should they take the cost of installing a separate metering station at Field B and convert to pro rata allocation? Who should be committed to take part in this investment? What is the correct procedure to uncover the exposure to economic loss for the owners in these fields?

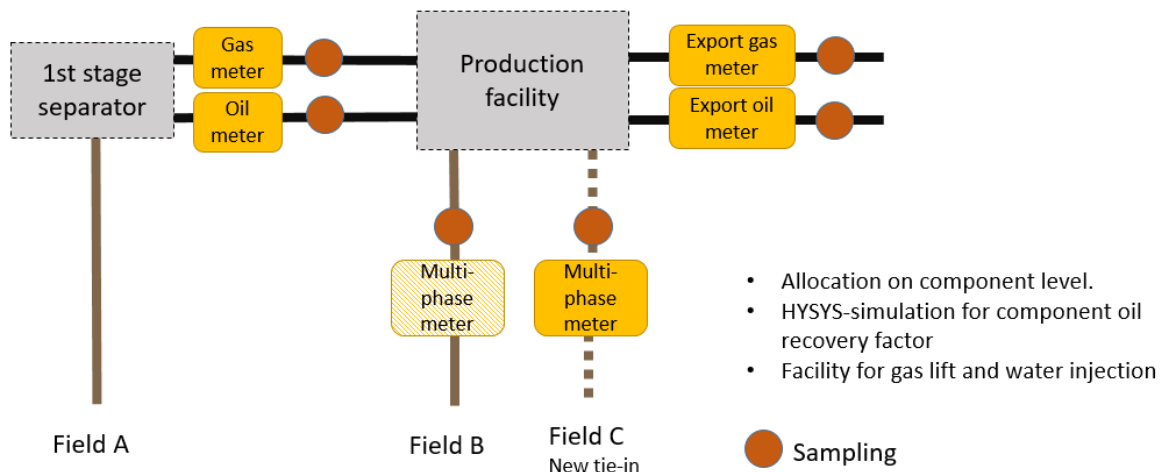
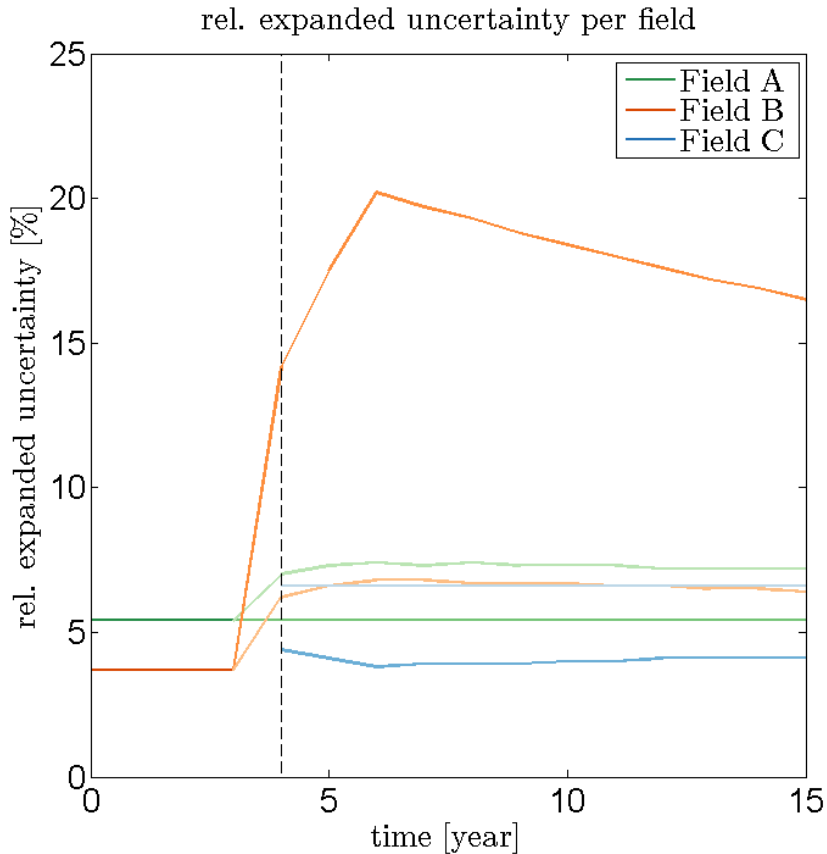


Figure 11: **Real-life example:** 2 existing fields, one new tie-in. 1st stage separators and multiphase flow meters.

In order to answer these important questions, an uncertainty analysis combined with a risk analysis are carried out. We assume the same ownership distribution as in the previous section, given in Table 1. The production rates follow the same

**Technical Paper**

profiles as in the previous examples besides that the rates of Field A are increased by a factor of five. Figure 11 gives the summary of the temporal evolution of the relative expanded uncertainty of the field allocation for the two different scenarios. The lighter colours represent pro rata allocation, the darker by difference.



*Figure 12: Temporal evolution of the relative expanded allocation uncertainty per field. The dashed vertical line indicates the start of production of Field C. The two different scenarios for the allocation system (continuing with by difference allocation or switching to pro rata) are indicated with different shades of the colour associated to the respective field, the darker shade represents by difference allocation, the lighter pro rata.*

In this example we will focus on the effects of correlation between the field allocated quantities in ownership allocation. To this end, we compare the lifetime risk for each owner calculated using correct ownership uncertainty to the results of the same calculations based on Equation (2). The results from this analysis are shown in Table 2. The first column of the table denotes the allocation principle applied and the different owners, while columns 2 and 3 show the exposure to risk accumulated over field lifetime (15 years) correctly accounting for correlations (column 2) or using the erroneous Equation (2). The rightmost column gives the difference between the two calculations. The relative expanded uncertainties for the metering stations A and B (if any), and C is set to 5 % (95% confidence interval) while the relative expanded uncertainty for the export metering station is set to 0.25 % (95 % confidence interval) in all cases. An oil price of 60 USD per barrel is assumed. Note that correlations only affect owners holding shares in several sources, i.e. Owner 2 in this example.

# 34<sup>th</sup> International North Sea Flow Measurement Workshop 25-28 October 2016

## Technical Paper

We see that the change in risk is, like in the previous example, dominated by the choice of allocation principle, but the effect of correlations between allocated streams is only one order of magnitude smaller and thus far from negligible. Depending on the allocation principle, using the ad hoc method following Equation (2) results in an overestimation of the risk exposure between 41 and 46 million dollars over the field lifetime. Furthermore, neglecting correlation yields also a slight overestimation of the benefit for Owner 2 in switching allocation principle, approximately 4.7 million dollars. While this figure may not seem dramatic compared to the overall risk, this is still in the order of magnitude of the total cost of a metering station.

**Table 2: Parameters for the two different scenarios considered in the realistic example system. The uncertainty numbers and oil price used in the different scenarios are chosen for illustration purposes only.**

		Exposure to risk [USD], accumulated over lifetime		
		with correlations	using Eq. (2)	difference
<b>By diff</b>	<b>Owner 1</b>	115 702 379	115 702 379	0
	<b>Owner 2</b>	544 899 752	590 653 852	45 754 100
	<b>Owner 3</b>	835 761 210	835 761 210	0
<b>Pro rata</b>	<b>Owner 1</b>	141 161 739	141 161 739	0
	<b>Owner 2</b>	246 653 591	287 723 559	41 069 968
	<b>Owner 3</b>	509 024 384	509 024 384	0

## 6 SUMMARY AND CONCLUSIONS

This paper describes the calculation of field and ownership allocation uncertainty for realistic measurement setups and allocation scenarios in a multi-field setting based on industrial projects. Furthermore, the exposure to losses due to misallocation is calculated and discussed for different metering setups.

Beyond illustrating exposed economic risk for each owner due to misallocation through realistic example systems, this paper has three main messages:

- The field allocation uncertainty will in many cases differ significantly from the individual metering station uncertainties (dependent on the system setup).
- In most real life setups, it is not intuitive to decide which owner(s) that are most exposed to economic loss due to misallocation.
- It is mandatory to take into account the correlation between the uncertainties in the field-allocated streams in order to estimate the owner allocation uncertainty correctly.

## 7 NOTATION

$U^*(x)$	Relative expanded uncertainty of a quantity x
$U(x)$	Absolute expanded uncertainty of a quantity x
$F_{field y}^{owner x}$	Ownership fraction for owner x in field y

# 34<sup>th</sup> International North Sea Flow Measurement Workshop 25-28 October 2016

## Technical Paper

$R$	Exposure to lost revenue
$V$	Value per unit of relevant quantity
$\bar{x}$	Average of quantity $x$
$k$	Coverage factor
$r_{A,B}$	Correlation coefficient between parameters $A$ and $B$
CAPEX	Capital expenditure or capital expense
OPEX	Operating expenditure or operational expense

## 8 REFERENCES

- [1] ISO/IEC Guide 93-3:2008/Supplement 1, «Propagation of distributions using a Monte Carlo method,» ISO/IEC, Geneva, 2008.
- [2] T. Aven, Pålitelighets- og risikoanalyse, Oslo: Universitetsforlaget, 1991.
- [3] P. Stockton, «Cost Benefit Analyses in the Design of Allocation Systems,» i *27th International North Sea Flow Measurement Workshop*, 2009.
- [4] ISO/IEC Guide 93-3:2008, , «Uncertainty of measurement - part 3: Guide to the expression of uncertainty in measurement (GUM:1995),» ISO/IEC, Geneva, 2008.
- [5] Stein W. Wallace, Carsten Helgesen and Arild Nystad, «Generating production profiles for an oil field,» *Mathematical modelling*, vol. 8, pp. 681 - 686, 1987.
- [6] A. Pobitzer, A. M. Skålvik og R. N. Bjørk, «Allocation System Setup Optimization in a Cost-Benefit Perspective,» *Journal of Petroleum Science and Engineering*, vol. In press, p. <http://dx.doi.org/10.1016/j.petrol.2016.08.025>, 2016.
- [7] Astrid Marie Skålvik, Ranveig Nygaard Bjørk, Kjell-Eivind Frøysa and Camilla Sætre, «A new methodology for cost-benefit-risk analysis of oil metering layouts,» i *33rd International North Sea Flow Measurement Workshop*, Tønsberg, 2015.

## **Technical Paper**

# **When Allocation “Back Out” Agreements can become “Lose Out” Agreements**

**Phil Stockton, Accord Energy Solutions Limited**

---

## **1 INTRODUCTION**

### **1.1 Overview**

When a newly developed third party field is tied back to existing infrastructure, such as a pipeline system, there is the potential for the new field’s production to cause an increase in back pressure and reduce the flow of the incumbent fields already producing through the system. This is termed “back-out” and in effect defers some of the incumbent fields’ production.

Back-out agreements are sometimes put in place, within the allocation system, to compensate the incumbent fields for the reduction in flow they experience. This may take the form of a transfer (or payment) from the third party of hydrocarbons to the incumbent fields so that in effect they do not experience deferment and suffer resultant economic loss.

As the production matures, the situation eventually reverses and the transfer (repayment) proceeds in the opposite direction from the incumbents to the third party. The assumption often made is that eventually the transfers will cancel one another and over their lifetime, all fields’ cumulative allocation will equal their cumulative production.

This paper presents the concept of how back-out calculations typically work and presents a simplified mathematical model of a system where an incumbent field is backed out by a new field introduced into a pipeline. This simplified model is used to illustrate potential problems with the concept of back-out, particularly in the repayment period and shows that there is the very real potential for “back-out” to become “lose out” for the new field.

Finally the paper discusses methods to overcome the pitfalls exposed by the analysis.

This paper specifically addresses back-out associated with gas reservoirs producing through shared pipeline infra-structure.

### **1.2 Structure of the Paper**

Section 2 describes a typical gas production system in which back-out occurs. This is used as an example to illustrate the issues associated with back-out. Though a fictitious system it is based on typical production rates and parameters from a real system to ensure it is reasonably representative of equivalent real systems in general. The values of the parameters used to generate the flows, pressures, etc. presented in the various charts are given in Section 6.5.

Section 3 describes a simplified mathematical model that is used to analyse the long term behaviour of the system. It thereby exposes a problem in that it

**Technical Paper**

appears it is impossible for the tied back field to be repaid, in any reasonable timeframe, the gas it has transferred to the incumbent field during the early back-out payment phase.

Section 4 examines options to address the problem of excessive repayment periods in an effort to ensure all fields receive the gas they have produced over the length of their lives.

Section 5 presents conclusions.

Section 6 provides a detailed description of the simplified mathematical model employed.

**2 DESCRIPTION OF A SYSTEM WITH BACKOUT**

**2.1 Physical System**

Consider the subsea gas pipeline system depicted in Figure 1:

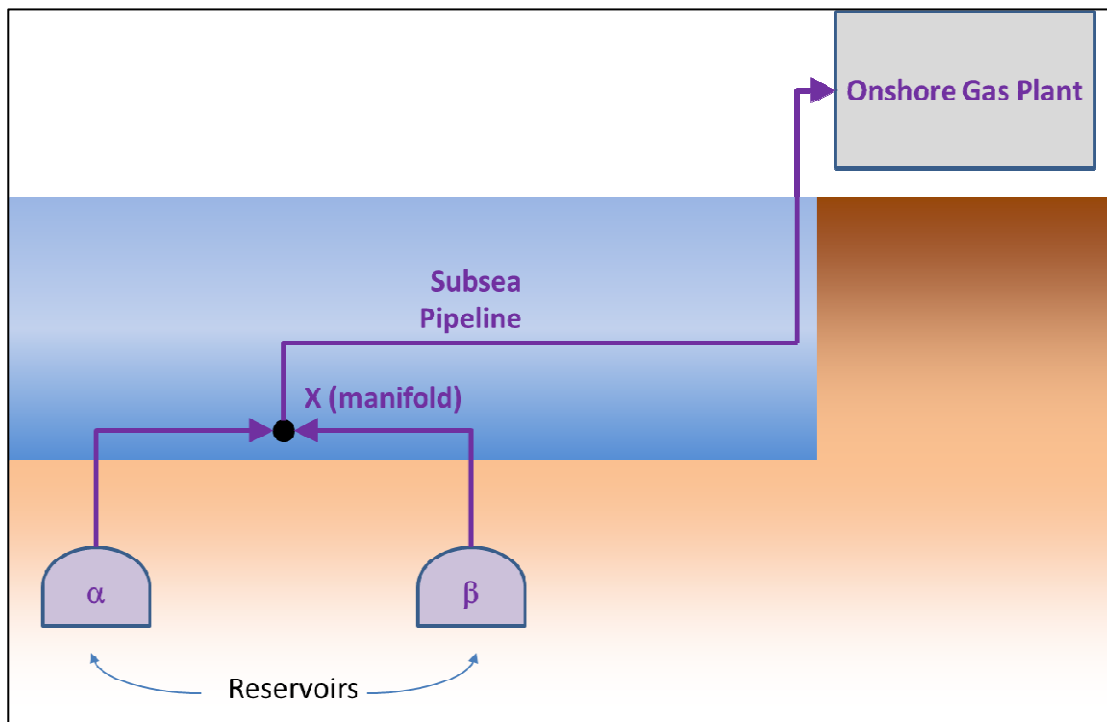


**Figure 1 – System Configuration**

The incumbent field has been labelled as Field Alpha ( $\alpha$ ). In order to utilise spare capacity and maximise the use of existing infrastructure it is often mutually beneficial for new developments to tie back into existing transportation and processing facilities.

A potential problem for the incumbent field is that the introduction of a new field, denoted Bravo ( $\beta$ ), increases the total flow down the shared pipeline resulting in a higher back pressure at Field Alpha's wellhead(s).

# 34<sup>th</sup> International North Sea Flow Measurement Workshop 25-28 October 2016

## Technical Paper

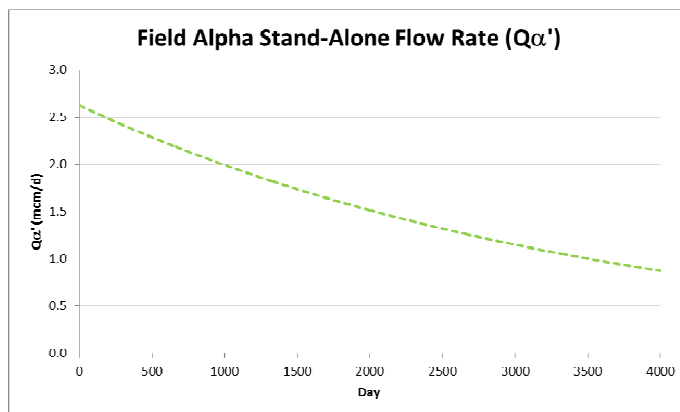
If Alpha's wells are off plateau, the increased back pressure will reduce production from the field and this is termed back-out. (Since new field tie-backs into existing infra-structure are usually taking advantage of spare capacity, it is likely that the incumbent fields' are off-plateau).

Unless the increased back pressure has a permanently deleterious impact on the incumbent wells, back-out does not result in lost production, it merely defers it. However, due to the time value of money the incumbent field would normally wish to produce its hydrocarbons sooner rather than later and back-out is considered to have an economic cost to the incumbent.

To understand the consequences of back out, it is instructive first to consider the behaviour of the incumbent field when it is producing alone, i.e. without back-out.

### 2.2 Stand-Alone Production

When Field Alpha is producing alone and it is off plateau, the pressure drop across the system, from the reservoir to the delivery point at the gas plant, will determine its flow. As the reservoir pressure drops, the driving-force decreases and Alpha's flow declines. This is illustrated in Figure 2.

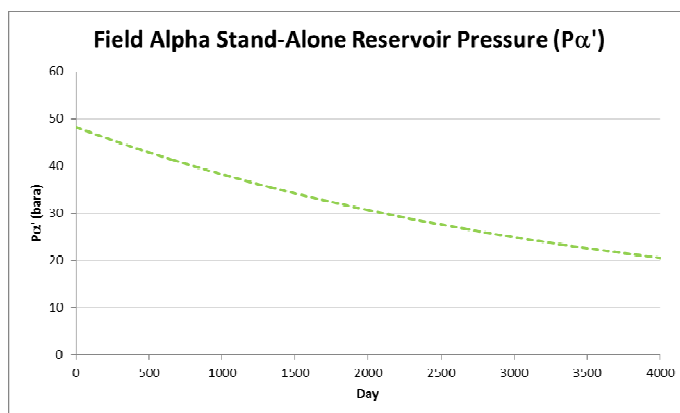


The dash ' in  $Q_{\alpha}'$  means this is the Stand-Alone volumetric flow for Field Alpha.

The horizontal scale ranges from 0 to 4,000 days, almost 11 years of production.

The reservoir pressure also declines as shown in Figure 3.

Figure 2 – Alpha Stand-Alone Flow Rate

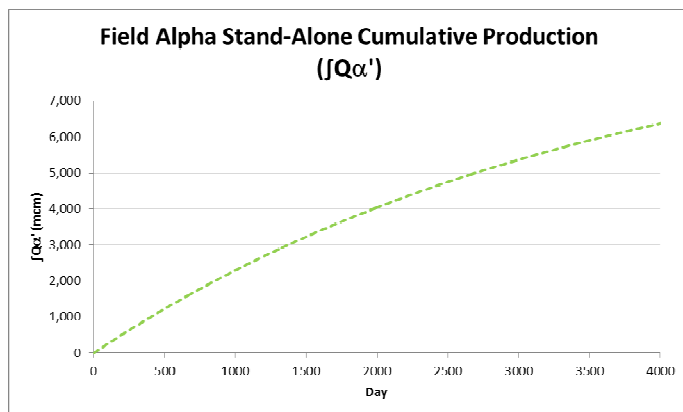


The reservoir acts like a pressurised tank. As gas is produced from the reservoir the pressure in it falls. As the pressure declines the driving force reduces, resulting in a lower flow rate.

The rate of pressure decline also falls as can be seen in the figure.

Figure 3 – Alpha Stand-Alone Reservoir Pressure

Technical Paper



The reservoir pressure tends asymptotically to the delivery pressure at the gas plant, which in this example is set at 6.75 bara.

The fall in the reservoir pressure is directly related to the cumulative production which is plotted in Figure 4.

Figure 4 – Alpha Stand-Alone Cumulative Production

The above plots represent the evolution of Alpha’s production with time in the absence of a new field being introduced. This is compared in the next section with the scenario of Shared Production with Field Bravo – a new third party tie-back.

### 2.3 Shared Production and Back-Out

In the Shared Production scenario, Alpha and Bravo are producing together. Alpha experiences a rise in back pressure due to the higher flow and resulting increased frictional pressure drop across the shared section of the subsea flow line. Alpha’s flow rate will therefore be lower when compared with the Stand-Alone case.

The Stand-Alone and Shared Production<sup>1</sup> flows are compared in Figure 5:

<sup>1</sup> The Stand-Alone and Shared Production scenarios or cases have been capitalised for convenience of reference throughout the paper.

Technical Paper

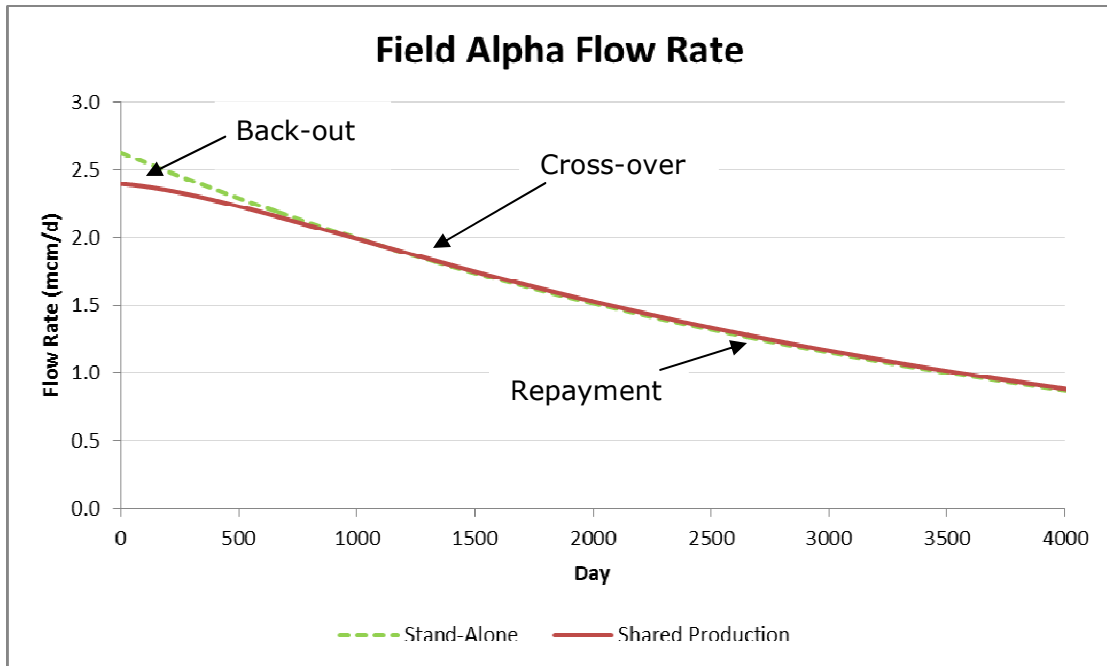


Figure 5 – Alpha Stand-Alone vs Shared Production Flow Rate

The locus of the green dashed line is identical to that in Figure 2. The red line shows the reduced flow experienced by Alpha in the early phase of the profile. The margin narrows until it becomes zero after 1,112 days, when Alpha's Shared Production exceeds its Stand-Alone level. The reason for this is revealed by comparing the difference in the reservoir pressures for the two scenarios in Figure 6:

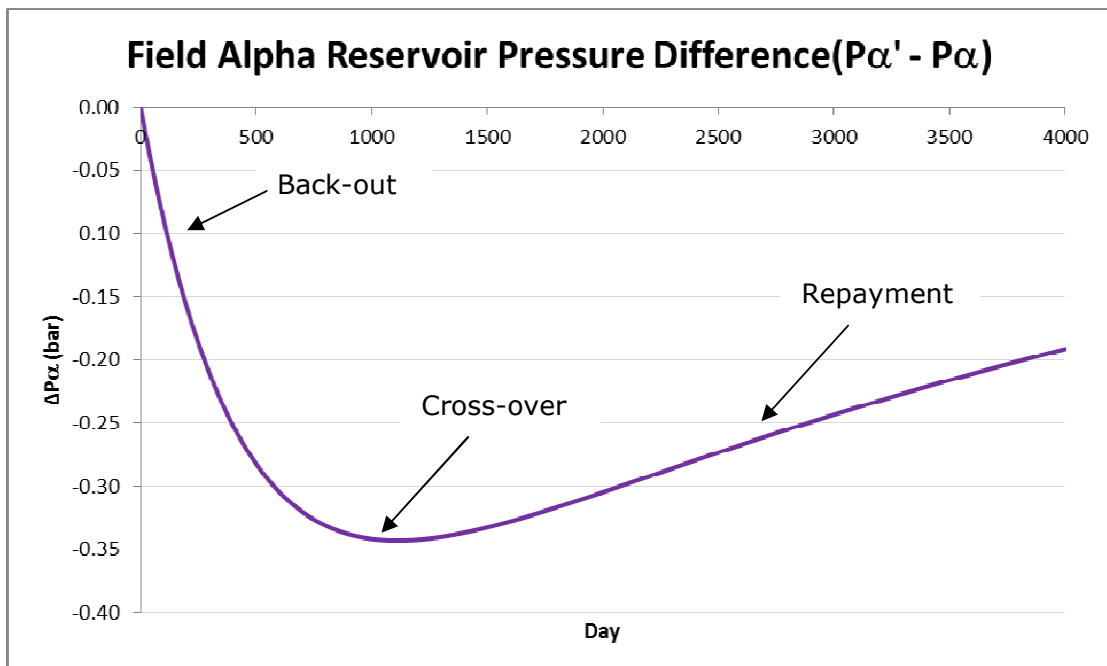


Figure 6 – Alpha Stand-Alone Minus Shared Production Reservoir Pressure

# 34<sup>th</sup> International North Sea Flow Measurement Workshop 25-28 October 2016

## Technical Paper

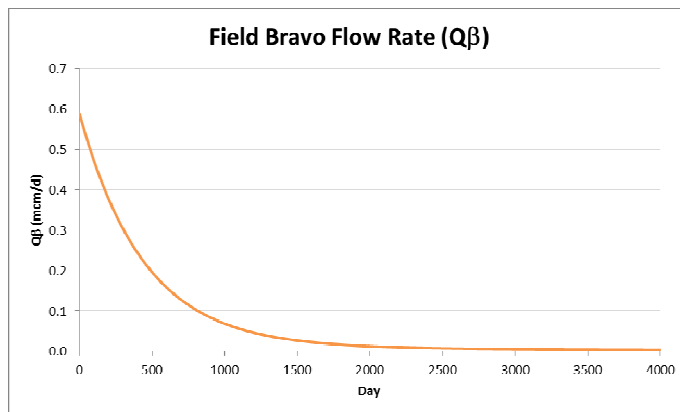
(The difference in pressure is presented as the plots of the two reservoir pressures almost lie over one another).

The plot shows that the Stand-Alone reservoir pressure is always lower than in the Shared Production case. This is because more gas has been taken out of the reservoir in the Stand-Alone case.

Though the back pressure experienced by Alpha is greater in the Shared case, the driving force at the reservoir is also greater and this eventually results in Alpha producing more in the Shared Production scenario.

This reservoir pressure difference between the two cases reaches its maximum at the cross-over point when Alpha's flow rate is identical in both scenarios.

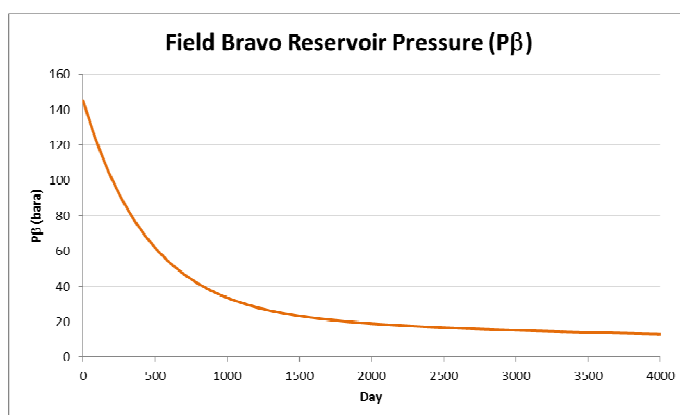
Also in the Shared case the production from Field Bravo is declining with time and therefore further reducing the back pressure.



The daily flow for Bravo is presented in Figure 7.

In the example, Bravo's production is less than Alpha's but its initial reservoir pressure is significantly greater as illustrated Figure 8.

**Figure 7 – Bravo Flow Rate**



Bravo's initial high reservoir pressure backs out Alpha but it declines rapidly as its reservoir is considerably smaller than Alpha's.

**Figure 8 – Bravo Reservoir Pressure**

Returning to Alpha, the difference in the Stand-Alone and Shared Production daily flow rates is compared in Figure 9:

Technical Paper

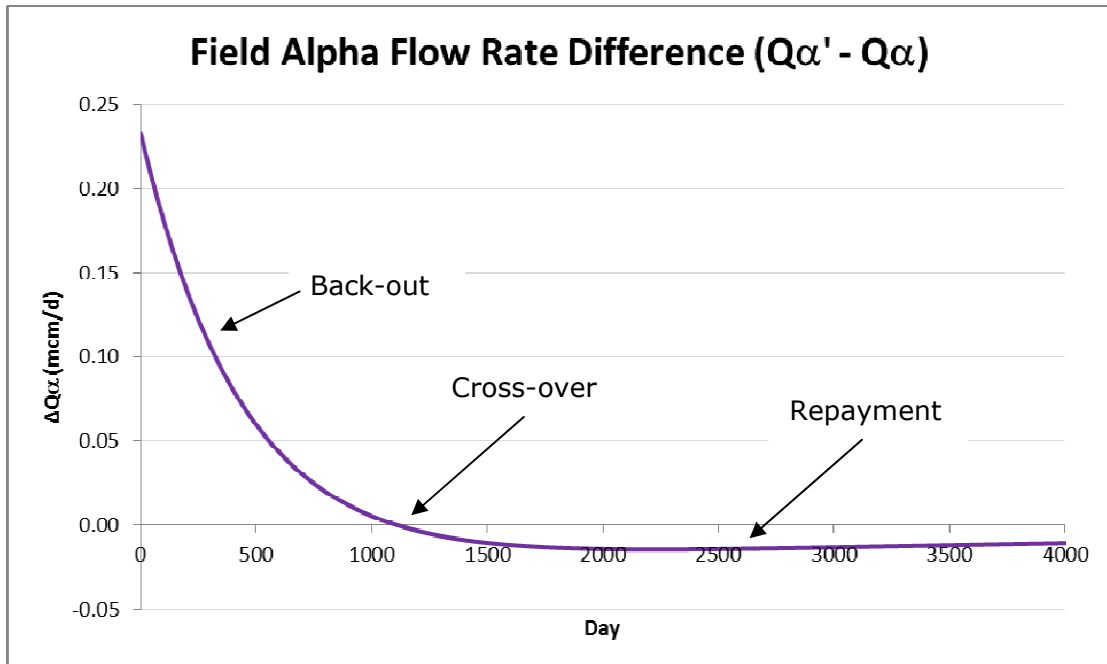


Figure 9 – Alpha Stand-Alone Production Minus Shared Production

The difference in the two daily flow rates, which is positive in the first 1,112 days, represents deferred production for Alpha and is termed the back-out.

Back-out agreements can be put in place to compensate incumbent fields (such as Alpha) for this deferred production.

## 2.4 Back-Out Agreement

A typical premise of back-out agreements is to allocate the incumbent field the quantity of gas it would have produced without the new field being present.

In the example, this entails calculating Alpha's deferred production as the difference between Alpha's measured (or allocated) production when co-producing compared with its estimated Stand-Alone production.

Gas is then transferred from Bravo to Alpha to compensate Alpha for the deferment, or back-out, and ensure it does not suffer economic loss.

An issue that immediately arises is the Stand-Alone Alpha production. This cannot be directly measured as it did not actually occur and is therefore hypothetical in nature. In order to overcome this, simulation models are used to calculate the hypothetical Stand-Alone production.

## 2.5 Back-Out Modelling

Back-out agreements usually stipulate the simulation modelling to be under-taken in order to calculate the back-out.

These simulations can vary in type and complexity but they usually involve modelling the reservoirs, wellbores and pipeline infrastructure to the point of

# **34<sup>th</sup> International North Sea Flow Measurement Workshop 25-28 October 2016**

## **Technical Paper**

delivery, e.g. at the inlet to a gas plant where the pressure may be considered fixed.

Commercial software programs [1], [2] such as MBAL and Eclipse model reservoirs, PROPSER and OFM model wells and GAP and PipeSim model pipeline networks. These may be integrated under a wider software framework. Such models are relatively sophisticated and require considerable expertise and effort to run.

In order to predict the level of back-out normally two models are run:

- The Shared Production case with both fields producing, i.e. mimicking reality and;
- The Stand-Alone hypothetical case with only the incumbent field producing.

The difference between the two then provides the predicted back-out experienced by the incumbent field.

At first sight, the model simulating reality appears superfluous. However, it serves two purposes:

- It allows the modelling environment to be calibrated against real production, i.e. by history matching the model against real data. The parameters calibrated in the Shared model can then be used in the Stand-Alone model and thereby improve estimates of back-out;
- It allows calculated daily back-out quantities to be projected into the future, the forecast back-out being used in the daily allocation in the forthcoming period until a new calibration exercise can be undertaken.

There are variations to the above approach but they all tend to include models that simulate both scenarios.

### **2.6 Deferment Back-Out is different to Hydrodynamic Back-Out**

It is worth noting that back-out, in the deferred production sense and addressed in back-out Agreements, cannot be measured directly.

At first sight it may appear that the back-out experienced by the incumbent field Alpha could be determined by physically shutting in Bravo and recording the change in Alpha's production as the back-out. But this is a different kind of back-out, termed here as hydrodynamic back-out.

Hydro-dynamically, at any instant in time, Bravo is backing out Alpha in the sense that if Bravo is shut in Alpha's flow will always increase.

However, this is not how deferred production back-out is defined in back-out agreements as Alpha's flow has to be compared with the hypothetical case of Alpha having produced up to this point in time without Bravo producing at all. In such a scenario, Alpha's reservoir pressure would be lower and it would be producing less on a Stand-Alone basis.

When determining back-out in the deferred production sense, the Shared Production case, however it is determined, has to be compared against a parallel, hypothetical scenario in which only Alpha has ever produced.

# 34<sup>th</sup> International North Sea Flow Measurement Workshop 25-28 October 2016

## Technical Paper

### 2.7 Back-Out Balances

There are three phases associated with back-out which are indicated on Figure 5, Figure 6 and Figure 9:

- Back-out payment
- Cross-over
- Repayment.

During the initial back-out payment phase the transfer of gas from Field Bravo to Alpha is normally recorded and accumulated as a back-out balance.

Once the cross-over point is reached the daily back-out payments will fall to zero and the back-out balance reaches its maximum.

The repayment phase ensues and Alpha commences transfer of gas back to Bravo. The back-out balance is decremented accordingly.

The back-out balance associated with the fictitious example introduced above is presented in Figure 10:

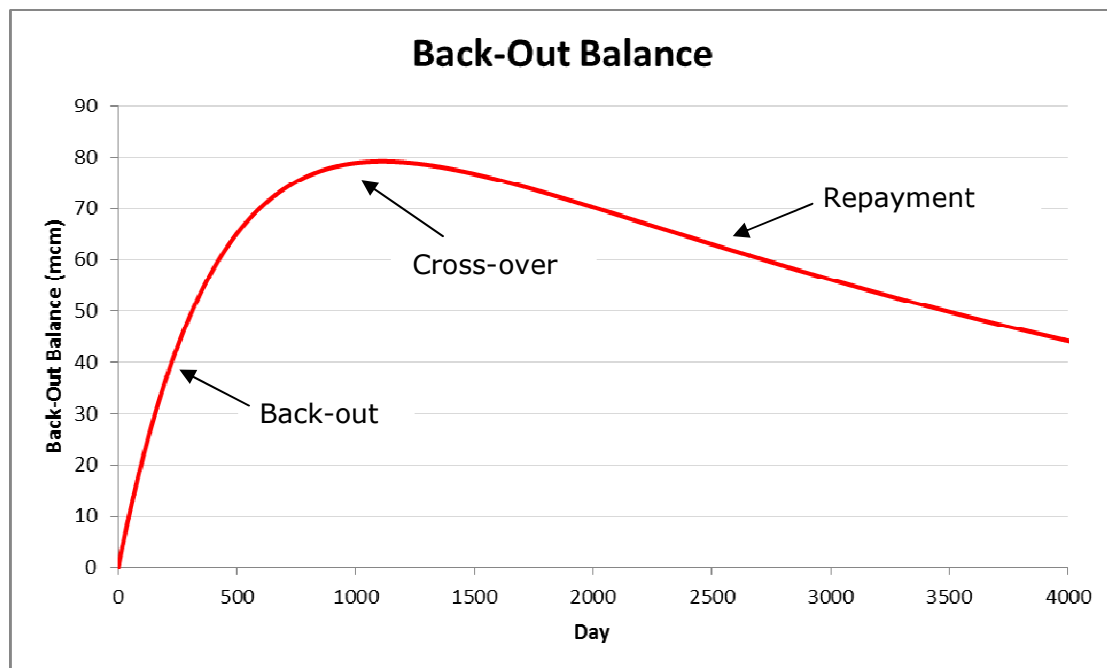


**Figure 10 – Back-Out Balance**

The back-out balance reaches its maximum value of 79.1 mcm at the cross-over point. This is the cumulative quantity of gas Bravo has transferred to Alpha to compensate for deferred production.

After the cross-over point Alpha Field is producing more gas than it would have been if it had produced on its own and the back-out becomes negative and repayment in the opposite direction from Alpha to Bravo takes place.

The back-out balance is then decremented by the repayment quantities.

# 34<sup>th</sup> International North Sea Flow Measurement Workshop 25-28 October 2016

## Technical Paper

When the back-out balance reaches zero the back-out payments will all have been repaid and the back-out calculations cease. However, how long does it take for the balance to return to zero?

Examination of Figure 10 shows that it took slightly over 3 years to build up the balance to its maximum value, but after almost a further 8 years, less than half the balance has been repaid.

In order to answer the question posed above, a simplified model of the system was developed and this is described, and its behaviour analysed, in the next section.

### 3 SIMPLIFIED MODEL

#### 3.1 Reasons for the Simplified Model

In order to assess the behaviour of the repayment phase and estimate the completion date, a simplified mathematical model of the system and associated back-out was developed. The derivation of the model is presented in Section 6.

This simplified model produces analytical equations that can solve the state of the system at any point in time.

Running the rigorous, complex models mentioned in Section 2.5, is considerably more time consuming and being numerical in nature, not so easily extended far into the future in order to examine the long term behaviour of the repayment phase.

The analytical solvable equations associated with the simplified model also provide a deeper understanding of the behaviour of the system.

#### 3.2 Model Development

The model is based on the following principles:

- the fall in reservoir pressure over a period of time is directly related to the cumulative production over that period
- the cumulative production is equal to the integrated flow rate over time
- the flow rate is equal to the rate of change of reservoir pressure.

Two principal sets of equations were developed. The first describes the behaviour of Alpha's reservoir pressure in the Stand-Alone case:

$$P_{\alpha}' = (P_{\alpha}^{\circ} - P_D)e^{-\mu t} + P_D \quad (1)$$

Where,

$P_{\alpha}'$	Stand-alone Alpha reservoir pressure (at time t). (The dash ' denotes the Stand-Alone case and is not the differential operator)
$P_{\alpha}^{\circ}$	Initial Alpha reservoir pressure
$P_D$	Delivery pressure (at gas plant)
t	time

# 34<sup>th</sup> International North Sea Flow Measurement Workshop 25-28 October 2016

## Technical Paper

$\mu$  is a constant determined by several system parameters; see Section 6 for its definition.

The second describes Alpha's reservoir pressure in the Shared Production case:

$$P_{\alpha} = C_1 e^{\lambda_1 t} + C_2 e^{\lambda_2 t} + P_D \quad (2)$$

Where,

$P_{\alpha}$  Shared Production Alpha reservoir pressure (at time t)

$C_1$ ,  $C_2$ ,  $\lambda_1$  and  $\lambda_2$  are all constants determined by the system parameters; see Section 6 for their definition.

Hence, at any point in time these equations provide the reservoir pressures for the two scenarios.

Two analogous equations provide the flow rate at any point in time. Alpha's flow rate in the Stand-Alone case is given by:

$$Q_{\alpha}' = \frac{\mu}{k_{\alpha}} (P_{\alpha}^{\circ} - P_D) e^{\mu t} \quad (3)$$

Where,

$Q_{\alpha}'$  Stand-alone Alpha flow rate (at time t)

$k_{\alpha}$  Constant relating Alpha's reservoir pressure to its gas volume

And for the Shared Production case:

$$Q_{\alpha} = \frac{\lambda_1}{k_w} C_1 e^{\lambda_1 t} + \frac{\lambda_2}{k_w} C_2 e^{\lambda_2 t} \quad (4)$$

Where,

$Q_{\alpha}$  Shared Production Alpha flow rate (at time t)

### 3.3 Cross-Over Point

The cross-over point occurs when  $Q_{\alpha}'$  and  $Q_{\alpha}$  are equal and hence the cross over time ( $t = \tau_X$ ) can be determined by combining equations (3) and (4) to give:

$$\mu (P_{\alpha}^{\circ} - P_D) e^{\mu \tau_X} = \lambda_1 C_1 e^{\lambda_1 \tau_X} + \lambda_2 C_2 e^{\lambda_2 \tau_X} \quad (5)$$

This equation has to be solved iteratively for  $\tau_X$ .

# 34<sup>th</sup> International North Sea Flow Measurement Workshop 25-28 October 2016

## Technical Paper

### 3.4 Repayment Completion Point

The repayment phase is completed when the back-out balance falls to zero.

The back-out balance (B) at any time (t) is calculated as the difference between Alpha's Stand-Alone and Shared cumulative production:

$$B = \int_0^t Q_{\alpha}^{\prime} dt - \int_0^t Q_{\alpha} dt \quad (6)$$

By substituting for the flow rates from equations (3) and (4) and integrating with respect to time:

$$B = \frac{1}{k_w} \left( (P_{\alpha}^{\circ} - P_D) e^{\mu t} - C_1 e^{\lambda_1 t} - C_2 e^{\lambda_2 t} \right) \quad (7)$$

Hence by equating B to zero, the right hand side can be solved for  $t = \tau_0$ , the repayment completion time. There are two solutions:

$$\tau_0 = 0$$

$$\tau_0 = \infty.$$

The back-out starts at zero, indicated by the first solution, but only returns to zero after an infinite time.

This explains the shape of the plot of the balance in Figure 10, which starts at zero, goes through a maximum at the cross-over point but then extends out with time. The second solution of the equation completes the picture suggested by the plot in that it shows that the balance returns asymptotically towards zero over an infinite time.

To further illustrate the slow rate of decline repayment, in this example after a further 10 years of production, there would still be approximately 20% of the balance unpaid.

The analysis illustrates that using this back-out approach, the new third party field (Bravo) is not going to be repaid its gas in any reasonable timeframe. Indeed, the fields will have become uneconomic to produce long before the back-out balance is appreciably repaid.

A further problem for the new third party field is that the back-out agreement may contain a clause that states that: should the incumbent field's production cease, or become uneconomic, any liability for back-out repayments ceases. This means that the new field will almost certainly be left with unpaid back-out gas.

In effect, the back-out agreement is a "Lose Out" agreement for the new field.

Technical Paper

3.5 Comparison with Complex Model

As noted in Section 6 the simplified model does make some simplifying assumptions in order to make the equations solvable analytically and allow the underlying physics of back-out to be analysed, in particular the long term behaviour.

However, it is important that the simplified model is reasonably representative of the more complex models (and indeed actual production) in order for the conclusions drawn from it to be credible.

Figure 11 is a plot of an incumbent field's production from a real system though the data is anonymised.

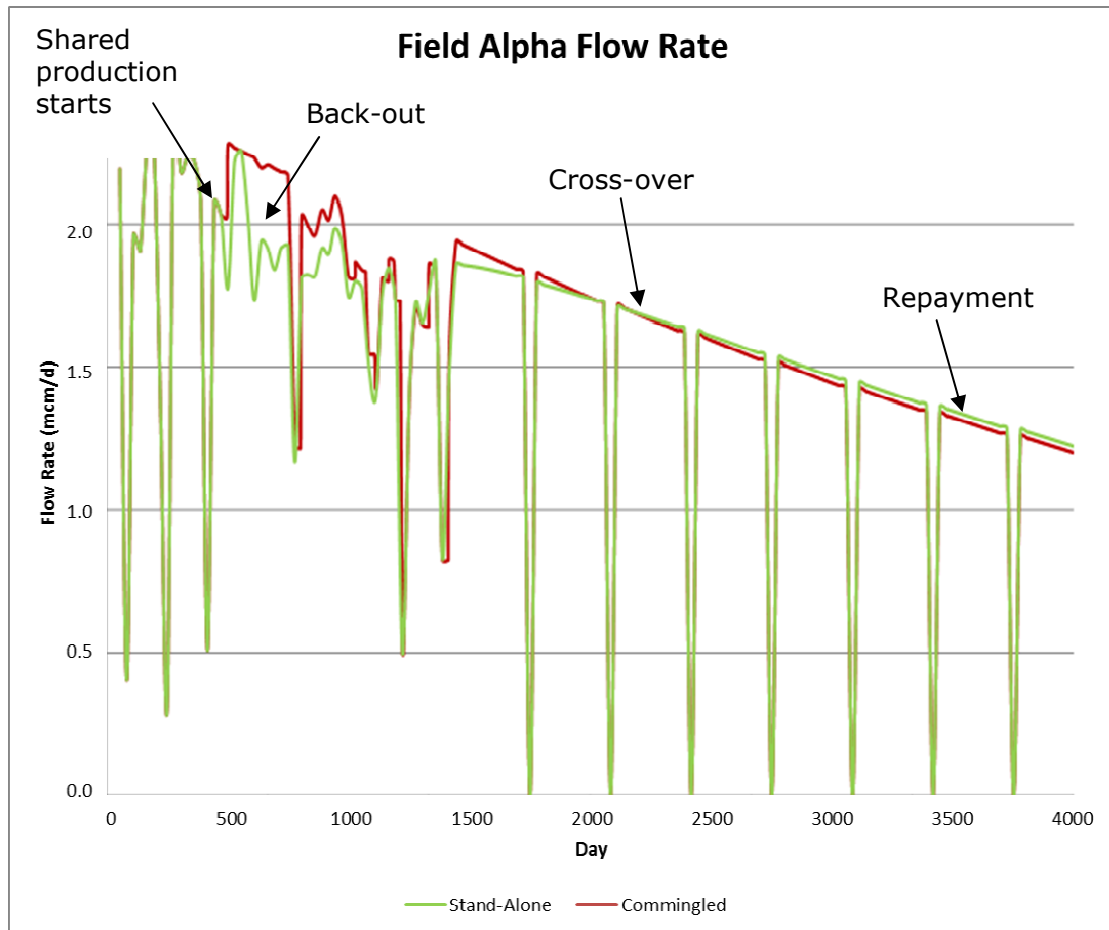


Figure 11 – Complex Model Flow Rate Results

The real system is different to that in the fictitious example used in the simplified model, which is why the timing of events is not the same when comparing the two.

# **34<sup>th</sup> International North Sea Flow Measurement Workshop 25-28 October 2016**

## **Technical Paper**

The Shared Production starts after around 500 days and the difference between the forecast Stand-Alone production (red line) and the Shared Production (green line) representing back-out is immediately observed.

The data is noisy up to around day 1,300 because the models have been matched to real historical production data up to that point. Beyond that the models are predicting into the future and appear smoother.

The cross-over is observed around day 2,100 and the slow repayment behaviour observed after that.

The downward spikes to zero represent planned shutdowns which are factored into the more complex models.

Though noisier the more complex model results display all same features as the simpler model.

The same slow repayment phase can be observed with the real data but the power of the simplified model is that it shows algebraically that repayment cannot be achieved in practice and certainly not on economic timescales for such gas fields.

In the author's experience this phenomenon does not appear to have been appreciated when these back-out agreements were historically developed. It seems apparent that the focus of the agreements is on the initial back-out experienced by the host fields.

The next section discusses options to address the repayment problem.

## **4 ALTERNATIVE REPAYMENT OPTIONS**

### **4.1 Contractual Agreement**

Though, once realised, the unreasonably long repayment phase appears easily corrected in a technical sense. However, if the methodology is written into a contractual agreement it may be extremely difficult to obtain agreement from the incumbent field's owners to modify the repayment mechanism.

The first option presented in Section 4.2 is a relatively straight forward approach. However, it is not necessarily consistent with the premise, frequently encountered in agreements, that: the incumbent field is allocated the quantity of gas it would have produced without the new field being present.

The second option in Section Incorporation of COP into Back-Out4.3 provides a methodology which is still arguably consistent with the premise.

### **4.2 Fixed Period Repayment**

The repayment phase could simply be based on an alternative method. For example running the balance repayments down over the same period they were built up, or some variation of this, and dispensing with the models altogether for the repayment phase.

# 34<sup>th</sup> International North Sea Flow Measurement Workshop 25-28 October 2016

## Technical Paper

Though pragmatic, the problem with this approach is that the incumbent field's allocated production is different to that which it would have experienced if it was produced alone as it is paying back the gas faster than the modelling predicts it should be.

### 4.3 Incorporation of COP into Back-Out

If the incumbent field becomes uneconomic and the repayment liability ceases before the balance is significantly repaid then in such a case the new tie-back field has effectively lost considerable volumes of gas.

However, the cessation of production (COP) does offer a route for the new field to receive repayment whilst being consistent with the agreement. The COP represents the point when the incumbent field's flow is so low that it is uneconomic to produce. So there is a definable COP flowrate. This COP flow rate would have been reached earlier in the Stand-Alone case so all the gas produced by the incumbent field between Stand-Alone COP time and Shared Production COP time should be transferred as repayment. This idea is illustrated in Figure 12:

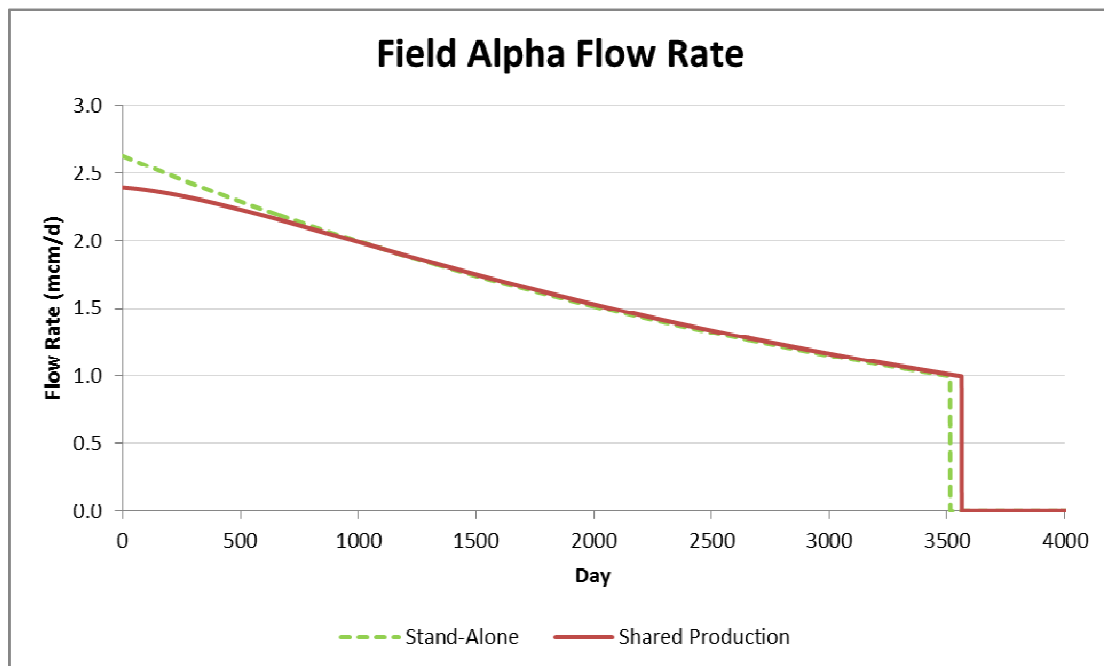


**Figure 12 – Alpha Stand-Alone vs Shared Production Flow Rate with COP**

Nominally, Field Alpha is considered to become uneconomic when its production falls to 1.0 mcm/d and this occurs on Day 3,562 for the Shared Production case, after which it is shut-in and its flow rate falls to zero. In the hypothetical Stand-Alone scenario this COP flow would have occurred on Day 3,513, 49 days earlier.

Hence the entire Alpha production for the last 49 days of its life should be transferred to Bravo as repayment.

The difference in the flow rates is plotted in Figure 13.

Technical Paper

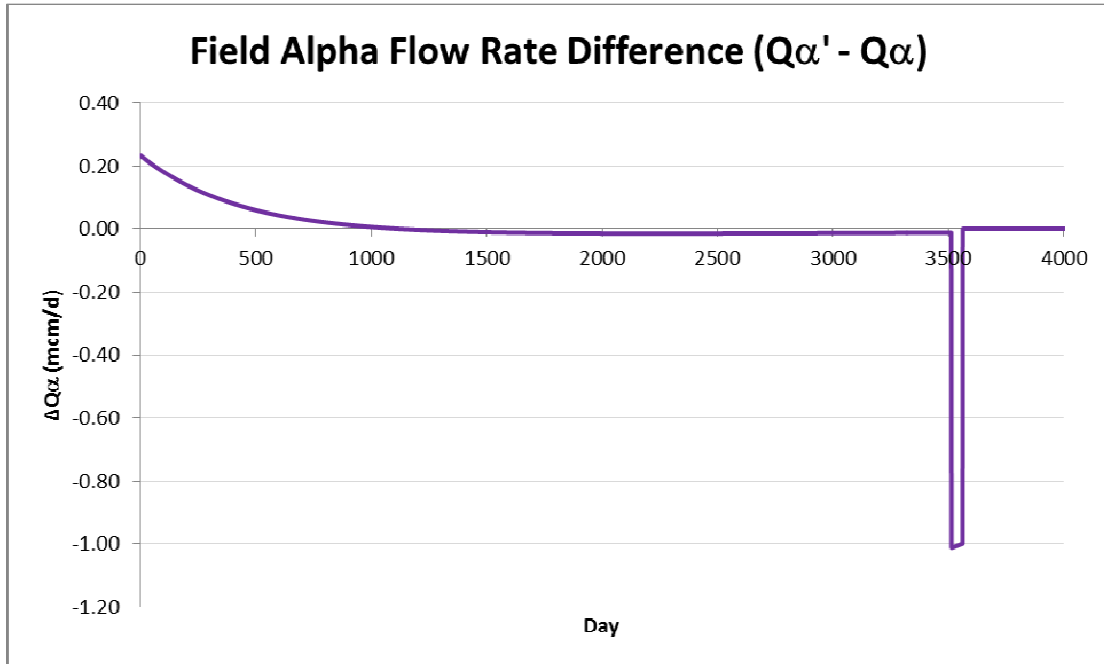


**Figure 13 – Alpha Stand-Alone Production Minus Shared Production with COP**

This plot graphically illustrates the slow repayment after cross over with a relatively short period of high repayment prior to Alpha's COP.

Finally Figure 14 shows the back-out balance rapidly falling to zero just prior to COP:

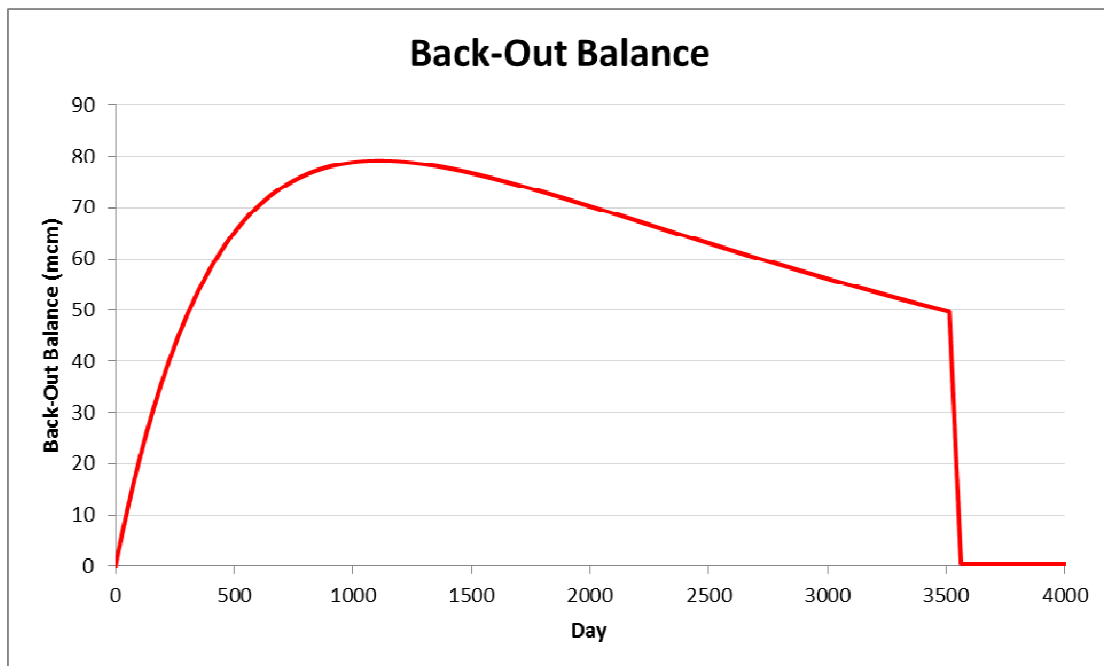


**Figure 14 – Back-Out Balance with COP**

# **34<sup>th</sup> International North Sea Flow Measurement Workshop 25-28 October 2016**

## **Technical Paper**

As can be seen most of the repayment occurs in a single block of production just prior to COP. This could be a significant amount of time after the cross-over date but it is a mechanism by which the new field can obtain repayment, whilst still being consistent with the concept that the incumbent field's allocation is unaffected by the new field.

### **5 CONCLUSIONS**

The paper has explored the behaviour of back-out payment and repayment mechanisms.

It has accomplished this with the use of simplified mathematical models which complement the more complex models but have the advantage that they are more tractable and readily predict the long term behaviour of such back-out systems.

The analysis has revealed that the repayment phase is so prolonged that the new third party field may not receive a significant proportion of repayment before the incumbent field's COP.

A mechanism has been suggested, that incorporates the COP, and ensures full repayment of gas. It achieves this whilst being consistent with the premise, frequently expressed in back-out agreements, that the incumbent field's allocated production is no different to that which it would have experienced if it was produced alone.

When they are written, some back-out agreements appear to focus on the initial back-out experienced by the incumbent field(s). Perhaps this is not surprising as this phase is in the near future. In contrast it appears that the consequences associated with the mechanisms for the repayment phase, are not fully realised. This can result in significant penalty of lost production for the new field.

Finally this paper has attempted to expose potential pitfalls associate with back-agreements and presented potential solutions to address them.

### **6 SIMPLIFIED BACK-OUT MATHEMATICAL MODEL**

#### **6.1 System**

Figure 15 depicts the two gas reservoirs ( $\alpha$  and  $\beta$ ) producing through a shared subsea pipeline to an onshore gas plant.

Technical Paper

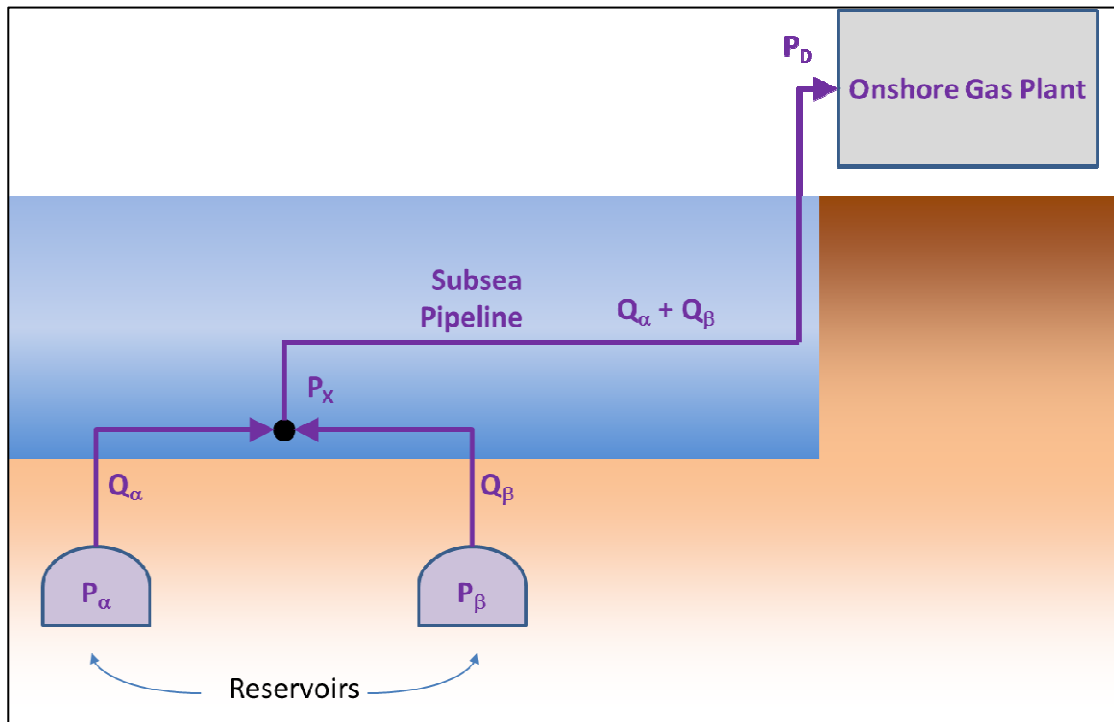


Figure 15 – System Configuration

The pressures and standard volumetric flows at various points in the system are indicated symbolically.

## 6.2 Simplifying Approximations

In order to render the system solvable analytically some simplifying approximations are made.

The frictional pressure loss in the pipelines is approximated to be linearly dependent on flow:

$$Q_{\alpha} \approx R_{\alpha}(P_{\alpha} - P_x) \quad (8)$$

$$Q_{\beta} \approx R_{\beta}(P_{\beta} - P_x) \quad (9)$$

$$Q_{\alpha} + Q_{\beta} \approx R_p(P_x - P_D) \quad (10)$$

The R terms represent the resistance to flow in each pipe segment and are assumed to be constants.

The typical correlation between cumulative gas produced to date (GPD) and reservoir pressure (divided by compressibility) is illustrated in Figure 16 below:

Technical Paper

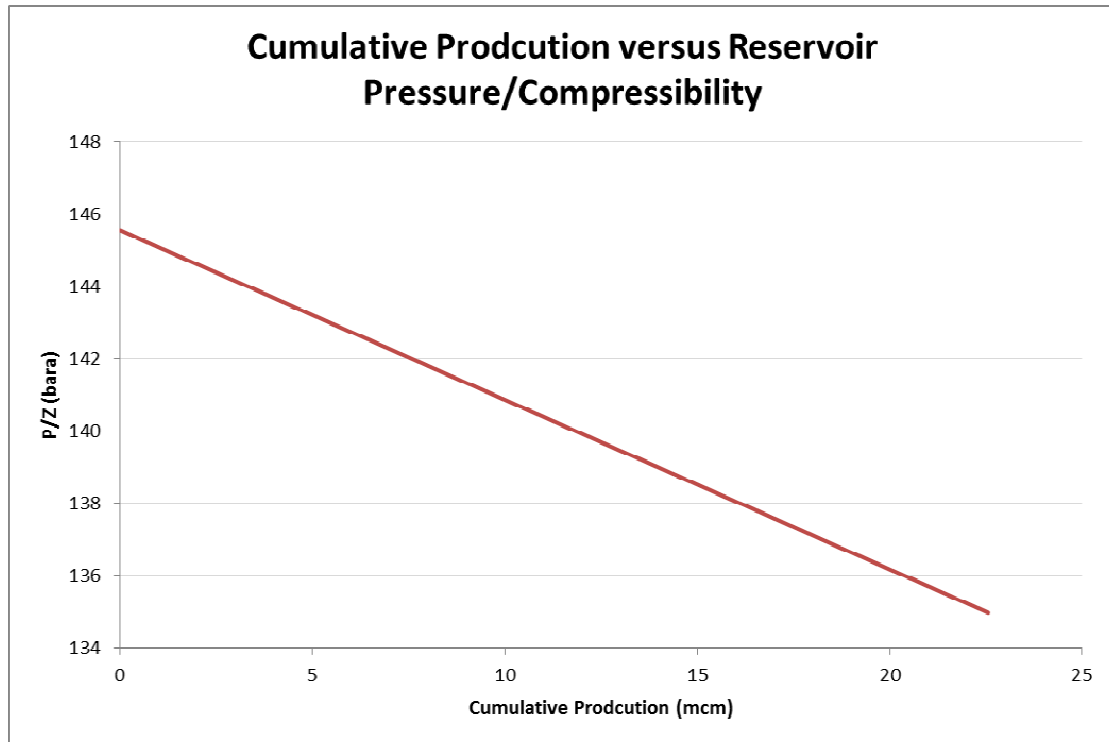


Figure 16 – Reservoir Pressure versus Cumulative Production

Again to simplify the mathematics gas compressibility (Z) is assumed to be constant over the pressure range and reservoir pressure can be expressed as a linear function of cumulative production according to:

$$P_{\alpha} \approx k_{\alpha} GPD_{\alpha} \quad (11)$$

### 6.3 Shared Production Scenario

Cumulative production is given by the integral of the flow rate over time:

$$GPD_{\alpha} = \int_0^t Q_{\alpha} dt \quad (12)$$

Rearranging (11) and substituting for GDP in (12), and rearranging in terms of reservoir pressure gives:

$$P_{\alpha} = k_{\alpha} \int_0^t Q_{\alpha} dt \quad (13)$$

Differentiating with respect to time:

**34<sup>th</sup> International North Sea Flow Measurement Workshop  
25-28 October 2016**

**Technical Paper**

$$\frac{dP_{\alpha}}{dt} = k_{\alpha}Q_{\alpha} \quad (14)$$

A similar relationship can be obtained for Bravo:

$$\frac{dP_{\beta}}{dt} = k_{\beta}Q_{\beta} \quad (15)$$

Substituting for flow  $Q_{\alpha}$  from (8) in (14):

$$\frac{dP_{\alpha}}{dt} = k_{\alpha}R_{\alpha}(P_{\alpha} - P_X) \quad (16)$$

Similarly for Bravo:

$$\frac{dP_{\beta}}{dt} = k_{\beta}R_{\beta}(P_{\beta} - P_X) \quad (17)$$

Rearranging equation (10) in terms of  $P_X$  and substituting for  $Q_{\alpha}$  and  $Q_{\beta}$  from (8) and (9) results in:

$$P_X = \frac{R_{\alpha}P_{\alpha} + R_{\beta}P_{\beta} + R_P P_D}{R_{\alpha} + R_{\beta} + R_P} \quad (18)$$

This can be substituted in (16) and (17) to obtain:

$$\frac{dP_{\alpha}}{dt} = \left( \frac{k_{\alpha}R_{\alpha}}{R_{\alpha} + R_{\beta} + R_P} \right) (P_{\alpha}R_P + P_{\alpha}R_{\beta} - P_{\beta}R_{\beta} - P_D R_P) \quad (19)$$

And:

$$\frac{dP_{\beta}}{dt} = \left( \frac{k_{\beta}R_{\beta}}{R_{\alpha} + R_{\beta} + R_P} \right) (P_{\beta}R_P + P_{\beta}R_{\alpha} - P_{\alpha}R_{\alpha} - P_D R_P) \quad (20)$$

Differentiating (19) with respect to time:

$$\frac{d^2P_{\alpha}}{dt^2} = \left( \frac{k_{\alpha}R_{\alpha}}{R_{\alpha} + R_{\beta} + R_P} \right) \left( \frac{dP_{\alpha}}{dt} (R_P + R_{\beta}) - \frac{dP_{\beta}}{dt} R_{\beta} \right) \quad (21)$$

Rearranging (21):

$$\frac{dP_{\beta}}{dt} = \frac{1}{R_{\beta}} \left( \frac{dP_{\alpha}}{dt} (R_P + R_{\beta}) - \frac{d^2P_{\alpha}}{dt^2} \left( \frac{R_{\alpha} + R_{\beta} + R_P}{k_{\alpha}R_{\alpha}} \right) \right) \quad (22)$$

**Technical Paper**

Rearranging (19) in terms of  $P_\beta$ :

$$P_\beta = \frac{1}{R_\beta} \left( P_\alpha R_P + P_\alpha R_\beta - P_D R_P - \frac{dP_\alpha}{dt} \left( \frac{R_\alpha + R_\beta + R_P}{k_\alpha R_\alpha} \right) \right) \quad (23)$$

Substituting (22) and (23) in (20) and rearranging produces:

$$\begin{aligned} \frac{d^2 P_\alpha}{dt^2} - \left( \frac{k_\alpha R_\alpha (R_P + R_\beta) + k_\beta R_\beta (R_P + R_\alpha)}{R_\alpha + R_\beta + R_P} \right) \frac{dP_\alpha}{dt} + \left( \frac{k_\alpha k_\beta R_\alpha R_\beta R_P}{R_\alpha + R_\beta + R_P} \right) P_\alpha = \\ \left( \frac{k_\alpha k_\beta R_\alpha R_\beta R_P}{R_\alpha + R_\beta + R_P} \right) P_D \end{aligned} \quad (24)$$

This is a second order linear differential equation in  $P_\alpha$ , which has the solution:

$$P_\alpha = C_1 e^{\lambda_1 t} + C_2 e^{\lambda_2 t} + P_D \quad (25)$$

This is an initial value problem, with initial conditions defined when  $t = 0$ :

$$\text{At } t = 0, P_\alpha = P_\alpha^\circ, P_\beta = P_\beta^\circ \quad (26)$$

The starting reservoir pressures  $P_\alpha^\circ$  and  $P_\beta^\circ$  are assumed to be known.

The various  $\lambda$  and C parameters in (25) are:

$$\lambda_1 = \frac{k_\alpha R_\alpha (R_P + R_\beta) + k_\beta R_\beta (R_P + R_\alpha) + \sqrt{(k_\alpha R_\alpha (R_P + R_\beta) - k_\beta R_\beta (R_P + R_\alpha))^2 + 4k_\alpha^2 R_\alpha^2 k_\beta^2 R_\beta^2}}{2(R_\alpha + R_\beta + R_P)} \quad (27)$$

$$\lambda_2 = \frac{k_\alpha R_\alpha (R_P + R_\beta) + k_\beta R_\beta (R_P + R_\alpha) - \sqrt{(k_\alpha R_\alpha (R_P + R_\beta) - k_\beta R_\beta (R_P + R_\alpha))^2 + 4k_\alpha^2 R_\alpha^2 k_\beta^2 R_\beta^2}}{2(R_\alpha + R_\beta + R_P)} \quad (28)$$

$$C_1 = \frac{1}{(\lambda_2 - \lambda_1)} \left( \frac{k_\alpha R_\alpha (P_\beta^\circ R_\beta - P_\alpha^\circ (R_P + R_\beta)) + P_D R_P}{(R_\alpha + R_\beta + R_P)} + \lambda_2 (P_\alpha^\circ - P_D) \right) \quad (29)$$

$$C_2 = \frac{-1}{(\lambda_2 - \lambda_1)} \left( \frac{k_\alpha R_\alpha (P_\beta^\circ R_\beta - P_\alpha^\circ (R_P + R_\beta)) + P_D R_P}{(R_\alpha + R_\beta + R_P)} + \lambda_1 (P_\alpha^\circ - P_D) \right) \quad (30)$$

Now  $P_\alpha$  is obtained all other variables:  $P_\beta$ ,  $Q_\alpha$  and  $Q_\beta$  can be determined.

#### **6.4 Stand Alone Production Scenario**

For the Alpha Stand-Alone case,  $Q_\beta$  is zero. Equation (10) now becomes:

# 34<sup>th</sup> International North Sea Flow Measurement Workshop 25-28 October 2016

## Technical Paper

$$Q'_\alpha \approx R_p(P_X - P_D) \quad (31)$$

Combining equation (8) and (31) to eliminate  $P_X$ :

$$Q'_\alpha = \frac{R_\alpha(P'_\alpha - P_D)}{\left(1 + \frac{R_\alpha}{R_p}\right)} \quad (32)$$

This is then substituted in (14) to obtain the first order differential equation in  $P'_\alpha$ :

$$\frac{dP'_\alpha}{dt} = \frac{k_\alpha R_\alpha(P'_\alpha - P_D)}{\left(1 + \frac{R_\alpha}{R_p}\right)} \quad (33)$$

With initial conditions defined when  $t=0$ :

$$\text{At } t=0, P'_\alpha = P_\alpha^\circ, \quad (34)$$

This has the solution:

$$P'_\alpha = (P_\alpha^\circ - P_D)e^{\mu t} + P_D \quad (35)$$

Where,

$$\mu = \frac{k_\alpha R_\alpha R_p}{(R_p + R_\alpha)} \quad (36)$$

Now  $P'_\alpha$  is obtained,  $Q'_\alpha$  can be determined.

### 6.5 Values of Parameters Used in Example System

$k_\alpha$	-0.004344 bar/mcm
$k_\beta$	-0.4683577 bar/mcm
$P_\alpha^\circ$	48.3 bara
$P_\beta$	145.3 bara
$P_D$	6.75 bara
$R_\alpha$	0.1047 mcm/bar
$R_\beta$	0.004911 mcm/bar
$R_p$	0.160105 mcm/bar.

# 34<sup>th</sup> International North Sea Flow Measurement Workshop 25-28 October 2016

## Technical Paper

### 7 NOTATION

B	Back-out balance	$P_X$	Manifold pressure
$C_1$	System parameter defined in (29)	$Q_\alpha$	Field Alpha Shared Production volumetric flow rate
$C_2$	System parameter defined in (30)	$Q_\alpha'$	Field Alpha Stand-Alone volumetric flow rate
$GDP_\alpha$	Field Alpha cumulative gas production to date	$Q_\beta$	Field Bravo Shared Production volumetric flow rate
$k_\alpha$	Constant relating Alpha's reservoir pressure to its gas volume	$R_\alpha$	Flow resistance factor Alpha to X (manifold)
$k_\beta$	Constant relating Bravo's reservoir pressure to its gas volume	$R_\beta$	Flow resistance factor Bravo to X (manifold)
$P_\alpha$	Field Alpha Shared Production reservoir pressure	$R_p$	Flow resistance factor X (manifold) to delivery point
$P_\alpha'$	Field Alpha Stand-Alone reservoir pressure	t	Time
$P_\alpha^\circ$	Initial Alpha reservoir pressure	Z	Gas compressibility
$P_\beta$	Field Bravo Shared Production reservoir pressure	$\lambda_1$	System parameter defined in (27)
$P_\beta'$	Field Bravo Stand-Alone reservoir pressure	$\lambda_2$	System parameter defined in (28)
$P_\beta^\circ$	Initial Bravo reservoir pressure	$\tau_0$	Repayment completion time
$P_D$	Delivery pressure	$\tau_X$	Cross-over time
		$\mu$	System parameter defined in (36)

### 8 REFERENCES

- [1] Petroleum Experts supply MBAL, PROPSEER and GAP, <http://www.petex.com/>
- [2] Schlumberger supply Eclipse, OFM and Pipesim, <https://www.software.slb.com/products>

## **Application of Data Validation and Reconciliation to Production Allocation**

**Amin Amin, Letton Hall Group  
Robert A. Webb, Letton Hall Group  
Boris Kalitventzeff, Belsim SA  
Georges De Vos, Belsim SA**

---

### **1 INTRODUCTION**

Generally, upstream oil and gas export measurements are made on separated and depressurized bulk oil and gas flow streams collected from a group of wells. In depressurized conditions, where phase separation can be ensured, single phase measurements can be made with the best possible accuracy. These measurements follow measurement standards and recommended practices, such as from the API MPMS, Chapter 20, Section 1.

Wherever export production contains fluids from more than one producer (or unique ownership group, whether it is for one well or several), there must be an equitable distribution of the production export to each and every contributing producer. The allocation process serves to determine in the most fair manner the quantities of oil and gas produced, flared, consumed for fuel, or otherwise spent out of the total export over a given time period for each contributing producer. The allocation process starts at the end of upstream production, from the point of custody transfer to the midstream transporter, and works back upstream to the source of production, the well. In determining each producer's fair share of the export production, the resulting revenues and costs, such as production handling service fees, royalties and other costs, can be completely resolved.

The allocation process of quantifying the volume or mass of fluids produced from each well applies similarly to non-fiscal activities, such as the management of well performance, process facility operations, and reservoir recovery. While these applications are also important, they generally do not involve the resolution of inter-company financial transactions in accordance with an agreement. The elements of upstream metering and allocation carried out for fiscal allocation often encompass most of the needs for well or fluid allocation; however, the unique measurement requirements of reservoir and production management should be considered separately in order to get a complete set of metering and allocation requirements for all end uses of the flow measurement data.

Finally, if the allocation fully serves its purpose, it should be auditable and defensible. A good allocation minimizes disputes between partners in a production agreement.

In practice, how is this achieved? Unmixing the mixed streams of hydrocarbons from different wells, zones and fields is not straightforward. It can be downright challenging, and it certainly can be done in different ways leading to different outcomes, which leads back to the possibility of dispute. A good allocation, therefore, is one that is agreeable to all parties involved.

For each producer to get a consistently good, equitable allocation, it requires:

1. a written agreement that defines the objectives and methods of the allocation
2. a metering system that can deliver the required flow and other measurements
3. an auditable, independent execution of the allocation process

## **34<sup>th</sup> International North Sea Flow Measurement Workshop 25-28 October 2016**

As with many physical phenomena, a deterministic approach to defining the outcome of certain pre-established procedures and agreements is not always realistic. Errors and uncertainties in measurements, processes, and models, visible and hidden are also critical to the allocation process requiring attention and understanding by all parties involved, the producers and regulator alike. Identifying and understanding the sources of measurements errors is a necessary step to minimize their impact on allocation.

The risk of revenue loss by any of the parties, big or small due to ill-defined statistical factors will strongly reflect on the sense of fairness felt by everyone. Such situation can trigger with individuals a sense of unfairness as they learn that the production allocated to their lease is deemed less certain than the one from next door despite the fact that they both use the same equipment to measure production! Can this knowledge be used to mitigate "unfairness" and reduce the exposure faced by producers and regulators in the execution of their duties?

Through the study of simulated production scenarios the paper highlights ways to detect and deal with errant data in production allocation data sets. It also proposes and evaluates a practical procedure that turns DVR error-qualifiable production data into allocated quantities the same way traditional PSM systems are used in production allocation. The difference is that in the latter approach the data qualification for potential data bias or imprecision is not integrated in the allocation process leaving room for production misallocation risks.

The evaluated approach is based on maximizing the use of all available process information (devices and fluids) in an attempt to "vote out" erroneous measurements once identified. Results are evaluated with and without the erroneous data in moderate cases where measurements cannot be replaced for cost or operational reasons.

The Data Validation and Reconciliation (DVR), as the name implies, is evaluated for measurement error identification (surveillance functionality), and for its ability to make production estimates that qualify as allocated quantities of a relatively complex multi-tiered commingled production system. The current work builds on earlier effort that aimed at studying the use of measurement uncertainty in production allocation; Pro-rata, Uncertainty-based, and DVR-based methodologies [1].

DVR background and basic theory are first reviewed then followed by a review of the steps employed to perform traditional proportional allocation of volumetric quantities using Process Simulation Modeling (PSM). A PSM-DVR approach to allocation is proposed in the paper and tested by comparing the results to the "True Values" of a Reference simulation and to the results obtained from the PSM-Proportional Allocation methodology. However before performing allocation calculations, various production scenarios are simulated with various types of measurement and fluids property errors to test DVR's surveillance capabilities. Proportional and DVR based allocation is carried out with and without errors and with varying amount of information to examine the robustness of allocation answers of each allocation methodology. The results are compared with the process "True Values".

The paper continues in summarizing practical considerations and recommendations on the use of DVR in surveillance and/or allocation applications. It is also shown that if DVR-based allocation is not adopted for commercial or contractual reasons, other allocation methodologies will continue to benefit from a parallel DVR implementation for surveillance applications. Moreover, while the determination of measurements uncertainties has direct relevance to monetary arrangements if DVR is used for allocation, the constraints in quantifying the uncertainty values can be relaxed if the DVR process is used for surveillance only.

# 34<sup>th</sup> International North Sea Flow Measurement Workshop

## 25-28 October 2016

### 2 DATA VALIDATION AND RECONCILIATION (DVR)

#### 2.1 Background [2]

Industrial process data validation and reconciliation, (DVR), is a technology that uses process information and mathematical methods in order to automatically correct measurements in industrial processes. The use of DVR allows for extracting accurate and reliable information about the state of industry processes from raw measurement data and produces a single consistent set of data representing the most likely process operation.

DVR has become more and more important due to industrial processes that are becoming more and more complex with applications aiming at closing material balances in production processes where raw measurements were available for all variables. At the same time the problem of gross error identification and elimination has been addressed. Later, unmeasured variables were taken into account and the process matured by considering general nonlinear equation systems coming from thermodynamic models. Quasi steady state dynamics for filtering and simultaneous parameter estimation over time were introduced by Stanley and Mah.[3] Dynamic DVR was formulated as a nonlinear optimization problem by Liebman et al. in 1992.[4] followed by the use of Interior Point SQP by Kalitventzeff et al. for large-scale process optimization in 1996.[5]

Data reconciliation is a technique that aims at correcting measurement errors that are due to measurement noise, i.e. random errors. From a statistical point of view the main assumption is that no systematic errors exist in the set of measurements, since they may bias the reconciliation results and reduce the robustness of the reconciliation. However, systematic errors will be flagged if they are the cause for measurements excessive deviation from the "expected" values that best balance the system

DVR finds application mainly in industry sectors where either measurements are not accurate or even non-existing, like for example in the upstream sector where flow meters are difficult or expensive to position; or where accurate data is of high importance, for example for security reasons in nuclear power plants. Another field of application is performance and process monitoring in oil refining or in the chemical industry.

The application of DVR to production allocation for fiscal or reservoir management received increased attention in past few years albeit for specific cases; Ref [6] used the basic linear solving algorithms to arrive at the formulation of Uncertainty Based Allocation methodology of developed in [7] and [8], while Ref [9] applied DVR error minimization technique to take advantage of the field's lower GOR uncertainty to improve the production allocation of commingled subsea fields/wells. On the other side, Ref [1] took a more general approach by evaluating DVR in the context of using measurement uncertainty with different allocation methodologies.

As DVR enables to calculate estimates even for unmeasured variables in a reliable way, the German Engineering Society (VDI Gesellschaft Energie und Umwelt) has accepted the technology of DVR as a means to replace expensive sensors in the nuclear power industry (VDI norm 2048) [10].

# 34<sup>th</sup> International North Sea Flow Measurement Workshop 25-28 October 2016

## 2.2 Basic Theory

Given  $n$  measurements  $y_i$ , data reconciliation can mathematically be expressed as an optimization problem of the following form:

$$\min \sum_{i=1}^n \left( \frac{y_i^* - y_i}{\sigma_i} \right)^2 \quad (1)$$

Subject to  $F(x, y) = 0$

where  $y_i^*$  is the reconciled (allocated) value of measurement  $y_i$ , and  $x_j$  is the unmeasured variable ( $j = 1$  to  $m$ ).

$\sigma_i$  is the absolute uncertainty (standard deviation) of measurement  $y_i$  and  $F(x, y) = 0$  are the  $r$  process equality constraints. (Figure 1)

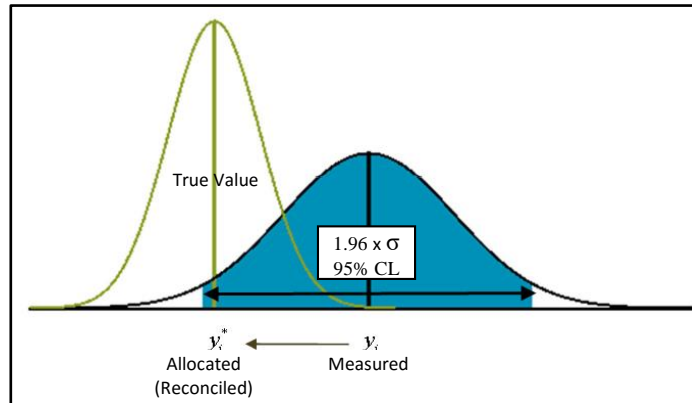


**Figure 1 Illustration of Measurement and Reconciled Values with their Uncertainties Assuming Gaussian Distributions**

The term  $\left( \frac{y_i^* - y_i}{\sigma_i} \right)^2$  is called the penalty of measurement  $i$ . The objective function is the sum of the penalties.

In other words, one wants to minimize the overall correction (measured in the least squares term) that is needed in order to satisfy the system constraints (mass, energy, component balances and phase equilibrium at each node). Additionally, each least squares term is weighted by the standard deviation of the corresponding measurement. In this formulation, both measurement bias and uncertainty (precision) are factored in the estimation of reconciled (validated) quantities.

Data reconciliation relies strongly on the concept of redundancy to correct the measurements as little as possible in order to satisfy the process constraints. Redundancy arises from combining sensor data with the model (algebraic constraints such as mass balance).

Redundancy can be used as a source of information to cross-check and correct the measurements  $y_i$  and increase their accuracy and precision. Further, the data reconciliation problem also includes unmeasured variables  $x_j$ . Based on information redundancy, estimates for these unmeasured variables (ex. missing flow measurement) can be calculated along with their accuracies. In industrial processes these unmeasured variables that data reconciliation provides are referred to as soft sensors or virtual sensors, where hardware sensors are not installed.

## 34<sup>th</sup> International North Sea Flow Measurement Workshop 25-28 October 2016

An important feature of DVR is results validation and gross error detection. Result validation may include statistical tests to validate the reliability of the reconciled values, by checking whether gross errors exist in the set of measured values. These tests can be for example:

1. The Global test of the entire system requiring that the summed penalties for a given number of constraints  $r$  should be less than the Chi-squared test criteria defined in VDI norm 2048 [10].
2. The Individual test compares each penalty term in the objective function with the critical values of the measurement's normal distribution. If the  $i$ -th penalty term is outside the 95% confidence interval of the normal distribution, then there is reason to believe that this measurement has a gross error as illustrated in Figure 1.

Advanced data validation and reconciliation is an integrated approach of combining data reconciliation and data validation techniques, which is characterized by:

1. Complex models incorporating besides mass balances also thermodynamics, momentum balances, and phase equilibria constraints etc. This is particularly applicable to complex allocation schemes where a Process Simulation Model (PSM) is used to account for mass transfer between phases in a commingled stream.
2. Gross error remediation techniques to ensure meaningfulness of the reconciled values in the presence of moderate biases.
3. Robust algorithms for solving the reconciliation problem.

### 2.3 DVR-based Production Allocation

In production allocation, the DVR approach differs from traditional methods by fully accounting for the system uncertainties associated with measurement devices, process parameters or fluids properties, and by allowing system redundancy to improve the accuracy and precision of the allocated quantities. This ensures that the allocated quantities are estimated in accordance with the physical principles/laws and constraints of the producing system. The approach can therefore be judged as more equitable where the allocated quantities are qualified by their degree of agreement with the original measurements (or lack thereof) in the form of global and individual penalties that can be monitored and quantified.

In production allocation schemes, where the balancing of multiple nodes may be required along the production path from subsea to sales, the minimization of Eq.(1) results in a series of equations that are solved simultaneously for the entire system to determine the adjustments vector  $\mathbf{v}$ . The adjustment is then added to the measurements vector  $\mathbf{y}$  in order to calculate the reconciled/allocated value  $\mathbf{y}^*$  (Eq.(2):

$$\mathbf{y}^* = \mathbf{y} + \mathbf{v} \quad (2)$$

In the majority of allocation cases involving straightforward mass or energy balances, the calculation is reduced to linear algebraic matrix operations solvable using spread sheets embedded functionalities. Such algorithm was incorporated in an allocation tool to perform this type of calculations.

On the other hand, more elaborate allocation schemes involving phase equilibrium calculations (PSM) will require the use of DVR software with built-in thermodynamics package and non-linear solver to allow for the simultaneous iterative solving of system's equations. A procedure to combine PSM and DVR methodologies is described in the following sections. The results are compared to the traditional PSM-Pro-rata approach.

# 34<sup>th</sup> International North Sea Flow Measurement Workshop 25-28 October 2016

## 3 FORMULATION OF COMPLEX ALLOCATION

### 3.1 Process Simulation Model (PSM)

Differences in the composition of the inlet streams and their respective process conditions will have an impact on the allocation due to material transfer between the commingled streams. Therefore, a Process Simulation Model (PSM) is used. The PSM calculates theoretical produced oil and gas volumes as well as Gas Energy Content for each separator(s) relative to the measured export quantities.

Commercial simulation packages are used in combination with an Equation of State (EOS), as provided in the PSM software, to generate the phase behavior and fluid properties and output results. The EOS is tuned to actual lab experiments for improved results.

Forward calculations are performed using the streams flowrates and fluid composition as inputs. Such inputs are obtained from "Allocation" single phase flow metering devices after separation or from physical or virtual multiphase flowmeters, and from fluids samples.

Additional measurements/samples are also performed at the Export/Sales point and in-between at various points/nodes in the process facility or production path. The Export measurements are usually custody transfer quality measurements of the stabilized hydrocarbon streams and are of high accuracy and precision.

For the purpose of this study, only the liquid streams (oil) are considered and shown in the following PFD diagram. The same treatment can also be applied to gas streams including liquid recovery from compression and vapor recovery processes.

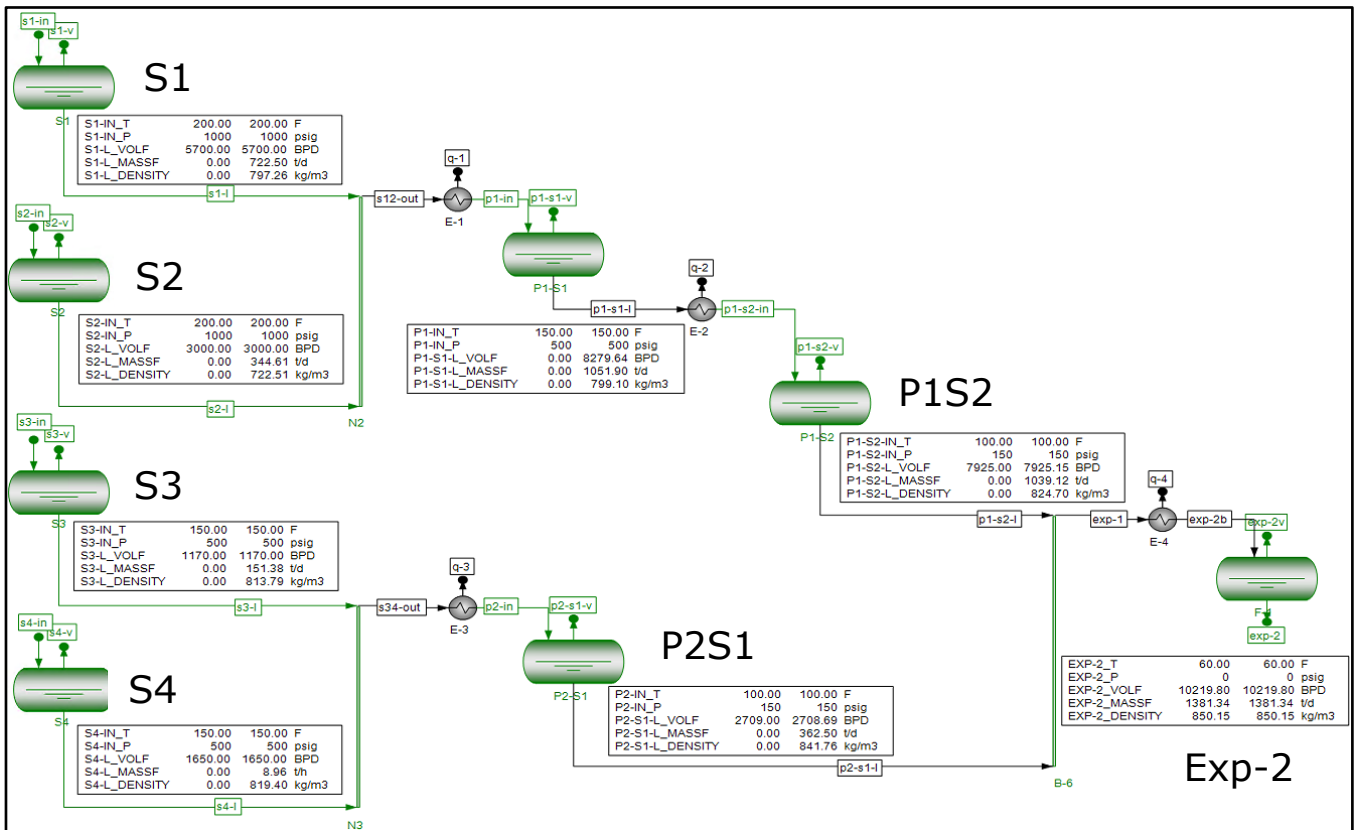


Figure 2 Reference oil process, 4 Inlet Separators, 2 Production Trains and Sales Meter

# 34<sup>th</sup> International North Sea Flow Measurement Workshop 25-28 October 2016

## 3.2 Proportional Allocation with PSM - The Traditional Way

Due to the differences in the fluid compositions, pressures, and temperatures, the use of a PSM is required. The PSM is used in multiple steps to allocate production measured and sold at the export meter to each of the inlet separators. The allocation is performed on volume quantities basis and is critically impacted by the phase transfer or inter-molecular mixing taking place between the streams as they travel from the inlet to the export point.

The common industry practice is to first determine the PSM results at the export point conditions when all inputs from the separator streams are included in the simulation (Combined PSM Run) [11]. The estimate of what a separator has contributed is the result of all separator streams simulated except one separator's streams (Exception PSM Runs). The Exception PSM run determines the Theoretical Volumes for the separator not being simulated (Figure 3). To balance the system volumetrically, the Volume Imbalance due to the difference between the Export meter and the sum of all Theoretical Volumes, is added or subtracted from each stream in pro-rata of the its Theoretical Volume.

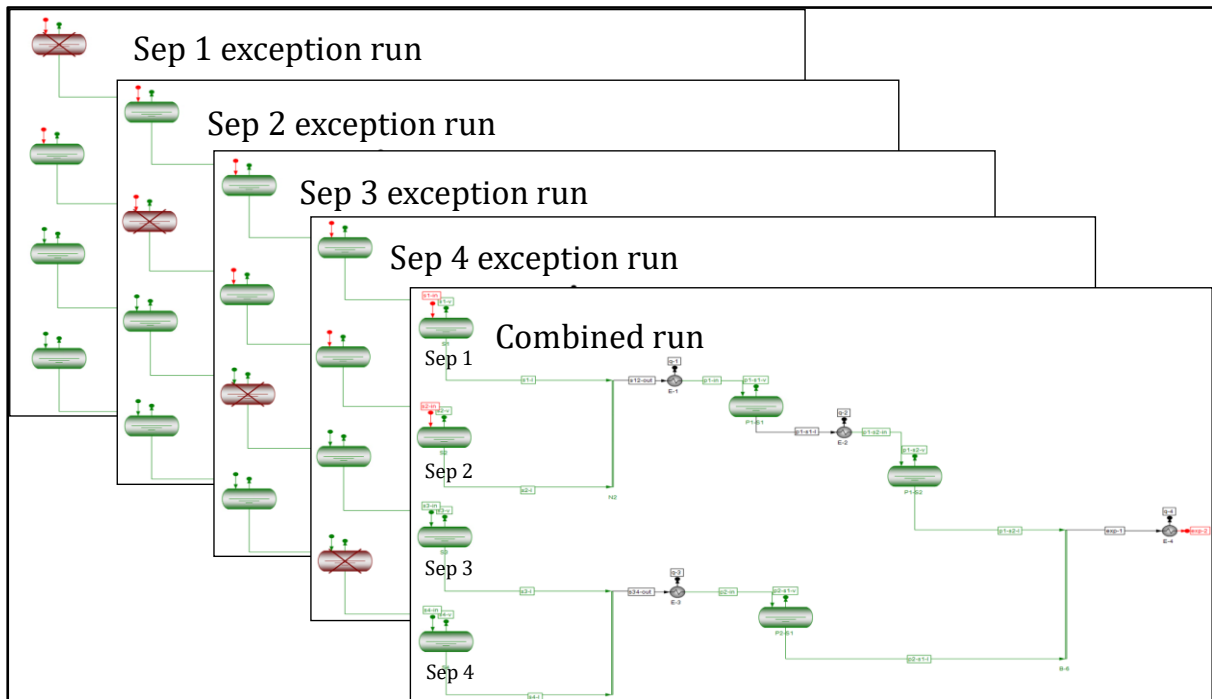


Figure 3 - Illustration of PSM Configuration for Combined and Exception Runs

## 3.3 Description of the Simulated Process

The process scenario used in the study is typical of a host facility consisting of two production trains, high and intermediate pressures. Two inlet separators (S1, S2 and S3, S4) are used on each train with additional production or bulk separation stages; two intermediate separation stages in the Train1 (P1S1, P1S2) and one (P2S1) in Train2. The mixed stream is taken down to standard or stock tank conditions using one more separation stage before the export point (Exp-2). The process pressure and temperature set conditions are shown underneath each separation vessel on Figure 2.

Allocation meters and fluids samples measurements are available from each inlet separator and at the Export point. The precision of the inlet measurements and samples is in the range of 4%-6% while it is specified at 0.1%-0.2% at the Export meter. In between, flow measurements are also available for each of the trains at P1S2 and P2S1.

## 34<sup>th</sup> International North Sea Flow Measurement Workshop 25-28 October 2016

These are of intermediate precision considering the relatively stabilized nature of the streams at this point.

While the process layout is mostly typical of a surface production host facility, a very similar layout can also be extended to subsea or subsea/surface production process using a combination of separators and physical or virtual flowmetering systems.

All measurements are performed and reported at the process conditions as is the case with any flowmeter used at the outlet of a separator. The next sections will discuss the procedures used to evaluate and report the flowrates at the Export point conditions (assumed standard conditions in this study).

The hydrocarbon fluids have varying compositions and are typical of deepwater production fields. The fluids characteristics obtained from PVT reports are summarized in the following Table 1:

**Table 1 - Main Fluid Parameters of Streams Used in Inlet Separators**

Inlet Separator	API°	MW (g/mol)	GOR (scf/stb)	Gas Gravity (Air=1)
S1	26.8	108.0	700	0.704
S2	43.2	28.5	18600	0.784
S3	25.4	174.3	220	1.014
S4	22.5	167.8	230	0.760

Because of the streams' relative distribution, extensive interaction is expected within Train1 and little material transfer between the two trains since they only combine after multiple separation stages at relatively low pressure and temperature.

The composition of the monophasic fluid flashed in each of the inlet separators was reduced for simplicity to N<sub>2</sub>, CO<sub>2</sub>, C<sub>1</sub> thru C<sub>6</sub>, C<sub>7-12</sub>, C<sub>12-20</sub>, C<sub>20-30</sub>, C<sub>30+</sub>. The key properties of the lumped components were available from the PVT reports.

#### 4 COMPARATIVE STUDY

The results of the above proportional allocation procedure with PSM will be evaluated using the process model and calculation method described in previous section.

The software package used in the study has the dual capability of working as pure PSM forward simulator and as a PSM-DVR engine. By switching between the two modes, it is possible to generate two sets of allocation results; from the PSM-Proportional Allocation (PSM-PROP) and from the PSM Validation and Reconciliation (PSM-DVR) methodologies.

Moreover, in this package, the results of the PSM runs are evaluated along with their uncertainties using the uncertainties specified for the input measurements/parameters: flowrates, fluid composition, process instrumentation, etc. The evaluation and use of allocated quantities uncertainties was addressed in [1] and is not repeated in this paper.

In addition, the PSM mode is used to generate a third set of results treated as Reference or True Values; the relative deviations of different allocation methods (PROP or DVR) are evaluated in reference to the True Values. In other instances the True Values determined by this initial simulation run are used as intermediate measurements to assess the impact of added information on the allocation or reconciliation results. This is mostly applicable to the DVR method where intermediate flowrates and Export sample results can be integrated with inlet measurements (new measurement Tags).

## **34<sup>th</sup> International North Sea Flow Measurement Workshop 25-28 October 2016**

The simulated process is a multi-tier allocation process consisting of three allocation nodes. In the absence of measurements at the trains' outlets, P1S2 and P2S1, the entire process is treated as a single tier allocation scheme by performing the Combined and Exception runs using the flow measurements at the inlet and export points. Including the intermediate measurement at the production separators (if available) is a matter of adding the measurement tags in the simulator when running in the PSM-DVR mode. The same cannot be done in PSM mode alone without doing multiple simulation runs and two proportional allocations to balance the system at the P1S2, P2S1, Export node and at the inlet separators nodes for Train1 and Train2. Such practice is not common. Instead a single balancing calculation is performed without making use of the intermediate measurements. Alternatively such measurements can still be used for quality check and measurement performance improvements before allocation calculations.

### **4.1 Evaluation Procedure and Objectives**

A number of cases (production scenarios) were run in the PSM-PROP and PSM-DVR modes where Combined and Exception runs were used to perform production allocation at export meter conditions. Such process was applied to the PSM runs as described before, and to the DVR results. In the case of DVR, the Combined and Exception simulation runs were done using the reconciled estimates obtained from the PSM-DVR mode. No further proration is required because the DVR results have already been balanced during the reconciliation/DVR run. The difference between the Combined and Exception runs are used directly as the allocated volume quantities for each of the inlet streams evaluated at the Export meter conditions and are compared to the PSM-PROP method and the Reference case as will be shown in other parts of the paper.

The analyzed production scenarios are used to assess the performance of the PSM-DVR mode to:

- Detect flow measurement bias
- Detect fluid samples errors (density and composition)
- Evaluate the impact of additional measurements (flowrates and fluid sample information) on the accuracy and precision of reconciled results
- Perform production allocation driven by measurement uncertainty and bias minimization
- Perform comparative evaluations with the traditional PSM-PROP mode and with the Reference "True Values"

### **4.2 Simulated Reference Case**

As noted before, the Reference case is a PSM simulated case using Reference inlet flowrates at metering conditions (Figure 2) and the fluids of Table 1. The simulated data provides the "True Values" for the flowrates at P1S2 and P2S1 and flowrate, fluid properties and composition at the Export point. The information can then be used as additional measurements (including uncertainties) when needed during the PSM-DVR runs, or as Reference measurement for the Export meter flowrate (similar to the LACT measurement).

The Reference case is also used as the benchmark "True Value" case to calculate the relative deviation of allocation quantities when influenced by the process and/or measurements errors; i.e. errors caused by flowrates, fluids properties or instrumentation. Combined and Exception runs are performed in PSM mode to evaluate the "Theoretical True Value" for each stream at the Export meter conditions. The Theoretical Quantity total matches well with the initial Export meter reading (less than 0.05% difference).

## **34<sup>th</sup> International North Sea Flow Measurement Workshop 25-28 October 2016**

As with the Reference case generated in PSM mode, similar results are obtained in DVR mode with negligible penalties confirming the consistent behavior of the software package when run in either PSM or DVR modes.

### **4.3 Simulated Production Scenarios**

#### **Case 1: Actual Case - Moderate Imbalance**

This case is identical to the Reference case except that the inlet separators' measurements were slightly increased to impart a positive 3.37% imbalance between the PSM-PROP Theoretical Quantity total and the Export measurement. Such imbalance is neutralized by prorating it to each of the inlet streams' Theoretical Quantity.

The model is then run in PSM-DVR mode where measurements are reconciled at their actual conditions. The reconciled values for each inlet separator are subsequently used in PSM mode to determine the DVR Theoretical Quantity at the Export meter. Because the system has been balanced prior to performing the Combined and Exception runs such run results in approximately the same value as the initial Export meter reading (less than 0.05% difference in most cases).

The DVR run is shown in Figure 4. The altered inlet streams are flagged according to the penalty values of Table 2. This is a key feature of the DVR processing as it allows the inspection of input data before considering the reconciled data for allocation. In this case three of the four inlet streams were identified as candidates for in depth investigation (flagged blue). Depending on the magnitude of measurement error and the number of variables (moderate in this case) the severity of corresponding penalties can change from one variable to another. In this software package, the streams with individual penalty higher than 1 are coded blue changing to red when it gets above 4 ( $1.96^2$ ) indicating that the reconciled value is outside the 95% confidence level range defined for this measurement. Note that the reconciled value for each of the selected tags shows to the right of the measured value in the PFD figures.

Table 2 summarizes the allocated values and their relative deviation from the True Values. The Theoretical Quantity totals and imbalances are also shown for the PSM-PROP and PSM-DVR runs. Moreover, the DVR run provides information about the uncertainty of the reconciled (allocated) values along with the penalties. They are shown to the right of the reconciled values.

# 34<sup>th</sup> International North Sea Flow Measurement Workshop 25-28 October 2016

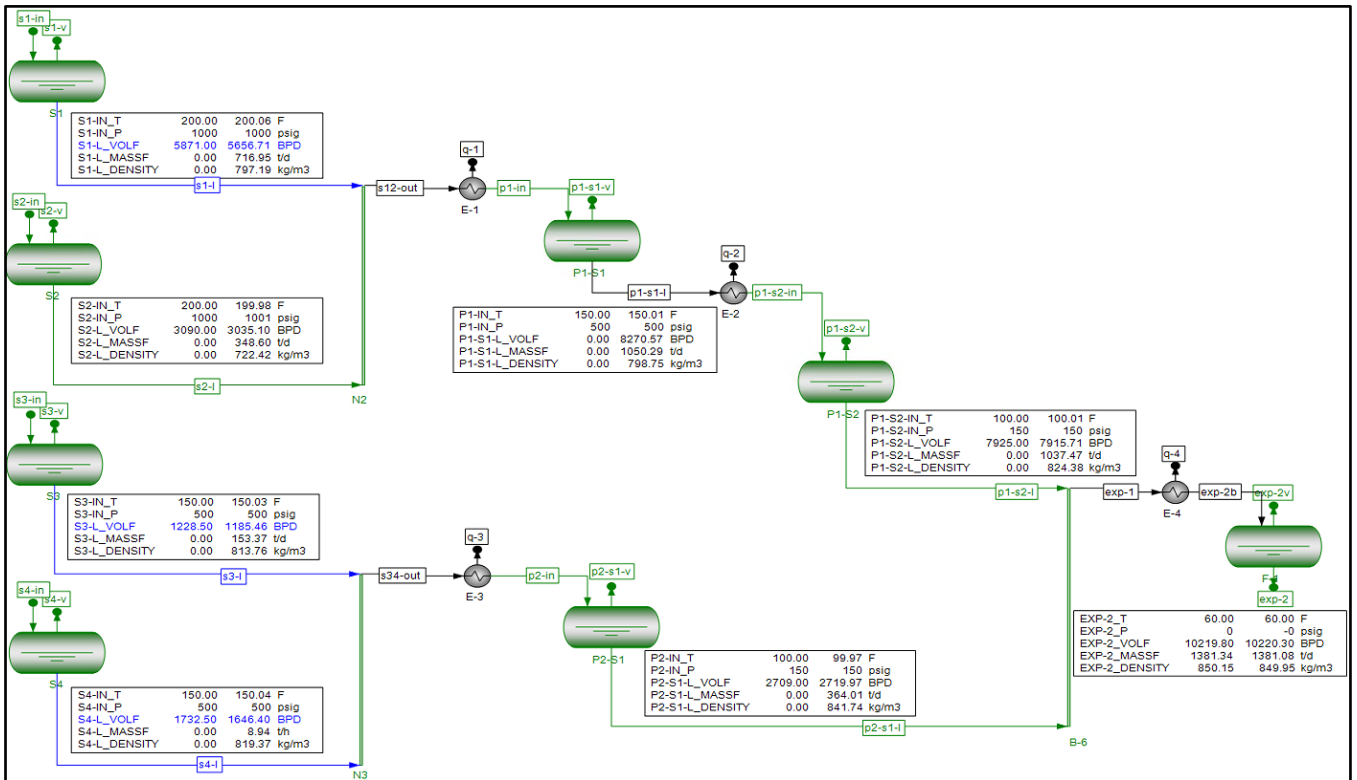
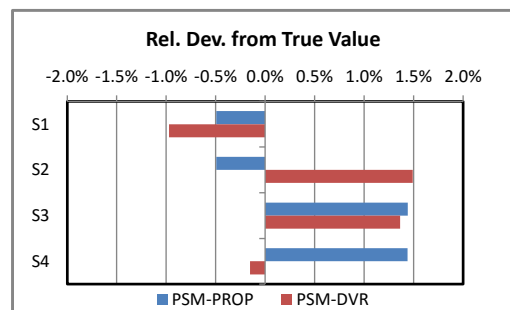


**Figure 4 - DVR Run of Actual Case with Moderate Imbalance and Penalties**

**Table 2 - Case 1 Result: Moderate Imbalance**

Case 1: Actual Case - Moderate Imbalance					
PSM-PROP		PSM-DVR			
STBD	%	STBD	%	Unc	Penalty
365.3	3.57%	7.6	0.07%		
10,585.1		10,227.4			
5,088.6	-0.49%	5064.2	-0.97%	2.0%	3.20
2,486.0	-0.49%	2535.6	1.49%	3.7%	0.76
1,092.0	1.44%	1091.2	1.36%	5.3%	1.31
1,553.2	1.44%	1528.8	-0.15%	4.1%	2.64



It can be seen from the graph of Table 2 that Proportional Allocation is done without consideration for the measurements' precision; the higher accuracy S1 and S2 measurements are allocated production volumes below the True Values to cover the gains of the less precise streams S3, and S4. This can somehow be justified by the fact that S1 and S2 streams were responsible for most of the positive imbalance in absolute terms.

The DVR reconciliation is driven and affected by the measurement uncertainty (Uncertainty Based Allocation - UBA) as was demonstrated in the simpler case of [1]. It is harder to interpret the results for each stream in this more complex case due to the number of variables including phase behavior and measurements uncertainties. However the measurements were reconciled to less than 2% deviation from the True Values as was the case with Proportional Allocation too. The added information about the uncertainties of the allocated quantities is a plus that is missing from the PSM-PROP run.

## 34<sup>th</sup> International North Sea Flow Measurement Workshop 25-28 October 2016

### Case 2: Actual Case with Export stream fluid sample composition measurement

Before proceeding to analyzing other cases, it was decided to study the impact of integrating the fluid sample information obtained at the Export meter sampling station (equivalent to LACT station). This exercise is applicable to the PSM-DVR mode since such information cannot be used directly in the conventional PSM-PROP mode.

In the previous case, no sample information was entered for the stream EXP-2. The fluid composition was calculated by the PSM as unmeasured variables using the measurement of the inlet streams' compositions. It was possible to perform these calculations because there was sufficient information redundancy (7) in the system to perform the calculations - i.e. number of equations exceeded the number of unmeasured variables as shown in Table 3. In Case 1 the calculation of EXP-2 stream composition added more unmeasured variable at the expense of reducing the system redundancy. The decrease in system redundancy reduced the accuracy and precision of the reconciled variable as will be shown later.

By including the 12 components composition obtained from lab analysis as measured variables, the number of equations and measurements increased by 12 raising the system redundancy from 7 to 19. This added redundancy makes the system more "over-specified" leading to improved reconciled values of the inlet streams in addition to improved precision as shown in Table 4.

**Table 3 - Number of Measurements and Redundancies**

	<b>Case 1 With Unmeasured Fluid Composition</b>	<b>Case 2 With Measured Fluid Composition</b>
Number of equations	306	<b>318</b>
Unmeasured variables	299	299
Measured variables	72	<b>84</b>
Number of redundancies	7	<b>19</b>

It can be noted from Table 4 that the reconciled results of S1 and S2 have improved compared to Case 1 along with improved uncertainty. In this particular case it was assumed that the precision of the sample components are in the range of 2% (i.e. higher quality sampling and analysis at the LACT sampling station) compared to the 5% uncertainty assigned to inlet separators samples.

The added advantage of including the sample information in the calculations as new equations enables the reconciliation of phase components across the system; this will be shown to provide the benefit to detect potential problems with the fluids sampling and analysis inputs and can be used as an important KPI in accepting or rejecting the samples according to industry standards [12].

Figure 5 shows that the S2 stream penalty was flagged in addition to the other streams; the penalty increase in this case is a direct result of the reconciled value improvement as it moves away from the biased measurement result and closer to the True Value. Before interpreting the penalty changes of a given measurement it is important to address and reduce other penalties to minimize their interference especially when the errors are relatively small.

# 34<sup>th</sup> International North Sea Flow Measurement Workshop 25-28 October 2016

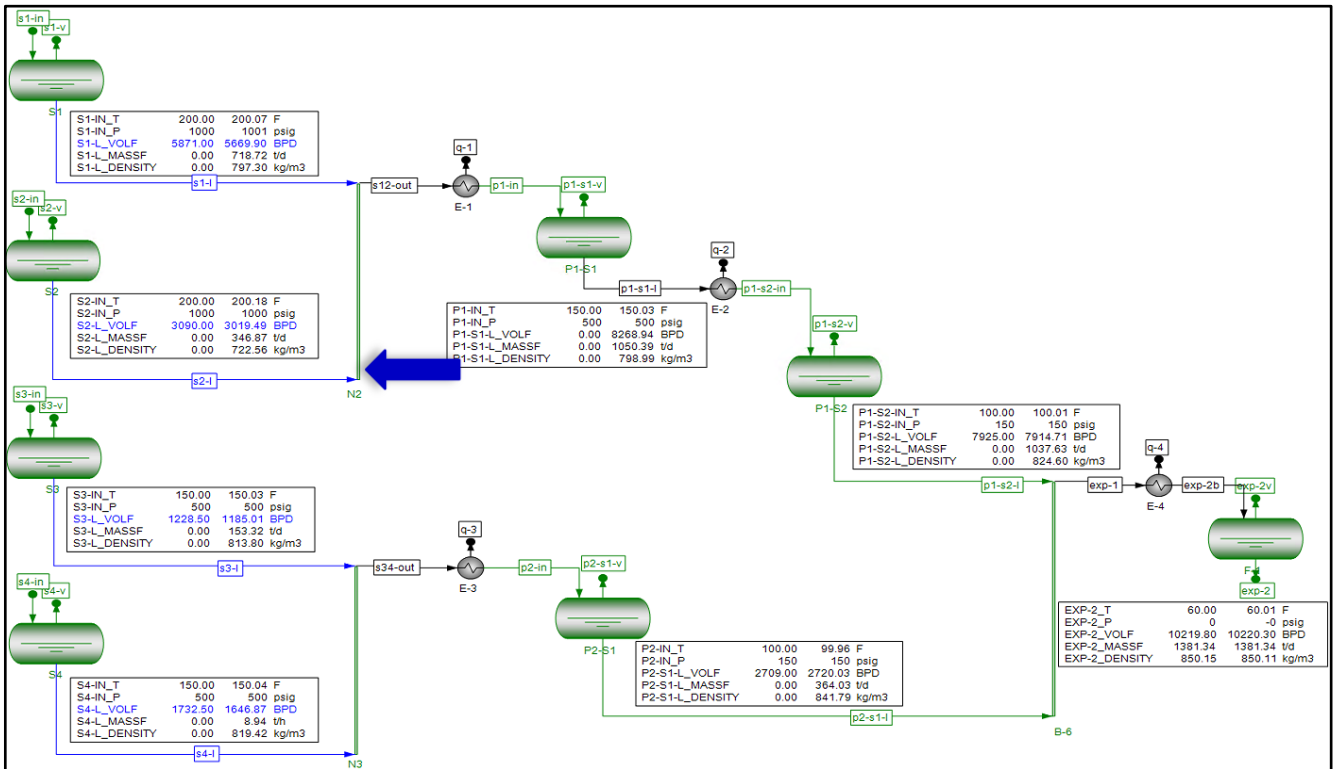
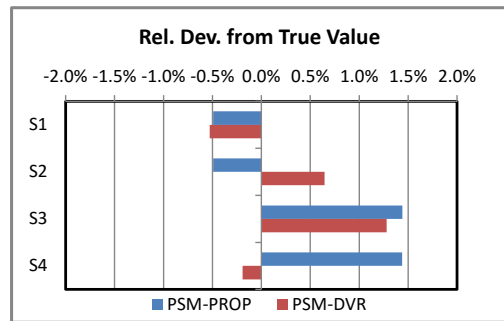


**Figure 5 - DVR Run Moderate Imbalance and with Composition Measurements at Exp-2**

**Table 4 - Case 2 Result: Export Meter Sample Composition Added as Measurements**

Case 2: Actual Case with Export fluid sample info.					
PSM-PROP		PSM-DVR			
STBD	%	STBD	%	Unc	Penalty
365.3	3.57%	6.3	0.06%		
10,585.1		10226.1			
5,088.6	-0.49%	5086.8	-0.53%	1.7%	2.82
2,486.0	-0.49%	2514.5	0.65%	2.9%	1.25
1,092.0	1.44%	1090.3	1.28%	5.2%	1.34
1,553.2	1.44%	1528.2	-0.19%	4.1%	2.61



### Case 3: Increased S4 flowrate bias (Gross Error) applied to Case 2

A "Gross Error" is introduced to S4 flowrate measurement by increasing this measurement's positive bias from 5% to 9%, i.e. increasing the error beyond the measurement's 95% confidence level range of 6%. The system imbalance has also increased from 3.47% to 4.17%.

In this case S4 stream is flagged red (Figure 6) due to its penalty (5.35) exceeding the 4 boundary level (the boundary for the reconciled value deviation from the measurement's 95% confidence level range of uncertainty). Other inlet separators' measurements are also influenced but still within moderate penalty ranges.

Errors of such magnitude are usually noticed and should be corrected first before proceeding with the production allocation process (meter recalibration or fluid density correction are possible solutions). However, in the event that such gross error was

# 34<sup>th</sup> International North Sea Flow Measurement Workshop 25-28 October 2016

overlooked and went undetected, it can be seen that the allocation results deteriorate significantly in the PSM-PROP mode as shown in Table 5.

The results of the PSM-DVR mode reflect the change in system reconciled profile due to the gross error but continued to be within the acceptable range of less than 2% deviation from the True Values.

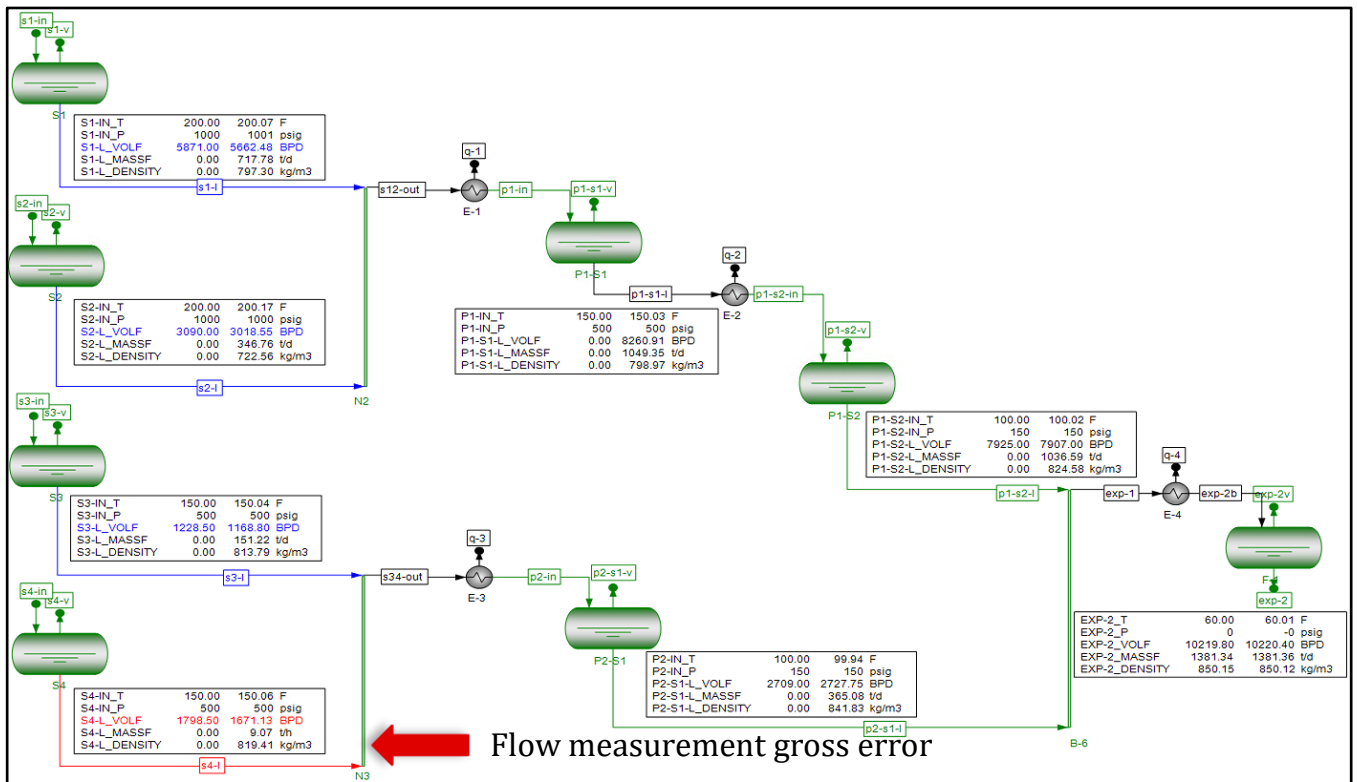
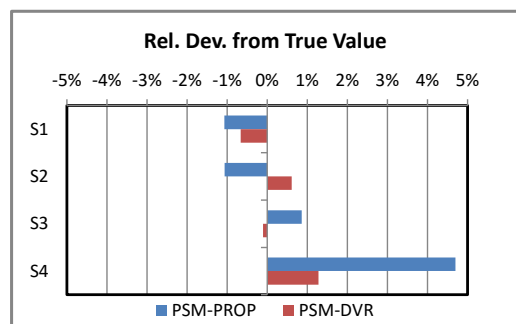


**Figure 6 - DVR Run: Gross Error Identified at S4 Due to Flowmeter Measurement Bias**

**Table 5 - Case 3 Result: Gross Error Due to Increased Flowmeter bias at S4**

Case 3: Actual with S4 Gross Error					
PSM-PROP		PSM-DVR			
STBD	%	STBD	%	Unc	Penalty
426.6	4.17%	6.6	0.06%		
10,646.4		10,226.4			
5,059.3	-1.07%	5080.1	-0.66%	1.7%	3.03
2,471.7	-1.07%	2513.7	0.61%	2.8%	1.28
1,085.7	0.86%	1075.3	-0.11%	5.3%	2.52
1,603.1	4.70%	1550.7	1.28%	4.1%	5.35



An obvious observation from the DVR results of Table 5 is that the damage caused by the gross error is mainly inflicted on the penalty parameter leaving the reconciled value almost unaffected. Furthermore, the measurement gets tagged for corrective action potentially leading to allocation results improvement. This contrasts with the PSM-PROP mode where the diagnostics features are lacking, and where much of the damage is inflicted directly on the allocated volume quantities.

# 34<sup>th</sup> International North Sea Flow Measurement Workshop 25-28 October 2016

## Case 4: S4 flowrate bias and S1 sample composition error applied to Case 3

Case 3 was further modified by introducing an error to S1 fluid sample. The error consisted of modifying the molar fraction by removing 0.7% from the molar fraction of C30+ component and adding it to the lighter component C6. In essence this led to the PSM erroneous treatment of S1 stream as having a lighter fluid, which is characterized by more shrinkage. The treatment was carried through the different separation stages to the Export meter. The net result is that the Theoretical Quantity total was reduced by approximately 12 STBD leading to an apparent lower imbalance compared to the previous case. This was the only observation made from the PSM-PROP run.

Conversely, the PSM-DVR run based on Figure 8, flagged three other streams red in addition to S4 indicating penalties in excess of 4. The three other streams are:

- S1-in: the feed stream of inlet separator S1 with erroneous sample
- S2-in: the feed stream of inlet separator S2
- Exp-2: the Export meter stream

By examining the tags windows of the above streams (Figure 7) it can be concluded by triangulation that the most likely cause for increased penalties at S1-in, S2-in and Exp-2 are erroneous molar fraction inputs at S1. Of course this assumes that the composition input in Exp-2 stream as discussed in Case 2 above, is accurate and of high quality.

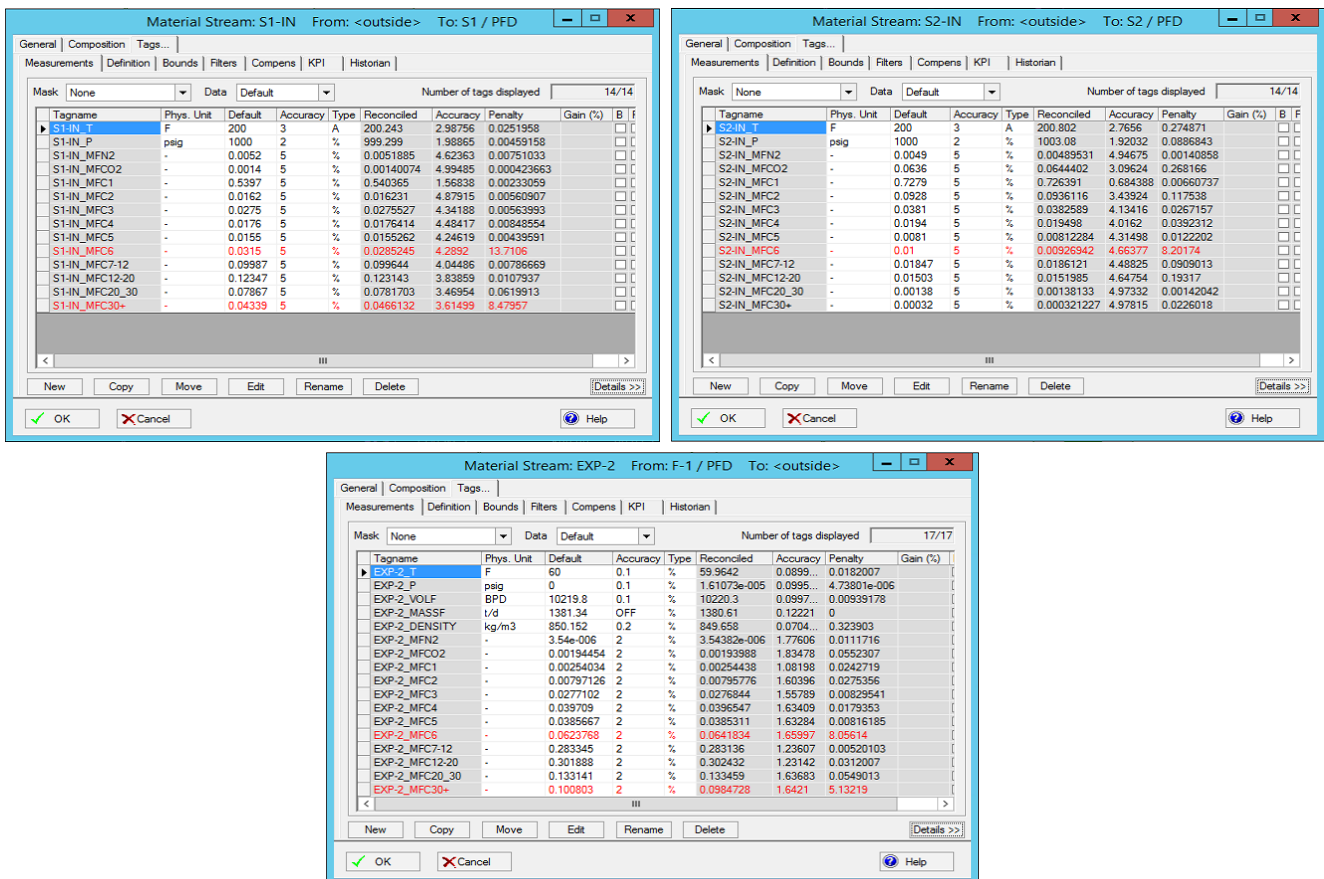
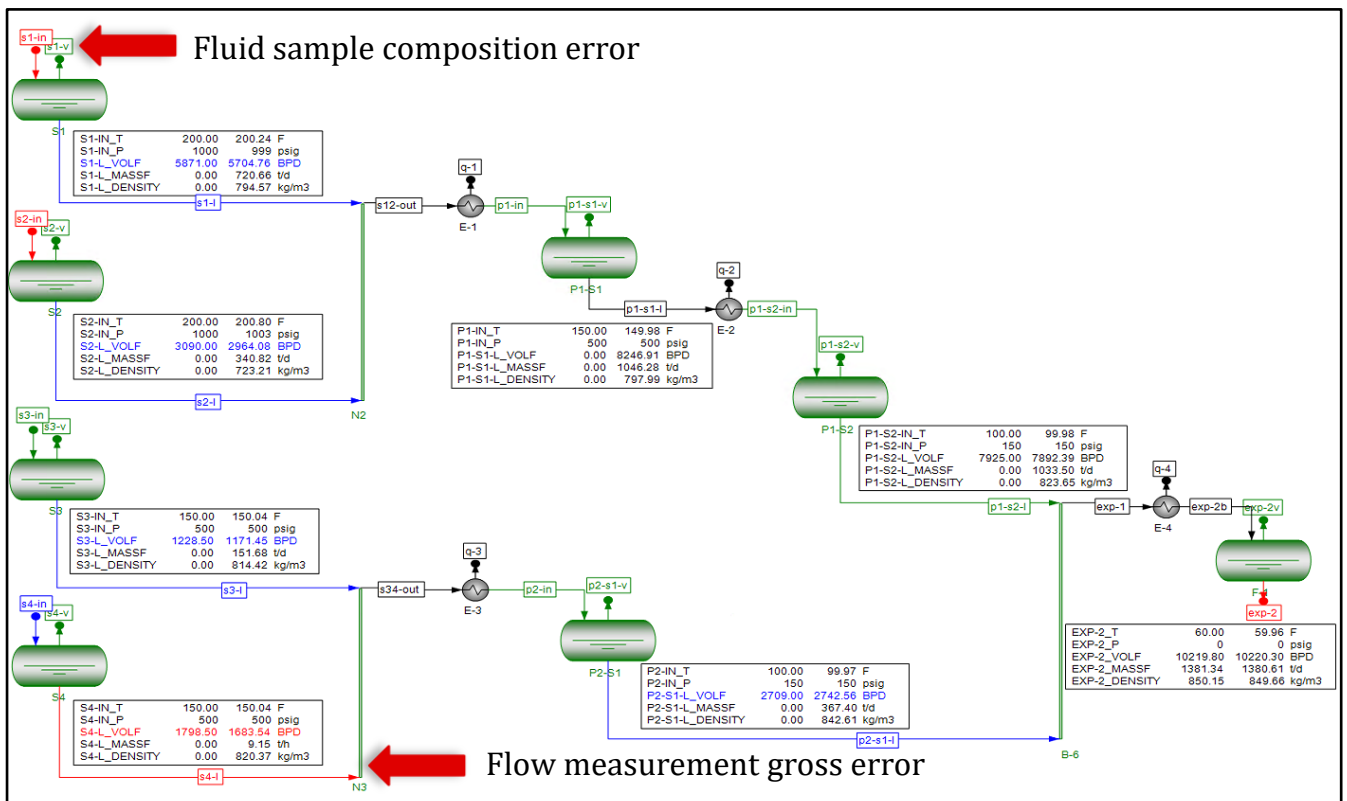


Figure 7 - Tags Windows of S1-in, S2-in and Expo-2 to Locate Source of Sample Error

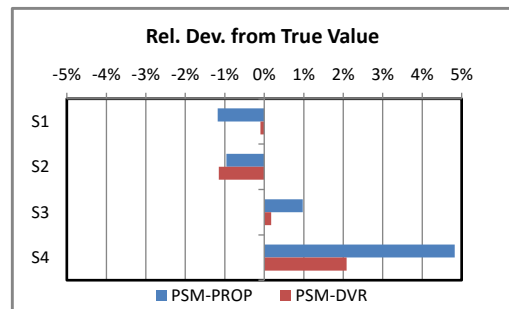
# 34<sup>th</sup> International North Sea Flow Measurement Workshop 25-28 October 2016



**Figure 8 - DVR Run of Case 4 with S4 Flowmeter Bias and S1 Sample Error with Expo-2 Comp.**

**Table 6 - Case 4 Result: S4 Flowmeter Bias and S1 Sample Error with Expo-2 Composition**

Case 4: S4 flow bias, S1 sample error, Exp. compo. & den.					
PSM-PROP		PSM-DVR		Unc	Penalty
STBD	%	STBD	%		
414.2	4.05%	1.1	0.01%		
10,634.0		10,220.9			
5,053.5	-1.18%	5108.9	-0.10%	1.7%	1.93
2,474.3	-0.96%	2469.5	-1.15%	2.9%	3.99
1,087.0	0.97%	1078.4	0.17%	5.3%	2.30
1,605.0	4.82%	1563.1	2.08%	4.1%	4.36



As expected, the results of the PSM-PROP run changed slightly because of the small reduction in the apparent imbalance assessed at the Export meter conditions. On the other hand, more adjustments are observed in the PSM-DVR results due to the integral use of the erroneous sample data in the reconciliation calculations. However, the results were still confined to about 2% deviation from the True Values.

It should be mentioned that such error detection was made possible by using the sample compositional analysis at the Export meter sampling station as input measurements. This in turn enabled the DVR reconciliation process to balance the streams' measured compositions rather than using computed or unmeasured compositions.

In the case of the PSM-PROP run, all compositions are forward-computed. Without a quality check procedure to compare the computed results with the actual composition at Exp-2 the erroneous sample data would not be identified.

# 34<sup>th</sup> International North Sea Flow Measurement Workshop 25-28 October 2016

## Case 4a: Same as Case 4 but with liquid density measurement at Export meter

The case builds on Case 4 by maintaining the sample error at S1 but replacing the 12 liquid components measurements at the Export meter with one liquid density measurement. This may be the case if sample analysis are not performed and only certain properties such as oil API° is available.

Again the results of the PSM-PROP run are not expected to change because the information at the Export meter is not included in the model's forward simulation. At best a comparison between the measured and calculated density values at the Export meter may reveal a discrepancy that could prompt actions to trace back the source of discrepancy and improve results.

The results of the PSM-DVR run are expected to be similar to Case 4 because in both cases the fluid density measurement was used to anchor the liquid properties at the Export meter. However it can be shown that the uncertainty of the reconciled flowrates increases slightly due to the reduction of system redundancy caused by the removal of composition measurements. Additionally, the absence of composition information limited the system's error detection capability by only indicating an increase of liquid density penalty at the Export meter (Figure 9) without making reference to the sample error at the inlet separator S1.

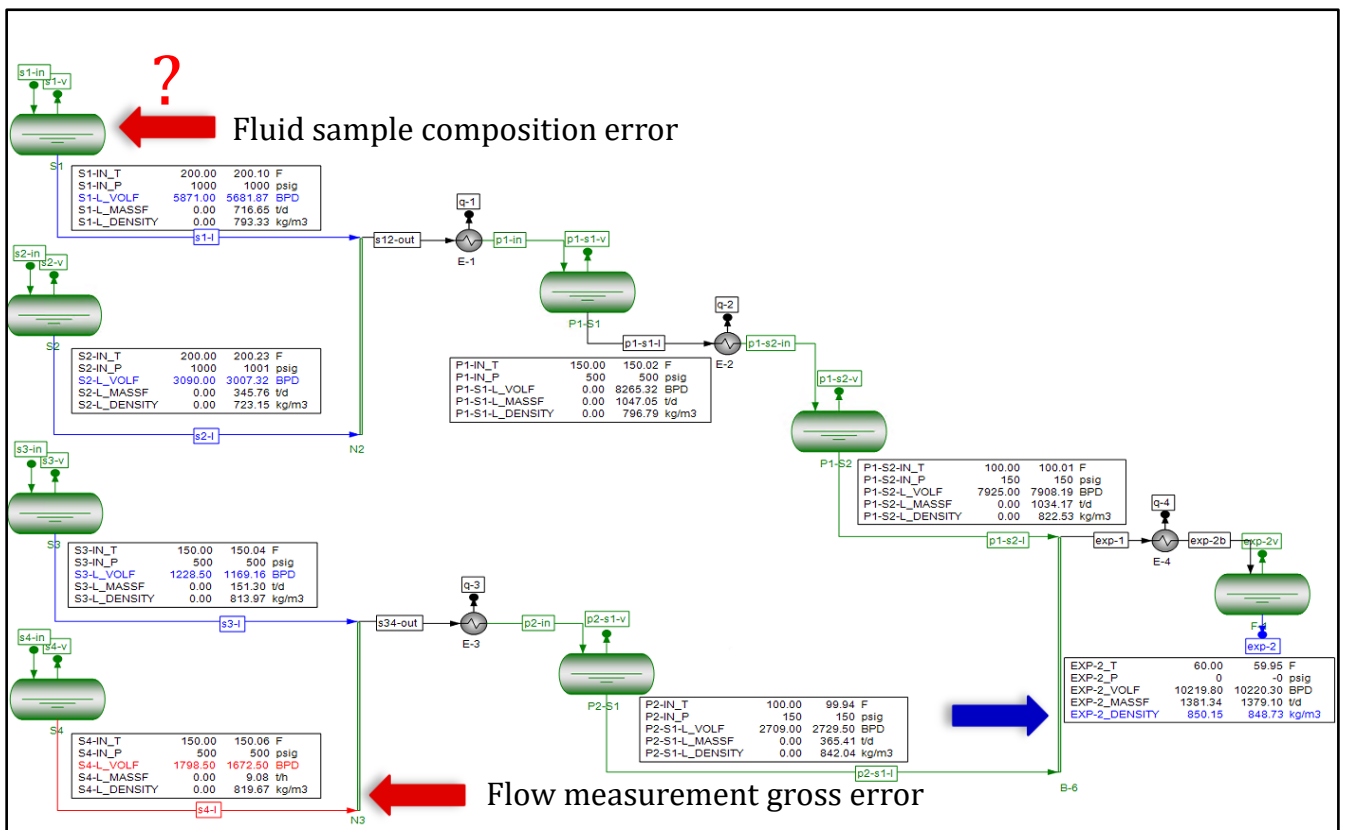


**Figure 9 - DVR Run of Case 4a with S4 Flowmeter Bias and S1 Sample Error with Expo-2 Liquid Density and No Sample Composition**

## 34<sup>th</sup> International North Sea Flow Measurement Workshop 25-28 October 2016

### Case 5: Analysis after flowmeter calibration and sample error elimination

With the ability to detect potential biases and errors in the flow measurement and/or fluid samples, the erroneous data can first be corrected before proceeding to the allocation phase. This was done in this case by using the information gained from the PSM-DVR surveillance results to eliminate the gross error in S4, remove the molar fraction errors in the fluid sample of S1, and recalibrate all inlet flowmeters. Compared to Case 1, the flowmeters performance has been improved according to Table 7, while their uncertainty specification (precision) remained unchanged (4%-6%):

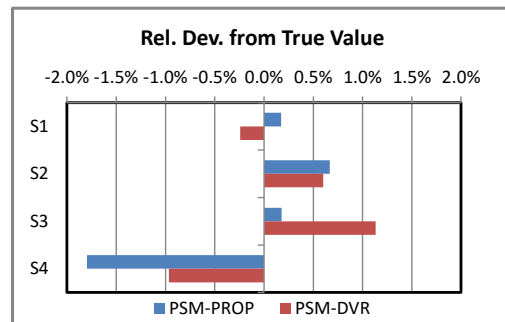
**Table 7 - Assumed Flowmeters Bias before and after calibration - % of True Values**

Inlet Separator	Case 2 (before calibration)	Case 5 (after calibration)
S1	3%	1.5%
S2	3%	2.0%
S3	5%	1.5%
S4	5%	-0.5%
Imbalance	3.57%	1.39%

Following the corrective action the improved measurements were used in both allocation schemes, PSM-PROP and PSM-DVR as shown in Table 8.

**Table 8 - Case 5 Result: After Flowmeters Calibration and Sample error Elimination**

Case 5: After meters calibration and sample error corr.					
PSM-PROP		PSM-DVR			
STBD	%	STBD	%	Unc	Penalty
141.8	1.39%	6.0	0.06%		
10,361.6		10,225.8			
5,122.8	0.17%	5101.4	-0.24%	1.7%	0.71
2,515.0	0.67%	2513.3	0.60%	2.8%	0.45
1,078.4	0.18%	1088.7	1.13%	5.0%	0.01
1,503.6	-1.80%	1516.4	-0.97%	4.0%	0.02



Noticeable improvements are seen in the allocation results, which translate to reduced average relative deviation from the True Values. Most individual streams deviations are contained within 1%. The larger negative excursion of S4 allocated quantity in the PSM-PROP mode is due to the "irregular" measurements bias contributions with negative bias assumed for S4.

The PSM-DVR run penalties are also reduced to below 1 indicating closer match between the reconciled measurements values ("True Values surrogate") and the actual flowrate measurements. Overall system consistency is achieved between the measurements, the input parameters and the system's physical model.

Regardless of the allocation formulation scheme adopted by the user, the above diagnostics and corrective steps are essential to achieve optimal and equitable allocation results.

## 34<sup>th</sup> International North Sea Flow Measurement Workshop 25-28 October 2016

### Case 6: Case of loss of inlet flowmeter

The case examines the impact of losing physical sensors due to equipment failure or unavailability. This may apply to any device in the system; however in the case of production allocation, the loss of an inlet flowmeter can be critical and highly disruptive.

The simultaneous inclusion of all system available information (flowmeters, fluid samples, process conditions, physical constraints) in the PSM-DVR model provides efficient and quantifiable way to recover from this situation - at least until the faulty meter is replaced. Provided sufficient data redundancy is present, the removal of a device from the system is automatically substituted for by its measurement reconciled value and associated uncertainty.

While other modeling approaches can also be used to perform this recovery task, the limited information (inlet flowrates and samples analysis and Export meter flowrate in the case of PSM-PROP methodology) may be insufficient to arrive at a unique estimate for the missing inlet flowrate. Iterative "by-difference" volumetric and mass based calculations will be required to obtain an estimate. However the results will be unquantifiable in the presence of even small errors in the other streams and/or other phases. Ultimately, all the other streams errors/biases, which cause production imbalance, will systematically accumulate in the estimated/unmeasured flowrate of the stream that is missing the inlet flowmeter.

The corrective action based on the PSM-PROP methodology was not attempted in this work, instead, comparative analysis was done using Case 5 configuration to recover S3 flowmeter (Table 9).

**Table 9 - Case 6 Result: Case of Loss of Flowmeter at S3**

Case 6: Comparison of Case 5 results with and without S3 flowmeter							
DVR <b>without</b> S3 flow measu.				DVR <b>with</b> S3 flow measu. (Case 5)			
STBD	%	Unc	Penalty	STBD	%	Unc	Penalty
6.0	0.06%			6.0	0.06%		
10,225.8				10,225.8			
5,103.0	-0.21%	1.7%	0.69	5101.4	-0.24%	1.7%	0.71
2,513.7	0.62%	2.8%	0.44	2513.3	0.60%	2.8%	0.45
1,079.3	0.26%	<b>9.3%</b>	0.00	1088.7	1.13%	<b>5.0%</b>	0.01
1,523.8	-0.48%	5.9%	0.00	1516.4	-0.97%	4.0%	0.02

Train2 is the most affected by the new estimate. The surprising result in this case is the reduced deviation from the True Value compare to the case with meter availability; with meter removal, the stream's bias (-0.5%) was also removed and with sufficient system redundancy the reconciliation was also improved. However the improvement is also tagged by increased uncertainty from 5% to 9.3%. The other streams estimates and uncertainties were almost unchanged especially S1 and S2 of Train1. This led to similar average deviation for both cases and confirms the fact that the PSM-DVR approach is not subjected to the "by difference" shortfalls.

Losing a flowmeter (or other devices) is a situation that production operations will likely face at one point in the life of a project. This can have serious consequences if such meter is irreplaceable in the short term. This situation is quite applicable to subsea MPFMs where substitute flowrate estimates by-difference or from Virtual Flowmeters (VFM) is often used. Adopting the DVR approach will add another level of rigor as shown in the above example; in this situation the simultaneous use of DVR in the well model (VFM) and the system model (PSM-DVR) will further improve the results at the well where the meter became unavailable, and at the system level for allocation and reservoir management.

# **34<sup>th</sup> International North Sea Flow Measurement Workshop**

## **25-28 October 2016**

### **5 DVR PRACTICAL CONSIDERATIONS AND SUMMARY**

#### **5.1 Surveillance versus Allocation; What is Needed?**

The use of a PSM and/or DVR software package depends on the intended application. For surveillance application the integration of PSM and DVR capabilities in single software is not required. This would be the case if a PSM software package is already employed to perform the PSM-PROP modeling and allocation calculations. The addition of a separate DVR package will be for surveillance and diagnostics applications. In this case DVR devised corrective actions and improvements can be implemented before proceeding with the PSM-PROP runs.

If a DVR-based allocation (Uncertainty Based Allocation for complex systems) is required, an integrated PSM-DVR software package will be required to perform the surveillance and allocation functions. As shown before, the initial PSM-DVR run is performed to check the system for erroneous data, and if none are found, the measurement reconciled values from this run are fed to the PSM standalone mode of the same package to perform the Combined and Exception runs. The allocated volume quantities are obtained directly by differencing each of the Exception runs from the Combined run. No further proration is required because the system has already been balanced during the initial PSM-DVR run.

The need to use an integrated PSM-DVR package stems for the fact that commercial PSM packages use different internal models / EOS versions. Residual differences won't cancel out if distinct software packages are used to perform DVR then PSM runs for the allocation application.

#### **5.2 Uncertainties of Allocated Quantities - Improvement with Redundancy**

In a DVR run uncertainties are calculated for all system variables, measured and unmeasured variables. This feature is only available in the PSM-DVR mode and is an important addition to the qualification of allocated volume quantities. In other words, the allocated quantities are qualified by their uncertainties in addition to their absolute values. This qualification will aid in reducing the risks associated with the measurement/data quality, or lack thereof, that is used in allocation calculations. An example was shown in Case 6 above where the use of unmeasured flowrate in S3 due to flowmeter unavailability resulted in much higher uncertainty for this variable.

Moreover, the DVR approach provides the added advantage of improving the allocated quantities uncertainties with the inclusion of as many measurements as available in the production system/facility. It was shown that more measurements lead to more system redundancies which in turn lead to improving the uncertainty of the reconciled values. In production environment, measurements sources are not limited to physical sensors, meters, or devices. They can be fluid composition from lab analysis and other fluids properties as well as any other production KPI's such as Gas Oil Ration (GOR) if deemed accurate and usable as another piece of information [9].

Figure 10 summarizes uncertainty improvements in the above studied cases as more measurements were added to the PSM-DVR model. It was also noted that depending on the type of added measurements, the model diagnostics capabilities can change. This was observed in Cases 4 and 4a.

# 34<sup>th</sup> International North Sea Flow Measurement Workshop 25-28 October 2016

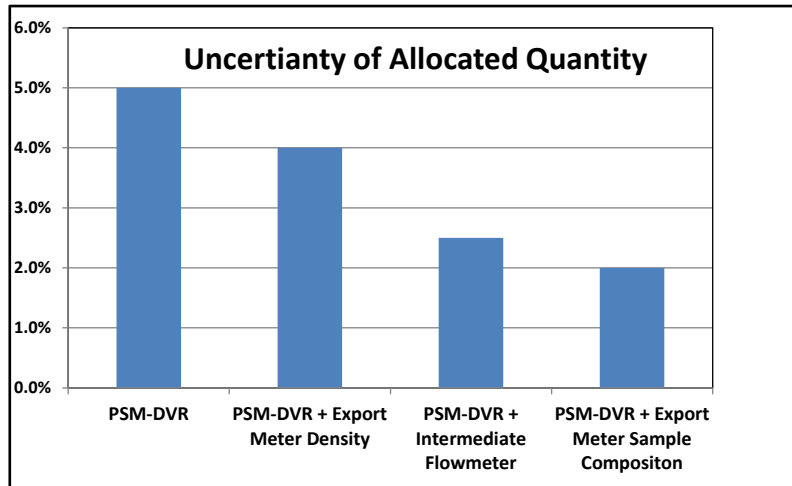


Figure 10 - DVR Run - Reduction of Allocated Quantities Due to Added Measurements

### 5.3 Penalties Trending for Surveillance

In the surveillance mode, DVR is best used by visualizing the trend of a measurement penalty. A schematic view of the penalties tracked in this study is shown in Figure 11.

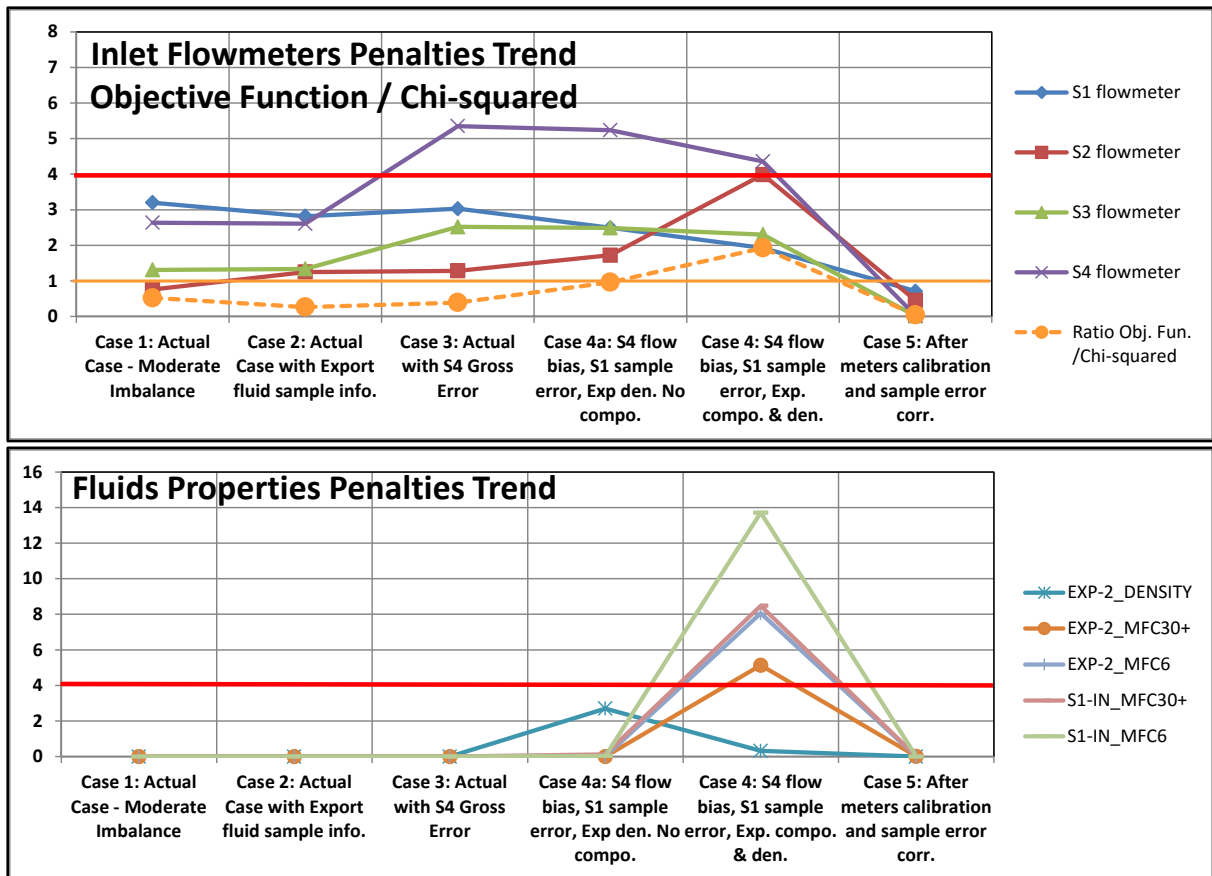


Figure 11 - Schematic Presentation of DVR Penalties in Surveillance Application

Only the affected measurements trends are shown for the inlet flowmeters and fluid samples at S1 separator and Export meter station. By correlating the trends from the two groups of measurements, the onset of different events can be detected and

## **34<sup>th</sup> International North Sea Flow Measurement Workshop 25-28 October 2016**

interpreted for their interaction with each other; the bias of S1 flowmeter is clear in Cases 3, 4a, and 4 while the anomaly on the Export meter density trend indicates potential fluids problems. It was not until the Export meter fluid composition was introduced as measurement that the source of fluids anomalies was attributed to S1 sample, and more particularly to the components C6 and C30+. Once all errors were removed and the meters calibrated to better accuracy, all trends returned closer to zero penalty in Case 5.

Another aggregate parameter, the Global Test, can also be monitored to assess the process overall health. This would be the first line of defense before looking things up in more details, tag by tag. The ratio of the Objective function over the Chi-square function is indicative of any anomalous trends, especially if it rises above 1 as shown in the upper graph of Figure 11. The more measurements / redundancies built in the process the more sensitive it is.

With the DVR approach, system surveillance and data trending to identify potential problem uses differential-data such as measurements penalties in addition to trending the measurements absolute values; this approach carries an important advantage because measurement values change with process changes, but differential-data trending is more sensitive to measurement anomalies. Isolating potential issues is made easier and better quantified by using penalties trends.

Compared to conventional process monitoring approaches, DVR fills an important void in any allocation process by providing a dynamic reference as close as possible to system's "True Values". The reference consists of the reconciled measurement surface (or topography) used by the penalties calculations to generate the differential-data; As long as the penalties are contained, the differential-data surface will remain low and gradually changing across the process. Any considerable rise in penalty values will translate in spikes easily detectable.

### **5.4 System Optimization and Analysis**

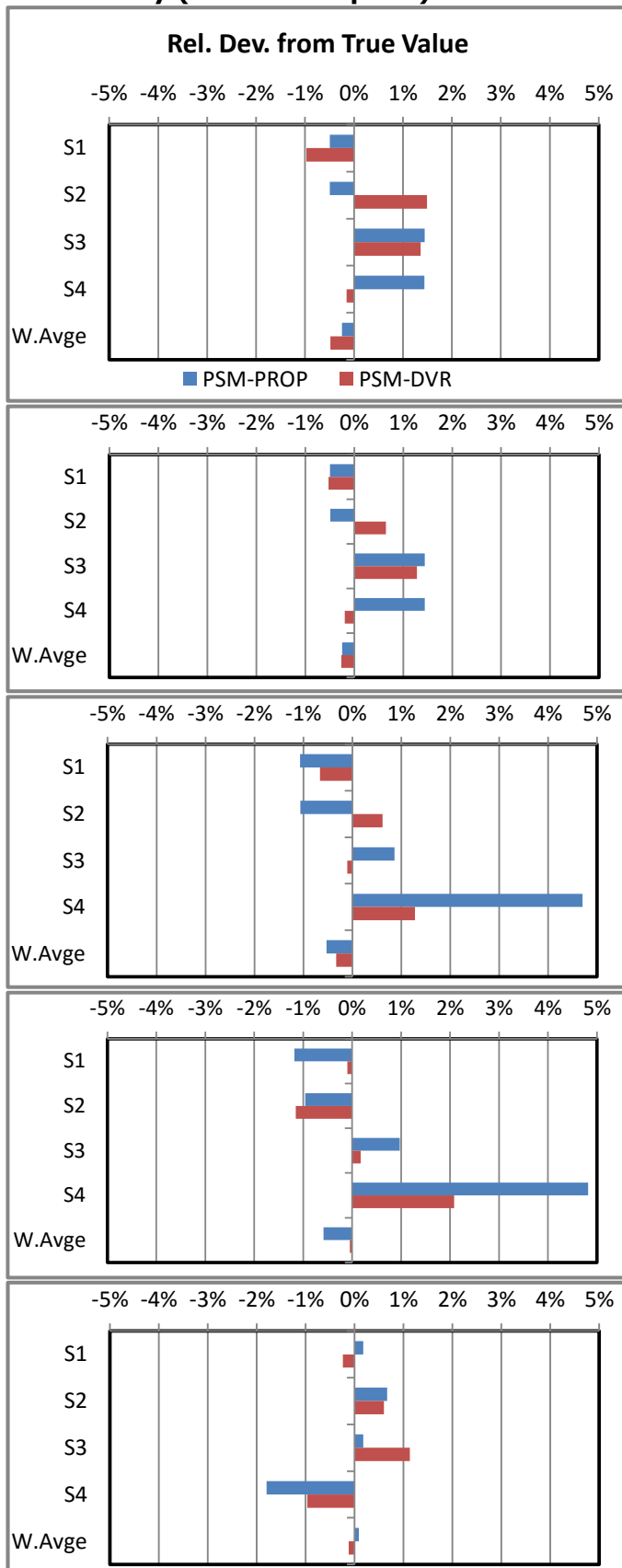
Because of the simultaneous solving of all measurements equations in a DVR model, the impact of any single measurement on the sought solution can be quickly studied by making the runs with and without the measurement in question. Other sequential approaches may also be used but will lack the accuracy and the automated features of a DVR model. This feature was highlighted in Case 6 and is addressed in more details in [13].

### **5.5 Cases Summary**

To better visualize the relative effect of different changes made to the PSM-DVR model in this study, the relative deviation plots are shown together using the same scale. A summary and comments are provided for each case next to the plot.

# 34<sup>th</sup> International North Sea Flow Measurement Workshop 25-28 October 2016

## Summary (same scale plots)



### 1) Actual Case

**Imbalance 3.37%**

#### Inlet flowrates:

S1 Ref flowrate plus 3% bias

S2 Ref flowrate plus 3% bias

S3 Ref flowrate plus 5% bias

S3 Ref flowrate plus 5% bias

**Fluids:** Same as Ref case

**Comments:** Allocated volumes are within 1.5% of Ref values.

Prop Allo: S1,S2 under allocated

S3,S4 over allocated

DVR results driven by evaluated measu. bias and precision, and process balances.

### 2) Actual Case with Export fluid composition

**Imbalance 3.37%**

**Inlet flowrates:** Same as case 1

**Fluids:** Exp Ref fluid composition used as measurements (12 added tags) in DVR reconciliation

**Comments:** Improved DVR reconciliation in S1, S2 with additional information. No change in Prop Allo; Added data not integrated and not used.

### 3) Actual Case and S4 increased bias

**Imbalance 4.17%**

**Inlet flowrates:** Same as case 1. Increased S4 4% - Total 9% bias

**Fluids:** Same as case 2

**Comments:** In Prop Allo, S4 is 4.8% over allocated due to significant imbalance in Train 2. Train 1 under-allocated by 1%.

DVR results moderately affected by S4 bias and remain below 1.3% deviation

### 4) Actual Case with S4 +bias and S1 sample composition error

**Imbalance 4.05%**

**Inlet flowrates:** Same as case 3. **Fluids:** Same as case 2 - S1 sample error 0.7% increase C6, decrease C30+

**Comments:** Only 16 BPD reduction in imbalance due S1 lighter apparent fluid (more shrinkage). Allocation adjustments with slight deviation increase from Ref case DVR within 2%.

### 5) After meters calibration, S4 bias and S1 sample error elimination

**Imbalance 1.39%**

#### Inlet flowrates: (residual bias after calib.)

S1 Ref flowrate +1.5% bias

S2 Ref flowrate +2.0% bias

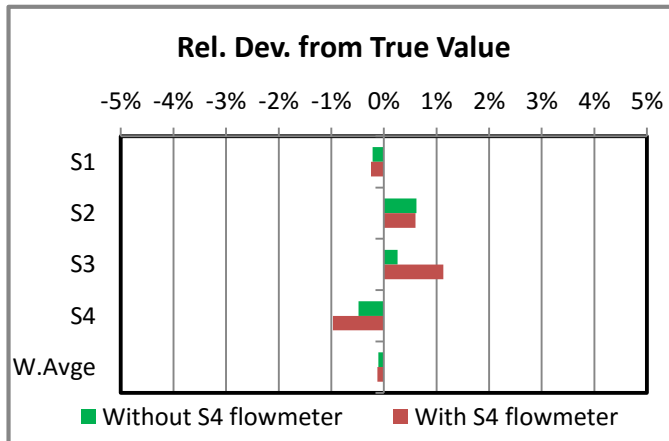
S3 Ref flowrate +1.5% bias

S3 Ref flowrate -0.5% bias

**Fluids:** same as Ref case

**Comments:** Improvements guided by DVR penalty evaluation. Not available in Prop Allo but helps improve either method. Prop Allo impacted by measurement bias irregularity

## 34<sup>th</sup> International North Sea Flow Measurement Workshop 25-28 October 2016



### **6) Loss of Inlet Flowmeter at S3 after error correction (Case 5).**

**Imbalance: 1.39%**

**Fluids:** same as Ref case

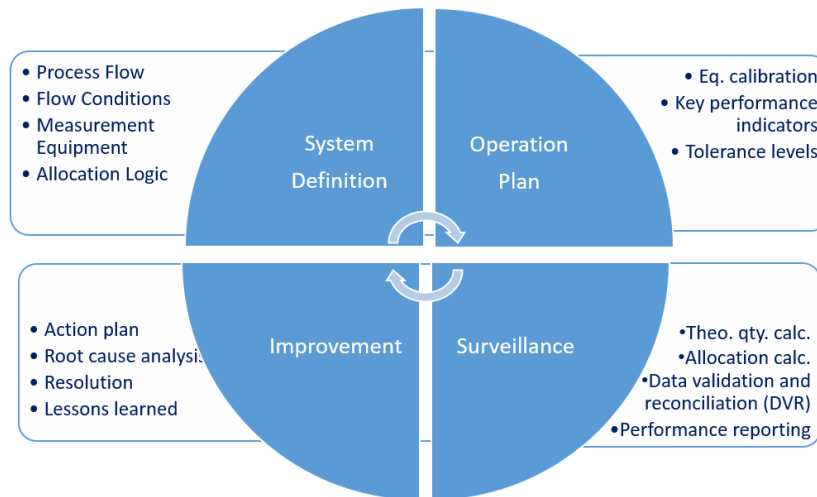
**Comments:** This is identical to Case 5 but after the loss of flowmeter at S3. Graph shows the results with and without the meter. With enough redundancy in the system soft sensors can be created. In this case, S3 flowmeter is substitute by a soft flowmeter that can be used in the allocation process.

# 34<sup>th</sup> International North Sea Flow Measurement Workshop 25-28 October 2016

## 6 CONCLUSIONS - RECOMMENDATIONS

### Production Allocation Measurement Management

Data validation and reconciliation (DVR) acts as an engine that drives the performance improvement and sustainability of the production allocation measurement system. DVR is the part of the surveillance program where data analysis adds value in identifying errors and performance shortfalls. However, while DVR is at the heart of production allocation measurement performance management, DVR needs to be combined with other parts of performance management in order provide complete the assurance cycle.



This figure illustrates the production allocation measurement assurance cycle. The upper activities define the production allocation measurement system and the operation plan used to maintain the systems performance. The lower activities use the system definition and operational activities as input surveillance and improvement activities. When the four activity sets, system definition, operational plan, surveillance, and improvement, are combined a complete production measurement system can be managed more effectively to assure performance.

### 1) System Definition

System definition is foundational to DVR efforts. It is essential that the DVR effort knows where the data being analyzed is coming from within the process flow.

The system definition activity defines the process flow, the associated measurement equipment and the allocation logic. The system definition is used to evaluate the capability of the equipment in terms of random uncertainty and bias tendencies considering the relative flow conditions. The system definition is especially helpful in providing non-operating parties and governmental agencies with a transparent view of the measurement and allocation parts of the system. It can also provide some insight into the performance expectation in terms of risk of measurement uncertainty and allocation inequity.

There are key documents that should be developed and maintained as part of the system definition. The primary document is called a "measurement" process flow diagram or MPFD. The MPFD describes both the process flow and the relative allocation measurement systems. Another key document is the allocation logic diagram. This document might take multiple forms, but ultimately the objective of the document is to describe the allocation formulation relative to the measurement data being created by the equipment and logged into the data historian. The diagram can also serve as a blueprint

## **34<sup>th</sup> International North Sea Flow Measurement Workshop 25-28 October 2016**

for the configuration of the allocation software and for subsequent audits of the allocation calculations.

### **2) Operational Plan**

The key point of the operational plan relative to the DVR effort is the defining of the key performance indicators (KPI) and the out-of-tolerance levels. These two basic elements help support DVR in defining what data to analyze, and identifying when there is a likely errant measurement. Conversely the DVR activity can also lead to changing the operational plan in both a more or less aggressive manner. DVR can demonstrate where the frequency of validation and calibration activities should be increased. But, DVR can also show where instrument stability justifies decreasing the verification and calibration frequency. The goal of the operation plan is to optimize human activity versus the associated financial and HSSE risks.

### **3) Surveillance**

For the most part surveillance is data validation and reconciliation. Because the other sections of this paper thoroughly discuss DVR, nothing more needs be said here. The end of the surveillance activities includes performance reporting. This rather simple step is a critical part of the process because it definitively ties the recognition of poor performance to the improvement activities that addresses it.

Often a step is inserted between surveillance and improvement activities. This step is best described as a justification and clarification step where a case to take action is presented with an estimation of activities (e.g. man-power, cost, schedule, etc.). This step is especially necessary in offshore and remote operations where extra technical staff and activities require a certain extra effort in logistics.

### **4) Improvement**

The work exerted in defining the system, operational planning, and surveillance, comes to fruition in the improvement segment of the assurance cycle. The improvement activities take action on the outcomes of the surveillance activities. It also utilizes all the system definition and operational plan information together with the wealth of data collected and analyzed by the surveillance / DVR activities. By using all the data as a resource the improvement activities can utilize root cause analysis and continuous improvement techniques to resolve measurement system errors and performance shortfalls.

By resolving the various issues, a variety of positive outcomes are realized. First, most often the integrity in terms of accuracy and stability of the measurement results are improved. Where improvements are limited, an evaluation of the technical limitation of the equipment is addressed, which may result in a modification of the capability assessments. Learned lessons are captured, which can lead to codification of procedures and processes or amending existing technical practices and standards. The ultimate object of the improvement activities is improved performance and future avoidance of like incidents.

Through the study of simulated production scenarios the paper highlights ways to detect and deal with errant data in production allocation data sets. It also proposes and evaluates a practical procedure that turns DVR error-qualifiable production data into allocated quantities the same way traditional PSM systems are used in production allocation. The difference is that in the latter approach the data qualification for potential data bias or imprecision is not integrated in the allocation process leaving room for production misallocation risks.

# 34<sup>th</sup> International North Sea Flow Measurement Workshop

## 25-28 October 2016

### 7 ACKNOWLEDGEMENT

The Authors extend their appreciation to Thomas Hurstell of Letton Hall Group for his help with the comparison of other commercial PSM results and general guidance on production allocation practices.

### 8 REFERENCES

- [1] Amin A., Using Measurement Uncertainty in Production Allocation, the UPM Forum, Houston, Texas, 24 – 25 February 2016.
- [2] Data validation and reconciliation - Wikipedia
- [3] Mah R.S.H., Stanley G.M., Downing D.W., Reconciliation and Rectification of Process Flow and Inventory Data, *Ind. & Eng. Chem. Proc. Des. Dev.* 15: 175–183, 1976.
- [4] Liebman M.J., Edgar T.F., Lasdon L.S., Efficient Data Reconciliation and Estimation for Dynamic Processes Using Nonlinear Programming Techniques, *Computers Chem. Eng.* 16: 963–986, 1992.
- [5] Kyriakopoulou D.J., Kalitventzeff B., Data Reconciliation using an Interior Point SQP, ESCAPE-6, Rhodes, Greece, 26-29 May 1996.
- [6] Stockton P., Experience of the Use of Uncertainty Based Allocation in a North Sea Offshore Oil Allocation System, Production and Upstream Flow Measurement Workshop, Houston, Texas, February, 2008.
- [7] American Petroleum Institute (API), Use of Subsea Wet-Gas Flowmeters in Allocation Measurement Systems, Recommended Practice RP 85.
- [8] Webb R.A., Letton W., AND Basil M., Determination of Measurement Uncertainty for the Purpose of Wet Gas Hydrocarbon Allocation, 20th North Sea Flow Measurement Workshop, St. Andrew's, Scotland, October 2002.
- [9] Corbet N., Johnston J., Sibbald R., Stockton P., Wilson Allan, Allocation in an Uncertain World: Maximising the Use of Data with UBA on Global Producer III, 31st North Sea Flow Measurement Workshop, Stavanger, Norway, October 2013.
- [10] VDI 2048 Measurement Uncertainties of Acceptance Measurements on Energy-conversion and Power Plants Basic Principles, 2000.
- [11] Webb R., Donkervoet W., Application of Phase Behavior Models in Production Allocation Systems, 22nd North Sea Flow Measurement Workshop, St. Andrew's, Scotland, October 2004.
- [12] API MPMS Draft Standard, Application of Hydrocarbon Phase Behavior Modeling in Upstream Measurement and Allocation Systems, First Edition, August 2016.
- [13] Heyen G., Kalitventzeff B., Process Monitoring and Data Reconciliation, ResearchGate Chapter, June 2008.

## **Technical Paper**

### **Determination of Optimal Calibration Intervals – A Risk Based Approach**

**Nadezhda Pashnina, Emerson Process Management  
Paul Daniel, Emerson Process Management**

---

#### **1 INTRODUCTION**

The current economic challenges facing the upstream oil and gas sector has driven an urgent need to reduce costs and improve efficiency. A reduction of operating costs may be achieved through the extension of the calibration intervals. The maintenance strategies associated with fiscal and custody transfer measurement systems have traditionally been based on a 'time-based' approach (maintenance activities are scheduled at fixed intervals), without much consideration to past equipment performance and the introduction of ever more intelligent diagnostic capabilities of modern instrumentation. However, custody transfer, fiscal and allocation metering are essentially the cash registers of the company and their performance must be assured to minimise financial exposure. Similarly, complying with EU regulation for the monitoring, reporting and verification of greenhouse gas emissions requires the operators to have in place a measurement plan defining the calibration and maintenance regime required in order to meet the specified uncertainty levels for activity data for the applied tiers.

It is this drive, to reduce costs, whilst maintaining control of the measurement uncertainty that has resulted in the Oil & Gas Authority (UK) to strongly urge operators to consider abandoning the traditional time-based maintenance in favour of a 'risk-based' or 'condition-based' maintenance, or combination of both [3]. It is suggested that a risk-based approach to maintenance, as outlined in section 5.2.5 of the current issue of the DECC Measurement Guidelines [1], should be the default methodology.

The impact of measurement bias is proportional to the time over which it exists without correction. The effect can be eliminated by calibration and adjustment at appropriate intervals, however, the determination of calibration intervals is a complex mathematical and statistical process requiring accurate and sufficient data taken during the calibration process [7]. There is no universally applicable single best practice and thus there is a need for a better understanding of the mechanism required for the determination of an appropriate calibration interval. There are very few official documents available which provide guidance on establishing the optimal calibration interval [2], [4].

This paper details the application of a risk-based approach to determine the optimal calibration interval.

Section 2 covers the concept of the risk-based approach. Section 2.1 introduces the term 'total costs' and provides insight as to how this can be established. Section 2.2 details the mechanism of measuring instrument ageing and introduces some models which can be used to define the evolution of the measurement bias over time. Section 2.3 describes the calculation of financial exposure in terms of the 'expected loss', considering the likelihood and consequences of the measurement bias, and the 'value flow rate'. Section 2.4 defines the measurement costs calculation. The methodology is demonstrated on the example of a gas ultrasonic meter, pressure and temperature transmitters using real anonymised data in Section 3. Section 4 provides conclusions.

# 34<sup>th</sup> International North Sea Flow Measurement Workshop 25-28 October 2016

## Technical Paper

### 2 RISK-BASED APPROACH CONCEPT

For deployment of the risk-based approach [1] the following parameters have to be evaluated:

- **the value flow rate** is the product of the relevant flow rate  $Q$  and the relevant measured product value  $PV$ .
- **the estimate of a measurement error** (measurement bias)  $\Delta(t)$  over a given period of time (refer to section 2.2).
- **the financial exposure**  $FE$  is the product of the expected loss and the value flow rate ( $Q \cdot PV$ ) accumulated over the period of time  $T$  during which the measurement error  $\Delta(t)$  may be expected to occur (refer to section 2.3).
- **the measurement costs**  $MC$  take account of the costs of ownership of a measuring instrument including calibration costs, repair costs, maintenance and metering service, depreciation and other costs (refer to section 2.4).

The concept of the risk-based approach is to balance the measurement costs against the financial exposure, determined by estimating the likelihood and consequences of the measurement error over a given period of time. The balance equation can be expressed as follows:

$$FE = MC \quad (1)$$

#### 2.1 Total Costs

For implementation of the risk-based approach the time-dependent total costs function is defined as the sum of financial exposure and the measurement costs as follows:

$$TC(t) = FE(t) + MC(t) \quad (2)$$

The optimal calibration interval will correspond to the minimum of the total costs function [6]. This can be calculated by differentiating equation (2) and setting the found derivative equal to zero, thus the optimal calibration interval is the one which satisfies the following condition:

$$\frac{d(FE(t) + MC(t))}{dt} = 0 \quad (3)$$

To solve the differential equation (3) for the optimal calibration interval  $T$ , the financial exposure and the measurement costs have to be defined as a function of time. In many cases obtaining such an analytical solution to equation (3) is infeasible and thus the solution can be determined graphically by observing a minimum of the total costs function.

This can be demonstrated by the following example. Substituting  $FE(t)$  from (11) and  $MC(t)$  from (21) in (3):

$$\frac{d}{dt} \left( \int EL(t) \cdot Q \cdot PV dt \right) + \frac{d(A \cdot t^B)}{dt} = 0 \quad (4)$$

## Technical Paper

Substituting  $EL(t)$  from (12) in to equation (4) differentiates to:

$$c \cdot \frac{\sqrt{2}}{\sqrt{\pi}} \cdot (\sigma_0 + v_\sigma \cdot t + a_\sigma \cdot t^2) + A \cdot B \cdot t^{B-1} = 0 \quad (5)$$

The optimal calibration interval  $T$  is the one which satisfies equation (5), but it is not possible to solve this equation in closed form, but it can be solved numerically.

### 2.2 Measurement Bias

Following the international vocabulary of metrology [5]:

- **systematic measurement error** is the component of measurement error that in replicate measurements remains constant or varies in a predictable manner and can be known (and be corrected) or unknown (considered as random).
- **random measurement error** is the component of measurement error that in replicate measurements varies in an unpredictable manner, which can be evaluated with the help of probability theory.
- **instrumental drift** or '**drift error**' is the continuous or incremental change over time in indication, due to changes in metrological properties of a measuring instrument. Instrumental drift is related neither to a change in a quantity being measured nor to a change of any recognized influence quantity, but related to an interaction of a measuring instrument with an operating environment and this process is defined in the paper as 'ageing'. Ageing does not depend on whether a measuring instrument is in operation or in storage. The drift error can be corrected at a given time and then again starts to age going forward from this point, thus repeated corrections are required over a measuring instrument life time. The rate of ageing depends on a manufacturing process, used materials and operating temperature of a measuring instrument.

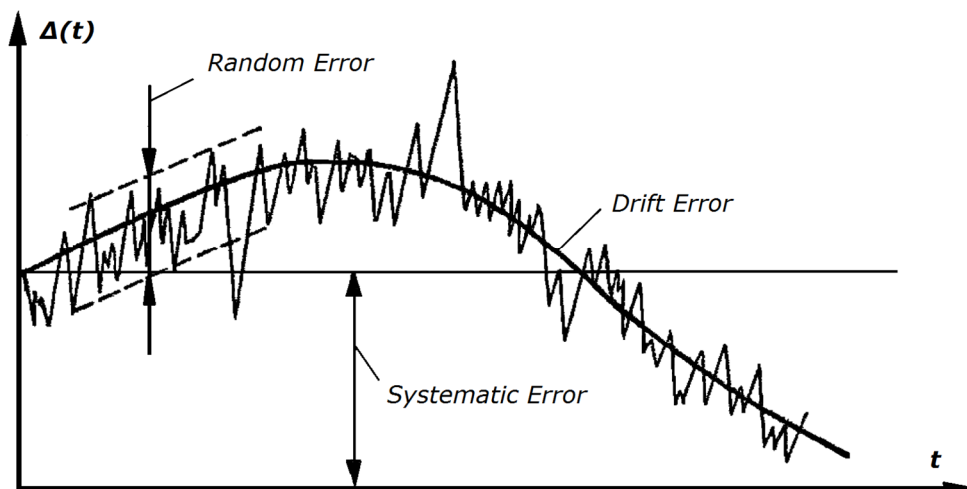


Figure 1 – Measurement Bias

**Technical Paper**

The systematic and random errors are characteristics of a stationary random process, but the drift error is characteristic of a nonstationary random process and varies continuously with time. In reality all these three types of errors are combined in the form of a seamless nonstationary random process shown on Figure 1 and within this paper its estimate is defined as a function of time using the term of measurement bias  $\Delta(t)$ . Note that the measurement bias term is broadened in comparison with the definition given in [5].

A measuring instrument after calibration can be characterized over its measurement range by the relation between the quantity  $Q$  and the measurement bias  $\Delta(t)$ . Figure 2 shows a one-to-many relation and the width of the strip provides a measuring instrument uncertainty which is supposed to be within the maximum permissible limits  $\pm\Delta_p$ . After initial calibration the relation tends to be as graph a) shows. Over the period of time  $T$  the joint action of the above mentioned errors causes an additive and multiplicative shift in relation as graph b) shows. The additive shift can be corrected by zero adjustment as graph c) shows but it has to be kept in mind that with zero adjustment expands the width of the strip. The multiplicative shift reflects the presence of the drift error and graph c) shows the most common situation for all subsequent calibrations. Consequently, it is more likely that a measuring instrument uncertainty exceeds the maximum permissible limit towards the end of its measurement range with half of all instruments failing calibration at these points [11].

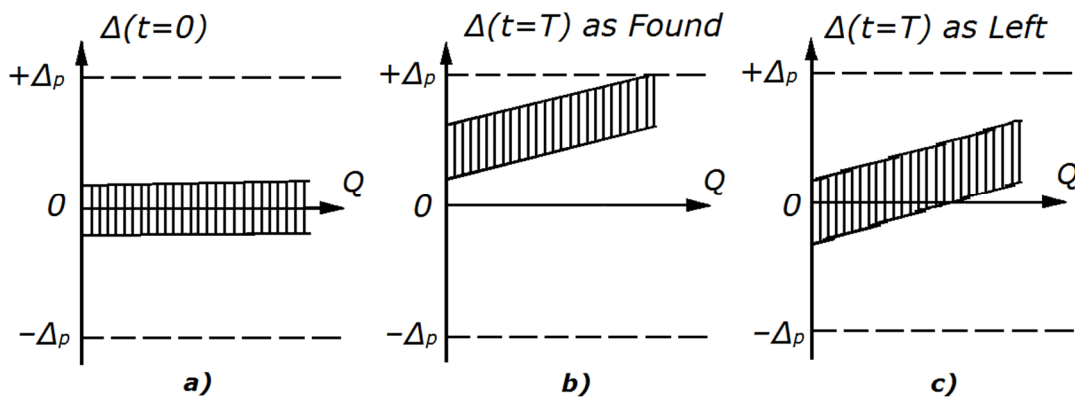


Figure 2 – Measurement Bias

Along with predictable calibration failure, that is those where the measurement bias  $\Delta(t)$  exceeds the permissible limits  $\pm\Delta_p$  due to drift error, unexpected calibration failure may also occur. As shown in [11] only 5 % of all calibration failures can be classified as unexpected and will not be considered in the present paper.

The measurement bias can be defined by several mathematical models based on a hypotheses of the continuous changing or ageing of a measuring instrument in the process of its operation or storage.

In general, the exponential model can be used and the measurement bias over the measuring instrument lifetime may be written in terms of time (an instrument age, years) as follows:

$$\Delta(t) = \Delta_0 + \Delta_m \cdot \frac{\omega_0}{a} \cdot (e^{a \cdot t} - 1) \quad (6)$$

**Technical Paper**

where  $\Delta_0$  is the measurement bias defined at initial calibration ( $t = 0$ ),  $\Delta_m = \Delta_p - \Delta_0$  is the difference between the measurement bias defined at initial calibration and the maximum permissible limit,  $\omega_0$  is the calibration failure frequency,  $a$  is the acceleration of the measuring instrument ageing.

Substituting function  $e^{a \cdot t} = 1 + a \cdot t + (a \cdot t)^2/2 + (a \cdot t)^3/3 + \dots$  by first three terms of its expansion, equation (6) can be approximated by a quadratic equation as follows:

$$\Delta(t) = \Delta_0 + v \cdot t + a_{\Delta} \cdot t^2 \tag{7}$$

where  $v = \Delta_m \cdot \omega_0$  is the velocity of the measuring instrument ageing (%/year),  $a_{\Delta} = (\Delta_m \cdot \omega_0 \cdot a)/2$  is the absolute acceleration of the measuring instrument ageing (%/year<sup>2</sup>).  $v$  and  $a_{\Delta}$  can be defined on the basis of experimental data (calibration results over a number of years) using least squares or any other suitable technique.

In terms of the standard deviation  $\sigma$  of the measurement bias, equation (7) can be expressed as follows:

$$\sigma(t) = \sigma_0 + v_{\sigma} \cdot t + a_{\sigma} \cdot t^2 \tag{8}$$

where  $\sigma_0$  is the standard deviation at initial calibration ( $t = 0$ ),  $v_{\sigma}$  and  $a_{\sigma}$  are the velocity and acceleration of the standard deviation which can be defined on the basis of experimental data (calibration results over a number of years).

If the calibration failure frequency is higher at the beginning of the measuring instrument life time and lower at the end as graph a) on Figure 3 shows, then the acceleration of ageing is a negative value. And vice versa, if the calibration failure frequency is increasing towards the end of the measuring instrument life time the acceleration of ageing is a positive value as graph b) on Figure 3 shows. With every adjustment at a time  $T_i$  the measurement bias is set to the value close to initial calibration  $\Delta_0$  but it continues to deviate following its ageing curve and showing the nature of the instrumental drift.

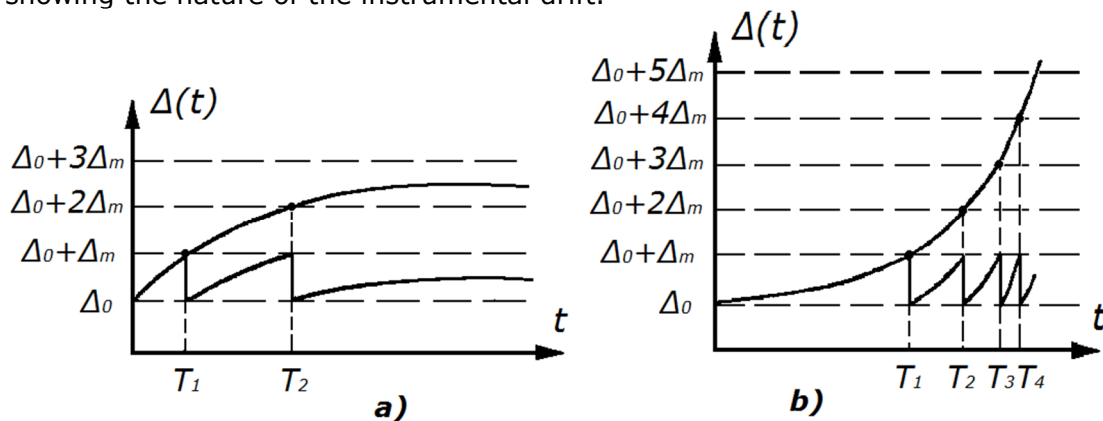


Figure 3 – Exponential Ageing Model

If the calibration failure frequency is roughly the same over a measuring instrument life time, then the linear mathematical model ( $a = 0$ ) describing the measurement bias behaviour can be assumed and equation (7) is reduced to:

# 34<sup>th</sup> International North Sea Flow Measurement Workshop 25-28 October 2016

## Technical Paper

$$\Delta(t) = \Delta_0 + v \cdot t \quad (9)$$

The measurement bias behaviour defined by the linear model is shown on Figure 4. In this case the calibration interval will remain constant over the measuring instrument life time. The linear model is referred to in [8] for optimal calibration interval determination.

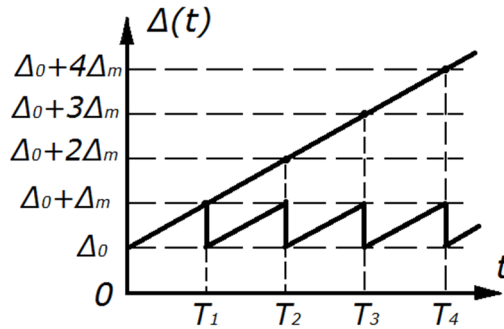


Figure 4 - Linear Ageing Model

Defining the errors on the grounds of their frequency (drift error – lower frequency, random error – higher frequency) refers them to different regions of the frequency spectrum and specifies the spectral properties of the measurement bias. It allows the prediction of the ageing peak maximum of a measuring instrument as a maximum of the measurement bias logarithmical spectrum [11] defined by the following function:

$$S(t) = \sqrt{S_i^2 + 2 \cdot v \cdot t \cdot e^{a \cdot t} \cdot \left[ S_i + \frac{v}{a} \cdot (e^{a \cdot t} - 1) \right]} \quad (10)$$

where  $S_i = \sigma_i^2 / \ln(T_i/t)$  is the value of the logarithmical spectrum at a particular time moment  $T_i$ ,  $\sigma_i$  is the standard deviation of the measuring instrument.

Summarising the models described in this section it should be noted that the linear model (9) facilitate the prediction of the measurement bias in the period from 1 to 5 years, the exponential model (6) in the period from 1 to 100 years and the logarithmic spectrum model may be used to predict the measurement bias behaviour in the range from 1 second to 100 years. The models can show good results if at least 5 calibration results are available, thus sufficient as-found and as-left data have to be available for a multiple of instruments of the same type.

### 2.3 Financial Exposure

The consequences of the measurement bias can be determined by a loss function and in conjunction with the likelihood of the measurement bias to occur, the expected loss can be calculated as detailed in Section 7.

The expected loss may include a penalty due to failure to deliver an agreed amount of product or an incorrect evaluation and forecasting of product.

The consequences of the measurement bias grow with time, the longer calibration interval the higher the expected loss. The accumulated product of the expected

# 34<sup>th</sup> International North Sea Flow Measurement Workshop 25-28 October 2016

## Technical Paper

loss and the value flow rate over the period of time  $T$  between two subsequent calibrations defines the financial exposure as follows:

$$FE(t = T) = \int_0^T EL(t) \cdot Q \cdot PV dt \quad (11)$$

where  $T$  is the number of days between two subsequent calibrations,  $Q$  is the product flow rate per day,  $PV$  is the product value per flow rate unit. The financial exposure is expressed in currency units.

Assuming the exponential model (8) of the normally distributed measurement bias and absolute loss function (29), the expected loss defined by equation (32) is expressed in terms of  $t$  as follows:

$$EL(t) = c \cdot \frac{\sqrt{2}}{\sqrt{\pi}} \cdot (\sigma_0 + v_\sigma \cdot t + a_\sigma \cdot t^2) \quad (12)$$

where  $\sigma_0$  is the measuring instrument standard deviation defined following the initial calibration.

Equation (12) allows the expression of the financial exposure in the following form:

$$\begin{aligned} FE(t = T) &= \int_0^T c \cdot \frac{\sqrt{2}}{\sqrt{\pi}} \cdot (\sigma_0 + v_\sigma \cdot t + a_\sigma \cdot t^2) \cdot Q \cdot PV dt = \\ &= Q \cdot PV \cdot T \cdot c \cdot \frac{\sqrt{2}}{\sqrt{\pi}} \cdot \left( \sigma_0 + \frac{1}{2} \cdot v_\sigma \cdot T + \frac{1}{3} \cdot a_\sigma \cdot T^2 \right) \end{aligned} \quad (13)$$

### 2.4 Measurement Costs

The measurement costs include capital and operating expenditures and the **annual** measurement costs  $MC$  (£/year) are calculated as follows:

$$MC = OPEX + EF \cdot CAPEX \quad (14)$$

where  $OPEX$  (£/year) is the operating expenditures,  $EF$  (1/year) is the efficiency factor of capital expenditures,  $CAPEX$  (£) is the capital expenditures.

The operating expenditures calculation can be formularized as follows:

$$OPEX = CalC + RepC + SalC + DepC + AsC \quad (15)$$

where  $CalC$  (£/year) is the calibration costs,  $RepC$  (£/year) is the minor repair or servicing costs,  $SalC$  (£/year) is the costs associated with the workforce (engineers and technicians assuring trouble-free operation of measuring instruments) salary,  $DepC$  (£/year) is the depreciation (allocation of an assets cost to periods in which the assets are used) costs,  $AsC$  (£/year) is the electrical energy consumption and processed materials supply costs.

The calibration costs  $CalC$  may include but not limited to:

- calibration at an accredited laboratory,

# 34<sup>th</sup> International North Sea Flow Measurement Workshop 25-28 October 2016

## Technical Paper

- attendance to witness a calibration by manufacturer's and operator's engineers,
- expenses related with the attendance,
- transportation of the measuring instrument to a calibration laboratory and back,
- removal and replacement of the measuring instrument,
- scaffolding over meter stream to allow removal and replacement,
- lagging removal and replacement,
- updating records

The minor repair or servicing costs are calculated as follows:

$$RepC = t \cdot RPC + Prt \quad (16)$$

where  $t$  (hours/year) is the average time spent for repair or service,  $RPC$  (£/hour) is the repair personnel costs,  $Prt$  (£/year) is the average cost of replaced parts.

The metering personnel salary costs are calculated as follows:

$$SalC = 12 \cdot \sum MPC \cdot K \quad (17)$$

where  $MPC$  (£/month) is the metering personnel costs,  $K$  is the personnel workload factor showing a fraction of time spent for the particular measuring instrument, 12 (month/year) is the constant.

The depreciation costs are calculated as follows:

$$DepC = K_D \cdot PC \quad (18)$$

where  $K_D$  (1/year) is the depreciation coefficient defining the period of the metering instrument life time,  $PC$  (£) is the measuring instrument purchase costs.

The electrical energy consumption  $EnC$  (£/year) and processed materials supply costs  $MSC$  (£/year) are calculated as the sum of two:

$$AsC = EnC + MSC \quad (19)$$

The capital expenditures calculation can be formularized as follows:

$$CAPEX = K_{PC} \cdot PC + K_{ICC} \cdot ICC + K_{RDC} \cdot RDC \quad (20)$$

Where  $K_{PC}$ ,  $K_{ICC}$  and  $K_{RDC}$  are the coefficients defining the part of the costs associated with the measurement of the specified process parameter and applicable if the measuring instrument is capable to measure more than one parameter,  $PC$  (£) is the measuring instrument purchase costs,  $ICC$  (£) is the installation and commissioning costs,  $RDC$  (£) is the research and development costs which include but not limited to:

- development of measurement, calibration and maintenance procedures,
- evaluation of uncertainty and obtaining of specified approval,
- upgrade and development of data control system and related software.

# 34<sup>th</sup> International North Sea Flow Measurement Workshop 25-28 October 2016

## Technical Paper

The estimate of the installation and commissioning costs is assumed as 20 % of the measuring instrument purchase costs or  $ICC = 0.2 \cdot PC$ . The estimate of the coefficients in (20) is assumed as  $1/n$ , where  $n$  is the number of process parameters the measuring instrument is capable to measure and control.

Considering the nature of the measurement costs nonlinearly decreasing with the calibration interval extension it can be approximated by a power function as follows:

$$MC(t) = A \cdot t^B \quad (21)$$

where  $A$  and  $B$  are the parameters of the approximation function which can be obtained using the least squares technique or any other suitable technique.

### 3 OPTIMAL CALIBRATION INTERVAL CALCULATION EXAMPLE

For illustration of the aspects covered in the paper let us consider a gas metering system incorporating an ultrasonic flow meter, pressure and temperature transmitters.

The mass flow rate,  $Q_m$  (kg/h), is calculated as follows:

$$Q_m = Q_v \cdot [1 + K_T \cdot (Ta - Ta_{cal})] \cdot [1 + K_P \cdot (P - P_{cal})] \cdot \rho \quad (22)$$

where  $Q_v$  ( $m^3/h$ ) is the measured gross volume flow rate,  $K_T$  is the material specific temperature coefficient of the meter body,  $K_P$  is the pressure coefficient of the meter body,  $Ta_{cal}$  and  $P_{cal}$  are the calibration absolute temperature and pressure respectively,  $\rho = \frac{M \cdot P}{Z \cdot R \cdot T}$  ( $kg/m^3$ ) is the flowing density of the gas,  $M$  is the molar mass,  $P$  is the absolute line pressure,  $Z$  is the compressibility factor,  $R$  is the gas constant,  $Ta$  is the absolute line temperature.

**As the first step** the measurement bias as a function of time is determined on the basis of available calibration data (refer to section 8) for the ultrasonic flow meter, pressure and temperature transmitters with no considerations of zero and span adjustments. The statement in section 2.2 that in 50 % of all cases the measurement bias exceeds the maximum permissible limit towards the end of the measurement range is proved by the results. Thus for the measurement bias development the following calibration points are considered: 2800 m<sup>3</sup>/h, 90 barg and 40 °C.

The exponential model as per equations (7) and (8) is used for the measurement bias determination. For the ultrasonic meter the ageing velocity is defined as positive value and the acceleration as negative value. The opposite situation was observed with pressure and temperature transmitters, but it should be noted that calibration results were only available for a period of two years, further data is required to establish a more reliable ageing model.

**The second step** supposes the calculation of the financial exposure using equation (13) and assuming the normally distributed measurement bias and absolute loss function. The following parameters were used for evaluation:

- natural gas is the fluid type
- 0.41 £/thm is the product value  $PV$

# 34<sup>th</sup> International North Sea Flow Measurement Workshop 25-28 October 2016

## Technical Paper

- 164,038.0 thm /day is the product flow rate  $Q$
- sensitivity coefficient on the basis of equation (22) is calculated as  $c = 1$  for ultrasonic flow meter,  $c = 0.99$  for pressure transmitter and  $c = 0.03$  for temperature transmitter.

**The third step** specifies the measurement costs calculation and in the current example operating expenditures (15) are limited by calibration and depreciation costs but the capital expenditures are defined by equation (20).

**The last step** directs us to balance the calculated measurement bias and measurement costs by searching the minimum of the total costs function defined by equation (2). Defining the values of the total costs function by varying the variable  $T$  in the range from 0 to 100 months and mapping it on the graph allows the determination of the optimal calibration interval corresponding to the minimum of the total costs function.

The total costs function minimum was identified at the level of 14 months for the ultrasonic flow meter (the current calibration interval is 12 months) as shown on Figure 5.

The total costs function minimum was identified at the level of 5 months for the pressure transmitter (the current calibration interval is 3 months) as shown on Figure 6.

The total costs function minimum was identified at the level of 13 months for the temperature transmitter (the current calibration interval is 2 months) as shown on Figure 7.

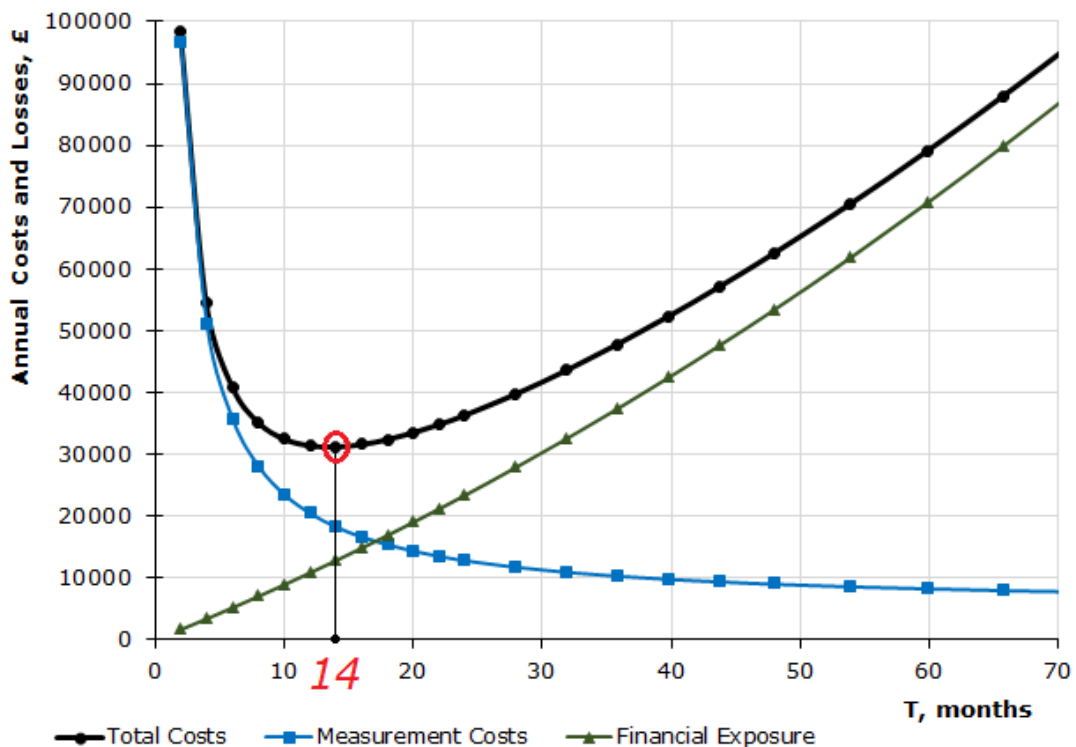


Figure 5 – Total Costs Function for Gas Ultrasonic Flow Meter

Technical Paper

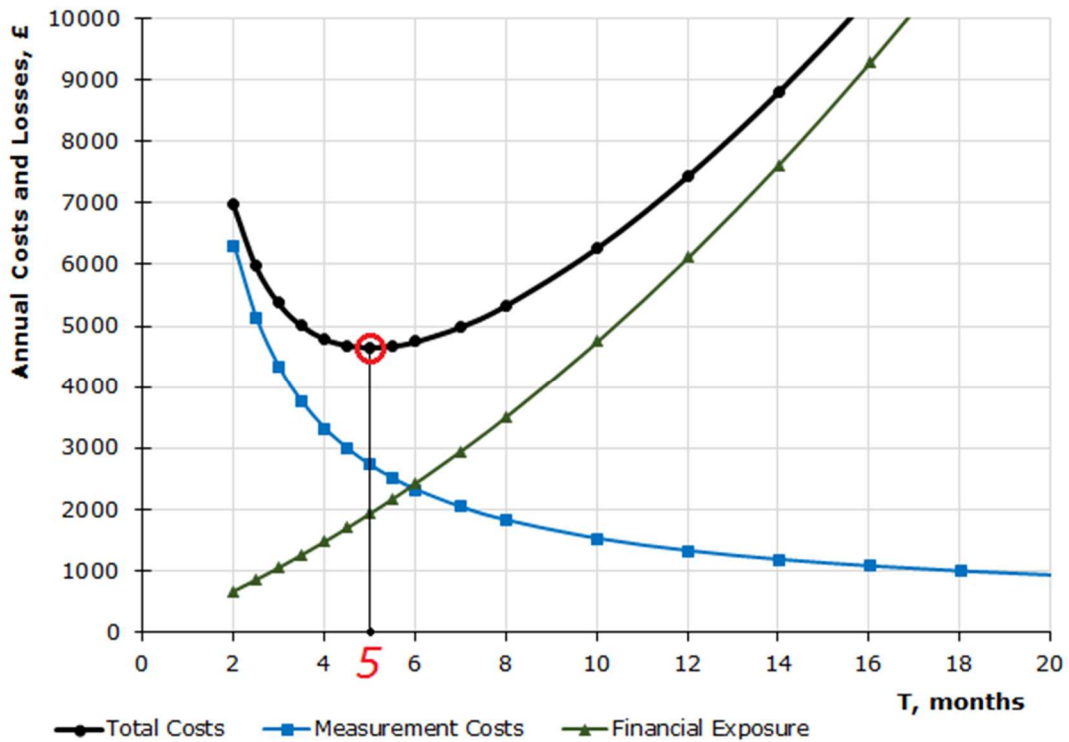


Figure 6 – Total Costs Function for Pressure Transmitter

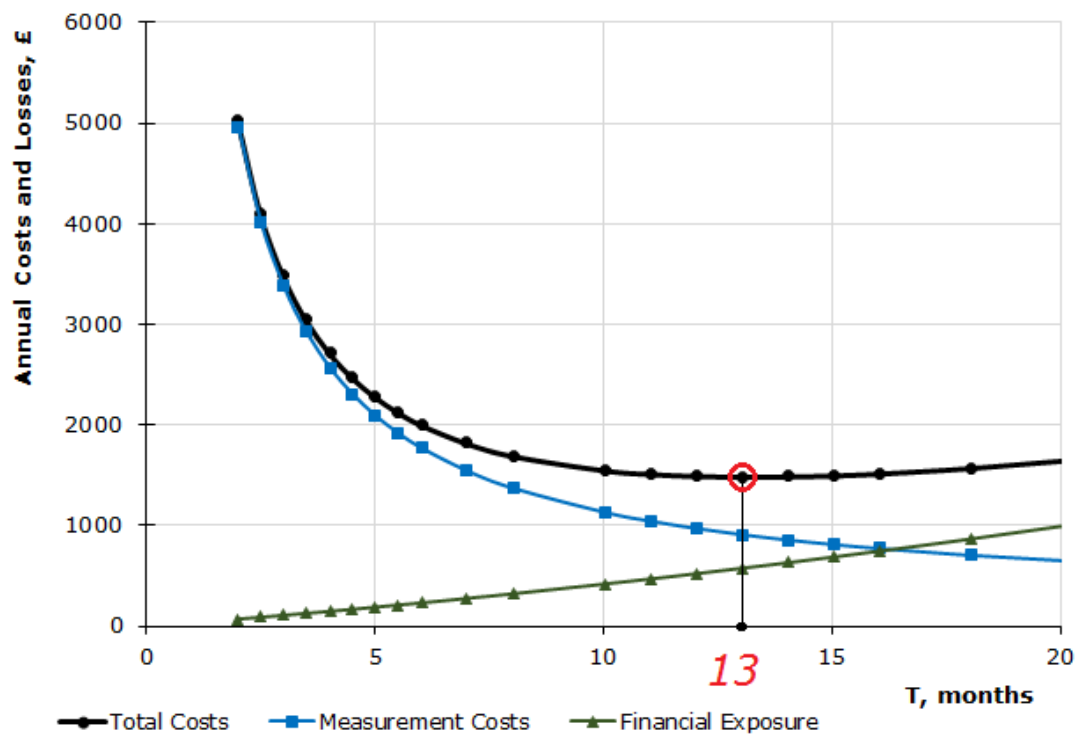


Figure 7 – Total Costs Function for Temperature Transmitter

# 34<sup>th</sup> International North Sea Flow Measurement Workshop 25-28 October 2016

## Technical Paper

### 4 CONCLUSIONS

The present paper details a risk-based approach to the maintenance of measuring instruments determining the optimal calibration interval. Each parameter of the risk-based concept is analysed separately, in particular, the models allowing the definition of the measuring instrument ageing process and the loss functions modifying the expected loss and consequently the financial exposure.

A step-by-step methodology has been provided which specifies how to implement the proposed risk-based approach. It has been shown on real data that the risk-based approach can play an important role and provide an efficient tool for the optimization of maintenance resources.

It is shown that the process of establishing an optimum calibration interval can be a complex endeavour requiring the use of mathematical and statistical processes and demanding a sufficient quantity of calibration data. The development of a standardised suite of tools to perform the process can make the process simpler but still retain the mathematical rigour to provide confidence that the resultant calibration intervals are optimal from a financial exposure perspective and the total costs are minimised.

In the current climate faced by the industry operators can obtain significant benefit by assessing the financial risk associated with an implemented maintenance methodology and therefore ensuring that the resultant financial exposure is properly understood.

### 5 NOTATION

The symbols defined and used within the section of the paper are not listed below.

$A, B$	Parameters of $MC$ approximation	$t$	time
$a$	Ageing acceleration of measurement bias	$T$	Period of time between calibrations
$a_\sigma$	Ageing acceleration of standard deviation	$TC$	Total costs
$a_\Delta$	Absolute acceleration	$Q$	Determined quantity value
$c$	Sensitivity coefficient	$v$	Ageing velocity of measurement bias
$CAPEX$	Capital expenditures	$v_\sigma$	Ageing velocity of standard deviation
$EF$	Efficiency factor of $CAPEX$	<b>Greek</b>	
$EL$	Expected loss	$\Delta$	Measurement bias
$FE$	Financial exposure	$\Delta_0$	Measurement bias at initial calibration
$MC$	Measurement costs	$\Delta_m$	difference between $\Delta_p$ and $\Delta_0$
$OPEX$	Operating expenditures	$\Delta_p$	Maximum permissible limit
$PV$	Product value	$\sigma_0$	Standard deviation at initial calibration
$S$	Measurement bias logarithmical spectrum	$\omega_0$	Calibration failure frequency

# 34<sup>th</sup> International North Sea Flow Measurement Workshop 25-28 October 2016

## Technical Paper

### 6 REFERENCES

- [1] DECC, Guidance Notes for Petroleum Measurement, Issue 9.2: for systems operating under the Petroleum (Production) Regulations, October 2015.
- [2] NCSL RP 1, Establishment and Adjustment of Calibration Intervals, 2010.
- [3] OGA policy statement – maintenance strategies on fiscal measurement systems 21.08.2015.
- [4] OIML D 10, Guidelines for the determination of calibration intervals of measuring instruments. Edition 2007 (E), 2007.
- [5] International Vocabulary of Metrology – Basic and General Concepts and Associated Terms. VIM 3rd edition, JCGM 200:2012.
- [6] David Deaver. Calibration intervals, a manufacturer's perspective. Available at: [http://assets.fluke.com/download/calibration/MSC2009\\_Deaver.pdf](http://assets.fluke.com/download/calibration/MSC2009_Deaver.pdf)
- [7] Donald W. Wyatt, Howard T. Castrup. Managing Calibration Intervals. Available at: [http://www.isgmax.com/articles\\_papers/mgcalint.pdf](http://www.isgmax.com/articles_papers/mgcalint.pdf)
- [8] Howard Castrup. Calibration Intervals from Variables Data, NCSL International Workshop and Symposium, 2005. Available at: [http://www.ncsli.org/i/c/TransactionLib/C05\\_20.pdf](http://www.ncsli.org/i/c/TransactionLib/C05_20.pdf)
- [9] Philip Stockton. Smith Rea Energy Limited, UK. Cost Benefit Analysis in the Design of Allocation Systems, North Sea Flow Measurement Workshop, 2009.
- [10] V.A. Bryuhanov. Methods of measurement accuracy improvement of measurements in industry (В.А. Брюханов Методы повышения точности измерений в промышленности, 1991).
- [11] P.V. Novitskiy, I.A. Zograf, V.S. Labunets. Dynamics of measuring instruments errors (П.В. Новицкий, И.А. Зограф, В.С. Лабунец. Динамика погрешностей средств измерений, 1990).

**Technical Paper**

**7 APPENDIX A**

**A.1 Expected Loss Calculation**

There is a relationship between a measurement bias,  $\Delta$ , and the associated change in the quantity value  $\Delta Q$  which can be formularized as  $\Delta Q = \Psi(\Delta)$ , where the function  $\Psi$  is known as a loss function (also known as a risk function). A loss (or cost – “the price paid for inaccuracy”) will arise if the measurement error turns to be different from agreed value and the larger the measurement error the greater the shift in the determined parameter and the greater the loss.

If the measurement bias remains constant or varies in a predictable manner, then the measurement bias is defined as systematic and the shift in the determined quantity value will have a particular sign. In practice, corrections are applied to compensate for a known systematic measurement error, but unknown systematic measurement errors are considered to be random. In this paper only unknown systematic and random measurement errors are considered and thus the shift in the determined quantity value  $\Delta Q$  is treated as a random variable as well.

Ideally the loss function has to be minimised, but it is incorrect to find an extremum of the function of a random variable. Instead, considering a large number of measurements a mean or expectation of the loss function  $\Psi(\Delta)$  can be minimised and an expected loss (a risk measure),  $EL$ , may be written as:

$$EL = E[\Psi(\Delta)] = \int_{-\infty}^{+\infty} \Psi(\Delta) \cdot f(\Delta) d\Delta \quad (23)$$

where  $f(\Delta)$  is a probability density function of the measurement bias  $\Delta$ .

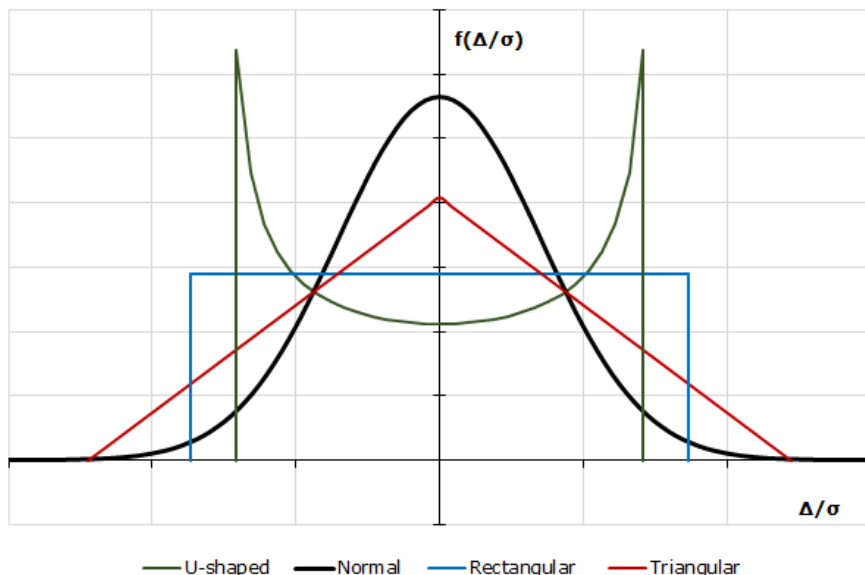


Figure 8 – Probability Density Functions

Most frequently the measurement bias  $\Delta$  is normally distributed because its components have similar significance. In practice, rectangular, triangular and U-shaped distribution of measurement bias may occur. Figure 8 shows probability

# 34<sup>th</sup> International North Sea Flow Measurement Workshop 25-28 October 2016

## Technical Paper

density function of these distributions, where  $\sigma$  is a standard deviation of the measurement bias.

In this paper, as the most common, the normal distribution will be considered with the probability density function written as follows:

$$f(\Delta) = \frac{1}{\sigma \cdot \sqrt{2\pi}} \cdot e^{-\frac{(\Delta-m)^2}{2\sigma^2}} \quad (24)$$

where  $m$  is the mean and  $\sigma$  is the standard deviation of the distribution.

There are three commonly used loss functions: squared, absolute and '0-1'. Additionally, the hybrid absolute function is also considered in the article and all of them are shown in Figure 9. Obviously, the expected loss will be calculated differently for each function as shown in the sections below.

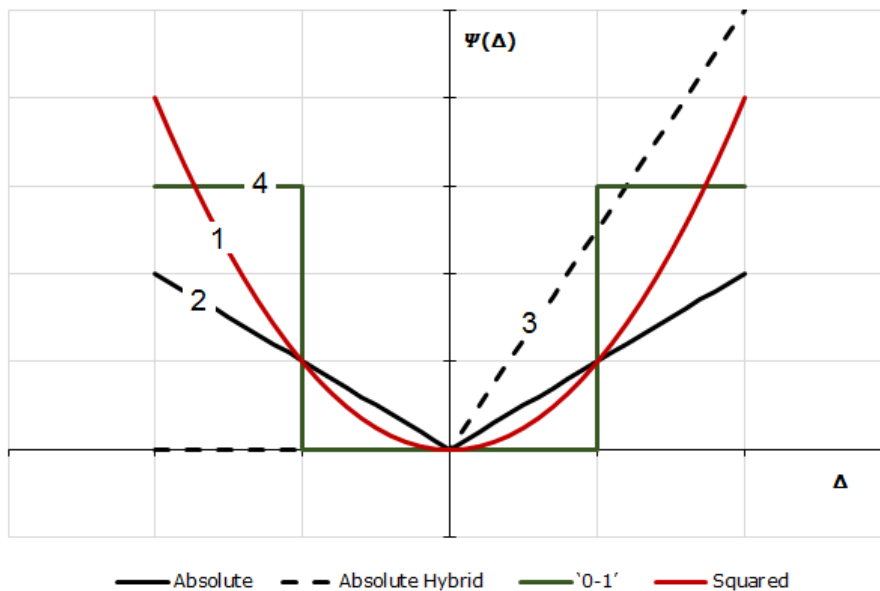


Figure 9 – Loss Functions

### A.2 Squared Loss Function

The squared loss function (curve 1 on Figure 9) is commonly used in mathematical optimization when the relationship between the measurement bias and the quantity value is explicitly nonlinear. The function that represents the squared loss is given by:

$$\Psi(\Delta) = c \cdot \Delta^2 \quad (25)$$

where  $c$  hereinafter is a coefficient, representing the sensitivity coefficient of the determined quantity value to the measurement bias. This is applicable to indirect measurements and elements of secondary instrumentation having an influence on the determined quantity.

Then the expected loss is calculated by substituting from (24) and (25) to (23):

**Technical Paper**

$$EL = \int_{-\infty}^{+\infty} c \cdot \Delta^2 \cdot \frac{1}{\sigma \cdot \sqrt{2\pi}} \cdot e^{-\frac{(\Delta-m)^2}{2 \cdot \sigma^2}} d\Delta \quad (26)$$

Making the substitution of a variable  $z = (\Delta - m)/(\sigma \cdot \sqrt{2})$  and considering that  $\Delta = z \cdot \sigma \cdot \sqrt{2} + m$  and  $d\Delta = \sigma \cdot \sqrt{2} \cdot dz$ , then equation (26) can be expressed in terms of  $z$  as follows:

$$\begin{aligned} EL &= \frac{c}{\sqrt{\pi}} \int_{-\infty}^{+\infty} (z \cdot \sigma \cdot \sqrt{2} + m)^2 \cdot e^{-z^2} dz = \\ &= \frac{c \cdot \sigma^2 \cdot 2}{\sqrt{\pi}} \int_{-\infty}^{+\infty} z^2 \cdot e^{-z^2} dz + \frac{c \cdot m^2}{\sqrt{\pi}} \int_{-\infty}^{+\infty} e^{-z^2} dz \\ &\quad + \frac{c \cdot \sigma \cdot 2\sqrt{2} \cdot m}{\sqrt{\pi}} \int_{-\infty}^{+\infty} z \cdot e^{-z^2} dz \end{aligned} \quad (27)$$

The third integral in equation (27) is equal to zero as the integral of an odd function over symmetric limits, the second integral is the Euler-Poisson (Gaussian) integral equal to  $\sqrt{\pi}$  and the first integrand can be integrated by parts with the result of  $\sqrt{\pi}/2$ . Hence, the expected loss is given by:

$$EL = \frac{c \cdot \sigma^2 \cdot 2}{\sqrt{\pi}} \cdot \frac{\sqrt{\pi}}{2} + \frac{c \cdot m^2}{\sqrt{\pi}} \cdot \sqrt{\pi} + 0 = c \cdot (\sigma^2 + m^2) \quad (28)$$

If the known systematic errors are excluded from the measurement results the number and values of positive and negative errors remaining is balanced and the mean is equal to zero. Thus, hereinafter  $m = 0$  is assumed.

**A.3 Absolute Loss Function**

The absolute loss function (curve 2 on Figure 9) is used when the relationship between measurement bias and the quantity value can be expressed in the form of piecewise linear function. The function that represents the absolute loss is given by:

$$\Psi(\Delta) = c \cdot |\Delta| \quad (29)$$

Then the expected loss is calculated by substituting from (24) and (29) to (23):

$$EL = \int_{-\infty}^{+\infty} c \cdot |\Delta| \cdot \frac{1}{\sigma \cdot \sqrt{2\pi}} \cdot e^{-\frac{(\Delta-m)^2}{2 \cdot \sigma^2}} d\Delta \quad (30)$$

Making the substitution of a variable  $z = (\Delta - m)/(\sigma \cdot \sqrt{2})$  and considering that  $\Delta = z \cdot \sigma \cdot \sqrt{2} + m$  and  $d\Delta = \sigma \cdot \sqrt{2} \cdot dz$ , then equation (30) can be expressed in terms of  $z$  assuming for simplification  $m = 0$  as follows:

$$EL = \frac{c}{\sqrt{\pi}} \int_{-\infty}^{+\infty} |z \cdot \sigma \cdot \sqrt{2} + m| \cdot e^{-z^2} dz = \frac{c \cdot \sigma \cdot \sqrt{2}}{\sqrt{\pi}} \int_{-\infty}^{+\infty} |z| \cdot e^{-z^2} dz \quad (31)$$

# 34<sup>th</sup> International North Sea Flow Measurement Workshop 25-28 October 2016

## Technical Paper

The integral in equation (31) is equal to one as the integral of an even function with symmetric limits. Hence, the expected loss is given by:

$$EL = \frac{c \cdot \sigma \cdot \sqrt{2}}{\sqrt{\pi}} \cdot 1 = c \cdot \frac{\sqrt{2}}{\sqrt{\pi}} \cdot \sigma \quad (32)$$

If the absolute hybrid loss function (curve 3 on Figure 9) is piecewise function defined by two sub-functions as follows:

$$\Psi(\Delta) = \begin{cases} 0, & \Delta < 0 \\ c \cdot \Delta, & \Delta \geq 0 \end{cases} \quad (33)$$

Then the expected loss is calculated by substituting from (24) and (33) to (23):

$$EL = \int_0^{+\infty} c \cdot \Delta \cdot \frac{1}{\sigma \cdot \sqrt{2\pi}} \cdot e^{-\frac{(\Delta-m)^2}{2\sigma^2}} d\Delta \quad (34)$$

Making the substitution of variable  $z = (\Delta - m)/(\sigma \cdot \sqrt{2})$  the equation (34) can be expressed in terms of  $z$  as follows:

$$\begin{aligned} EL &= \frac{c}{\sqrt{\pi}} \int_0^{+\infty} (z \cdot \sigma \cdot \sqrt{2} + m) \cdot e^{-z^2} dz = \\ &= \frac{c \cdot \sigma \cdot \sqrt{2}}{\sqrt{\pi}} \int_0^{+\infty} z \cdot e^{-z^2} dz + \frac{c \cdot m}{\sqrt{\pi}} \int_0^{+\infty} e^{-z^2} dz \end{aligned} \quad (35)$$

Hence the integration interval is half of the interval in equation (31), and the expected loss is given by:

$$EL = \frac{c \cdot \sigma \cdot \sqrt{2}}{\sqrt{\pi}} \cdot \frac{1}{2} + \frac{c \cdot m}{\sqrt{\pi}} \cdot \frac{\sqrt{\pi}}{2} = c \cdot \left( \frac{\sigma}{\sqrt{2 \cdot \pi}} + \frac{m}{2} \right) \quad (36)$$

Obviously, the expected loss evaluated using equation (36) is only half as large as the expected loss evaluated using equation (32). In this case the loss occurs when the measurement bias deviates only in one direction and it means that the systematic measurement bias shall be greater than  $0.66 \cdot \sigma$  at the 90 % confidence level [11]. Assuming freedom from the known systematic errors  $m = 0$  and the loss function slope  $a = 1$ , equation (36) takes on the form of the "risky misallocation exposure" calculation equation presented in paper [9].

### A.4 '0-1' Loss Function

The '0-1' loss function (curve 4 on Figure 9) is used when the relationship between measurement error and the quantity value has a form of discontinuous change if the error is found outside of its permissible limits. The function that represents the '0-1' loss is given by:

$$\Psi(\Delta) = \begin{cases} 0, & -\Delta_p \leq \Delta \leq \Delta_p \\ \Delta Q_p, & |\Delta| > \Delta_p \end{cases} \quad (37)$$

**34<sup>th</sup> International North Sea Flow Measurement Workshop  
25-28 October 2016**

**Technical Paper**

where  $\Delta_p$  is a maximum permissible error,  $\Delta Q_p$  is a deviation of the quantity value caused by error  $\Delta_p$ .

Then the expected loss is calculated by substituting from (24) and (37) to (23) and assuming the even loss function:

$$\begin{aligned}
 EL &= \int_{-\infty}^{-\Delta_p} \Delta Q_p \cdot \frac{1}{\sigma \cdot \sqrt{2\pi}} \cdot e^{-\frac{(\Delta-m)^2}{2\sigma^2}} d\Delta + \int_{\Delta_p}^{+\infty} \Delta Q_p \cdot \frac{1}{\sigma \cdot \sqrt{2\pi}} \cdot e^{-\frac{(\Delta-m)^2}{2\sigma^2}} d\Delta \\
 &= 2 \int_{\Delta_p}^{+\infty} \Delta Q_p \cdot \frac{1}{\sigma \cdot \sqrt{2\pi}} \cdot e^{-\frac{(\Delta-m)^2}{2\sigma^2}} d\Delta
 \end{aligned} \tag{38}$$

Making the substitution of variable  $z = (\Delta - m)/(\sigma \cdot \sqrt{2})$  the equation (38) can be expressed in terms of  $z$  as follows:

$$\begin{aligned}
 EL &= \Delta Q_p \cdot \frac{2}{\sqrt{\pi}} \int_{\frac{\Delta_p - m}{\sigma \cdot \sqrt{2}}}^{+\infty} e^{-z^2} dz = \Delta Q_p \cdot \left[ erf(+\infty) - erf\left(\frac{\Delta_p - m}{\sigma \cdot \sqrt{2}}\right) \right] \\
 &= \Delta Q_p \cdot \left[ 1 - erf\left(\frac{\Delta_p - m}{\sigma \cdot \sqrt{2}}\right) \right]
 \end{aligned} \tag{39}$$

where  $erf$  is the error function and  $erf(+\infty) = 1$ .

**A.5 Conclusion**

In terms of relative expanded uncertainty  $U$  at a defined confidence level the expected loss can be expressed as shown in Table 1. In practice, the most common is the confidence level of 95 %.

Table 1 – Expected Loss in terms of Uncertainty

Confidence Level	Coverage Factor $k$ (for Normal Distribution)	Expected Loss		
		Squared (25)	Absolute (29)	Absolute hybrid (33)
68 %	1.0	$1 \cdot c \cdot U^2$	$0.8 \cdot c \cdot U$	$0.4 \cdot c \cdot U$
90 %	1.6	$0.39 \cdot c \cdot U^2$	$0.5 \cdot c \cdot U$	$0.25 \cdot c \cdot U$
<b>95 %</b>	<b>2.0</b>	<b><math>0.25 \cdot c \cdot U^2</math></b>	<b><math>0.4 \cdot c \cdot U</math></b>	<b><math>0.2 \cdot c \cdot U</math></b>
99 %	2.58	$0.15 \cdot c \cdot U^2$	$0.31 \cdot c \cdot U$	$0.15 \cdot c \cdot U$
99.7 %	3.0	$0.11 \cdot c \cdot U^2$	$0.27 \cdot c \cdot U$	$0.13 \cdot c \cdot U$

It is not shown in the paper but it should be noted that if the normal distribution is considered for the measurement bias without a good reason, then the calculated expected loss may differ from real value by 2 to 3 times [10]. Thus, prior to choosing a type of distribution the behaviour of the random variable (measurement bias) needs to be investigated.

It has to be noted that the confidence level of 90 % has a unique property in that the coverage factor does not depend on the type of distribution and is equal to  $k = 1.6$  or  $U = 1.6 \cdot \sigma$ . If the distribution is not known, it is recommended to report uncertainty at the 90 % confidence level [11].

Technical Paper

8 APPENDIX B

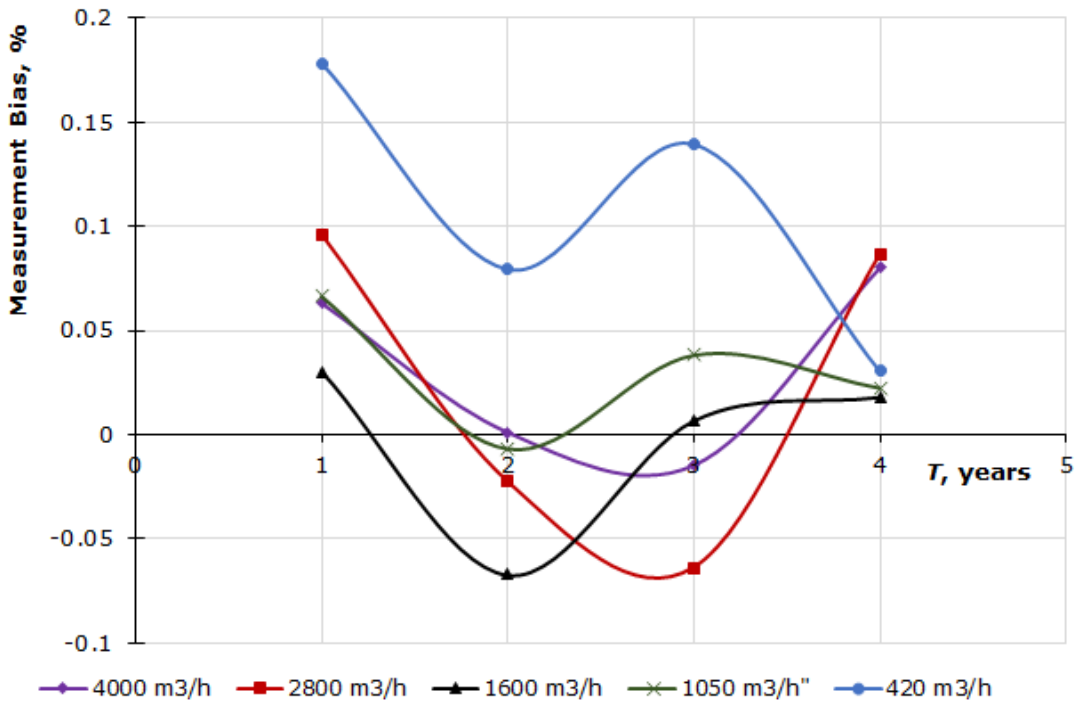


Figure 10 – Ultrasonic Flow Meter Calibration Results

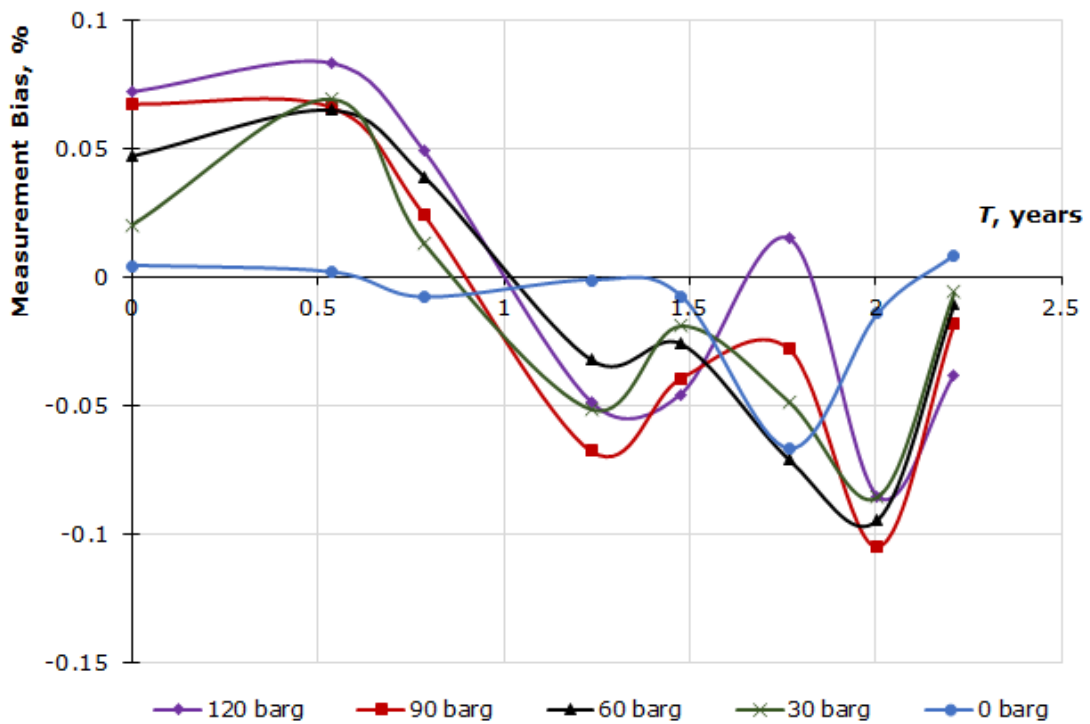


Figure 11 – Pressure Transmitter Calibration Results

34<sup>th</sup> International North Sea Flow Measurement Workshop  
25-28 October 2016

Technical Paper

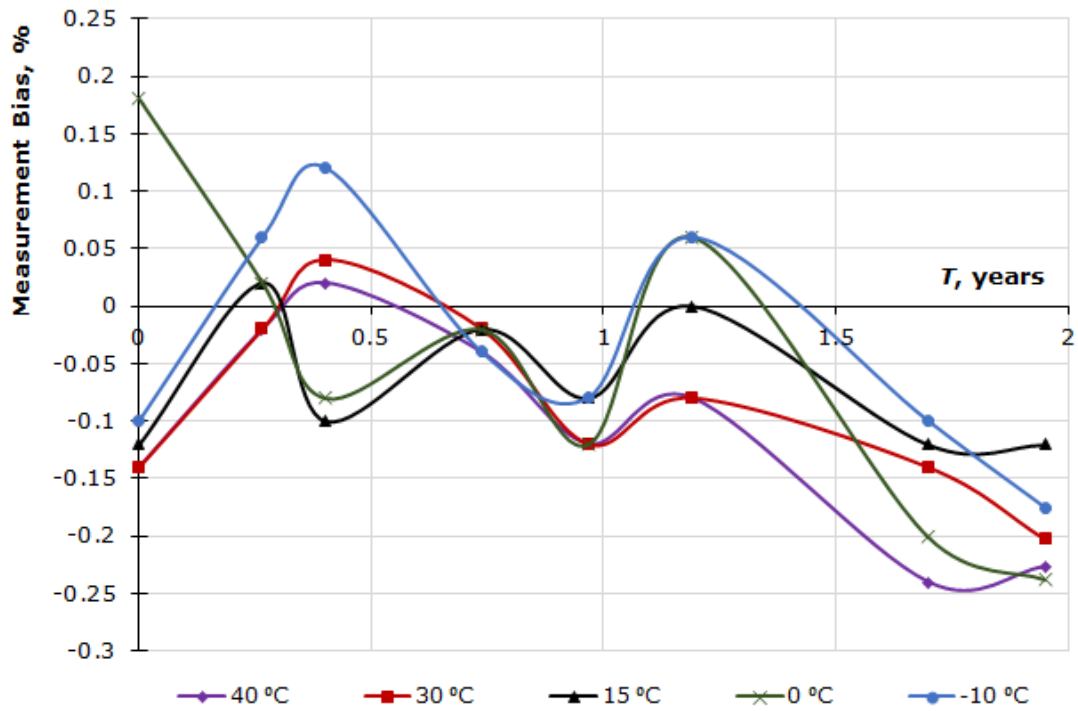


Figure 12 – Temperature Transmitter Calibration Results

## **Technical Paper**

# **Reynolds Number, the Correct Calibration, Characterization and Proving of Flow Meters**

**T. Cousins, CEESI**

### **ABSTRACT**

The flow world has forgotten the importance of Reynolds number for determining the performance of flow meters. Many users and even manufacturers do not understand the meaning or implication of this concept. The implication of the reality that flow meter performance is dictated by the Reynolds number is that meter manufacturers with in-house water calibration laboratories have to send their meters to third party independent calibration facilities in order for many of their meters to be properly calibrated for their applications. In turn operators have to pay more for a correctly calibrated meter. This has resulted in some cases as total denial by the flow meter manufacturers who do not want their meters to be dictated by Reynolds number, with the consequent extra calibration expense. API MPMS chapter 4, one of the better standards assiduously avoids any mention of Reynolds number by saying the meters should be reproved if there is a significant change in viscosity. This implies Reynolds number but does not explicitly use it. We know that all meters used on gas and liquid measurement, Turbines, Coriolis, USMs, differential pressure meters have variations in their calibration determined by Reynolds number to a greater or lesser extent depending on the type and design. Previous papers have described the methods and issues of correcting for Reynolds number and pointed out the pitfalls, which can cause unexpected bias, with consequent financial implications. This paper builds on the issues to show with real data the implications of not considering Reynolds number when designing calibrating and operating meters. It further points out the flaws of using flowrate, velocity, correction methods, where Reynolds number is the predominant physical property determining the meter performance. Finally the paper discusses the pitfalls attendant on using extrapolation, when there is little or no knowledge of the meter performance in the extrapolated area. A number of examples will be shown of the effect of not recognizing the potential problems.

### **1 INTRODUCTION**

This is the culmination of series of papers designed to show used in the Hydrocarbon industry are influenced by Reynolds number, and the effect that ignoring this phenomena can have on their performance. For many years it has been accepted that the installation of meters is of primary importance when using flow meters. The installation effects can be changes in flow profile which will effect some meter types or mechanical installation which will affect others. What has not been accepted universally is that before even the installation there are basic fluid mechanical issues, particularly Reynolds number which must be confronted to obtain reliable and low uncertainty measurement. When combined the installation effect and Reynolds number become a complex interacting set of variables that make the understanding of how meters work under site operating conditions very difficult. Some issues can be easily resolved, orifice plates installed back to front, control valves immediately upstream of the meter, blockage of the meter or flow conditioner etc. But many discrepancies in measurement turn out to be complex, not obvious and sometimes insoluble. Many of these complex problems ultimately revolve around how the meter really operates and in particular the effect of Reynolds number on the process fluid, the meter and the method that the meter uses to combat the consequences of Reynolds number on the meter operation. The only sensible way around Reynolds number is first to accept that it is important,

# 34<sup>th</sup> International North Sea Flow Measurement Workshop 25-28 October 2016

## Technical Paper

then to find stable and acceptable methods to correct the meter. It generally starts with a good calibration, representative of the flow conditions to allow for a good characterization of the meter, and then some method to carry this characterization successfully into the field. Making assumptions about the characteristics of the meter curve brings us firmly into the area of extrapolation. Fluid mechanics is a graveyard of best intentions, where we have assumed that fluid phenomena continue to react in a way that is simply predictable only to find that changes happen to totally discredit the concept. how all of our main meters

## 2 REYNOLDS NUMBER

This has been defined many times, and in previous papers on the subject but to clarify it again, it is defined as the ratio of inertia forces in a fluid to the viscous forces. At low Reynolds numbers the viscous forces predominate and at higher Reynolds numbers the inertia forces are in the ascendency.

The simple equation that determines Reynolds number is given in equation 1, showing that it is a function of a characteristic dimension  $D$ , usually in the case of flow measuring taken as the pipe diameter, the fluid velocity,  $v$ , and the kinematic viscosity,  $\nu$ , the ratio of the absolute viscosity to the fluid density.

$$R_D = vD/\nu \dots\dots\dots 1$$

As a general rule but not always true the changes in fluid mechanics are greater at low Reynolds numbers than high. So at low Reynolds numbers' particularly through transition, as the fluid becomes laminar, and for example the flow profile in a pipe changes rapidly as the Reynolds number changes, shown by the ratio of the mean to the maximum velocity of the profile, [1] figure 1. At higher Reynolds numbers the fluid is turbulent and the profile changes flatten out. The change ratio is usually seen as around 1% per decade. Figure 1 shows also the change in profile experienced by a four path ultrasonic meter, as can be seen the curve is very similar.

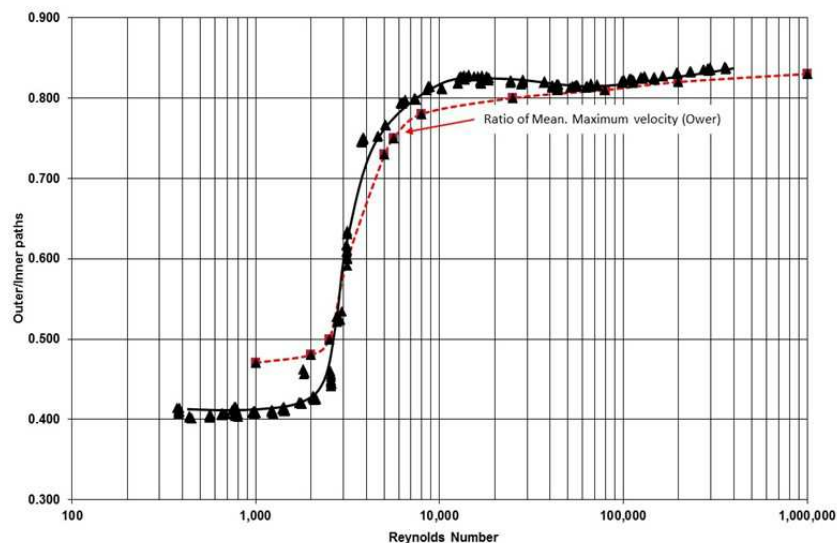


Figure 1 - Variation in Flow Profile velocity Ratio with Reynolds Number

# 34<sup>th</sup> International North Sea Flow Measurement Workshop 25-28 October 2016

## Technical Paper

As stated at higher Reynolds numbers generally the forces induced by fluid phenomena are more stable and so for example Gas Ultrasonic meters tend to be more linear with Reynolds number, and other factors such as Mach number become an issue. Be aware that everything is relative. As Gas meters begin to claim better and better performance there is still an underlying Reynolds number deviation, which needs to be corrected. Some manufacturers assume the non-linearity is velocity, it is not. With the current specifications for gas meters this probably works without taking the meter outside of the specification, but when the claims get to the level of their liquid cousins this will become more of an issue.

An idea of the real span of Reynolds number as it effects the natural world is shown in Table 1, giving some feel for the vast expanse of Reynolds that nature has to resolve methods of motion to accommodate.

	Reynolds number
A large whale swimming at 10 m/s	300,000,000
A tuna swimming at the same speed	30,000,000
A duck flying at 20 m/s	300,000
A large dragon fly going 7 m/s	30,000
A copepod in a speed burst of 0.2 m/s	300
Flapping wings of the smallest flying insects	30
An invertebrate larva, 0.3 mm long, at 1 mm/s	0.3
A sea urchin sperm advancing the species at 0.2 mm/s	0.03
A bacterium, swimming at 0.01 mm/s	0.00001

**Table 1 Spectrum of Reynold Number in Nature**

### **Usain Bolt averages a Reynolds number of around 800,000 during his Olympic medal runs!!!**

The really big problem with Reynolds number is that for complex fluid machines there are a variety of Reynolds numbers affecting the performance. This is because we choose to take a single dimension and velocity in the equation, usually in the case of flow metering the diameter and mean pipe velocity. Changes however appear at different Reynolds numbers if we do this. For example the simple orifice plate goes through a variety of changes, the change in profile, based on diameter, change in the boundary layer on the plate surface, this should be the plate length to the throat, but we use diameter again, and finally the changes in the separated boundary layer forming the jet. This should be some function of the jet, but again for convenience we use pipe diameter. Similarly with velocity. If the right dimension and velocity were used for each process then they would all happen at similar Reynolds number, but by virtue of using a single dimension they happen at different Reynold number values resulting in the apparently complex shaped curves with several changes across their range for many of our meters produce during calibration.

The issue of whether we see changes happen at higher Reynolds numbers can be seen in the case of the vortex meter. The majority of meters now have sharp edges to define the separation of flow from the bluff body. Early designs and patents concentrated on using a circular cylinder, because it was an easy shape to manufacture. Unfortunately if we look at the calibration of a circular cylinder vortex shape we see that there is a change in the calibration, Strouhal number, at a high Reynolds number, figure 2. At the low Reynolds numbers the change is due to the separated boundary layer changing from

Technical Paper

laminar to turbulent. At the higher Reynolds number the boundary layer on body itself changes from laminar to turbulent. The layer now has more energy to battle against the adverse pressure gradient around the body, and so the separation point moves, changing the vortex frequency. The use of sharp edges stops this effect, by determining physically the separation point.

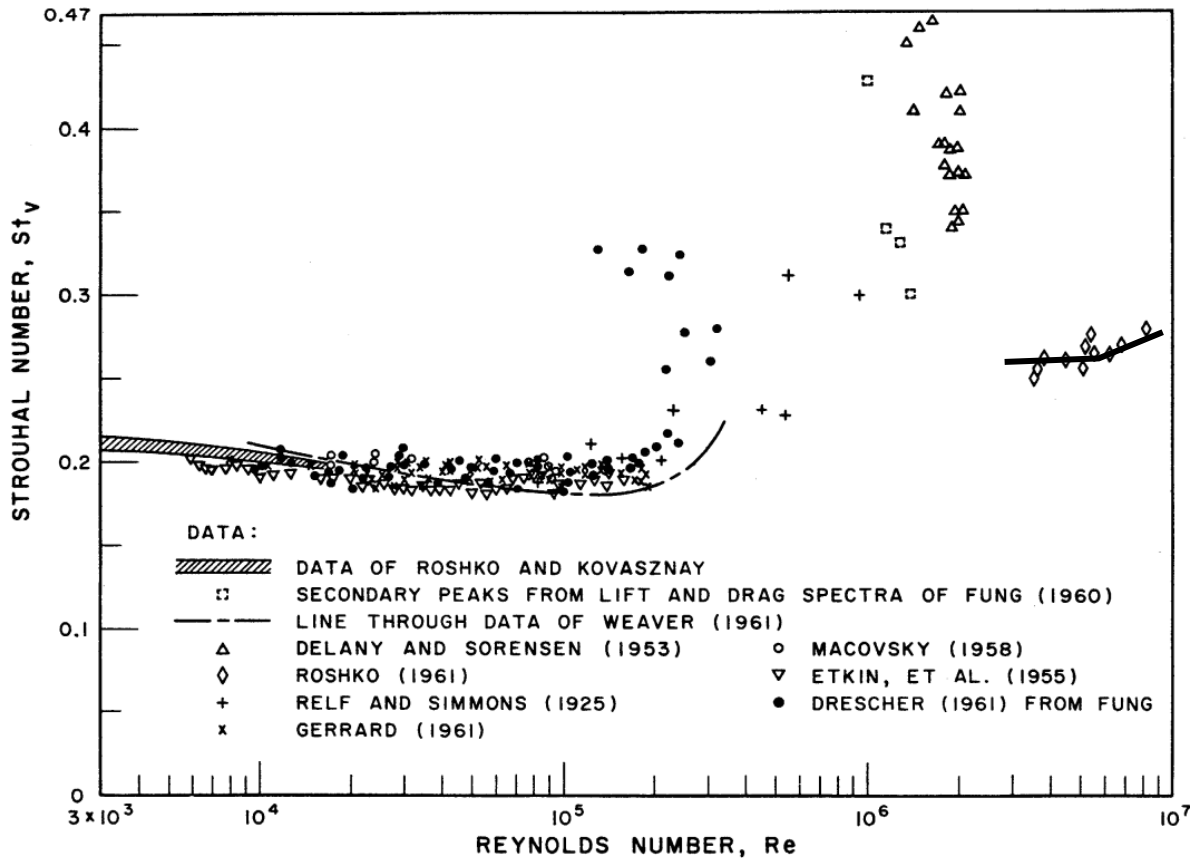


Figure 2 - Change in Calibration of a Circular Cylinder Vortex Meter

The major issues to note about Reynolds number are:

- All meters are beholden to Reynolds number in some form or another.
- It can jump up and bite you if you have not done the proper investigation into its effect on a product, for example for years it was said that the Coriolis meter was not subject to Reynolds number, and now we know that it is a mere mortal like the rest of other meters in this respect.
- Reynolds number effects are different not only for different meters types, but also designs and even within the same design, largely because it is difficult to manufacture meters that are so identical that Reynolds number effects are exactly the same when we are trying to produce low uncertainty measurement.

It should be emphasized that Reynolds number is not the only effect, bearings, resolution velocity effects can all contribute to meter errors.

Technical Paper

3 HOW DOES THIS RELATE TO FLOW MEASUREMENT

All of this is great in theory but how does this effect measurement? The issue is not a new one, Reynolds number correction of meters goes back to the very earliest days of flow measurement as an accepted need and science. Looking at the early standards for differential pressure meters Reynolds number correction is an essential part of the meter performance. In BS 1042, the earliest standards relating to differential pressure measurement clearly show in graphical form the corrections, figure 3, and further discuss the increase in uncertainty.

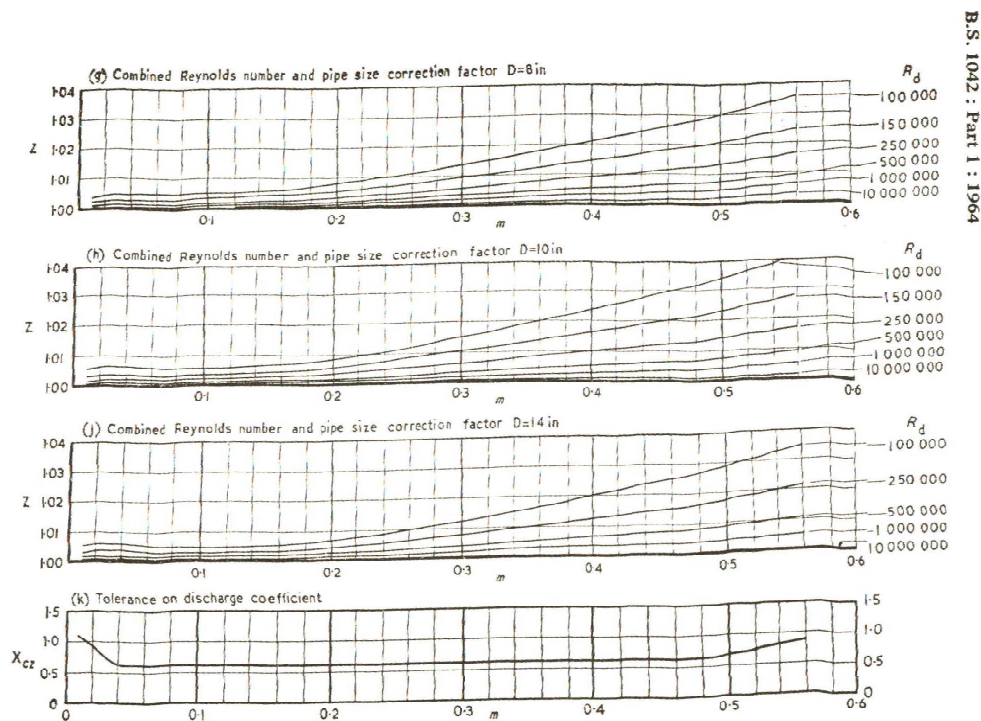


Fig. 41. Data for orifice plate with flange tapings—continued

Figure 3 - Reynold Number Correction of Orifice BS1042

When presented in this form it is easy to see the correction, particularly as we also then had to do a hand correction and so its relevance to measurement was very clear, now we have a complex equation used in most times in a computer and so the relevance is less obvious. More often than not now the extra uncertainty that results from the calculation of Reynolds number and the shape of the calibration curve is entirely forgotten. In fact it is now ignored completely largely because the corrections are hidden entirely within a "black box" and the methodology is hidden. Without knowing the methodology it is largely impossible to determine any extra uncertainty, or even how good the method is at correcting the changes due to Reynolds number.

# 34<sup>th</sup> International North Sea Flow Measurement Workshop 25-28 October 2016

## Technical Paper

In fairness there is more openness within the gas measurement industry. The methods used to calibrate and linearise Gas USMs are very clear, in fact CEESI now does the corrections for most manufacturers, and in fact the calibration is shown as an "as found" and as "as left", figure 4, so that it can be easily seen how much correction is applied and how it is applied. Many manufactures still use velocity as the base correction which is not correct, but at least from the calibration data feasible to understand and calculate the possible extra uncertainty.

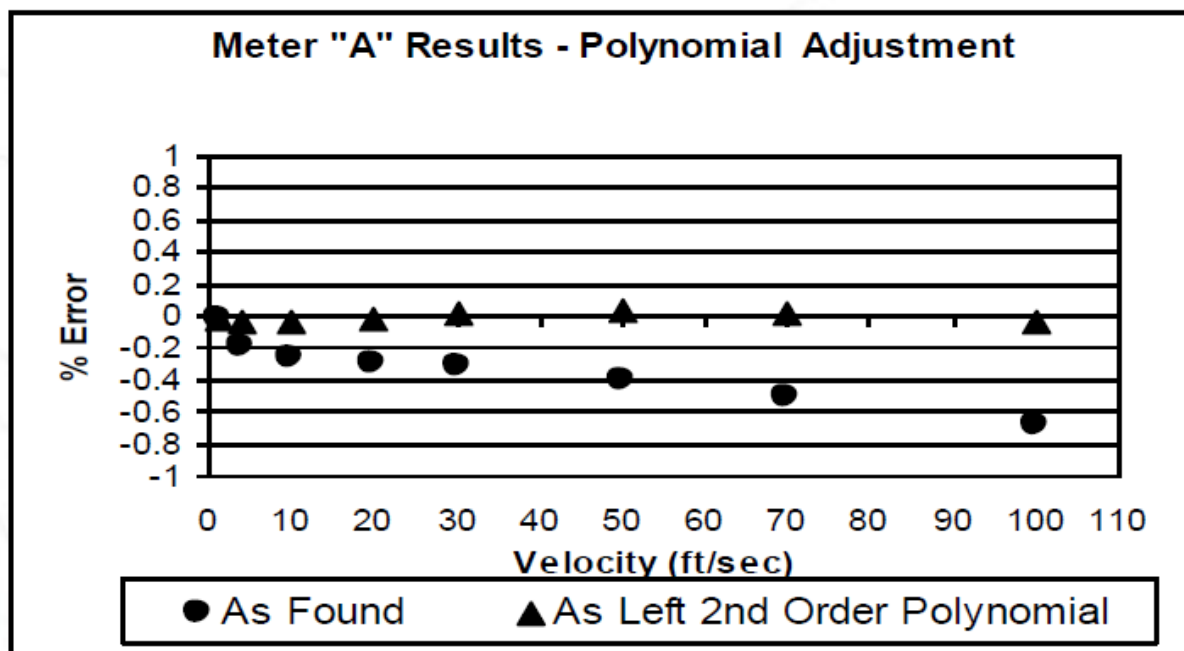


**Figure 4 - Correction of a Gas Ultrasonic Flow meter using a Polynomial Velocity Fit.**

It should be noted that for Gas USMs the method of calibration is laid out in standards, for example AGA 9. They call for an "as found" and "as left" calibration. The "as left" is after the corrections are applied. It should be noted, however, that while at least they call for both bits of data to be supplied, unlike the graph in figure 4 they only call for two or three points for the "as found", when this is the curve that is really important piece of information to the user!!

The real difference between the liquid and gas methods seems to have come from history. Gas meters have very little opportunity for calibration checks on site, whereas for liquids there has for many years been the ability to prove the meter, and hence check the meter calibration on site. This has developed a mentality that proving will solve all ills, and that the minimum is required for the calibration of the meter before it is installed. This as will be shown has led to some potential errors in measurement, and lax procedures that could be costing metering uncertainty.

On the liquid side the methods of correction is generally hidden, and even denied either explicitly or by non-discussion. Most USM manufacturers, although there are still some exceptions, recognize the need for a proper calibration that covers the operational parameters, most importantly Reynolds number, of the meter, figure 5. To ignore this means that the calibration must be extrapolated, and either the curve is ignored or

# 34<sup>th</sup> International North Sea Flow Measurement Workshop 25-28 October 2016

## Technical Paper

assumed. Particularly at lower Reynolds numbers the curve of a USM can, depending on the design, produce large linearity errors. Machining does not easily reproduce the detailed shape of for example the transducer ports, and so the calibration curve will change in detail from meter to meter. Remember we are looking for a total uncertainty in the order of 0.2% for liquid custody transfer meters, and so these small changes will matter, and proving does not necessarily solve the problem. Perhaps the biggest problem is the methods used. These have been previously described [1], and can still be very fragile.

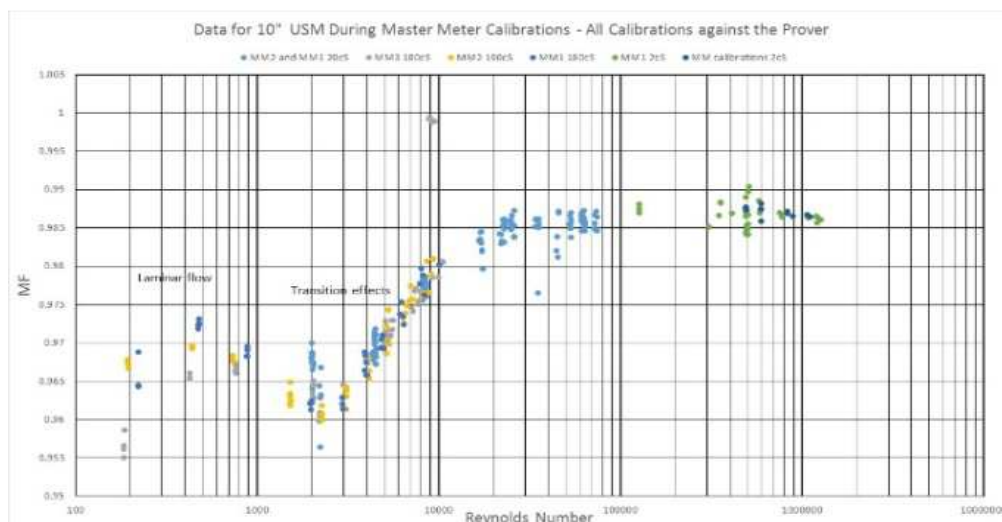


**Figure 5 - Calibration of a 10" 4 Path USM**

The same is true for the Coriolis meter, but probably more hidden than for a USM. It took over 20 years to discover the fact that a Coriolis meter is subject to a Reynolds number non linearity at low Reynolds numbers, figure 7. Once eventually found it would be expected that we would have heard about solutions to the problem. These may be design, for example tests seem to show that lower frequency, smaller meter seem to have less susceptibility, or how the problem is being solved. Only one manufacturer has shown their solutions. Others must be solving the problem but are not willing to share the methodology. This leaves a feeling of suspicion as to how the method works. Further the majority of Coriolis meters are calibrated on water, which will not allow for anything other than an assumed correction for the meter at low Reynolds numbers.

The turbine meter has now several detailed descriptions of the method used to linearise the meter [2]. Particularly Helical bladed meters are usually now calibrated on hydrocarbon, to be able to improve the linearity of the meter under operational conditions. As described they can be modified fluid dynamically to account for the eccentricities of the calibration, and bring the curve close to linear relationship over the operational range.

# 34<sup>th</sup> International North Sea Flow Measurement Workshop

## 25-28 October 2016

### Technical Paper

#### 4 PROVING

Proving should solve the problem! Proving is a very effective method for ensuring that the meter calibration is corrected for the vagaries of site installation. It does however present several practical problems. If as we see meters are non-linear with Reynolds number and not corrected properly we are left with several scenarios:

1. If the flowrate is nominally constant but the viscosity changes, for example due to ambient temperature then:
  - I. Using the API philosophy of proving every time there is a change in viscosity, but how often should it be proved? It is not clear as to how much and how often this should be done?
  - II. In most cases in the US, proving is done by contract prove companies, maybe every 3 months, how do you get the prover company to come in for example every day. In the Northeast of USA on in winter the temperature can change from day to day up to 20°C. Even between night and day this can vary by the same amount in parts of the world. How many times do you prove?
  - III. You could correct it by proving against Reynolds number, but few manufacturers allow you to get into their electronics and put in the correction.
  - IV. There are now some Flow computers that allow for Reynolds number correction, but how do you know the Reynolds number (Viscosity)?
2. If you have a linear range that is a combination of changing flowrate and viscosity this becomes even harder to deal with:
  - I. Have to linearise with Reynolds number somehow, but how?
  - II. How often do we calibrate, the API definition should be based on Reynolds number not just viscosity!
3. If the meter is properly calibrated and linearized for Reynolds number then:
  - I. If that linearisation is good, and the method holds up under operation, then proving will be straight forward.
    1. Note however if you use traditional proving flowrate linearising methods to "improve the calibration on site, the meter will still need to be corrected for Reynolds number not flow rate.
  - II. If, as can easily be the case, the linearisation method does not work well, then we are back to a more disconcerting case 2, but with the added complexity of uncovering the effects of linearization.

Two examples that come easily to mind are the case of USMs operating at low Reynolds numbers at startup [2]. In this case the meters had to be essentially re-linearised on site, a costly and time consuming exercise. Another example is the case of a USM operating in the non-linear range with a poor determination of viscosity. This meant the corrections were being applied at the wrong Reynolds numbers, figure 6. It was located in the North east of the US. The nominal viscosity was 4cS, but through the year the viscosity changed, as it was supplied from storage tanks, from 1.5-6cS, a Reynolds number variation at a constant flow of 4:1. The user was disconcerted to see his proves varied through the year at "constant flow rate" by as much as 0.4%. His turbines he replaced changed by 0.2%, he was expecting to do better with the USM.

Technical Paper

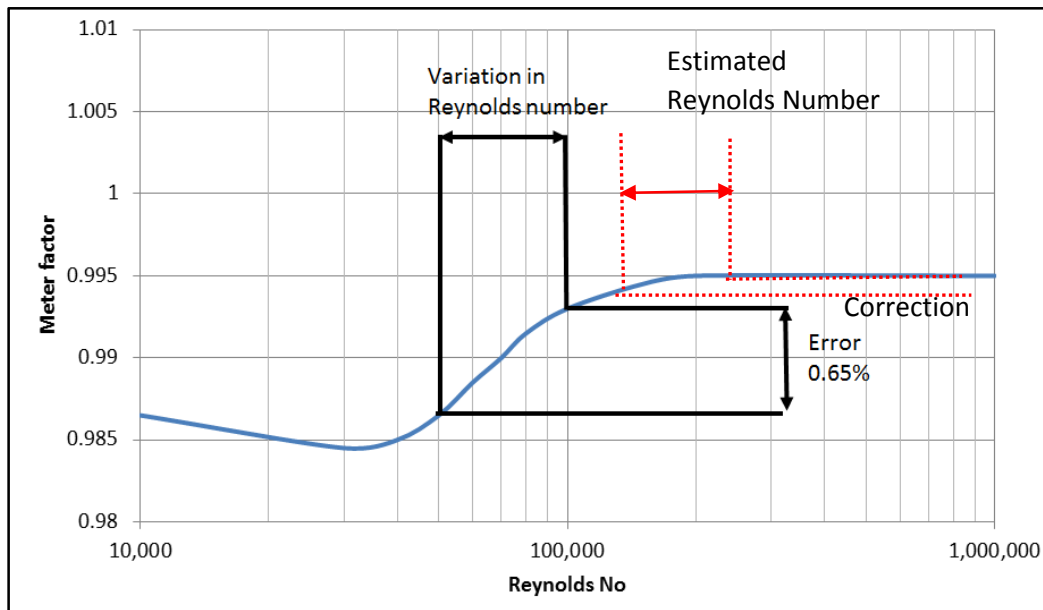


Figure 6 - Mis-Linearisation of a USM

## 5 EXTRAPOLATION

If we accept that the meter is basically non-linear and needs to be corrected, we then must accept that we need to know the shape of the curve that is to be linearized. The basic method to do this is by calibrating the meter. If the non-linearity is a function of Reynolds number then we must accept that we need to know the shape of the calibration curve across the operational Reynolds number range. Here we walk into the issue of what uncertainty do we require, and how big is the correction. To ensure the best uncertainty it is essential that the meter be characterized over the full operational range of Reynolds numbers, but what happens if we do not. If for example we chose to calibrate an 8" meter to operate on 40cS oil with water. The bottom Reynolds number on water will be around 170,000 and the top Reynolds number for oil will be 56,000. The Calibrations do not even overlap. So any non- linearity in the curve will not be caught by the water calibration. An **uneducated extrapolation** of a 4" meter is shown in figure 7, the potential difference in calibration curves can be clearly seen.

# 34<sup>th</sup> International North Sea Flow Measurement Workshop 25-28 October 2016

## Technical Paper

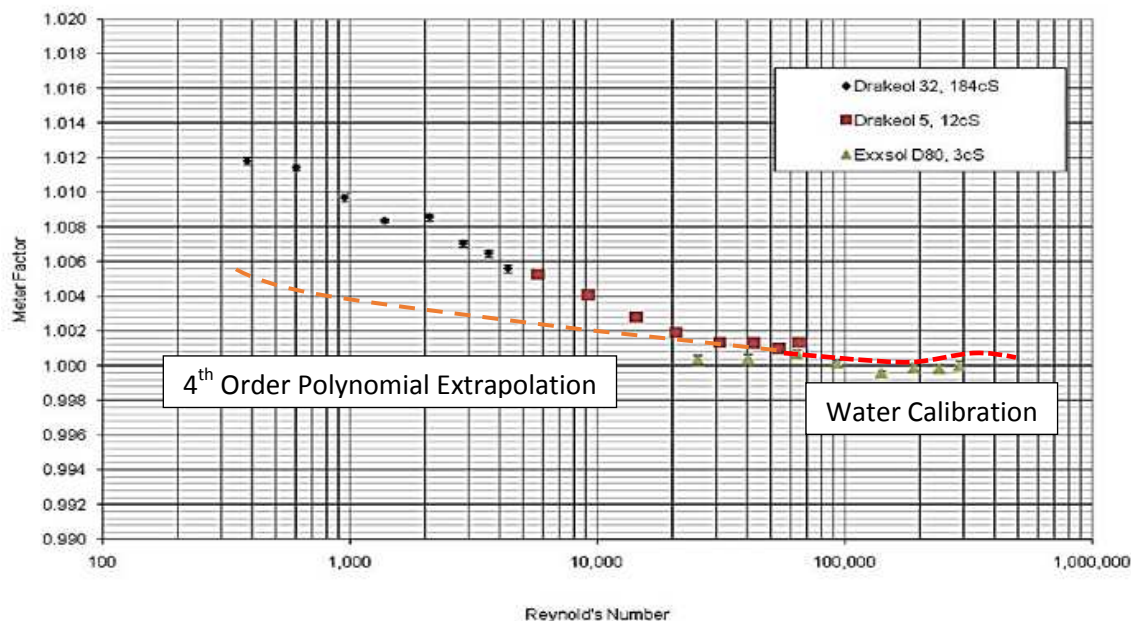


Figure 7 - Calibration of a 4" Coriolis Meter

It may be said that this is an uneducated extrapolation and we know the shape of the calibration of our meter. This would be for example the principle used for using an orifice plate without calibration, using ISO 5167. However, the uncertainty level is not 0.1%. It must be recognized that there is an extra uncertainty that must be included for the extrapolation. The viability of such extrapolations depends on the meter type, the manufacturing processes and the backlog of collected data. It therefore takes a long time and is a costly process to produce sufficient proof of the veracity of such a method. As far back as 1964 in the BS1042 standard for orifice plates the authors clearly recognized the fact that meter reproducibility was a problem in determining the effect of Reynolds number, figure 8.

Technical Paper

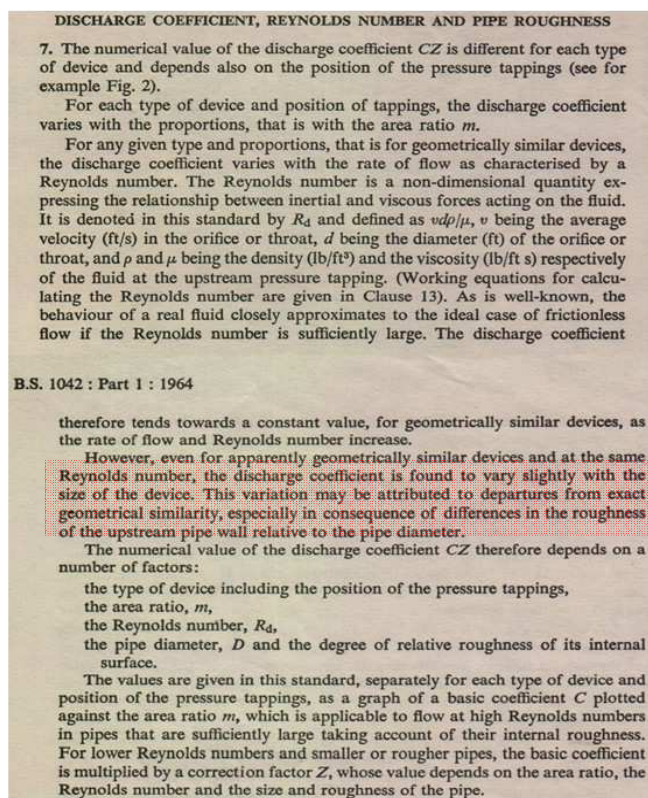


Figure 8 - BS1042 Statement on Reynolds Number Correction

We have concentrated on extrapolation in the downwards direction of Reynolds number, but also it should be pointed out the same is true for upward extrapolation. We have said that in general the higher the Reynolds number the more stable to operation of fluid mechanics. This is not always the case and such an assumption can be fraught. In the past such orifice plates as the conical entry plate were designed to have a good low Reynolds number performance. It was assumed that once a good linear meter had been produced it would continue to high Reynolds numbers. In fact there is a 1% change in the calibration at high Reynolds numbers due to the change in surface boundary layer from laminar to turbulent. A similar issue was shown in figure 2, with vortex shedding. Thus the current propensity for assuming that a meter calibrated on water will operate in the same way for LNG at much higher Reynolds numbers may not be true!

To summarize, the assumption that has to be made is, the extrapolated data follows the curve of the meter at the end of calibration. Often the assumption is that the meter is now completely linear, a feature of many Reynolds number based meters as they increase in Reynolds number. The problem comes if there is an unexpected discontinuity in the calibration. This of course will never be known until tests can be carried out at the extrapolated flowrates, or the meter shows differences to the expected performance, by for example a mass balance of the system. If this method has to be used then it is imperative that supplier shows:

- The method in detail.
- The data to back up the extrapolation.
- And importantly an independent assessment of the extrapolation method and how strong it will be in the application.

# **34<sup>th</sup> International North Sea Flow Measurement Workshop 25-28 October 2016**

## **Technical Paper**

**The uncertainty for extrapolated meters will always be greater than for a meter calibrated over the operational range.**

### **6 CALIBRATION**

It is hopefully clear now that meters with Reynolds number non-linearity in applications where we are looking for low uncertainty need to be calibrated, as far as possible over the operational range. At present there is no good independent proof to tell us that any of the meters can be calibrated by "assumption". This unfortunately requires the user to pay more money because calibrating liquid meters over a wide Reynolds number range is not inexpensive, water is much easier and cheaper. These meters are, however, the only source available to measure the dollars passing through a flow line, particularly hydrocarbon. Without the proper calibration, even with proving there is always a risk the calibration will change with time. This drops down to dollars moving in an unknown direction (The definition of uncertainty). At least with the correct calibration, it is possible to understand where the meter is starting from and to determine the attention that needs to be made to the operation and linearization of the meter.

The quality of calibration is also an issue. Poor calibration can be as damaging as no calibration. Initially of course calibrations should be carried out at facilities that are independently audited to an international standard. This does not necessarily require that it be an independent facility, although that may add credibility. The methods and requirements at least have a standard in AGA, particularly for Gas USMs, although as previously stated this leaves much to be desired. The concept of only producing 2 or 3 "as left" points is odd to say the least. In fact in some recent liquid calibrations of USMs using the same principle, it was clear that points could be chosen that appeared to make the curve much better than it actually was. For liquid measurement there is very little current discussion in standards as to the method of calibration and its requirements. This leaves it in the hands of the manufacturer and possibly the calibration facility if independent. While a calibration facility can give advice, in general its purpose is to do the calibration in line with the customers (often the manufacturer) order.

### **7 CONCLUSIONS**

- Reynolds number must be acknowledged as a major factor in the performance of flow meters.
- All meters are subject to non-linearity due to Reynolds number and generally have to be corrected.
- This correction should be more transparent to the user.
- When extrapolation is used it will always increase the measurement uncertainty.
- This can be alleviated by the correct calibration of the meters.

### **8 REFERENCES**

- [1] Cousins T. "HOW SAFE IS LINEARISATION OF FLOW METERS?" ISSFM 2011
- [2] Cousins T. "Is Linearisation Safe for Custody Transfer?" NSFMS 2014
- [3] BS 1042: Part 1:1964

# **34<sup>th</sup> International North Sea Flow Measurement Workshop 25-28 October 2016**

## **Technical Paper**

- [4] T. Cousins "VISCOSITY AND ITS APPLICATION IN LIQUID HYDROCARBON MEASUREMENT" ISHM CLASS 2013.
- [5] T. Cousins "The Reynolds Number Correction of Liquid Ultrasonic Meters and Coriolis Meters" CEESI/VSL Conference 2014 Lisbon.
- [6] Liptak B.G - Editor in Chief "Instrument-Engineers-Handbook-Fourth-Edition-Volume-One-Process-Measurement-and-Analysis" Fourth edition CRC publication for ISA
- [7] Baker R.C "Flow-Measurement-Handbook" Cambridge University Press.
- [8] Augenstein D. & Cousins T. "Validating the Accuracy of Multi-Path Transit Time Ultrasonic Flowmeters" ISSFM, Alaska, 2010
- [9] Cousins T. "EFFECT OF SWIRL ON 8 PATH METERS" CEESI Workshop Singapore 2010.
- [1-] Augenstein D & Cousins T. "THE PERFORMANCE OF A TWO PLANE MULTI-PATH ULTRASONIC FLOWMETER" Northsea Flow Measurement Workshop, 2010.
- [11] Brown G, Estrada H, Augenstein D, Cousins T, "LNG Allocation Metering Using 8-Path Ultrasonic Meters" Northsea Flow Measurement Workshop, 2007
- [12] Brown G, Augenstein D, Cousins T. " The relative Merits of Ultrasonic Meters Employing Two to Eight Paths", SEAWS, 2006.
- [13] Liptak B.G - Editor in Chief "Instrument-Engineers-Handbook-Fourth-Edition-Volume-One-Process-Measurement-and-Analysis" Fourth edition CRC publication for ISA
- [14] Baker R.C "Flow-Measurement-Handbook" Cambridge University Press.
- [15] Augenstein D. & Cousins T. "Validating the Accuracy of Multi-Path Transit Time Ultrasonic Flowmeters" ISSFM, Alaska, 2010
- [16] Cousins T. "EFFECT OF SWIRL ON 8 PATH METERS" CEESI Workshop Singapore 2010.
- [17] Augenstein D & Cousins T. "THE PERFORMANCE OF A TWO PLANE MULTI-PATH ULTRASONIC FLOWMETER" Northsea Flow Measurement Workshop, 2010.
- [18] Brown G, Estrada H, Augenstein D, Cousins T, "LNG Allocation Metering Using 8-Path Ultrasonic Meters" Northsea Flow Measurement Workshop, 2007
- [19] Brown G, Augenstein D, Cousins T. " The relative Merits of Ultrasonic Meters Employing Two to Eight Paths", SEAWS, 2006.

## Estimating Gas Ultrasonic Meter Field Error

Randy Miller, Energy Transfer  
Ed Hanks, CEESmaRT  
John Lansing, CEESI

### 1 INTRODUCTION

For nearly a decade the North American Fluid Flow Measurement Council (NAFFMC) has investigated a variety of ultrasonic meter effects on both low and high-pressure ultrasonic meters. The NAFFMC is comprised of 5-6 industry experts that request testing be performed and subsequently published at the annual CEESI Ultrasonic Conference.

During the 10+ years of the NAFFMC's existence, research has studied effects ranging from header designs, upstream piping configurations, various meter tube end-treatments, and inline filters. While this paper examines some of the history behind the NAFFMC research, much of the data used for the final analysis is not included in order to keep the paper to a manageable length. Thus this paper will summarize some of the tests, and then focus on the use of an ultrasonic meter's diagnostics to determine the health and predict the meter's uncertainty based on the diagnostic parameters.

### 2 HEADER EFFECT ON USM, T TYPE HEADER INSTALLATION

There were two NAFFMC studies performed on the installation effects of headers. The first discussed is a presentation developed by Jonatan Mustafa (Kinder Morgan) and Joel Clancy (CEESI), and presented by Reese Platzer (Enterprise Products). The research was titled "Header Effects on USM, Type Header Installation."

Due to the difficulty of transporting the headers to a test calibration facility, ultrasonic meters are commonly calibrated individually then placed on a meter skid with multiple runs. Because of this, there has been interest from the industry to test the effect of headers on ultrasonic meters. The purpose of these tests is to determine the effect a "T-type" header has on ultrasonic meter performance. Figure 2.1 shows the dimensions of the header used for this series of tests.

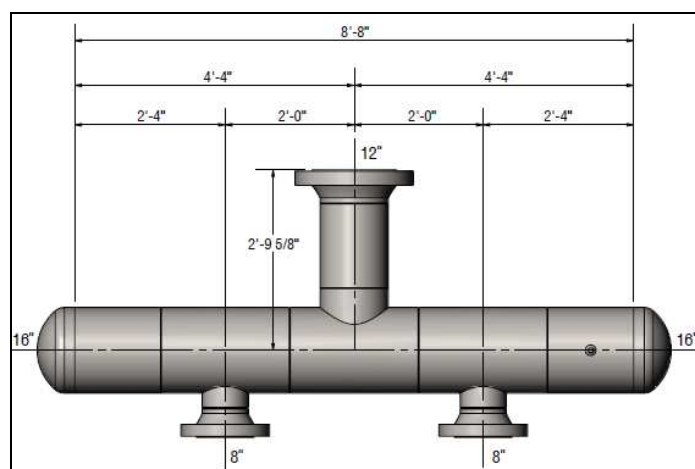


Fig. 2.1. - T-Header

## 34<sup>th</sup> International North Sea Flow Measurement Workshop 25-28 October 2016

Figure 2.2 shows the “Elongated Attenuating Tees (EA T’s)” testing which included the following:

- Test at three flow rate points for run one at 7.5, 15 and 23 m/s (no header).
- Install both meter runs with EA Tees in the header.
- Take the same three points with just run one flowing.
- Take the same three points with both runs flowing.

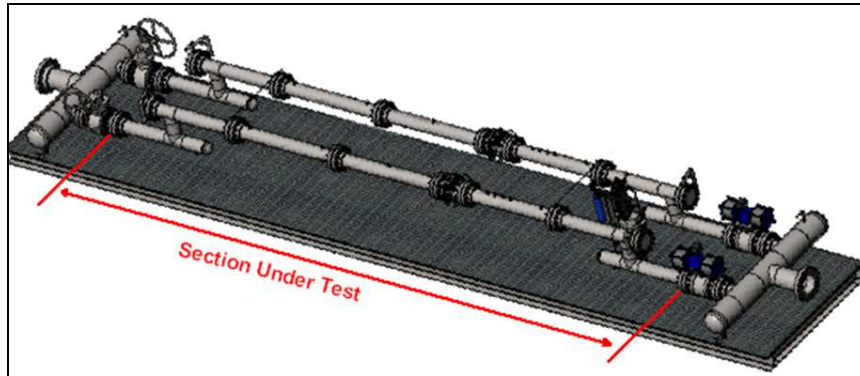


Fig. 2.2. Elongated Attenuating Tees (EA T’s)

Figure 2.3 shows the “Straight Pipe Header Effect” testing which included the following:

- Test at three points for run one at 7.5, 15 and 23 m/s.
- Install both meter runs in the header (no tees).
- Take the same three points with only run one flowing.
- Take the same three points with both runs flowing.

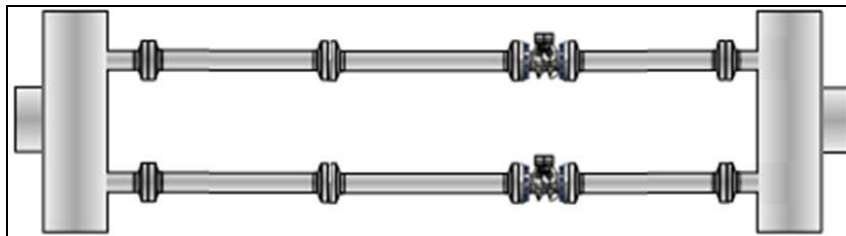


Fig. 2.3. Straight Pipe Header Effect

The final set of tests run in this series was with AGA-9 Tees with an Elbow to a Header. The piping configuration is illustrated in Figure 2.4. The tests included the following:

- Test at three points for run one at 7.5, 15 and 23 m/s (no header).
- Install both meter runs with AGA-9 tees + elbow in the header.
- Take the same three points with only run one flowing.
- Take the same three points with both runs flowing.

**34<sup>th</sup> International North Sea Flow Measurement Workshop  
25-28 October 2016**

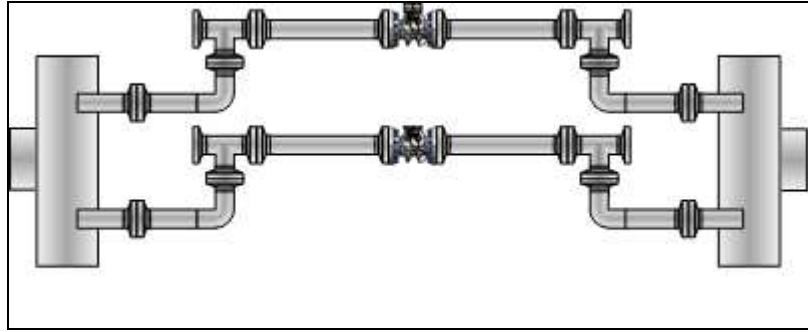


Fig. 2.4. AGA-9 Tees + Elbow Header Effect

For this series of tests, a 16-inch header and two each 8-inch SICK FLOWSIC600, Daniel SeniorSonic and Instromet Q.Sonic-Plus meters were all fitted with typical AGA 9 meter piping which consisted of 10D, CPA 50E, 10D, Meter, and 5D meter tubes. Figures 2.5 through 2.10 show the various piping configurations and meters. The straight pipe test runs were all used for the baselines. For this series of testing, results displayed are as found, (not adjusted to a baseline test run result). All tests used the same pipes.



Fig. - 2.5. Straight Pipe No Header



Fig. - 2.6. - Elongated Attenuation Tees



Fig. 2.7. - AGA 9 Tee w/Elbow



Fig. 2.8. - Parallel Runs Straight Pipe

# 34<sup>th</sup> International North Sea Flow Measurement Workshop 25-28 October 2016



Fig. 2.9. - Elongated Tees



Fig. - 2.10. - AGA 9 Tees W Elbows

Figure 2.11 shows the test results for the SICK meter. The test with the header and elongated tees created the most deviation from baseline in the SICK meter. Using the straight pipe data for a baseline, the shift was just over 0.1% at the 23 m/s test point, but on the order of 0.05% for the 7.5 m/s test point. Figure 2.12 shows the percent shift in profile factor for the various test runs.

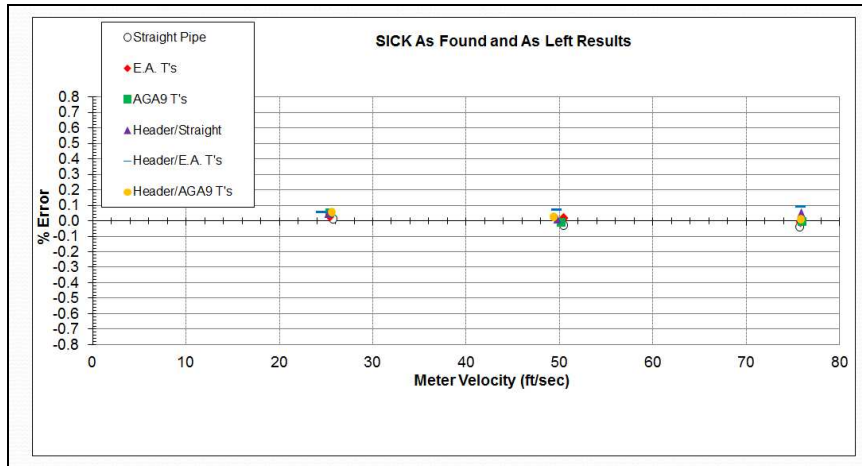


Fig. 2.11. - SICK Meter Test Results

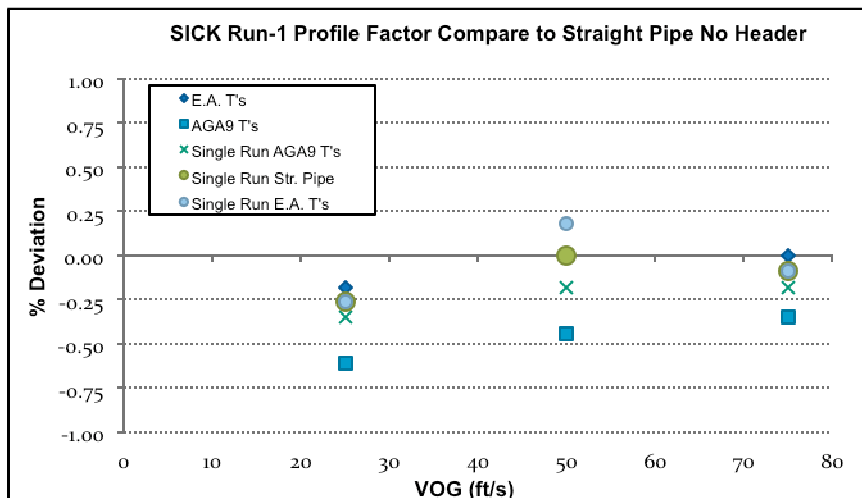


Fig. 2.12. SICK Meter Profile Factor Percent Shift

## 34<sup>th</sup> International North Sea Flow Measurement Workshop 25-28 October 2016

Figure 2.13 shows the test results for the Instromet meter. For the Instromet meter test, there was no significant difference between the test runs with the elongated tees and no header at 23 m/s, and the elongated tees with the header at 15 m/s. These two tests created the most measurement shift from baseline with an effect of just over 0.1%. Figure 2.14 shows the profile factor percent shift from baseline. The profile factor shifts were minimal but the elongated tee with a header test runs had the greatest profile factor shift around 0.5%.

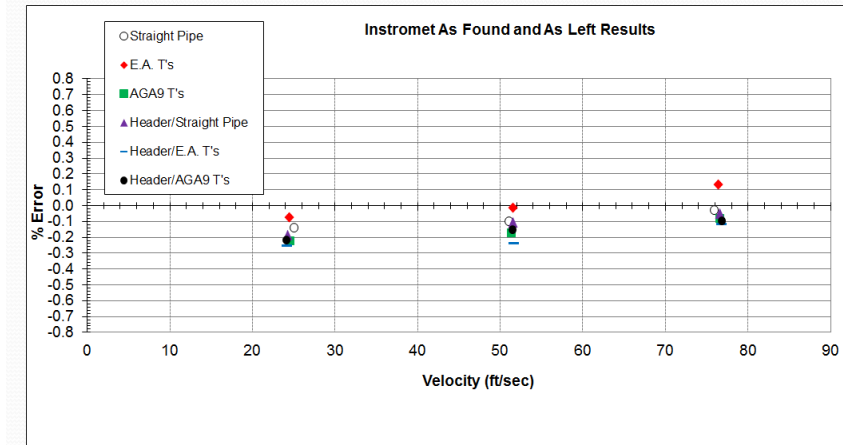


Fig. 2.13. - Instromet Meter Test Results

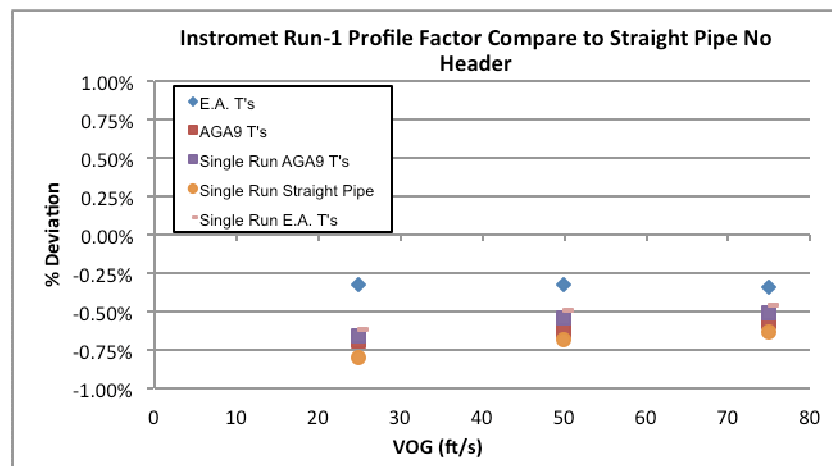


Fig. 2.14. - Instromet Meter Profile Factor Percent Shift

Figure 2.15 shows the Daniel test results. For the Daniel meter the test run with the AGA 9 Tees and the Header shifted the meter approximately +0.25% at the 23 m/s velocity. Figure 2.16 shows the profile factor percent shift was -0.42% for the test run with the AGA 9 Tees and for the Header.

# 34<sup>th</sup> International North Sea Flow Measurement Workshop 25-28 October 2016

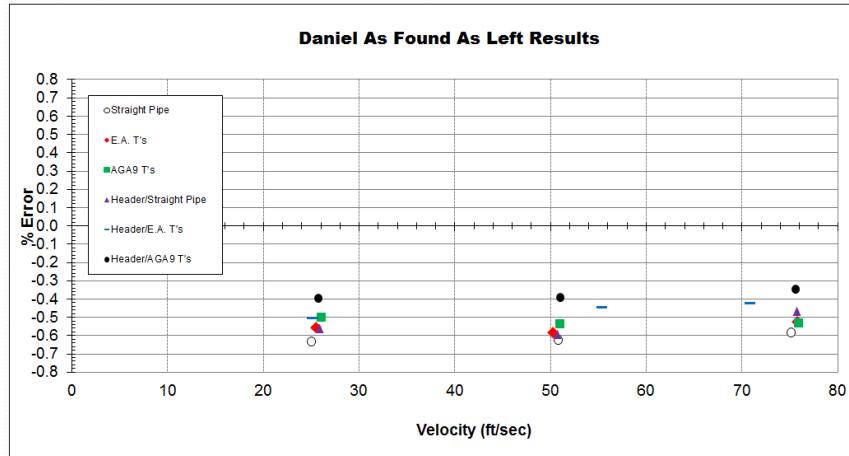


Fig. 2.15. - Daniel Meter Test Results

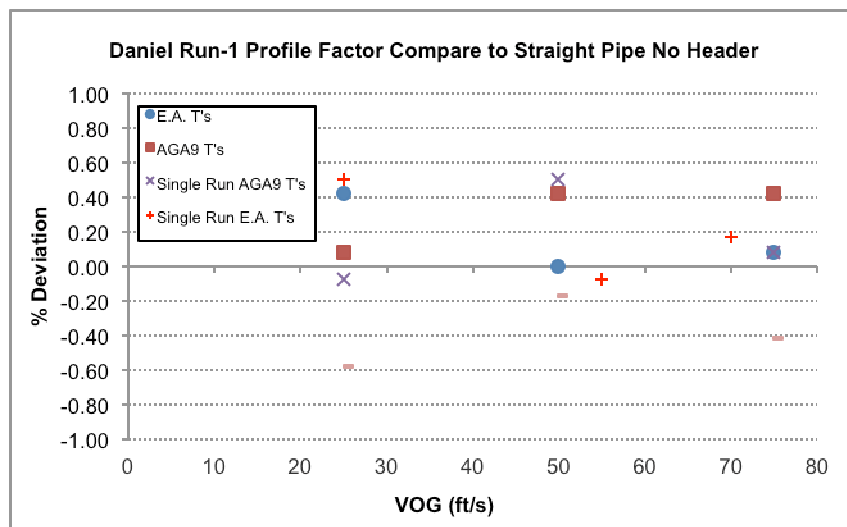


Fig. 2.16. - Daniel Meter Profile Factor Percent Shift

### 3 EIGHT-INCH USM INSTALLATION EFFECTS

The next NAFFMC research overview is on a presentation given by Randy Miller (Energy Transfer) titled "NAFFMC 2013 Testing." This test was the result of a customer approaching CEESI to perform some research. They wanted to study erratic behavior occasionally experienced when a meter was equipped with close-coupled tees and a Yale inspection closure on the upstream and downstream ends of the meter tube. The customer had two identical meters, meter tubes, and end-treatments. During calibration one meter displayed the erratic behavior, and the other did not.

The CEESI flow lab staff has seen this phenomenon before, so it was hoped this this issues could be re-created in order to study the problem closer. In this series of tests, researched various piping "end-treatments" on 8-inch Daniel and SICK meters were researched. This Instromet meter was not included in this testing as the NAFFMC chose to test only the Daniel and SICK meters. The baseline, as well as all end-treatment tests, were performed on both brands 8-inch meters with typical AGA 9 meter tube configuration of 10D, CPA 50E flow conditioner, 10D, Meter, 5D. The following bullets summarize the wide variety of end-treatment test configurations.

## 34<sup>th</sup> International North Sea Flow Measurement Workshop 25-28 October 2016

- Elbow and Blinded Tee - Elbow and Flat Closure
- Elbow and Blinded Tee - Elbow and Yale Closure
- Tee and Blinded Tee - Tee and Yale Closure
- Tee and Blinded Tee - Tee and Flat Closure
- Tee and Blinded Tee - Extended Tee and Flat Closure
- Tee and Yale Closure - Tee and Yale Closure
- Tee and Yale Closure - Tee and Yale Closure with Elliptical Deflector upstream
- Extended Tee and Yale Closure - Extended Tee and Yale Closure
- Extended Tee and Yale Closure - Extended Tee and Yale Closure with Elliptical Deflector downstream
- Extended Tee and Yale Closure - Extended Tee and Yale Closure with Elliptical Deflector upstream
- Elbow and Yale Closure - Elbow and Yale Closure

Figures 3.1 through 3.9 illustrate some of the different piping configurations and shows the Elliptical Deflector.



Fig. 3.1. Tee / Tee Flat Closure Left



Fig. 3.2. - Elbow / Tee Blind Flange Right



Fig. 3.3. - Tee/Tee Blind Flange Right



Fig. 3.4. - Tee/Tee Yale Closure Left



Fig. 3.5. - Extended Tee/Yale Closure



Fig. 3.6. - Elbow/Tee Yale Closure

## 34<sup>th</sup> International North Sea Flow Measurement Workshop 25-28 October 2016

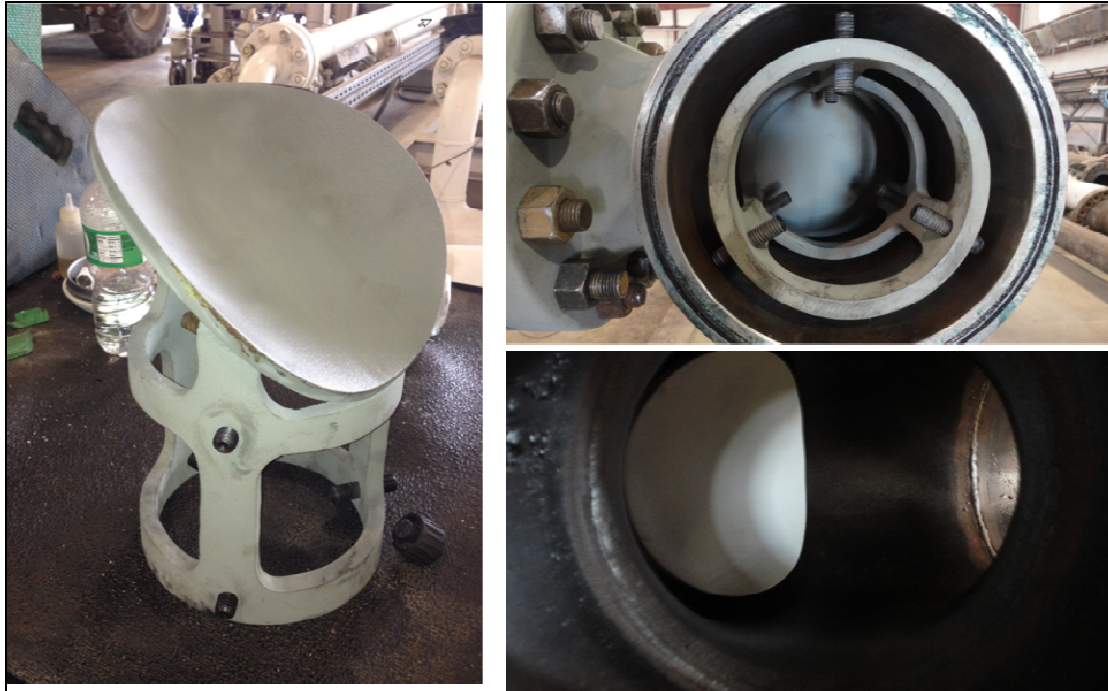


Fig. - 3.7, 8 & 9. Eight-Inch Elliptical Deflector Designed for Closure Caped Tees

The first objective was to look at the disturbances of each type of end treatment and to ultimately recreate the erratic behavior that had been seen in the customer's meter. While we were unable to achieve this erratic behavior to the point seen in the past, we were able to create some substantial disturbances worth studying. In Figures 3.10 and 3.11 the error vs. velocity is plotted on the graph for both meters.

Of note, both meters shifted up in (over-registered) every case as the upstream and downstream piping was modified. This may be due to the fact that the piping configurations always generated the swirl in the same direction throughout this series of tests.

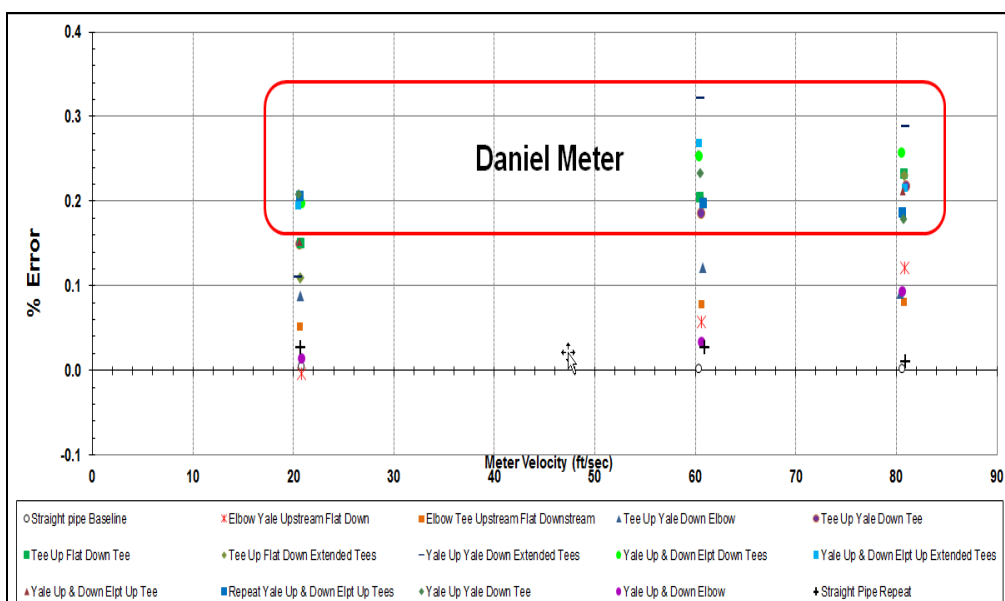


Fig. 3.10. - Eight-Inch Daniel Meter Test Results

## 34<sup>th</sup> International North Sea Flow Measurement Workshop 25-28 October 2016

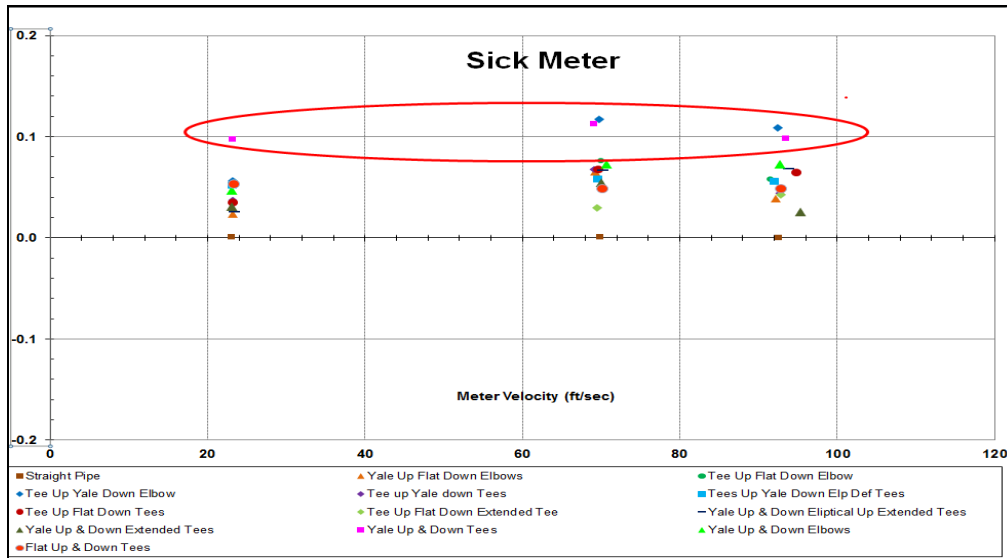


Fig. 3.11. - Eight-Inch SICK Meter Test Results

In the case of both meters, any combination of two close-coupled tees, installed on the inlet of the meter, created the highest measurement shift and instability and turbulence in the meters.

### 4 2014/2015 8-INCH USM DIAGNOSTIC DATA

In 2014 CEESI presented diagnostic maintenance logs from different brands of USMs taken during the test runs that created the greatest shift in each meter. Because the exact same tests were conducted in 2014 and 2015, with the exception of the swirl direction, it was decided to summarize diagnostics from both years of testing for each meter's extreme test case. Examining the measurement shift in these next tests, the reader should be aware that many of these tests created extreme conditions for the meters. These extreme conditions would not normally be found in the field, but do provide us with some indication of the meter's performance under severe conditions.

In 2014, a special device called a CPA Swirl Generator (CSG) was setup to create clockwise swirl (more in Section 5 on the CSG). For the SICK meter the most severe condition was created with the CSG set at 72-degrees and the valve wide open. Figure 4.1 shows the results from the 2014 test run and Figure 4.2 is from the 2015 data. The diagnostic graphs quickly indicate the difference between the two sessions. The CSG was setup to create counterclockwise swirl for the first series of tests (2014). Both conditions created similar error and in the same direction even though the Path Velocity Ratios were inverted (different swirl direction).

The SICK software was used to summarize the diagnostics that follow. The profile factors in both cases were 1.06, which is a 4.5% shift from the baseline profile factor. The symmetry factors shifted substantially more and in the opposite direction. The 2014 symmetry factor was 0.827, which is a 17% shift from the baseline, and the 2015 symmetry factor was 1.26, which was a 25% shift from the baseline. The turbulence values were extremely high in both tests. For this series of tests, the asymmetry and turbulence were the two indicators of measurement issues. The performance, speed of sound comparison and profile factor values were all within typical alarm limits.

# 34<sup>th</sup> International North Sea Flow Measurement Workshop 25-28 October 2016

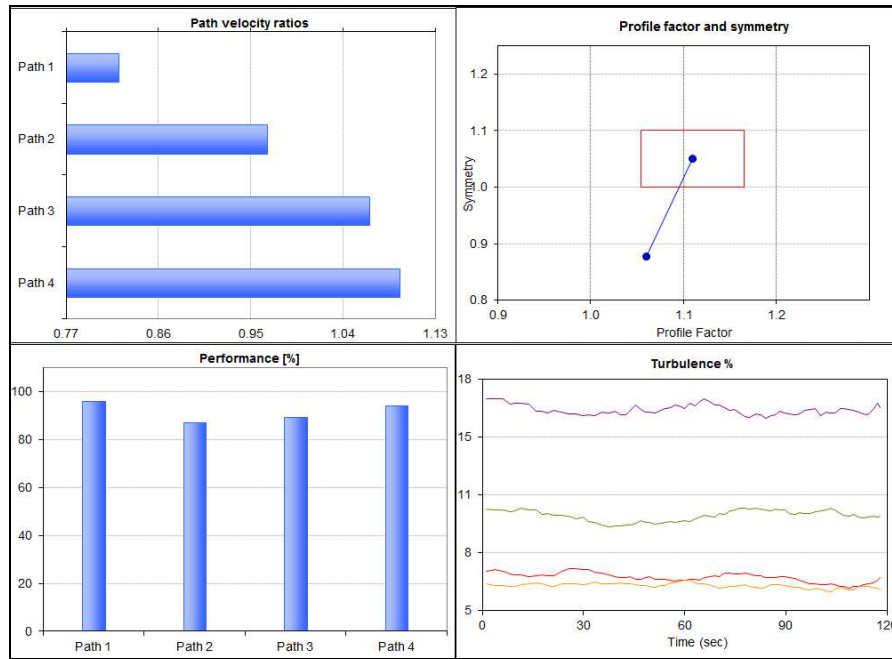


Fig. 4.1. - SICK Meter 2014 Data High Swirl Significant Symmetry Shift

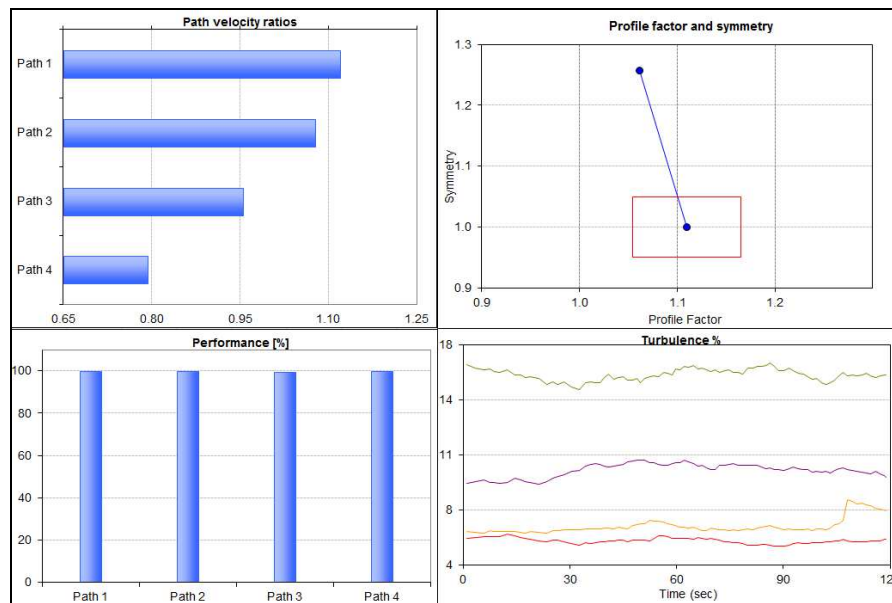


Fig. 4.2. - SICK Meter 2015 Data High Swirl Significant Symmetry Shift

For the Daniel meter the NAFFMC examined the maintenance logs from the CSG set at 72-degrees, and valve pinch set at 30%. Figure 4.3 is from the 2014 test data, and Figure 4.4 is from the 2015 data. Again, the diagnostic graphs quickly indicate the difference between the two sessions. As with the SICK meter in 2014, our CSG was setup to create clockwise swirl, and in 2015 the CSG was setup to create counterclockwise swirl.

The counterclockwise swirl created more measurement shift in the meter, and the errors were in opposite directions. The profile factor in 2014 was 1.259, a 9% shift from the baseline profile factor. In 2015 the profile factor for this same test scenario was 0.9, a shift of 22%. The symmetry factors shifted quite differently as well. The 2014, symmetry factor was 0.92, an 8% shift from the baseline and the 2015 symmetry factor was 0.99, a 1% shift from the baseline.

# 34<sup>th</sup> International North Sea Flow Measurement Workshop 25-28 October 2016

In this instance the profile factor and turbulence were the two indicators of measurement issues for both years, as well as the symmetry in the 2014 test. The performance and speed of sound comparison values were within typical alarm limits.

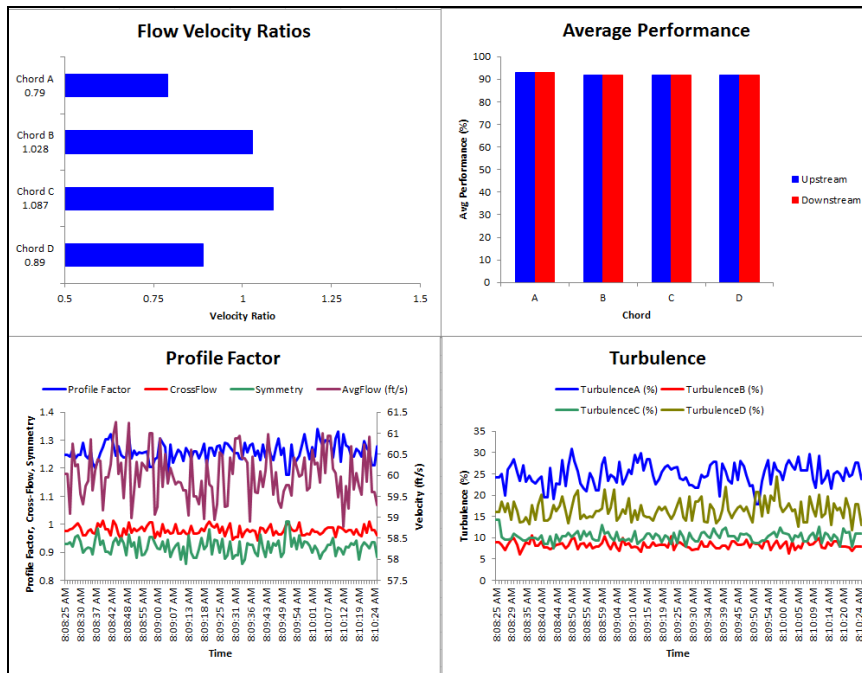


Fig. 4.3. - Daniel Meter 2014 Data High Swirl & High Symmetry

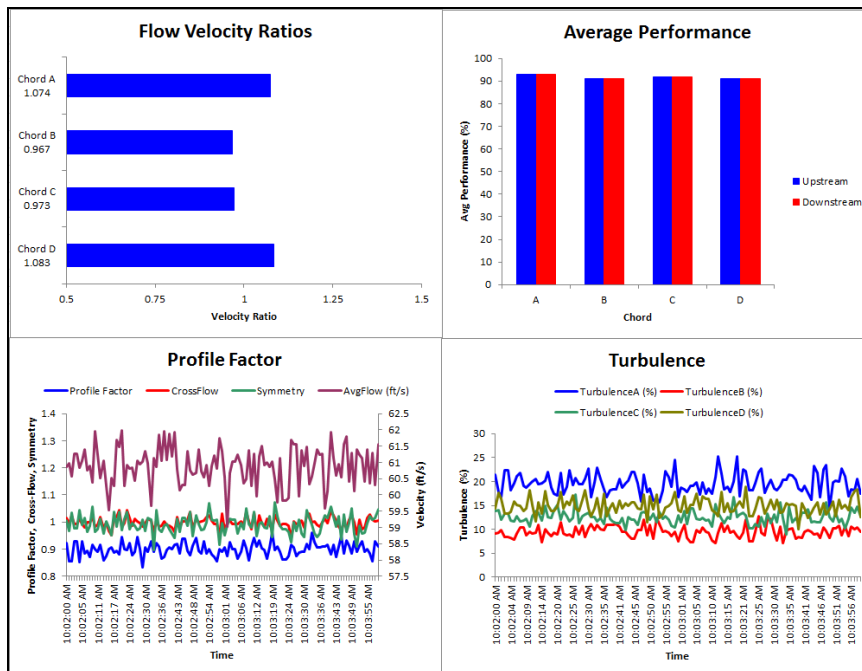


Fig. 4.4. - Daniel Meter 2015 Data High Swirl & High Symmetry

Next the NAFFMC looked at the diagnostics from the 2014 and 2015 Instromet Q.Sonic-Plus maintenance logs. The test runs were with the CSG set at 72-degrees, and the valve pinch set at 30%. Graphs in Figure 4.5 are the diagnostics for the 2014 test and in Figure 6.6 are the diagnostics for the 2015

## 34<sup>th</sup> International North Sea Flow Measurement Workshop 25-28 October 2016

test. As with the other meters, it is quite easy to see the difference in the diagnostics due to the change in swirl direction.

The error was somewhat higher for the 2015 test than it was in 2014, but both errors were in the same direction. The profile factor was 1.009 in 2014, a 3.26% shift from the baseline. The profile factor was 1.013 in 2015, a 3.0% shift from the baseline. The symmetry factor from the 2014 data was 0.82 which was calculated by the clockwise swirl paths divided by the the counterclockwise swirl paths. This was a 18% shift from the baseline. The symmetry factor from the 2015 data was 1.14, a 14% shift from baseline.

The primary indicators of measurement shift from both the 2014, and 2015 data were the symmetry factors which were 18% and 14% shifts from the baseline and the profile factors, that while under 5% from the baseline, were in alarm in the Sonic Explorer Health Care Report. Of note, the symmetry calculated from the axial paths were within limits, but the symmetry calculated from the swirl paths were not. The speed of sound comparisons were within their alarm limits.

Since the Instromet meter computes a value for swirl, this data is another diagnostic tool that can be used as an indicator of potential error. In the 2014 test, the meter measured +4 degrees of swirl, and in 2015 the meter measured a value of -6 degrees of swirl. In both cases the swirl values fell outside of normal alarm limits.

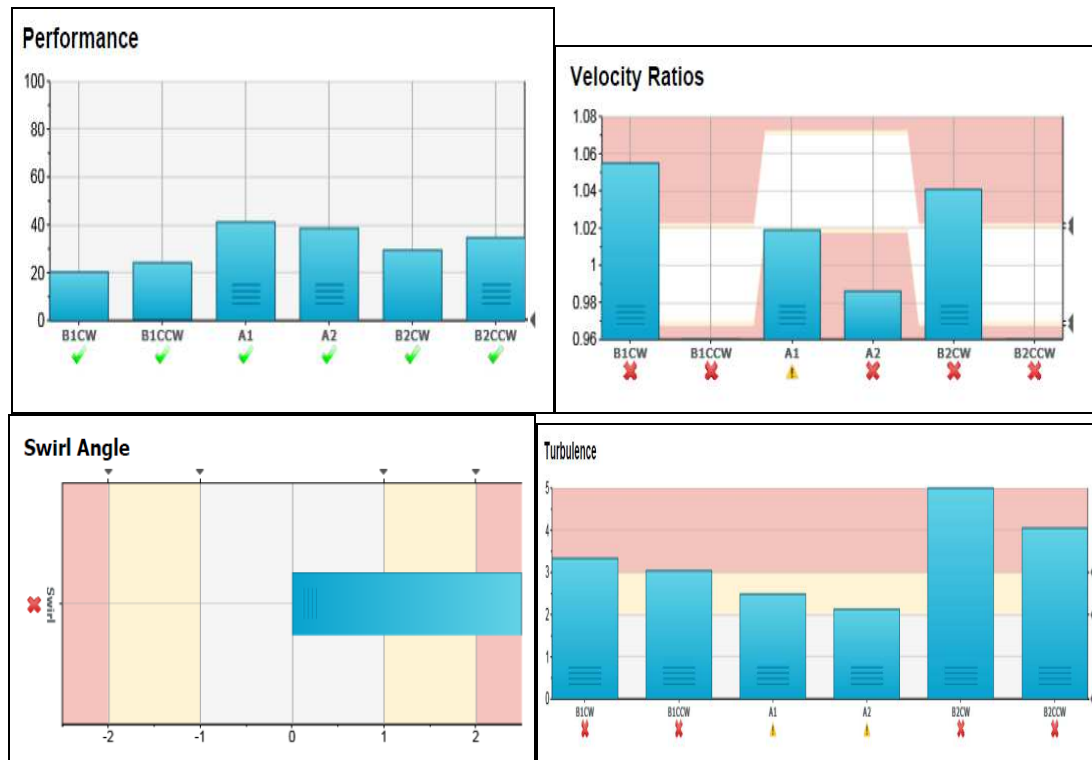


Fig. 4.5. - Instromet Meter 2014 Data High Swirl & High Symmetry

## 34<sup>th</sup> International North Sea Flow Measurement Workshop 25-28 October 2016

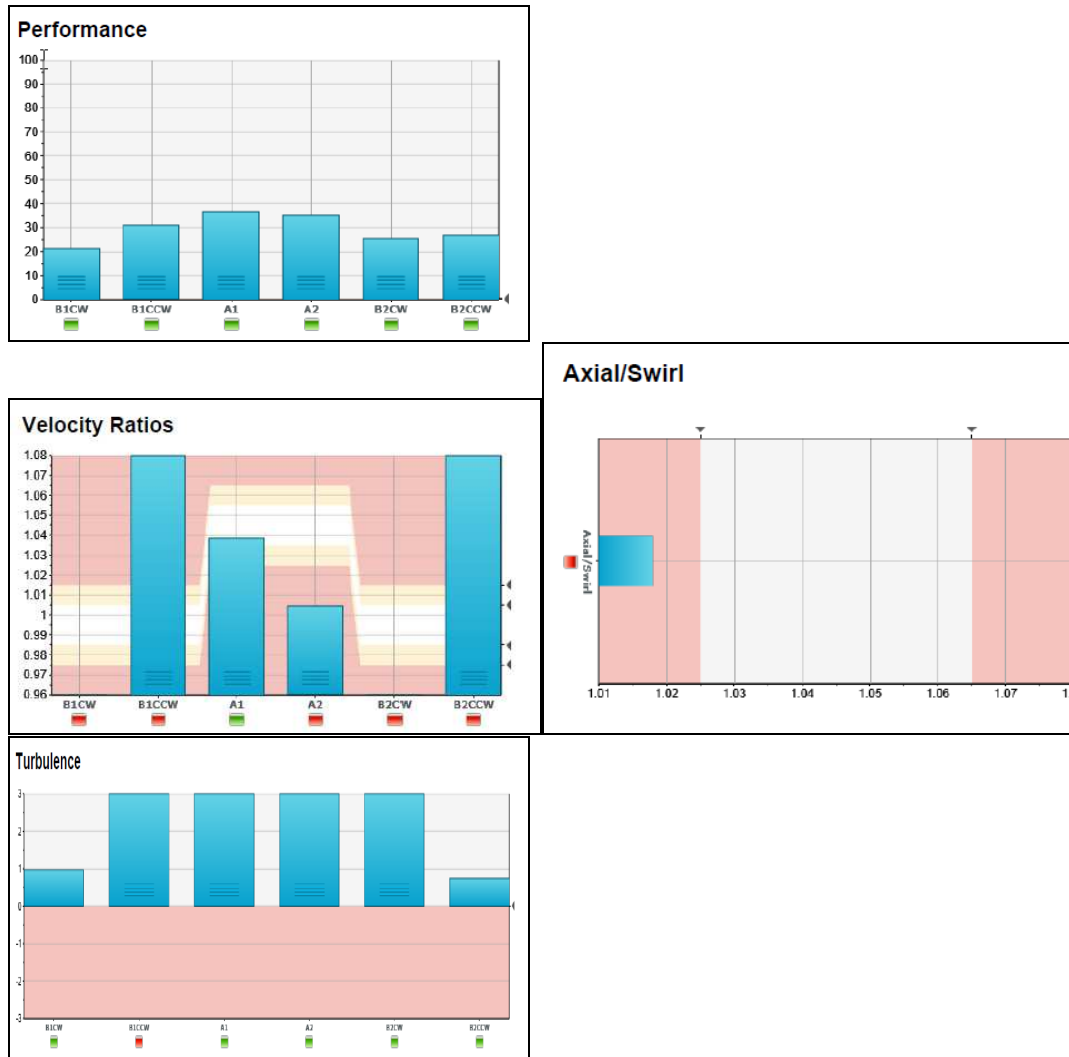


Fig. 4.6. - Instromet Meter 2015 Data High Swirl & High Symmetry

### 5 2004-2015 12-INCH USM DIAGNOSTIC DATA

The NAFFMC next examined installation effects research with a look at each meter’s diagnostic indicators. Using the vast amount of data available on 12-inch ultrasonic meter installation effects, the group wanted to see if it could create models to provide approximate measurement shift indicators. The objective of this research is to analyze and present the ultrasonic meter diagnostics in a manner the user can employ to better manage their measurement risk associated with diagnostic shifts from the calibration to the field.

As stated in the previous section, in some cases the measurement shift in these tests created extreme conditions for the meters. These extreme conditions would be unusual to see in the field when the installation included a flow conditioner, but do provide data outside of normal conditions that was used to improve our modeling of the measurement shift and diagnostic parameters. Subsequently, the extreme perturbation testing performed also gave a valuable overall look at how these meters operate under such extreme conditions. In the case of all three meters under test, they performed with a reasonable amount of uncertainty while being pushed to excessive limits.

## 34<sup>th</sup> International North Sea Flow Measurement Workshop 25-28 October 2016

Data collected from installation effects testing in 2004, 2009, 2011, 2014 and 2015 was used the following analysis. All of the testing done in 2004, 2009 and 2011 involved combinations of tees and elbows upstream and downstream of a typical AGA 9 piping configuration of 10D, CPA 50E flow conditioner, 10D, Meter, 5D, to create disturbed flow profiles. The NAFFMC decided to utilize the same 8-inch CPA Swirl Generator (CSG) for testing on 12-inch meter.

The 2014 and 2015 piping configuration consisted of the CSG and a pinched block valve located 5D from the meter with no flow conditioning. In 2015 the CSG was configured to create swirl in the opposite direction as the 2014 tests.

Figure 5.1 is a picture of the CSG, one offset paddle plate is welded to the horizontal flat plate and the other offset paddle plate is then rotated to create variable degrees of swirl. Figure 5.2 is an upstream view of the ball valve pinched at 30-degrees which was used to create variable amounts of asymmetrical swirling profile.

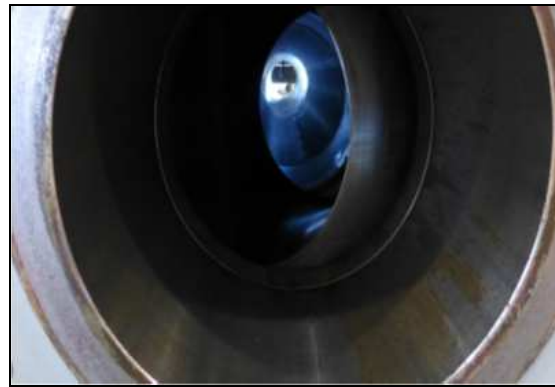


Fig. 5.1. CSG CPA Swirl Generator      Fig. 5.2. Upstream Ball Valve 30% Pinch

Figures 5.3 and 5.4 illustrate the 2004 test-piping configuration using elbows and tees to induce various installation effects. 2009 testing was a repeat of the 2004 installation effects testing.



Fig. 5.3. - 2004 DOOP Elbows      Fig. 5.4. - 2004 DOOP Elbows/Tee

In 2011 upstream piping simulations, again using tees and elbows to reproduce common installation effects, were tested. As seen in Figures 5.5 and 5.6, two meters were bolted back-to-back and tested. They were also rotated, in combination with the different tee and elbow piping configurations, to create different upstream disturbance installation effects.

## 34<sup>th</sup> International North Sea Flow Measurement Workshop 25-28 October 2016



Fig. 5.5. - 2011 Meters Horizontal



Fig. 5.6. - 2011 Meters Rotated 90°

Figure 5.7, shows the CSG position during the 2014 testing. Figure 5.8 shows the CSG position during the 2015 testing. The opposite rotation of the downstream paddle plate allowed us to create varying degrees of clockwise or counterclockwise swirl. Figure 5.9, is the piping setup for the baseline tests. Figure 5.10, shows the CSG, 5D, pinched valve, 5D, Meter, piping configuration.



Fig. 5.7. - 2014 CSG CW Swirl Setup



Fig. 5.8. - 2015 CSG CCW Swirl Setup



Fig. 5.9. - 2015 Baseline Testing



Fig. 5.10. - 2015 CSG, 5D, Pinched Valve

Figure 5.11 shows the CSG, 5D, pinched valve, CPA, 10D, Meter, piping configuration. Figure 5.12 is the CSG, 5D, pinched valve, 5D, CPA 50E, 10D, CPA50E, 10D, Meter piping configuration. Figure 5.13 is the tee and elbow-piping configuration used for the final day of 2015 testing.

**34<sup>th</sup> International North Sea Flow Measurement Workshop  
25-28 October 2016**



Fig. 5.11. - 2015 CSG, 5D, Pinched Valve, 5D, CPA 50E, 10D, Meter



Fig. 5.12. CSG, 5D, Pinched Valve, 5D, CPA 50E, 10D, CPA 50E, 10D, Meter

## 34<sup>th</sup> International North Sea Flow Measurement Workshop 25-28 October 2016



Fig. 5.13. 2015 Final Day Testing With Elbows and Tees

### **6 INSTALLATION EFFECT ERROR DIAGNOSTIC MODELING ANALYSIS**

This section provides the following information:

- Analyzes the installation effect research.
- Develops installation effect estimate models based on diagnostics.
- Applies diagnostic control limits to the models to demonstrate a method to control installation effect uncertainty.

Only the 2014 and 2015 data was used to generate the models. The models were used to estimate installation effect for the 2011 data.

Since the research took place over multiple years, a new Baseline was obtained each year. The baseline piping consisted of considerable straight upstream piping and a CPA 50E flow conditioner installed at 10D. The error recorded for each test run was adjusted by the Baseline error for that particular year of testing. This reduced the uncertainty caused by changes in the meter and/or laboratory over time. The adjusted error is referred to as Meter %Dev. from Baseline or simply Meter %Dev. throughout this section of the paper.

Shifts in the velocity ratio diagnostics such as the Profile Factor, Symmetry, and Swirl Ratios were all measured from the 2015 baseline ratios (not adjusted each year like the error).

## 34<sup>th</sup> International North Sea Flow Measurement Workshop 25-28 October 2016

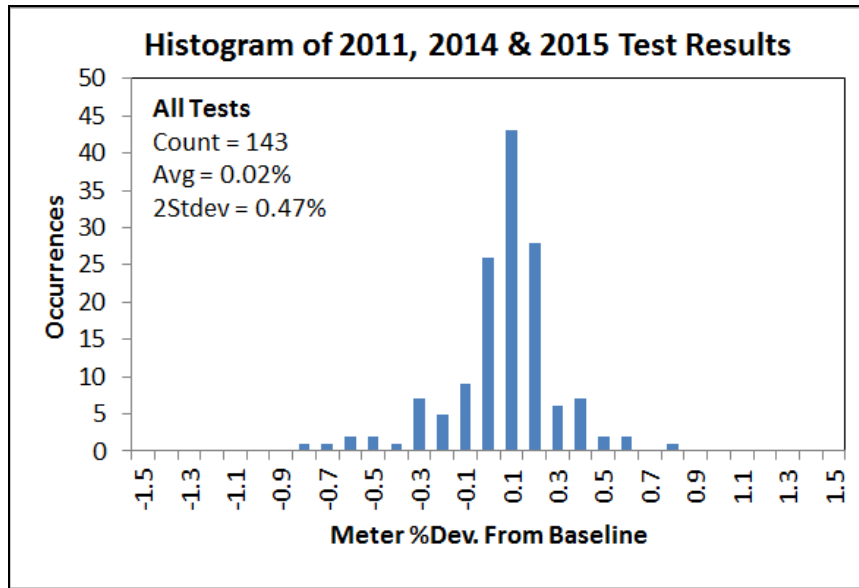


Fig. 6.1. - Histogram of 2011, 2014, and 2015 Test Results

Figure 6.1 illustrates the results of the 143 Installation Effects testing conducted between 2011 and 2015. The results include all three meter brands tested: Daniel SeniorSonic, Instromet Q.Sonic-Plus, and SICK FLOWSIC600. The histogram shows that the average error was near zero and reasonably symmetric. The variance was  $\pm 0.47\%$  (at 2 Standard Deviations). The meters handled extreme, harsh, non-real world installation effects typically not seen when a flow conditioner is utilized.

### 6.1 Daniel Seniorsonic Modeling

Linear regression modeling techniques were applied to the Daniel data. The Profile Factor, Symmetry, and Cross Flow were tested as regressors to model the Meter %Dev. from Baseline. The analysis found a strong inverse linear relationship between the Meter %Dev. and the Profile Factor. Figure 6.2 below illustrates the relationship. The F-statistic for the model was 31. The  $R^2$  was 51%. The slope of the line was  $-1.42 \pm 0.51$  (95% CI). Thus, on the average, for every 1% change in the Profile Factor the Meter %Dev. changed by  $-0.014\%$ .

The Symmetry and Cross Flow ratios did not correlate with the Meter %Dev. For example, the  $R^2$  for the model including the Profile Factor, Symmetry, and Cross Flow only increased 4% from the  $R^2$  for the Profile Factor only model.

# 34<sup>th</sup> International North Sea Flow Measurement Workshop 25-28 October 2016

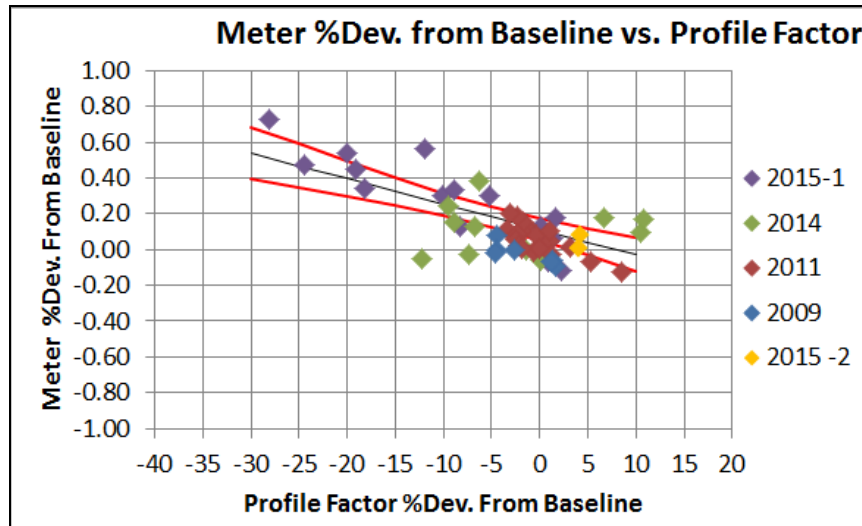


Fig. 6.2. - Daniel SeniorSonic Meter %Dev vs. Profile Factor

## 6.2 Instromet Q.Sonic-Plus Modeling

The analysis of the Instromet Q.Sonic-Plus data indicated a relationship between the Meter %Dev. and the Profile factor. The analysis suggested that for Profile Factor shifts less than  $\pm 2\%$  the installation effect error could be estimated as  $0.0\% \pm 0.15\%$  (at 2 Standard Deviations). For Profile Factor shifts  $> \pm 2\%$ , the analysis indicates that the error could be estimated at  $-0.24\% \pm 0.42\%$  (at 2 Standard Deviations). Figure 6.3 illustrates the relationship.

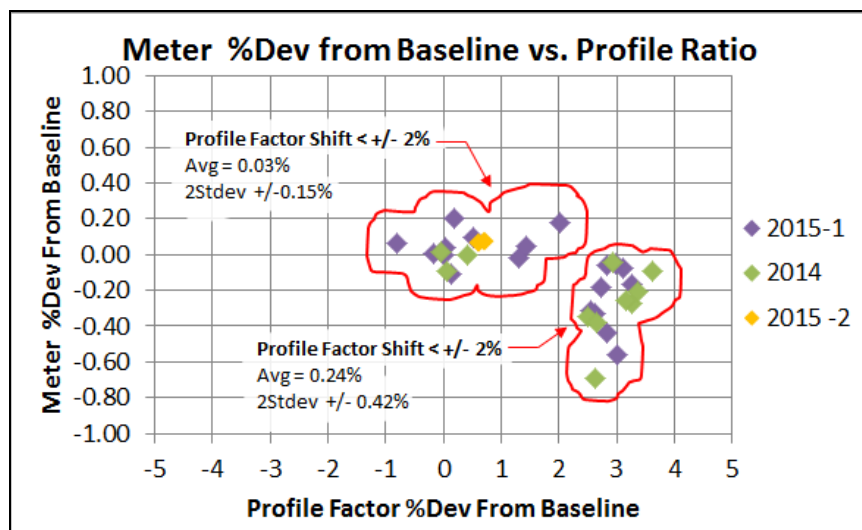


Fig. 6.3. - Instromet Q.Sonic-Plus Meter %Dev vs. Profile Factor

Linear regression modeling techniques were also applied to the Instromet data. Various velocity ratios were tested as regressors. The most statistically significant ratios were found to be either the ratio of the Clockwise velocities or the ratio of the Counterclockwise velocities. Modeling the Meter %Dev. from Baseline as a function of the Clockwise Velocity Ratio yielded a model with an F-statistic of 31 and an  $R^2$  of 53%.

Figure 6.4 illustrates the relationship. The slope of the line was  $-29.6 \pm 10.5$  (95% CI). Thus, on the average, for every 0.05% change in the Clockwise Velocity Ratio the Meter %Dev. changed by  $-0.15\%$ .

# 34<sup>th</sup> International North Sea Flow Measurement Workshop 25-28 October 2016

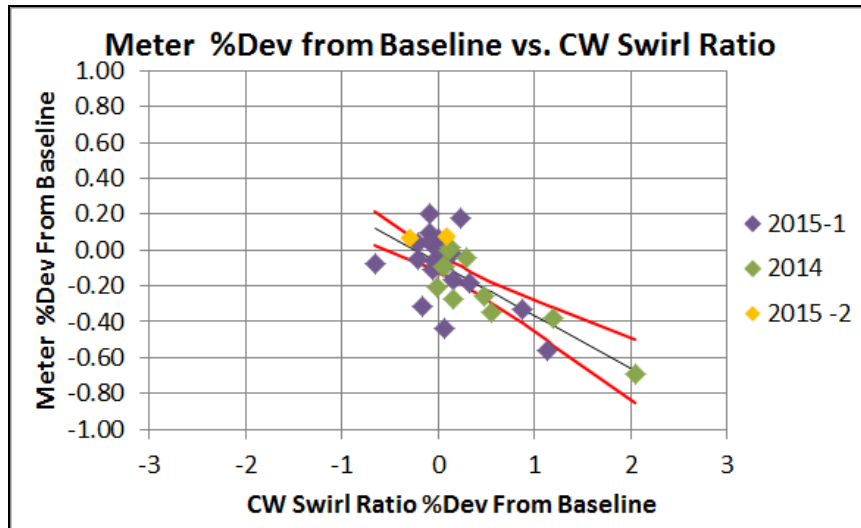


Fig. 6.4. - Instromet Q.Plus Meter %Dev vs. Clockwise Velocity Ratio

The analysis suggests a 2-step approach to estimating the Instromet Q.Sonic-Plus installation effect error. First, check the Profile Factor. If the shift is less than  $\pm 2\%$ , consider the error not detectable. If the shift is  $> \pm 2\%$ , estimate using either  $-0.24\%$  or the Clockwise Velocity Ratio model. The  $> \pm 2\%$  estimate using the  $-0.24\%$  criteria simply tells us if we have a profile factor shift greater than  $\pm 2\%$  the data analysis indicates the measurement shift will be in excess of  $\pm 0.2\%$ . Because the Profile Factor diagnostic is available in Q.3 and Q.5 meters, it may also be a good indicator of installation effect uncertainty for those meters."

### 6.3 Sick Flowsic600 Modeling

Figure 6.5 below illustrates the relationship between the Sick Meter %Dev. from Baseline and the Symmetry. Both the Symmetry and Profile Factor were tested as regressors and the Symmetry relationship was found to be significant. Figure 6.5 shows Symmetry shifts away from the baseline Symmetry (regardless of whether the shift was positive or negative) correlated with increasing, negative installation effect error.

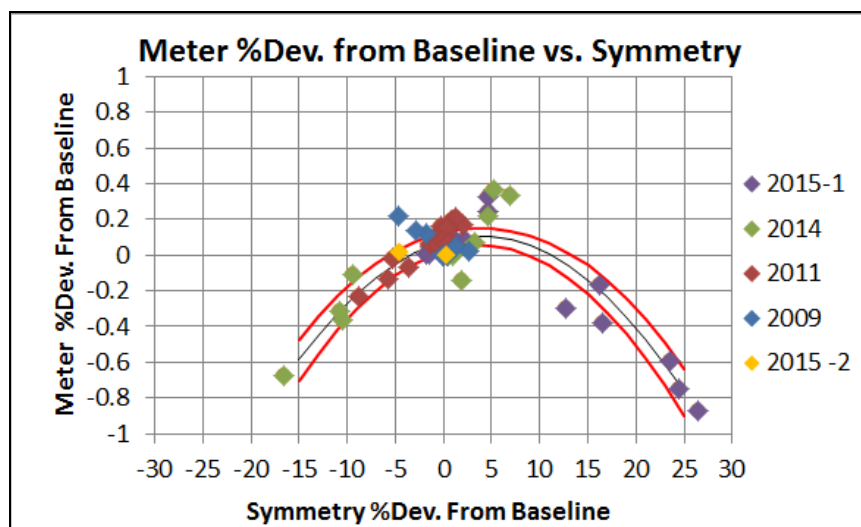


Fig. 6.5. - SICK FLOWSIC600 Meter %Dev vs. Symmetry

## 34<sup>th</sup> International North Sea Flow Measurement Workshop 25-28 October 2016

Figure 6.5 illustrates that Symmetry also shows swirl direction. The green data points to the left are clockwise swirl test points, while the purple points to the right are counterclockwise test points. The points that fall outside the 95% Confidence Region at the +5% Symmetry shift were high symmetry tests. The model does not fit these points well. Other diagnostics, such as turbulence, would have identified installation issues associated with the high symmetry points.

Figure 6.5 also suggests that modeling the Meter %Dev. as a function of the absolute value of the symmetry shift would transform the parabolic relationship into a linear relationship. Figure 6.6 illustrates the results of the transformation.

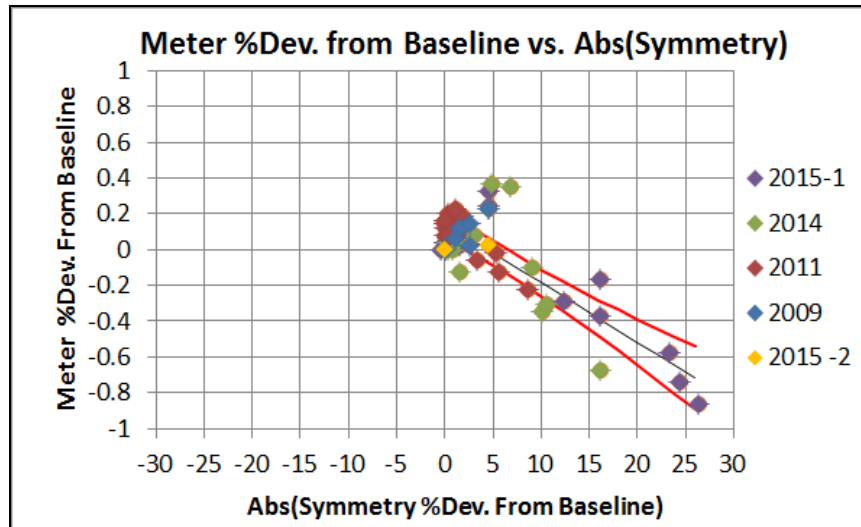


Fig. 6.6. - SICK FLOWSIC600 Meter %Dev vs. Symmetry

The transformation shown above exhibits a strong, inverse linear relationship. The F-statistic for the model was 66. The  $R^2$  was 69%. The slope of the line was  $-3.31 \pm 0.82$  (95% CI). Thus, on the average, for every 1% change in the Symmetry, the Meter %Dev. Changed by  $-0.033\%$ .

### 6.4 Applying Control Limits to the Models

From the modeling results, the following control limits were selected to identify installation effect tests with high Meter %Dev. The tests elimination criteria were as follows:

- Daniel SeniorSonic: Profile Factor shift  $> \pm 5\%$  from Baseline.
- Instromet Q.Sonic-Plus Profile Factor shift  $> \pm 2\%$  from Baseline.
- SICK FLOWSIC600 Symmetry shift  $> \pm 4\%$  from Baseline.

The criteria eliminated 59 of the 143 installation effect tests yielding a distribution with an average of  $0.06\% \pm 0.15\%$  (at 2 Standard Deviations). The orange data series in Figure 6.7 below illustrates the resulting Meter %Dev. distribution. The illustration shows that the elimination criteria effectively controlled the installation effect uncertainty.

## 34<sup>th</sup> International North Sea Flow Measurement Workshop 25-28 October 2016

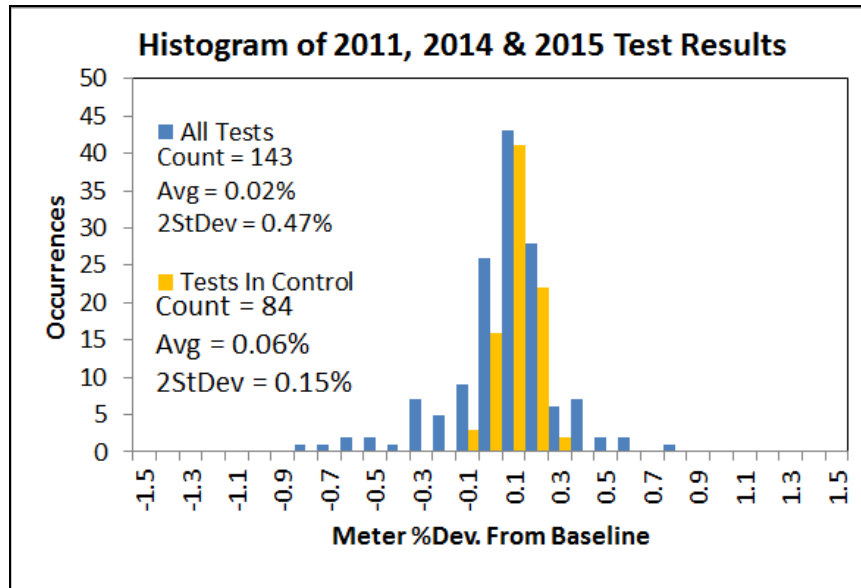


Fig. 6.7. - Histogram of Meter %Dev. from Baseline

## 7 ANALYSIS AND MODELING CONCLUSIONS

The research continues to point towards the feasibility of creating diagnostic models to estimate installation effect error and developing diagnostic criteria from the models to control installation effect uncertainty. **However, the analysis and modeling presented in the paper should not be generalized.** Further research could determine if the modeling can be generalized to other sizes, types of meters, and velocity ranges, and could provide guidance to AGA 9 with regards to installation effect uncertainty. Testing is on going and each year new information is obtained from the testing directed by the NAFFMC, and presented at the annual CEESI Custody Transfer Conference.

## 8 REFERENCES

- [1] AGA Report Number 9, Measurement of Gas by Multipath Ultrasonic Meters
- [2] Bill Frasier, Ned Davis, *Bill\_Frasier\_Ned\_Davis\_-\_InstallationEffectDirtyClean.pdf*, presented at the CEESI Ultrasonic Workshop 2011
- [3] Ed Hanks, *EdHanks\_CEESINAFFMCRsearch\_24HeaderAnd12FilterTesting.pdf*, presented at the CEESI Ultrasonic Workshop 2013
- [4] Randy Miller, *NAFFC 2013.ppt*, presented at the CEESI Ultrasonic Workshop 2013
- [5] Ed Hanks, *Ed\_Hanks\_-\_InstallationEffectsNAFFMC.pdf*, presented at the CEESI Ultrasonic Workshop 2011

## **34<sup>th</sup> International North Sea Flow Measurement Workshop 25-28 October 2016**

- [6] Jonatan Mustafa, Joel Clancy, *2012 NAFFMC\_Research Testing Header Effects on USMs.pptx*, presented at the CEESI Ultrasonic Workshop 2012 by Reese Platzer
- [7] Randy Miller, *2014 NAFFMC Ultrasonic Meter Testing.pptx*, presented at the CEESI North American Custody Transfer Measurement Conference 2014.
- [8] 2015 NAFFMC Director Board; Bob Wurm – Tallgrass Energy, Reese Platzer – Enterprise Products Company, Gary McCargar – Oneok Partners, Jonatan Mustafa – Sunoco, Dan Rebman – Universal Pegasus, Randy Miller – Energy Transfer, Ed Hanks – CEESmaRT, John Lansing – CEESI, Joel Clancy – CEESI.

## **Clamp on Ultrasonic Flow Meters vs A Fiscal Orifice Station.**

### **How Accurate Are Clamp on Meters Out of The Box?**

**Andrew Runcie, PX Limited  
Paul Daniel, METCO | Emerson Process Management**

---

#### **1 INTRODUCTION**

Total E&P operated the St Fergus Gas Terminal and Associated Pipelines from 1977 till March 2016 when operations were transferred over to PX limited on behalf of North Sea Mid stream Partners.

There are 2 pipelines that feed the terminal where Natural Gas is processed, Metered and Exported to the National Grid Network.

##### **1.1 FUKA (Frigg UK Pipeline)**

The Frigg UK pipeline (FUKA) currently transports gas from the following fields to the phase 3 process trains at St Fergus Gas Terminal:

- Alwyn Area fields
- Bruce Area Fields
- Buzzard Field
- Captain Field
- Ross Area fields
- Claymore/Piper/Tartan

Gas from these fields is metered prior to entering the FUKA pipeline. The Gas is then processed at the St Fergus Gas terminal to meet the National Grid Transportation specifications. The Gas is metered immediately prior to entering the National Grid.

##### **1.2 Vesterled Pipeline:**

Gas from the Heimdal area is transported through the GASSCO Transportation network and is routed through the Heimdal riser platform where it is metered prior to Entering the Vesterled platform. Upon entering St Fergus the Gas is then passed through the Phase 2 Process trains and then metered immediately prior to being exported to the National Grid Gas transportation Network.

# 34<sup>th</sup> International North Sea Flow Measurement Workshop 25-28 October 2016

A high level block diagram of the St Fergus terminal is presented in Figure 1, showing the location of the sales gas metering. Immediately prior to the Sales Gas meters there is a cross over facility to enable Phase 2 Gas to be comingled with the Phase 3 Gas and exported via either the Sales gas 1 or Sales Gas 2 Metering stations.

## ST. FERGUS SCHEMATIC DIAGRAM (NO PRETREATMENT CROSSOVERS AVAILABLE)

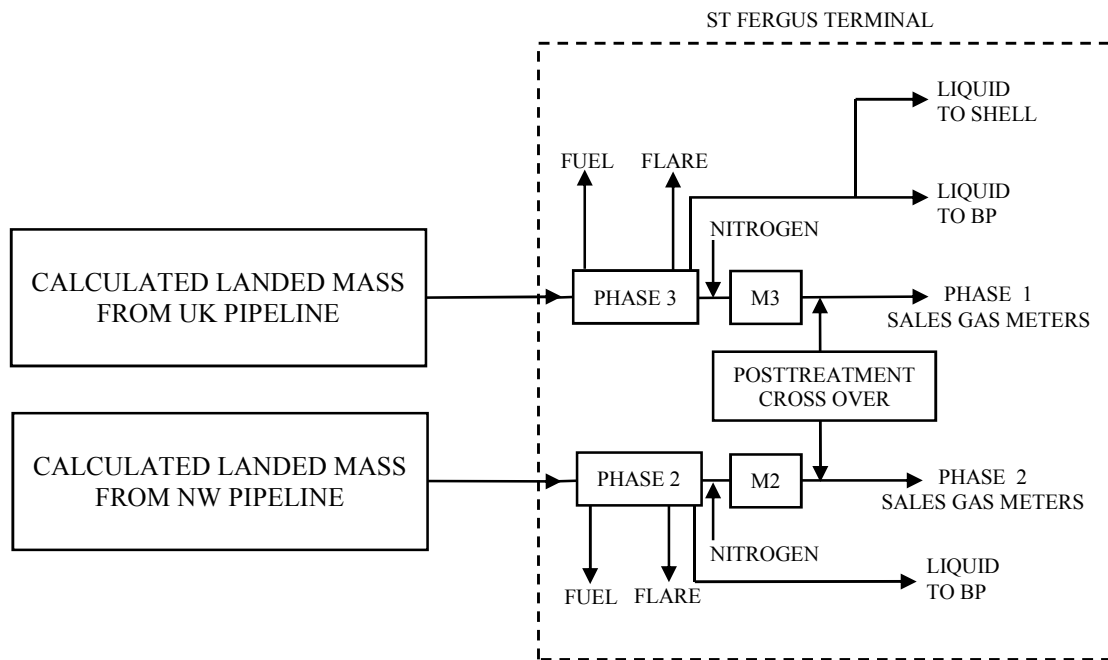


Figure 1 : St Fergus Process Schematic Diagram

With an ultimate aim to facilitate allocation during periods when the cross-over is in use Siemens FUG1010 single channel clamp on Ultrasonic Meters were installed in 2011 by Able instruments in 3 of the Ph2 Process trains along with a new Daniels 700XA chromatograph. The Meters were installed on 24" Carbon Steel Flow lines flowing natural gas at around 45BarA and 10°C with a Gas velocity between 0 and 20m/s.

This Paper describes some of the key measurement issues experienced by the operator in recent years and the steps taken to meet these challenges.

The areas covered in this paper are:

- a) Use of a Clamp on meter straight out of the box
  - Initial performance tests with comparisons against the Sales gas metering station
- b) Further work carried out to improve the meter performance with comparison tests against the fiscal metering station

# 34<sup>th</sup> International North Sea Flow Measurement Workshop 25-28 October 2016

## 2 SYSTEM DESIGN AND OPERATION

The meters are clamped onto the outlet of each process stream along with a strap on Temperature RTD.

A common Pressure transmitter exists at the outlet of the Ph2 Process system. The Volume flow rate and stream Temperature from each Flow Meter is communicated to a Dedicated S600 flow computer via serial link as well as the unnormalised Gas composition from a dedicated Emerson 700XA Gas chromatograph and the Ph2 outlet Pressure.

Using the composition from the Gas chromatograph, the flow computer calculates the density and compressibility at stream conditions in accordance with AGA8 (1994) [1]. The Mass flow rate for each stream is then calculated and summed to give the total Phase 2 Mass flowrate.

The St Fergus Sales Gas 2 Export Metering station consists of 6 x 24" Orifice plate meter runs with Daniels type Senior Sonic Orifice Plate Carriers.

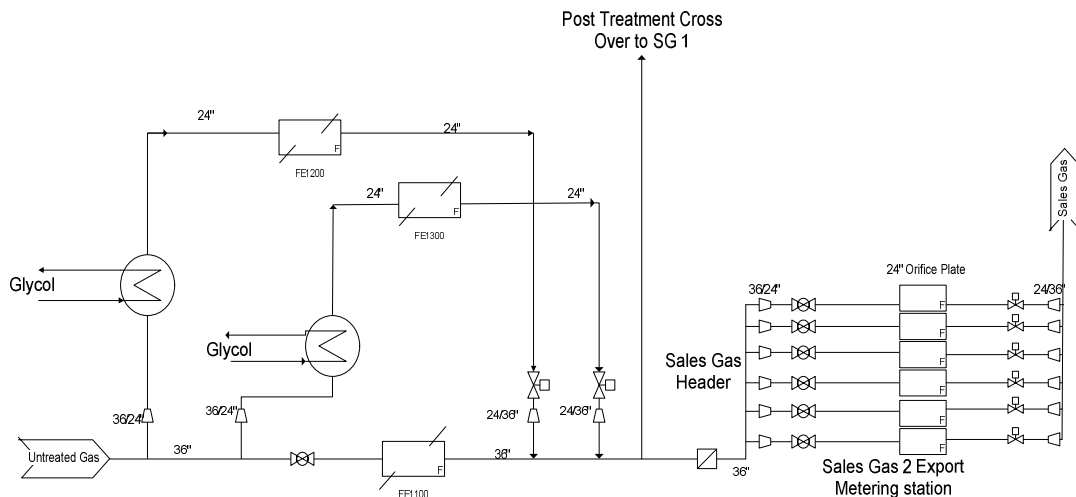


Figure 2 : St Fergus Phase 2 Process Schematic Diagram

During normal operations, the Clamp-on flow meters are in series with the Sales gas Metering station and can be directly compared, however there are occasions when the Phase 2 Gas is comingled with the Phase 3 Gas and is exported via either the Sales gas 1 or Sales Gas 2 Metering stations.

# 34<sup>th</sup> International North Sea Flow Measurement Workshop 25-28 October 2016

The meters installed on streams 1200 & 1300 are shown in Figures 3 & 4.



Figure 3 : Stream 1200 clamp on meter installation



Figure 4 : Stream 1300 clamp on meter installation

Figure 5 below shows a plot of both the Sales Gas Export 2 Daily reported mass and the Phase 2 Process Gas Daily reported mass for a period in 2012/2013. The clamp-on USM meters match the sales gas metering station very well.

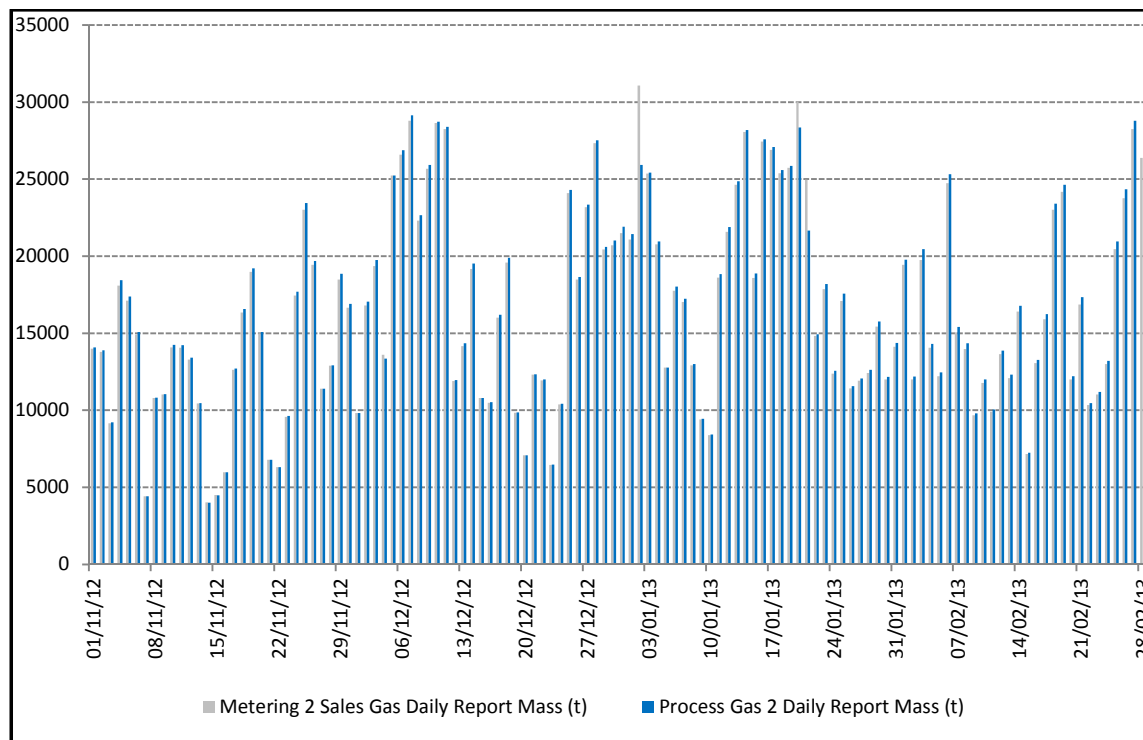


Figure 5 : Production data

# 34<sup>th</sup> International North Sea Flow Measurement Workshop 25-28 October 2016

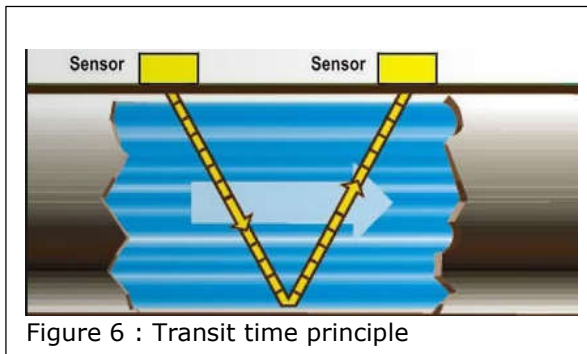
## 3 MEASUREMENT THEORY

For Clamp on ultrasonic Meters two principles are generally available, these are; Doppler or time transit principle. For this application the more common time transit principle was used.

### 3.1 Transit-Time Measuring Principle

The principle is based on the time difference it takes for an ultrasonic pulse to travel a defined distance both with and against flow.

As the medium in which the signals propagate is flowing, the transit time of the ultrasonic signals in the flow direction is shorter than against the flow direction. The transit time difference,  $\Delta t$ , is measured and facilitate the determination of the average flow velocity along the propagation path of the ultrasonic signals.



A flow profile correction is then performed in order to obtain the area averaged flow velocity, which is proportional to the volumetric flow rate. Figure 6 shows a single reflective path design.

The received ultrasonic signals are checked for their usefulness for the measurement and the plausibility of the measured values evaluated. The complete measuring cycle is controlled by integrated microprocessors. Disturbance signals will be eliminated.

The clamp-on ultrasonic meter may be mounted and configured in a Reflective mode (Figure 7) or Diagonal mode (Figure 8). For a single reflective path, both of the transducers are mounted on the same side of the pipe making correct positioning of the transducers easier.

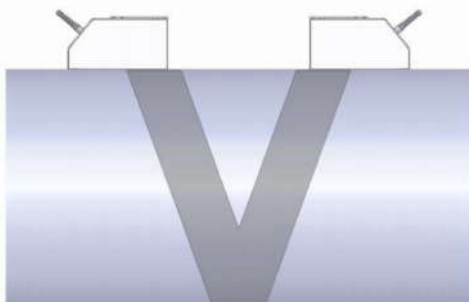


Figure 7 : Reflection mode

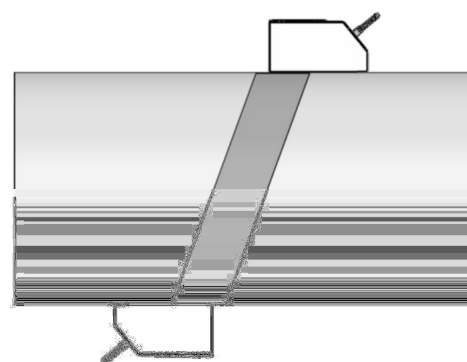


Figure 8 : Diagonal mode

For a Diametric paths, the transducers are mounted on opposite sides of the pipe. In the case of high signal attenuation by the medium, pipe and coatings, a diagonal mode with 1 sound path may be most appropriate.

## **34<sup>th</sup> International North Sea Flow Measurement Workshop 25-28 October 2016**

The preferred method of installation depends on the application. As the transducers can be mounted with the transducer mounting fixture in reflection mode or diagonal mode, the number of sound paths can be adjusted optimally for the application.

### **3.2 Flow Calibration Factor**

Normally, the flow stream is parallel to the axis of the pipe. On this basis, the calibration factor of a clamp-on ultrasonic flow meter is proportional to the cosine of the beam angle relative to the pipe axis (ref Siemens FUG1010 operating instruction manual). However, this reveals that if the angle of flow stream is not in line with the pipe axis, the flow calibration factor could be compromised. This most often occurs when the sensor mounting location is within close proximity of a bend or other pipe obstruction.

### **3.2 Achievable Accuracy**

Within the industry many of the meter manufacturers claim that a level of uncertainty of  $\pm 2\%$  is achievable at a calibration facility, however for industrial applications it is thought within the industry that the achievable level of performance with a typical clamp-on meter, with a good installation base, is typically between 1–3 % of reading.

# 34<sup>th</sup> International North Sea Flow Measurement Workshop 25-28 October 2016

## 4 INITIAL CLAMP ON METER PERFORMANCE TESTS

During 2012 the performance of the flow meters against the Sales gas 2 Metering system was monitored. This itself posed some problems in how this could be achieved since the individual data points were not fed in the Total PI system and were therefore not available in the historian. Since the Mass for the combined Phase 2 Meters is reported in the Flow computer as a daily Total, it was decided to compare the reported daily Mass from both systems. Figure 9 shows the Percentage Difference between the Reported Sales Gas 2 Metering station versus the Combined Phase 2 Process Gas Daily Mass Total. Figure 9 also shows the periods when the cross over is opened, hence the large % differences during these periods. With the Cross over periods removed the average % difference for the period in the graph in figure 9 is given as -1.058%.

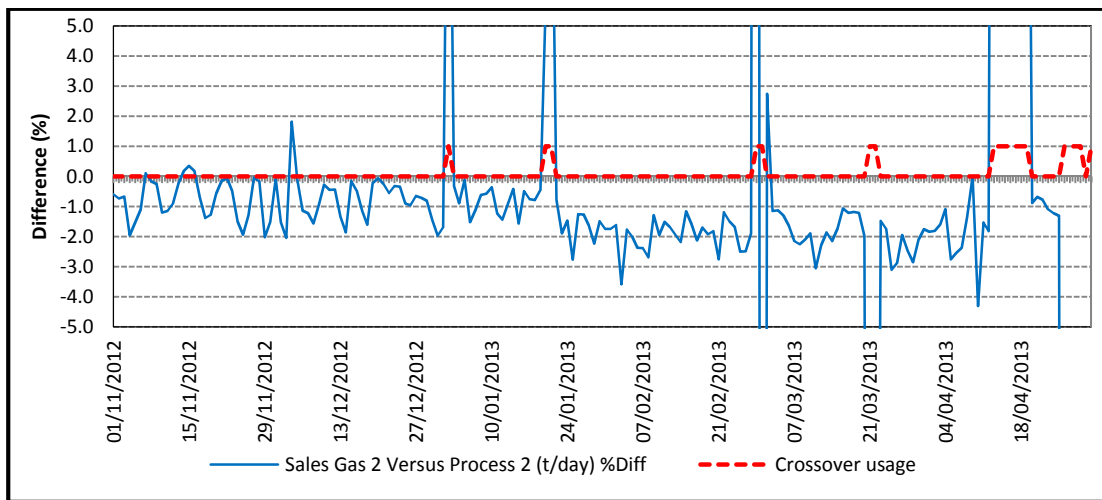


Figure 9 : Sales Gas vs Process Gas: 2012 -2013 trend

From the Trend, it is clear that there is a negative bias in the Phase 2 Process gas flow meters.

The Mass totals for Phase 2 against the percentage difference between the phase 2 clamp-on meters and the sales gas metering station was also compared. The results can be seen on Figure 10.

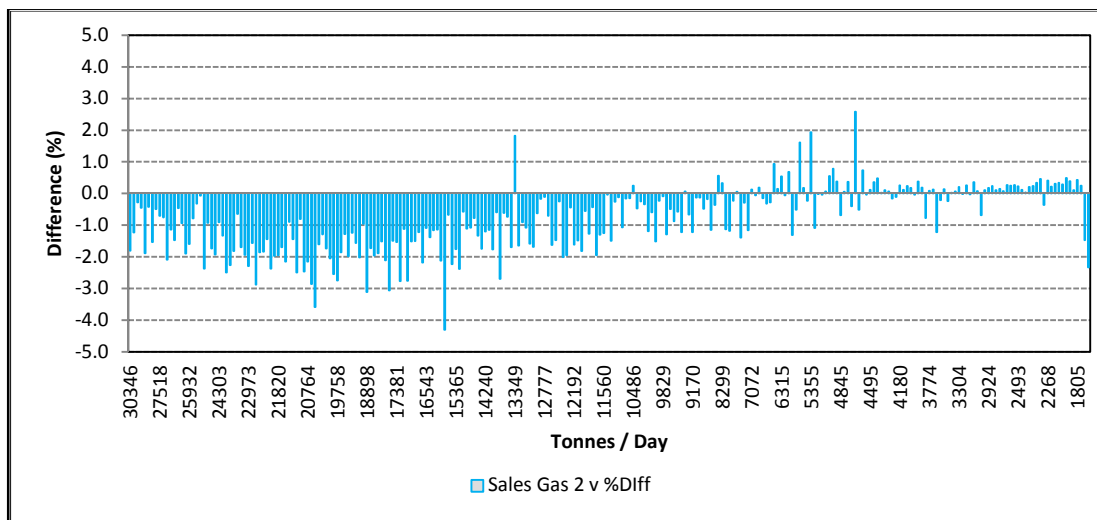


Figure 10 : Sales gas vs Process gas post 2012 -2013 trend

## 34<sup>th</sup> International North Sea Flow Measurement Workshop 25-28 October 2016

The results in figure 10 clearly show that the meters appear to perform around  $\pm 1\%$  at the lower flow rates up to 5000 tonnes/day, however the performance starts to degrade after this point at flows up to 20000 tonnes/day as can also be seen in figure 5.

After reviewing the data, it was decided to contact the Vendor, Able instruments, with a view to try and tune the Meters to Match the output from the Sales gas metering station to within  $\pm 1\%$  so that the meters can be used for Allocation purposes.

Within the Flow Meters there is an option to adjust the meter output to match that of an external or reference meter by entering a Calibration Factor(Kc factor). The factor Kc (slope correction) assumes that the flow range produces a linear response.

The Kc factor is calculated as follows:

$$Kc = \left[ \frac{\text{Actual Rate}}{\text{Indicated Rate}} - 1 \right] \times 100 \quad (1)$$

There is also another Option within the Flow meter to select a methodology by which the response can be linearized or optimised by tabulating the results of a series of calibration points into a table. The Flow meters were originally set with a KC value of 4%.

During June 2013, the vendor re-positioned the transducers on all 3 streams and adjusted the Kc value to 3.0 & 3.3% on stream 1200 and 1300. It was decided not to adjust stream 1100 since it is rarely used.

This is seen in the Graph in figure 11 below, where the error bias shifts from negative to Positive.

# 34<sup>th</sup> International North Sea Flow Measurement Workshop 25-28 October 2016

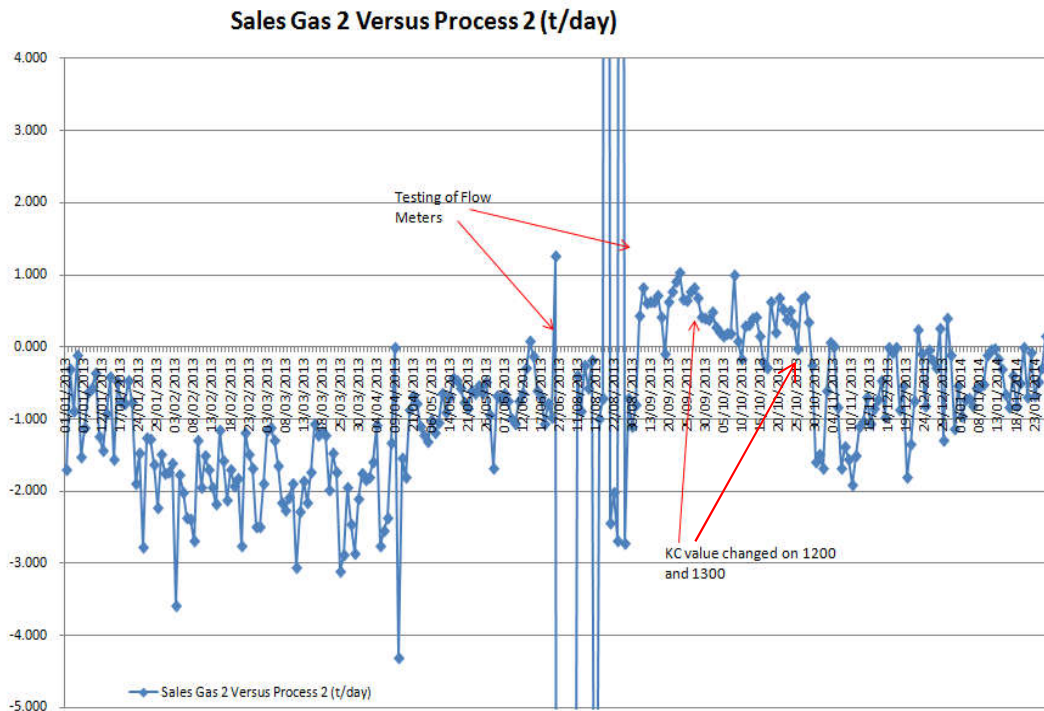


Figure 11 : Sales gas vs Process gas post 2013 -2014 trend

After a period of collecting more data, it was decided to again adjust the KC values on both streams. Stream 1200 was adjusted to 2.8 % and stream 1300 was increased to 3.4%.

This change appeared to have shifted the Bias so that is was more evenly distributed however during the period after the change, the flow rates were significantly increased and the error became more negatively biased. This is possibly due to the use of stream 1100 and other process related activities’.

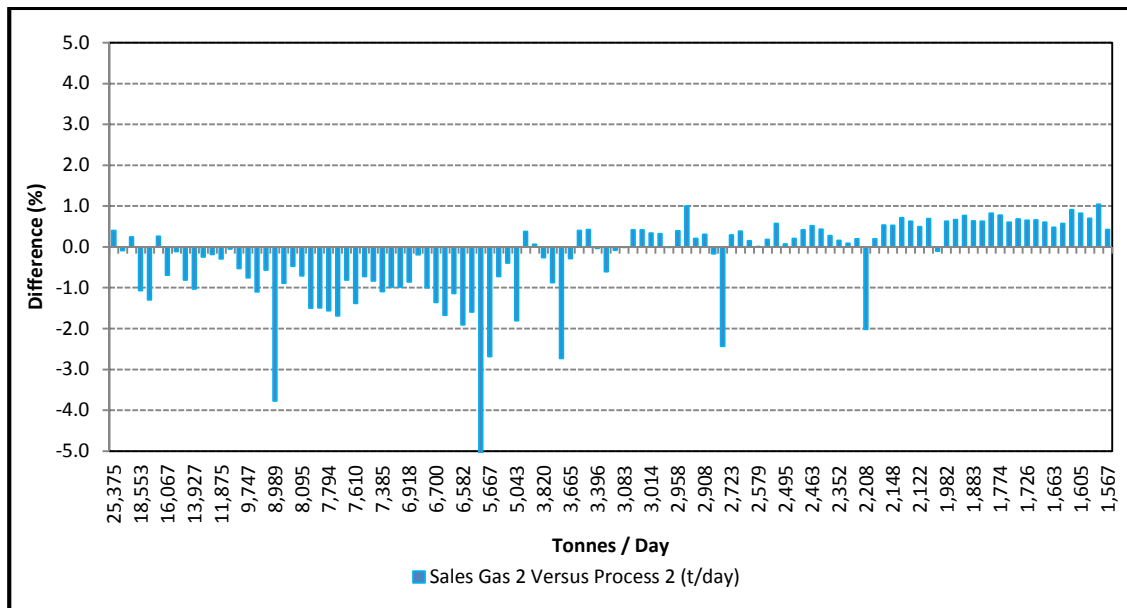


Figure 12 : Sales gas 2 vs %Diff post Able Testing –June 2013 to Jan 2014

## 34<sup>th</sup> International North Sea Flow Measurement Workshop 25-28 October 2016

Figure 12 above shows the change in meter performance after the KC Factor changes from June 2014 till January 2014. It can be seen there that there is a slight increase in performance over the operating range

### 5 CLAMP ON METER OPTIMISATION

To further improve the performance of the meters, the meters were upgraded to dual channel meters during 2014 and the KC Factors were adjusted again.

The strap on RTD's were removed and insertion RTD's were fitted just downstream of the meters during 2015.

The results however were mixed, on stream 1200 the performance was greatly improved however on stream 1300 the performance was varied over the operating range of the meter as can be seen in figure 13.

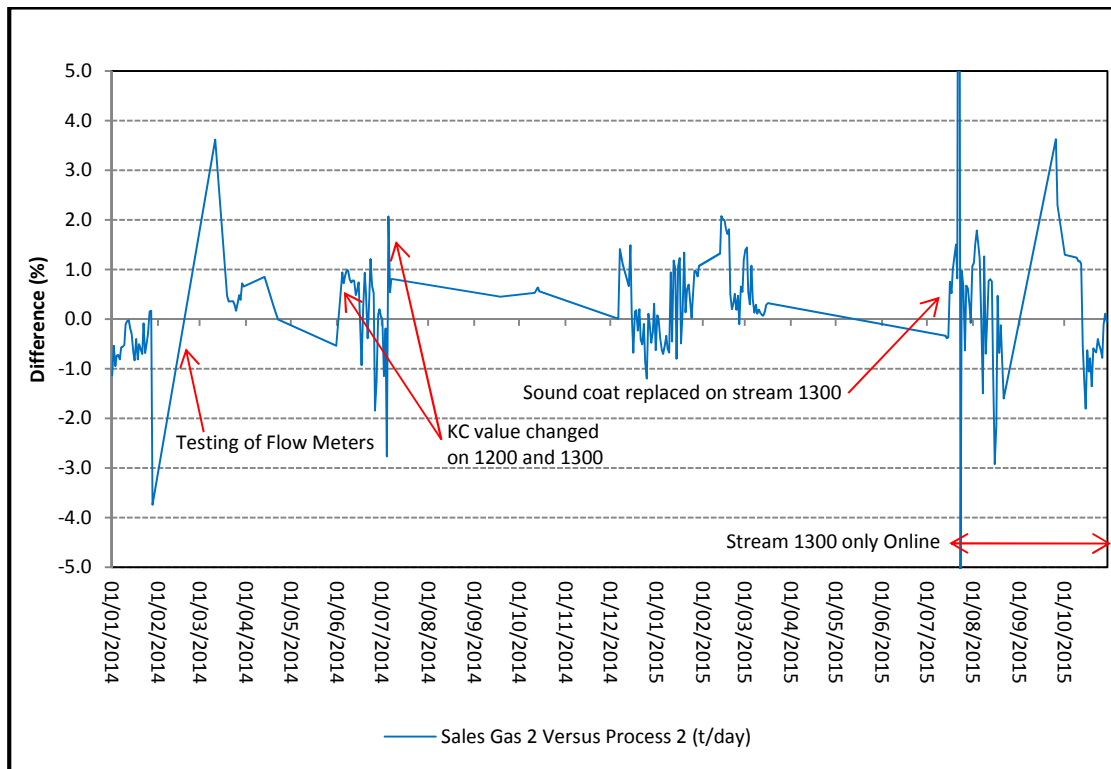


Figure 13 : Sales gas vs Process gas post 2014 -2015 trend

After some investigation work it was clear that there were problems with the installation of the stream 1300 meter. The Sound coating of the meter was removed and re-applied to the pipe and the meter re-fitted. The correct thickness of the sound coat was also entered into the Meter configuration. This has led to a significant an improvement in the performance of the clamp-on meters as can be seen in figures 14 and 15.

# 34<sup>th</sup> International North Sea Flow Measurement Workshop 25-28 October 2016

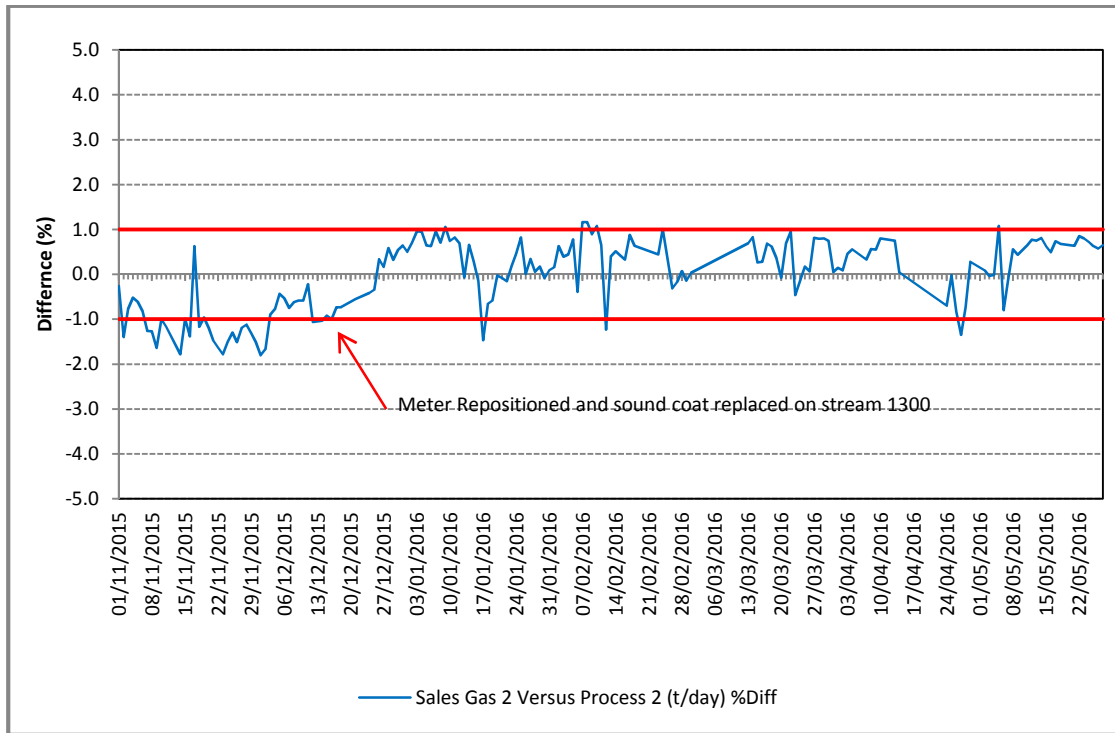


Figure 14 : Sales gas vs Process gas post 2015 -2016 trend

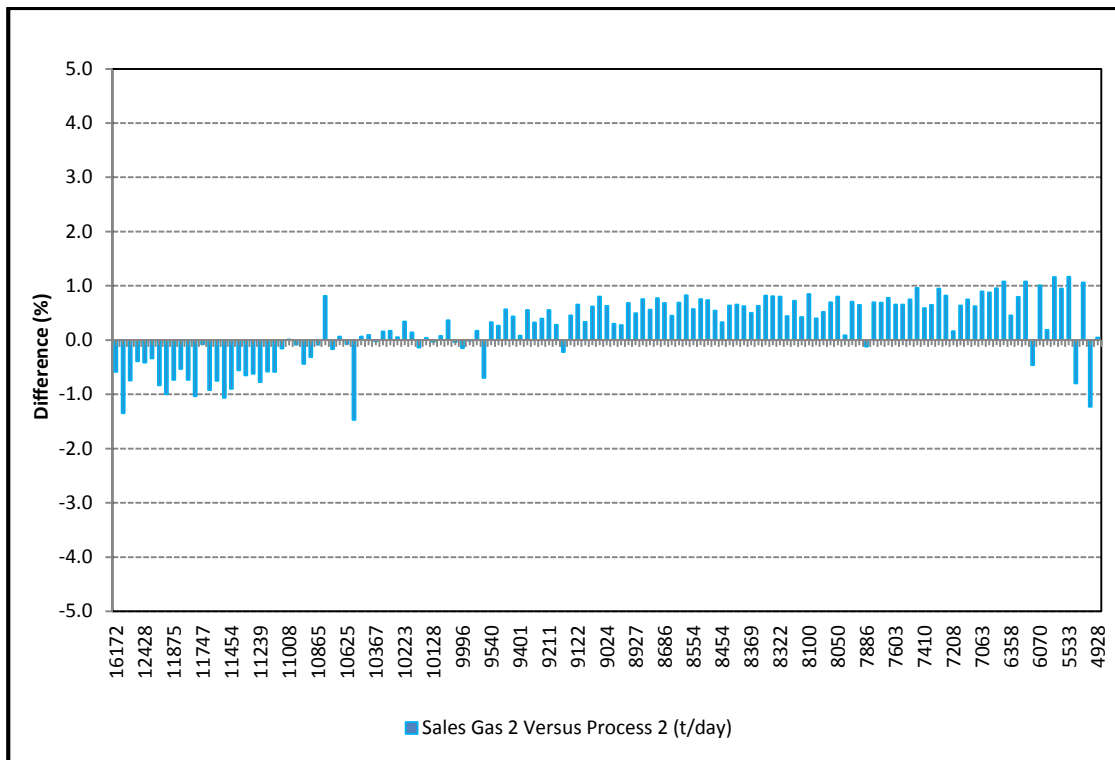


Figure 15 : Sales gas 2 vs %Diff December 2015 –May 2016

Figure 15 shows the difference versus the sales gas 2 flow rate since the stream 1300 sound coat was re-applied and the meter setup correctly. From the graph it is clear that there is a significant improvement across the flow range, and the meters tend to perform within 1% of the Sales gas 2 daily mass total.

# **34<sup>th</sup> International North Sea Flow Measurement Workshop**

## **25-28 October 2016**

### **6 SUMMARY AND CONCLUSION**

The Clamp on meter has proven itself to be capable in delivering a performance of better than  $\pm 1\%$  of reading when compared to the Gas Export metering system. However, it is clear that the most important factor in achieving an acceptable level of performance is ensuring that the meters are installed correctly and sited at a suitable location ensuring that the meter is located where there is little or no effect of noise from the process. The meters should also be located where disturbances in the flow such as bends that can cause changes to the flow profile is avoided.

The addition of flow linearization curves within the flow computer for the individual meters may also improve the performance of the meters over the operating range and is an option currently being considered.

# 34<sup>th</sup> International North Sea Flow Measurement Workshop 25-28 October 2016

## 7 NOTATION

The notation used in this paper is as follows:

m/s	Metres per second	KC	Calibration Factor
°C	Degrees Centigrade		
t	Mass (tonnes)		

## 8 REFERENCES

- [1] AMERICAN GAS ASSOCIATION , Compressibility Factor of Natural Gas and Related Hydrocarbon Gases. American Gas Association Transmission Measurement Committee Report No. 8 (1994)
- [2] AMERICAN GAS ASSOCIATION. Measurement of Gas by Multithread Ultrasonic Flow meters. American Gas Association Transmission Measurement Committee Report No.9,2000.
- [3] BSI British Standards. Guide to the Selection, installation, operation and calibration of diagonal path transit time ultrasonic flow meters for industrial gas applications. BS 7965:2009
- [4] SEMINAR ON ULTRASONIC FLOW METER CONDITION BASED MONITORING. Organised by the United Kingdom Department of Energy and Climate change(DECDC), aberdeen Exhibition and conference centre(AECC),2011.
- [5] JWF Survey of Bruce Gas Export Meters by clamp on Meters using Flexim Clamp on Meters Report.
- [6] Survey report for St Fergus Clamp on meters By Able Instruments UK Ltd.
- [7] TUV NEL Good Practice Guide - An introduction to non-invasive ultrasonic flow metering

## 9 ACKNOWLEDGEMENTS

The authors would like to thank the following for their input to the issues described in this paper:

**TOTAL UK Ltd**  
Ian Bates

**EMERSON**  
Jonathan Ritchie

**GASSCO**  
Frode Bjellend

## **Technical Paper**

# **Diagnostics and Orifice Plates: Experimental Work**

**Michael Reader-Harris and David Addison, NEL  
Julian Barnett and Ketan Mistry, National Grid**

---

## **1 INTRODUCTION**

Differential-pressure meters, including orifice plates, Venturi tubes and cone meters have been and remain the group of flowmeters most commonly used in industry. Orifice plates in particular provide the mainstay of gas fiscal metering systems worldwide. While ultrasonic meters have been installed in many installations in recent years, orifice plates continue to serve a useful function owing to their advantage of not requiring flow calibration and of having a dependence on the square root of density to provide mass flow (rather than the mass flow being directly proportional to the density).

One of the features of an ultrasonic flow meter is its ability to provide additional diagnostic information on the nature of the flow and the condition of the meter. This information can be used to check for the presence of additional uncertainty in the measured flow caused by, for example, swirl induced by upstream flow disturbances, a change in pipe roughness or damage to or degradation of the transducers. The ability to provide diagnostics is not limited to ultrasonic meters: the same opportunity can arise with differential pressure meters. This has been known for many years. In 1986 Martin [1] showed that the use of an additional upstream pressure measurement would give the possibility of correcting the measured flowrate to account for the effect of different upstream installations. He measured the ratio of the pressure rise into the upstream corner of an orifice plate to the differential pressure: a change in this pressure rise ratio is proportional to the change in discharge coefficient due to certain upstream flow conditions. In more recent years Steven [2] and Skelton et al [3] have shown the benefits of using an additional pressure tapping around  $6D$  downstream of an orifice plate so that the permanent pressure loss can be combined with the differential pressure to give information on the acceptability of the measurement. Departures from the anticipated pressure loss ratio can be attributed to different meter fault conditions or potential errors in measurement. This principle can be extended to other differential pressure devices such as Venturi meters and cone meters. This patented finding has been developed into a commercial software monitoring tool called 'Prognosis', which can be used to monitor the different measurement values, compare them with predicted or baseline measurements and then indicate departures from the norm as a diagnostic tool.

## **2 OBJECTIVES AND APPROACH**

The main objective of this project for National Grid was to investigate the use of an additional pressure loss measurement in an orifice plate installation to generate diagnostic information. The usual differential pressure is measured from the flange tappings. An additional differential pressure is measured from the upstream (and the downstream) tapping to an additional tapping located some diameters downstream: a distance of six pipe diameters ( $6D$ ) from the orifice plate is used as it is around the first location at which the pressure has recovered. A particular question to be addressed was whether a change in the discharge

# 34<sup>th</sup> International North Sea Flow Measurement Workshop 25-28 October 2016

## Technical Paper

coefficient can be related to a change in the measured ratio of pressure loss to differential pressure.

A paper on the theory [4] written as a result of this project covers Computational Fluid Dynamics (CFD) simulations and other calculation methods to determine the ratio between the pressure loss and the standard differential pressure and to see how the ratio is correlated with change in discharge coefficient. The flow simulations covered the effects of axisymmetric profiles (both flatter and more peaked than that in a long straight pipe), an asymmetric profile and a swirling profile. They also covered the effect of a deposit on the upstream surface of an orifice plate, a fault condition which is a different type of poor installation and may occur during service. A common fault of having an orifice plate installed incorrectly by reversing the plate was also examined. This latter fault condition gives rise to large measurement errors which are undetectable through the normal measurement process.

This paper describes the experiments that have been carried out to measure the effect of a series of fault conditions described in detail in Section 3.2.

The experiments were carried out using the NEL water flow test facility. The data were collected from the NEL data acquisition system. This recorded the average of the differential pressures, six in all, the flowrate and the water temperature taken across defined test periods with a reference flowmeter measuring the continuous flowrate. A network diagram of the flow loop is shown as Figure 1 and a photograph of the orifice meter as Figure 2.

The six differential pressures were transmitted in real time to the commercial 'Prognosis' software where they were recorded and analysed against pre-set fault limits.

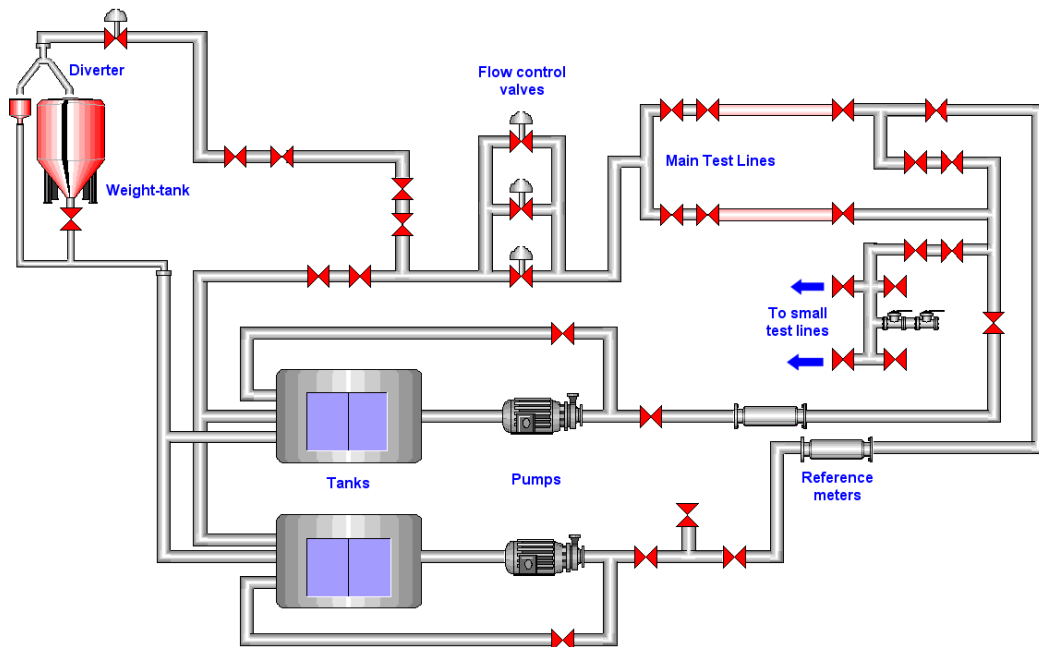


**Figure 1 Diagram of the flow loop: the orifice meter was installed in the main test lines; reference meters were used**

Technical Paper

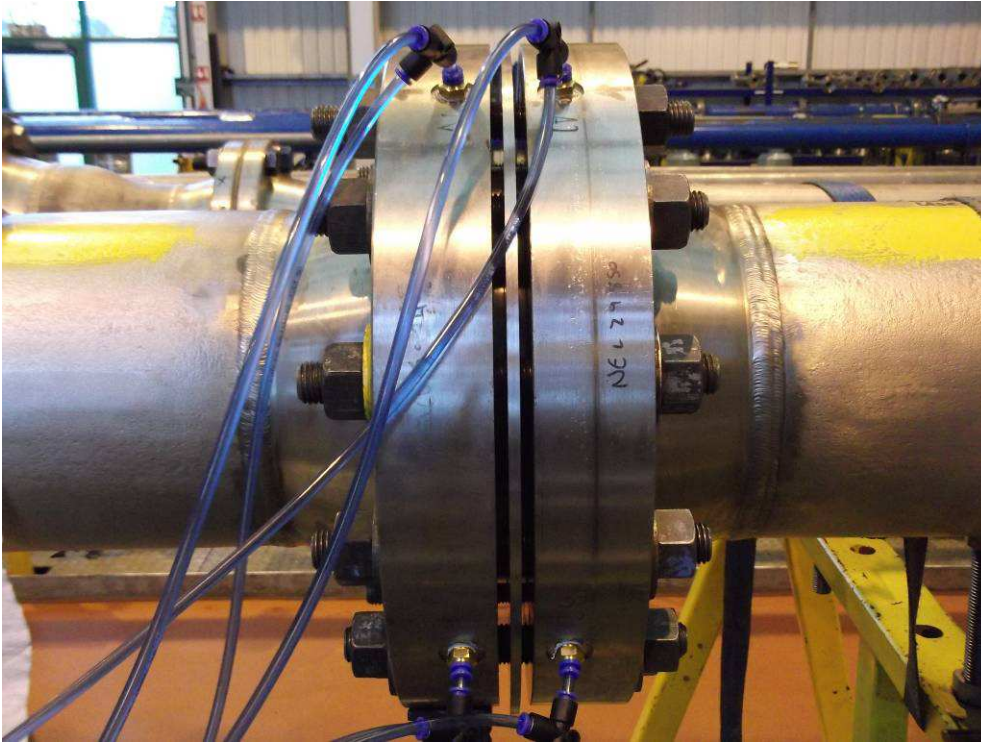


Figure 2 The orifice meter

### 3 EXPERIMENTAL WORK

#### 3.1 General

Existing 8" (200 mm) diameter pipes manufactured as an orifice plate metering assembly with flange tappings were used: the internal diameter  $D$  was 202.56 mm. Upstream of the orifice plate there was  $70D$  of straight pipe to a perforated plate flow conditioner and then  $10D$  to a bend. The last  $9D$  of the upstream pipe before the orifice plate was machined internally. Downstream of the orifice plate there was a  $4D$  machined length and then a further length of matching machined pipe,  $6D$  in length for the initial tests (see also 5.2). The assembly had pressure tappings available in two planes  $90^\circ$  apart.

To the additional pipe, bosses were added  $6D$  downstream of the orifice plate so that the pressure loss could be measured. Data were collected in two planes perpendicular to each other (referred to as horizontal and vertical, although they were  $30^\circ$  below horizontal and  $30^\circ$  from vertical up; the dowel pins were located top and bottom). Seven orifice plates were manufactured ( $\beta = 0.2, 0.4, 0.6$  (4 off) and  $0.75$ ) by a specialist fabricator. Care was taken to adhere strictly to the requirements of ISO 5167 and the orifice bores were spark eroded to ensure sharp edges. Multiple plates were required because some were to be damaged in order to produce fault conditions and could not be used subsequently.

Three differential pressures were measured:

1. the differential pressure: from the upstream flange to the downstream flange,  $\Delta P$
2. the measured pressure loss: from the upstream flange to  $6D$  downstream of the orifice plate (not the actual pressure loss), PL

**Technical Paper**

3. the measured pressure recovery from the downstream flange to  $6D$  downstream of the orifice plate, PR

These measured differential pressures were taken as shown in Figure 3.

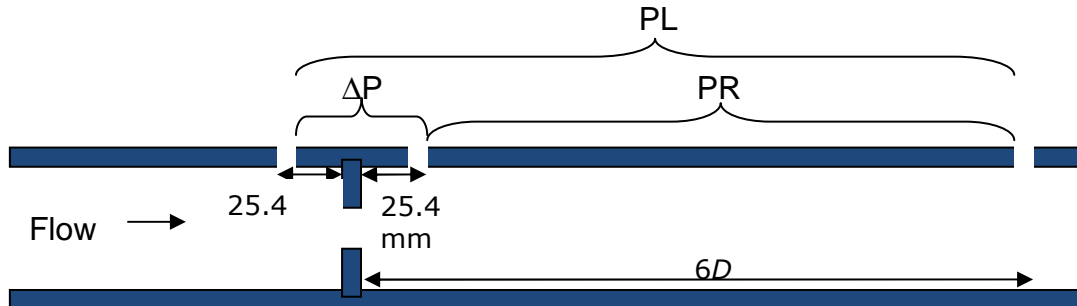


**Figure 3 Measured differential pressures**

From these measurements three diagnostic ratios are computed.

Pressure Loss Ratio (PLR) = Ratio of PL to  $\Delta P$

Pressure Recovery Ratio (PRR) = Ratio of PR to  $\Delta P$

Pressure Recovery to Pressure Loss (PRL) = Ratio of PR to PL

Throughout the project the difference between the differential pressure across the orifice plate and the sum of the measured pressure loss and the measured pressure recovery was calculated. The value of this sum relative to the measured differential pressure provides a strong diagnostic test. During testing 95% of the good points were within about 0.05%. This ratio was used to indicate the presence of air in the impulse lines. Because of the good agreement between the three differential pressures in this project there is very little need to consider pressure recovery data separately from pressure loss data except in two situations: for  $\beta = 0.2$  where the pressure recovery is about 5% of the pressure loss (see 4.1) and where there was a deliberately introduced error in differential pressure.

### **3.2 Tests Undertaken**

The actual tests undertaken were as follows:

- 1) Error in orifice plate diameter (entered value 1% higher than the true value)
- 2) Error in pipe diameter (entered value 2% higher than the true value)
- 3) Drift in differential pressure transmitter (measured value 2% higher than the true value)

NOTE 2% of value could, for example, be 0.2% of span when the transmitter is operated at 10% of span.

- 4) Incorrectly positioned orifice plate (offset by 6.3 mm (an eccentricity of 3.1% of  $D$ ) towards the horizontal tappings) – see Figure 4 (there was no leak around the outside of the orifice plate).

NOTE If this offset was due to the orifice plate not being fully seated at the bottom of the meter tube then the 'vertical' tappings would be on the side of the orifice meter and the 'horizontal' tappings would be on the top.

Technical Paper

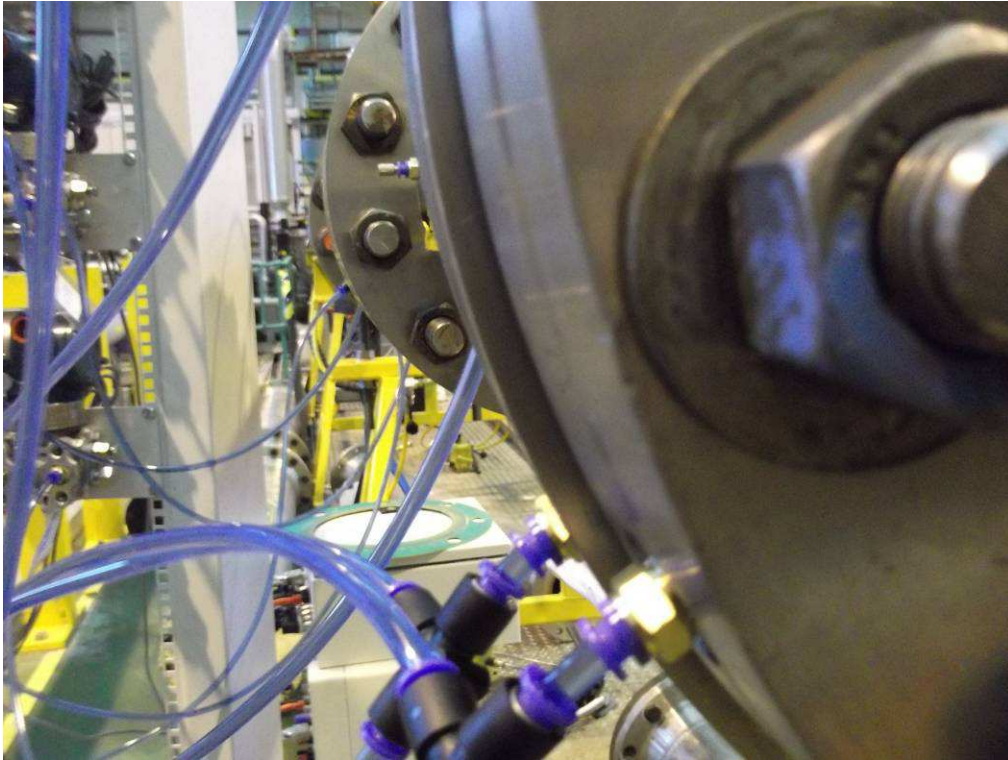


**Figure 4 Orifice plate offset towards the 'horizontal' tapplings**

- 5) Rounded orifice edge (edge radius = 0.23 mm, i.e.  $r/d = 0.0019$ )
- 6) Rounded orifice edge (edge radius = 0.42 mm, i.e.  $r/d = 0.0035$ ) – see Figure 5



**Figure 5 Rounded edge of orifice plate**

- 7) Unexpected drain hole (drain hole of radius =  $0.1d$  not included in calculation) – see Figure 6

**Technical Paper**

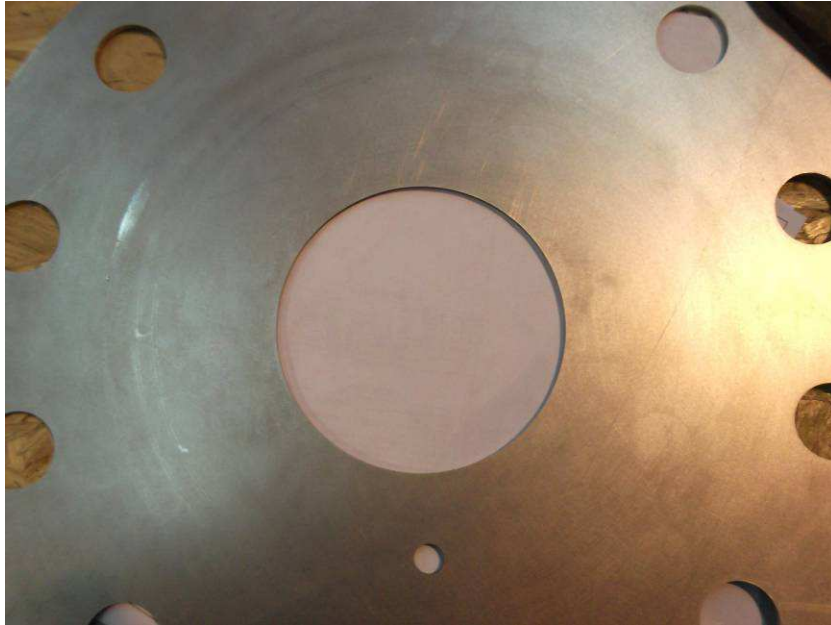


**Figure 6 Orifice plate ( $\beta = 0.6$ ) with drain hole**

- 8) Deposit on the face of the orifice plate, simulating face contamination (a gasket of thickness 1.5 mm covering most of the upstream face leaving a clear zone of width 7 mm) – see Figure 7
- 9) Deposit on the face of the orifice plate, simulating face contamination (a gasket of thickness 1.5 mm covering most of the upstream face leaving a clear zone of width 5.25 mm)
- 10) Deposit on the face of the orifice plate, simulating face contamination (a gasket of thickness 1.5 mm covering most of the upstream face leaving a clear zone of width 4.8 mm)

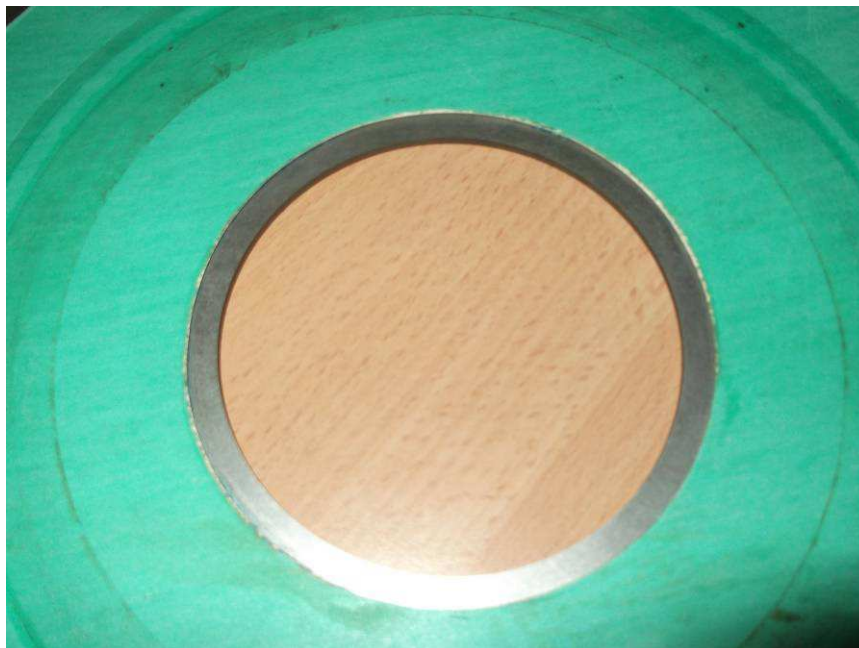


**Figure 7 Orifice plate with gasket simulating face contamination**

**34<sup>th</sup> International North Sea Flow Measurement Workshop  
25-28 October 2016**

**Technical Paper**

- 11) Two phase flow (adding bubbles to the water)
- 12) Plate installed backwards
- 13) Simulation of a partially blocked flow conditioner (using a gate valve 1/3<sup>rd</sup> closed, downstream end 7D from orifice plate) – see Figure 8
- 14) Simulation of a partially blocked flow conditioner (using a gate valve 2/3<sup>rd</sup> closed, downstream end 7D from orifice plate)



**Figure 8 Simulation of a partially blocked flow conditioner (using a partly closed gate valve)**

- 15) Bent plate (deviation from flat approximately linear with distance from pipe wall, maximum deviation from flat about 5 mm) – see Figure 9

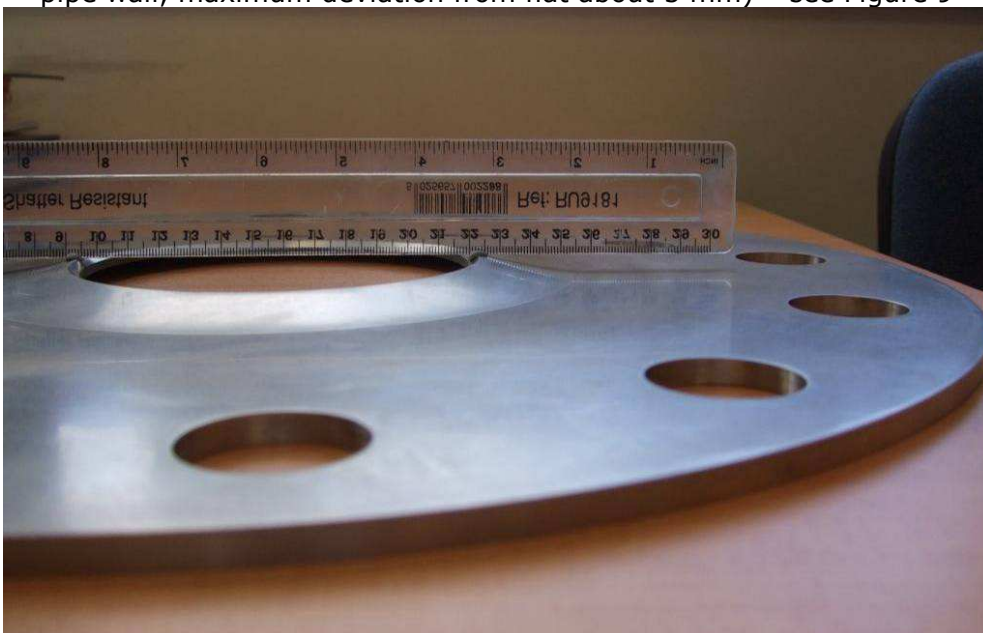


**Figure 9 Bent orifice plate**

# 34<sup>th</sup> International North Sea Flow Measurement Workshop 25-28 October 2016

## Technical Paper

All these tests were carried out using a  $\beta = 0.6$  orifice plate except tests 4), 10) and 13), which were only done with  $\beta = 0.75$ .  $\beta = 0.75$  was used instead of  $\beta = 0.6$  for tests 4) and 13) to give a larger shift in discharge coefficient.

Test 7) was carried out with  $\beta = 0.2, 0.6$  and  $0.75$ .

Test 12) was carried out with  $\beta = 0.2$  and  $0.6$ .

Test 14) was carried out with  $\beta = 0.6$  and  $0.75$ .

To present the data, a baseline test was provided without any fault condition. In each case the baseline data were fitted as a function of  $(10^6/Re_D)^{0.5}$  and the mean deviation from the fitted line calculated for inclusion in subsequent work. An example from the orifice plate deposit tests is shown in Figures 10 and 11. This shows both the baseline calibrations and the results when the fault is introduced. Figure 10 shows the change in discharge coefficient whereas Figure 11 shows the change in measured pressure loss.

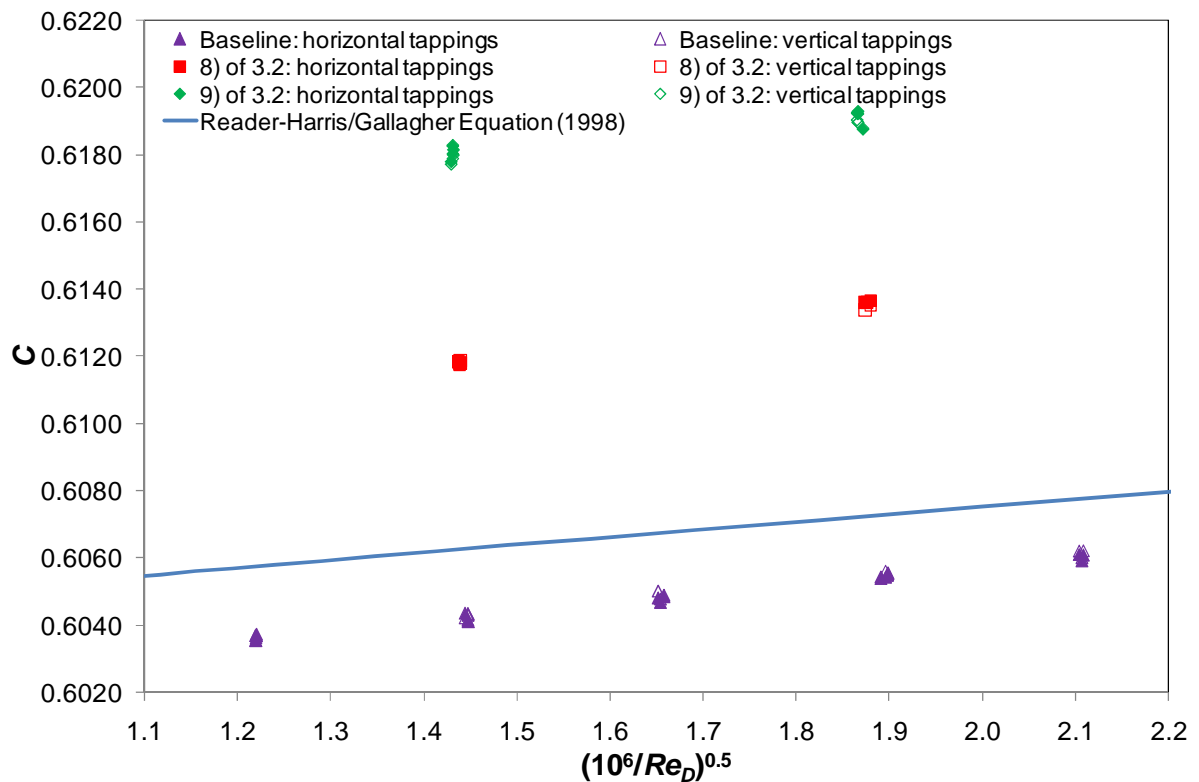


**Figure 10 Effect of the deposit on the orifice plate on the discharge coefficient:  $\beta = 0.6$**

Technical Paper

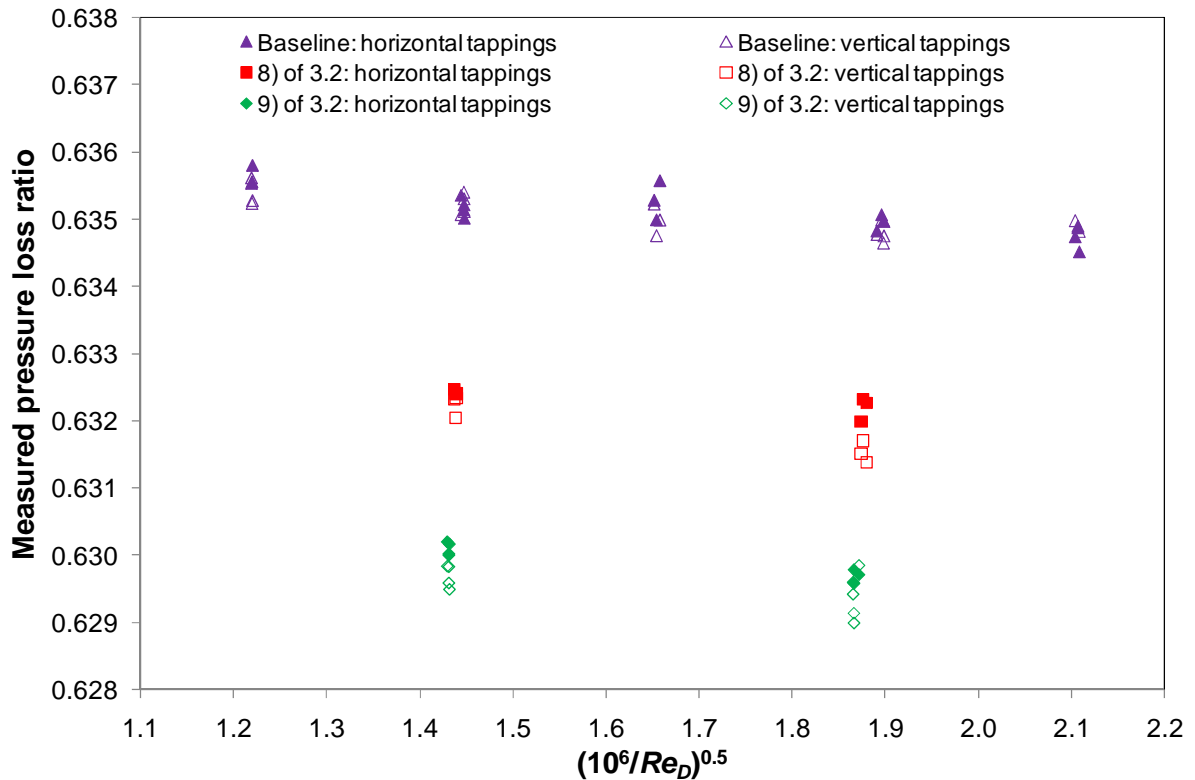


**Figure 11 Effect of the deposit on the orifice plate on the measured pressure loss ratio:  $\beta = 0.6$  (data corrected)**

From these measured data, the relative changes in discharge coefficient and pressure loss were derived and presented as the result of the experiment.

Correction to the data has been carried out: the correction is related to the manufacture of the downstream pressure tapping and is fully explained in section 5.2. For analyses against an established base line the correction makes very little difference.

#### 4 WITH AN INITIAL BASELINE

##### 4.1 General

Where an orifice plate is installed and records of the pressure ratios are taken across the flow range, a baseline can be established. Departures during service from these baseline values can then be attributed to a fault developed on the system, i.e. the PLR trends can be monitored in service to identify developing faults. Potential faults have been simulated in the testing programme in order to determine the difference from the baseline.

##### 4.2 With an Initial Baseline: Single-Phase Flow $\beta = 0.2$ Orifice Plate

The  $\beta = 0.2$  plate was tested during test 7) – unexpected drain hole - and test 12) - reversed plate. These results are shown in Figure 12. An unexpected drain hole fault will be caused by installing a plate with a drain hole, but not including the hole in the calculation software. A similar fault condition (but causing an error of opposite sign) is a drain hole becoming blocked in service.

Technical Paper

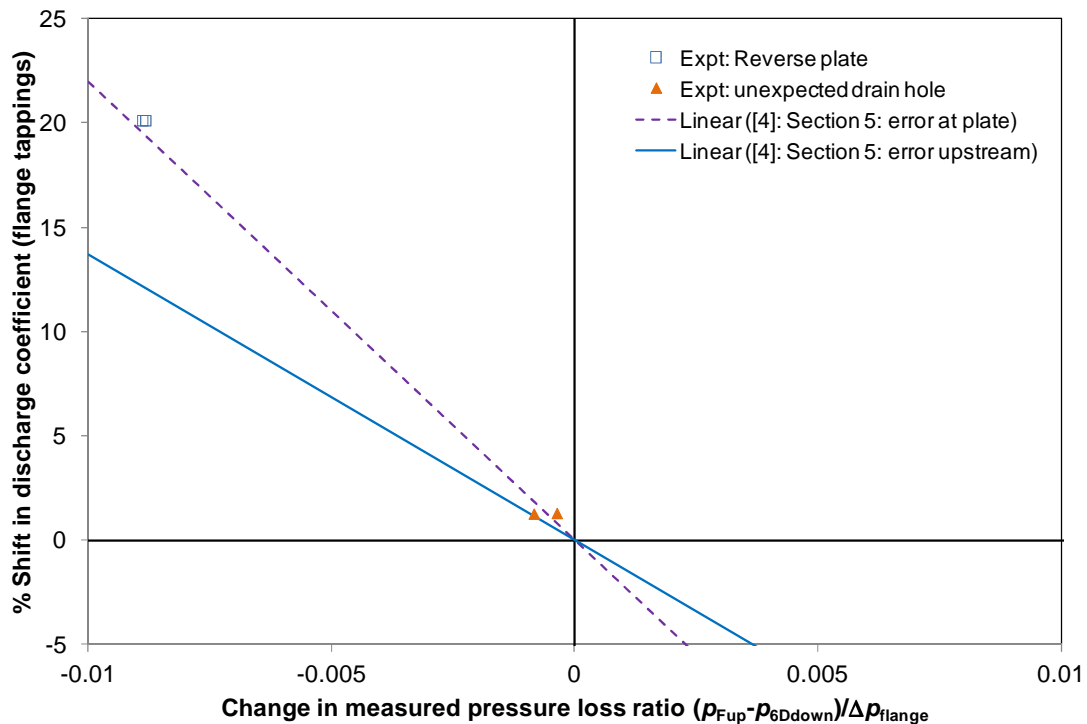


**Figure 12 Shift in discharge coefficient from baseline vs Change in measured pressure loss ratio:  $\beta = 0.2$  orifice plate**

The two results for each condition are derived from the two sets of pressure tappings 90° apart.

For each plate the Computational Fluid Dynamics (CFD) results taken from a theoretical study previously reported [4] have been shown. These results have been included to demonstrate that the experimental and the CFD results are in good agreement with each other. The calculated values as derived in Section 5 of [4] are also included.

Installing an orifice plate in the reverse direction gives a change in discharge coefficient of about 20%. It is clearly shown by a change in pressure loss ratio of about -0.009. This can be measured.

The drain hole gives a change in discharge coefficient of about 1.3%. The pressure loss data are shown in Figure 13: it would be very difficult from the PLR data in the case of the unexpected drain hole for the  $\beta=0.2$  orifice plate to be sure that there is a problem.

In this case because the pressure recovery is so much smaller than the pressure loss more discrimination can be obtained by considering the pressure recovery ratio (PRR). The pressure recovery data are shown in Figure 14: it might be possible from the PRR data in the case of the unexpected drain hole to be sure that there is a problem.

Technical Paper

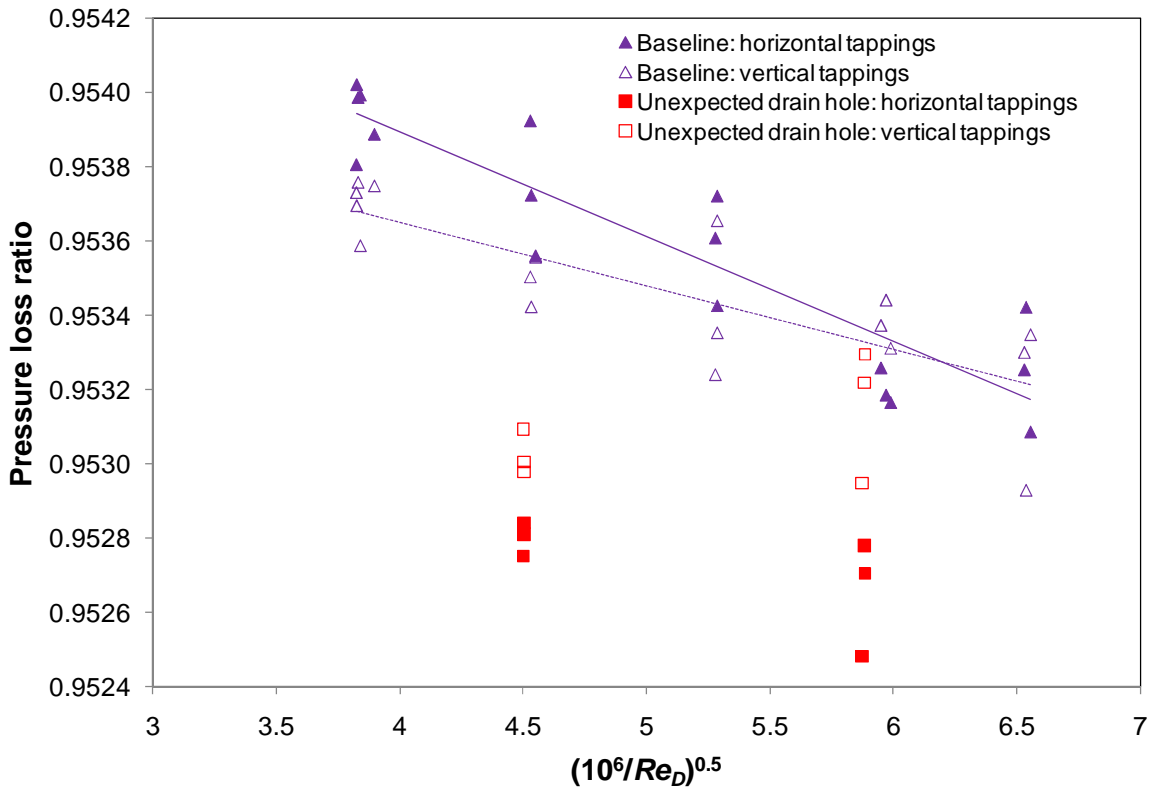


Figure 13 Effect of unexpected drain hole of diameter  $0.1d$  on measured pressure loss ratio:  $\beta = 0.2$  orifice plate

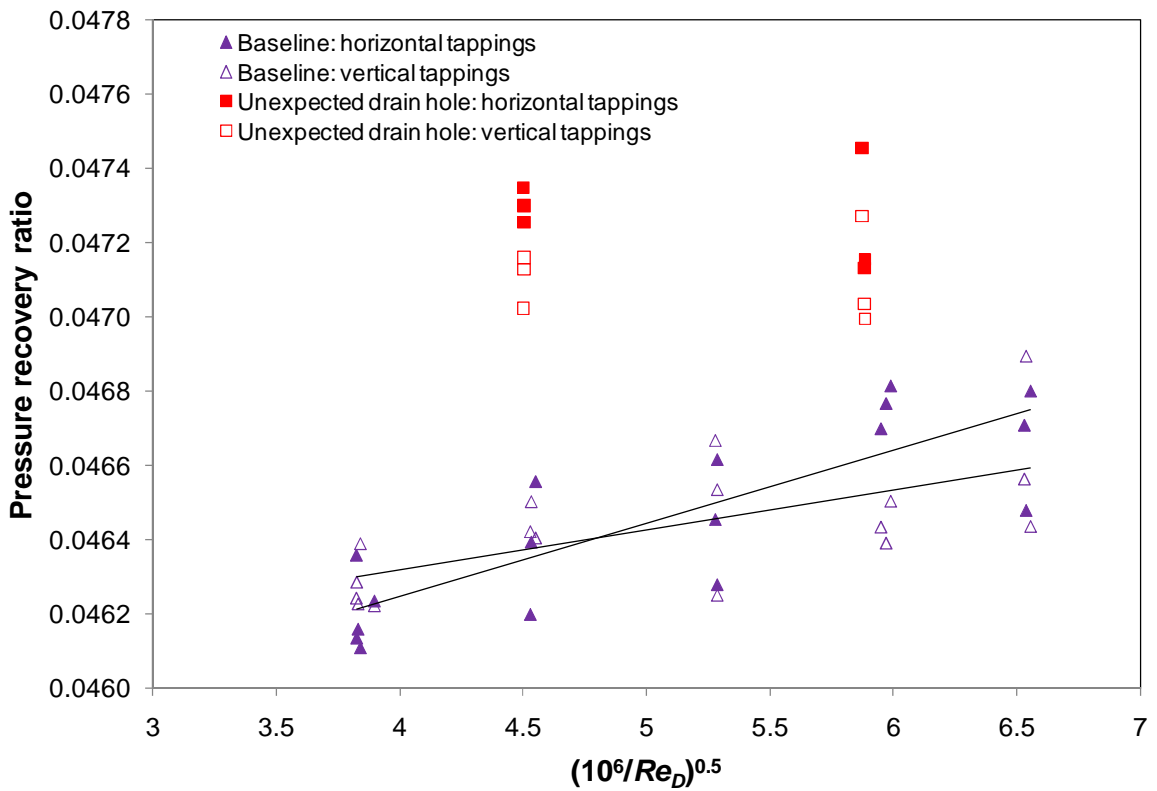


Figure 14 Effect of unexpected drain hole of diameter  $0.1d$  on measured pressure recovery ratio:  $\beta = 0.2$  orifice plate

Technical Paper

4.3 With an Initial Baseline: Single-Phase Flow with  $\beta = 0.6$  And  $\beta = 0.75$  Orifice Plates

Again the initial baseline differential pressures were established prior to testing and changes from the baseline were determined for each orifice plate and fault condition.

The  $\beta = 0.6$  orifice plates were tested in single-phase flow during tests 1) to 3), 5) to 9), 12), 14) and 15). Tests 5) and 6) use the same symbol; similarly tests 8) and 9) use the same symbol. The results are shown in Figure 15a. To give additional clarity Figure 15b shows the same data except for those with a reversed plate. This allows the remaining results to be shown with higher resolution.

In practice the error in differential pressure ('dp error') led to a failure to achieve the balance  $PL + PR = \Delta P$  (see the final paragraph of 3.1); so this point on Figures 15a and 15b is irrelevant.

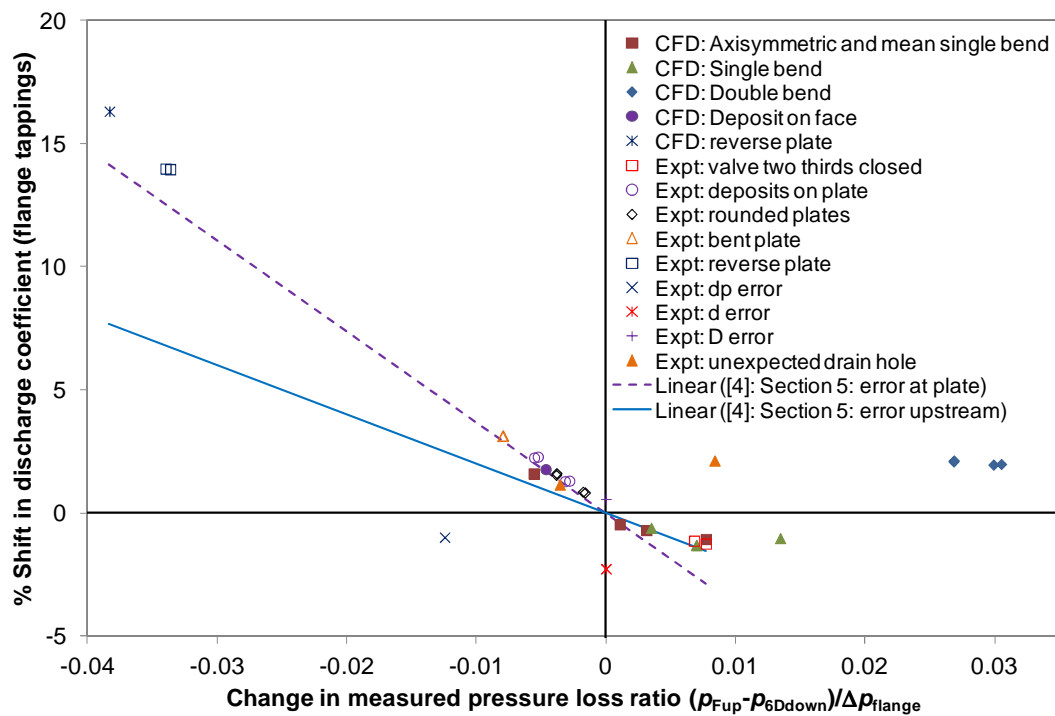
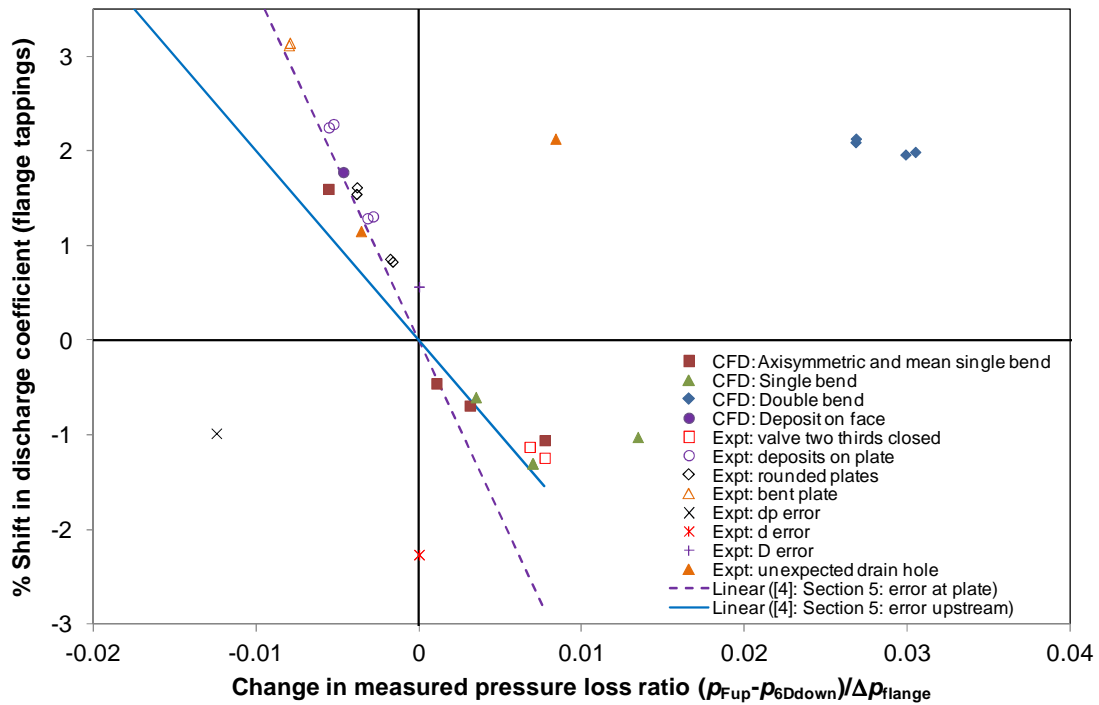


Figure 15a Shift in discharge coefficient from baseline vs Change in measured pressure loss ratio:  $\beta = 0.6$  orifice plate

Technical Paper



**Figure 15b Shift in discharge coefficient from baseline vs Change in measured pressure loss ratio:  $\beta = 0.6$  orifice plate (omitting reversed plate)**

The Prognosis image for the bent plate is shown as Figure 16. The fact that the points lie outside the box show that Prognosis would find this problem. Further details about the interpretation of the Prognosis image can be found in [3]. The date in the Figure is that when the image was produced, not when the data were taken.

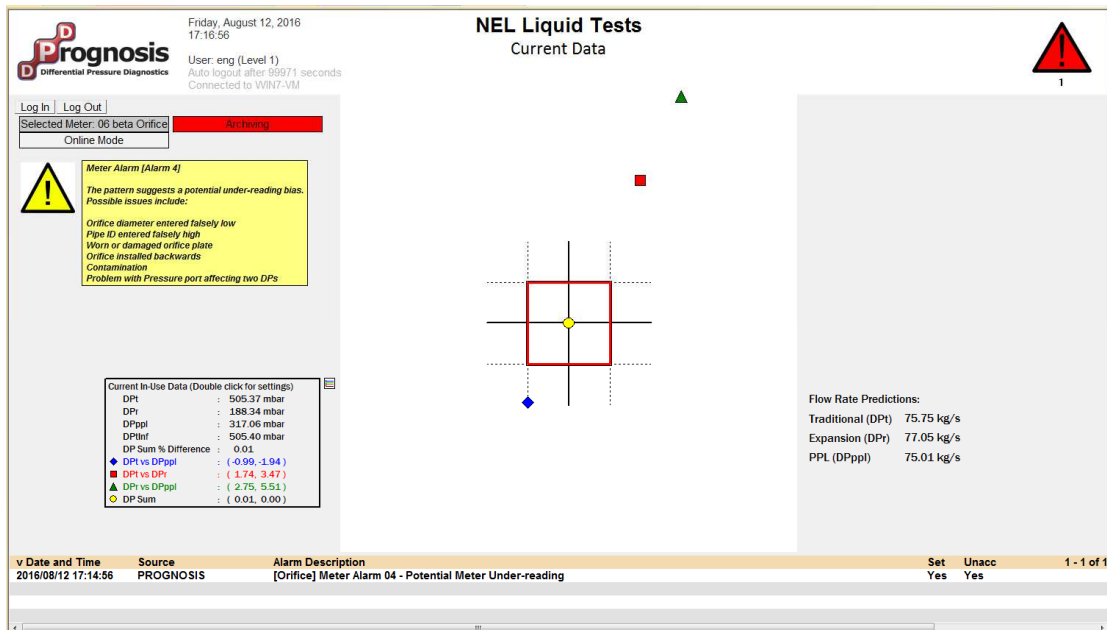


**Figure 16 Prognosis image for flow downstream of a bent plate:  $\beta = 0.6$  orifice plate**

# 34<sup>th</sup> International North Sea Flow Measurement Workshop 25-28 October 2016

## Technical Paper

The  $\beta = 0.75$  orifice plates were tested in single-phase flow during tests 4), 7), 10), 13), and 14). The results are shown in Figure 17.

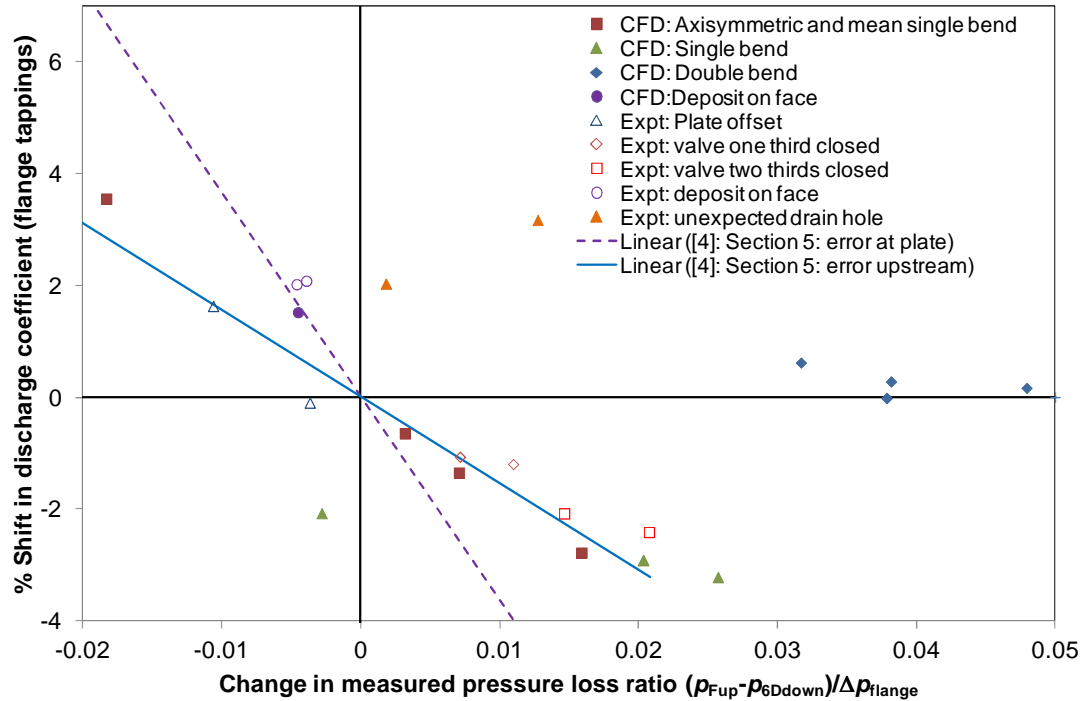


**Figure 17 Shift in discharge coefficient from baseline vs Change in measured pressure loss ratio:  $\beta = 0.75$  orifice plate**

The Prognosis images for a valve one third closed and two thirds closed are shown as Figures 18a and 18b. The fact that the points lie outside the box show that Prognosis would find both these problems.

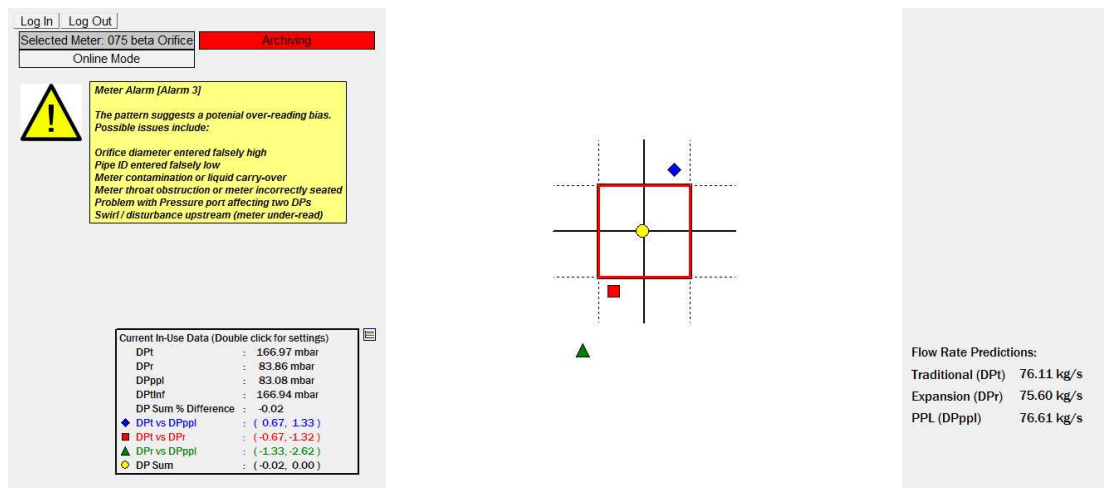


**Figure 18a Prognosis image for flow downstream of a valve one third closed:  $\beta = 0.75$  orifice plate**

Technical Paper

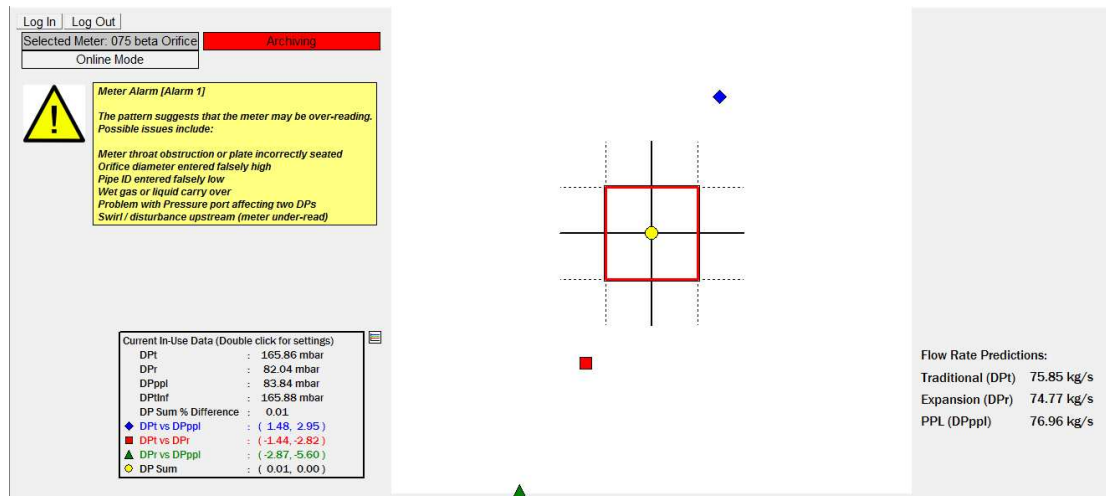


Figure 18b Prognosis image for flow downstream of a valve two thirds closed:  $\beta = 0.75$  orifice plate

From Figures 15 and 17 it is clear that, for  $\beta = 0.6$  and  $0.75$ , if a change of less than  $0.0025$  in measured pressure loss ratio is measured, then provided that there is not a mistake (wrong entry of diameters, presence of unexpected drain hole) it is unlikely that there is a shift in discharge coefficient greater than  $1\%$  from the original condition.

As expected from the report on the theory [4] the effect of many types of installation is proportional to the difference in the pressure loss ratio; however, as expected, the constant of proportionality depends on whether the fault is at the orifice plate itself or in the upstream pipework.

So it is clear that a shift in discharge coefficient can be spotted by looking at the change in the pressure loss ratio. Moreover, if errors due to mistakes (wrong entry of diameters, presence of unexpected drain hole) are avoided and the orifice plate is known from inspection to be in good condition it may be possible to assume the error is upstream (e.g. a partially blocked conditioner or a roughened pipe) and to estimate the error.

The challenge in practice is to ensure that the sensitivity of the pressure measurements can resolve a change in PLR to within  $0.0025$ . It is also important to recognise that this sensitivity is based on a comparison with measured and recorded baseline values of PLR rather than on comparison with a standard prediction of the PLR in good conditions.

PRR gives a little more discrimination than PLR, but the pattern is almost identical. PRL gives a further improvement in discrimination, but again with a very similar pattern.

#### 4.4 With an Initial Baseline: with Added Gas Bubbles

For liquid flows it is possible that gas can be entrained in the flow. The presence of gas is known to give errors in the measurement. Gas volume fractions of up to approximately  $1.5\%$  were produced by introducing air to the water flow. This produced errors in discharge coefficient of up to  $2.5\%$  for pressure tappings near the top of the pipe.

**34<sup>th</sup> International North Sea Flow Measurement Workshop  
25-28 October 2016**

**Technical Paper**

The data with added gas bubbles cannot easily be shown on the same graph as the other data since the data were taken over a range of gas volume fractions. The data are shown in Table 1. It is clear that in general there is good agreement between the differential pressure and the sum of the measured pressure loss and the measured pressure recovery, but that as air accumulates in the pressure tapping near the top of the pipe the agreement becomes less good. This diagnostic measurement may indicate the presence of gas gathering at the top of the pipe when the tappings are also near the top of the pipe.

From Figure 19 for both pairs of tappings the PLR clearly indicates the presence of gas in the flow. It can be seen that using the pressure tappings just below the horizontal the relationship between the shift in  $C$  and the change in measured pressure loss ratio is similar to that in Figure 15 with the error upstream: the performance of the orifice plate with these pressure tappings is much better than its performance with pressure tappings near the top of the pipe because in the former case gas does not accumulate in the impulse lines (impulse lines for liquid metering should always slope downwards lest gas accumulate within the pressure tappings and cause errors, as found, for example, in Table 1 with vertical tappings). The relationship between shift in discharge coefficient and PLR for the vertical tappings probably reflects more the amount of air held within the tapping and impulse line than the gas volume fraction.

**Table 1 Data collected with added gas bubbles**

Water $Re_D$	% Gas Volume Fraction	% difference in sum of pressure loss and pressure recovery from differential pressure		% shift in $C$ from baseline		Change in measured pressure loss ratio from baseline	
		Horizontal tappings	Vertical tappings	Horizontal tappings	Vertical tappings	Horizontal tappings	Vertical tappings
471594	No gas injection	0.02	-0.01	0.03	0.04	0.0004	0.0000
471256	0.04	0.02	-0.01	0.00	-0.01	0.0003	-0.0017
470357	0.11	0.03	-0.01	-0.02	0.00	0.0003	-0.0012
470284	0.14	0.02	-0.01	-0.06	-0.07	0.0007	-0.0016
351946	No gas injection	0.01	-0.03	-0.03	-0.02	0.0001	-0.0037
347068	0.41	0.01	-0.03	-0.21	-0.24	0.0014	-0.0087
340432	1.16	0.00	-0.03	-0.53	-0.23	0.0016	-0.0062
275989	No gas injection	0.01	-0.04	-0.02	0.85	0.0006	-0.0035
265898	1.57	0.00	-0.06	-0.57	2.13	0.0032	0.0088
269013	1.11	0.01	-0.05	-0.23	2.43	0.0014	0.0092

Technical Paper

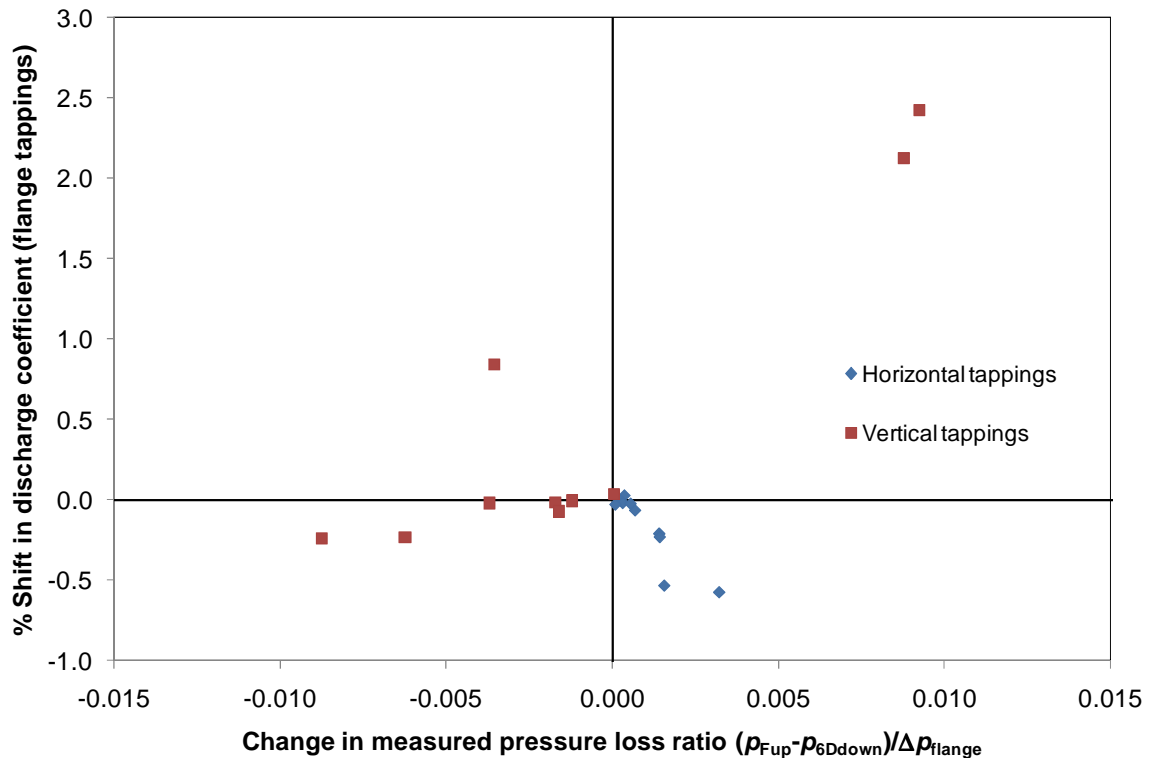


**Figure 19 Shift in discharge coefficient from baseline vs Change in measured pressure loss ratio for tests with added gas bubbles:  $\beta = 0.6$  orifice plate**

## 5 WITHOUT AN INITIAL BASELINE

### 5.1 General

It is more difficult to know whether an orifice metering system is functioning correctly when there is no preliminary measurement of pressure ratios when the installation is first installed and put into service with, presumably, correctly designed pipe, plate and associated instrumentation.

To carry out diagnostic tests with no baseline, the various pressure ratios are tested against those predicted for the installation. This in effect creates a (theoretical) baseline. Comparing against a theoretical baseline will, however, potentially lose significant sensitivity in comparison with establishing and using a measured baseline.

### 5.2 Effect of Pipework

An important finding in relation to the installation of the additional  $6D$  pressure tapping was made during the testing and shows how important the condition of the downstream pipe is if diagnostics without a measured baseline are not to be misleading.

The orifice meter used in this project was very well made; the downstream pipe with the additional tappings was made by taking an existing high-quality length of machined pipe and welding additional tappings to it: a reputable pipework

# 34<sup>th</sup> International North Sea Flow Measurement Workshop 25-28 October 2016

## Technical Paper

contractor spark-eroded the  $6D$  tapplings to ensure the tapping ports and locations were of the highest quality.

On inspection it was noticed, only by very careful examination of the clean pipe, that the heat from welding had locally distorted the pipe creating an inward bulge at the tapping. The distortion was discernible to the eye and by a finger, but was measured as only about a 0.8 mm inward bulge. An attempt was made to heat the pipe and reduce the distortion. This reduced the distortion to about 0.6 mm. Once this fault in the pipe had been observed, a fault which could easily occur when a tapping is added to a pipe and the pipe is not subsequently machined, the effect on the diagnostic information was investigated. The exact size of the bulges is difficult to determine because the heat has made the pipe slightly oval.

Firstly CFD was carried out to check the effect. This suggested that with a hump or bulge of 0.65 mm with the tapping centrally located on the bulge the difference in measured pressure loss from that measured with a tapping on a pipe without a bulge would be unacceptably large.

While this work was being carried out, experimental testing continued with the pipe with the bulge. The diagnostics showed almost all the pressure loss ratio baselines as unacceptable. To investigate further and to provide correct results a new pipe with no distortion (that is with the tapplings welded on and then the pipe machined and then the tapplings spark eroded) was manufactured. The new pipe was of length  $4D$ .

Most of the data were taken with the original downstream pipe, but some were collected with the new pipe; so it was necessary to correct all the results to what they would have been using the new pipe.

Accordingly baselines were taken for  $\beta = 0.75, 0.6$  and  $0.4$  orifice plates with both downstream pipes in turn so that it was possible to calculate the correction required: see Figure 20. Then all the results presented in this report were corrected to the values that would have been obtained with the new pipe. Corrections to the measured pressure loss ratio were around  $-0.014$  and  $-0.021$  for  $\beta = 0.75$  with the horizontal and vertical tapplings respectively, and  $-0.0043$  and  $-0.0062$  for  $\beta = 0.6$  with the horizontal and vertical tapplings respectively. No measured corrections for  $\beta = 0.4$  have been included in Figure 20 as their uncertainty is too high (although corrections based on extrapolation from Figure 20 corrected the baseline for the pipe with the bulge to within around 0.0003 of the baseline with the new pipe). The correction for  $\beta = 0.2$  is negligible.

Technical Paper

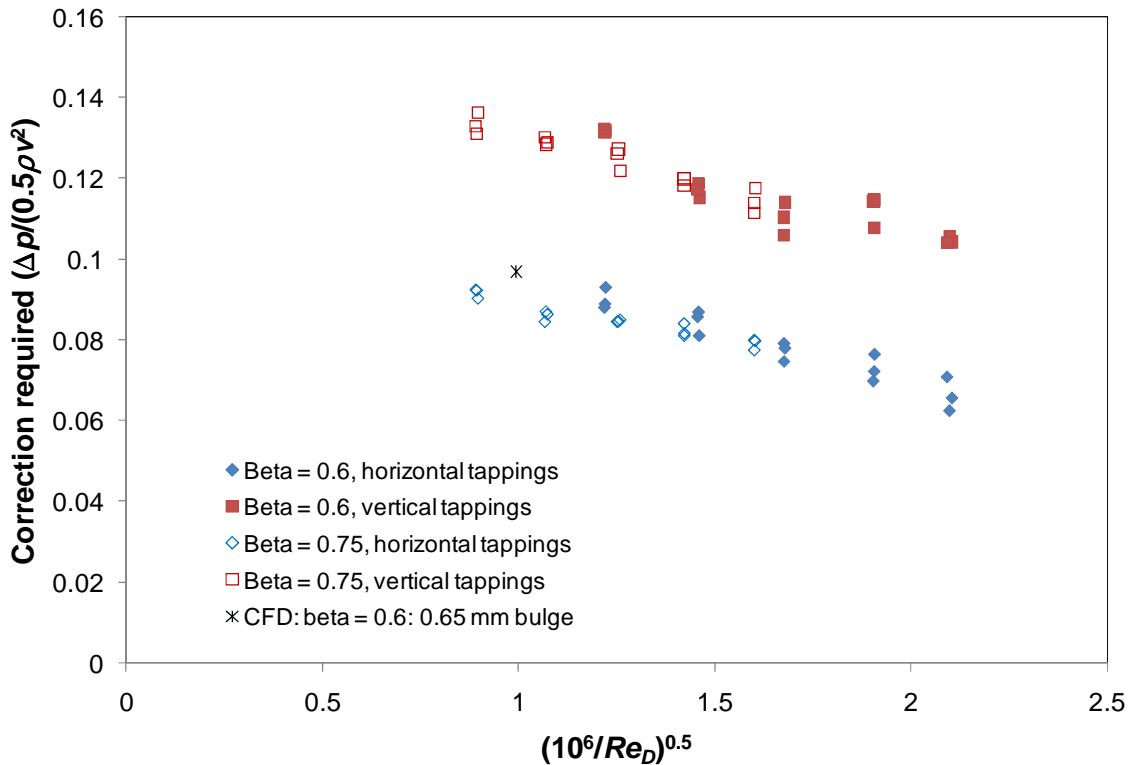


Figure 20 Correction required to the measured pressure loss ( $v$  is the mean velocity in the pipe)

### 5.3 Pressure Measurement Locations

Calculation of the discharge coefficient and hence the flowrate in an industry installation is done using the appropriate prediction from a standard – normally the Reader-Harris/Gallagher (1998) Equation as in ISO 5167-2:2003 [5]. A prediction of the pressure loss is also given in ISO 5167-2:2003, in particular the equation given in section 5.4.1 as:

$$\frac{\Delta \varpi}{\Delta p} = \frac{\sqrt{1 - \beta^4(1 - C^2)} - C\beta^2}{\sqrt{1 - \beta^4(1 - C^2)} + C\beta^2} \quad (1)$$

This applies for a pressure loss measured using tappings approximately  $D$  upstream of the orifice plate and  $6D$  downstream of the orifice plate. It is not specified what tappings should be used when determining  $C$ . This prediction is provided to allow the determination of total pressure loss for piping design purposes and is not provided for diagnostic purposes. It is entirely adequate for determining the pressure loss required to determine the temperature change from the downstream temperature measurement location to upstream of the plate (regardless of the choice of tappings for the determination of  $C$  in Equation (1)). It has an as yet unquantified uncertainty. Since this pressure loss prediction is based on the loss from approximately  $1D$  upstream of the orifice plate to approximately  $6D$  downstream of the plate, in practice this means that the measured upstream pressure if used for diagnostics will not match that required by the prediction if flange (or corner) tappings are used.

# 34<sup>th</sup> International North Sea Flow Measurement Workshop 25-28 October 2016

## Technical Paper

The deviation in measured PLR was evaluated from the NEL test work using the theoretical baseline derived in Equation (1) with  $C$  taken as the discharge coefficient using flange tappings as predicted by the Reader-Harris/Gallagher (1998) equation in ISO 5167-2: the results given in Figures 21 to 24 were obtained. As stated in 3.2 many more tests were carried out for  $\beta = 0.6$  than for other values of  $\beta$ . Figures 21 and 22 show that this method works well for  $\beta = 0.2$  and  $0.4$ , but Figures 23 and 24 show that it works poorly for  $\beta = 0.6$  and  $0.75$  since they imply that good flowrate measurements might be shown as errors and some poor flowrate measurements shown as acceptable. This is as expected from [4]. Error in mass flowrate has been shown in these figures rather than discharge coefficient since that relates better to the final use of the orifice measurement.

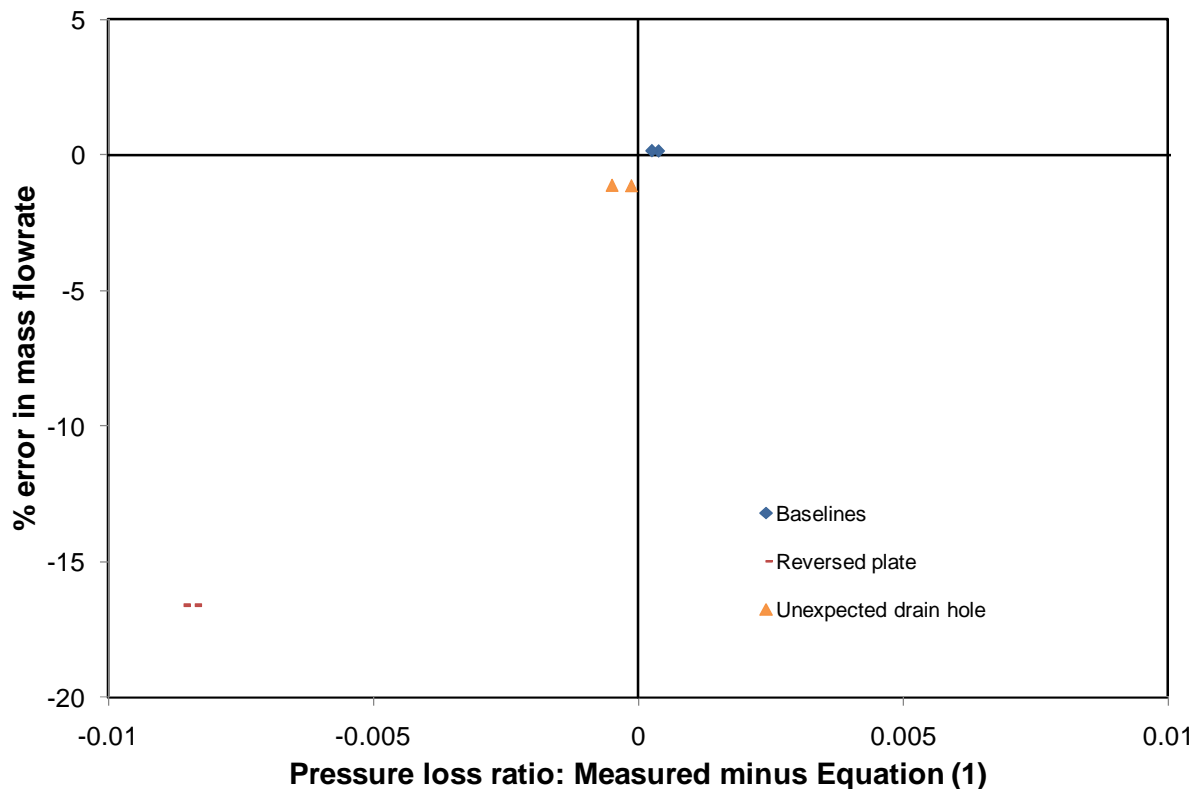


**Figure 21 Error in mass flowrate using Reader-Harris/Gallagher (1998) Equation vs Deviation in measured pressure loss ratio from Equation (1):  $\beta = 0.2$  orifice plate**

Technical Paper

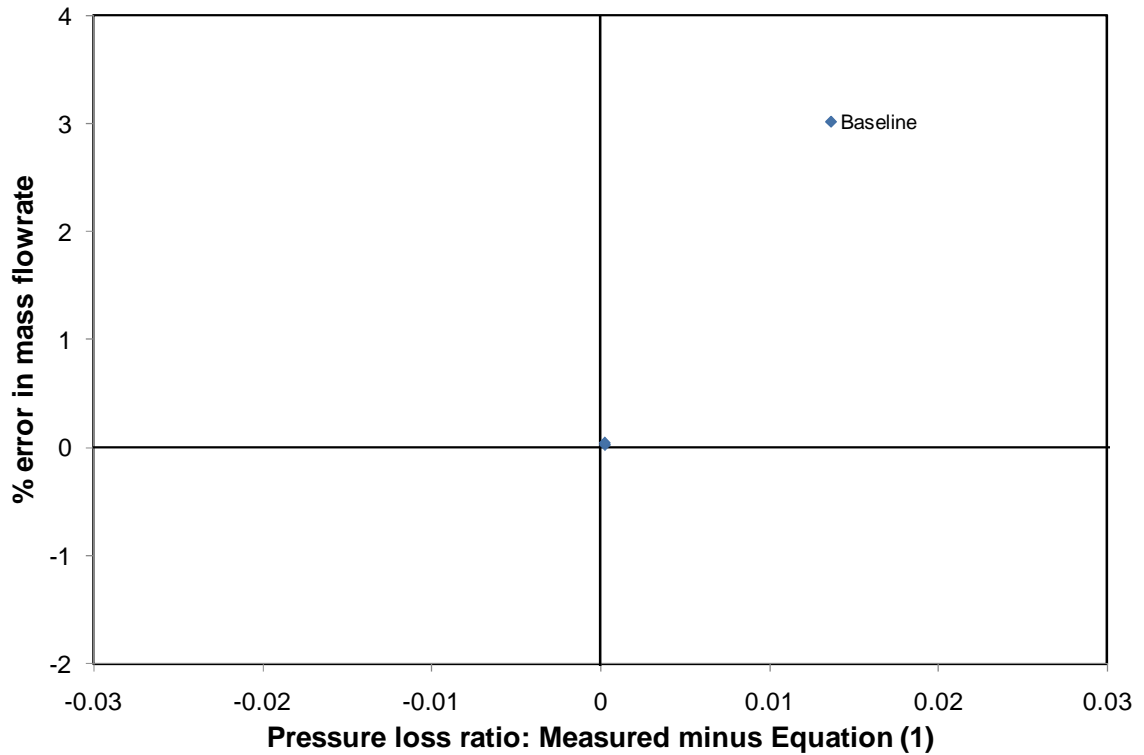


**Figure 22 Error in mass flowrate using Reader-Harris/Gallagher (1998) Equation vs Deviation in measured pressure loss ratio from Equation (1):  $\beta = 0.4$  orifice plate**

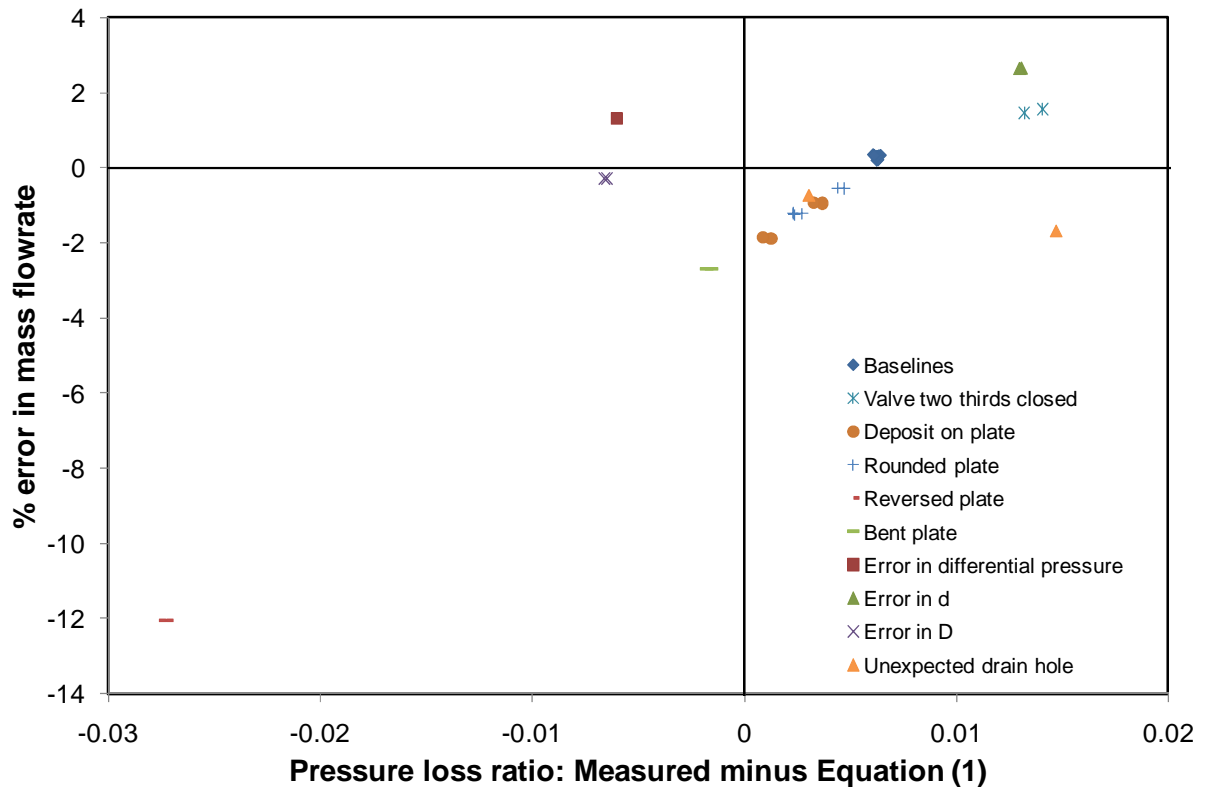


**Figure 23 Error in mass flowrate using Reader-Harris/Gallagher (1998) Equation vs Deviation in measured pressure loss ratio from Equation (1):  $\beta = 0.6$  orifice plate**

Technical Paper

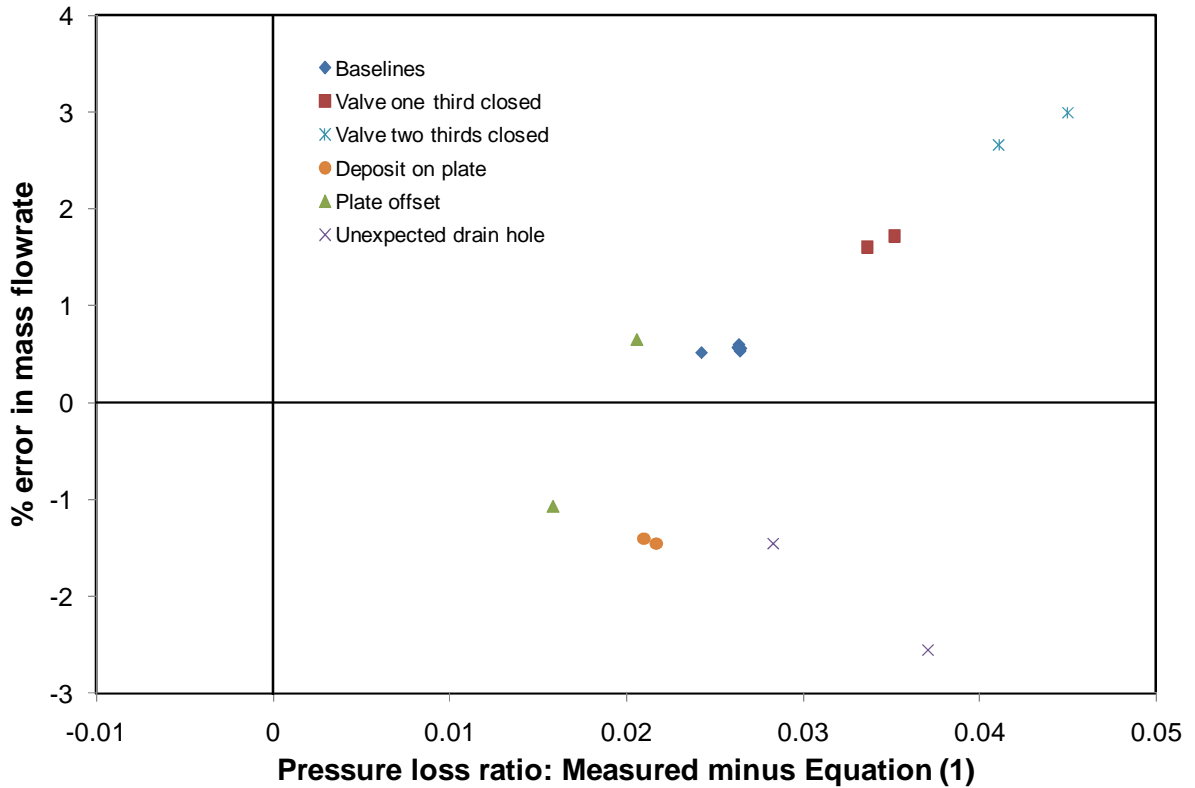


**Figure 24 Error in mass flowrate using Reader-Harris/Gallagher (1998) Equation vs Deviation in measured pressure loss ratio from Equation (1):  $\beta = 0.75$  orifice plate**

A better option is to assume that the equation in 5.4.1 of ISO 5167-2:2003 (Equation (1) of this paper) is correct using tappings  $D$  upstream, at some point  $P$  downstream and around  $6D$  downstream. Then

$$\begin{aligned} \Delta \bar{w}_{meas} &= p_{rise} + \Delta \bar{w} \\ &= p_{rise} + \frac{\sqrt{1 - \beta^4 (1 - C_{DandP}^2)} - C_{DandP} \beta^2}{\sqrt{1 - \beta^4 (1 - C_{DandP}^2)} + C_{DandP} \beta^2} \Delta p_{DandP} \end{aligned} \quad (2a)$$

$$\Delta p_{flange} = \Delta p_{DandP} + p_{rise} - \Delta p_{fdowntoP} \quad (2b)$$

where  $\Delta \bar{w}_{meas}$  is the pressure loss from the upstream flange tapping to  $6D$  downstream,  $p_{rise}$  is the pressure rise from  $D$  upstream to the upstream flange tapping,  $\Delta p_{flange}$  is the differential pressure using flange tappings,  $\Delta p_{DandP}$  is the differential pressure using tappings  $D$  upstream and at  $P$  downstream,  $C_{DandP}$  is the discharge coefficient with tappings in those locations, and  $\Delta p_{fdowntoP}$  is the pressure drop from the downstream flange tapping to the point  $P$ .

Then

**34<sup>th</sup> International North Sea Flow Measurement Workshop  
25-28 October 2016**

**Technical Paper**

$$\frac{\Delta \bar{\omega}_{meas}}{\Delta p_{flange}} = \frac{\frac{P_{rise}}{\Delta p_{DandP}} + \frac{\sqrt{1 - \beta^4(1 - C_{DandP}^2)} - C_{DandP}\beta^2}{\sqrt{1 - \beta^4(1 - C_{DandP}^2)} + C_{DandP}\beta^2}}{1 + \frac{P_{rise}}{\Delta p_{DandP}} - \frac{\Delta p_{fdowntoP}}{\Delta p_{DandP}}}. \quad (3)$$

From the Reader-Harris/Gallagher (1998) Equation

$$\frac{\Delta p_{fdowntoP}}{\Delta p_{DtoP}} = \frac{2}{C_{DandP}} 0.031 \left( M_{2P}' - 0.8 \times M_{2P}'^{1.1} - (M_{2flange}' - 0.8 \times M_{2flange}'^{1.1}) \right) \beta^{1.3}, \quad (4)$$

where  $M_2' = 2L_2'/(1-\beta)$  and  $L_2'$  is the quotient of the distance of the downstream tapping (or point P) from the downstream face of the orifice plate and the pipe diameter.

A reasonable result is obtained with point P 0.125D downstream of the plate.

As far as the data collected in this project are concerned this is almost equivalent to following the simpler model in [4], but the attraction of using the model here is that it is more consistent when different pipe diameters are used. It also puts the downstream pressure tapping at a smaller value of  $M_2'$  for smaller  $\beta$ .

There is also an additional loss term which should be included. It is reasonable to suppose that there is a loss equivalent to between 0 and 7D of pipe and that, given that the recirculation zone is shorter for larger  $\beta$ , the loss (in terms of number of pipe diameters) should increase with  $\beta$ . The effect of static hole error will be small compared with this pressure loss and is not included explicitly. Then a reasonable equation is:

$$\frac{\Delta \bar{\omega}_{meas}}{\Delta p_{flange}} = \frac{\frac{P_{rise}}{\Delta p_{DandP}} + \frac{\sqrt{1 - \beta^4(1 - C_{DandP}^2)} - C_{DandP}\beta^2}{\sqrt{1 - \beta^4(1 - C_{DandP}^2)} + C_{DandP}\beta^2}}{1 + \frac{P_{rise}}{\Delta p_{DandP}} - \frac{\Delta p_{fdowntoP}}{\Delta p_{DandP}}} + \frac{a\beta^{b+4}C_{DandP}^2}{1 - \beta^4}, \quad (5a)$$

where  $C_{DandP}$  is determined from the Reader-Harris/Gallagher (1998) Equation with  $L_1 = 1$  and  $L_2' = 0.125$ .  $L_1$  is the quotient of the distance of the upstream tapping from the upstream face of the orifice plate and the pipe diameter.

$a = 0.05625$  and  $b = 1$ , which correspond to a loss due to a pipe of length  $4.5\beta D$  of friction factor  $\lambda = 0.0125$ , have been used.

$$\frac{P_{rise}}{\Delta p_{DandP}} = \frac{2}{C_{DandP}} 1.033 \left( 0.123e^{-7L_1} - 0.080e^{-10L_1} - 0.00011 \right) \frac{\beta^4}{1 - \beta^4} \quad (5b)$$

$$\frac{\Delta p_{fdowntoP}}{\Delta p_{DtoP}} = \frac{2}{C_{DandP}} 0.031 \left( M_{2P}' - 0.8 \times M_{2P}'^{1.1} - (M_2' - 0.8 \times M_2'^{1.1}) \right) \beta^{1.3}. \quad (5c)$$

In Equations (5b) and (5c)  $L_1$  and  $M_2'$  are based on the actual tapping positions and  $M_{2P}'$  on  $L_2' = 0.125$ .

**Technical Paper**

Using this approach the difference in the measured pressure loss ratio (using flange and 6D tappings) from the theoretical baseline in Equation (5) is determined and shown in Figures 25 to 28.

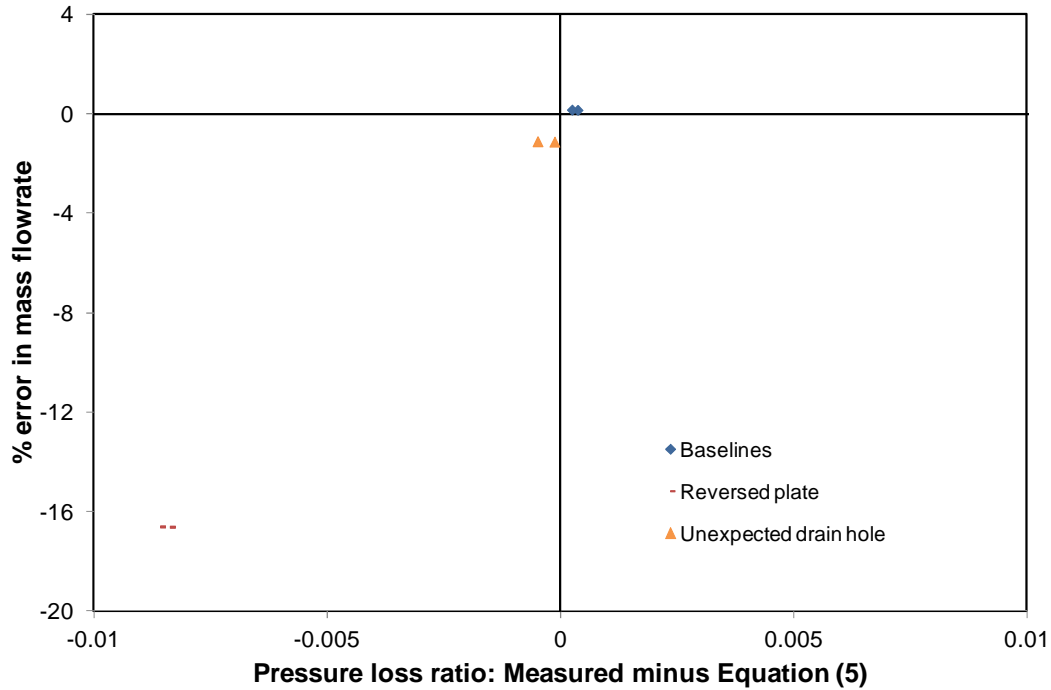


**Figure 25 Error in mass flowrate using Reader-Harris/Gallagher (1998) Equation vs Deviation in measured pressure loss ratio from Equation (5):  
 $\beta = 0.2$  orifice plate**

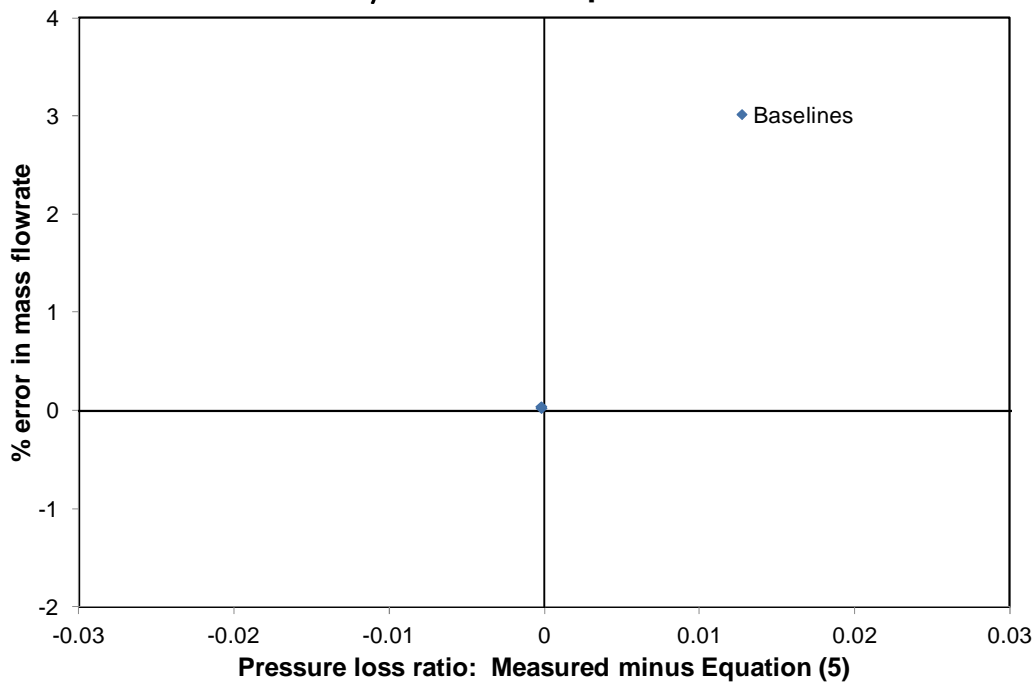


**Figure 26 Error in mass flowrate using Reader-Harris/Gallagher (1998) Equation vs Deviation in measured pressure loss ratio from Equation (5):  
 $\beta = 0.4$  orifice plate**

Technical Paper

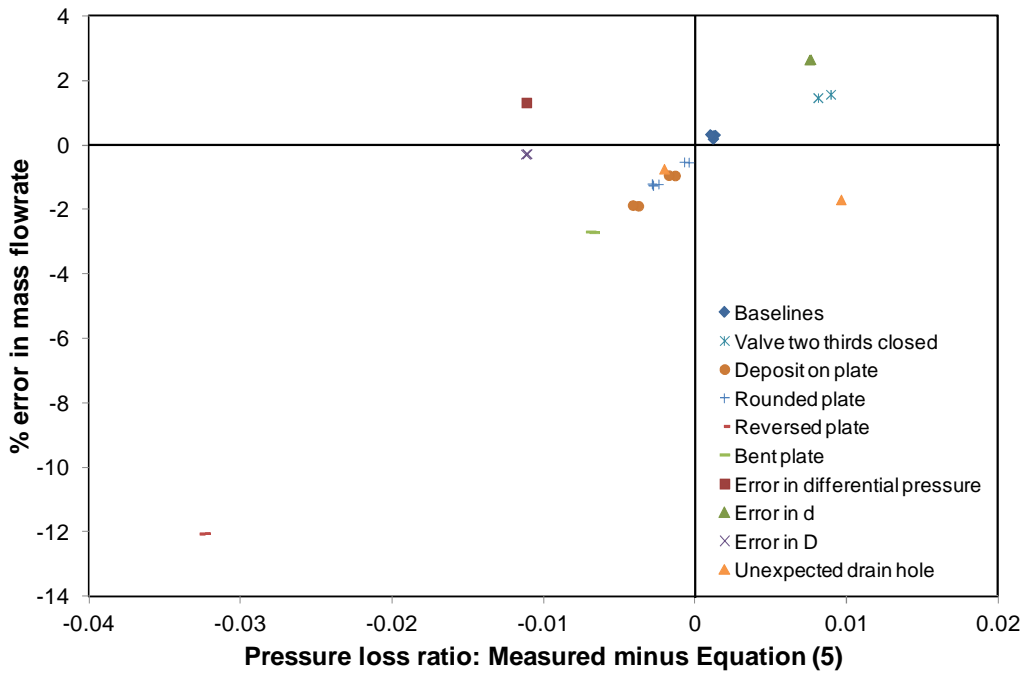


**Figure 27 Error in mass flowrate using Reader-Harris/Gallagher (1998) Equation vs Deviation in measured pressure loss ratio from Equation (5):  $\beta = 0.6$  orifice plate**

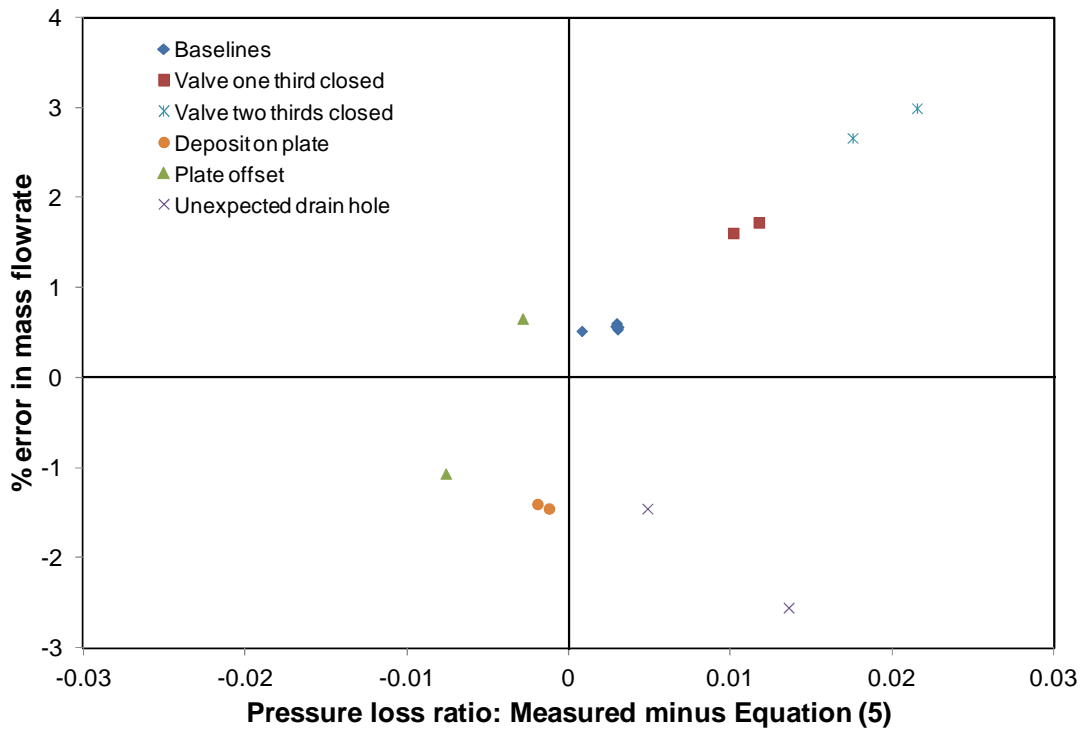


**Figure 28 Error in mass flowrate using Reader-Harris/Gallagher (1998) Equation vs Deviation in measured pressure loss ratio from Equation (5):  $\beta = 0.75$  orifice plate**

**Technical Paper**

Figures 25 to 28 show that Equation (5) performs well. To give more confidence in Equation (5) it would be necessary to have more data on pressure losses to analyse. More data would give a much clearer view of what is a significant deviation of measured PLR from that given by Equation (5).

In Figure 29 Equation (5) is compared with the data collected by CEESI as part of their Wet Gas JIP. These data were collected in 4" (100 mm) diameter pipe with flange tapplings and a tapping 6D downstream. The data from [6] have been used here although the data appear to be also presented in [2] but with different values.

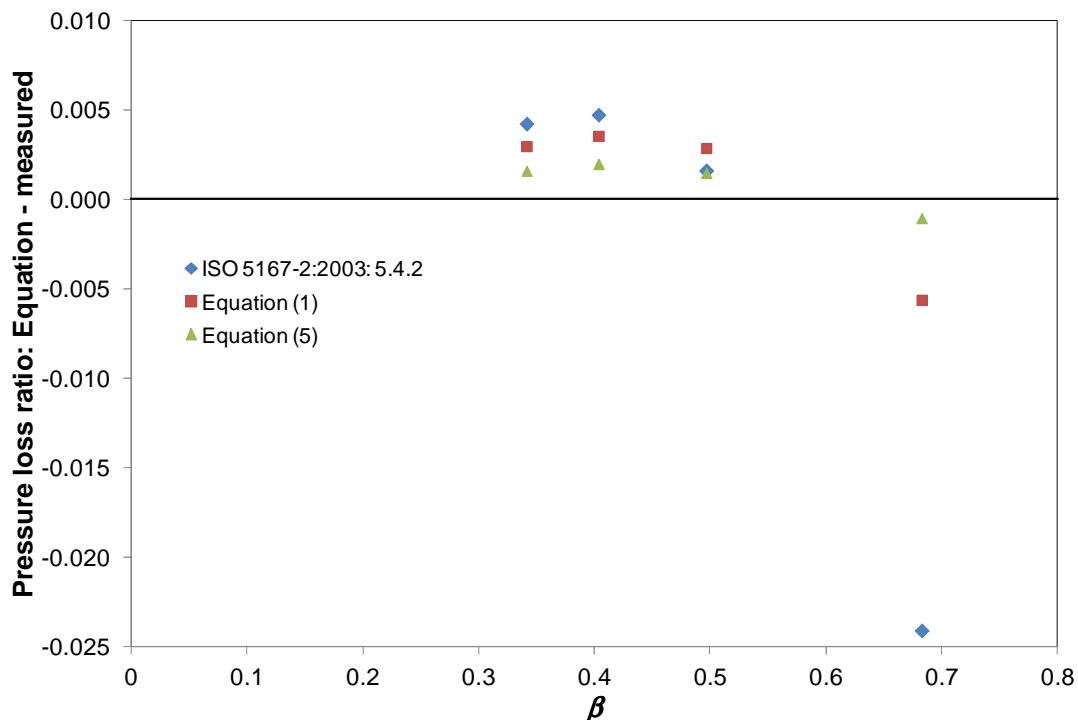


**Figure 29 Different equations compared with measured values of measured pressure loss ratio in 4" (100 mm) diameter pipe [6]**

The data in Figure 29 suggest that the correction to the equation for PLR to reflect the use of flange tapplings with a 6D downstream tapping is small but not negligible at values of  $\beta$  up to 0.5, whereas as  $\beta$  increases above 0.5 the correction must be considered necessary if a theoretical baseline PLR is to be used.

The applicability of Equation (1) was also discussed by Steven et al. [7]: they presented a large quantity of PLR data and showed that Equation (1) fitted their data well for  $\beta \leq 0.55$  but that a bias was observed for  $\beta > 0.55$ . Steven et al. obtained an empirical equation for PLR as a function of  $\beta$  for use for  $\beta > 0.55$  and applicable across the range of their data.

**6 CONCLUSIONS**

The work in this project has shown that an additional downstream pressure tapping can be used to provide a powerful diagnostic method. A shift in discharge coefficient due to a fault can in many cases be spotted from a change in the measured pressure loss ratio and in some cases the value of the shift estimated.

# 34<sup>th</sup> International North Sea Flow Measurement Workshop 25-28 October 2016

## Technical Paper

The simple diagnostic of summing the measured pressure loss and the measured pressure recovery and comparing with the measured differential pressure is surprisingly powerful.

When a measured baseline is available the 'Prognosis' method works very well in discerning problems. However, it is desirable to be able to use this system when no measured baseline is available: a simple application of equation (7) in 5.4.1 of ISO 5167-2:2003 is unsatisfactory for large  $\beta$  when flange tapplings are used.

When a measured baseline or an appropriate empirical prediction is not available an improved diagnostic calculation based on the work in [4] gives much better results.

When a measured baseline is not available the quality of the downstream pipe in which the pressure loss ratio is measured is of great importance. Apparently small deviations can affect the measured pressure loss ratio very significantly. Spark eroding the tapplings (to avoid burrs or rounded edges) is not sufficient.

If it were desired not only to predict the presence or absence of a fault but the value of the shift in discharge coefficient the use of an additional tapping  $D$  upstream of the orifice plate would be helpful. Then the ratio of the shift in discharge coefficient to the pressure loss ratio would not depend on whether the fault is at the orifice plate or upstream of it.

## 7 RECOMMENDATIONS FOR FURTHER WORK

Further work to determine measured pressure loss ratios in a wide variety of pipes of different diameter is required. The need is to know how well the measured pressure loss ratio can be predicted in good flow conditions, so that errors of 1% or less can be spotted.

## 8 NOTATION

$C$	discharge coefficient
$C_{DandP}$	discharge coefficient using tapplings $D$ upstream and at $P$ downstream
$D$	pipe diameter
$d$	orifice diameter
$L_1$	quotient of the distance of the upstream tapping from the upstream face of the orifice plate and the pipe diameter
$L_2'$	quotient of the distance of the downstream tapping from the downstream face of the orifice plate and the pipe diameter
$M_2'$	quotient of the distance of the downstream tapping from the downstream face of the orifice plate and the dam height: $M_2' = 2L_2' / (1 - \beta)$
PLR	pressure loss ratio (see 3.1)
$p_{rise}$	pressure rise from $D$ upstream to the the upstream flange tapping
$v$	mean velocity in the pipe
$\beta$	diameter ratio
$\Delta p_{DandP}$	differential pressure using tapplings $D$ upstream and at $P$ downstream

# 34<sup>th</sup> International North Sea Flow Measurement Workshop 25-28 October 2016

## Technical Paper

$\Delta p_{f_{down}toP}$	pressure drop from the downstream flange tapping to the point P
$\Delta p_{flange}$	differential pressure using flange tappings
$\Delta \bar{w}$	pressure loss from the upstream $D$ tapping to $6D$ downstream
$\Delta \bar{w}_{meas}$	pressure loss from the upstream flange tapping to $6D$ downstream
$\lambda$	friction factor

## 9 ACKNOWLEDGMENTS

This paper is published by permission of the Managing Director, NEL.

The authors are grateful for funding from the Innovation Funding Initiative (IFI).

## 10 REFERENCES

- [1] MARTIN, C. N. B. Effects of upstream bends and valves on orifice plate pressure distributions and discharge coefficients. NEL Report No 702. East Kilbride, Glasgow: National Engineering Laboratory, February 1986.
- [2] STEVEN, R. Diagnostic methodologies for generic differential pressure flow meters. In Proc. 26<sup>th</sup> Int. North Sea Flow Meas. Workshop, St Andrews, October 2008. East Kilbride, Glasgow: TUV NEL, 2008.
- [3] SKELTON, M., BARRONS, S., AYRE, J., and STEVEN, R. Developments in the self-diagnostic capabilities of orifice plate meters. In Proc. 28<sup>th</sup> Int. North Sea Flow Meas. Workshop, St Andrews, October 2010. East Kilbride, Glasgow: TUV NEL, 2010.
- [4] READER-HARRIS, M. J., LEE, W. K., BARNETT, J., and MISTRY, K. Diagnostics and orifice plates: theoretical and computational work. To be published at FLOMEKO, Sydney, Australia, September 2016.
- [5] INTERNATIONAL ORGANIZATION FOR STANDARDIZATION. Measurement of fluid flow by means of pressure differential devices inserted in circular cross-section conduits running full - Part 2: Orifice plates. ISO 5167-2: 2003.
- [6] STEVEN, R., BRITTON, C., and STEWART, D. CEESI Wet Gas JIP Data Release. EI/CEESI Wet Gas Metering Seminar Aberdeen, 2007.
- [7] STEVEN, R., KINNEY, J., ADEJUYIGBE, B., and LEWIS, K. Expanded knowledge on orifice meter response to wet gas flows. In Proc. 32<sup>nd</sup> Int. North Sea Flow Meas. Workshop, St Andrews, October 2014. East Kilbride, Glasgow: TUV NEL, 2014.

## **Technical Paper**

# **Errors Due to Use of the AGA8 Equation of State Outside of Its Range of Validity**

**Norman Glen, TUV NEL  
David Mills, Oil and Gas Systems Ltd  
Douglas Griffin, UK Oil and Gas Authority  
Steinar Fosse, Norwegian Petroleum Directorate**

---

## **1 INTRODUCTION**

In any measurement system (apart from the most trivial) the model(s) used to convert the basic outputs of transducers to the final quantity of interest form an integral part of the system and will have an impact on the overall uncertainty of measurement achievable. For example, a resistance-temperature device such as a platinum resistance thermometer makes use of an equation relating the resistance of platinum wire to temperature. Similarly, an ultrasonic flow meter makes use of a model describing the time of flight of the ultrasonic signal across the flowing fluid. In both these cases (and many others), the direct influence of the models are reduced, through calibration of the complete measurement system. However, in the case of gas metering systems, for example those used to account for production in the North Sea, this is not necessarily the case.

For custody-transfer standard flow measurement of dry, processed gaseous hydrocarbons in the UK sector of the North Sea, OGA's 'Guidance Notes for Petroleum Measurement' specify that the flow rate measurements may be in either volumetric or mass units [1]. They also stipulate that where volume is the agreed measurement unit, it should be referred to the standard reference conditions of 15 °C temperature and 1.01325 bar absolute pressure (bar (a)). This requires determination of the gas density at the flow meter, which may be achieved by

- continuous direct measurement by an on-line densitometer or
- calculation, using a recognised equation of state together with measurements of gas composition, temperature and pressure.

If the calculation method is used, the performance of the model (the equation of state) will have a direct impact on the uncertainty of the parameter of interest, the quantity of flowing gas.

Numerous equations of state have been developed, including cubic models such as the Peng-Robinson [2] and Redlich-Kwong-Soave [3] models or corresponding-states models such as that of Lee and Kesler [4] and used for the calculation of gas density from composition.

More recently, the AGA 8 [5] method has been fairly universally adopted for the calculation of natural gas density and, for example, forms an integral part of the measurement infrastructure in the North Sea, being programmed in to flow computers and written in to many gas sales agreements. However, gas compositions may or may not lie within the pipeline quality gas specifications required to obtain the lowest uncertainty with the AGA 8 method, possibly due to the compositional changes from ageing fields or for complex fields exhibiting non-

# 34<sup>th</sup> International North Sea Flow Measurement Workshop 25-28 October 2016

## Technical Paper

standard gas compositions. This leads to the requirement to review the use of the AGA 8 method and investigate possible alternatives.

### 2 BACKGROUND

The AGA 8 method is based on a residual Helmholtz free energy equation of state which enables the calculation of thermodynamic properties of natural gases consisting of up to 21 components. The structure of the equation of state is based on a total of 58 polynomial terms and polynomial terms in combination with exponential functions which require 860 different parameters. The current version of the method, AGA 8-1992 [5], is the method recommended in ISO 12213:2005 [6] when a detailed composition is available.

Although the range of validity of the AGA 8 method is limited to the gas phase, it is most often applied to the supercritical state, but, despite this, it generally performs sufficiently well. If all the components are within the specified composition ranges for pipeline quality gas [5], calculated densities will have an uncertainty of the order of 0.1 % (at  $k=2$ ) for temperatures between -10 and 65 °C at pressures up to 120 bar (a). Table 1 summarises the limits required to obtain the 0.1 % uncertainty in calculated density.

**Table 1 – AGA 8 Applicability Limits (Pipeline Quality Gas)**

Parameter	Min	Max	Parameter	Min	Max
pressure / MPa	0	12	butanes / mol%	0.0	1.5
temperature / K	263	338	pentanes / mol%	0.0	0.5
superior cal value / MJ m <sup>-3</sup>	30	45	hexanes / mol%	0.0	0.1
relative density / -	0.55	0.80	heptanes / mol%	0.0	0.05
methane / mol%	70.0	100.0	octanes+ / mol%	0.0	0.05
nitrogen / mol%	0.0	20.0	hydrogen / mol%	0.0	10.0
carbon dioxide / mol%	0.0	20.0	carbon monoxide / mol%	0.0	3.0
ethane / mol%	0.0	10.0	helium / mol%	0.0	0.5
propane / mol%	0.0	3.5	water / mol%	0.0	0.015

However, for mixtures with components in the extended composition range and / or at temperatures and pressures outside the above limits (see Table 2), the uncertainty increases to between 0.2 and 0.5 % (at  $k=2$ ) and is effectively indeterminate for compositions outside the extended range of applicability (see Annexes E and F in ISO 12213:2005 Part 2 [6]).

# 34<sup>th</sup> International North Sea Flow Measurement Workshop 25-28 October 2016

## Technical Paper

**Table 2 – AGA 8 Wider-Range Applicability Limits  
(Extensions highlighted in red)**

Parameter	Min	Max	Parameter	Min	Max
pressure / MPa	0	65	butanes / mol%	0.0	1.5
temperature / K	225	350	pentanes / mol%	0.0	0.5
superior cal value / MJ m <sup>-3</sup>	20	48	hexanes / mol%	0.0	0.1
relative density / -	0.55	0.90	heptanes / mol%	0.0	0.05
methane / mol%	50.0	100.0	octanes+ / mol%	0.0	0.05
nitrogen / mol%	0.0	50.0	hydrogen / mol%	0.0	10.0
carbon dioxide / mol%	0.0	30.0	carbon monoxide / mol%	0.0	3.0
ethane / mol%	0.0	20.0	helium / mol%	0.0	0.5
propane / mol%	0.0	5.0	water / mol%	0.0	0.015

To overcome these limitations, Ruhr-Universität Bochum developed a new wide-range equation of state for natural gases and other mixtures, covering the same 21 components as the AGA 8 method. The method, explicit in the Helmholtz free energy, was adopted by GERG in 2004 [7] and a revised version was adopted in 2008 [8]. The mixture model uses accurate equations of state in the form of fundamental equations for each mixture component along with formulations developed for binary mixtures that take into account the residual mixture behaviour. Although the quoted uncertainty in density for the gas phase is similar to that for the AGA 8 method [5,6], the GERG-2008 method achieves this over a wider range of temperatures, pressures and compositions. The GERG-2008 method has now been adopted as an ISO standard, ISO 20765-2 [9].

The Peng-Robinson model [2] is a cubic equation of state of general applicability and has been widely used to model the phase behaviour of hydrocarbon systems. One common requirement for all phase equilibria models is for binary interaction parameter (BIP) information. BIPs represent the deviations from ideality for interactions between a given binary pair. Since the general approach to mixtures is the treatment of a mixture as a combination of binary pairs, the BIPs are extremely important for the representation of correct behaviour. For the Peng-Robinson model, for example, the results obtained, in particular for the location of the vapour – liquid phase boundary, are sensitive to the availability and exact values of the BIPs. Furthermore, particularly in regions close to the phase boundary, the uncertainties in key properties such as the density and compressibility of a mixture can become quite large.

In addition to having access to the GERG-2008 method (through the Bochum University implementation), TUV NEL has its own package, PPDS, for the calculation of thermophysical properties of fluids and fluid mixtures. All of the methods used in PPDS are taken from open literature and the user can select which method(s) to apply for each calculation. For the case studies presented in this paper the Peng-Robinson method was used with the PPDS default BIP values and the PPDS implementation of the AGA 8 method was used.

# 34<sup>th</sup> International North Sea Flow Measurement Workshop 25-28 October 2016

## Technical Paper

A key limitation of both the AGA 8 and GERG-2008 methods is the fixed 21-component data set. This means that components present in a real gas mixture which are not within this list must be assigned to existing components. Guidance is provided on appropriate assignments [5,6]; for example, benzene is assigned to *n*-pentane, toluene to *n*-heptane. However, there still remains the problem of dealing with components for which no specific assignments are given; for case study two, for example, two of the compositions included pseudo-components. These are effectively unidentified petroleum fractions obtained from laboratory analysis and defined by boiling point and molecular weight.

To overcome this limitation, TUV NEL has implemented a Petroleum Fractions package within its PPDS package. A petroleum fraction is a pseudo-component composed of a mixture of components, usually hydrocarbons. It is usually defined by some of its physical properties, particularly boiling point and density. The Petroleum Fractions package is a subroutine of prediction and estimation methods which calculates the thermodynamic and transport properties from this input. For example, liquid density is calculated using the Hankinson and Thomson method [10]. In the PPDS implementation, pseudo-components can be mixed with pure components from the PPDS System Pure databank to create representative mixtures.

### 3 CASE STUDIES

Two case studies are presented which illustrate potential problems when using the AGA 8 method outside its range of validity. Case study one is an example of where some of the components have compositions outside even the extended composition ranges allowed by the AGA 8 method whilst case study two examines the effect of mixtures with components not in the 21-component AGA 8 list.

#### 3.1 Components Concentrations Outside Allowed Ranges

This case study represents a system in which export gas is produced by two stages of separation of the hydrocarbon fluid recovered from the well and subsequent compression of the flashed gas to a pressure to enable export to be completed. In normal operation gas from the second stage separation goes for final compression and export. Special cases occur where the gas from the second stage (low pressure) separator does not go through to export, resulting in a lighter gas being exported.

Calculations were carried out for six cases, three for normal operation and three for the situation when the low pressure separator was off. For all six cases the density and compressibility at base conditions ( $T = 15^{\circ}\text{C}$ ,  $P = 1.01325 \text{ bar(a)}$ ) and average line conditions ( $T = 37.22^{\circ}\text{C}$ ,  $P = 117.46 \text{ bar(a)}$ ) were calculated by the various methods and the results compared.

For normal operation, the three compositions used were average data representing an extended period of operation plus data for two compositions corresponding to samples with the minimum and maximum methane contents respectively.

Similarly, for operation with the low pressure separator off, the same three input compositions were used.

# 34<sup>th</sup> International North Sea Flow Measurement Workshop 25-28 October 2016

## Technical Paper

Table 3 shows the input compositions (full 21 component AGA 8 requirement) and Table 4 the calculated values of the outputs (molecular weights, densities and compressibilities) from the AGA 8 method.

Tables 5 and 6 show the differences between the results calculated by the AGA 8 method and the Peng-Robinson method and between the AGA 8 method and the GERG-2008 method respectively.

### 3.1.1 Discussion

At base conditions all three calculation methods produce very similar values, with a maximum difference of -0.05 % in density for one composition. However, at line conditions significant differences are observed, with a maximum of 2.30 % for one composition between the AGA 8 and Peng-Robinson methods and 4.14 % between the AGA 8 and GERG-2008 methods for the same composition.

These differences are consistent with the observation that for all the compositions studied, several of the components had mole fractions significantly outside even the extended AGA 8 ranges, with the errors having an almost linear dependence on the methane and propane concentrations, as shown in Figures 1 and 2 respectively.

**Table 3 – Case Study 1: Input Compositions (mol %)**

Component	Normal operation			LP off		
	Average	CH <sub>4</sub> min + C <sub>3</sub> H <sub>8</sub> max	CH <sub>4</sub> max + C <sub>3</sub> H <sub>8</sub> min	Average	CH <sub>4</sub> min + C <sub>3</sub> H <sub>8</sub> max	CH <sub>4</sub> max + C <sub>3</sub> H <sub>8</sub> min
Methane	48.76	41.00	51.57	55.41	49.02	60.72
Nitrogen	1.11	0.84	1.18	1.27	1.05	1.41
Carbon Dioxide	2.76	2.51	2.91	3.02	2.75	3.21
Ethane	15.93	16.27	16.06	15.78	15.76	15.68
Propane	20.04	24.24	18.71	16.51	19.67	14.11
Water	0.00	0.00	0.00	0.00	0.00	0.00
Hydrogen	0.00	0.00	0.00	0.00	0.00	0.00
Sulphide						
Hydrogen	0.00	0.00	0.00	0.00	0.00	0.00
Carbon Monoxide	0.00	0.00	0.00	0.00	0.00	0.00
Oxygen	0.00	0.00	0.00	0.00	0.00	0.00
i Butane	3.52	4.66	3.03	2.55	3.53	1.79
n Butane	5.77	7.80	4.81	3.98	5.81	2.53
i Pentane	0.96	1.25	0.82	0.65	0.97	0.29
n Pentane	0.83	1.05	0.69	0.56	0.85	0.22
Hexane	0.27	0.33	0.23	0.23	0.41	0.04
Heptane	0.04	0.05	0.02	0.06	0.15	0.00
Octane	0.04	0.00	0.00	0.01	0.03	0.00
Nonane	0.00	0.00	0.00	0.00	0.00	0.00
Decane	0.00	0.00	0.00	0.00	0.00	0.00
Helium	0.00	0.00	0.00	0.00	0.00	0.00
Argon	0.00	0.00	0.00	0.00	0.00	0.00

**34<sup>th</sup> International North Sea Flow Measurement Workshop  
25-28 October 2016**

**Technical Paper**

**Table 4 – Case Study 1: AGA 8 Results**

	Normal operation			Normal operation		
	Average	CH <sub>4</sub> min + C <sub>3</sub> H <sub>8</sub> max	CH <sub>4</sub> max + C <sub>3</sub> H <sub>8</sub> min	Average	CH <sub>4</sub> min + C <sub>3</sub> H <sub>8</sub> max	CH <sub>4</sub> max + C <sub>3</sub> H <sub>8</sub> min
Molecular weight / amu	29.978	32.734	28.812	27.530	30.062	25.399
Density <sub>base</sub> / kgm <sup>-3</sup>	1.278	1.398	1.227	1.172	1.281	1.080
Compressibility <sub>base</sub> / -	0.9923	0.9905	0.9929	0.9936	0.9922	0.9948
Density <sub>line</sub> / kgm <sup>-3</sup>	314.52	378.09	284.13	250.29	316.56	200.64
Compressibility <sub>line</sub> / -	0.4338	0.3941	0.4616	0.5006	0.4323	0.5762

**Table 5 - Case Study 1: Differences Between AGA 8 and PPDS Calculations**

	Normal operation			LP off		
	Average	CH <sub>4</sub> min + C <sub>3</sub> H <sub>8</sub> max	CH <sub>4</sub> max + C <sub>3</sub> H <sub>8</sub> min	Average	CH <sub>4</sub> min + C <sub>3</sub> H <sub>8</sub> max	CH <sub>4</sub> max + C <sub>3</sub> H <sub>8</sub> min
$\delta MW$ / %	0.00	0.00	0.00	0.00	0.00	0.00
$\delta \rho_{base}$ / %	-0.03	-0.02	-0.04	-0.05	-0.03	-0.05
$\delta Z_{base}$ / %	0.03	0.02	0.04	0.04	0.03	0.05
$\delta \rho_{line}$ / %	1.68	2.30	0.84	0.08	1.84	-0.81
$\delta Z_{line}$ / %	-1.66	-2.25	-0.83	-0.08	-1.81	0.81

**Table 6 - Case Study 1: Differences Between AGA 8 and GERG-2008 Calculations**

	Normal operation			LP off		
	Average	CH <sub>4</sub> min + C <sub>3</sub> H <sub>8</sub> max	CH <sub>4</sub> max + C <sub>3</sub> H <sub>8</sub> min	Average	CH <sub>4</sub> min + C <sub>3</sub> H <sub>8</sub> max	CH <sub>4</sub> max + C <sub>3</sub> H <sub>8</sub> min
$\delta MW$ / %	0.01	0.00	0.00	0.00	0.00	0.00
$\delta \rho_{base}$ / %	0.04	0.04	0.03	0.03	0.04	0.02
$\delta Z_{base}$ / %	-0.03	-0.03	-0.03	-0.02	-0.03	-0.02
$\delta \rho_{line}$ / %	2.91	4.14	2.08	1.40	3.02	0.75
$\delta Z_{line}$ / %	-2.82	-3.98	-2.03	-1.38	-2.93	-0.74

Technical Paper

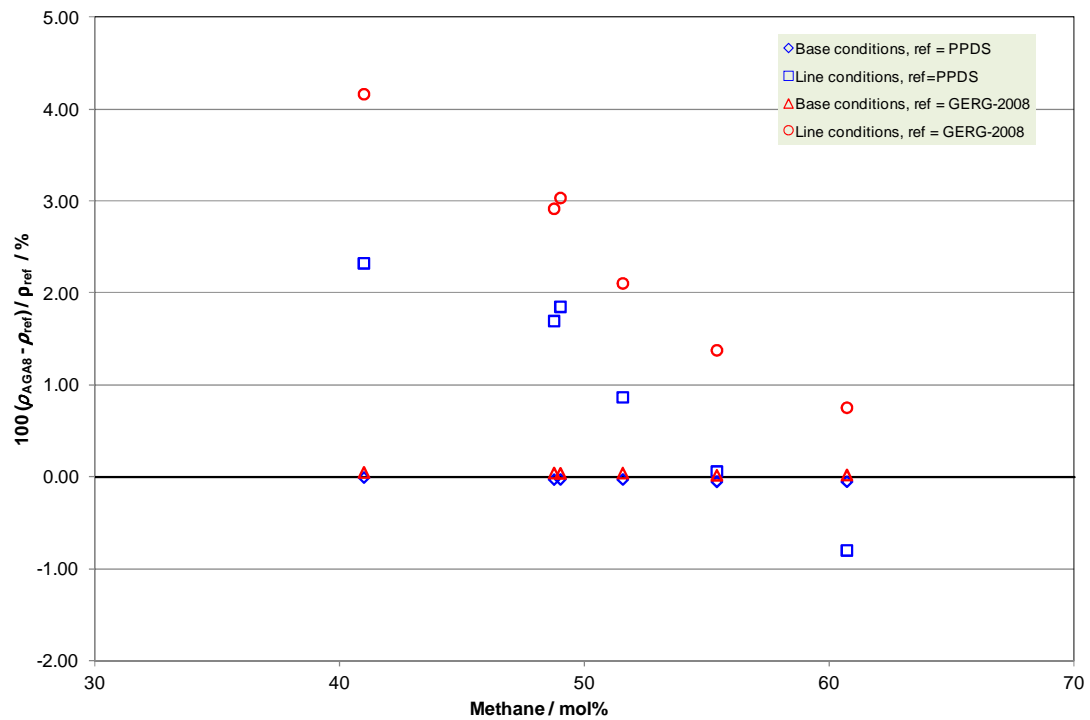


Fig. 1 – Case Study 1: AGA8 Differences as a Function of Methane Concentration at Line Conditions

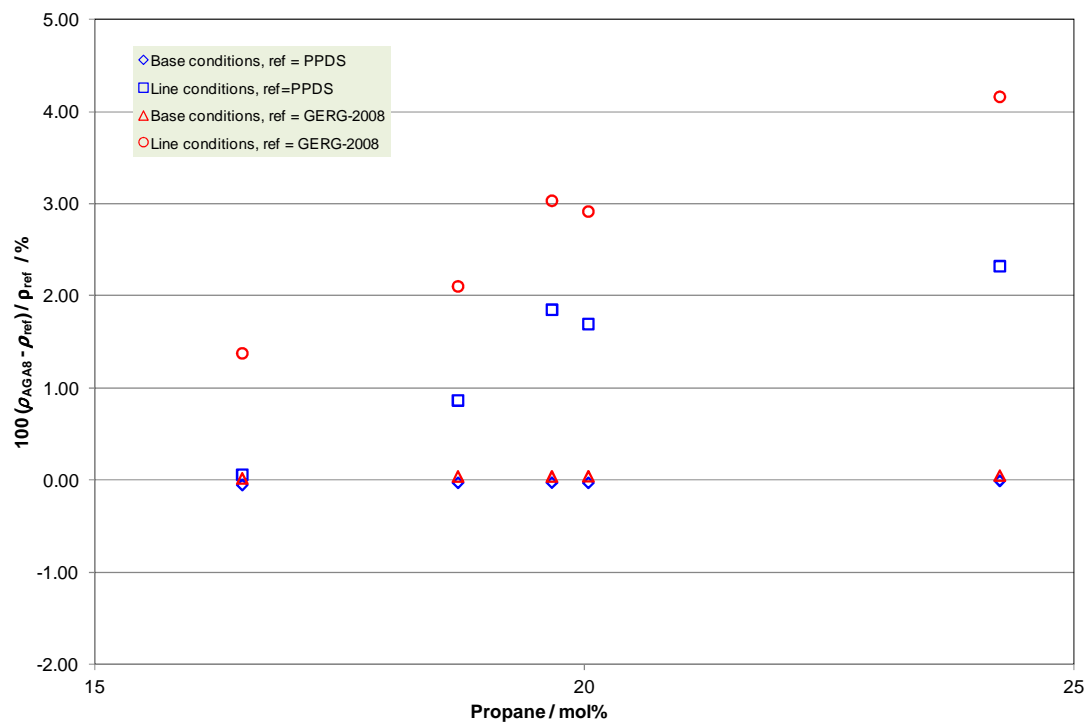


Fig. 2 – Case Study 1: AGA8 Differences as a Function of Propane Concentration at Line Conditions

# 34<sup>th</sup> International North Sea Flow Measurement Workshop 25-28 October 2016

## Technical Paper

### 3.2 Components not in AGA 8 List.

This case study examined the impact of changes in gas composition on the calculated properties (in particular the density and compressibility) of gas mixtures entering a gas processing plant from a number of different fields. For this case study it was assumed that the feed gas custody transfer metering package was based on the use of an in-line ultrasonic flow meter, to provide volumetric flow rate data, and a gas chromatograph, to enable density to be calculated from composition. However, depending on which fields are producing, there may be components in the feed gas stream that are not in the 21 component set covered by the AGA 8 method [5,6]. If a number of partners were involved in such a project, it would be important that whatever method was used to determine the gas density, it was accepted by all partners and also by the regulator.

For the five mixtures examined in this case study, phase envelopes were calculated using TUV NEL's PPDS implementation of the Peng-Robinson method and compared with those obtained using the Bochum University implementation of the GERG-2008 method. In addition, for each case the density and compressibility of the gas was calculated at its normal operating temperature and pressure using all three methods, with the AGA 8 values being taken as the reference.

For the first two mixtures, pseudo-components were added to the feed gas compositions by creating PPDS pseudo-components based on representative boiling point, molecular weight and density data.

To examine the impact of components such as hydrogen sulphide and the 'BTEX' components (benzene, toluene, ethyl-benzene and xylene), calculations were done for three variations for each of the five mixtures:

1. H<sub>2</sub>S etc + BTEX all set to representative maximum values,
2. H<sub>2</sub>S etc + BTEX all set to 0.5 x representative maximum values, and
3. H<sub>2</sub>S etc + BTEX all set to 0.

Table 7 shows the input compositions for these three variations for Mixture 1. The compositions for Mixture 2 were broadly similar, the main difference being that the methane content was about two percent lower, with the balance being made up of slightly higher ethane and propane contents. Mixture 3 was mainly methane (96.24 mol% excluding BTEX components) whilst Mixtures 4 and 5 had methane contents of ~66 and ~78 mol% respectively, with most of the remainder of these mixtures being ethane and propane.

Calculations were carried out for the three variations for all five mixtures. For all of the compositions all the components are available within the System Pure databank in TUV NEL's PPDS package or had been created as pseudo-components and hence calculations using the Peng-Robinson model could be undertaken using the input compositions.

When using the AGA 8 and GERG-2008 models it was necessary to assign 'missing' components. Specifically, this relates to the BTEX components, undecane and the pseudo-components. For the BTEX components, the assignments were done in accordance with Table 1 in ISO 12213:2005 [2], as shown in Table 8.

**34<sup>th</sup> International North Sea Flow Measurement Workshop  
25-28 October 2016**

**Technical Paper**

**Table 7 – Case Study 2: Input Compositions for Mixture 1  
(mol %)**

<b>Component</b>	<b>H<sub>2</sub>S etc and BTEX set to max values</b>	<b>H<sub>2</sub>S etc and BTEX set to 0.5 x max values</b>	<b>H<sub>2</sub>S etc and BTEX set to 0</b>
Nitrogen	0.272	0.275	0.279
Methane	87.540	88.660	89.810
Ethane	5.272	5.339	5.409
Propane	2.621	2.655	2.689
i-Butane	0.411	0.416	0.421
n-Butane	0.657	0.666	0.674
i-Pentane	0.217	0.220	0.223
n-Pentane	0.209	0.212	0.215
Hexane	0.067	0.068	0.069
Heptane	0.033	0.033	0.034
Octane	0.013	0.013	0.013
Nonane	0.003	0.003	0.003
Decane	0.001	0.001	0.001
Undecane	0.000	0.000	0.000
PseudoComp1	0.019	0.019	0.019
PseudoComp2	0.081	0.082	0.083
PseudoComp3	0.031	0.031	0.031
PseudoComp4	0.022	0.022	0.022
PseudoComp5	0.004	0.004	0.004
Hydrogen sulphide	1.478	0.748	0.000
Carbon dioxide	0.735	0.372	0.000
Water	0.035	0.018	0.000
Benzene	0.178	0.090	0.000
Toluene	0.075	0.038	0.000
Ethyl benzene	0.013	0.007	0.000
o-Xylene	0.013	0.007	0.000

**Table 8 – Case Study 2: Assignment of Minor Components  
(as per ISO 12213:2005)**

<b>Minor or Trace Component</b>	<b>Assigned to</b>
Benzene	<i>n</i> -pentane
Ethyl-benzene	<i>n</i> -hexane
Xylene	<i>n</i> -hexane
Toluene	<i>n</i> -heptane
Undecane	<i>n</i> -decane

Mixtures 1 and 2 included the pseudo-components. Since neither the AGA 8 nor GERG-2008 methods have defined methods for dealing with such components, three allocation methods were used:

1. to provide a worst case, all the pseudo-components were summed with *n*-decane,
2. to show the effect of ignoring pseudo-components, their compositions were set to zero, and
3. to provide the most realistic case, the pseudo-components were assigned by boiling point, as shown in Table 9.

# 34<sup>th</sup> International North Sea Flow Measurement Workshop 25-28 October 2016

## Technical Paper

**Table 9 – Case Study 2: Assignment of Pseudo-components**

Pseudo-component	Assigned to
PseudoComp1	<i>n</i> - hexane
PseudoComp2	<i>n</i> -hexane
PseudoComp3	<i>n</i> - heptane
PseudoComp4	<i>n</i> -heptane
PseudoComp5	<i>n</i> -octane

### 3.2.1 Effect of assignment of pseudo-components – mixtures 1 and 2.

For both cases the effects of assigning the pseudo-components are significant. For Mixture 1 the density difference between the AGA 8 and GERG-2008 methods changes from -0.52 % to +0.10 % whilst the density difference between the AGA 8 and the Peng-Robinson methods changes from -0.59 % to -0.16 %. The corresponding changes for Mixture 2 are slightly smaller, from -0.09 % to +0.07 % and -0.38 % to -0.09 % respectively, probably due to the slightly lower amounts of the pseudo-components in the Mixture 2 composition.

The effect of totally ignoring the pseudo-components is even more significant. Even taking the most realistic assignment, i.e. by boiling point, shifts of about 1.0 % and 0.7 % are seen for Mixtures 1 and 2 respectively for all three methods. Clearly, if such components are present, they must be accounted for, ideally in the most realistic manner possible. Although the AGA 8 and GERG-2008 methods do not explicitly include assignments for such components, since the shifts in density observed for all three models were consistent, assignment by boiling point would appear to be the best approach. However, this recommendation must be treated with some caution, since the amounts of the pseudo-components in these mixtures were relatively small.

The extreme effect of assigning the pseudo-components to *n*-decane for the GERG-2008 method on the phase envelopes can be seen by comparing Figures 3 and 4. For each sub-set within a case, the solid and dashed curves for each colour compare the phase envelopes calculated by the GERG-2008 and Peng-Robinson methods respectively.

For the base case (the green curves), the phase envelopes calculated by the two methods are fairly similar. As expected, adding the pseudo-components increases the size of the two phase region, moving the cricondbar to higher pressure and the cricondtherm to higher temperature. However, the shifts are very much more significant when the pseudo-components are assigned to *n*-decane rather than being assigned by boiling point, e.g. comparing the solid red curves in Figures 3 and 4 shows that the cricondbar has increased from about 115 bar(a) to over 140 bar(a). Similar effects were seen for Mixture 2.

Technical Paper

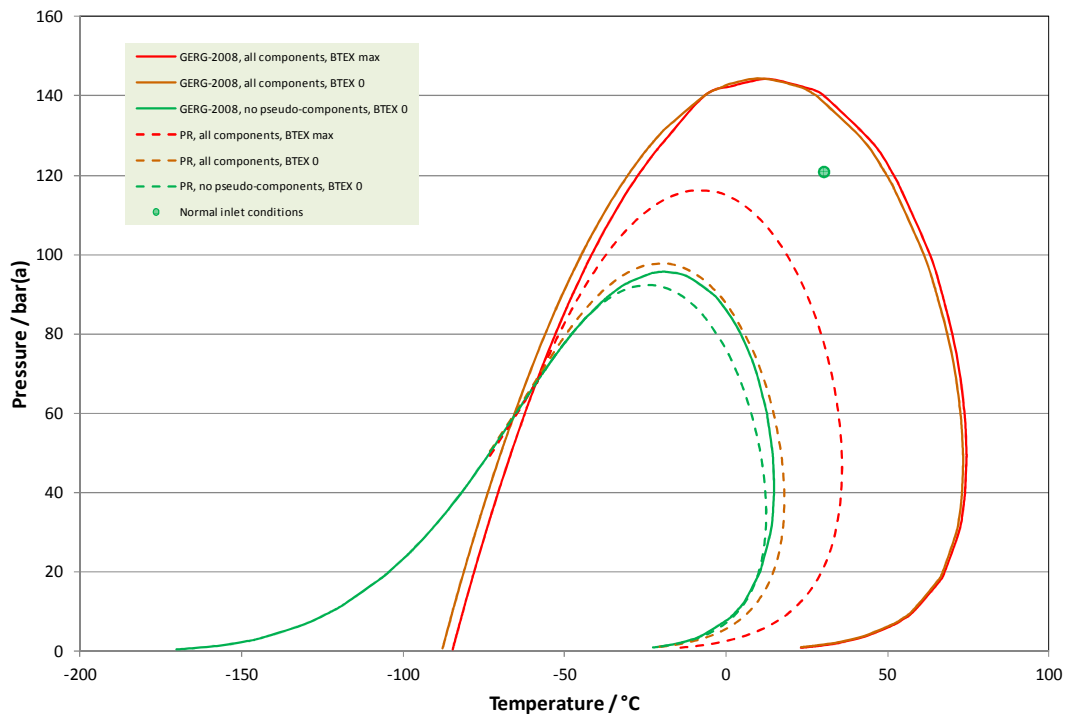


Fig. 3 – Case Study 2: Phase Envelopes for Mixture 1:  
Pseudo-components Assigned to C<sub>10</sub>

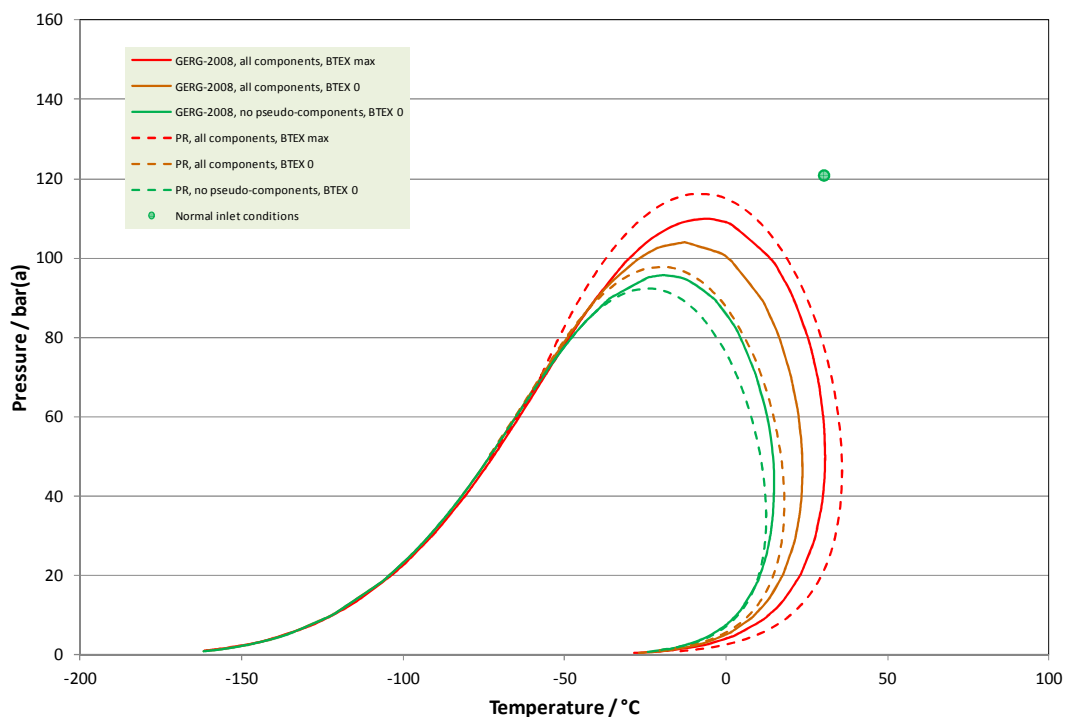


Fig. 4 – Case Study 2: Phase Envelopes for Mixture 1:  
Pseudo-components Assigned by Boiling Point

# 34<sup>th</sup> International North Sea Flow Measurement Workshop 25-28 October 2016

## Technical Paper

### 3.2.2 Effects of other minor components – mixtures 3 to 5.

Although there are none of the pseudo-components present in the compositions for Mixtures 3 to 5, the effects of the other minor components can be clearly seen on the calculated densities and phase envelopes.

Since Mixture 3 is mainly methane (96.24 mol% excluding BTEX components), all the other components are essentially minor components, so significantly altering any of them will have a large effect. For all three methods, the differences in density between setting the H<sub>2</sub>S etc and BTEX component compositions to their maximum values or to zero causes changes in density of between 5.8 % and 6.2 %. This also results in significant shifts in the calculated phase envelopes, as shown in Figure 5, resulting in much larger two-phase regions and shifts in the cricondbar and cricondtherm.

An apparent anomaly in the performance of the GERG-2008 and Peng-Robinson methods with regard to the effects of the minor components on the phase envelope and calculated densities is worth examining, as it illustrates some of the difficulties inherent in undertaking such calculations.

For Mixture 3, when all the minor components are set to their maximum concentrations, the densities calculated by the GERG-2008 and Peng-Robinson methods are in close agreement (89.210 and 89.205 kgm<sup>-3</sup> respectively, i.e. less than 0.1 %) even though the calculated phase envelopes are quite different. On the other hand, when all the minor components are set to zero, although the calculated phase envelopes are similar, the calculated densities differ by 0.36 % (84.301 and 83.998 kgm<sup>-3</sup> for the GERG-2008 and Peng-Robinson methods respectively).

These differences are believed to arise from the method of calculating the density. With both methods, the equation of state is solved at the specified conditions to determine the phase split and the phase compositions, based on the input compositions. In the GERG 2008 method the equation of state is also used to directly calculate the density. PPDS can also operate in this mode ('Consistent') but due to the known limitations of simple cubic equations of state, there is also an option to operate in 'Accurate' mode, in which the properties required are calculated by equations chosen to provide better representations of the those properties. Throughout this work PPDS was used in 'Accurate' mode, meaning that densities were calculated by applying a Lee-Kesler correction from the density calculated by the equation of state at the phase boundary to the required conditions.

For Mixture 3, the differences in the calculated phase boundaries between the GERG-2008 and Peng-Robinson methods when all the minor components are set to their maximum values reflects the differences in the BIPs used by the two methods for these minor components. The significant shift in the position of the phase boundary between the two extreme sub-cases (all minor components set to zero or set to maximum values) as calculated by the Peng-Robinson method makes a big difference in the magnitude of the correction applied by the PPDS calculation for the density. This is the likely origin of the apparent anomaly with regard to the performance of the two methods and clearly illustrates the importance of understanding the calculation methods in sufficient detail to explain such discrepancies. With PPDS, the user has full control over the calculation modes and all the key parameters (including BIPs) and the package also provides quality codes that provide information on corrections applied.

Technical Paper

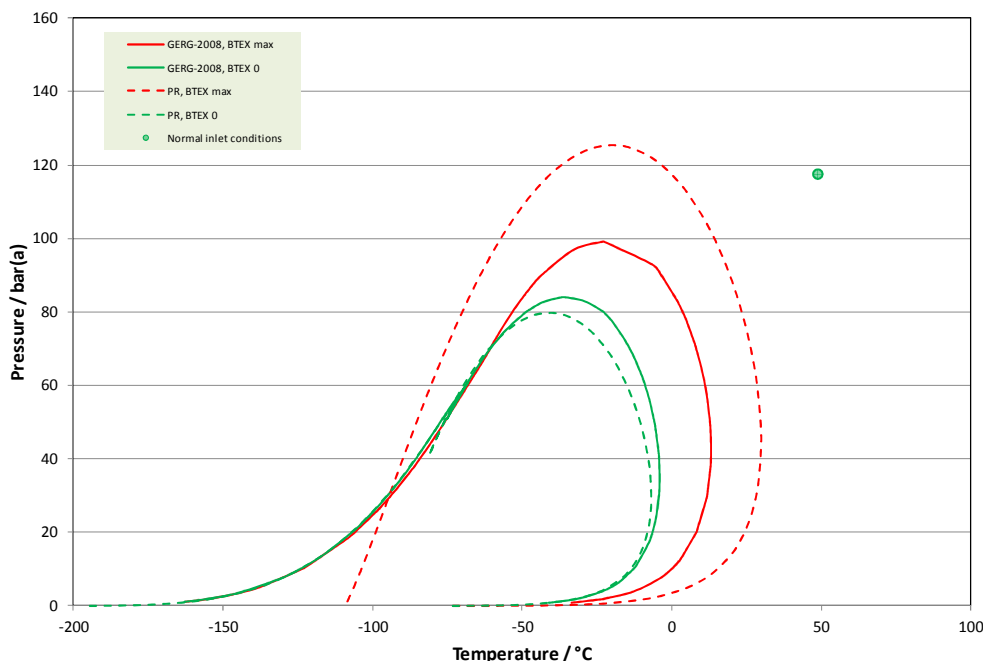


Figure 5 – Case Study 2: Phase Envelopes for Mixture 3

For Mixtures 4 and 5 the methane content is much lower than for the other three cases. For Mixture 4 it is actually below the normal limit for the AGA 8 method (70 mol%) and although it is within the extended range (down to 50 mol%), the propane content (almost 14 mol%) is significantly above even the extended limit (5.0 mol%). For Mixture 5, although the propane content is just above the extended limit (5.2 mol%), the butanes content (3.0 mol%) is double the limit (1.5 mol%). Not surprisingly, this leads to significant differences in the densities calculated by the three methods but, as with the first three cases, the trends are not immediately obvious.

For both cases, ignoring the minor components causes the calculated densities to change by between 3.3 % and 4.7 % from the values when all the components are set to their maximum values. The most extreme effects are seen with Mixture 4, where the density difference between the AGA 8 and GERG 2008 methods changes from -0.79 % to -0.63 % while the density difference between the AGA 8 and Peng-Robinson methods changes from +0.59 % to -0.12 %, again indicating the sensitivity of the properties to BIPs and calculation modes. For Mixture 5 the corresponding shifts are from -0.20 % to -0.12 % for the AGA 8 / GERG-2008 differences and from +0.44 % to -0.10 % for the AGA 8 / Peng-Robinson differences.

In contrast to Mixture 3 however, the shifts in the phase boundaries for Mixtures 4 and 5 are much less significant when the BTEX components are ignored, as shown in Figures 6 and 7.

Technical Paper

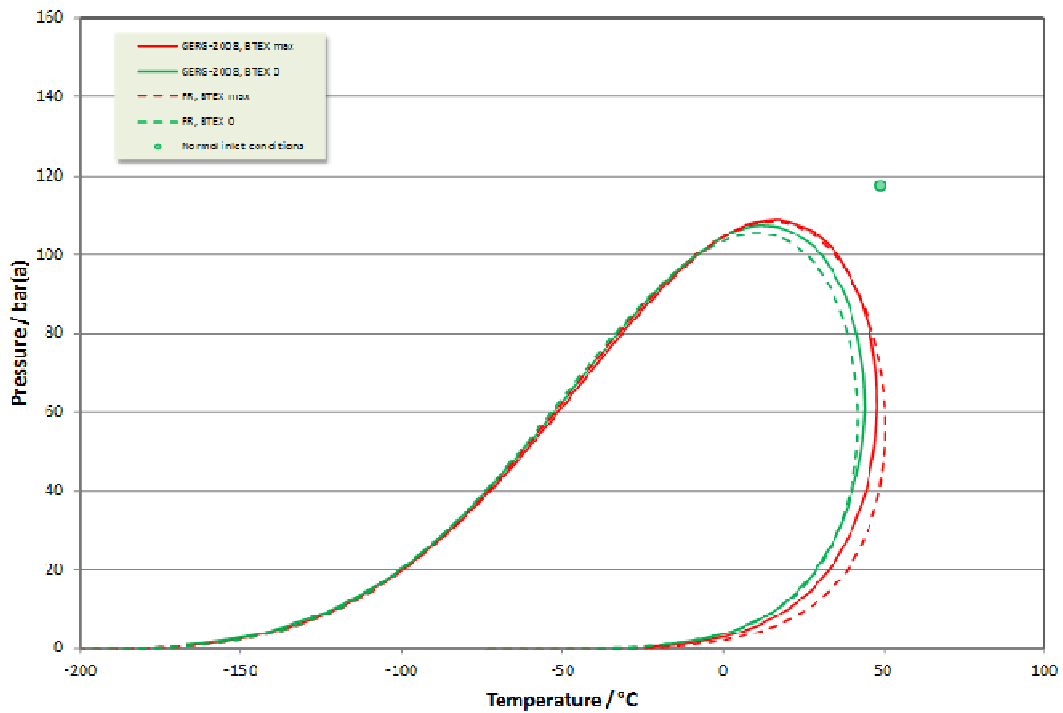


Figure 6 – Case Study 2: Phase Envelopes for Mixture 4

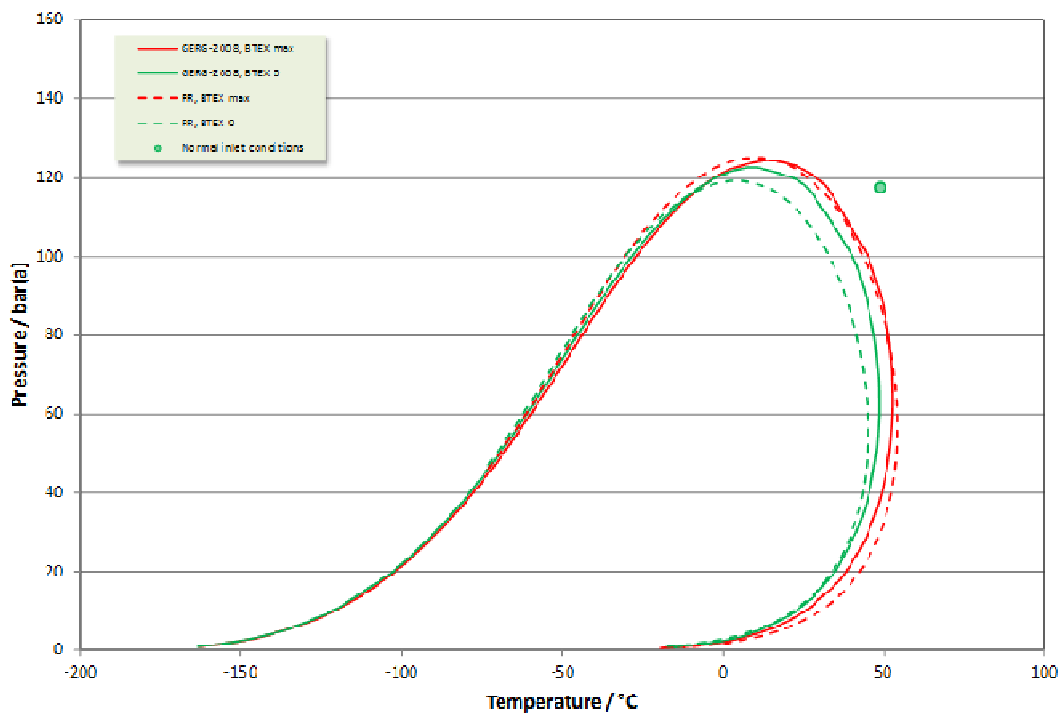


Figure 7 – Case Study 2: Phase Envelopes for Mixture 5

# 34<sup>th</sup> International North Sea Flow Measurement Workshop 25-28 October 2016

## Technical Paper

### 4 CONCLUSIONS

If all the components are within the specified composition ranges for pipeline quality gas, densities calculated using the AGA 8 method are claimed to have an uncertainty of 0.1 % (at  $k=2$ ) for temperatures between -10 and 65°C at pressures up to 120 bar(a). However, for mixtures with components in the extended composition range and / or at temperatures and pressures outside the standard limits, the uncertainty increases to between 0.2 and 0.5 % (at  $k=2$ ) and is effectively indeterminate for compositions outside the extended range of applicability. Comparison with values calculated using the GERG-2008 method generally confirms these claims. However, even for compositions that are within the extended AGA 8 range, the differences can exceed 1 % and the effect of ignoring pseudo-components or components not in the 21-component data set can cause differences of over 5 %.

Given the known limitations of the AGA 8 method and the lack of clarity of the likely uncertainties in calculated densities and compressibilities when used in its extended range, the use of an alternative method would be preferable.

Although the GERG-2008 method still has the same 21-component data set as the AGA-8 method, it is claimed to retain its uncertainty (0.1 %) over a much wider range of compositions. However, it is of course important that all minor and trace components are accounted for to ensure uncertainties are minimised and measurements are as accurate as possible. This is successfully achieved by assigning them by boiling point to the corresponding component in the data set. To increase accuracy, this should also be done for pseudo-components known to be present. However, this recommendation must be treated with some caution, as it has only been tested for mixtures with relatively small amounts of pseudo-components so far.

A further problem is that of ensuring that all the components in the gas stream are measured. This is because the majority of on-line gas chromatographs only discriminate hydrocarbons up to heptanes ( $C_7$ ), although some newer models are now able to discriminate up to undecane ( $C_{11}$ ), with all higher hydrocarbons being lumped in with the highest carbon number discriminated. Although the total amounts of higher hydrocarbons may be small, as with pseudo-components, even this can cause percentage errors in calculated properties. Furthermore, additional sensors are also necessary to allow for components such as hydrogen sulphide and carbon dioxide.

One solution to this is sampling and off-line analysis, which can provide much more detailed compositional information. However, this method is obviously not capable of providing real-time information for input to a flow computer. In addition, obtaining representative samples and ensuring that they do not change composition (due to flashing of high volatile components) presents significant challenges and potential safety risks.

Furthermore, it is not possible to simply assume that ignoring one component in a mixture will always have the same effect on the calculated properties as the error will depend on the temperature and pressure of the mixture and how far those conditions are from the phase boundary, with positive or negative errors being possible. This significantly complicates the application of corrections to on-line calculations of gas properties based on off-line analysis of samples, particularly for systems where conditions change on a frequent basis.

# 34<sup>th</sup> International North Sea Flow Measurement Workshop 25-28 October 2016

## Technical Paper

However, these issues must be addressed when dealing with gas fields whose compositions are outside the pipeline quality gas specification required by the AGA 8 method, as the potential financial exposure can run to hundreds of millions of dollars per annum for a region such as the North Sea.

### 5 REFERENCES

- [1] Guidance Notes for Petroleum Measurement, Issue 9.2. Oil and Gas Authority, Aberdeen, October 2015.
- [2] Peng, D.J. and Robinson, D.B. A New Two-Constant Equation-of-state. *Ind. Eng. Chem. Fundam.* **15**, 59-64, 1976.
- [3] Soave G. Equilibrium Constants for Modified Redlich-Kwong Equation-of-state. *Chem. Eng. Sci.* **27**, 1196-1203, 1972.
- [4] Lee, B.I. and Kesler, M.G. A Generalized Thermodynamic Correlation based on Three-parameter Corresponding States. *AIChE J.* **21**, 510-527, 1971.
- [5] Starling, K.E. and Savidge, J.L. Compressibility Factors of Natural Gas and Other Related Hydrocarbon Gases. Transmission Measurement Committee Report No.8, American Gas Association (1515 Wilson Boulevard, Arlington, Virginia 22209, USA), 2<sup>nd</sup> Edition, November, 1992.
- [6] BS EN ISO 12213-2:2005 Natural gas - Calculation of compression factor - Part2: Calculation using molar-composition analysis. BSI, London.
- [7] Zunz, O., Klimeck, R., Wagner, W., and Jaescke, M. The GERG-2004 Wide-Range Equation of State for Natural Gases and Other Mixtures. GERG Technical Monograph 15 and Fortschr.-Ber. VDI, Reihe 6, Nr. 557, VDI Verlag, Düsseldorf, 2007.
- [8] Kunz, O. and Wagner, W. The GERG-2008 Wide-Range Equation of State for Natural Gases and Other Mixtures: An Expansion of GERG-2004. *J. Chem. Eng. Data*, **57** (11), 3032-3091, 2012.
- [9] ISO 20765-2:2015 Natural gas -- Calculation of thermodynamic properties -- Part 2: Single-phase properties (gas, liquid, and dense fluid) for extended ranges of application.
- [10] Hankinson, R. W. and Thomson, G. H. A New Correlation for Saturated Densities of Liquids and Their Mixtures. *AIChE Journal* **25** (4): 653-663, 1979.

## Technical Paper

**Venturi vs. Ultrasonic Meter Comparisons  
– The Heretical Unauthorized Version**Richard Steven, CEESI  
Gary Fish, Solartron ISA**1 INTRODUCTION**

Industry has a wealth of experience with Venturi Differential Pressure (DP) meters (e.g. see Fig. 1). Used for over a century their physical principles of flow measurement are fundamental, well understood, reliable and *beautifully* simple. The development of the popular Venturi meter technology has kept pace with competing flow meter technologies. However, there has been virtually no marketing of Venturi meters in the last twenty years. This has resulted in widespread Venturi meter performance misperceptions. The highly competitive modern Venturi meter performance specifications are hidden in plain sight, described clearly in standards, manuals and text books for the few that care to look, but they are seldom directly compared to competing technologies. Venturi meters are therefore seen falsely by many as old stagnant technology.



Fig. 1 - Venturi Meter



Fig. 2 - Ultrasonic Meter

Industry now has extensive experience with ultrasonic meters, or 'USMs', (e.g. see Fig. 2). Available for more than a quarter of a century their highly competitive performance specifications are well known through years of extensive marketing by multiple corporations. They have been marketed as offering many potential benefits over more traditional flow meters, such as Venturi meters, with three key specifications being:

- a low flow rate prediction uncertainty
- a high turndown (while maintaining a low permanent pressure loss)
- an excellent diagnostic / meter verification ability.

The ultrasonic meter is a marketing triumph as well as a technical achievement. Ultrasonic meters are therefore seen by many as the *obvious* future of flow meter technology. With no significant rebuttal of these claimed performance advantages they have slowly become accepted as axioms, as self-evident truths responsible for the often heard phrase "... we are upgrading our DP meter to an ultrasonic meter". To question this widely believed metering doctrine (i.e. dogma) by requesting technical proof, is becoming 'metering heresy'. However, there is a problem. A technical review shows that none of these claimed ultrasonic meter advantages over the modern Venturi meter are actually true.

Although USM proponents may view it as such, this paper is **not** meant to be an attack on ultrasonic meters. The authors generally agree with most of the

# 34<sup>th</sup> International North Sea Flow Measurement Workshop 25-28 October 2016

## Technical Paper

impressive ultrasonic meter performance specifications. The issue is that the modern Venturi meter performance specifications *are just as impressive*. It is the *marketing claims* of the ultrasonic meter superiority that is being questioned. In this paper the modern Venturi & ultrasonic meter specifications are compared. Using mathematics, hydraulic theory, standards, published manufacturer manuals, and 3<sup>rd</sup> party end user papers the results and conclusions will likely surprise many. Considering the very different physical principles on which these flow meters are based the equally good Venturi & ultrasonic meter performance specifications are *remarkably* similar.

## 2 ULTRASONIC & VENTURI METER FLOW RATE UNCERTAINTIES

Gas flow must ultimately be metered by mass flow<sup>1</sup> (e.g. kg/hr, MMSCFD<sup>2</sup> etc.). A gas mass flow rate reading is an absolute statement on the quantity of gas flowing in a pipeline. A volume flow rate reading is not. Gas volume flow and gas density both change with the local thermodynamic (i.e. pressure & temperature) conditions, and hence a volume meter's volume flow rate prediction is only applicable at the meter. Therefore, most gas meter designs (ultrasonic & Venturi meters inclusive) require an independent gas density prediction to be available (and trustworthy) at the meter location. Many volume flow meter's ambiguous 'flow rate' prediction uncertainty statements are volume based. This can be confusing, or even misleading. The required mass flow rate prediction uncertainty is higher and often not stated.

A typical generic flow meter's *mass* flow rate prediction uncertainty (ultrasonic & Venturi meter inclusive) is  $\leq 0.7\%$ . This may seem *very* high to many, but this is reality. The reader may be used to hearing that an ultrasonic meter has "a gas flow rate uncertainty  $< 0.2\%$ " but this is a marketing idealised velocity / volume flow rate prediction uncertainty quote, not the actual required mass flow rate uncertainty of most meters in the field.

"There is a lot of uncertainty about uncertainty". Industry follows guidelines laid down by documents such as ISO 5168 [1]. These guidelines advise that an uncertainty analysis should consist of the following steps:

- a) establish a mathematical model for the measurement process
- b) list & qualify the contributory variances
- c) combine variances into a composite statement of uncertainty

While there is agreement on these generic steps, in practice for each specific scenario there is usually debate over what contributory factors need be considered, what the variance of these factors are, and how to mathematically combine inter-connected contributory factors. Such is the case with published flow meter mass flow rate uncertainty calculations. For example, AGA 9 [2] & ISO 17089 [3] both offer worked examples of ultrasonic meter flow rate uncertainty. They have some differences in what contributory variances to include (ISO 5168 part b), and how to combine the variances (ISO 5168 part c). This is typical of flow meter flow rate prediction uncertainty calculations. They are all to an extent debatable and difficult to prove.

---

<sup>1</sup> Strictly speaking natural gas must ultimately be metered by energy content which is achieved by combining mass (*not* volume) flow and gas composition information.

<sup>2</sup> Million standard cubic feet per day (MMSCFD) is a volume of gas at a defined density. Therefore, although MMSCFD superficially looks like a volume flow rate unit it is actually a mass flow rate unit.

# 34<sup>th</sup> International North Sea Flow Measurement Workshop 25-28 October 2016

## Technical Paper

Ultrasonic and Venturi meters operate according to very different physical principles. As such their respective uncertainty calculations are quite different, each containing contributory factors only relevant to their own respective uncertainty calculations. Hence, it is difficult to directly compare these uncertainty calculations. It is practically only possible to compare the final output, and there will always be scope for debate regardless of what respective assumptions are used in each meter's uncertainty calculation.

This paper is not dedicated to detailed discussion of ultrasonic & Venturi meter uncertainty calculations. As such, with limited space the authors have chosen to take ISO 17089 Section 7.7 and the orifice meter API 14.3.1 (modified for Venturi meters<sup>3</sup>) as sample uncertainty calculations to be discussed. On such a potentially contentious subject these choices seemed as open and transparent as any.

The aim of this exercise is not to argue over tenths of a percent uncertainties. It is to show that the actual mass flow rate uncertainty predictions of ultrasonic and Venturi meters are remarkably similar.

### 2a. Ultrasonic Meter Mass Flow Rate Prediction Uncertainty

The multipath ultrasonic meter mass flow rate ( $Q_m$ ) calculation is shown as equation 1.

$$Q_m = \rho Q_v = \rho A V_{av} = \rho K A \sum_{i=1}^n W_i V_i \quad \text{-- (1)}$$

Note:

- $Q_m$  - mass flow rate (kg/s)
- $Q_v$  - volume flow rate (m<sup>3</sup>/s)
- $A$  - inlet area to the meter, i.e.  $A = (\pi/4)D^2$  (m<sup>2</sup>)
- $\rho$  - fluid density (kg/m<sup>3</sup>)
- $V_{av}$  - average flow velocity (m/s)
- $K$  - meter factor (from calibration)
- $n$  - no. of paths
- $W_i$  - weighting factor for path 'i'
- $V_i$  - measured velocity across path 'i' (m/s)

The average flow velocity ( $V_{av}$ ) is predicted by the sum of the products of the individual measured path velocities ( $V_i$ ) and their corresponding weighting factors ( $W_i$ ). ISO 17089 Section 7.3.3.5 states "... $W_i$  to  $W_n$ , are determined on the basis of documented *numerical integration methods*." Hence, as with all flow meters, Venturi meter inclusive, the actual mass flow rate calculation routine of an ultrasonic meter is complicated relative to the average training of the typical end user. Thankfully, nowadays the complexity of flow meter calculation routines are embedded in the flow computer and the average end user (and even the calibration lab) never has to worry about such detail. However, Equation 1 is shown here to help make sense of the following uncertainty discussion.

Stating that the ultrasonic meter mass flow rate prediction uncertainty is in the order of 0.7% is not the author's opinions, but away from marketing claims, it is published industry wisdom. ISO 17089 [3] Section 7.7 shows two different ultrasonic meter *volume* flow rate uncertainty examples using different scenarios and assumptions. The contributory variances considered by ISO are:

---

<sup>3</sup> Considering the long term popularity of the Venturi meter it is curious that unlike ultrasonic & orifice DP meters there are no well-known standard board's Venturi meter flow rate uncertainty calculation examples.

# 34<sup>th</sup> International North Sea Flow Measurement Workshop 25-28 October 2016

## Technical Paper

- the reproducibility of the USM as specified by the manufacturer (including all intrinsic factors but excluding the calibration)
- the uncertainty of the calibration facility
- installation effects
- data fitting / calibration curve uncertainty
- other extrinsic factors.

**Table 1 - Various Ultrasonic Meter Mass Flow Rate Uncertainty Calculations**

contributory variances	Sensitivity Coeff	ISO 17089 example 1	ISO 17089 example 2	Authors moderate example 3
reproducibility	1	0.2	0.3	0.25
calibration facility uncertainty	1	0.2	0.3	0.23
installation influences	1	0	0.3	0.3
calibration data 'K' fitting	1	0	0.3	0.2
handling (other extrinsic factors)	1	0.1	0.1	0.1
RSS % volume flow uncertainty	N/A	<b>0.300</b>	<b>0.608</b>	<b>0.505</b>
Independent Density uncertainty	1	0.4	0.4	0.4
RSS % mass flow uncertainty	N/A	<b>0.500</b>	<b>0.728</b>	<b>0.645</b>

Table 1 shows the two ISO 17089 volume flow rate uncertainty calculations, with the addition of a 3<sup>rd</sup> moderate example by these authors. ISO consider the reproducibility of an USM to be practically between 0.2 & 0.3% (see examples 1 & 2). Hence the authors consider a reasonable compromise to be 0.25%.

All gas flow calibration facilities have inherent reference uncertainties. As with flow meters, calibration laboratories are in competition to quote ever lower reference uncertainties. However, in practice most industrial grade calibration facilities have mass flow rate prediction uncertainties > 0.25%. In 2010 Zanker et al [4] commented of such facilities: "These have typical uncertainties of 0.2% to 0.3%, so it is difficult [for USMs] to achieve higher absolute accuracies", and "... the product cannot have a stated uncertainty that is better than the laboratory". CEESI Iowa, a leading natural gas flow meter calibration facility, quotes a reference volume flow rate prediction uncertainty as 0.23%. This practical value has therefore been used in the author's example.

AGA 9's [2] Section 7.2.2<sup>4</sup> on installations states that the meter manufacturer should specify the maximum allowable disturbance "...that will not create an additional flow rate measurement error of more than 0.3% due to the installation configuration." It goes on to say: "This recommendation shall be supported by test data" (i.e. 'type testing'). ISO 17089's [3] Section 5.9.3.2 states that the minimum straight upstream pipe length required for the USM to have a maximum additional error due to flow perturbations of 0.3% should be stated. Such is the USM sensitivity to disturbances (i.e. shifts in the velocity profile) that Chan et al [5] state "Operators have to increase their awareness over profile parameters and its influence on [ultrasonic] flowmeter performance." It is advised by AGA & ISO that an USM be calibrated with the upstream & downstream spools in place, with the strong recommendation that the flow conditioner being kept installed in the

<sup>4</sup> At the time of writing, it is being proposed by the AGA9 technical committee that this explicit statement in the main text of AG9 Ed 1 be demoted to an implicit statement in the Appendices in AGA 9 Ed 2. Nevertheless, regardless of this less prominent position in the text, this does not change the fact that USMs should have 0.3% added to their flow rate prediction uncertainties to account for velocity profile differences between calibration and field installations.

# 34<sup>th</sup> International North Sea Flow Measurement Workshop 25-28 October 2016

## Technical Paper

same orientation as that of the calibration. Even so various piping configurations upstream of this inlet run & flow conditioner can cause shifts in USM performance, hence the 0.3% additional uncertainty advised by AGA & ISO. This is commented on by Chan [5]: "Even calibrating the [ultrasonic] meter with up/downstream pipe spools and a flow conditioner may not solve the problem, as the profile entering the spool is different between calibration and on-site." Chan goes on to say that "Any non-compensated profile anomaly will result in [an USM] systematic [flowrate] mis-measurement." Chan also states that "Operators need to resist the urge to think of the ISO 17089 type test as a guarantee that the [USM] flowmeter performs under all upstream configurations."

As such manufacturers, AGA9 & ISO 17089 state that the USM can be calibrated for any pipework configuration, and in that scenario there would be *no* additional installation uncertainty. However, it is important to realize that this is not a statement / quality specific to ultrasonic meters. The same is true for other flow meters, *inclusive* of the Venturi meter. But, as special pipework configuration calibrations are not the norm for any meter type, USM & Venturi meter inclusive, the authors consider it not representative of the vast majority of cases to ignore the 0.3% installation effect for USMs on the premise that it *could* be (at least partially) calibrated out. It usually is *not* calibrated out. It is therefore fair and representative to keep the 0.3% installation uncertainty component in the generic moderate USM flow rate uncertainty example in Table 1.

The most common method of curve fitting (i.e. 'linearizing') both USM & Venturi meter calibration data is almost certainly "piece-wise linear interpolation". This means fitting a linear line to bridge the unknown between two adjacent calibration points. Figure 3 shows an example of such a practice. This figure uses hypothetical USM data as copied from a hypothetical sample data set given in AGA 9 Section 5.1.2. The piece-wise linear interpolation is shown. This 'data fit' technique (also used for Venturi meters) *by definition* produces a result that appears to have no residual error. However, it is only an *illusion* of no error.

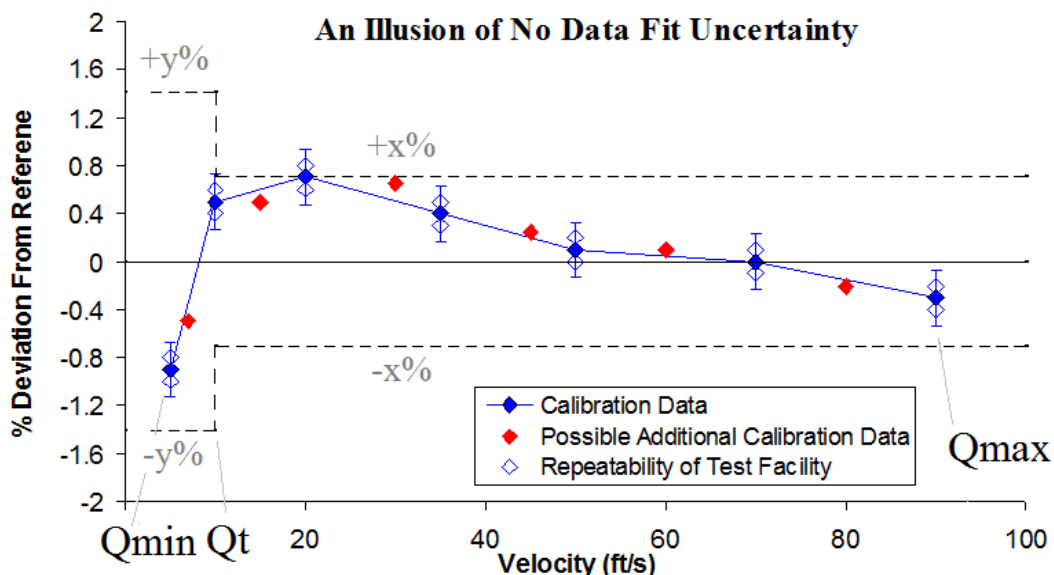


Fig. 3 - Hypothetical Example of Piece-Wise Linear Interpolation

Along with reputable gas flow calibration facilities having a flow reference uncertainty (in the order of 0.25% as indicated by the error bands in Figure 3), they also have a repeatability in the order of  $\leq 0.1\%$ . Such repeat points are indicated in Figure 3. (These are slightly simplified, in reality repeat points have

# 34<sup>th</sup> International North Sea Flow Measurement Workshop 25-28 October 2016

## Technical Paper

repeatability variances in the x & y axes.) The linear fits tend to be between either single points or averages of repeat points, and hence these have an inherent uncertainty of 0.1%. Linear interpolation is defined<sup>5</sup> as "... *an estimation* of a function by *assuming* a straight line between known values". The premise of the linear fits is that when the meter is operated between calibration points the meter performance can be *estimated* by *assuming* the performance falls on this linear line. In reality it is likely to be close to the line, but it is not realistic to assume it will always be on the line. Therefore, it is not realistic to claim that after data fitting a flow meter has no calibration uncertainty (see Table 1 Example 1). When considering the calibration facility repeatability and the limitations of the piece-wise linear interpolation technique, the authors think a calibration data fit uncertainty of 0.2% is realistic and fair (see Table 1 Example 3).

In order to predict the required mass flow rate USMs, like Venturi meters, depend on the gas density being supplied by an independent source. These meter's mass flow rate prediction uncertainty is *wholly* dependent on the gas density uncertainty. ISO 17089's USM examples only predict volume flow prediction uncertainty. The extension to the required mass flow in Table 1 is added by these authors. The density prediction usually comes from a gas chromatograph (GC), with a pressure & temperature reading, & an equation of state / 'PVT' software package (usually AGA8 [6] or GERG [7]). Unfortunately, gas density uncertainty is not widely published or discussed.

API 14.3 [8] suggests this independent gas density prediction has an uncertainty of 0.6%. However, this is undoubtedly a conservative estimate based on obsolete instrumentation and methods. Modern systems should perform better than this. Gas density is calculated by equation 2, where P is the pressure, T is the temperature, R is the universal gas constant, m is the gas molecular weight, and Z is the gas compressibility factor, itself a function of gas composition and the pressure & temperature.

$$\rho = \frac{mP}{ZRT} \quad (2)$$

AGA 9 Appendix E suggests that reasonable pressure & temperature reading uncertainties are 0.1% & 0.17% at  $\sigma = 1$  respectively. That is 0.2% & 0.34% at  $\sigma = 2$  respectively. Ifft [9] uses a pressure transmitter manual to give an uncertainty example that approximately agrees with this AGA estimate. For a known molecular weight the gas constant is known to an extremely low uncertainty, so practically compressibility is the final component in gas density prediction uncertainty. AGA 9 suggests that compressibility uncertainty is 0.05% to  $k=1$ , so 0.1% for  $k=2$ . Therefore, the root sum square of the pressure, temperature, & compressibility uncertainties shows that AGA 9 is effectively saying gas density uncertainty is approximately 0.4% at 95% confidence. This is a realistic uncertainty for best practice gas density measurements in the field.

As with *all* flow meter designs the uncertainty of the mass flow rate prediction of an ultrasonic meter is subjective, i.e. dependent on the assumptions made. ISO 17089 gives two examples with different scenarios / assumptions. Through reasoning described above it is seen that the first example is rather optimistic, while the second is rather pessimistic. The authors have argued (not surprisingly) that reality is between these extremes, and a fair and honest ultrasonic gas meter volume flow rate is 0.49% (i.e. approximately 0.5%) and an associated mass flow rate uncertainty specification of 0.645% (i.e. approximately 0.65%).

---

<sup>5</sup> Merriam-Webster Dictionary

# 34<sup>th</sup> International North Sea Flow Measurement Workshop 25-28 October 2016

## Technical Paper

### 2b. Venturi Meter Mass Flow Rate Prediction Uncertainty

The Venturi meter is a generic DP meter that measures mass flow rate like all DP meters, i.e. by the simple and reliable method of cross-referencing the physical laws of conservation of mass and energy. The Venturi meter uses the generic DP meter mass flow equation set (see equations 3 thru 6). Note equation 3 is ISO 5167-4 2003 equation 1, and the form of equation 6 is shown by ISO 5167-4 2003 equation 2.

$$Q_m = \frac{C_d}{\sqrt{1-\beta^4}} \varepsilon \frac{\pi}{4} d^2 \sqrt{2\rho\Delta P} \quad (3)$$

$$\beta = \frac{d}{D} \quad (4)$$

$$\tau = 1 - \frac{\Delta P}{P_1} \quad (5)$$

$$\varepsilon = f(\beta, \kappa, \tau) \quad (6)$$

Note:

- $Q_m$  - mass flow rate (kg/s)
- $\beta$  - beta, i.e. diameter ratio, see equation 4
- $D$  - inlet diameter (m)
- $d$  - Venturi throat bore (m)
- $\varepsilon$  - expansibility, alternatively denoted by 'Y', unity for liquids
- $C_d$  - discharge coefficient,
- $k$  - isentropic exponent of the fluid (-)
- $\tau$  - ratio of Venturi throat to inlet pressure
- $\rho$  - fluid density (kg/m<sup>3</sup>)
- $P_1$  - inlet pressure (Pa)
- $\Delta P$  - differential pressure between inlet and throat (Pa).

The following flow rate prediction uncertainty discussion is based on the API 14.3 orifice meter example modified to be applicable to Venturi meters. The contributory variances to a Venturi meter's uncertainty are:

- uncertainty of the calibration facility
- uncertainty in the expansibility
- data fitting / calibration curve uncertainty
- uncertainty in the independent density prediction
- uncertainty in the DP primary signal reading
- installation effects

**Table 2 - Sample Venturi Meter Mass Flow Rate Uncertainty Calculation**

contributory variances	Uncertainty (U <sub>95%</sub> )	Sensitivity Coefficient	(U <sub>95%</sub> S) <sup>2</sup>
calibration facility uncertainty	0.23	1	0.053
calibration data 'C <sub>d</sub> ' fitting	0.2	1	0.040
Expansibility (ε)	0.2	1	0.040
Density (ρ)	0.4	0.5	0.040
DP reading (ΔP)	1.0	0.5	0.250
Sum of Squares			0.423
% Mass Flow Rate Uncertainty			<b>0.65</b>

# 34<sup>th</sup> International North Sea Flow Measurement Workshop 25-28 October 2016

## Technical Paper

There are differences between the USM & Venturi meter contributory variances. Some differences are only apparent, others are real. This is a consequence of comparing meter designs that work on different physical principles.

Like ultrasonic meters, Venturi meters should be calibrated. Like an USM's inlet area measurement, the Venturi meter geometry measurement uncertainties are systematic uncertainties that are accounted for in the calibration's discharge coefficient uncertainty. Venturi meters are calibrated in the same facilities as USMs. Hence the calibration facility uncertainty is the same, i.e. say 0.23%. Likewise, Venturi meters rely on the same independent density prediction as USMs, and hence the gas density uncertainty is the same, i.e. 0.4%.

The Venturi meter expansibility ( $\epsilon$ ) uncertainty ( $U_\epsilon$ ) is quoted by ISO 5167-4 [10] as calculated by equation 7:

$$U_\epsilon = \left(4 + 100\beta^8\right) \frac{\Delta P_t}{P} \% \quad (7)$$

The uncertainty in the Venturi meter's expansibility is obviously case dependent. Table 3 shows a small sample of expansibility uncertainties. The worst expansibility uncertainties occur with a combination of high beta, low pressure, and high DP. For example, a high  $0.7\beta$  at 25 Bar and a high DP of 1 bar / 400"WC would have an expansibility uncertainty of 0.39%. However, *Venturi meter designers are of course aware of this*, and a geometry is chosen to minimise such increase in uncertainties. In most high pressure, high flow rate, high monetary value natural gas flows expansibility uncertainty is not a significant handicap. Table 3 shows that the mid-beta Venturi meter ( $0.55\beta$ ) at a relatively low production or transmission pressure of 25 Bar while at a relatively high DP of 1 bar / 400"WC has an ISO predicted expansibility uncertainty of 0.19%. This is typical of the expansibility uncertainty in the field, and 0.2% is used as a reasonable estimate in the uncertainty calculation in Table 2.

**Table 3 - Sample Venturi Meter Expansibility Uncertainties**

Beta	0.4	0.4	0.6	0.6	0.7	0.7	0.55	0.55
DP (Bar)	1	0.25	1	0.25	1	0.25	1	0.25
P (Bar)	25	100	25	100	25	100	25	100
U exp	0.163	0.010	0.227	0.014	0.391	0.024	0.193	0.012

Some Venturi meter manufacturers (and end users) can and do play the same specmanship<sup>6</sup> games as USM manufacturers (and end users). As with USMs, "piece-wise linear interpolation" is a common way of data fitting Venturi meter  $C_d$  vs. Reynolds number data. This suffers the same issues as with the USM. Figure 4 shows a Solartron ISA ISO compliant 6",  $0.4\beta$  Venturi meter during calibration. Figure 5 shows the resulting real data. The repeat points are shown as hollow diamonds. The average results are shown as solid squares with the linear fits. The triangles show hypothetical points between the real data added by the authors. The error bars show the 0.1% repeatability of the test facility. Again, as with the USM, a reasonable data fit uncertainty for the Venturi meter is therefore 0.2%.

It could be argued that the Venturi meter DP reading uncertainty is equivalent to the USM reproducibility uncertainty. Figure 5 shows that each  $C_d$  vs. Re point (solid square) is an average of a set of repeat points (hollow diamonds). This data

<sup>6</sup> "Specmanship"- the linguistic subterfuge used to manipulate data / results in order to improve the apparent specifications of a product or device.

# 34<sup>th</sup> International North Sea Flow Measurement Workshop 25-28 October 2016

## Technical Paper

set is typical of Venturi meters with modern digital DP transmitters. These data points repeated to <0.1%, which is comparable to other meter technologies. AGA9 sets the allowable USM repeatability at  $\leq 0.2\%$ , but USM's also typically have a lower repeatability.



Fig. 4 - Solartron 6", 0.4 Beta Ratio Venturi Meter During Calibration.

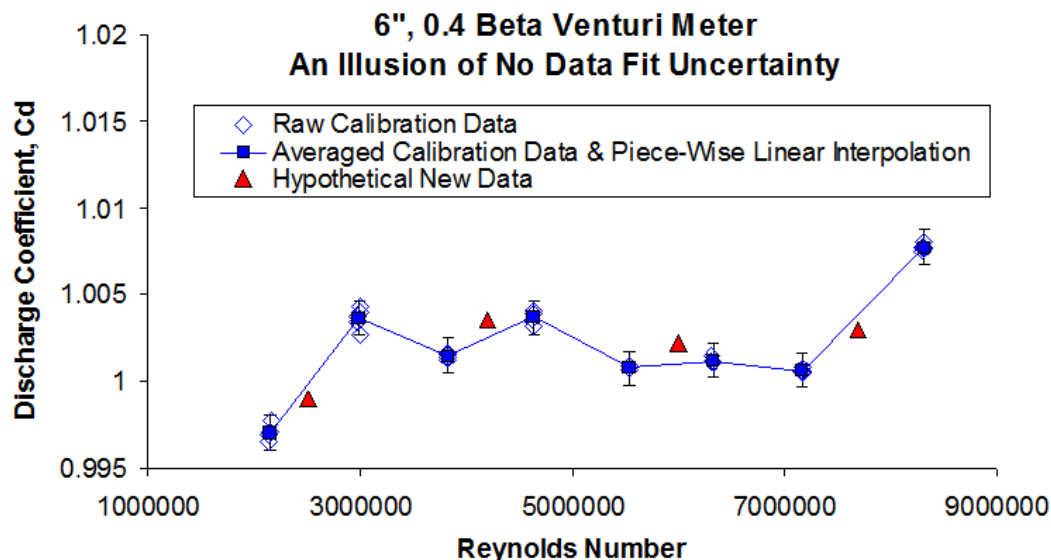


Fig. 5 - Actual Calibration Example of 6", 0.4 Beta Venturi Meter with Piece-Wise Linear Interpolation

The uncertainty of the DP reading is dependent on several factors, including the decision to stack digital DP transmitters, the range of these transmitters, the temperature swing etc. This will be discussed in some detail in section 3 when we consider permanent pressure loss and turndown. The Venturi meter mass flow rate is proportional to the square root of the DP (and density) meaning that a DP (or density) reading uncertainty has half that effect on the mass flow rate prediction uncertainty. For now, let us consider Table 2. In order to achieve a mass flow rate uncertainty equivalent to the USM in Table 1, i.e. 0.645%, the Venturi meter uncertainty calculation shows that the DP uncertainty must be  $\leq 1\%$ . As will be discussed in Section 3, according to most reputable DP transmitter manufacturers this is a very achievable DP reading uncertainty across a wide range of DP.

The USM mass flow rate uncertainty calculation (Table 1) includes a 0.3% uncertainty associated with installation influences. The Venturi meter uncertainty calculation (Table 2) does not. ISO 5167-4 Section 6 [10] produces a table (partly

# 34<sup>th</sup> International North Sea Flow Measurement Workshop 25-28 October 2016

## Technical Paper

reproduced here as Table 4) showing experimentally found minimum lengths for a Venturi meter, *without* a flow conditioner, installed downstream of common pipe components producing flow disturbances. The lengths stated are those required for there to be *no* change in the Venturi meter flow rate uncertainty. Unlike a USM, a Venturi meter is rather resistant to flow disturbances. When discussing data from Venturi and ultrasonic meters in series, Chan et al [5] stated that they had a "... suspicion that the USMs are influenced by the different in-situ flow profiles, while the Venturi meter is not." ISO 5167-4 Section 6.2.1 says of this matter that "This is due to the attenuation of flow non-uniformities taking place within the contraction section of the classical Venturi tube." Such resistance to flow disturbances is effectively helping prevent the problem that a flow conditioner helps cure, and prevention is generally better than cure.

**Table 4 - ISO 5167-4 Required Upstream Lengths (in Multiples of Pipe Diameter) to Ensure No Additional Uncertainty**

Beta	Single Bend	Double Bend (in or out of plane)	Reducer 1.33D to D over length 2.3D	Expander 0.67D to D over length 2.5D	Reducer 3D to D over length 3.5D	Expander 0.75D to D over length D	Full Bore Gate or Ball Valve Full Open
0.3	8	8	4	4	2.5	2.5	2.5
0.4	8	8	4	4	2.5	2.5	2.5
0.5	9	10	4	5	5.5	2.5	3.5
0.6	10	10	4	6	8.5	3.5	4.5
0.7	14	18	4	7	10.5	5.5	5.5
0.75	16	22	4	7	11.5	6.5	5.5

The Venturi meters resistance to flow disturbances would be further enhanced if a flow conditioner was added, but in most applications this is not required. Flow conditioners require a significant length of upstream pipe, e.g. CPA advise installing the flow conditioner in a 10D upstream pipe run. Table 4 shows only the Venturi meters with the highest betas combined with the most severe disturbances have a recommended upstream length >10D. In these rare cases a flow conditioner can be installed. Also, as with a USM, if there was an especially difficult installation the Venturi meter could be calibrated with that pipework. However, as with USMs, this is the minority of calibrations. In summary, unlike USMs, there is no automatic required installation uncertainty component required for a Venturi meter flow rate uncertainty calculation.

Hence a fair Venturi gas meter mass flow rate uncertainty specification is in the order of 0.65%. Which leads to a conclusion some in industry may find startling:

**A review of ultrasonic and Venturi meters shows both meters have very similar flow rate prediction uncertainties. There is no significant difference between the meters in this specification. Properly calibrated ultrasonic and Venturi meters both have a state of the art gas mass flow rate prediction uncertainty in the order of 0.65%.**

### 3 FLOW TURNDOWN

The operational flow range of a flow meter is described as the "turndown". The turndown is defined as the *ratio* of the largest to smallest flow rate that can be metered to the meter's stated flow rate prediction uncertainty at a stated confidence level. Flow meters, ultrasonic & Venturi meters inclusive, continue to

# 34<sup>th</sup> International North Sea Flow Measurement Workshop 25-28 October 2016

## Technical Paper

operate below this minimum at higher flow rate prediction uncertainties. Low flows with flow prediction uncertainties that exceed the meter's stated flow rate uncertainty are *by definition* outside the turndown specification.

For operational reasons most natural gas pipelines cap the maximum flow to 30 m/s. Hence, generic natural gas flow meters are seldom designed for continuous flows at >30 m/s. Most gas meter designs, ultrasonic & Venturi meter inclusive, can easily be designed for a nominal maximum of 30 m/s, and hence turndown is in reality defined by how much lower than 30 m/s the meter can read within its stated prediction uncertainty. This general case will be discussed in Section 3a & 3b for ultrasonic and Venturi meters respectively, with the special case of surge flow, i.e. the case where the flow occasionally exceeds 30 m/s for short periods discussed in Section 3c.

### 3a. Ultrasonic Meter Turndown

Figure 3 shows a hypothetical ultrasonic meter calibration result based on an AGA9 example. Hypothetical uncertainty limits are also shown indicating that uncertainty is dependent on the required turndown. Figure 3 shows that as the flow rate reduces from the maximum ( $Q_{\max}$ ) there is some threshold flow rate ( $Q_t$ ) before the meter's flow prediction uncertainty of  $x\%$  rises. From this threshold flow down to the minimum flow ( $Q_{\min}$ ) the flow rate uncertainty is  $y\%$ , where  $y\% > x\%$ . Whereas AGA9 shows such uncertainty limits for an uncalibrated USM, the universal rule of a reducing measurand resulting in the instrument output having an increasing measurement uncertainty holds for all calibrated flow meters, ultrasonic and Venturi meter inclusive. Hence, as with all flow meter designs different turndown ranges should have different associated uncertainties assigned to them.

The nominal maximum flow rate ( $Q_{\max}$ ) usually corresponds to 30 m/s (i.e.  $\approx 100$  ft/s). The ultrasonic meter may be calibrated for higher flow rates in order to give some surge flow capability, but this is not within normal operational parameters, and this scenario will be dealt with separately in Section 3c. As end users do not tend to deliberately run gas at >30 m/s any ability to operate at higher flows is of academic interest only and (with the exception of surge flow) not of practical importance. Hence, any practical turndown statement should be based on this industrially set maximum flow. The threshold flow rate ( $Q_t$ ) is determined by the USM manufacturer. It is often the flow rate corresponding to approximately 1.5 m/s ( $\approx 5$  ft/s). The minimum / cut off flow varies, but a common minimum calibration volume flow is that giving approximately 0.75 m/s ( $\approx 2.5$  ft/s). Therefore, as for a set density and cross sectional area the velocity turndown is equivalent to volume & mass flow turndown, a reasonable turndown for an ultrasonic meter is 30 m/s to 1.5 m/s, i.e. 20:1 at  $x\%$ , or 30 m/s to 0.75 m/s, i.e. 40:1 at  $y\%$ , where  $y\% > x\%$ . That is, if the operator wishes to maintain the highest mass flow rate prediction uncertainty across the meter range (i.e. typically of 0.65% at 95% confidence, see Section 2a), the ultrasonic meter turndown is practically 20:1. This is a competitive flow range specification that more than covers the majority of industrial applications.

Unfortunately, as both manufacturers and end users like to keep equipment specifications simple all too often a flow meter's turndown is described as a single ratio with no associated uncertainty & confidence level stated. This has led to USM manufacturers claiming USM turndowns of 40:1 or higher. With no mention of the associated uncertainty the end users all too often falsely assume these high turndowns maintain the low flow rate uncertainty. These inflated turndown claims have led many in industry to claim that an ultrasonic meter's turndown is

Technical Paper

significantly better than that of a Venturi meter system. However, as we will see this is not in fact true.

3b. Venturi Meter Turndown

A Venturi meters primary signal, i.e. the DP ( $\Delta P$ ), has theoretical parabolic relationship with the flow rate ( $Q_m$ ), as shown in equation 8. This relationship is a consequence of the physical laws of the conservation of mass and energy and is therefore *precisely* understood. The ultrasonic meter's theoretical primary signal (difference in time of flight,  $\Delta t$ ), is linear with flow rate. The authors have repeatedly heard USM proponents claim that the USM derives some (undefined) advantage from this linear relationship compared to the Venturi meter's parabolic relationship. However, in reality, as long as the relationship between a meter's primary signal and the flow rate is precisely mathematically defined there is no theoretical advantage. The only potential practical advantage would be that for a given flow rate range the primary signal's range is wider for a parabolic relationship than for a linear relationship, meaning the Venturi meter primary signal (DP) range can be large. That is, if the Venturi meter's uncertainty is to match that of the USM, this wide DP range must be read to an acceptably low uncertainty, i.e. 1% as shown in Section 2b.



Fig. 6 - Manometer, Bourdon Gauge & Stacked Modern DP Transmitters.

Early Venturi meter systems read DPs by manometer or Bourdon type devices (see Figure 6). These early DP measurement methods had a *DP turndown* of approximately 10:1. This means the maximum measurable DP was ten times larger than the minimum measurable DP. Hence **early** DP meters were said to have a corresponding *flow rate turndown* (due to equations 3 & 8) of  $\sqrt{10}:1$ , i.e.  $\approx 3:1$ , i.e. the maximum measurable flow rate was three times larger than the minimum measurable flow rate. Hence **long ago**, before the advent of modern instrumentation, before USMs even existed, the Venturi meter *used to have* a flow rate turndown of 3:1. This is where the flawed perception of the modern Venturi meter turndown limitation originates.

$$Q_m \propto \sqrt{\rho \Delta P} \text{ -- (8)}$$

In the modern world with stacked digital DP transmitters this limitation has long been consigned to history. One of the most significant (and understated) improvements in flow metering equipment in the last twenty years is the vast improvement of DP transmitters. Modern DP transmitters are designed by some of the same corporations that have developed USMs. Today's digital DP transmitters are individually capable of measuring the same or larger DP ranges more accurately than these archaic traditional methods.

# 34<sup>th</sup> International North Sea Flow Measurement Workshop 25-28 October 2016

## Technical Paper

The relatively low cost of these modern mass produced digital DP transmitters makes it in most cases economically attractive to 'stack' DP transmitters rather than consider other more expensive metering technologies. 'Stacking', i.e. adding DP transmitters that are for different DP ranges, is simple and approved by industry, e.g. API 14.3 [8] discusses DP transmitter stacking in its Section 1.12.2. This significantly increases the DP meter's measurable DP range and hence the associated flow rate turndown to an order of magnitude greater than the historic 3:1 turndown. To prove the point we consider a worked example using published DP transmitter manual specifications in Section 3b.1.

First though, note that a Venturi meter's mass flow rate prediction is proportional to the square root of both DP **and** density. Therefore, compared to linear meters like the USM where the flow prediction is linear to density, the Venturi meter flow rate prediction uncertainty is less sensitive to biases in the estimated fluid density. Hence, it is rather disingenuous of USM marketers to claim a practical advantage due to the Venturi meter's flow prediction square root relationship with DP, when the same associated square root relationship with density practically counters any such claimed advantage.

### 3b.1 Worked example

Consider the flow of a natural gas (with a molecular weight of 18) at 60 Bar & 20°C in an 8", schedule 80 pipe. The density is 49.6 kg/m<sup>3</sup>. The maximum expected flow rate is 176 MMSCFD (i.e. a Reynolds number of 26.2e6, a velocity of 30 m/s). A 0.566β Venturi meter is selected and calibrated across the Reynolds number range. The maximum DP corresponding to the maximum flow rate at a C<sub>d</sub> of 1.01 is 200 kPa (i.e. 800"WC). What flow rate turn down is achievable using stacked modern DP transmitters? (USM proponents may now be shouting 800"WC!? What about the permanent pressure loss!? We will deal with that fallacy later in Section 3d.)

In order to be realistic let us assume an application where the DP transmitters are outside exposed to a seasonal 28K (50°F) temperature swing. (If a transmitter was housed in a temperature controlled building the DP reading & corresponding flow rate uncertainties reduce significantly.) As the flow rate and the associated DP reduces the uncertainty in the DP reading increases. The modern DP transmitter products all have similar specifications which are stated in their respective manuals. In the following example the Yokogawa EJA product series is used as a generic example of modern DP transmitter capabilities.

Figure 7 shows the DP reading uncertainty if a stack of three DP transmitters are used, i.e. a 'H capsule' upper range limit (URL) of 500 kPa (≈2000"WC) spanned to 500 kPa (0), a 'M capsule' URL of 100 kPa (≈400"WC) spanned to 50 kPa (≈200"WC), and a 'L capsule' URL of 10 kPa (≈40"WC) spanned to 5.5 kPa (≈22"WC). The component uncertainties that cannot be 'zeroed out'<sup>7</sup> are combined using root sum square technique (as instructed by Yokogawa).

Yokogawa states uncertainty in 3σ (i.e. 99.7% confidence). To keep these results comparable with the USM results and the rest of the DP meter uncertainty components Figure 7 shows these uncertainties converted to 2σ (i.e. 95% confidence). Table 2 shows that the DP must be read to ≤1%. The transmitters

---

<sup>7</sup> Long term drift is a universal problem with all flow meters. Here, just as USM drift over the years between re-calibration is an unaccounted for uncertainty, the authors have also not accounted for any long term drift of DP transmitters. For both meter designs these uncertainty component are *assumed* to be small.

Technical Paper

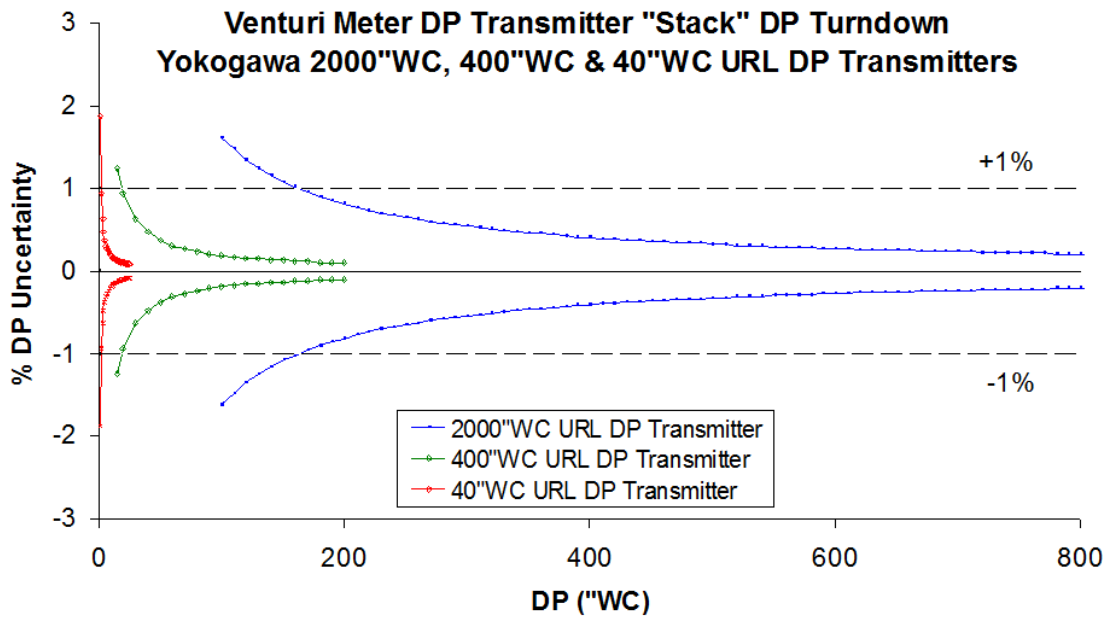


Fig. 7 - DP Reading Uncertainty of Three DP Transmitter Stack

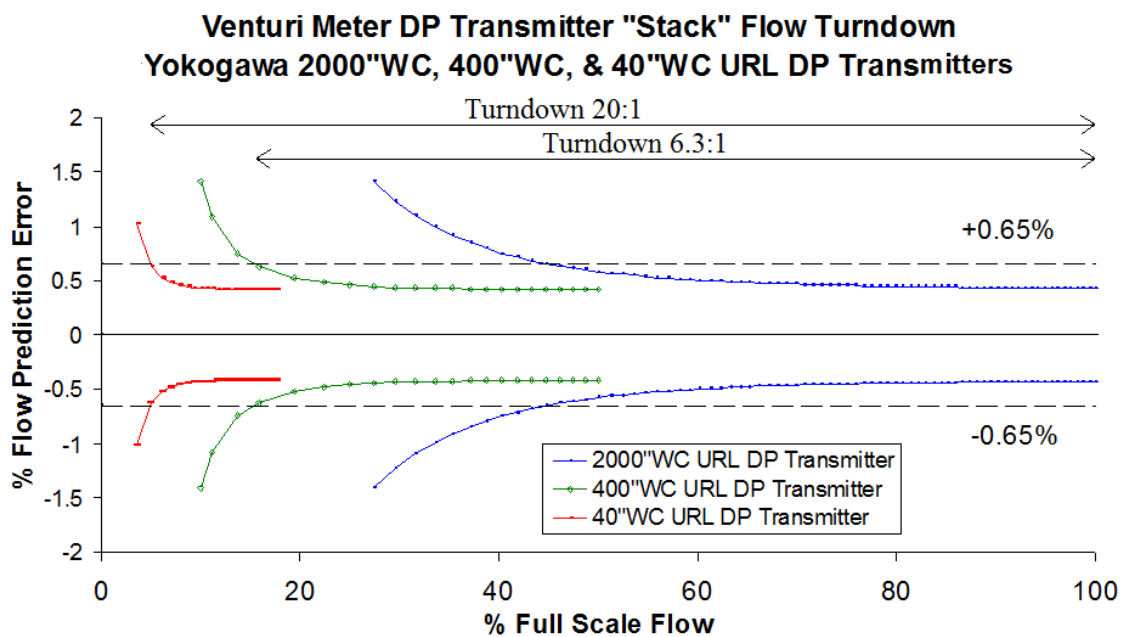


Fig. 8 - Flow Reading Uncertainty Associated With A Three DP Transmitter Stack

overlap such that between the DP range of 200 kPa ( $\approx 800$ \"WC) and 0.5 kPa ( $\approx 2$ \"WC) the DP is never read to  $>1\%$  uncertainty. Figure 8 shows the corresponding flow rate turndown for 0.65% uncertainty at 95% confidence. The three DP transmitter stack has produced a 200:0.5, i.e. 400:1 DP turndown at 1% at 95% confidence, and a corresponding flow rate turndown of  $\sqrt{400}$ :1, i.e. 20:1 at 0.65% uncertainty at 95% confidence. Hence, with the simple, common, relatively inexpensive, and approved practice of stacking digital DP transmitters, a modern Venturi meter system has the same turndown capability as an ultrasonic meter.

The majority of real applications do not require a huge flow rate turndown range. Often, real applications don't need more than two DP transmitters in a stack. If

**Technical Paper**

only the H & M capsules were used, then the DP transmitters overlap such that between the range 200 kPa ( $\approx 800''\text{WC}$ ) to 4.7 kPa ( $\approx 19''\text{WC}$ ) the DP is always read to  $<1\%$ . This produces a 42:1 DP turndown at 1% at 95% confidence, and a corresponding flow rate turndown of 6.5:1 at 0.65% uncertainty at 95% confidence. As we will discuss in 2c, although this may sound like a relatively narrow flow range it is wider than many end users realise and often more than is actually required by industry in many applications.

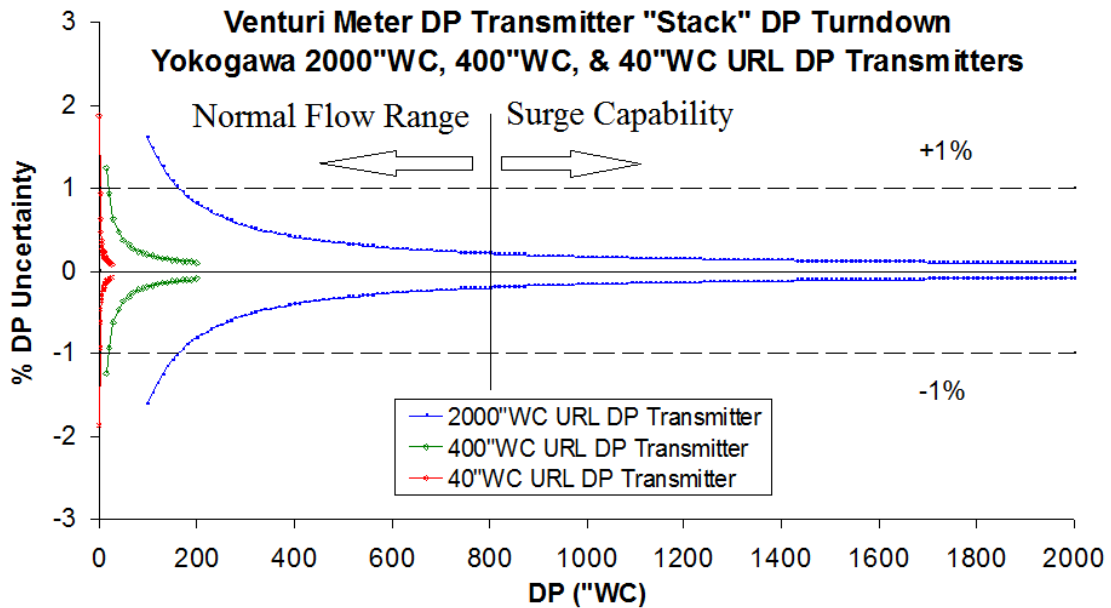


Fig. 9 - DP Transmitter Stack's Capability to Measure Higher Than Expected DPs

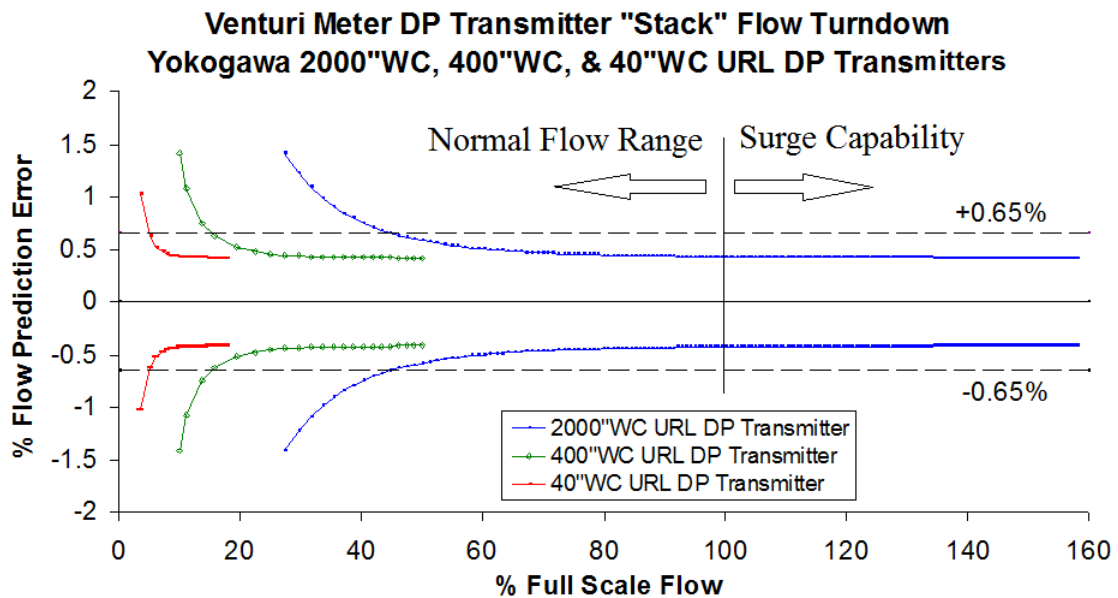


Fig. 10 - Surge Capability of Venturi Meter With a DP Transmitter Stack

The Venturi meter & USM turndown is restricted not by flow meter technology but by the pipeline cap on the maximum velocity. However, it is inevitable that applications may see periodic higher velocities, or 'surge flows'. It is advantageous for a flow meter to continue to operate in this state of 'surge flow'. The ultrasonic meter marketers make a great play about the USM's ability to cope with surge flows. This is cited as a major selling point of USM technology. It is

# 34<sup>th</sup> International North Sea Flow Measurement Workshop 25-28 October 2016

## Technical Paper

common practice for USM calibrations to include calibration points in excess of 30 m/s in case the meter has to cope with surge flow. The typical maximum calibrated flow velocity is about 50% higher than the stated nominal maximum flow velocity, e.g. if a maximum velocity of 30 m/s is expected the USM may be calibrated up to 45 m/s. It is unusual for a USM to be calibrated with significantly higher flows still as somewhere above this rule of thumb limit the USM begins to fail due to excessive background noise, i.e. low signal-to-noise ratio (SNR).

The authors agree that USMs can cope with surge flow well compared to many meter designs, e.g. orifice meters (which may buckle) or turbine meters (where over-speed can damage the rotor bearings). However, no flow meter design, *ultrasonic meter inclusive*, copes with surge flow better than a Venturi meter. In our example, if the flow exceeded 30 m/s, where the DP produced is 200kPa ( $\approx 800$ "WC), the Venturi metering system will continue to operate within the stated performance specification up to a maximum DP of 500 kPa ( $\approx 2000$ "WC), or whatever maximum DP the transmitter is rated for. Figures 9 & 10 show this scenario for the DP and flow rate turndowns respectively. In this case the 3 DP transmitter stack would have a DP turndown of 500 kPa to 0.5 kPa, i.e. 1000:1, which corresponds to a flow rate turndown of  $\sqrt{1000}$ :1, i.e. 31.6:1. Figure 10 shows the 'surge flow' capability this provides. In this example the Venturi meter can operate within its stated flow rate uncertainty at >50% more flow than the expected maximum. This is equivalent to USM surge flow capability.

If the end user is concerned about potential surge flow then there are some precautions that can be taken. Although it is common for USM calibrations to include over-speed calibration points this is not a capability unique to USMs. Venturi meter calibrations can also include over-speed calibration points. This practice supplies an accurate discharge coefficient in the event of surge flows. However, if this is not done ISO 5167-4 Table B2 offers approximate discharge coefficient predictions for machined convergent section Venturi meters to a Reynolds number dependent stated uncertainty.

Pipeline maximum flow velocity limits aside, the practical limit of a Venturi meters maximum flow velocity is set by the maximum readable DP and the limit of applicability of the Venturi meter expansibility equation. There are DP transmitter products capable of reading huge DPs so the DP reading limit is set by the choice of DP transmitter. The ISO Venturi meter expansibility equation is applicable when  $(P_1 - \Delta P) / P_1 \geq 0.75$ . In our worked example with an inlet pressure ( $P_1$ ) of 60 Bar, the maximum  $\Delta P$  allowed is therefore a *huge* 15 bar. Furthermore, the Venturi meter by design is one of the most sturdy meters on the market that suffers no specific damage concern with extreme surge flow. Hence, there is no practical limitation to Venturi meters potentially metering extreme surge flows. Any implication that a Venturi meter cannot cope with surge flow is rather disingenuous.

**A review of ultrasonic and Venturi meter flow rate turndowns shows that both meters have very similar turndowns. There is no significant difference between the meters in this specification. Ultrasonic meters and Venturi meters with stacked digital DP transmitters both have a flow rate turn down in the order of 20:1. Furthermore, both meters can cope well with over-speed / surge flows.**

A common way to decry such a description of Venturi meter flow rate turndown capability is to claim that it comes hand in hand with the significant disadvantage of producing a high permanent pressure loss compared to an ultrasonic meter. If this was true it would mean that a Venturi meter would incur significantly more

# 34<sup>th</sup> International North Sea Flow Measurement Workshop 25-28 October 2016

## Technical Paper

operating expense in the form of gas compression or liquid pumping costs. However, we will see in Section 3d that rather surprisingly this is not the case. First though, it is worth stopping to note that the flow turndown specification of any generic flow meter is often exaggerated by flow meter marketing beyond its true importance.

### 3c Large Turndown Specifications Are Often Over-Rated

The meaning of 'turndown' is not well understood. Say Meter A has flow range of 100 to 1 units of flow (i.e. 99 units of flow). The turndown is 100:1. Say Meter B has flow range of 100 to 10 units of flow (i.e. 90 units of flow). The turndown is 100:10, i.e. 10:1. Unfortunately, because Meter A has ten times the turndown of Meter B, it is often falsely assumed that Meter A has ten times the flow range of Meter B. It does not! Meter A only covers  $90/99 * 100\% = 9.1\%$  more range than Meter B. The difference in flow range between 100:1 and 10:1 turndown is not 10 times difference as often assumed but only about 10% difference!

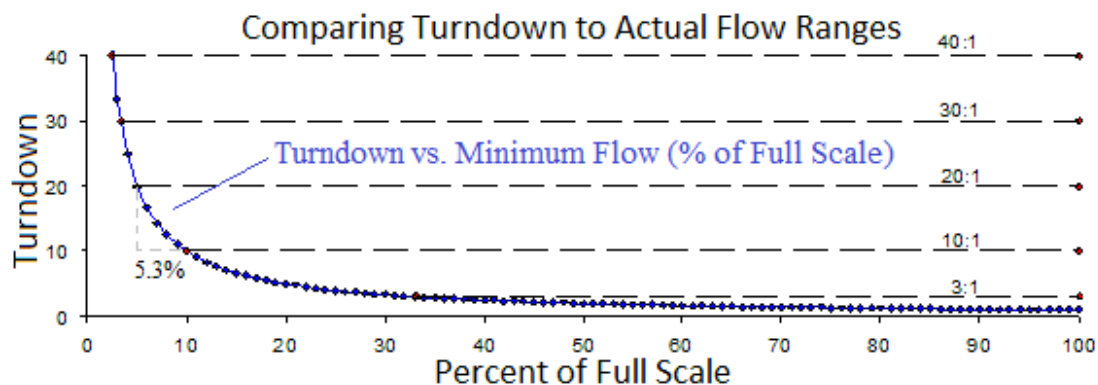


Fig. 11 - Flow Rate Range to Turndown Comparisons

Most flow meters, Venturi & ultrasonic meters inclusive, can be designed for the nominal maximum flow rate (i.e. 100% full scale). The difference in turndown therefore represents how low a flow they can respectively meter within their stated uncertainties. For a set maximum flow Equation 9 calculates the percentage difference in absolute flow range ( $\lambda\%$ ) achieved by Meter A with a turndown of  $x:1$  compared to Meter B with a turndown of  $y:1$ , where  $x > y$ .

$$\lambda\% = \left[ \frac{x - y}{y(x - 1)} \right] * 100\% \quad (9)$$

Taking the above example of Meter A with a turndown of 100:1 ( $x=100$ ) compared to Meter B with a turndown of 10:1 ( $y=10$ ), we see that  $\lambda\%$  is 9.1% (as required). Figure 11, graphical representing Equation 9, shows the difference in range between 20:1 ( $x=20$ ) & 10:1 ( $y=10$ ) turndowns is not double as is often assumed, but a meagre 5.3%. If we consider the flow range difference in the worked example in Section 3.b.1 between using three or two DP transmitters in the stack, i.e. a flow turndown of 20:1 ( $x=20$ ) and 6.5:1 ( $y=6.5$ ) respectively, the difference in absolute range is only 10.9%.

Figure 11 shows that as turndown increases for a set maximum flow rate a *law of diminishing returns* exists. Each step increase in turndown creates a smaller increase in flow range attained. The only practical issue with any meters flow turndown is whether it can cover the required flow range for a particular application, not what maximum turndown a manufacturer claims.

# 34<sup>th</sup> International North Sea Flow Measurement Workshop 25-28 October 2016

## Technical Paper

### 3d Comparison of Ultrasonic & Venturi Meter Permanent Pressure Loss

A full bore ultrasonic meter has no permanent pressure loss (PPL). However, ISO & AGA both repeatedly state the benefits a flow conditioner brings to an USM. For example, ISO 17089 Section 5.9.1 states "In order to achieve the desired meter performance, it may be necessary for the installation designer to alter the original piping configuration or include a flow conditioner as part of the meter run". AGA 9 [2] Section 5.2.1 states "...the use of flow conditioning is recommended to provide the basis for a repeatable and stable metering package". That is, most USM systems include a flow conditioner<sup>8</sup> and therefore most USM systems do have an associated PPL.

ISO 17089 Section 5.9.3.5 states "One of the main advantages of USMs is the absence of a pressure drop. The use of a flow conditioner introduces a pressure drop and negates this advantage." That is, ISO is stating that one of the main *theoretical* advantages of an USM is lost *in practice* by the USM's dependence on flow conditioning. Flow conditioners produce a significant PPL. Therefore, in most cases it is rather disingenuous to claim an USM has no PPL.

A flow conditioner must be installed in an upstream straight run of pipe, e.g., the CPA 50E requires a straight run of  $\geq 10D$ . A USM should therefore have a straight inlet run  $\geq 10D$  containing the flow conditioner. In contrast, ISO 5167-4's minimum required Venturi meter inlet run lengths to *assure no additional uncertainty* (reproduced here as Table 4) is  $\leq 10D$  for all but the highest betas with the most extreme disturbances (which is a relatively uncommon scenario). Therefore, if you have  $\geq 10D$  upstream run length, most Venturi meters in most applications can *and do* operate satisfactorily *without* a flow conditioner. Hence, when comparing the PPL of ultrasonic and Venturi meter systems it is a fair and realistic comparison to consider the USM with a flow conditioner package vs. the stand-alone Venturi meter (with no flow conditioner). However, the examples will consider the Venturi meter with and without a flow conditioner.

Returning to our worked example in Section 3.b.1, let us now consider the PPL consequences of using a Venturi or ultrasonic meter. Most gas flow meters are not continuously run at their maximum nominal flow of 30 m/s, so let us consider the same 8", schedule 80 pipe flow conditions with a gas density of 49.6 kg/m<sup>3</sup> flowing at say, 20 kg/s, i.e. 80.1 MMSCFD, 13.7 m/s, 11.9e6 Reynolds number. (N.B. the relative PPL results are the same regardless of flow rate.) The "minor loss coefficient" ( $K_{loss}$ ) of pipe components states the PPL ( $\Delta P_{loss}$ ) of that pipe component in multiples of the flow's dynamic pressure, i.e.

$$\Delta P_{loss} = K_{loss} * \frac{\rho V_{av}^2}{2} \quad (10)$$

ISO 5167-1 [11] Annex C states that the minor loss coefficients ( $K_{loss}$ ) of the Spearman, Zanker, and NOVA flow conditioners are equal to 3.2, 3, & 2 respectively. The Laws / CPA flow conditioner minor loss coefficient is stated by manufacturers to be equal to 2 (at Reynolds number  $> 100,000$ ). Hence, the NOVA or CPA flow conditioner is the low PPL choice. In this example, the PPL of an USM with a CPA flow conditioner would be:

---

<sup>8</sup> An USM meter operating without a flow conditioner may have diagnostics that can tell the operator if the flow profile is not as expected, but crucially this only notes the problem, it doesn't correct for it. An USM diagnostic package is no substitute for a flow conditioner.

**34<sup>th</sup> International North Sea Flow Measurement Workshop  
25-28 October 2016**

**Technical Paper**

$$\Delta P_{loss} = 2 * \frac{(49.6)(13.7^2)}{2} = 9.28kPa = 37.3''WC \quad (10a)$$

Hence, a **USM with a flow conditioner produces a significant PPL**, but how does this relate to the Venturi meter? The Venturi meter is specifically designed to be streamlined, i.e. to be a low loss DP meter. The literature does not directly state the minor loss coefficient of a Venturi meter, but there are other published forms of this information. ISO 5167-4 states that the Venturi meter PPL is accepted as being  $5\% \leq DP \leq 20\%$ . This examples 8", 0.566 $\beta$  Venturi meter with a  $C_d$  of 1.01 produces a DP of 40.1 kPa, and hence ISO predicts a maximum PPL of 8 kPa (i.e. 32.2"WC). However, more precise Venturi meter PPL predictions exist. Miller [12] published Venturi meter PPL predictions for 7° & 15° divergent angle diffusers. The Miller equations relate the Pressure Loss Ratio (PLR), i.e. the PPL to DP ratio, to beta,  $\beta$ :

Miller 7° divergent angle diffuser: 
$$\frac{\Delta P_{loss}}{\Delta P} = 0.218 + (-0.42\beta) + (0.38\beta^2) \quad (11)$$

Miller 15° divergent angle diffuser: 
$$\frac{\Delta P_{loss}}{\Delta P} = 0.436 + (-0.86\beta) + (0.59\beta^2) \quad (12)$$

In the worked example, a 0.566 $\beta$  Venturi meter with a 7° diffuser losses 10.2% of the DP, i.e. a PPL of 4.1kPa/ 16.4"WC. A 0.566 $\beta$  Venturi meter with a 15° diffuser losses 13.8% of the DP, i.e. a PPL of 5.55kPa / 22.3"WC. If a flow conditioner was installed (which is not usually required) the overall PPL would be the sum of the flow conditioner & Venturi meter, i.e. a PPL of 13.48 kPa or 14.84 kPa for the 7° & 15° respectively.

It can be shown that the equivalent minor loss coefficient prediction to Miller's PLR prediction is given by equation 13, where a, b, & c are constants set for a specific beta, e.g. see equations 11 & 12. In the worked example 7° & 15° diffuser Venturi meters (with a  $C_d$  of 1.01 & expansibility of 0.995) are predicted to have a minor loss coefficients of 0.88 & 1.20 respectively, with a corresponding PPL of 4.1 kPa & 5.5kPa (as required).

$$K_{loss} = \frac{(1 - \beta^4)(a + b\beta + c\beta^2)}{(\beta^2 \epsilon C_d)^2} \quad (13)$$

Neither the flow conditioner minor loss coefficient or Miller Venturi meter PLR prediction have a published uncertainty. Figure 12 shows the ISO PLR predicted limits, the Miller PLR predictions, and an approximate interpolated PLR prediction for a 12° diffuser angle. Superimposed on this are sample CEESI PLR vs.  $\beta$  data sets from representative gas flow Venturi meters. All data sets are for a pressure tap at 6D downstream of the diffuser exit. All Venturi meters were calibrated with >10D upstream length but without flow conditioners – as is common practice. All data falls within the ISO predicted range although the data is not particularly reproducible. The black diamonds represent a batch of seven 6", 0.6 $\beta$  ISO compliant Venturi meters with 12° diffusers that are nominally identical. There is a spread between meters of  $0.07 < PLR < 0.107$ . Nevertheless, this data tends to show that the Miller predictions are conservative. On average the Venturi meter PPL is *slightly less* than the predictions.

Technical Paper

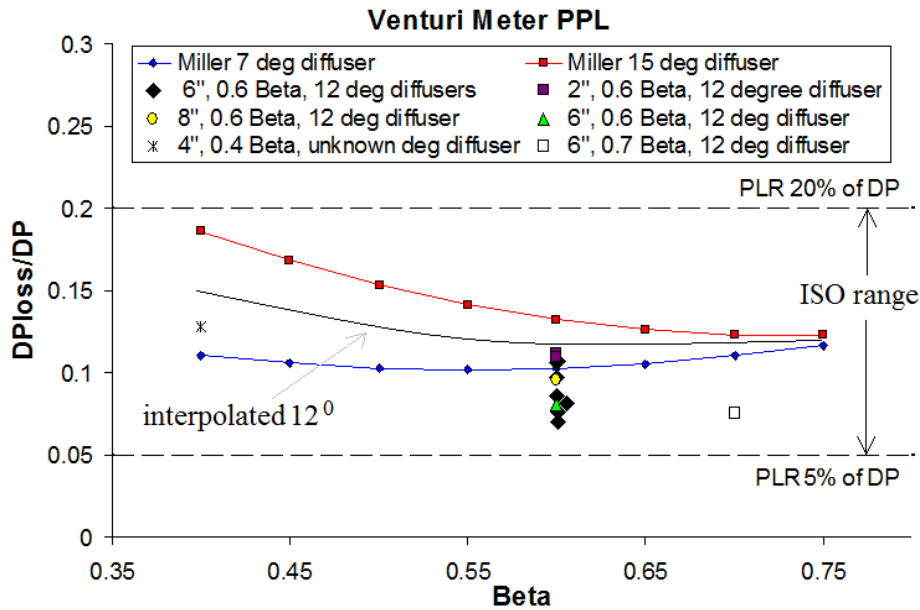


Fig. 12 - Venturi Meter PPL Predictions and Data Sets

Hence, typical Venturi meter systems (without flow conditioners) tend to have slightly less PPL than USM systems. This worked example is not cherry picked. The reader is invited to try such calculations themselves using any flow conditions. The general results will be the same. In hindsight, after considering that a flow conditioner is a perforated plate, whereas a Venturi meter is an aerodynamically designed low PPL converging / diverging tube, perhaps it should not be that surprising that a flow conditioner, and hence the USM metering package, tends to have a higher PPL than a Venturi meter.

**A review of ultrasonic and Venturi meter systems shows that both have very low pressure loss characteristics. There is no significant difference between the meters in this specification.**

A perception has permeated into industry that a smaller USM does the job of a larger Venturi meter. This belief seems to originate from claims that compared to a generic DP meter the USM has a significantly higher maximum velocity limit and a lower PPL even at that higher velocity limit. But, we have now seen that the Venturi meter has a *similar* maximum velocity limit and similar (or lower) PPL to an USM system. Hence, as a consequence, it is not true to say that a smaller USM does the job of a larger Venturi meter. For a given flow metering application a USM and a Venturi meter would be the same size.

#### 4 ULTRASONIC & VENTURI METER VERIFICATION SYSTEMS

Both meter users and manufacturers talk up the concept of flow meter diagnostics to facilitate meter verification, but in practice they are as yet sparingly used. The reasons for this are complex and diverse, and discussed in some detail by Cousins et al [14]. Nevertheless, a comprehensive diagnostic system (or 'suite') is now seen as a prerequisite for a flow meter to be considered a cutting edge, state of the art, modern flow meter. As such, most meter designs are touted as having a diagnostic suite. But not all flow meter diagnostic systems are created equal.

The USM diagnostic suite has been shown to be comprehensive and capable with mass laboratory and field examples. Such is the exposure of the USM diagnostic suite that many in industry assume it to have a better diagnostic suite than *all*

# 34<sup>th</sup> International North Sea Flow Measurement Workshop 25-28 October 2016

## Technical Paper

competing meter designs. Whereas this is a reasonable proposition when comparing the USM diagnostic suite to those of turbine, Coriolis, & vortex meters, it is certainly *no longer true* of the Venturi (and generic DP) meter. Whereas the Venturi meter is a beautifully simple traditional technology, quite counter-intuitively, it now has one of the most modern, comprehensive, and easy to understand diagnostic suite of all flow meters. This Venturi meter diagnostic system has also been proven with multiple laboratory and field examples (e.g. see Vijay & Rabone [15, 16]). The ultrasonic and Venturi meter both have state of the art diagnostic systems. It is not possible or necessary to give a full description of the USM & Venturi meter diagnostic suites here. All that is possible and required here is a basic summary of each of the meters diagnostic suites. However, before that it is helpful to consider types of diagnostics.

### 4a Objective and Subjective Diagnostics

Diagnostic techniques can be categorized as either *subjective* or *objective*. In theory and in practice *subjective* diagnostics compare the diagnostic result to an *estimated*, but fundamentally uncertain diagnostic baseline representing a serviceable system. Subjective diagnostics do not offer black & white, yes / no results, but various 'shades of grey' results. An example of a subjective diagnostic technique is monitoring the standard deviation of an instrument reading and comparing it to some rule of thumb baseline value based on experience rather than some physical law.

In theory *objective* diagnostics compare the diagnostic result to a *guaranteed* diagnostic baseline set not by experience but by say a physical law or a calibration result representing a serviceable system. Theoretically, objective diagnostics give black & white, yes / no results. An example of an objective diagnostic technique is check metering, where the physical law of conservation of mass dictates there shall be no difference in mass flow rate predictions between two mass meters in series. However, in practice all diagnostic techniques rely on instrument readings, and all instruments have uncertainty. Setting a reasonable uncertainty limit to instrumentation is a subjective act. Hence, theoretically objective diagnostic techniques are in practice somewhat subjective.

Nevertheless, it is desirable to have a theoretically objective diagnostic technique. The level of uncertainty is then reduced to the instrument uncertainty only. In contrast, subjective diagnostic techniques have both instrument and operator dictated baseline setting uncertainties. In reality all diagnostic techniques fall along an objective / subjective spectrum. Therefore, not all diagnostics are created equal. Thus, a fundamental rule of diagnostics is: **All diagnostic techniques are subjective, but some are more subjective than others.** Unfortunately, with diagnostic interpretation being subjective there is a tendency for some to see what they want to see, and not what is actually there. Or, there is a tendency to claim that the diagnostic system identified a specific problem *after* maintenance had *independently* confirmed the problem source, and they have subconsciously then weaved a narrative fallacy around the diagnostic result and the maintenance report. Nevertheless, generally, the less subjective / more objective a diagnostic technique the more powerful a diagnostic tool it is.

Regardless, all diagnostic techniques are somewhat subjective, and hence the results are by definition interpreted by opinionated end users. It is therefore beneficial to have multiple different diagnostic techniques for the end user to cross reference and therefore build a more confident picture. The Venturi / DP and ultrasonic meter respective diagnostic suites are two of the very best diagnostic suites of all flow meter designs. Both have an impressive blend of subjective and

# 34<sup>th</sup> International North Sea Flow Measurement Workshop 25-28 October 2016

## Technical Paper

theoretically objective diagnostic techniques where the whole is greater than the sum of its parts. There is no obvious overall diagnostic capability advantage between the two meter designs.

### 4b Ultrasonic Meter Diagnostic Suite Summary

USMs have a set of paths across which the local flow velocity is found for each, e.g. see Fig 13 for a sketch of a 4 path USM cross section, where the paths ( $P_n$ ) are between the transducers A & B. The average velocity and hence volume flow is predicted from these velocity measurements across the paths. What's more, the path information tells the operator a lot more than the local velocity.

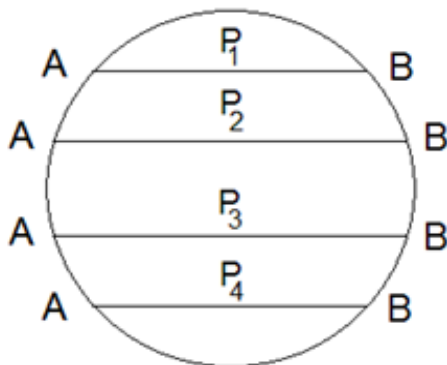


Fig. 13 - A 4 Path USM

The fluid speed of sound is also predicted for each path. This allows a path speed of sound inter-comparison check, and an average speed of sound prediction check against an external speed of sound measurement. The velocity predictions across each path give an idea of the actual velocity profile which can be compared to that of hydraulic theory. Two geometric velocity profile factors used for such a comparison are the profile factor and symmetry.

Each path also has a set of diagnostic tools. The paths "turbulence" is the standard deviation of the velocity ( $\Delta t / \text{path length}$ ) reading. The "gain" of a path is effectively the power required to maintain a clear signal. The paths "signal to noise ratio", or "SNR", is the ratio of the strength of the signal to the background noise. The paths "performance" is the ratio of the number of successful attempts to measure the velocity across the path in a unit time to the number of attempts made. Therefore, there is:

- internal speed of sound measurement comparison (theoretically objective)
- internal/external sound measurement comparison (theoretically objective)
- profile factor & symmetry checks (theoretically objective)
- path turbulence levels (subjective consideration)
- path gain (subjective consideration)
- path SNR (subjective consideration)
- path performance (subjective consideration)

USM diagnostics are often set to a baseline found after field installation as the baseline, or "footprint", can change between calibration and the field. E.g. when describing a real world USM diagnostic example Chan et al [5] stated that the "... [USM diagnostic] footprint as described in ISO 17089 is available, but usually not monitored as even small changes in flow profiles lead to significant changes in the footprint".

There is no standardized USM diagnostic suite presentation. Each USM manufacturer has developed their own form of diagnostic display. Figure 14 reproduces one such display. (The external speed of sound check is not displayed.) Unfortunately, the lack of standardization of the USM diagnostic display has contributed to some end users finding USM diagnostics difficult to understand, as each USM diagnostic display containing fundamentally the same core information can look different and complex. Nevertheless, some end users

Technical Paper

and consultants can and do use USM diagnostics to great effect. For examples of this diagnostic system in operation see Lansing [17].

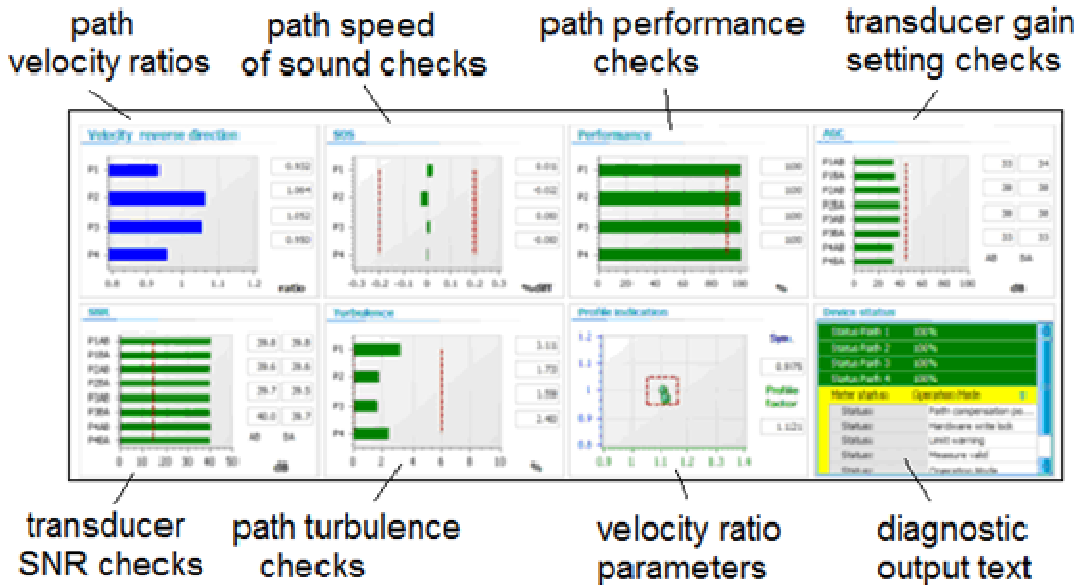


Fig. 14 - Example of a Ultrasonic Meter Diagnostic Screen

4c Venturi Meter ("Prognosis") Diagnostic Suite Summary

Venturi meters can have a downstream tap added, as shown in Figure 15's sketch of a genetic Venturi meter and its associated pressure field. This allows the patented concept of Venturi meter pressure field diagnostics (called "Prognosis"). Three separate DP's can be read, the traditional upstream to throat DP ( $\Delta P_t$ ), the downstream to throat DP ( $\Delta P_r$ ), & the PPL across the meter ( $\Delta P_{PPL}$ ), as shown in Figure 15.

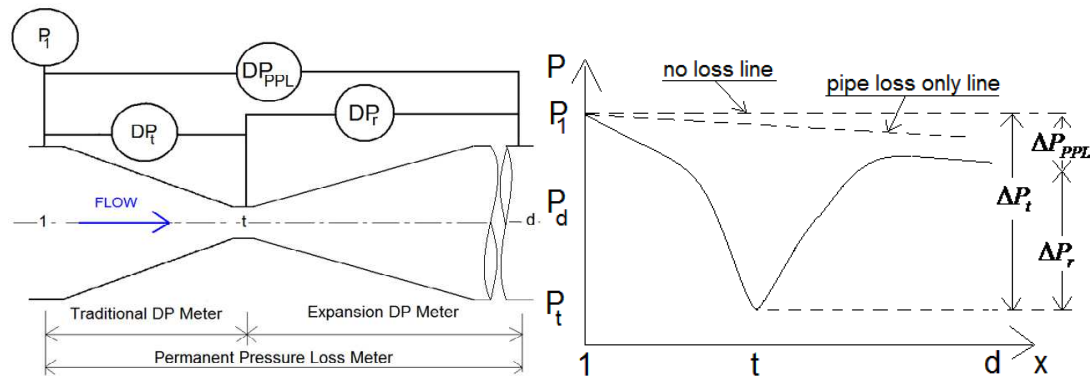


Fig. 15 - Venturi Meter with Instrumentation Sketch and Pressure Field Graph.

These three DPs are inter-related (as shown in Figure 15). It is a consequence of the 1<sup>st</sup> law of thermodynamics that the sum of the recovered and PPL DPs equates to the traditional DP, i.e.  $\Delta P_t = \Delta P_r + \Delta P_{PPL}$ . This simple relationship produces an extremely useful DP reading integrity check.

For each of these three DPs an independent flow rate prediction can be obtained. Hence, the Venturi meter effectively becomes the three flow meters in series in one point in space, i.e. the traditional meter (using  $\Delta P_t$ ) has two check meters, the expansion meter (using  $\Delta P_r$ ) and the PPL meter (using  $\Delta P_{PPL}$ ). Conservation of

# 34<sup>th</sup> International North Sea Flow Measurement Workshop 25-28 October 2016

## Technical Paper

mass dictates that the three flow rate predictions must be the same, and hence comparing the three flow rate prediction pairs give three diagnostic checks.

With these three DPs there are three pairs of DPs, and hence three DP ratios (ignoring the reciprocals). Hydraulic theory dictates that these DP ratios are effectively constant. While the individual DPs change with flow conditions these three DPs change in proportion. Hence, the three as found DP ratios can be compared to their calibrated values to give three diagnostic checks.

Modern DP transmitters have internal diagnostics. This usually consists of a variation on one common theme, namely the standard deviation of the DP signal. Therefore, there is:

- DP integrity / i.e. DP summation check (theoretically objective)
- Expansion / Traditional meter prediction check (theoretically objective)
- PPL / Traditional meter prediction check (theoretically objective)
- Expansion / PPL meter prediction check (theoretically objective)
- $\Delta P_{PPL} / \Delta P_t$  actual to calibration check (theoretically objective)
- $\Delta P_r / \Delta P_t$  actual to calibration check (theoretically objective)
- $\Delta P_r / \Delta P_{PPL}$  actual to calibration check (theoretically objective)
- DP transmitter signal standard deviation levels (subjective consideration)

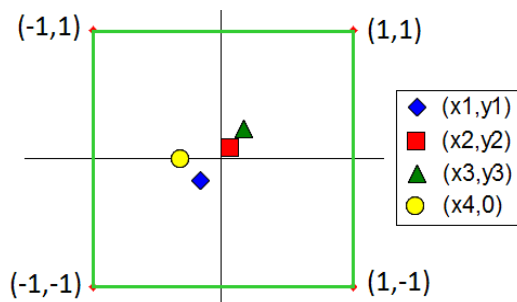


Fig. 16 - Venturi Meter Diagnostic Display

The Venturi meter diagnostic baselines are often set at the calibration. With the exception of the DP reading standard deviation diagnostic check the calibrated diagnostic baseline is transferable to the field. The single subjective diagnostic baseline can be set in the field.

For ease of use the Venturi meter diagnostic display (see Fig 16) is standardized. Four points on a graph,

i.e.  $(x_1, y_1)$ ,  $(x_2, y_2)$ ,  $(x_3, y_3)$  &  $(x_4, 0)$  represent seven diagnostics results. Coordinates  $x_1$ ,  $x_2$ ,  $x_3$  represent three flow rate comparisons. Coordinates  $y_1$ ,  $y_2$ ,  $y_3$  represent three DP ratio comparisons. Coordinate  $x_4$  represents the DP integrity check. (The transmitter standard deviation diagnostics are not displayed.) If the points are within the box drawn around the origin then the Venturi meter is serviceable. One or more points lying outside the box indicates the meter is in-serviceable. Industry can and does use Venturi meter diagnostics to great effect. For examples of this see Rabone [16].

**A review of ultrasonic and Venturi meter diagnostic / verification systems shows that although the operating principles are very different both are comprehensive. The USM & Venturi / DP meters have arguably the best diagnostic systems of all flow meter designs. There is little difference between the meters in this specification.**

It is not possible to directly compare the diagnostic suites of flow meters that operate according to different physical principles. Nevertheless the authors have heard a few comments that imply you can. A relatively common argument is to say that the USM diagnostics can see minor flow profile disturbances and hence are inherently better. But this argument relies on both meters being equally affected by minor flow disturbances. They are not. As the standards imply, USMs are far more sensitive to minor flow disturbances than Venturi meters. Hence,

# 34<sup>th</sup> International North Sea Flow Measurement Workshop 25-28 October 2016

## Technical Paper

Chan's [5] statement of a "...suspicion that the USMs are influenced by the different in-situ flow profiles, while the Venturi meter is not." So it is imperative an USM diagnostic suite can see minor flow disturbances, while this is not imperative for a Venturi meter. This of course works both ways. A Venturi meter diagnostic suite is good at seeing a DP transmitters leaking 5 way manifold valve. But USMs don't measure DPs and therefore need no such diagnostic capability. In summary, it is not possible to directly compare flow meter diagnostic systems, that would be comparing "apples and oranges". All that can be practically said is a flow meter of a specific physical principle has or has not a good associated diagnostic system. Both ultrasonic and Venturi meters certainly do.

### 5 ULTRASONIC VS. VENTURI METER IMAGE

Flow meters are required to meter flow as accurately, reliably, and as economically as possible. Flow metering should be influenced by technical and economic facts, and not be influenced by popular trends, fashions etc. Although in reality, to an extent it is. *Everything is*. The influence of peer pressure, perception via marketing, jumping on the bandwagon, not wanting to be controversial, wanting to go with the flow (no pun intended), are universal and of course exist in the flow metering world. USMs have the image of being ultra-modern, exciting, fashionable, slick & futuristic. Venturi meters do not have that image. Hence, regardless of the pros and cons of USMs & Venturi meters, USMs are without doubt currently more trendy than Venturi meters.

Twenty-five years ago the ultrasonic meter *promised a future of*:

- a lower flow rate prediction uncertainty
- a meter that did not require a flow conditioner
- a meter with no permanent pressure loss
- a meter that was so reproducible that it did not require calibration
- a diagnostic system that would identify most problems as they arose
  - and sometimes predict the biases and required corrections.

Today mature ultrasonic meters have only *partially* fulfilled these early promises:

- the flow rate prediction uncertainty is comparable with a Venturi meter
- a flow conditioner is strongly advised by AGA, ISO, and manufacturers
- flow conditioner permanent pressure loss is more than for a Venturi meter
- calibration is required (just like a Venturi meter)
  - with the cumbersome pipe run and flow conditioner included
- the diagnostic system does indicate when *something* is wrong, but for the vast majority of non-metering specialist operators it's difficult to interpret, & generally does not give a precise indication of the cause of alarms or associated metering biases.

Furthermore, Zanker [4], states that such are the challenges facing the USM development that any further improvement in the USM flow rate prediction uncertainty will need to be achieved by incremental advances in different aspects. That is, the days of large jumps in USM specification improvements are over, and further improvements can be expected to be achieved with slow incremental steps.

We have seen that the Venturi meter and the USM have similar specifications, so what is it about the USM that makes it seem so much more desirable: *Marketing*. The USM has a great *marketing* advantage. The USM marketers have done a superb job of promoting the USM. It is a marketing triumph. Through marketing,

# 34<sup>th</sup> International North Sea Flow Measurement Workshop 25-28 October 2016

## Technical Paper

the USM has an image of being a meter at the cutting edge of technology. Even though the early promise of USMs has not fully materialized the setbacks, such as continuing to require use of a flow conditioner and calibration, have been slow to be realised. They have been countered by the fact that many manufacturers and end users were by then financially, emotionally, and by reputation heavily invested in the USM concept. Curiously, no such technical set back seems to have dampened enthusiasm for the USM concept. After years of having no counter arguments on the behalf of Venturi meters the lines between USM sales pitch and what is taken as actual technical reality are worrying blurred. Nevertheless, the USM is now perceived by many to offer many advantages. People can only act on their perception of reality, not actual reality.

The lack of Venturi meter marketing has led to the image of the Venturi meter being an 'old technology', perceived as an unremarkable 'commodity'. It has an image of the 'plain old Venturi meter'. Familiarity has to an extent breed contempt. End users tend not to buy complete Venturi meters systems from manufacturers, but rather they buy components and fit (or 'cobble') the Venturi meter system together from the separately bought components, i.e. the Venturi body, DP transmitter/s, tubing, five way manifolds, flow computer etc. All too often the result looks more like an unruly contraption, and not a slick modern flow meter. This problem goes all the way to the standards. ISO 5167-4 is said to be the Venturi meter standard. But if you look at it critically you may realise this is not a complete system document. It is a description of the Venturi meter primary element (i.e. the meter body) and associated fluid flow issues. It says little about the rest of the system, i.e. DP transmitters, manifolds, or the flow computer. However, this is the way industry seems to think of Venturi meters. End users prefer to purchase individual components and install Venturi meter systems. Nevertheless, this does not stop many then saying the Venturi meter is complicated to install, has a large footprint etc. This is in contrast to the USM image.

No end user would contemplate buying USM components and fitting together their own USM system. Fitting together your own USM would be considered a ridiculous idea. USMs are purchased as a complete system. They are packaged to have a small footprint, be installed with minimal effort, and be, well... sexy. Not surprisingly the end users like this. But it is the same end users that tend to refuse to consider purchasing similarly packaged Venturi meter systems. Apparently **not** fitting together your own Venturi meter would be considered a novel idea. It is only user perception that stops Venturi meter systems being packaged as complete systems equivalent to USMs. This is a legacy issue. At the core of the 'problem' is Venturi meters are so simple, so well understood, that end users feel comfortable fitting together a Venturi meter system. In contrast the USM is much more of a mystery, a black box, and hence they do not feel as comfortable fitting together a USM from its constituent components. And **bizarrely** this is seen as a USM pro / Venturi meter con!?

## 6 AUTHOR'S EDITORIAL/OPINION

The USM has an image of being superior to that of the humble Venturi meter. Image is powerful, but image is superficial. Real comparisons of flow meters are far more complex than marketing tends to portray. It is relatively easy to prove or disprove the specifications of many mechanical devices, e.g. the maximum weight a crane can lift, or the maximum speed of a vehicle etc. These specifications are very visible, easily observable. This is not so with flow meter specifications.

# 34<sup>th</sup> International North Sea Flow Measurement Workshop 25-28 October 2016

## Technical Paper

Flow meters outwardly appear as inanimate objects. Their performance is invisible to the bystander, i.e. not directly observable. Meter performances, and differences in respective meter performances, are only indirectly visible through laboratory calibration, check metering etc. Hence, although meter end users may think they have carried out due diligence when comparing and selecting competing metering technologies, in reality most are not meter subject specialists and it is inevitable that marketing will have a strong influence on them. Hence, often the best marketed meter tends to be favoured. Whether a flow meter actually meets its claimed specifications in service is often difficult to prove, so the end user tends to just *assume* it does. Unfortunately this is even true for many meters with diagnostic systems, as such diagnostic systems cannot be guaranteed to see all small problems, and regardless, many end users just ignore diagnostic outputs. Hence, the perception of good performance is in some ways more commercially important than actual performance.

This mindset of USM superiority perhaps derives not just from marketing but also the early (only partially fulfilled) promises of USMs seducing many end user managers to 'hang their hat' on USM technology, and now their reputation is inextricably bound up with USMs. Whatsmore, such was the commercial drive to develop the USM that many engineers were hired into the flow meter industry via USM engineering jobs, and have therefore been conditioned to unquestionably assume the USM as superior.

The agenda for discussing the technological past, present, and future is often set by the promoters of new technologies, in this case USM marketers. For all these USM marketing claims reflect what industry has been repeatedly told, and therefore what they think they know, they are not necessarily as well founded as might be superficially supposed. USMs have been from the outset a highly marketed and intensely discussed technology. As a result it can be argued that the prominence & importance of this technology has been somewhat exaggerated.

Well intentioned efforts to improve technologies can go awry when questionable technical claims are shaped (even subconsciously) by commercial interests rather than scientific facts. With a performance equivalent to Venturi meters the USM is indeed an excellent meter. But it is of course a manmade device whose superior performance to more traditional mature technologies should not be treated as preordained. The USM does have pros and cons. Nevertheless, industry seldom discusses USM cons, or in the rare occasions these cons are discussed they tend to be played down. Meanwhile discussions on USM pros abound. This does not give industry a well balance view.

While many may acclaim the qualities of the USM over the Venturi meter there is a dearth of defensible proof that the USMs permeation into the hydrocarbon production industry has significantly altered productivity or reduced costs of hydrocarbon production. Economic historians argue that the significance of a technology is the difference between cost or benefit of using that technology and that of its best alternative. The Venturi meter is an obvious candidate for that best alternative to USMs. Contrary to popular opinion, it is yet to be shown if use of USMs will make industry richer or poorer than use of Venturi meters once *all* costs and benefits are properly accounted for.

Ultrasonic meter proponents may reject these comments out of hand. Cognitive dissonance will no doubt result in some finding these technical defensible results preposterous, and worthy of disdain and dismissal. There may be a tendency to want to shoot the messenger rather than seriously consider these facts. The more they have riding on their judgement, the more they are likely to ignore or

# 34<sup>th</sup> International North Sea Flow Measurement Workshop 25-28 October 2016

## Technical Paper

manipulate any new evidence that calls that judgment into question. The most effective cover ups are not perpetrated by those that are covering their backs, but by those who don't even realize they have anything to hide. But, as John Adams stated "...facts are stubborn things; and whatever may be our wishes, our inclinations, or the dictates of our passions, they cannot alter the state of facts". Reality sometimes delivers painful truths. The state of facts shows that far from the ultrasonic meters being superior to the humble Venturi meter, in reality these competing flow meter types have remarkably similar capabilities.

## 7 CONCLUSIONS

Contrary to a widely held belief Venturi and ultrasonic meter mass flow rate prediction uncertainties are on a par. The turndown capabilities and permanent pressure loss characteristics are similar. Both meters have cutting edge excellent diagnostic systems each based on cross-referencing multiple objective and subjective diagnostic methods to give a comprehensive picture of the meter system performance and health. Venturi and ultrasonic meters are *both* state of the art flow meters. Considering the very different physical principles used their performance specifications are *remarkably* similar.

## 8 REFERENCES

1. ISO 5168 - 2015 "Measurement of fluid flow - Procedures for the evaluation of uncertainties"
2. AGA Report No. 9, Measurement of Gas by Multipath Ultrasonic Meters (2007)
3. ISO 17089 - 2010: Measurement of fluid flow in closed conduits - Ultrasonic meters for gas -- Part 1: Meters for custody transfer and allocation measurement
4. Zanker et al "Limits on Achieving Improved Performance from Gas Ultrasonic Meters and Possible Solutions", NSF MW 2012, St Andrews, Scotland, UK
5. Chan P. et al "In-situ effects on ultrasonic gas flowmeters", North Sea Flow Measurement Workshop October 2015, Tonsberg, Norway.
6. AGA 8AGA Report No. 8, Compressibility Factor of Natural Gas and Related Hydrocarbon Gases (1994)
7. Groupe Européen de Recherches Gazières (GERG) 2008
8. 14.3 Report No. 3, 3<sup>rd</sup> Edition, 1990
9. Ifft S., "Orifice Plate Flow Meters – a Century of Success Hidden in Plain Sight, 100 Years of Experience and Development", SE Asia Hydrocarbon Measurement Conference, Kuala Lumpur, 2016.
10. International Standard Organisation, "Measurement of Fluid Flow by Means of Pressure Differential Devices, Inserted in circular cross section conduits running full", no. 5167, Part 4 - 2003.
11. International Standard Organisation, "Measurement of fluid flow by means of pressure differential devices inserted in circular cross-section conduits running full - Part 1: General principles and requirements", No. 5167, Part 1 - 2003.
12. Miller, R. "Flow Measurement Engineering Handbook" Ed 3, ISBN-10: 0070423660, Published by McGraw Hill.

**34<sup>th</sup> International North Sea Flow Measurement Workshop  
25-28 October 2016**

**Technical Paper**

13. Skelton M. et al, "Diagnostics for Large High Volume Flow Orifice Plate Meters", North Sea Flow Measurement Workshop October 2010, St Andrews, Scotland.
14. Cousins T., "Setting the STANDARD - Integrating Meter Diagnostics Into Flow Metering Standards", North Sea Flow Measurement Workshop October 2015, Tonsberg, Norway.
15. Ayre J. Vijay, Deverapalli., et al, "A Diagnostic System for Venturi Meters in Single Phase and Wet Gas Flow Applications", North Sea Flow Measurement Workshop, October 2011, Tonsberg, Norway.
16. Rabone J., "DP Meter Diagnostic Systems – Operator Experience", North Sea Flow Measurement Workshop October, 2012, St Andrews, Scotland.
17. Lansing J., "Basics of Gas Ultrasonic Meter Diagnostics", International School of Hydrocarbon Measurement, Oklahoma City, OK, USA, May 2014.
18. Lansing J., "Advanced Gas Ultrasonic Meter Diagnostics", International School of Hydrocarbon Measurement, Oklahoma City, OK, USA, May 2014.

## **Extended Abstract**

### **Performance of Coriolis Flowmeter for Metering of CO<sub>2</sub> with Impurities in CCS Applications**

**Mahmoud Nazeri and M.Mercedes Maroto-Valer, Heriot-Watt University  
Edward Jukes, KROHNE LTD**

---

#### **EXTENDED ABSTRACT**

Transportation of CO<sub>2</sub> by pipelines plays an important role in carbon capture and storage (CCS) operations, as the captured CO<sub>2</sub> from power plant / industries needs to be transported to the geological storage locations. However, the CO<sub>2</sub> stream may contain impurities, e.g. nitrogen, hydrogen, argon, oxygen and other gases, depending on the capture technology used. The presence of impurities can impact the thermophysical properties of the CO<sub>2</sub>-rich mixture, particularly density and viscosity. This impact can be significant in the vicinity of the critical point of CO<sub>2</sub>-rich mixtures. The temperature and pressure conditions likely to be experienced in the transportation of CO<sub>2</sub> with impurities by pipelines are close to the critical point of CO<sub>2</sub>-rich mixtures. Therefore, small gradients in pressure and temperature can significantly change the physical properties of the mixture. This can challenge the precise flow measurement of CO<sub>2</sub> mixtures, as the performance of the flowmeters is strongly dependent on the thermophysical properties of the transported fluid [1]. This is particularly important as European Union Emission Trading Scheme (EU ETS) regulations state that the uncertainty of fiscal metering in CCS must be within the range of  $\pm 1.5$  mass percent.

Under DECC-funded COMET project at Heriot-Watt University, a unique mass flow rig was designed and constructed based on the gravimetric calibration, i.e., comparison of mass recorded by the flowmeter with the mass measured by high robust weighing scale. The chosen flowmeter is OPTIMASS 6000-S08, provided by KROHNE Ltd with twin V-shaped measuring tubes which can work up to 600 kg/h. Briefly, the main components include the Coriolis mass flowmeter model OPTIMASS 6000-S08 from Krohne with twin V-shaped measuring tubes and flow range up to 600 kg/h, a gas-driven CO<sub>2</sub> pump model Maximator M22 with a cooling jacket, a pressure pulsation dampener model PulseGard SoG-SS with a PTFE/EPDM membrane, a back-pressure control valve model High-Tech EL-Press P-522C from Bronkhorst Ltd, source and receiving cylinders with 5 litres volume and 30 MPa design pressure, two pressure relief valves with the set pressure of 10 MPa, a robust weighing balance model ViBRA HJ-K with an accuracy of  $\pm 0.1$  g. The flow rig was then calibrated using pure dense liquid CO<sub>2</sub>. The trials conducted at different pressure, temperature and flow rates demonstrated that Coriolis meter can achieve an average measurement accuracy of 0.1% with an experimental measurement error of 0.025% [2].

Accordingly, in this work, the performance of the Coriolis mass flowmeter was evaluated for CCS applications using several gas mixtures representing the fluids captured by different technologies, i.e. pre-combustion, post-combustion and oxyfuel processes. A binary mixture of 1.97 mol% nitrogen and balanced CO<sub>2</sub> representing post-combustion, a multi-component mixture of 1.5 mol% hydrogen, 1.0 mol% nitrogen, 0.5 mol% argon and balanced CO<sub>2</sub> representing pre-combustion, as well as two multi-component mixtures with oxygen, nitrogen and

# 34<sup>th</sup> International North Sea Flow Measurement Workshop 25-28 October 2016

## Extended Abstract

argon as impurities with 2 mol% and 15 mol% representing oxyfuel, were used to investigate the performance of the chosen flowmeter. The tests were conducted in start / stop operations at different conditions of constant pressure and transient operations of ramp-up and depressurisation conditions. In addition to the mass and volume flow rates, the operational pressure and temperature as well as velocity and density were recorded for the test monitoring. The differential mass collected in the receiving cylinders then, were compared to the differential mass recorded by the mass flowmeter to obtain the deviation of each test. Experimental operation conditions are temperature and pressure from 288.6 to 293.3 K and 1.00 to 6.10 MPa with the flow range up to 32.1 kg/h and turndown of 53.5. The deviations of conducted tests varied within the range of -2.1% to +0.7% and -2.0% to +2.0% for the post-combustion and pre-combustion fluids, respectively. The Absolute Average Deviation (AAD) for both fluids was 1.0%. For oxyfuel fluids, the deviations vary in the range of -1.8% to +1.8% with AAD of 1.5% and -0.3% to 2.3% with AAD of 1.4% for oxyfuel I and II, respectively. In the investigated work, although the impurities can increase the uncertainty of flow measurement in CCS applications, they can still be within the range of EU ETS requirements with a suitably sized Coriolis mass flowmeter.

## REFERENCES

- [1] L. Hunter and G. Leslie, "A Study of Measurement Issues for Carbon Capture and Storage (CCS)," TUV NEL Rep. 2009/54, NEL, East Kilbride, 2009.
- [2] C.-W. Lin, M. Nazeri, A. Bhattacharji, G. Spicer, and M. M. Maroto-Valer, "Apparatus and method for calibrating a Coriolis mass flow meter for carbon dioxide at pressure and temperature conditions represented to CCS pipeline operations," *Appl. Energy*, vol. 165, pp. 759–764, Mar. 2016.

## **34<sup>th</sup> International North Sea Flow Measurement Workshop 25-28 October 2016**

### **Technical Paper**

# **A New Approach to Measuring the Gas and Formation Water Flow Rates in Wet Gas**

**Rolf Rustad and Andrew Charles Baker, OneSubsea, a Schlumberger company**

---

## **1 INTRODUCTION**

Many gas wells are producing very little liquid. For these wells it is not uncommon to use a simple differential pressure flow meter to measure production. Many correlations and correction factors are available to correct over-reading caused by the presence of liquids. These require the liquid fraction, or some derivative of the liquid fraction like the Lockhart-Martinelli parameter to be known. As long as a gas well is not producing any reservoir water, it may be possible to calculate the liquid fraction from the water saturation pressure and PVT calculations. This allows the liquid fraction to be estimated and the gas rate to be corrected.

Formation water production cannot be derived from the gas rate directly. First, it is necessary to know whether formation water is being produced or not. Second, when formation water is present, it needs to be quantified by other means than just measuring the gas rate. This usually means that a wet gas or multiphase flowmeter is needed if gas production is to continue after the onset of formation water production. The rate of formation water may be much higher than the rate of condensed water and hydrocarbons, but may still constitute only a small fraction of the total flow. As a result, the formation water rate measurement may have a large relative uncertainty. This uncertainty will propagate through the correction of the gas rate and make the estimates of gas rate and total water rate uncertain as well.

In this paper we present how a measurement of the conductivity of the water phase may be used to detect the presence of formation water and to estimate the fraction of formation water as a function of the condensed water. The fraction of liquid hydrocarbons may be added to obtain a total liquid fraction at metering conditions. This liquid fraction is used to correct the over-reading of the gas rate. In this way a differential pressure measurement and a measurement of the conductivity of the water phase are combined into a full 3-phase wet gas flowmeter. The applicability of this approach to different gas reservoirs is also discussed.

## **2 GAS AND WET GAS RESERVOIRS**

Oil and gas reservoirs can in very general terms be classified according to Figure 1. Gas reservoirs have reservoir temperatures higher than the cricondentherm and stay in single phase even when the pressure is reduced as a result of production. The PT trajectory from reservoir to standard conditions, represented by the curve A-A' in the figure, will usually cross the dew line, meaning that some liquid hydrocarbon will condense out of the gas as it

# 34<sup>th</sup> International North Sea Flow Measurement Workshop 25-28 October 2016

## Technical Paper

travels through the wellbore and flow line, and ultimately through the process system. Whether a gas reservoir is considered “wet” or “dry” depends on how much liquid is being produced, but there is no clear boundary between the two.

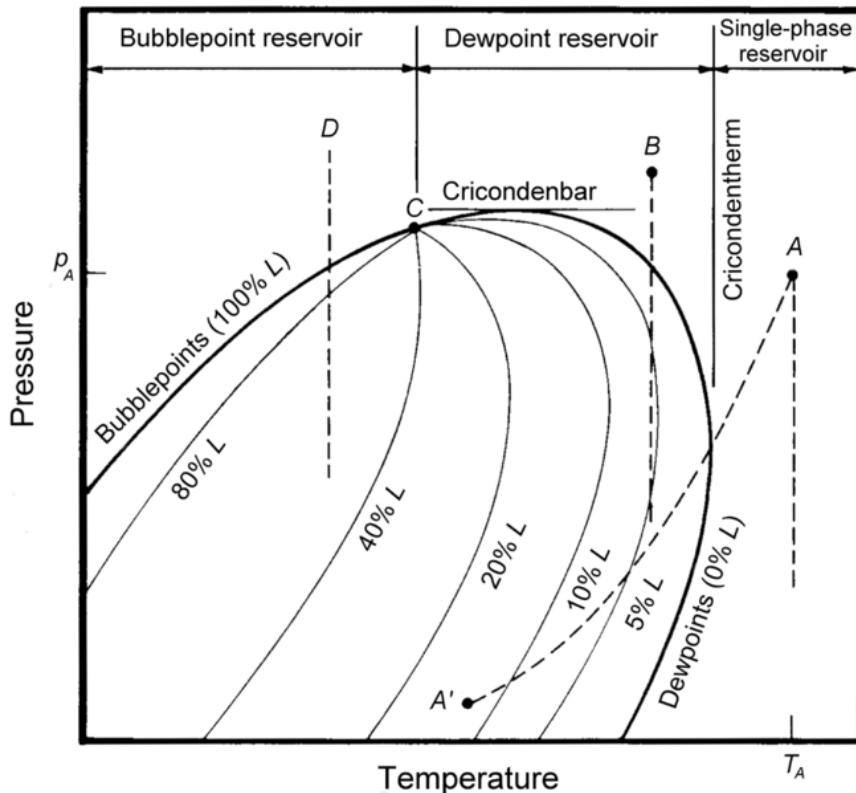


**Figure 1** Oil and gas reservoir types relative to a phase envelope

Most gas reservoirs also contain water vapour in equilibrium with condensed water in the source rock. Some of this water will condense out of the gas phase and the volume of water in the liquid phase typically increases as the temperature and pressure is reduced. This is of particular concern in subsea gas production because of the risk of hydrate formation in subsea flow lines.

The reservoir rock will contain liquid water in addition to the gas; formation water. This water will normally contain some salt and other dissolved solids. This water may or may not be produced, depending on the properties of the rock, the reservoir, and the production. Onset of formation water, or formation water break through, is a key decision point in the production of gas wells. In some cases it is not seen as economical to continue production when formation water breaks through, while it in other cases will be desirable to continue production with formation water. The presence of salt water in the process stream causes new flow assurance risks like corrosion and scaling in addition to hydrates, and the mitigation of these is key in order to continue production.

Gas reservoirs may also be in contact with aquifers. Gas wells will normally be shut in if an aquifer breaks through into a producing well. The main risk in this case is the rapid increase

# 34<sup>th</sup> International North Sea Flow Measurement Workshop 25-28 October 2016

## Technical Paper

in water production. It may be important to identify this at an early stage in order to avoid flooding the production system with water.

### 3 CONDENSED WATER IN PRODUCED GAS

An important objective of subsea wet gas flowmetering is often to provide data for flow assurance purposes, in particular hydrate risk mitigation. Flow assurance issues in gas production are often caused by produced water. Water comes out of the reservoir in vapour phase in association with the gas because the gas in the reservoir contains water vapour in equilibrium with condensed water. The water fraction in the gas can in this case be calculated from the saturation pressure.

For simplicity we assume ideal gases in the following. The fraction of water vapour in the gas in the reservoir is

$$F_{w,vap,r} = \frac{q_{w,vap,r}}{q_{g,r}} = \frac{P_w(T_r)}{P_r} \quad (1)$$

The water vapour is considered a component of the gas in  $q_{g,r}$ .

The partial pressure of water vapour in the gas at reservoir temperature,  $P_w(T_r)$  may be calculated from [4][6]

$$P_w(T_r) = P_c e^{(a_1\vartheta + a_2\vartheta^{1.5} + a_3\vartheta^3 + a_4\vartheta^{3.5} + a_5\vartheta^4 + a_6\vartheta^{7.5})\frac{T_c}{T}} \quad (2)$$

with:

$$\vartheta = \left(1 - \frac{T}{T_c}\right), \quad T_c = 647.096 \text{ K}, \quad P_c = 22.064 \text{ MPa}, \quad a_1 = -7.85951783, \quad a_2 = 1.84408259, \\ a_3 = -11.7866497, \quad a_4 = 22.6807411, \quad a_5 = -15.9618719, \quad \text{and} \quad a_6 = 1.80122502.$$

The fraction of water vapour in the gas increases with reservoir temperature and decreases with reservoir pressure. Figure 2 shows the vapour pressure of water as a function of temperature. The vapour pressure is 1bar at a temperature of 100°C and the water content declines rapidly at lower temperatures.

# 34<sup>th</sup> International North Sea Flow Measurement Workshop 25-28 October 2016

## Technical Paper

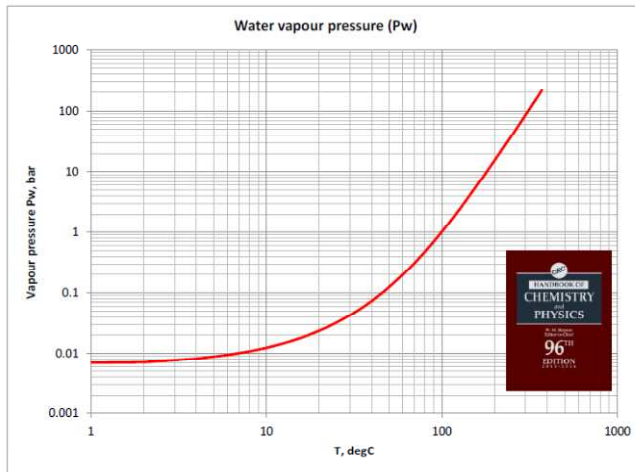


**Figure 2** Vapour pressure of water as a function of temperature. From the Handbook of Chemistry and Physics, 96<sup>th</sup> Edition.

The volumetric rate of water vapour being produced can be expressed as a function of the total volumetric gas rate, which includes the water vapour.

$$q_{w,vap,r} = F_{w,vap,r} q_{g,r} = \frac{P_w(T_r)}{P_r} q_{g,r} \quad (3)$$

We now convert the measured volumetric gas rate  $q_{g,m}$  to reservoir conditions and express the produced water vapour in terms of mass flow.

$$Q_{w,vap,r} = \rho_{w,vap}(P_r, T_r) q_{w,vap,r} = \rho_{w,vap}(P_r, T_r) \frac{P_w(T_r)}{P_r} \frac{P_m T_r}{P_r T_m} q_{g,m} \quad (4)$$

If hydrocarbons also condense out of the gas phase between reservoir and measurement conditions the relationship becomes a bit more complicated. In this case it will usually be necessary to create an Equation of State model to describe the PVT behaviour and find the gas rate at reservoir conditions. We will not discuss this further in this paper.

In the absence of formation water and with the qualifiers already mention, equation (4) gives the total quantity of water coming out of the well and that needs to be handled with respect to flow assurance.

The temperature of the gas will decrease as the gas enters the wellbore and travels upwards to the well head. The pressure will also decrease. As a result, some of the water vapour will usually condense into liquid water. Knowing the measured volumetric gas rate  $q_{g,m}$ , we can now calculate the mass rate of water still in vapour phase at measurement conditions (still ignoring any condensed hydrocarbons)

$$Q_{w,vap,m} = \rho_{w,vap}(P_m, T_m) \frac{P_{w,vap}(T_m)}{P_m} q_{g,m} \quad (5)$$

**34<sup>th</sup> International North Sea Flow Measurement Workshop  
25-28 October 2016**

**Technical Paper**

The mass and volumetric rates of the water that is condensed to the liquid phase at measurement conditions are then

$$Q_{w,cond,m} = Q_{w,vap,r} - Q_{w,vap,m}$$

$$= \left( \rho_{w,vap}(P_r, T_r) \frac{P_w(T_r) P_m T_r}{P_r P_r T_m} - \rho_{w,vap}(P_m, T_m) \frac{P_w(T_m)}{P_m} \right) q_{g,m} \quad (6)$$

$$q_{w,cond,m} = \frac{Q_{w,cond,m}}{\rho_{w,vap}(P_m, T_m)} \quad (7)$$

This condensed water is in itself free of ions and is non-conductive. There may be constituents in the gas, such as CO<sub>2</sub> or organic acids that will dissolve in the water and cause it to become slightly conductive. This needs to be assessed for each individual reservoir, and we will not discuss this further here.

If the well now starts producing formation water, it is no longer possible to estimate the total water production from a measurement of the gas rate alone. Additional measurements are needed.

**4 FINDING THE RATE OF FORMATION WATER FROM MEASURING THE WATER CONDUCTIVITY**

The rate of formation water may be calculated from a measurement of the conductivity of the liquid water if the salinity of the formation water and the rate of condensed water are known. We assume that the mass transfer of water from the liquid formation water to the gas phase between the reservoir and measurement conditions is negligible.

Let  $S_f$  be the salinity of the formation water and  $S_m$  be the salinity of the liquid water at measurement conditions. The latter is the formation water diluted by condensed water, so  $S_m < S_f$ . The salinity of the combined liquid water is the quantity of salt being produced with the formation water divided by the sum of formation water and condensed water.

$$S_m = \frac{S_f Q_{w,f}}{Q_{w,f} + Q_{w,cond,m}} \quad (8)$$

The mass rate of formation water is then

$$Q_{w,f} = \frac{S_m}{S_f - S_m} Q_{w,cond,m} \quad (9)$$

# 34<sup>th</sup> International North Sea Flow Measurement Workshop 25-28 October 2016

## Technical Paper

We see immediately that this method depends on the rate of produced formation water versus the rate of condensed water at measurement conditions. If the rate of condensed water is small, the measured salinity  $S_m$  will be very close to the salinity of the formation water  $S_f$ , and the calculated water rate will be very uncertain. It is necessary to analyse each case separately to determine the accuracy that can be achieved and the range of flow rates where it is applicable.

To give an idea about conditions where this method is applicable, we have calculated the measurement temperature  $T_m$  at which the rate of condensed water at measurement conditions is  $q_{w,cond,m} = 0.2$  bbl/MMscf as a function of reservoir temperature  $T_r$  at different measurement pressures. The value of 0.2 bbl/MMscf is somewhat arbitrary, but with this rate of condensed water it will in most cases be possible to achieve estimates of the formation water rate with good accuracy over a wide range of formation water salinities and rates. The reservoir pressure is  $P_r = 250$ bar in this example.

Measurement pressures above 200 bar represent cases where the measurement is made upstream the production choke valve, while the lower pressures represent measurement locations downstream the choke valve.

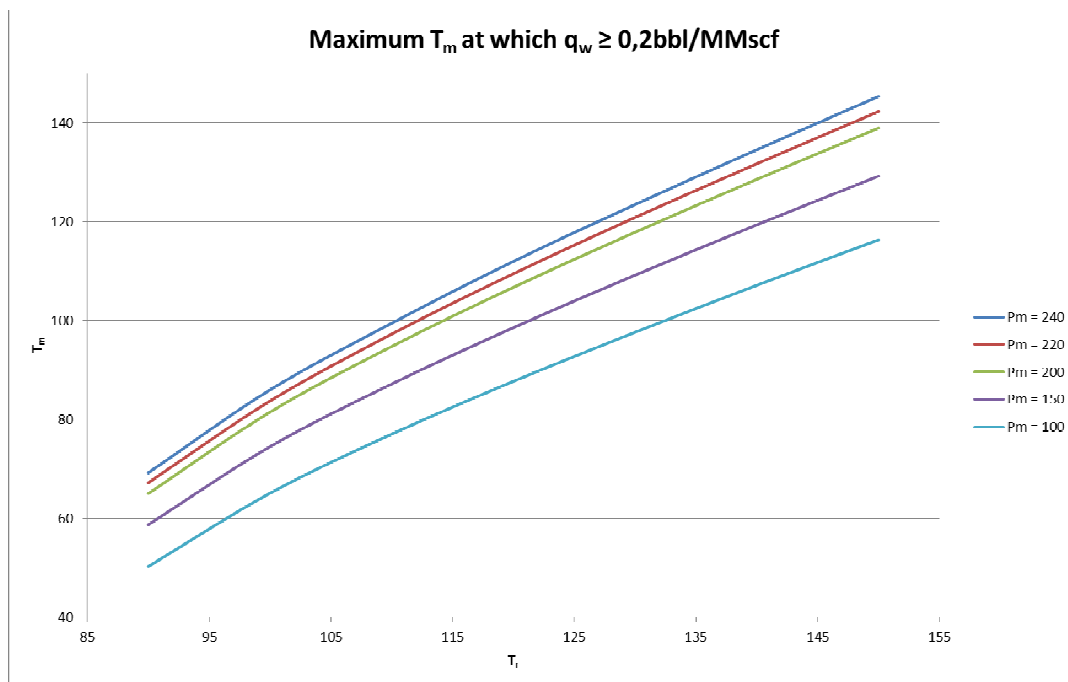


**Figure 3** The measurement temperature  $T_m$  for which the rate of condensed water is  $q_{w,cond,m} = 0.2$ bbl/MMscf as a function of reservoir temperature  $T_r$  at different measurement pressures  $P_m$ . The reservoir pressure is 250 bar.

Let us now look at a simple example. Assume a gas well with the parameters shown in

Table 1. The measurement is made at the wellhead upstream the choke.

# 34<sup>th</sup> International North Sea Flow Measurement Workshop 25-28 October 2016

## Technical Paper

**Table 1 Gas well parameters**

Parameter	Symbol	Unit	Value
Reservoir Temperature	$T_r$	°C	140
Reservoir Pressure	$P_r$	bar	250
Gas rate	$q_{gas}$	MMscf/d	50
Measurement Temperature	$T_m$	°C	115
Measurement Pressure	$P_m$	bar	220
Formation water salinity	$S_f$	g/l	70

The resulting mass rate of water coming out of the reservoir in the gas phase is according to (4) 627 kg/h. This is equivalent to ~94 bbl/d at standard conditions. In normal operations and in the absence of formation water, an operator would decide the injection of hydrate inhibitors based on the lowest expected flowline temperature and this value including a healthy safety margin.

At measurement conditions the rate of condensed water is 295 kg/h equivalent to ~44.6 bbl/d. This represents a Water Volume Fraction of 833 ppm or 0.08 %. In the absence of condensed hydrocarbons and formation water, the Gas Volume Fraction would be 99.92 %.

First we determine the smallest formation water rate that may be detected. The conductivity of the water may be measured with an uncertainty of less than 0.2 S/m at low conductivities [5]. This is equivalent to a salinity of a bit less than 0.5 g/l at these measurement conditions. If the formation water has the salinity of seawater, which is 35g/l, it would require a formation water flow rate of less than 0.5 bbl/d to increase the salinity of the water at measurement conditions by this amount. Formation water with a salinity of 70 g/l would be detectable at a flow rate of less than 0.25 bbl/d.

We now calculate the formation water flow rate from the measured conductivity according to (9) and using the parameters in Table 1. Figure 4 shows the formation water flow rate as a function of measured conductivity.

# 34<sup>th</sup> International North Sea Flow Measurement Workshop 25-28 October 2016

## Technical Paper

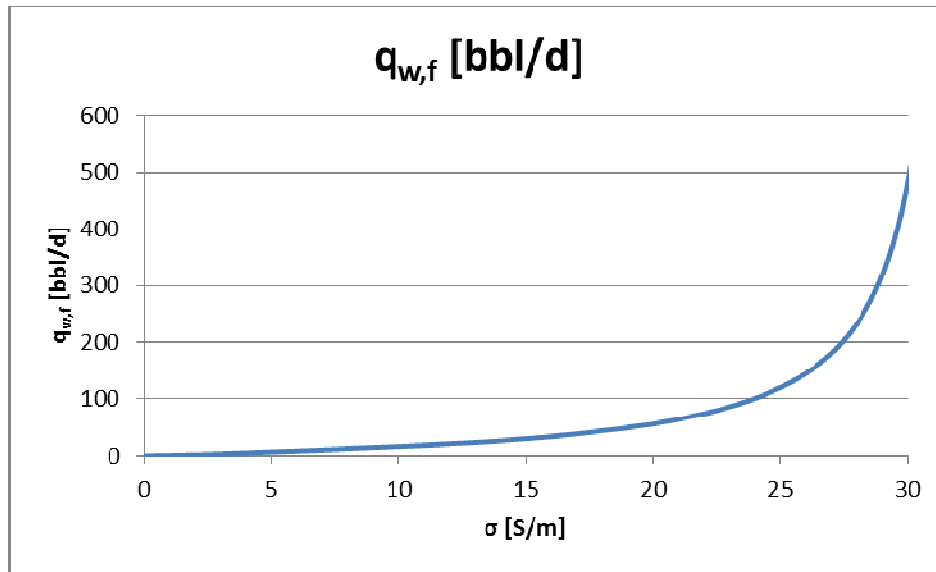


**Figure 4** Formation water flow rate as a function of measured water conductivity.

When the formation water flow rate in this example exceeds 500 bbl/d, the measured salinity  $S_m$  starts approaching the formation water salinity  $S_f$  and uncertainties increase rapidly. The maximum formation water rate that can be reliably estimated in this way needs to be assessed for each individual case.

## 5 MEASURING THE GAS RATE

Differential pressure devices like Venturi tubes and V-Cones are widely used to measure gas and wet gas flow. The presence of liquid in the gas causes additional differential pressure and will cause the gas rate to be overestimated. This is known as over-reading.

There is a very rich literature on the topic of correcting the gas flow rate based on knowing the liquid rate, including *ISO/TR 11583:2012(en) Measurement of wet gas flow by means of pressure differential devices inserted in circular cross-section conduits*, and *ISO/DTR 12748:2014 Wet gas flow measurement in natural gas operations*. We do not intend to discuss the validity or accuracy of the various correction factors and correlations in this paper. The methods we describe do not depend on this, and the user may choose his or her favourite correlation.

The liquid rates at metering conditions are often very small and may constitute much less than 1% of the total volume. This makes it very difficult to measure them accurately. The liquid fraction may be calculated from PVT models and water saturation if the composition and the reservoir conditions are well known, but this is only applicable if there is no formation water. The ability to estimate the gas rate accurately then depends on whether formation water is present or not.

**34<sup>th</sup> International North Sea Flow Measurement Workshop  
25-28 October 2016**

**Technical Paper**

If there is no formation water it is sufficient to measure the differential pressure. Everything else can be calculated. In this case it is very important to detect the first formation water. We have already shown that the presence of formation water can be detected at very low levels by measuring the conductivity of the water, and in most cases we can assume that the uncertainties in the estimates of condensed water and hydrocarbon are much larger.

The most widely used correlations for correcting the gas flow rate measurement include the Lockhart-Martinelli parameter:

$$X = \frac{Q_{l,m}}{Q_{g,m}} \sqrt{\frac{\rho_{g,m}}{\rho_{l,m}}} \quad (10)$$

In the absence of formation water, and still ignoring condensation of hydrocarbons from reservoir to measurement conditions, we get

$$\begin{aligned} Q_{l,m} &= Q_{w,cond,m} \\ &= \left( \rho_{w,vap}(P_r, T_r) \frac{P_w(T_r) P_m T_r}{P_r P_r T_m} - \rho_{w,vap}(P_m, T_m) \frac{P_w(T_m)}{P_m} \right) q_{g,m} \end{aligned} \quad (11)$$

and

$$Q_{g,m} = \rho_{g,m} q_{g,m} \quad (12)$$

hence

$$\begin{aligned} X &= \frac{Q_{l,m}}{Q_{g,m}} \sqrt{\frac{\rho_{g,m}}{\rho_{l,m}}} \\ &= \frac{\rho_{w,vap}(P_r, T_r) \frac{P_w(T_r) P_m T_r}{P_r P_r T_m} - \rho_{w,vap}(P_m, T_m) \frac{P_w,vap(T_m)}{P_m}}{\rho_{g,m}} \sqrt{\frac{\rho_{g,m}}{\rho_{l,m}}} \end{aligned} \quad (13)$$

The Lockhart-Martinelli parameter does not depend on the liquid rate but solely on densities and fractions that can all be calculated from the fluid properties and pressure and temperature in the reservoir and at metering conditions. This is true also if hydrocarbons condense out of the gas, but as already mentioned we will not discuss this complication in this paper.

The liquid density is the density of the condensed water (ignoring condensed hydrocarbons).

A commonly used correlation for horizontal Venturi tubes is that of *de Leeuw*. The corrected gas mass flow rate is given as

$$Q_{g,m}^{corr.} = \frac{Q_{g,m}^{meas.}}{\phi} \quad (14)$$

**34<sup>th</sup> International North Sea Flow Measurement Workshop  
25-28 October 2016**

**Technical Paper**

where  $\phi$  is a correction factor based on *Chisholm's* correlation [1],[2]

$$\phi = \sqrt{1 + C_{Ch}X + X^2} \quad (15)$$

with

$$C_{Ch} = \left(\frac{\rho_{l,m}}{\rho_{g,m}}\right)^n + \left(\frac{\rho_{g,m}}{\rho_{l,m}}\right)^n \quad (16)$$

*Chisholm* originally used  $n = 0,25$ , but *de Leeuw* introduced a modification of  $n$  based on the gas densimetric Froude number [3]

$$Fr_{gas} = \frac{v_{g,m}}{\sqrt{gD}} \sqrt{\frac{\rho_{g,m}}{\rho_{l,m} - \rho_{g,m}}} \quad (17)$$

with

$$n = 0.41 \quad \text{for} \quad 0,5 \leq Fr_{gas} < 1.5 \quad (18)$$

$$n = 0.606(1 - e^{-0,746Fr_{gas}}) \quad \text{for} \quad Fr_{gas} \geq 1.5$$

The densimetric Froude number does include the superficial gas velocity, but the error introduced by calculating this from the uncorrected gas rate is insignificant. All the other parameters depend on fluid properties, reservoir conditions, and measurement conditions.

If formation water is being produced, it is necessary to quantify the rate of formation water. We showed that this can be calculated from the rate of condensed water, which again can be calculated from the measured gas rate and the salinity. The salinity is found from the measured conductivity. The Lockhart-Martinelli parameter is then modified to

$$X = \frac{\left(1 + \frac{S_m}{S_f - S_m}\right) \left(\rho_{w,vap}(P_r, T_r) \frac{P_w(T_r) P_m T_r}{P_r T_m} - \rho_{w,vap}(P_m, T_m) \frac{P_{w,vap}(T_m)}{P_m}\right)}{\rho_{g,m}} \sqrt{\frac{\rho_{g,m}}{\rho_{l,m}}} \\ = \left(1 + \frac{S_m}{S_f - S_m}\right) \frac{f(P_r, T_r, P_m, T_m)}{\rho_{g,m}} \sqrt{\frac{\rho_{g,m}}{\rho_{l,m}}} \quad (19)$$

This does not depend on rates either. The liquid density depends on the salinity and fraction of formation water. Again ignoring condensed hydrocarbons, we find that

# 34<sup>th</sup> International North Sea Flow Measurement Workshop 25-28 October 2016

## Technical Paper

$$\begin{aligned}\rho_{l,m} &= \frac{Q_{w,cond,m} + Q_{w,f}}{q_{w,cond,m} + q_{w,f}} = \frac{Q_{w,cond,m} + Q_{w,f}}{\frac{Q_{w,cond,m}}{\rho_{w,cond,m}} + \frac{Q_{w,f}}{\rho_{w,f}}} = \\ &= \frac{1 + \frac{S_m}{S_f - S_m}}{\frac{\rho_{w,f}}{\rho_{w,cond,m}} + \frac{S_m}{S_f - S_m}} \rho_{w,f} \quad (20)\end{aligned}$$

Determining the liquid density depends only on knowing the formation water salinity and the salinity of the water at measurement conditions.

The Froude number and the Chisholm parameter are also updated with the new liquid density.

## 6 A NEW TYPE OF THREE-PHASE WET GAS FLOWMETER

We have so far shown that we, in wet gas flow, can measure the gas rate with a differential pressure meter and correct the over-reading. The correction can be made without additional measurements if we can verify that the well is not producing any formation water.

If formation water is being produced, we have shown that it is sufficient to measure the conductivity of the liquid water at the measurement conditions in order to determine the total liquid rate and correct the gas rate, at least when there is sufficient condensed water. This requires, however, that the reservoir conditions and fluid properties are known.

The workflow can be summarized as follows:

- Characterize fluid behaviour, if needed by building Equation of State models covering reservoir and well measurement conditions.
- Measure pressure, temperature, and differential pressure at measurement conditions
- Calculate the fluid densities at measurement conditions
- Measure reservoir pressure and temperature
- Calculate the liquid fractions at measurement conditions
- Measure the conductivity of the liquid water
- If formation water is present, estimate the fraction of formation water and update the liquid fraction and liquid density
- Calculate a corrected gas rate
- Calculate the liquid rates from the corrected gas rate

# 34<sup>th</sup> International North Sea Flow Measurement Workshop 25-28 October 2016

## Technical Paper

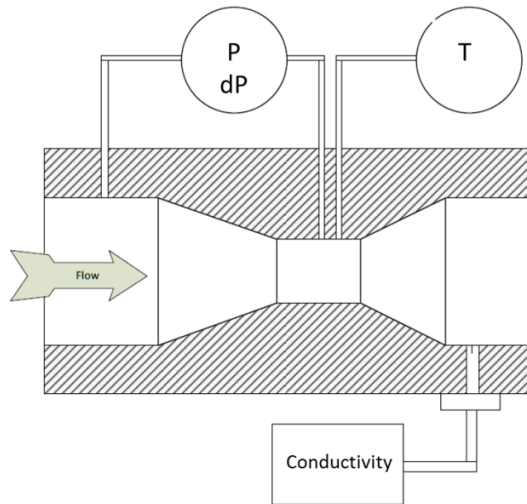


**Figure 5** Wet gas flowmeter combining a differential pressure flowmeter and a water conductivity measurement.

## 7 EXAMPLE

Let us now return to the example from section 5 and look at the effect of increasing formation water rates. We have calculated the over-reading in the gas rate and the salinity and conductivity of the water that is liquid at measurement conditions, that is – the mixture of formation water and condensed water. We have then applied the workflow from section 7 starting with the gas rate and the water conductivity as they would be measured.

The condensed water rate of 44,6 bbl/d will cause an over-reading in the gas rate of 0.5%. As the formation water rate increases from 0 to 550 bbl/d the Lockhart-Martinelli parameter increases to 0,0342, and the over-reading increases to 7%.

Figure 6 shows the measured gas rate as a function of formation water rate. The true gas rate is 50 MMscf/d. The line labelled "Corrected, ignoring form. w." shows the gas rate corrected for the condensed water only, and the line labelled "Corrected" shows the gas rate corrected for both the condensed water and the formation water based on the measured water conductivity. The deviation between the corrected gas rate and the reference is caused by cumulative errors through the forward and inverse modelling and amounts to ~0.25% at 550 bbl/d of formation water.

The corrected gas rate is a function of many parameters, and many uncertainties are involved, but we will now focus on the sensitivity to the uncertainty associated with the measurement of the water conductivity. We have assumed a maximum measurement error of 0.5 S/m. This is conservative, in particular at low water salinities. In Figure 6 the resulting gas rate estimates are labelled "Corrected, S +0.5" and "Corrected, S -0.5" respectively. Note that if the measured water conductivity is higher than the true water conductivity the

# 34<sup>th</sup> International North Sea Flow Measurement Workshop 25-28 October 2016

## Technical Paper

water rate will be over-estimated and the correction will be too large. The corrected gas rate will in this case be too small.

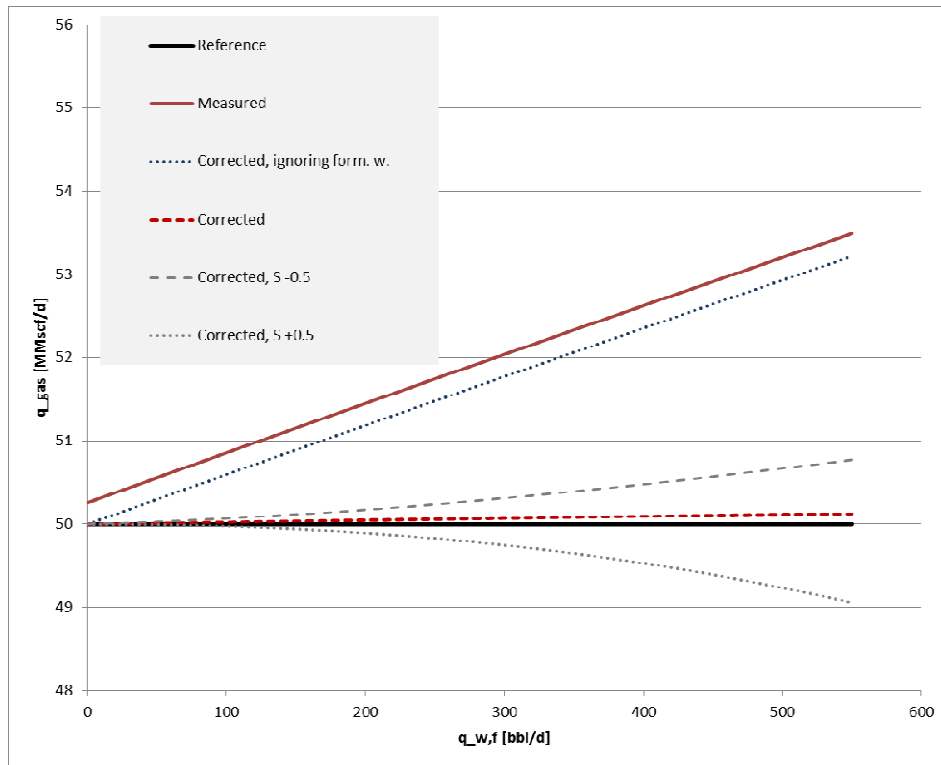


**Figure 6** Estimated gas rate as a function of the formation water rate.

We also note that the sensitivity is higher when the measured conductivity is too high than when it is too low. This is caused by the increasing slope of the formation water as a function of water conductivity, as seen in Figure 4.

## 8 CONCLUSIONS

Gas and wet gas wells are producing from formations where all the produced fluids initially are in the gas phase, with the exception of possible formation water. If no formation water is being produced, it is possible to calculate all liquid fractions from composition and knowledge about reservoir conditions and measurement conditions. These liquid fractions may be used to correct a differential pressure gas rate measurement.

Additional measurements are required when formation water is being produced. In this paper we have shown that it is sufficient to measure the conductivity of the water. We have described a workflow for estimating the formation water fraction, and then using this to correct a differential pressure gas rate measurement and the liquid rates derived from the gas rate.

# 34<sup>th</sup> International North Sea Flow Measurement Workshop 25-28 October 2016

## Technical Paper

### 9 NOTATION

The following notation is used for variables and parameters being measured or calculated:

$C_{ch}$	Chisholm's parameter
$D$	diameter
$F$	volume fraction
$Fr$	densimetric Froude number
$P$	pressure
$P_w$	vapour pressure of water
$q$	volumetric flow rate
$Q$	mass flow rate
$\rho$	mass density
$S$	salinity of water
$T$	temperature
$v$	velocity
$X$	Lockhart-Martinelli parameter
$\phi$	gas mass rate correction factor

The following subscripts are used to indicate which fluid is being measured or calculated:

$g$	gas
$l$	liquid
$w$	water
$f$	formation water

The following subscripts are used to indicate the conditions where a variable is measured or calculated:

$r$	reservoir condition
$m$	metering conditions, normally at or near the well head
$C$	conditions of the critical point of water

The following subscripts indicate the phase of the liquid being measured or calculated:

$cond$	liquid water that was in vapour phase in the reservoir but is now condensed
$vap$	water in vapour phase

**34<sup>th</sup> International North Sea Flow Measurement Workshop  
25-28 October 2016**

**Technical Paper**

**10 REFERENCES**

- [1] Chisholm, D. Flow of Incompressible Two-Phase Mixtures through Sharp-Edged Orifices, *Journal of Mechanical Engineering Science*, Vol 9, No. 1, 1967
- [2] Chisholm, D. Research Note: Two-Phase Flow through Sharp-Edged Orifices, *Journal of Mechanical Engineering Science*, Vol. 19, No. 3, 1977
- [3] de Leeuw, H. Liquid Correction of Venturi Meter Readings in Wet-Gas Flow, *Proc. of the 15th North Sea Flow Measurement Workshop*, Paper 21, 1997
- [4] Saul, A., & Wagner, J. *Phys. Chem. Ref. Data* 16, 893, 1987
- [5] Solheim, H. Conductivity measurement for multiphase and wet gas flow conditions, for both oil and water continuous flows, *Underwater Technology Conference*, 2015
- [6] Wagner, W., & Pruss, A. *J. Phys. Chem. Ref. Data*, 783, 1993

## Modelling of Wet Gas flow in Venturi Meters to Predict the Differential Pressure

H.R.E. van Maanen, Hint B.V.  
H. de Leeuw, Shell Global Solutions B.V.

### 1 INTRODUCTION

Fossil fuels will remain to provide a large fraction of the world's energy needs in the decades to come. As natural gas is a relatively clean fuel and because of its abundance, it is expected to be a major contributor. However, virtually all gas-wells produce not only gas, but also liquids, both hydrocarbon condensates as well as water. The latter consists of condensed water and often also formation water. Such flows of gas and liquids are usually referred to wet-gas. In this paper, we will use the term wet-gas for such flows where the Lockhart-Martinelli (LM) parameter is below 0.35 and the flow is not slugging or unstable (e.g. churn flow).

Flow rate measurement of wet-gas streams with a dedicated multi-phase/wet-gas flow meter would be beneficial as this is simpler and cheaper than the use of test-separators.

We think the performance of such flow meters in general could improve significantly, but it would require a much better understanding of the physics governing the measurement process than is currently available in the public domain. This paper is intended to make a start by disclosing our models for horizontal and vertical Venturis. We hope this will inspire others to come forward with further contributions bringing our collective understanding to a higher level.

### 2 THE BASIC EQUATIONS

Differential pressure flow meters are based on the Bernoulli equation, which states that specific kinetic energy and pressure (specific static energy) are interchangeable:

$$p + \frac{1}{2} \rho v^2 = C \quad (1)$$

Differential pressure flow meters are designed in such a way that the velocity of the fluid is changed, leading to a change in pressure. The differential pressure is a measure for the flow rate:

$$Q = C_D \varepsilon \frac{\beta^2}{\sqrt{1 - \beta^4}} A_D \sqrt{\frac{2\Delta p}{\rho}} \quad (2)$$

The actual gas volume fraction is defined as:

$$GVF_a = \frac{Q_{gas}}{Q_{gas} + Q_{liquid}} \quad (3)$$

The superficial velocities are defined as:

$$v_{sg,l} = \frac{Q_{g,l}}{A_D} \quad (4)$$

## 34<sup>th</sup> International North Sea Flow Measurement Workshop 25-28 October 2016

The gas Froude number is defined as:

$$Fr_g = \sqrt{\frac{\rho v_{sg}^2}{(\rho_l - \rho_g)gD}} \quad (5)$$

The liquid Froude number is defined as:

$$Fr_l = \sqrt{\frac{\rho v_{sl}^2}{(\rho_l - \rho_g)gD}} \quad (6)$$

With the Lockart-Martinelli parameter defined as:

$$LM = \frac{Fr_l}{Fr_g} = \frac{v_{sl}}{v_{sg}} \sqrt{\frac{\rho_l}{\rho_g}} = \frac{Q_l}{Q_g} \sqrt{\frac{\rho_l}{\rho_g}} = \frac{w_l}{w_g} \sqrt{\frac{\rho_g}{\rho_l}} \quad (7)$$

The overreading of a differential pressure flow meter in wet-gas is defined as:

$$Overreading = \sqrt{\frac{\Delta p_{tp}}{\Delta p_{go}}} \quad (8)$$

It is possible to derive the overreading analytically under the assumption that the flow is either fully stratified or when it is a homogeneous mist flow in which the liquid is fully dispersed as small droplets. The results are given below without derivation. These can be found elsewhere. The overreading in a stratified flow is:

$$Overreading = 1 + LM \quad (9)$$

The correlation of Murdock<sup>[1]</sup> is based on this equation, but a constant was added to fit his experimental data better. The overreading of a mist flow is:

$$Overreading = \sqrt{1 + \left[ \left( \frac{\rho_g}{\rho_l} \right)^{0.5} + \left( \frac{\rho_l}{\rho_g} \right)^{0.5} \right] \cdot LM + LM^2} \quad (10)$$

Note that the overreading of the stratified flow can be rewritten as:

$$Overreading = 1 + LM = \sqrt{1 + 2 \cdot LM + LM^2} = \sqrt{1 + \left[ \left( \frac{\rho_g}{\rho_l} \right)^0 + \left( \frac{\rho_l}{\rho_g} \right)^0 \right] \cdot LM + LM^2} \quad (11)$$

The overreading has been described in several correlations and we will discuss two of these here. The first is the correlation of Chisholm<sup>[2]</sup>. His correlation reads:

$$Overreading = \sqrt{1 + \left[ \left( \frac{\rho_g}{\rho_l} \right)^{0.25} + \left( \frac{\rho_l}{\rho_g} \right)^{0.25} \right] \cdot LM + LM^2} \quad (12)$$

As Chisholm did the experiments, on which his correlation is based, at relatively low pressures and with air-water, it is likely that his flow regime was stratified entrained. So his value of 0.25 in the above equation, halfway between zero and 0.5, seems not unrealistic.

De Leeuw<sup>[3]</sup>, having gathered a large set of experimental data up to higher pressures and gas Froude numbers and subsequently building on the above equations, modified it by introducing a parameter "n":

## 34<sup>th</sup> International North Sea Flow Measurement Workshop 25-28 October 2016

$$\text{Overreading} = \sqrt{1 + \left[ \left( \frac{\rho_g}{\rho_l} \right)^n + \left( \frac{\rho_l}{\rho_g} \right)^n \right] \cdot LM} + LM^2 \quad (13)$$

In which  $n$  is taken as a function of the gas Froude number:

$$\begin{aligned} n &= 0.41 & 0.5 < Fr_g < 1.5 \\ n &= 0.606 \cdot (1 - e^{-0.746 Fr_g}) & Fr_g > 1.5 \end{aligned}$$

Both the correlations of Chisholm and De Leeuw predict the overreading in the limiting cases of  $LM \downarrow 0$  and the dense phase  $\rho_g \uparrow \rho_l$  correctly. An interesting aspect of the correlation of De Leeuw is that it predicts an overreading *above* the overreading for the homogeneous mist flow which, at first sight, seems to be the upper limit for the overreading. We will park this question for the moment and come back to this issue later. We will first discuss the limitations of correlations.

### 3 THE LIMITATIONS OF CORRELATIONS

Correlations are basically mathematical curve fits through experimental data points. Some correlations, like those of Chisholm and De Leeuw, use a basic equation for the phenomenon they want to curve-fit, whereas others, like the one of Steven<sup>[4]</sup>, use equations which are not necessarily related to a basic equation. Although some speak of "models" in this case, this is incorrect as it is not based on physics.

Strictly speaking, correlations are only valid within the range of the experimental data on which they are based and validated. Therefore it is possible that correlations do not predict limiting cases correctly when these lay outside the range of the experimental data. As stated before, the correlations of Chisholm and De Leeuw predict the limiting cases correctly and a requirement for correlations could be that these include the limiting cases for which the behaviour is known.

However, a large problem with correlations is that these include a number of parameters to enable the use of the correlations with fluids with different physical properties. The selection of the parameters is educated guesswork and is often enforced by the limitation of the fluid properties which could be used during the experiments on which the correlation is based. However, there is no guarantee that all essential parameters are included in the correlation. In general, it is impossible to include all important properties in the experiments: the number of required data-points will simply become too large. So unless a better understanding of the physics, which govern the measurement process, is obtained, no guarantee can be given that correlations give correct and accurate predictions when the physical properties of the fluids used in the application are different from those in the experiments (and they always will). As a consequence, a narrow fit in a tested range does not imply any accuracy in other ranges and or other fluids.

Only when there is a good understanding of the governing physics, the essential physical properties can be revealed and it will become possible to predict the overreading in application with different conditions, e.g. pipe diameters, different  $\beta$ -ratios and different fluids. Also, applications outside the range of the experimental data become more trustworthy, thereby greatly extending the possibilities to apply wet-gas flow rate measurement in practice.

# 34<sup>th</sup> International North Sea Flow Measurement Workshop

## 25-28 October 2016

To avoid the use of correlations this paper presents the models developed for a wet gas flow through a horizontal Venturi and through a vertical upward Venturi. Both models will be described in the sections below.

### 4 THE EXTENSION OF THE BERNOULLI EQUATION

The Bernoulli equation is only valid for systems with no energy loss. When energy losses do occur, correction term(s) need to be added. This is illustrated by e.g. the orifice meter. It is well known that the discharge coefficient of an orifice is roughly 0.6, which can be interpreted in the following way:

$$\Delta p_o = \Delta p_B + \Delta p_d \quad (14)$$

It can be remarked that (eq. 2)

$$\Delta p_B = C_D^2 \Delta p_o \quad (15)$$

Reworking the two equations above yields:

$$\begin{aligned} \Delta p_o &= C_D^2 \Delta p_o + \Delta p_d \\ \Delta p_d &= (1 - C_D^2) \cdot \Delta p_o \end{aligned} \quad (16)$$

So with a discharge coefficient of 0.6, the contribution of the ideal Bernoulli equation to the differential pressure is 36% and 64% is generated by dissipation.

This explains why the pressure recovery of an orifice is only minor. A Venturi with a discharge coefficient of 0.995 thus has only 1% of the differential pressure generated by dissipation, so it is expected that its pressure recovery is significantly higher than that of an orifice. However, in the divergent section, significant turbulence is generated, leading to additional dissipation. Which is why the Venturi still has a noticeable total pressure loss, which depends on its construction.

Therefore it is clear that, in order to describe the differential pressure of a Venturi in a wet-gas flow, a dissipation term needs to be added to the Bernoulli equation. Implicitly, the rising of the "n" value above 0.5 in the correlation of De Leeuw is the inclusion of such a dissipation term. It does, however, not describe the size and the cause(s) of the dissipation. The given that the "n" value can become larger than 0.5 and knowing that the total pressure loss ratio of a Venturi is in a wet-gas flow significantly higher than in a single phase flow, reveal that already energy is dissipated upstream of the throat pressure tap. This will have to be included in the model.

It is to be expected that the dissipation mechanisms in a horizontal and a vertical upward Venturi are different. Because of the size limitation, it is not possible to include all the details and all the required equations into this paper. The crucial steps, however, will be described and discussed. For more details, the authors can be approached. As we do not have the possibilities to develop these models further on our own, we welcome any person or institution to bring this work further. We can provide the current state of the development and may provide data-sets from tests under realistic conditions.

### 5 MODELLING OF HORIZONTAL FLOW IN VENTURIS

The modelling of the differential pressure inlet – throat is based on an extension of the Bernoulli equation and will include the contributions by the gas, the

## 34<sup>th</sup> International North Sea Flow Measurement Workshop 25-28 October 2016

dispersed liquid(s), dissipation terms and some smaller contributors. This approach leads to the following equation:

$$N_t = \frac{I}{2} \left[ \rho_g v_g^2 A_g + \rho_l v_d^2 A_{lg} + \rho_l v_{lf}^2 A_{lf} \right] + N_{st} + N_{pl} + N_{diss} + P \quad (17)$$

Note that for the calculation of  $v_g$ ,  $A_g$ ,  $v_d$ ,  $A_{lg}$ ,  $v_{lf}$  and  $A_{lf}$  the local hold-up is required. Its calculation has been done by the authors, but this not included in this paper to limit its length.

The challenge is to determine the different contributors to this equation under realistic conditions. To indentify these, several parameters need to be known. Therefore, we will give a description of the wet-gas flow upstream and moving into the Venturi up to the throat pressure tap.

Upstream of the Venturi, a partly entrained, partly stratified-wavy flow regime is maintained. The energy of the moving fluids upstream of the Venturi is dependent on the entrained fraction. Correlations for the entrained fraction can be found in literature<sup>[7]</sup>, we used the Shell Vassiliadou relationship<sup>[5]</sup>:

$$E_f = E_M \frac{factor}{1 + factor} \quad (18)$$

in which:

$$E_M = \max \left( 0, \frac{w_l - w_{l,c}}{w_l} \right) \quad (19)$$

and *factor* is:

$$factor = 1.27 \frac{\eta_g}{(\rho_l - \rho_g) \rho_l \sigma g} (\rho_l \rho_g)^{1.5} v_{sg}^5 f_{sg} \quad (20)$$

and  $f_{sg}$  is the friction factor, smooth pipe, turbulent flow, based on superficial gas velocity:

$$f_{sg} = \frac{0.046}{Re_{sg}^{0.2}} \quad (21)$$

and  $Re_{sg}$  is:

$$Re_{sg} = \frac{v_{sg} D \rho_g}{\eta_g} \quad (22)$$

Once the entrained fraction is determined, the energy of the moving fluids can be found using the quasi Lockhart-Martinelli parameter, derived in Appendix 1:

$$E = \frac{I}{2} \rho_{mix} v_{s,mix}^2 (1 + LM_q) + \frac{I}{2} \rho_l (1 - E_f)^2 v_{sl}^2 \left( \frac{1 + LM_q}{LM_q} \right) \quad (23)$$

When the fluids move into the convergent section of the Venturi, the gas will start to accelerate. Due to the inertia of the droplets, these will lag the gas. This has two major consequences: the first is dissipation because of an increase in the velocity difference between the gas and the droplet, the second is an increase of the drag force on the droplet. When the drag force exceeds the surface tension,

## 34<sup>th</sup> International North Sea Flow Measurement Workshop 25-28 October 2016

the droplet is no longer able to withstand the increasing force and it will break up into smaller droplets.

In the calculation, this is approximated by the split of the droplet into two with identical sizes. This phenomenon also explains why the Venturi acts like a nozzle and the average droplet diameter in the throat is smaller than upstream of the Venturi. A major consequence of this description is that the surface tension is an important parameter, which now will be included.

The accelerating gas also creates an increasing shear on the gas-liquid interface, which will enhance the entrainment of droplets itself. The Vassiliadou relationship yields unrealistically high values for the entrained fraction, certainly at higher liquid loadings, as it is impossible to entrain so much liquid in the short time that the fluids stay in the convergent section of the Venturi. However, no reference which describes these phenomena has been found in the open literature, therefore, a novel correlation has been introduced, based on the SINTEF and CEESI data-sets:

$$er = 0.285 \left( \frac{\rho_g}{\rho_l} \right)^{0.29} \quad (24)$$

Note that the entrainment rate has the dimension of m/s, in order to calculate the actual volumetric entrainment, the value needs to be multiplied by the surface area from which the entrainment takes place.

The entrainment rate thus shows to be a shallow function of the ratio of the gas and liquid densities. Although these assumptions are only an approximation of reality, we think that this is the best approach available at the moment, although we realise that future work might bring better relationships. However, the complete model described here has been tested with experimental data from K-lab with a different Venturi, a different  $\beta$ -ratio and different fluids and it performed very well.

### 5.1 The Dissipation of the Gas Flow Around the Droplets

The normalised dissipation energy  $N_{diss}$  has two contributing components:

$$N_{diss} = N_{dg} + N_{sr} \quad (25)$$

The above described mechanisms enables the calculation of the contribution to the differential pressure by the Bernoulli effect of the gas, the entrained liquid and the liquid in the film and the dissipation due to the gas flow around the droplets. However, the contributions caused by the dissipation due to the interfacial roughness, the increase in potential energy of the stratified liquid (the throat is at an elevated level) and the energy stored in the surface tension (in the throat more and smaller droplets are present) still need to be included.

The drag force on the droplet is equal to:

$$F_d = C_w \left( \frac{1}{4} \pi d^2 \right) \left( \frac{1}{2} \rho_g v_r^2 \right) \quad (26)$$

The drag coefficient is found from:

$$C_w = \frac{24}{Re} + 0.44 \quad (27)$$

# 34<sup>th</sup> International North Sea Flow Measurement Workshop

## 25-28 October 2016

in which  $Re$  is:

$$Re = \frac{v_r d \rho_g}{\eta_g} \quad (28)$$

This is a well-known and often used correlation for spherical bodies and has been used here<sup>[6]</sup>.

### 5.2 Other Contributors to the Differential Pressure

It is assumed that the entrainment and deposition of the droplets upstream of the Venturi are in equilibrium and that at the entrance of the convergent section of the Venturi the droplets move with the gas velocity. If they would not, the gas would exert a force on the droplet until they did. This assumption does not take into account that the droplets have a limited "lifetime", i.e. are created with a velocity below the average gas velocity and are re-deposited in the liquid film after a certain time (which is probably random). However, the entrained fractions in the pipe, upstream of the Venturi, are relatively low and therefore the error in the determination of the kinetic energy of the entrained liquid will be small. On top of this, the kinetic energy of the moving fluids upstream of the Venturi is only a small term in the energy balance and hence has a small effect, except for a relatively large  $\beta$ -ratio (say  $> 0.7$ ).

The droplets which are entrained in the convergent section of the Venturi are given an initial velocity equal to the velocity of droplets already entrained. Although this is not completely realistic, it is a reasonable assumption and it simplifies the calculations. Note that the surface of the liquid layer, from where the droplets are torn from the liquid film, has a velocity which is roughly twice the average velocity of the liquid film due to the linear velocity profile in the liquid film. On top of that, the gas velocity close to the gas-liquid interface is lower than the average gas velocity, due to the friction at the gas-liquid interface. Thus, the velocity difference between the newly entrained droplets and the gas surrounding these, should therefore be in the same order of magnitude as that of the already entrained droplets. This velocity difference is more important than the absolute velocity and in case it would be significantly larger, it would result in break-up of the droplets.

The liquid film in the convergent section and the throat gives rise to a rough surface, which causes viscous dissipation in a similar way as in normal pipe flow. The surface roughness is taken as  $0.085 m$ ;  $m$  = liquid film thickness; the film is assumed to have a constant thickness across the circumference. However, the contribution to the dissipation is small but increases with decreasing gas density. The reason is that at the lower gas densities the hold-up is higher and the entrained fraction is lower. Both result in an increased surface roughness and thus friction factor.

The surface tension of the droplets represents an amount of energy, which increases as the total surface of the droplets increases when the fluids move through the Venturi up to the throat. The calculation of this contribution can be found in Appendix 3.

When the liquid is lifted from the lower half of the pipe into the throat of the Venturi, the potential energy of the liquid increases. This energy is delivered by the flow, thus increasing the pressure change. The liquid will -in the majority of the cases- be partly stratified. The potential energy of the liquid which stays in

## 34<sup>th</sup> International North Sea Flow Measurement Workshop 25-28 October 2016

the liquid layer at the bottom will increase due to the higher level of the throat. The potential energy of the liquid, entrained into the gas, increases even more as it is lifted from the liquid layer.

This results in relatively more significant contributions at the low gas Froude numbers. At the lowest gas Froude number, the liquid is damming up against the throat, which means that the raise in potential energy is already partly completed by the time the liquid reaches the upstream pressure tap as is illustrated in fig. 1.

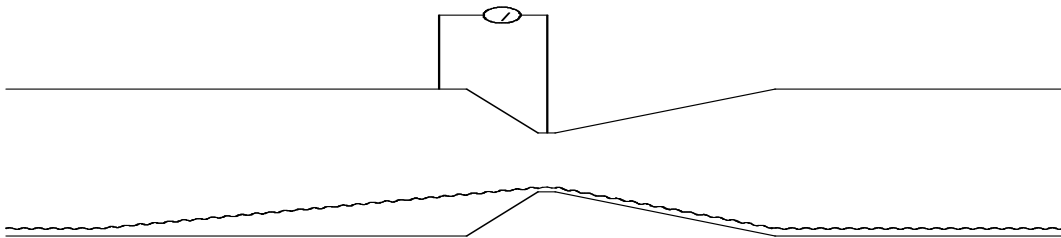


**Figure 1:** *The damming of the liquid up against the throat. Note the compression of the horizontal scale to elucidate the effect.*

Note that due to this liquid build-up, the gas velocity at the upstream pressure tap is higher than without it. So far, this phenomenon is not included in the model and could give rise to an over-prediction of the differential pressure at low gas Froude numbers.

## 6 MODELLING OF UPWARD FLOW IN VENTURIS

In a vertical upward wet-gas flow, the gas is the "continuous phase". The liquids are partly dispersed as droplets in the gas, partly moving as a film at the wall. Due to turbulence in the gas core, droplets will be deposited in the film at the wall and droplets will be torn off the wavy gas-liquid interface. Due to gravity, the liquids will move slower than the gas as the gas has to lift the liquids against the gravitational force. We will refer to this velocity difference as the "slip velocity".

The realization of the inlet-throat differential pressure has a number of different contributors:

- The Bernoulli dP caused by the gas
- The Bernoulli dP caused by the liquid droplets
- The Bernoulli dP caused by the liquid film
- The dissipation of the gas flow around the droplets
- The dissipation due to viscous forces in the liquid film
- The increase in potential energy of the liquid
- The energy, stored in the surface tension of the droplets

The modeling will require a description to quantify the different contributions. Note that some contributions are irreversible, which means that the total pressure loss (ratio), the outlet-inlet differential pressure, will be larger than in a single-phase system. The modeling will be described below in several separate steps.

### 6.1 The Dissipation of the Gas Flow Around the Droplets

The droplets are lifted against gravity by the friction of the gas flow around them. However, there are some limitations. The first question is the maximum droplet diameter which will occur in such a flow under the given conditions.

## 34<sup>th</sup> International North Sea Flow Measurement Workshop 25-28 October 2016

Basically, there are three forces acting on the droplet: the drag force of the gas flow around the droplet, the gravitational force and the surface tension. With increasing droplet diameter, the gravitational force increases rapidly (with the third power of its diameter), which has to be balanced by the same increase in the drag force. But this force is acting on the surface of the droplet and it is not hard to see that at a given diameter the surface tension is no longer able to maintain the integrity of the droplet: the drag force simply tears it apart. Using this reasoning, we can predict the maximum size of the droplet: it is the diameter at which the surface tension balances the drag force (which balances the gravitational force).

The gravitational force, acting on the droplet, consists in itself on two forces: one is the gravitational force, caused by its mass and the Earth's gravitational acceleration, the second is the hydrostatic force because the droplet is immersed in gas phase. It is not hard to combine these two and the result (net) gravitational force is:

$$F_g = \frac{\pi}{6} d^3 (\rho_l - \rho_g) g \quad (29)$$

The drag force, acting on the droplets is proportional to the cross-sectional area of the droplet, the kinetic energy of the gas phase, relative to the droplet velocity, i.e. the slip velocity and the so-called drag coefficient. In equation;

$$F_d = C_w \left( \frac{\pi}{4} d^2 \right) \left( \frac{1}{2} \rho_g v_r^2 \right) \quad (30)$$

We will use the same drag coefficient as in the model for the horizontal Venturi.

The surface tension creates a pressure differential with the surrounding gas, which is described for a stationary (relative to the gas) spherical droplet given by the Young-Laplace equation:

$$\Delta p = \sigma \left( \frac{2}{r_d} \right) \quad (31)$$

The force can be found by multiplying the pressure differential by the surface area, but we are not talking about a stationary droplet, but a droplet which is moving through the gas phase. Also, we are looking at a droplet which is at its maximum diameter under such conditions, i.e. at the verge of break-up. Therefore we need to take into account that the surface tension is counteracting the drag force, which acts on the lower half of the droplet and that the droplet, under these conditions, is not spherical anymore, but elongated. Therefore, the Young-Laplace equation cannot be used directly and a different radius has been chosen, related to the lower half of the surface area and the volume related to it to compensate for the above mentioned effects:

$$r_e = \frac{\frac{4}{3} \pi \cdot r_d^3}{2 \pi \cdot r_d^2} = \frac{2}{3} r_d \quad (32)$$

This radius represents the curvature at the "tip" of the ellipsoid, we will use for the radius at middle of the ellipsoid (where the drag force is the largest and will split the droplet as twice this value. The force subsequently becomes

$$\Delta p \cdot 2 \pi \cdot r_d^2 = \sigma \left( \frac{2}{2 \cdot r_e} \right) \cdot 2 \pi \cdot r_d^2 = \sigma \left( \frac{2}{\frac{4}{3} r_d} \right) \cdot 2 \pi \cdot r_d^2 = \frac{3}{2} \pi \cdot \sigma \cdot d \quad (33)$$

Equating this with the drag force yields:

**34<sup>th</sup> International North Sea Flow Measurement Workshop  
25-28 October 2016**

$$C_w \left( \frac{\pi}{4} d^2 \right) \left( \frac{1}{2} \rho_g v_r^2 \right) = \frac{3}{2} \pi \cdot \sigma \cdot d \quad (34)$$

or

$$C_w d \left( \frac{1}{2} \rho_g v_r^2 \right) = 6 \cdot \sigma \quad (35)$$

which is the equation used to determine the maximum diameter of the droplet under dynamic conditions. We will also use this equation to determine the locations of break-up of droplets in the accelerating flow in the convergent section of the Venturi, which will be discussed below.

The relation between  $v_r$  and  $d$  can be found by balancing the equations for the drag and gravitational forces and solving  $C_w$  from these:

$$C_w = \left( \frac{\pi}{6} d^3 \right) (\rho_l - \rho_g) g \left( \frac{4}{\pi} d^{-2} \right) (2 \rho_g^{-1} v_r^{-2}) \quad (36)$$

from which follows:

$$C_w = \frac{4}{3} d (\rho_l - \rho_g) g \rho_g^{-1} v_r^{-2} \quad (37)$$

Multiply both sides with  $Re^2$ :

$$C_w Re^2 = \frac{4}{3} d (\rho_l - \rho_g) g \rho_g^{-1} v_r^{-2} \frac{v_r^2 d^2 \rho_g^2}{\eta_g^2} \quad (38)$$

Substituting the correlation for  $C_w$  in the above equation yields:

$$\left( \frac{24}{Re} + 0.44 \right) Re^2 = \frac{4}{3} d^3 (\rho_l - \rho_g) \rho_g g \eta_g^{-2} \quad (39)$$

Using this quadratic equation,  $Re$  can be solved directly at a given diameter and thus  $v_r$ , yielding starting values for the determination of the maximum diameter using e.g. the Newton-Raphson technique.

A correction is applied for the elongated shape of the droplets. Under the assumptions, described above, the mass of the droplet is twice of that of a spherical droplet with the same radius of curvature at the bottom.

The dissipation around the droplet is calculated in the same way as in the model for a horizontal Venturi as described in Appendix 2. This algorithm is also used in the convergent section of the Venturi. The contribution to the differential pressure is found by multiplying the energy dissipation for each (initial drop) with the number of drops per  $m^3$ . However, two problems arise at this point:

- not all the liquid is entrained as droplets as a part is flowing in the liquid film at the wall, so the "entrained fraction" needs to be determined and
- the droplets move slower than the gas, which needs to be corrected for.

The first is rather trivial, the second less, but it can be understood by looking at a situation in which the gas velocity is so low that it can not lift the droplets (i.e.  $v_g = v_r$ ). In such a case, the dissipation for each droplet would be infinite, as the dissipation will continue, but the droplet will never pass the throat tap.

## 34<sup>th</sup> International North Sea Flow Measurement Workshop 25-28 October 2016

There is a further complication as the gas velocity is higher than the superficial gas velocity. But is also higher than the superficial gas velocity divided by the gas volume fraction (GVF), because that would only be valid if gas and liquid would move with the same velocity. But because the liquid lags the gas, a correction needs to be made by the hold-up or slip between the phases. Note that because of the high GVF in wet-gas flows (>95 %), the corrections are not very large, so we can use some approximations:

- we will assume that all liquid is entrained as droplets
- we will use the superficial gas velocity to do the initial calculation of the slip velocity

Using these approximations, the gas velocity can be calculated using:

$$v_g = \frac{v_{gs} \cdot (Q_g + \frac{v_{gs}}{v_d} \cdot Q_l)}{Q_g} \quad (40)$$

If desired, one can use this value as a first estimate for the actual gas velocity and subsequently use this value to get a better estimate for the gas velocity by replacing  $v_{gs} / v_d$  by  $v_g / v_d$  as this yields a more accurate result. However, even at 95% GVF and a gas velocity only three times the slip velocity, the second iteration is only 0.2% different from the first value, which is a negligible difference as in most other cases the correction will even be smaller.

The contribution of the dissipation to the differential pressure inlet-throat of the Venturi thus becomes:

$$\Delta p_d = P_d \cdot E_f \cdot N_d \cdot \left(\frac{v_g}{v_d}\right) \quad (41)$$

The number of droplets per cubic meter of gas can be found directly from the liquid volume fraction (LVF) and the droplet diameter:

$$N_d = \frac{Q_l}{(Q_l + Q_g) \cdot \left(\frac{\pi}{6} d^3\right)} \quad (42)$$

### 6.2 The Liquid Film Modeling

To model the liquid, flowing in the film at the wall, is the most difficult part of the wet-gas modeling. Therefore, we will first give a qualitative description of the phenomena, which take place and subsequently describe how these can be quantified.

There are four forces acting on the liquid, flowing in the film:

- the gravitational force
- the shear force, caused by the gas flowing along the gas-liquid interface
- viscous forces, caused by the velocity gradient in the liquid film, a consequence of the stationary wall.
- Pressure forces due to the Kelvin-Helmholtz phenomenon.

The gravitational force will tend to induce a downward flow in the liquid, which is counteracted by the shear of the upward moving gas at the gas-liquid interface. To get a feeling for these forces, let us write down the basic equations under the

## 34<sup>th</sup> International North Sea Flow Measurement Workshop 25-28 October 2016

assumption that the thickness of the liquid layer is very small, compared to the internal pipe diameter. The gravitational force will then be:

$$F_g = \pi \cdot D \cdot D_{lf} \cdot L \cdot \rho_l \cdot g \quad (43)$$

The shear force can be calculated using the pressure drop for pipe flow:

$$\Delta p = 4f \left( \frac{L}{D} \right) \left( \frac{1}{2} \rho_g (v_g - v_i)^2 \right) \quad (44)$$

From this, the wall shear stress can be derived using the balancing of the wall shear stress and the pressure drop:

$$\frac{\pi}{4} D^2 4f \left( \frac{L}{D} \right) \left( \frac{1}{2} \rho_g (v_g - v_i)^2 \right) = \pi \cdot D \cdot L \cdot \tau_i \quad (45)$$

from which follows:

$$\tau_i = \frac{f}{2} \rho_g (v_g - v_i)^2 \quad (46)$$

So the problem boils down to the calculation of the Fanning friction factor  $f$ . In literature, the Colebrook correlation<sup>[8]</sup> is often used. It is an implicit correlation, which, however, gives good results. The Colebrook correlation reads:

$$\frac{1}{\sqrt{f}} = -2 \cdot \log_{10} \left( \frac{k}{3.7D} + \frac{2.51}{\text{Re} \sqrt{f}} \right) \quad (47)$$

In this case, the waves on the gas-liquid interface act as the surface roughness for the gas flow. We will assume that the amplitude of the waves is 0.75 times the average thickness of the liquid layer, so the peak-to-peak value is 1.5 times the average thickness and we will use this value for the surface roughness  $k$ . Basically, the internal diameter should be corrected for the reduction due to the liquid film, which has a double influence on the Reynolds number: both by the internal diameter and the gas velocity. But because the Fanning friction factor is, at higher Reynolds number, virtually independent of the Reynolds number, we can use the "dry" internal diameter and the superficial gas velocity.

The Colebrook correlation can be solved by iteration. Usually, within 4 or 5 steps, the result has converged to its final value. This is simpler than using the Newton-Raphson method and about as fast. Using the thus obtained value of the Fanning friction factor, we can calculate the maximum liquid film thickness which can be held up by the interfacial shear stress against gravity. By assuming that  $v_i$  is 0 (zero) both the interfacial wall shear stress and the gravitational force can be calculated. Using the Newton-Raphson method, the maximum thickness can be calculated. Good starting values are e.g. 0.1, 1 and 5 mm thickness for the liquid film.

The shear on the interface, however, can tear off droplets from the liquid film. We will model this as follows:

- The wavelength of the waves on the gas-liquid interface is proportional to the amplitude (and thus of the liquid film thickness, as we assume that the amplitude is 0.75 times the average liquid film thickness, see above) and proportional to the dynamic viscosity of the liquid.

## 34<sup>th</sup> International North Sea Flow Measurement Workshop 25-28 October 2016

- When the shear force exceeds the surface tension at the wave crest, a droplet is torn off, which will thus limit the liquid film thickness.

It is not unrealistic to assume that the waves scale with the liquid film thickness and as the waves induce liquid motion, it is likely that the wavelength will increase with the liquid viscosity. Whether this is proportional is not unrealistic, but unproven. However, as the range of viscosities in wet-gas well flows is not that high, it is likely to be a good starting point. As a starting value, to be refined by validation with experimental values, we will use the viscosity of water at 20°C as reference value. The equation for the wavelength is:

$$\lambda = 2 \cdot \pi \cdot (0.75d_{lf}) \frac{\eta_l}{\eta_{w,20}} \quad (48)$$

The  $r_w$  is the radius of curvature at the wave crest is:

$$r_w = \frac{\lambda^2}{4\pi^2 a} \quad (49)$$

By using the Young-Laplace equation in its two-dimensional form:

$$\Delta p = \sigma \left( \frac{1}{r_w} + \frac{1}{r_y} \right) \quad (50)$$

and noting that  $r_y$ , the curvature in the tangential direction, is very high, it can be written as:

$$\Delta p = \sigma \left( \frac{1}{r_w} \right) = \frac{4\pi^2 a \sigma}{\lambda^2} = \frac{\sigma}{0.75d_{lf}} \cdot \left( \frac{\eta_{w,20}}{\eta_l} \right)^2 \quad (51)$$

When this value exceeds the wall shear stress, droplets are torn off, thus limiting the liquid film thickness. As the wall shear stress also depends on  $d_{lf}$ , the use of the Newton-Raphson method to find the maximum liquid film thickness, allowed by the surface tension, is recommended.

The third limitation for the thickness of the liquid layer at the wall comes from the velocity gradient in the liquid layer in combination with the liquid viscosity. We will assume that we have a linear velocity gradient in the liquid layer and the shear stress at the wall is given by:

$$\tau_w = \eta_l \frac{\partial v_z}{\partial r} \quad (52)$$

In a steady-state condition, this is equal to the interfacial shear stress and the gravitational force on the liquid. Assuming a linear velocity profile in the liquid film,  $v_i$  becomes:

$$v_i = \frac{\partial v_z}{\partial r} \cdot d_{lf} \quad (53)$$

As  $v_i$  increases with increasing  $d_{lf}$ ,  $(v_g - v_i)$  decreases. As the interfacial shear stress decreases with decreasing  $(v_g - v_i)$ , this puts an upper limit on the liquid film thickness, which can be determined using the Newton-Raphson method.

The downward force in the liquid film consists of two components: the gravitational force and the viscous force due to the velocity gradient in the film. If we assume a linear velocity profile in the film, the viscous force is equal to:

**34<sup>th</sup> International North Sea Flow Measurement Workshop  
25-28 October 2016**

$$F_v = \frac{v_i}{d_{lf}} \cdot \eta_l \cdot \pi \cdot D \cdot L \quad (54)$$

The gravitational force is equal to:

$$F_g = \pi \cdot D \cdot L \cdot d_{lf} \cdot \rho_l \cdot g \quad (55)$$

The total downward force thus becomes:

$$F_{dt} = \left[ \frac{v_i}{d_{lf}} \cdot \eta_l + d_{lf} \cdot \rho_l \cdot g \right] \cdot \pi \cdot D \cdot L \quad (56)$$

Now an interfacial velocity needs to be chosen which balances the downward force and is just not able to tear off droplets from the interface:

$$\tau_i = \frac{v_i}{d_{lf}} \cdot \eta_l + d_{lf} \cdot \rho_l \cdot g \quad (57)$$

The criterion for the tearing of droplets from the film is:

$$\tau_i = \frac{\sigma}{0.75d_{lf}} \cdot \left( \frac{\eta_{w,20}}{\eta_l} \right)^2 \quad (58)$$

Equating both equations to eliminate the interfacial shear stress yields:

$$\frac{v_i}{d_{lf}} \cdot \eta_l + d_{lf} \cdot \rho_l \cdot g = \frac{\sigma}{0.75d_{lf}} \cdot \left( \frac{\eta_{w,20}}{\eta_l} \right)^2 \quad (59)$$

which is an explicit equation of the liquid film thickness as a function of the interface velocity. From this follows:

$$0.75g \cdot \rho_l \cdot d_{lf}^2 = \sigma \left( \frac{\eta_{w,20}}{\eta_l} \right)^2 - 0.75v_i \cdot \eta_l \quad (60)$$

The interface velocity can be calculated using the equation above and the Colebrook correlation.

$$\tau_i = \frac{f}{2} \rho_g (v_g - v_i)^2 \quad (61)$$

The Fanning friction factor is a function of the liquid film thickness and the liquid viscosity. So combining this equation with the equation for the downward force yields:

$$\frac{v_i}{d_{lf}} \cdot \eta_l + d_{lf} \cdot \rho_l \cdot g = \frac{f}{2} \rho_g (v_g - v_i)^2 \quad (62)$$

is an explicit equation for  $v_i$  with a given  $d_{lf}$ .

A fourth mechanism is responsible for the limitation of the liquid film thickness, especially at higher velocities. This is caused by the Kelvin-Helmholtz mechanism. An undulation on the liquid film will lead to a pressure undulation because the gas velocity will vary. When this pressure undulation exceeds the surface tension, it will tear off droplets and thus reduce the film thickness. This can be quantified by the equations below.

For the derivation of the equations, we will first assume that the waves at the gas-liquid interface are encircling the complete circumference of the pipe. The concept is that the force, generated by the increase of the gas velocity over the wave crests, has to be balanced by the surface tension. If this force exceeds the

## 34<sup>th</sup> International North Sea Flow Measurement Workshop 25-28 October 2016

surface tension, drops will be torn off the surface, reducing the liquid film thickness. The differential pressure, generated by the surface tension, has been derived above:

$$\Delta p = \frac{\sigma}{0.75d_{lf}} \cdot \left(\frac{\eta_{w,20}}{\eta_l}\right)^2 \quad (63)$$

The differential pressure, caused by the Kelvin-Helmholtz effect is equal to:

$$\Delta p = \frac{1}{2} \rho_g v_{\max}^2 - \frac{1}{2} \rho_g v_{\min}^2 \quad (64)$$

$$v_{\max} = \frac{Q_g}{\frac{\pi}{4} D_{\min}^2} \quad (65)$$

$$v_{\min} = \frac{Q_g}{\frac{\pi}{4} D_{\max}^2} \quad (66)$$

in which:

$$\begin{aligned} D_{\min} &= D - 2 \cdot d_{lf, \max} \\ D_{\max} &= D - 2 \cdot d_{lf, \min} \end{aligned} \quad (67)$$

Using the assumption that the wave amplitude is 0.75 of the average liquid film thickness (see above), the following relations hold:

$$\begin{aligned} D_{\min} &= D - 3.5 \cdot d_{lf} \\ D_{\max} &= D - 0.5 \cdot d_{lf} \end{aligned} \quad (68)$$

When we square these diameters we will assume that  $d_{lf} \ll D$ , we will ignore terms of  $d_{lf}^2$  which results in:

$$\begin{aligned} D_{\min}^2 &\approx D \cdot (D - 7 \cdot d_{lf}) \\ D_{\max}^2 &\approx D \cdot (D - d_{lf}) \end{aligned} \quad (69)$$

Knowing that

$$Q_g = \frac{\pi}{4} D^2 v_{sg} \quad (70)$$

we obtain:

$$v_{\max}^2 = \left(\frac{D}{D - 7 \cdot d_{lf}}\right)^2 v_{sg}^2 \quad (71)$$

$$v_{\min}^2 = \left(\frac{D}{D - d_{lf}}\right)^2 v_{sg}^2 \quad (72)$$

Again ignoring the quadratic terms of the small fractions and using the approximation:

$$\frac{1}{1 - \delta} \approx 1 + \delta \quad (73)$$

when  $\delta \ll 1$ , we obtain:

## 34<sup>th</sup> International North Sea Flow Measurement Workshop 25-28 October 2016

$$\Delta p = \frac{1}{2} \rho_g \frac{12 \cdot d_{lf}}{D} v_{sg}^2 \quad (74)$$

If we assume that the wave covers only  $\frac{1}{4}$  of the circumference of the wall, the equation becomes:

$$\Delta p = \frac{3}{2} \rho_g \frac{d_{lf}}{D} v_{sg}^2 \quad (75)$$

Equating this to the differential pressure, created by the surface tension leads to:

$$\frac{3}{2} \rho_g \frac{d_{lf}}{D} v_{sg}^2 = \frac{\sigma}{0.75 d_{lf}} \cdot \left( \frac{\eta_{w,20}}{\eta_l} \right)^2 \quad (76)$$

Solving  $d_{lf}$  from this equation and putting  $1.125 \approx 1$  (as there are a number of "guessed" values in this number anyway), we obtain:

$$d_{lf} = \sqrt{\frac{\sigma \cdot D}{\rho_g \cdot v_{sg}^2}} \cdot \left( \frac{\eta_{w,20}}{\eta_l} \right) \quad (77)$$

The determination of the liquid film thickness using the Kelvin–Helmholtz mechanism limits the liquid film thickness at the higher liquid flow rates and results in more realistic entrained fractions. In this way, a fourth criterion for the determination of the liquid layer is introduced. The criteria so far are:

1. The balance of the gravitational force, the wall shear stress and the gas-liquid interfacial shear force.
2. The transportation capacity of the liquid film as determined by the first criterion.
3. The tearing of droplets from the gas-liquid interface due to the shear force.
4. The liquid film thickness as determined by the Kelvin–Helmholtz mechanism.

It is obvious that the lowest value of the four limitations on the maximum thickness should be chosen. Once this has been done, the liquid velocity ( $v_i$ ) at the gas-liquid interface can be determined. From this, the volumetric flow rate of the liquid in the film can be calculated under the assumptions of the linear velocity profile in the film and  $d_{lf} \ll D$ , the internal pipe diameter:

$$Q_{lf} = \pi \cdot D \cdot d_{lf} \cdot \frac{v_i}{2} \quad (78)$$

Note that because the above mentioned assumptions the average velocity in the liquid film is  $v_i / 2$ .

The entrained fraction is:

$$E_f = \frac{Q_l - Q_{lf}}{Q_l} \quad (79)$$

Note that the entrained liquid moves as droplets, dispersed in the gas.

### 6.3 The Prediction of the Differential Pressure of the Venturi

Using the above obtained information, the actual gas velocity, the velocity of the droplets, dispersed in the gas and the velocity of the liquid in the film can be calculated and the Bernoulli contributions to the differential pressure can be

## 34<sup>th</sup> International North Sea Flow Measurement Workshop 25-28 October 2016

calculated, taking the break-up of the droplets in the Venturi into account. Similarly, the dissipation contribution can be calculated as described in sec. 3.2 and also the contribution of the surface tension (note that the significant drop in the diameter of the droplets increases the energy, stored in the surface tension). The raise in potential energy can also be calculated, but one should realize that for the droplets, the difference in density between the gas and the liquid needs to be used whereas for the liquid in the liquid film, the liquid density only should be used, because it is not immersed in the gas. The final contribution comes from the friction of the liquid at the pipe wall because of viscosity.

### The Bernoulli contributions

For the calculations of the Bernoulli contributions of the different phases, several aspects need to be taken into account. These are:

1. The actual velocities of the phases need to be used, both in the pipe as in the throat of the Venturi.
2. The fraction of the cross sectional area, taken up by the phases need to be included in the calculation.
3. The contribution of the liquids needs to be separated in the entrained liquid and the film. Both require the weighted average density of the liquid, which is different for the film and the droplets.
4. It is assumed that the phases do not change while traveling through the Venturi, i.e., no gas comes out of solution from the oil and the entrained fractions remain the same.

### Ad 1

As the kinetic energy directly depends on the velocity, this is logical. So the superficial velocities need to be converted to actual velocities. For the gas, this means that the effective diameter of the pipe is reduced, due to the presence of the liquid film and the gas velocity is further increased because of the presence of droplets, which also move slower than the gas. The latter acts as an increase of the liquid volume fraction. Both effects can be described by the following equation:

$$v_g = \frac{Q_g}{\frac{\pi}{4}(D_p - 2d_{lf})^2} \left(1 + \frac{v_g}{v_g - v_s} \cdot E_f \cdot LVF\right) \quad (80)$$

Note that the entrained fraction in the above equation is the entrained fraction for the total liquid flow rate. The same holds for the liquid volume fraction. The calculation of the liquid film thickness and the slip velocity needs to be done for the pipe and the throat and the resulting velocities need to be used for the calculation of the Bernoulli contribution of the gas, which subsequently needs to be corrected for the fraction of the cross sectional area, taken up by the gas (see Ad 2 below).

The slip velocities for the droplets can be calculated using the equations as described in sec. 3.1 and 3.2. Note that the slip velocity in the pipe is influenced by the parameter (currently chosen to be 0.7, see sec. 3.4.2 below) which corrects for the droplet size distribution and that the droplet velocity in the throat still lags the equilibrium velocity.

The average velocity of the liquid film is the interface velocity divided by 2. The interface velocity in the throat is significantly different from that in the pipe, but both can be calculated using the theory as described in sec. 3.3.

## 34<sup>th</sup> International North Sea Flow Measurement Workshop 25-28 October 2016

### Ad 2

The contribution to the Bernoulli differential pressure needs to be corrected for the fraction of the cross-sectional area, taken up by the fluid. This is logical, because if that would not be done, a few drops of liquid would result in a major increase in the differential pressure, which is not realistic. The following equations can be used:

$$A_g + A_d + A_{lf} = 1 \quad (81)$$

$$A_g = \frac{v_{sg}}{v_g} \quad (82)$$

$$A_d = E_f \cdot LVF \cdot \left( \frac{v_g}{v_g - v_s} \right) \quad (83)$$

$$A_{lf} = \frac{4d_{lf}}{D_p} \quad (84)$$

The resulting  $dP_B$  thus becomes:

$$dP_B = A_g dP_{Bg} + A_d dP_{Bd} + A_{lf} dP_{Blf} \quad (85)$$

### Ad 3

Because the liquid consists of two immiscible fluids (oil and water), with different entrained fractions, the weighted densities of the liquid in the film at the wall and dispersed as droplets in the gas are different. These can be calculated using:

$$\rho_d = \frac{Q_o \cdot E_{f,o} \rho_o + Q_w \cdot E_{f,w} \rho_w}{Q_o \cdot E_{f,o} + Q_w \cdot E_{f,w}} \quad (86)$$

$$\rho_{lf} = \frac{Q_o (1 - E_{f,o}) \rho_o + Q_w (1 - E_{f,w}) \rho_w}{Q_o (1 - E_{f,o}) + Q_w (1 - E_{f,w})} \quad (87)$$

### Ad 4

When the fluids move through the Venturi, the velocities and pressure change. Also, the geometry is not "straightforward", which –in principle– all have an effect on the gas-liquid ratio and entrained fractions. The drop in pressure between the inlet and the throat of the Venturi will lead to gas, coming out of solution from the oil. This process is very hard to describe on the time scales of the fluids moving through the Venturi and therefore, it is recommended that the pressure changes are modest, compared to the absolute pressure (< 2%). In this way, it is expected that the effects remain negligible.

In the convergent section of the Venturi, several phenomena will take place. Because of the decrease of the cross-sectional area, droplets will be deposited in the liquid film at the wall, but because of the increase in the gas velocity, droplets will be torn off the liquid film more easily. The entrance of the throat will act as a nozzle, increasing the entrained fraction. This is very hard to model and therefore, because of the countering effects, we will assume that the net-effect is zero.

## 6.4 Refinement of the Initial Conditions

Direct application of the equations, as outlined above, will result in a droplet diameter at the entrance of the Venturi which is at its maximum. This is probably

## 34<sup>th</sup> International North Sea Flow Measurement Workshop 25-28 October 2016

not realistic as due to turbulence, differences will occur. In general, the droplets will show a size distribution with a maximum value as calculated above. But it is very hard to measure the droplet size distribution. Using a droplet size distribution would also complicate the calculations so it is simplified by using a single value of the droplet diameter at the entrance of the Venturi, albeit smaller than the maximum value. A diameter, which is 0.7 times the maximum possible diameter will be used. Fortunately, the calculated dissipation is not strongly dependent on the initial conditions, but it tends to decrease slightly with decreasing diameter at the entrance of the Venturi. It may require some "fine tuning" using experimental data.

### 6.5 Refinement of the Presence of Three Phases

In reality, the flow will be three-phase (gas, oil and water). The question is what will happen to the liquid phase as oil and water are immiscible. Modelling with different alternatives yields, of course, different results, but for the time being, the best results have been obtained when the liquid density is taken as the flow rate weighted average of oil and water. Similarly for the surface tension. It is not unlikely that the strong mixing forces in an upward wet-gas flow lie at the basis for this result, but it is certainly a subject for further study and modelling.

### 6.6 Contribution Due to the Surface Tension of the Droplets

The Young – Laplace equation for the differential pressure of a droplet is

$$\Delta p = \sigma \left( \frac{2}{r_d} \right) \quad (88)$$

This translates for the pressure itself as:

$$\Delta p = \sigma_{o,g} \left( \frac{2}{r_d} \right) E_{f,o} \cdot OVF + \sigma_{w,g} \left( \frac{2}{r_d} \right) E_{f,w} \cdot WVF \quad (89)$$

It is assumed (see above) that the droplet diameters of the oil and water droplets are identical. The surface tension used is the flow rate weighted average of the gas – oil and gas – water values.

### 6.7 Contribution Due to the Wall Shear Stress

The wall shear stress yields a pressure loss which is equal to

$$\Delta p = 4 \left( \frac{v_i}{d_{if}} \right) \eta_l \left( \frac{L}{D} \right) \quad (90)$$

which has to be integrated from the pipe (upstream) pressure tap to the throat pressure tap.

An impression of the different contributions to the differential pressure as predicted by the model for one of the conditions at 20 bar:

Potential energy	46 Pa
Dissipation	12,191 Pa
Bernoulli gas	19,430 Pa
Bernoulli droplets	26,414 Pa
Bernoulli liquid film	864 Pa
Total modelled differential pressure	58,945 Pa

# 34<sup>th</sup> International North Sea Flow Measurement Workshop 25-28 October 2016

## 7 COMPARISON WITH TEST-LOOP DATA

For the initial calibration and verification of the model for the horizontal flow, the data from the Sintef facility in Norway, on which the correlation of De Leeuw was based, have been used. The fluids were Nitrogen and diesel. The same Venturi, 4",  $\beta$ -ratio of 0.4, was subsequently tested at CEESI as part of the wet-gas JIP. Although the fluids at CEESI were significantly different from those at Sintef, the fluids were natural gas and Decane, the model predicted the overreading very well. The next comparison was with a newly built 6",  $\beta$ -ratio 0.739 Venturi which was tested at K-lab, together with a vertical upward Venturi. The fluids at K-lab were natural gas, Sleipner condensate and water. No modifications to the model were made. The physical properties of the fluids were calculated using the Shell STFlash software, a PVT simulator.

### 7.1 Horizontal Venturi Comparison

The model predicted the overreading of the horizontal Venturi correctly for a wide range of conditions. The results are shown in the six figures below, which are a representative sample of the test points at K-lab at respectively 25 bar, 55 bar and 90 bar.

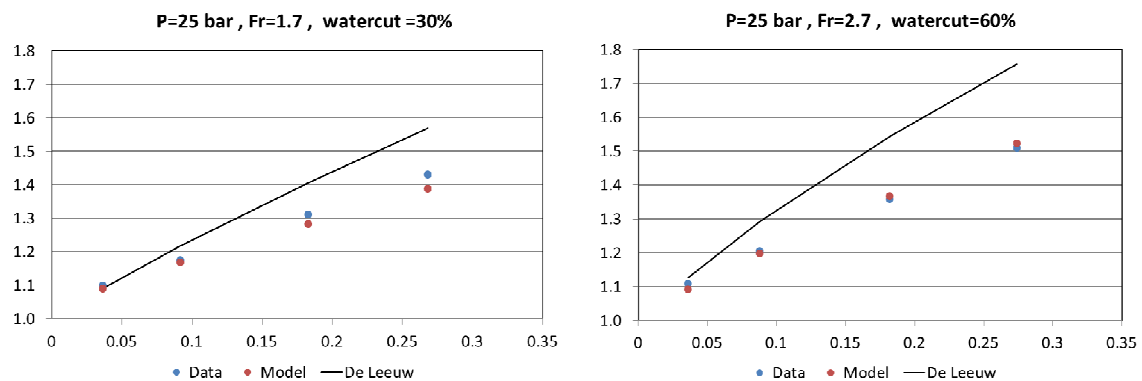


**Figure 2:** Overreading comparison between the measured data, the Venturi model, and the De Leeuw correlation.

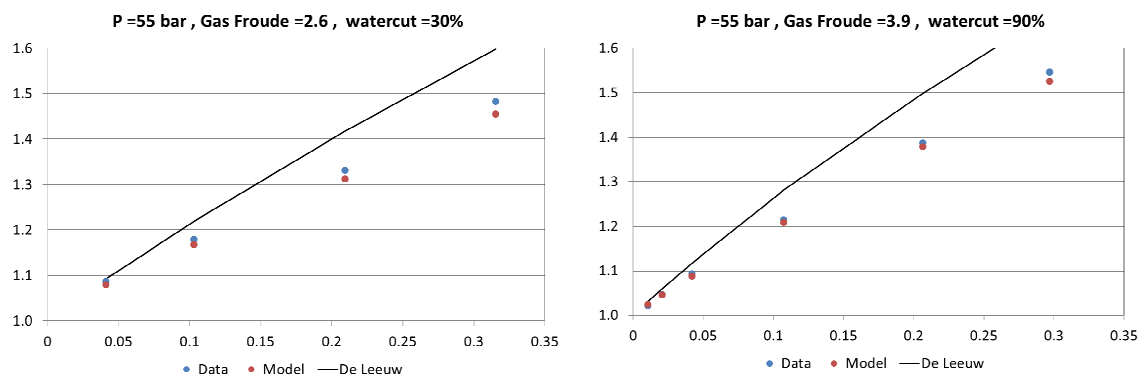


**Figure 3:** Overreading comparison between the measured data, the Venturi model, and the De Leeuw correlation.

# 34<sup>th</sup> International North Sea Flow Measurement Workshop 25-28 October 2016

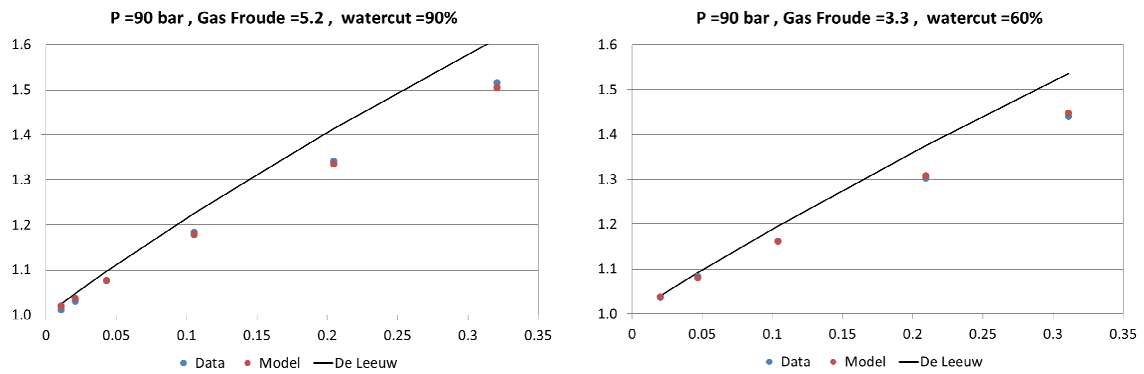


**Figure 4:** Overreading comparison between the measured data, the Venturi model, and the De Leeuw correlation.

## 7.2 Vertical Venturi Comparison

The model for the vertical upward Venturi was developed with a limited propriety data-set. Verification of the model was done using the Shell data-set acquired at K-lab. The fluids and pressures were different from those which were used to develop the model. The results are shown in the figures below.

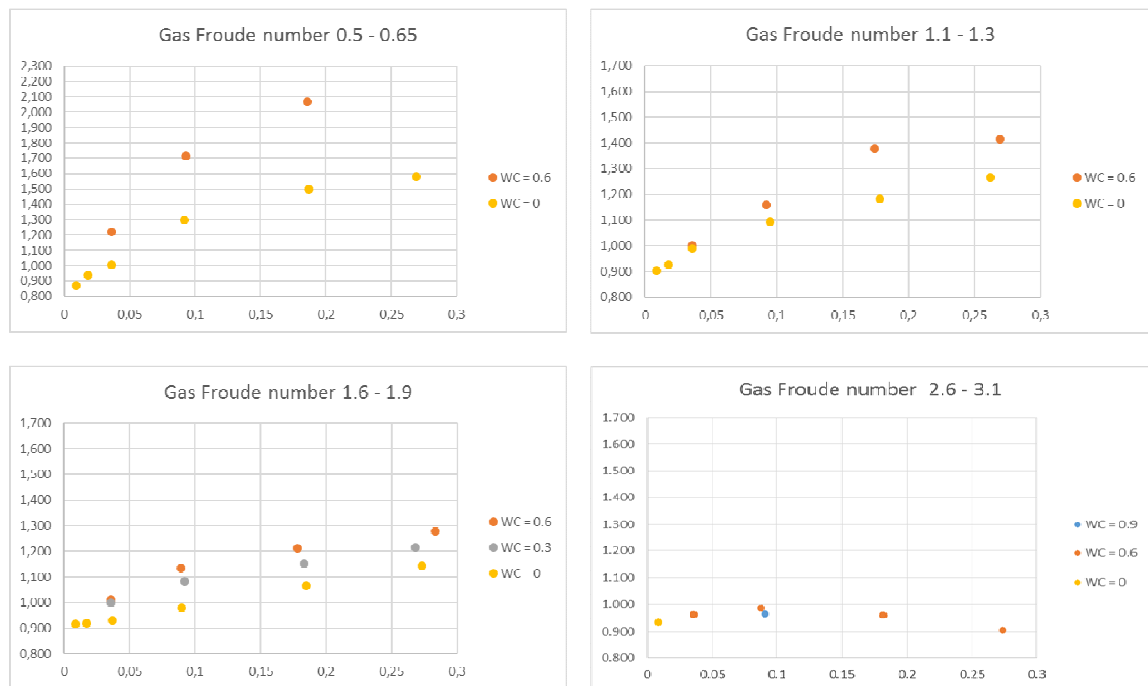


**Figure 5:** Horizontal axis: Lockhart-Martinelli parameter, vertical axis: ratio of modelled differential pressure and measured differential pressure. 25 bar.

# 34<sup>th</sup> International North Sea Flow Measurement Workshop 25-28 October 2016

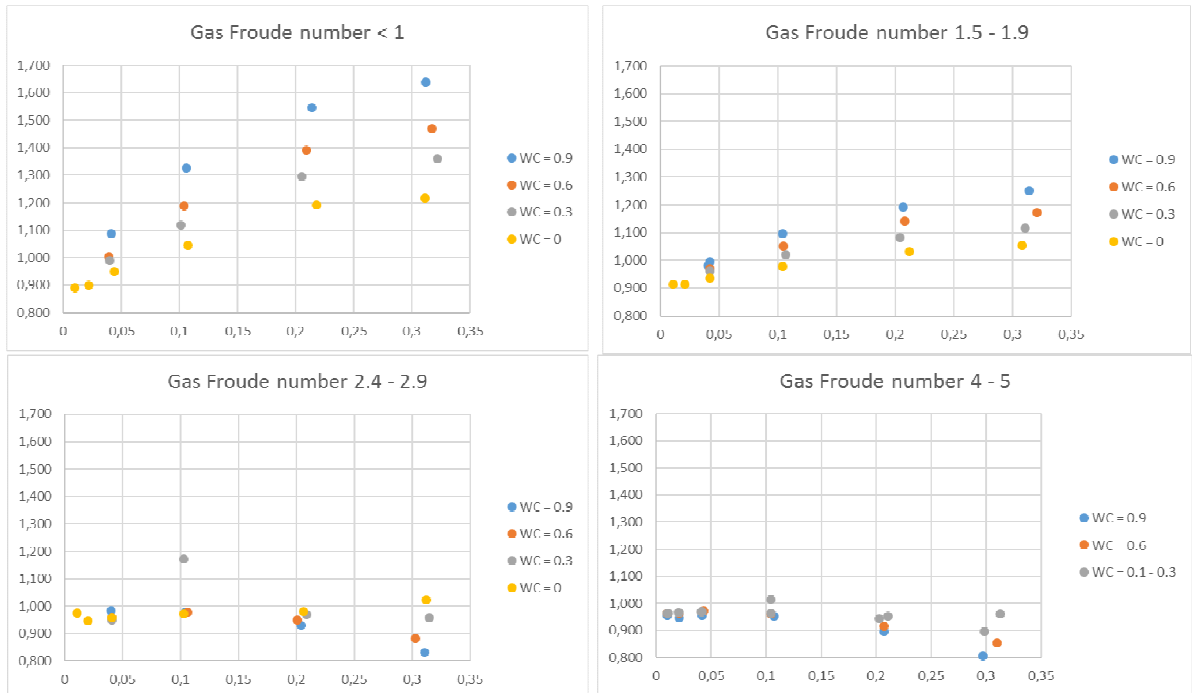


**Figure 6:** Horizontal: Lockhart-Martinelli parameter, vertical: ratio of modelled differential pressure and measured differential pressure. 55 bar.

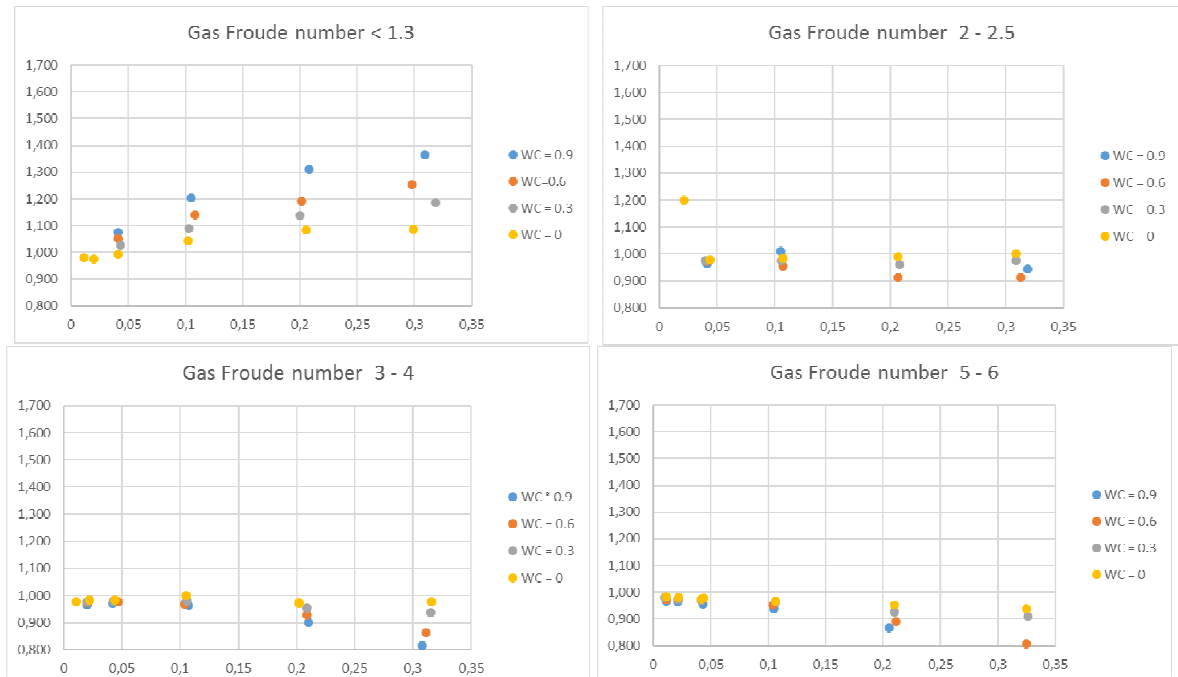


**Figure 7:** Horizontal: Lockhart-Martinelli parameter, vertical: ratio of modelled differential pressure and measured differential pressure. 90 bar.

These results show that the predictions deviate when the gas Froude number is low and the Lockhart-Martinelli parameter is high. There is also a trend with the water cut. The gas density plays a role too as the deviations are larger at 25 bar than at 55 and 90 bar. However, these differences can be understood.

## 34<sup>th</sup> International North Sea Flow Measurement Workshop 25-28 October 2016

Both models assume a “steady state” flow of the three phases. In a horizontal flow line, this condition is fulfilled as long as any intermittent flow regime is avoided. For horizontal wet-gas flows this means that the Lockhart-Martinelli parameter should be below 0.35. For the vertical upward flow, however, this alone is an insufficient requirement. As the liquid has to be transported upward by the gas, hence only specifying that the LM-parameter should be below 0.35 includes the conditions with low gas flow rates: the LM parameter is based on the *ratio* of the liquid and gas flow rates.

It is easy to see that at low flow rates the gas will be unable to lift the liquid in a steady fashion. At that moment, the flow becomes intermittent (e.g. churn). In a qualitative way, this is confirmed by a typical two-phase flow map, taken from the internet. See figure 8 below. As can be seen, there is a minimum gas flow rate requirement for non intermittent conditions, possibly expressed by the gas Froude number.

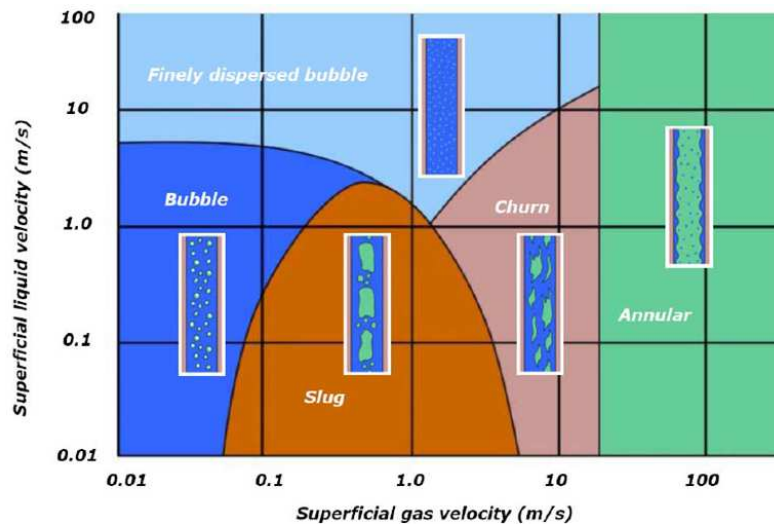


**Figure 8:** Two-phase flow map of vertical upward flow (Dahl, 2005).

As stated above, modelling of the liquid layer is the most difficult part. One of the modelled parameters is the velocity of the liquid at the gas-liquid interface. At a high gas velocity, the liquid will have a distinct velocity in the upward direction. However, lowering the gas velocity will mean a lower velocity in the liquid layer, down to a point where, theoretically speaking, the liquid in the wall layer will come to a stand-still because the friction from the gas moving upward balances the gravitational force downward. But it is obvious that in a realistic system, such a standstill will not occur, but this will be the onset to instability.

When the predicted differential pressure starts to deviate from the measured value, the model calculates a virtual standstill of the liquid in the wall layer, corresponding to instability in realistic systems. We can therefore conclude that the model is unable to predict the differential pressure of the Venturi at those conditions, but it is able to predict the onset of instability.

It shows that with low gas velocities and at low liquid loadings, the model predictions are in agreement with the measured values. When the LM-parameter is lower than 0.04, the amount of liquid is probably small enough to be transported by droplets, dispersed in the gas, and there is no build-up of liquid, inducing the instability. At least at the gas velocities / gas Froude numbers which have been covered by these tests.

## **34<sup>th</sup> International North Sea Flow Measurement Workshop 25-28 October 2016**

In general, the higher the gas density, the lower the gas velocity can be before the onset of instability and the higher the LM-parameter value can be. Although the number of data-points is limited, it seems that at higher water-cuts, the maximum allowable LM-parameter values before the instability starts, are lower. Whether this is caused by the higher density of water or the higher surface tension with the gas or both remains to be seen. Further modelling and experiments should shed light on this question.

When the predictions are in line with the measured differential pressure, a small but systematic difference can be discerned: the predicted differential pressure is a bit too small. There are a number of contributors to this phenomenon:

1. The discharge coefficient of the vertical upward Venturi is unknown. It has been taken as 1 (one) in the model predictions. When a value of 0.995 would be used, the predicted differential pressure should be increased by 1%, a value of 0.99 would result in a 2% correction.
2. It should be noted that the pressure, temperature and physical properties of the fluids are determined at the location of the horizontal Venturi during these tests. As the vertical upward Venturi was located downstream of the horizontal Venturi, the wedge meter and the V-cone meters, the conditions at the vertical upward Venturi were systematically different from the conditions at which the physical properties of the fluids were determined: lower pressure, thus higher volumetric gas flow rate and lower density of the gas. In differential pressure flow meters, the differential pressure is inversely proportional to the density at the same mass flow rate, so this has a systematic effect on the measured differential pressure.
3. It is not unlikely that also the gas volumetric flow rate was further increased by gas, coming out of solution from the oil. This would also have consequences for the oil density. Both would have a systematic influence on the results, both in the same direction as can be discerned from the tests.

## **8 DISCUSSION**

The modelling of the differential pressure, generated by a wet-gas flow in a Venturi, both horizontally and vertically upward, has shown to be successful. Comparison with test-loop data show a good (vertical) or an excellent (horizontal) agreement, which underpin the physics included in the models. Only a few, low level relationships are required to overcome the limited knowledge of some aspects. E.g. the drag force on droplets has been described with the correlation used for decades and can be regarded as well-established. The correlation, used for the entrainment rate in the accelerating flow in the convergent section of the horizontal Venturi, is novel and this could be subject to further study and investigation.

The model for the vertical upward Venturi requires less closure relationships than the model for the horizontal Venturi. It includes the Colebrook correlation for the friction factor on the rough gas-liquid interface<sup>[8]</sup>, this correlation is well established.

The modelling reveals which physical properties are essential to calculate the differential pressure. Therefore, the model includes physical properties, hitherto not, or only in an obscure way, included in the wet-gas overreading correlations.

# 34<sup>th</sup> International North Sea Flow Measurement Workshop

## 25-28 October 2016

For example, the models make clear why, and in what respect, the surface tension between gas and the liquids is important. At the same time, it explains why the differential pressure can be higher than in the case of a homogeneous mist flow. On the other hand, the models show that the essential physical properties of the fluids have been included in the model. Something which one can never be sure of when a correlation is made.

Because the modelling includes the physics which govern the measurement process, these are not limited to the range of the verification data. So the models can be used for more significantly different conditions as well, as can happen in reality.

As the overreading of a horizontal Venturi is, at the same conditions, always smaller than that of a vertical upward Venturi, it is possible to combine the two in order to create a wet-gas flow meter. This will yield two equations with two unknowns, which can be solved. As the overreadings, calculated by the models, are more accurate and reliable than those, predicted by correlations, the results for the gas and liquid flow rates will also be more accurate. Possibly, by using additional information, like the total pressure loss ratios of the Venturis, it might become possible to estimate the water flow rate as well.

The modelling of the total pressure loss of a Venturi in a wet-gas flow can basically be modelled in a similar way. This has not been done by the authors. However, the authors hope that their results, presented here, will inspire and stimulate others to develop such models. This would further enhance the possibilities of creating a wet-gas flow meter.

## 9 CONCLUSIONS, WAY FORWARD

The present paper has shown that physical modelling of wet-gas flow through horizontal and vertical Venturis is feasible. The models are capable of predicting the differential pressure generated by a three-phase wet gas flow in both cases. Comparison with test-loop data show an excellent agreement, which underpins the physics included in the models. Moreover, the modelling reveals which physical properties are essential to calculate the differential pressure.

The models can be applied outside the range of experimental data in pressure, temperature and physical properties of the fluids and still provide useful results. This is a major improvement over correlations, which rarely include all the required physical properties.

Further work to improve the understanding could include a better understanding of the entrainment in the convergent section of the horizontal Venturi and a better understanding of the physics of the water-oil mixture in the vertical upward flow. The flow measurement community is challenged to publish further contributions to these models, which would benefit the overall performance of multi-phase flow meters.

## 10 NOTATION

$a$	Wave amplitude	m
$A_D$	Cross sectional area of pipe	m <sup>2</sup>
$A_d$	Fraction of cross-sectional area, occupied by the droplets	

## 34<sup>th</sup> International North Sea Flow Measurement Workshop 25-28 October 2016

$A_g$	Fraction of cross-sectional area, occupied by the gas	
$A_{le}$	Fraction of cross-sectional area, occupied by the liquid film	
$A_{lf}$	Fraction of cross-sectional area, occupied by the liquid film	
$A_{lg}$	Fraction of cross-sectional area, occupied by droplets	
$C$	Constant	Pa
$C_D$	Discharge coefficient	
$C_w$	Drag coefficient	
$D$	Pipe internal diameter	m
$d$	Diameter of droplet	m
$D_{lf}$	Thickness of liquid film	m
$d_{lf}$	Thickness of liquid film	m
$d_{lf,max}$	Maximum thickness of liquid film due to the wave	m
$d_{lf,min}$	Minimum thickness of liquid film due to the wave	m
$D_{max}$	Maximum diameter available for the gas flow	m
$D_{min}$	Minimum diameter available for the gas flow	m
$dP_B$	Differential pressure contribution, due to Bernoulli effect	Pa
$dP_d$	Differential pressure contribution, due to Bernoulli effect of the droplets	Pa
$dP_g$	Differential pressure contribution, due to Bernoulli effect of the gas	Pa
$dP_{lf}$	Differential pressure contribution, due to Bernoulli effect of the film	Pa
$E$	Energy	J
$E_f$	Entrained fraction	
$E_{f,o}$	Entrained fraction of oil	
$E_{f,w}$	Entrained fraction of water	
$E_M$	Maximum liquid entrainment, modelled as eq. 18	
$e_r$	Entrainment rate	m/s
$f$	Fanning friction factor	
$F$	Force on sphere	N
$F_d$	Force on droplet	N
$F_g$	Net gravitational force	N
$Fr_g$	Gas Froude number	
$Fr_l$	Liquid Froude number	
$f_{sg}$	Friction factor, smooth pipe, turbulent flow, modelled as eq. 21	
$g$	Gravitational acceleration	m/s <sup>2</sup>
$GVF_a$	Actual gas volume fraction	
$h$	Height above reference surface	m
$k$	Surface roughness	
$L$	Length of pipe	m
$LM_q$	Quasi Lockhart-Martinelli parameter	
$LVF$	Liquid Volume Fraction	
$m$	Mass of sphere	kg
$N_d$	Number of droplets per m <sup>3</sup>	m <sup>-3</sup>
$N_d$	Number of droplets per m <sup>3</sup> of liquid entrained	
$N_{dg}$	Normalised energy of the dissipation of the gas, flowing around the drops	Pa
$N_{diss}$	Normalised energy of the dissipation	Pa
$N_{pl}$	Normalised energy of the potential energy of the liquid	Pa

## 34<sup>th</sup> International North Sea Flow Measurement Workshop 25-28 October 2016

$N_{sr}$	Normalised energy of the dissipation, caused by the interfacial roughness	Pa
$N_{st}$	Normalised energy of the surface tension of the entrained droplets	Pa
$N_t$	Normalised total energy	Pa
$N_t$	Number of droplets per second	s <sup>-1</sup>
$OVF$	Oil Volume Fraction	
$p$	Static pressure	Pa
$P_{st}$	Pressure generated by the surface tension	N/m <sup>2</sup>
$P_{st,act}$	Actual pressure, generated by the surface tension	N/m <sup>2</sup>
$Q$	Volumetric flow rate	m <sup>3</sup> /s
$Q_g$	Gas flow rate at actual conditions	m <sup>3</sup> /s
$Q_{gas}$	Gas volume flow rate at actual conditions	m <sup>3</sup> /s
$Q_l$	Liquid flow rate at actual conditions	m <sup>3</sup> /s
$Q_{lf}$	Volumetric flow rate in liquid film at the wall	m <sup>3</sup> /s
$Q_{liquid}$	Liquid volume rate at actual conditions	m <sup>3</sup> /s
$Q_o$	Oil flow rate at actual conditions	m <sup>3</sup> /s
$Q_w$	Water flow rate at actual conditions	m <sup>3</sup> /s
$r$	Distance to the wall (perpendicular to the wall)	m
$r$	Radius of droplet	m
$\rho_\delta$	Weighted average density of droplets	kg/m <sup>3</sup>
$r_d$	Droplet diameter	m
$Re$	Reynolds number of flow around droplet, eq. 28	
$r_e$	Effective radius of droplet under dynamic conditions	m
$Re_d$	Reynolds number of flow around droplet:	
$Re_{sg}$	Reynolds number, based on the superficial gas velocity, eq. 22	
$SA_d$	Surface area of droplet	m <sup>2</sup>
$t$	Time	s
$v$	Velocity of fluid	m/s
$v_d$	Velocity of droplets	m/s
$V_d$	Volume of droplet	m <sup>3</sup>
$v_e$	Terminal velocity of sphere	m/s
$v_g$	Actual gas velocity	m/s
$v_g$	Gas velocity at location of droplet	m/s
$v_{gs}$	Superficial gas velocity	m/s
$v_i$	Liquid velocity at the gas-liquid interface	m/s
$v_{lf}$	Velocity of liquid in the liquid film	m/s
$v_r$	Velocity difference between gas and droplet	m/s
$v_r$	Slip velocity	m/s
$v_r$	Velocity difference between gas and droplet (= $v_g - v_d$ )	m/s
$v_{s,mix}$	Superficial velocity of the mixture	m/s
$v_{sg}$	Superficial gas velocity	m/s
$v_{sg,l}$	Superficial gas or liquid velocity	m/s
$v_{sl}$	Superficial liquid velocity	m/s
$v_z$	Liquid velocity in the z (upward) direction	m/s
$w_l$	Liquid mass flow rate	kg/s
$w_{l,c}$	Critical liquid mass flow rate = 0.157 $\pi D$	kg/s

# 34<sup>th</sup> International North Sea Flow Measurement Workshop

## 25-28 October 2016

<i>WVF</i>	Water volume fraction	
$\Delta p$	Differential pressure due to surface tension at the wave crest	Pa
$\Delta p_d$	Differential pressure contribution due to dissipation	Pa
$\eta_l$	Dynamic viscosity of liquid	Pa.s
$\eta_g$	Dynamic gas viscosity	Pa s
$\eta_{w,20}$	Dynamic viscosity of water at 20 °C	Pa.s
$\lambda$	Wavelength of wave on gas-liquid interface	m
$\rho_d$	Weighted average density of droplets	kg/m <sup>3</sup>
$\rho_g$	Gas density	kg/m <sup>3</sup>
$\rho_l$	Liquid density	kg/m <sup>3</sup>
$\rho_{l,f}$	Weighted average density of liquid film	kg/m <sup>3</sup>
$\rho_o$	Oil density	kg/m <sup>3</sup>
$\rho_w$	Water density	kg/m <sup>3</sup>
$\sigma$	Surface tension	N/m
$\sigma_{o,g}$	Surface tension oil-gas	N/m
$\sigma_{w,g}$	Surface tension water-gas	N/m
$\tau_w$	Wall shear stress	Pa
$\Delta p$	Differential pressure	Pa
$\Delta p_B$	Differential pressure caused by the Bernoulli effect	Pa
$\Delta p_d$	Differential pressure caused by dissipation	Pa
$\Delta p_{go}$	Differential pressure if only the gas was flowing	Pa
$\Delta p_O$	Differential pressure over the orifice	Pa
$\Delta p_{tp}$	Differential pressure in two or three phase flow	Pa
$\varepsilon$	Compressibility factor	
$\rho$	Density	kg/m <sup>3</sup>
$\rho_l$	Liquid density, actual	kg/m <sup>3</sup>
$\rho_{mix}$	Mixture density, actual	kg/m <sup>3</sup>

### 11 REFERENCES

1. J.W. MURDOCK, "Two phase flow measurements with orifices", Journal of Basic Engineering, December 1962.
2. D. CHISHOLM, "Two phase flow through sharp-edged orifices", Research note, Journal of mechanical engineering science, 1977.
3. H. DE LEEUW, "Liquid correction of Venturi Meter Readings in Wet Gas Flow", Proceedings of the North Sea Flow Measurement Workshop, October 1997 (Kristiansand, Norway).
4. R. STEVEN, "Wet Gas Metering", Ph.D. Thesis, University of Strathclyde, department of Mechanical Engineering, Glasgow, UK, April 2001.
5. E. VASSILIADOU, "A model for liquid entrainment for horizontal annular and stratified gas/liquid flow based on the data measured in the high pressure gas/condensate test facility at Bacton (UK)", Internal Shell report AMGR.89.243., 1989.

**34<sup>th</sup> International North Sea Flow Measurement Workshop  
25-28 October 2016**

6. R.V.A. OLIEMANS, "Applied Multiphase Flows", Delft University of Technology, Faculty of Applied Sciences, Department of Applied Physics, Kramers' Laboratory (November 1998).
7. TOMIO OKAWA, TSUYOSHI KITAHARA, KENJI YOSHIDA, TADAYOSHI MATSUMOTO, ISAO KATAOKA, "Novel entrainment rate correlation in annular two-phase flow applicable to wide range of flow condition", Intl. Journal of Heat and Mass transfer 45 (2002) pp. 87 - 98.
8. COLEBROOK, C.F. Turbulent flow in pipes with particular reference to the transition region between the smooth and rough pipe laws. J. Inst. Civil Eng. 11(4), pp. 133-156. 1939.

# 34<sup>th</sup> International North Sea Flow Measurement Workshop 25-28 October 2016

## APPENDIX 1

### DERIVATION OF THE QUASI LOCKHART-MARTINELLI PARAMETER

The quasi Lockhart-Martinelli parameter is based on mixture properties and calculated from:

$$v_{s,mix} = v_{sg} + E_f v_{sl} \quad (A-1)$$

and

$$\rho_{mix} = \frac{v_{sg} \rho_g + E_f v_{sl} \rho_l}{v_{sg} + E_f v_{sl}} \quad (A-2)$$

From which follows:

$$LM_q = \frac{(1 - E_f) v_{sl}}{v_{s,mix}} \sqrt{\frac{\rho_l}{\rho_{mix}}} \quad (A-3)$$

# 34<sup>th</sup> International North Sea Flow Measurement Workshop 25-28 October 2016

## APPENDIX 2

### DISSIPATION DUE TO DRAG AROUND THE DROPLETS

The droplets are accelerated in the convergent section and the throat of the Venturi and decelerated in the divergent part. The viscous forces which are responsible for these changes in velocity are also responsible for the dissipation of energy. This can be illustrated as follows:

Imagine a steel sphere which is moving through a viscous fluid. After a while the sphere will reach its terminal velocity and in that case the forces of gravity and viscous drag are in balance. The dissipation will then equal the loss of potential energy of the sphere per unit time:

$$\frac{dE}{dt} = \frac{d(mgh)}{dt} = \frac{d(mgh)}{dh} \frac{dh}{dt} = mgv_e = F v_e \quad (\text{B-1})$$

In the case of the droplets:

$$F(v_g - v_d) dt = dE_d \quad (\text{B-2})$$

and

$$E_d = \int F_d (v_g - v_d) dt \quad (\text{B-3})$$

The force on the droplet is calculated as follows:

$$F_d = C_w (\pi r_d^2) \left( \frac{1}{2} \right) \quad (\text{B-4})$$

The drag coefficient is calculated by:

$$C_w = \frac{24}{Re_d} + 0.44 \quad Re_d > 43 \quad (\text{B-5})$$

$$C_w = 1 \quad Re_d \leq 43 \quad (\text{B-6})$$

in which  $Re_d$  is the Reynolds number of flow around droplet:

$$Re_d = \frac{v_r d_r \rho_g}{\eta_g} \quad (\text{B-7})$$

In order to calculate the  $\Delta p$  caused by this dissipation, the dissipation (which is calculated for an individual droplet) has to be multiplied by the number of droplets per  $m^3$  which can be found by calculating the number of droplets per second:

$$N_t = \frac{Q_l E_f}{\frac{4}{3} \pi r^3} \quad (\text{B-8})$$

and dividing this by the total volume flow rate:

$$Q_t = Q_l + Q_g \quad (\text{B-9})$$

**34<sup>th</sup> International North Sea Flow Measurement Workshop  
25-28 October 2016**

$$N_v = \frac{Q_l E_f}{(Q_l + Q_g) \left( \frac{4}{3} \pi r^3 \right)} \quad (\text{B-10})$$

For the calculation, the diameter of the droplets is assumed to be equal to the average diameter in the pipe upstream of the Venturi. As soon as the fluids enter the Venturi, the gas will accelerate and thus exert a drag force on the droplet. As soon as the drag force exceeds the surface tension of the droplet, the droplet is assumed to split into two identical droplets. As the drag force on the droplet increases with the droplet diameter (due to the larger surface area and the larger inertia of the droplet) and the surface tension decreases with increasing droplet diameter (due to the reduced curvature, see also Appendix 3), the calculation of the droplet velocity is not very sensitive to the initial value of the droplet diameter: the forces on the droplet will result in droplets of similar diameter, virtually independent on the initial conditions.

# 34<sup>th</sup> International North Sea Flow Measurement Workshop

## 25-28 October 2016

### APPENDIX 3

#### DIFFERENTIAL PRESSURE CAUSED BY SURFACE TENSION

The droplets, dispersed in the gas, represent a potential energy, caused by the surface tension: in order to create a droplet, the surface tension has to be overcome. Imagine a m<sup>3</sup> of liquid, split up into droplets with a diameter  $d$  ( $= 2r$ ). The surface area of such a droplet is:

$$SA_d = 4\pi r^2 \quad (C-1)$$

The volume of such a droplet is:

$$V_d = \frac{4}{3}\pi r^3 \quad (C-2)$$

The m<sup>3</sup> of entrained liquid thus yields a number of droplets equal to:

$$N_d = \frac{1}{\frac{4}{3}\pi r^3} \quad (C-3)$$

The total surface area of the m<sup>3</sup> entrained liquid is:

$$SA_T = N_d SA_d = \frac{4\pi r^2}{\frac{4}{3}\pi r^3} = \frac{3}{r} = \frac{6}{d} \quad (C-4)$$

The pressure generated by the surface tension is:

$$P_{st} = \frac{6}{d} \sigma \quad (C-5)$$

However, the flow is two-phase, and thus the pressure is:

$$P_{st,act} = LVF \left( \frac{6 \sigma}{d} \right) E_f \quad (C-6)$$

The reason is that the decrease in pressure is independent of the amount of liquid: if the fluid consisted of liquid only, the pressure decrease would be independent whether it was 1 ml or 1 m<sup>3</sup>. However, the smaller the fraction of liquid dispersed, the less the pressure decreases.

## **Technical Paper**

# **Evaluation of the SONAR Meter in Wet Gas Flow for an Offshore Field Development**

**Angela Floyd, BP  
Siddesh Sridhar and Gabriel Dragnea, Expro Meters**

---

## **1 INTRODUCTION**

The ABC project is a high pressure gas condensate development currently in the implementation stage. Platform top-side surveillance is considered critical for better reservoir management, production optimization and flowline integrity management. After investigating different options, the SONAR clamp-on meter was identified as the solution to provide individual, real time production surveillance for ten flow lines (12-inch pipe) upstream of the production manifolds and the high-pressure (HP) separator.

In order to determine the wet gas flow uncertainty over the anticipated gas and liquid flow range, testing was performed at the NEL, Wet Gas Facility in Scotland. The results and conclusions from the testing are detailed in this paper.

The main requirement of the test program was to evaluate the SONAR meter for provision of real time gas rates and inferred oil and water rates across a range of flow conditions anticipated across the life of high pressure gas condensate development. This testing was limited to lab capabilities of;

- Measure max pressure of 63 Barg at 2 flow rates of 780 ACMH and 1040 ACMH
- 0 – 10% WLR
- Volumetric Gas rate accuracy – 5-10%
- Volumetric Liquid Rate Accuracy 10-15%.
- Mass Bulk flow accuracy dependent on density measurement

## **2 SONAR Technology**

SONAR technology involves observing the naturally-occurring coherent vortical structures within the flow (generated due to turbulence) by monitoring interactions of externally-generated acoustic pulses (pulse arrays) with those coherent structures. The subsequent processing algorithms involve analysis of the spatial wavelength (distance) and temporal frequency (time) of the sensor signals over a range of values.

Multiple spatial and temporal wavelengths are plotted to generate a k-omega plot which is essentially a high energy region called the vortical ridge. The slope of this ridge determines the flow velocity. The volumetric flow rate at standard conditions can then be calculated using the pipe cross-sectional area, pressure and temperature.

Technical Paper

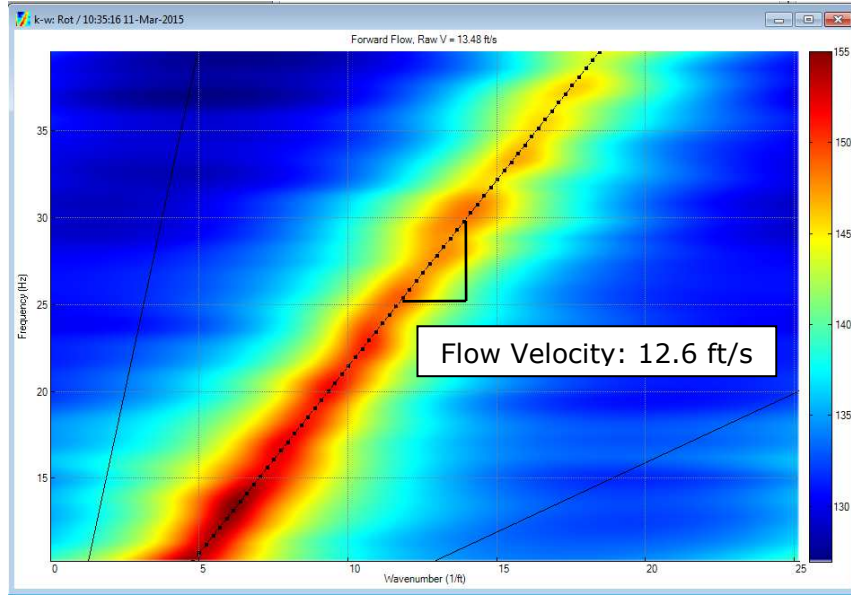


Fig.1 - SONAR Diagnostics: k- $\omega$  ridge

### 3 SONAR OVERREADING CORRELATION - BACKGROUND

In wet gas flow measurement, the flow meter generally over reads the gas flow rate due to wetness addition. The over-reading is defined as

$$OR = \frac{Q_g}{Q_g^{ref}} \quad (1)$$

where  $Q_g$  is the gas volumetric flow rate measured by the flow meter and  $Q_g^{ref}$  the actual gas volumetric flow rate given by the reference system in line condition.

Based on empirical data collected in flow loop testing conducted on 4-in Sch 40 and Sch 80 pipes, the over-reading of the 4-in ActiveSONAR™ flow meter can be characterized by the the following correlation:

$$OR = 1 + \beta \left( \frac{\sqrt{LVF}}{1 + Fr^m} \right) + \phi \left( \frac{\sqrt{LVF}}{1 + Fr^m} \right)^2 \quad (2)$$

where  $\beta = 2.5249$ ,  $\phi = -3.9043$  and

$$m = \begin{cases} Fr - 0.5, & 0.5 < Fr < 1.5 \\ 1, & Fr \geq 1.5 \end{cases} \quad (3)$$

The  $Fr$  number is defined as

$$Fr = \frac{V_{sg}}{\sqrt{gL}} \sqrt{\frac{\rho_g}{\rho_L - \rho_g}} \quad (4)$$

where  $V_{sg}$  is the superficial velocity of the gas flow,  $g$  the gravitational acceleration,  $L$  the characteristic length of the pipe (ID of the pipe here),  $\rho_g$  the gas density in line conditions and  $\rho_L$  the liquid density in line conditions.

# 34<sup>th</sup> International North Sea Flow Measurement Workshop 25-28 October 2016

## Technical Paper

The Liquid Volume Fraction ( $LVF$ ) is defined as

$$LVF = \frac{Q_L}{Q_L + Q_g} \quad (5)$$

where  $Q_L$  is the liquid volumetric flow rate in line conditions. For low liquid loading,  $Q_L \ll Q_g$ , Eq. (5) is simplified as the ratio of the liquid volumetric rate to the gas volumetric rate

$$LVF \approx \frac{Q_L}{Q_g} \quad (6)$$

The over-reading correction shown in Eq. (2) enables the 4-in ActiveSONAR™ meter to report gas rates to within  $\pm 3\%$  for  $0 < LVF < 0.106$  and  $0.5 < F_r < 5.78$ .

There is another important dimensionless parameter for liquid fraction broadly used in wetness flow metering is Lockhart-Martinelli number, which is defined as

$$X_{LM} = \frac{Q_L}{Q_g} \sqrt{\frac{\rho_L}{\rho_g}} \quad (7)$$

For low liquid loading, we have

$$X_{LM} \approx LVF \sqrt{\frac{\rho_L}{\rho_g}} \quad (8)$$

## 4 TEST SETUP

Testing was performed in the NEI high pressure wet gas facility in 2 phases, Oct-2014 and Mar-2015. The flow meter was clamped onto a 12" sch 160 pipe spool with class 600 raised face flanges. The meter was mounted approximately 14.5 D (4.3m) downstream from the 12-in straight pipe upstream flange face. This setup was used in order to replicate the expected installation setup at the platform conditions.

The test section pressure tapping was located 1.5 m from the downstream flange and the temperature probe was located 643 mm from the downstream flange. The flow computer was installed on a vertical grating adjacent to the meter location. An identical test setup was used for both phases of testing.

Phase 1 testing used Nitrogen gas via 6" ultrasonic meters and kerosene via 1/2", 1" and 3" turbine meters. Testing followed a defined test matrix and maintained a  $\sim 63$  bar(g) pressure, 15 °C and gas volumetric flow rates of 780 – 1040 m<sup>3</sup>/hr.

During the 6 month time from Phase 1 - Phase 2 testing, the NEL lab had been updated to a multiphase flow lab and incorporated the use of a 3" and 1 1/2" Coriolis meter as the liquid kerosene reference meters. The 6" USM remained the gas reference meter and maintain a  $\sim 63$  bar(g) pressure, 15 °C and gas volumetric flow rates of  $\sim 500 - 1600$  m<sup>3</sup>/hr.

The flow was wet gas, 100% nitrogen mixed with kerosene oil. After the geometric parameters of the pipe were obtained, the flow meter was configured. The driving frequency of the transducers and demodulation delay were obtained by using the built-in optimizer. The configuration of the flow meter was fixed

# 34<sup>th</sup> International North Sea Flow Measurement Workshop 25-28 October 2016

## Technical Paper

during the whole test period and identical configurations were used for both rounds of testing. The line pressure and temperature for both phases of testing ranged from 60-62 barg and 15-20°C respectively.

The flow rate, pressure and temperature were stabilized before a 30-second pre-test point was logged. The CGR (condensate-gas ratio) for each test point was then provided to Expro for input into the flow computer. The actual test point was then logged for a period 240 seconds (4 minutes).

Meter performance criteria was defined as 5% to 10% for the gas flow rate measurement and 10% to 15% for liquid flow rate measurement.

## 5 TEST RESULTS

### 5.1 1st Testing Phase

Testing was conducted for 65 data points in total with 5 dry gas points and 60 wet gas points. For the dry gas test points, 2 points were tested before the wet gas test points and 3 points were tested after the wet gas test points. The testing was conducted at gas flow rates of 620 and 800 m<sup>3</sup>/h (at actual conditions). The Froude Numbers (Fr) range for the test points ranged from 0.69 to 0.89 and the Liquid Volumetric Fraction (LVF) ranged from 0 – 10.7%.

After NEL reference data was obtained, a comparative analysis was done between Expro and NEL gas and liquid rates for all the test points. For dry gas test points, the difference in Q<sub>gas</sub> at actual conditions was less than  $\pm 1\%$  which is within the SONAR meter specifications as shown in Figure 2.

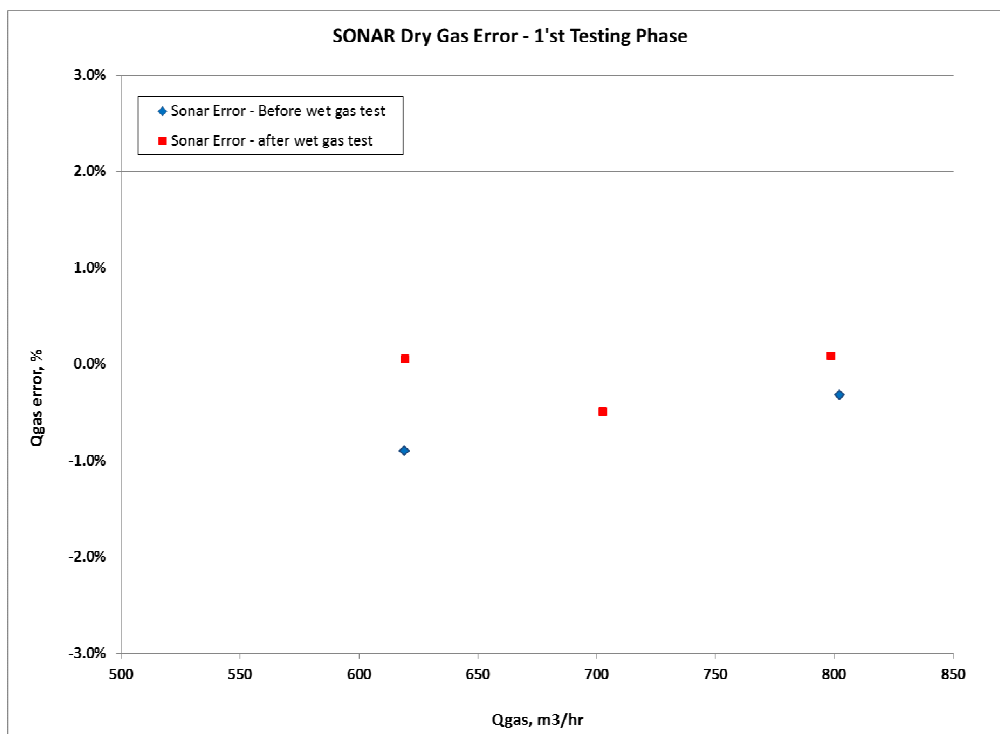


Fig. 2 - Dry Gas Error (SONAR vs. NEL) 1'st Testing Phase

# 34<sup>th</sup> International North Sea Flow Measurement Workshop 25-28 October 2016

## Technical Paper

For the wet gas test points, the average difference between Expro Qgas (at Actual conditions) and NEL Reference Qgas (Actual) was approximately -15% (Figure 3). Upon further investigation this error was attributed primarily due to the over-reading correlation. A secondary source of error was a mismatch in CGR (condensate gas ratio) for some of the test points and the actual CGR at flowing conditions. A modified over-reading correlation was developed and this has been detailed in section 5.2

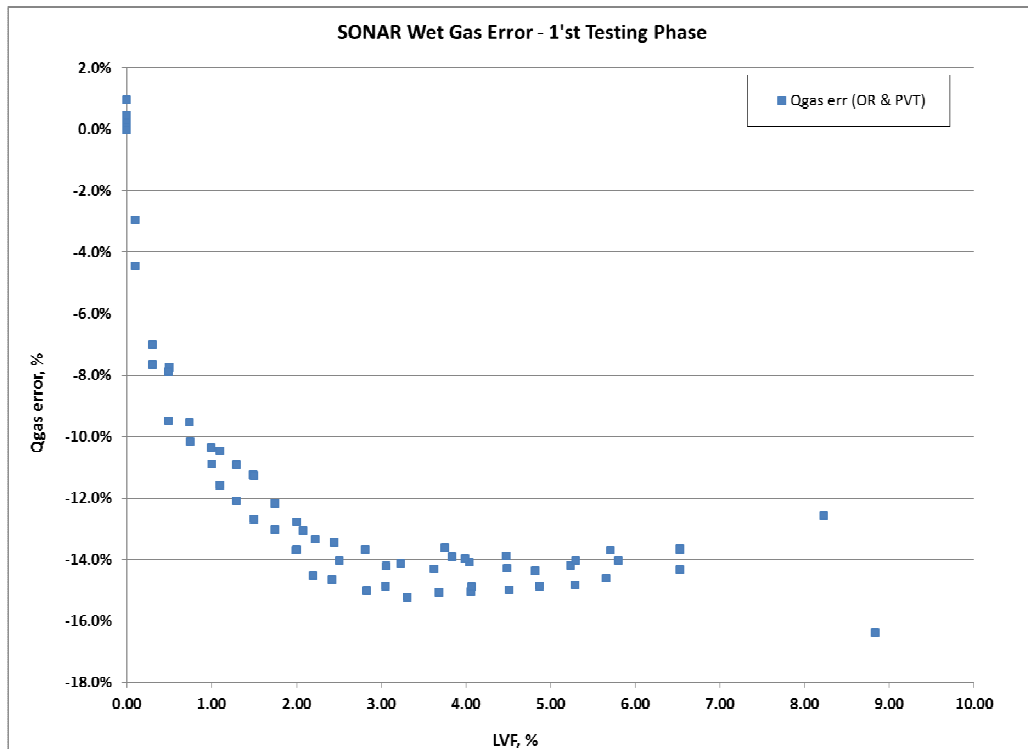


Fig. 3 - Wet Gas Error (SONAR vs. NEL) 1'st Testing Phase

### 5.2 Modified Overreading Correlation

For the first phase of testing, the over-reading correlation for 4-in wet gas flow shown in Eq. (2) and Eq. (3) (incorporated in the flow computer) was applied to the 12-in wet gas test points. Fig. 4 - 1 compares the actual over-reading for the NEL test points (OR NEL) and the reported over-reading using the existing 4" correlation (OR SONAR). The error in gas rate has been plotted on the Y-axis. It is evident that the actual over-reading is considerably lower than the 4" over-reading correlation and follows a linear trend. This indicates that the over-reading correction is pipe size dependent. Since the original correlation was developed for a 4" pipe and the NEL testing was conducted on a 12" pipe, the meter over-reading seems to decrease as the pipe size is increased.

Technical Paper

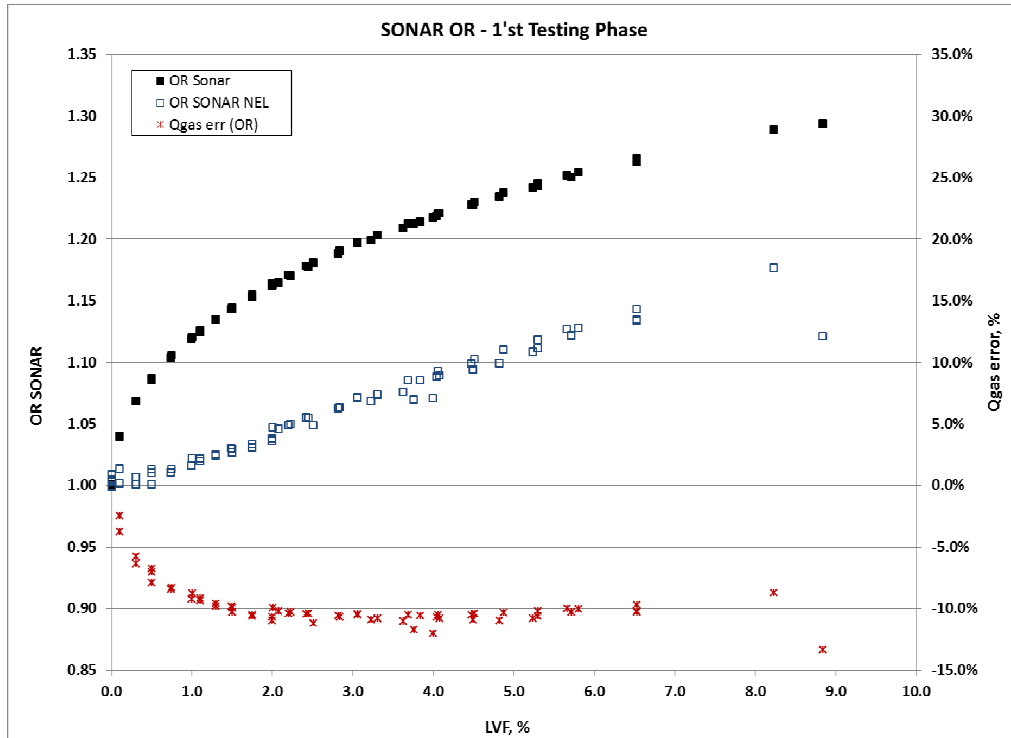


Fig. 4 - 1SONAR over reading versus LVF (1<sup>st</sup> Testing Phase)

Upon further analysis of the data, it was determined that the over-reading for the 12-in wet gas flow can be characterized by modifying the coefficients of Eq. (2). After a curve-fitting exercise, the following correlation was obtained for the 12-in wet gas flow:

$$OR = 1 + \beta \left( \frac{\sqrt{LVF}}{1 + Fr^m} \right) + \phi \left( \frac{\sqrt{LVF}}{1 + Fr^m} \right)^2 \quad (12)$$

where  $\beta = 0.037467$ ,  $\phi = 6.168157$  and

$$m = \begin{cases} Fr - 0.5, & 0.5 < Fr < 1.1 \end{cases} \quad (13)$$

The above correlation has been developed only up to  $Fr = 1.1$  and  $LVF \leq 8\%$ . Additional reference data was needed to validate the correlation at higher Froude numbers. The modified over-reading correlation was then applied to all the test points. Fig. 2 shows the curving fitting of the test points.

Technical Paper

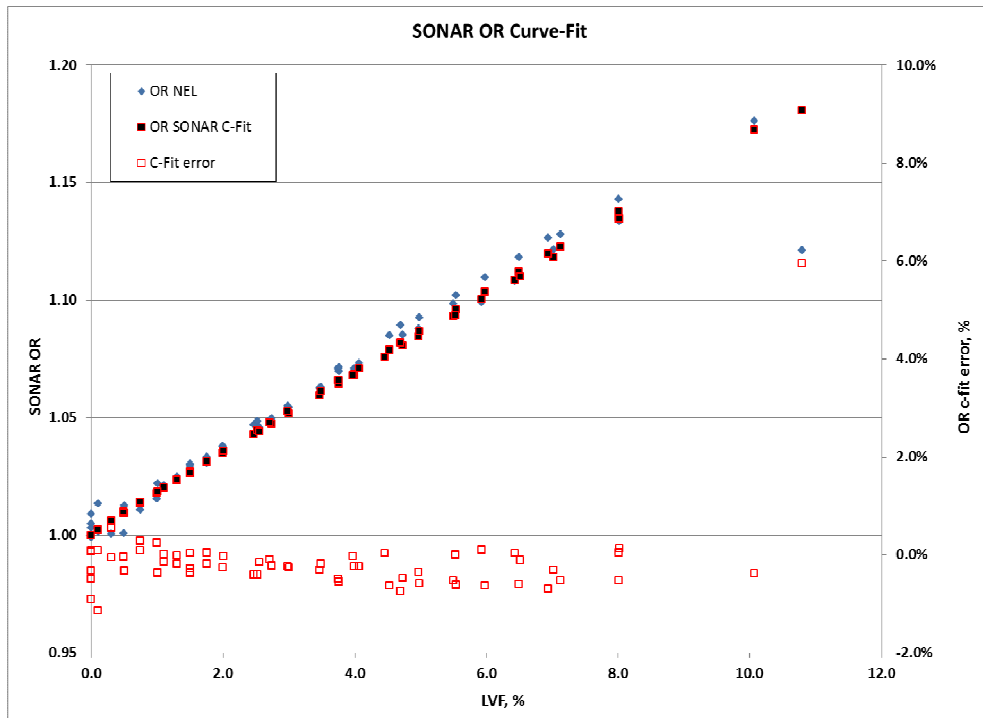


Fig. 2 - Over-reading curve-fitting for 12-in meter in wet gas flow

**Error! Reference source not found.** shows the Qgas error (SONAR vs. NEL) after applying the modified over-reading correlation to the test data. As evident from the graph, the difference between the SONAR gas rates and NEL gas rates was within  $\pm 2\%$  for most test points.

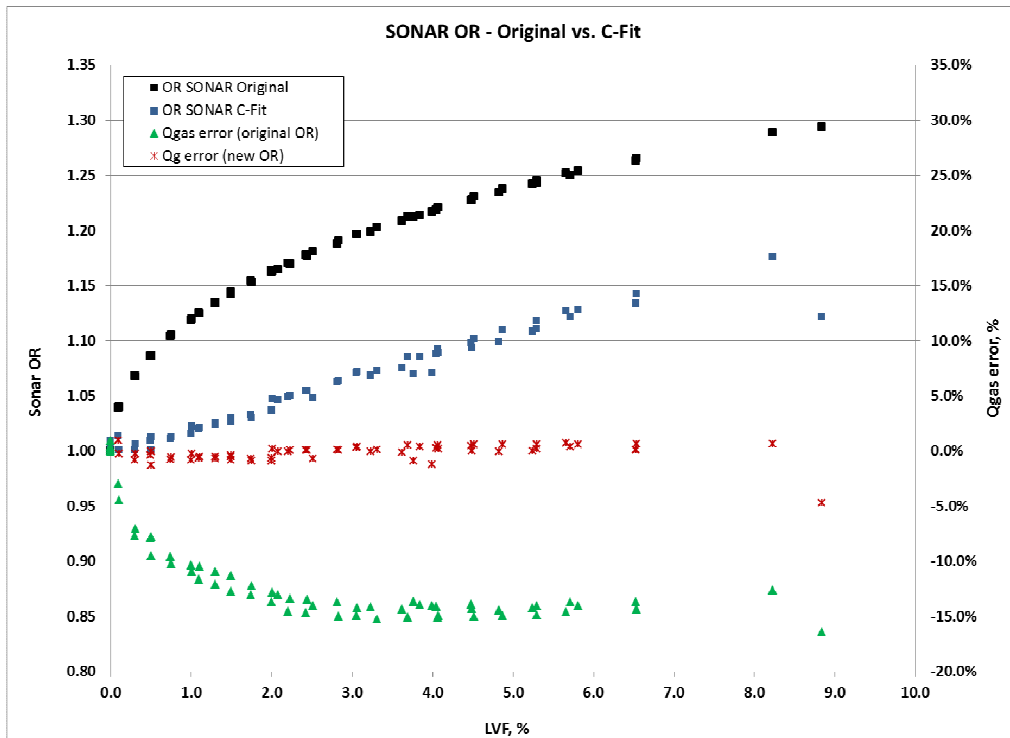


Fig. 6 - SONAR OR and Qgas Error versus LVF – C-Fit vs. Original OR

# 34<sup>th</sup> International North Sea Flow Measurement Workshop 25-28 October 2016

## Technical Paper

### 5.3 2<sup>nd</sup> Testing Phase

The 2<sup>nd</sup> round of testing at NEL was conducted in March 2015. The primary purpose of the test was to validate the over-reading correlation developed for the 12" meter based on the data analysis after the 1<sup>st</sup> round of testing. The new over-reading correlation was implemented in the flow computer prior to the commencement of the test.

As stated earlier, the meter and flow computer setup was identical to the previous setup in order to maintain repeatability of operating conditions. The test matrix was however condensed to 43 test points, 6 dry gas points and 37 wet gas test points. The Q<sub>gas</sub> (actual) range for the test points was 500 - 1000m<sup>3</sup>/hr. The Froude Numbers (Fr) range for the test points ranged from 0.69 to 1.1 and the Liquid Volumetric Fraction (LVF) ranged from 0 - 10.2%.

Figure 7 shows the comparison between the actual over-reading for the test points and the reported over-reading using the modified correlation using curve-fitting. It is evident from the chart that the modified over-reading correlation follows the same trend as the actual over-reading with increasing LVF.

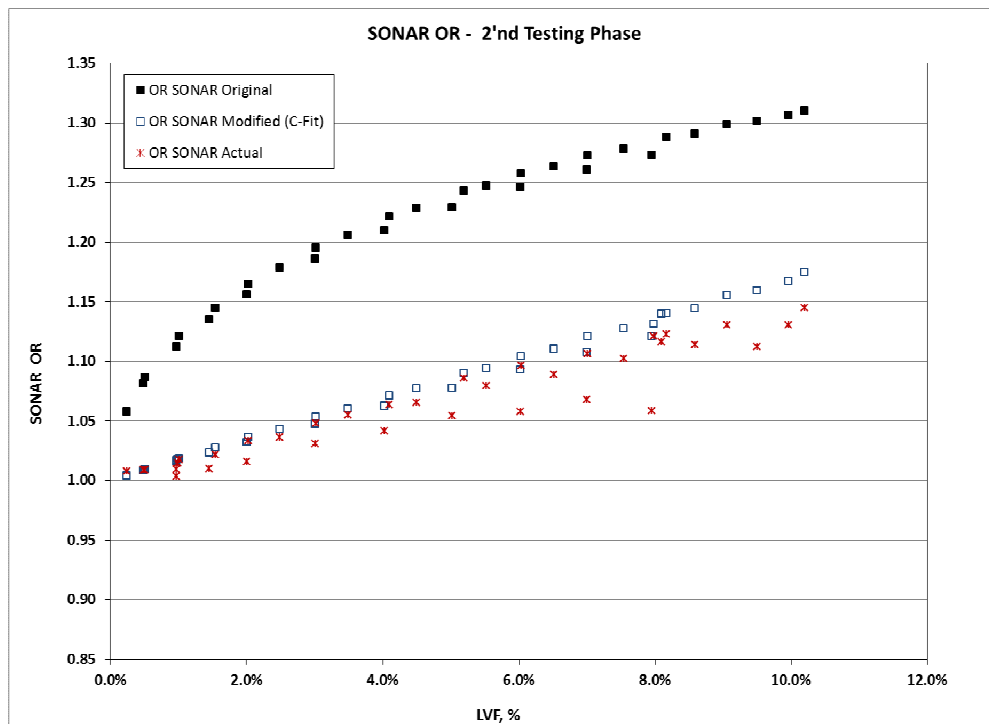


Fig. 7 - SONAR over reading versus LVF (2<sup>nd</sup> Testing Phase)

Figure 8 shows the comparison between SONAR Q<sub>gas</sub> actual and NEL reference Q<sub>gas</sub> actual versus LVF. As can be seen in the chart, 93% of the SONAR reported gas rates were within  $\pm 5\%$  of the reference rates. The remaining points were within 10% of the reference rates. The liquid rates are directly inferred from the gas rates using the CGR and hence are within the same error bands (Figure 9).

Technical Paper

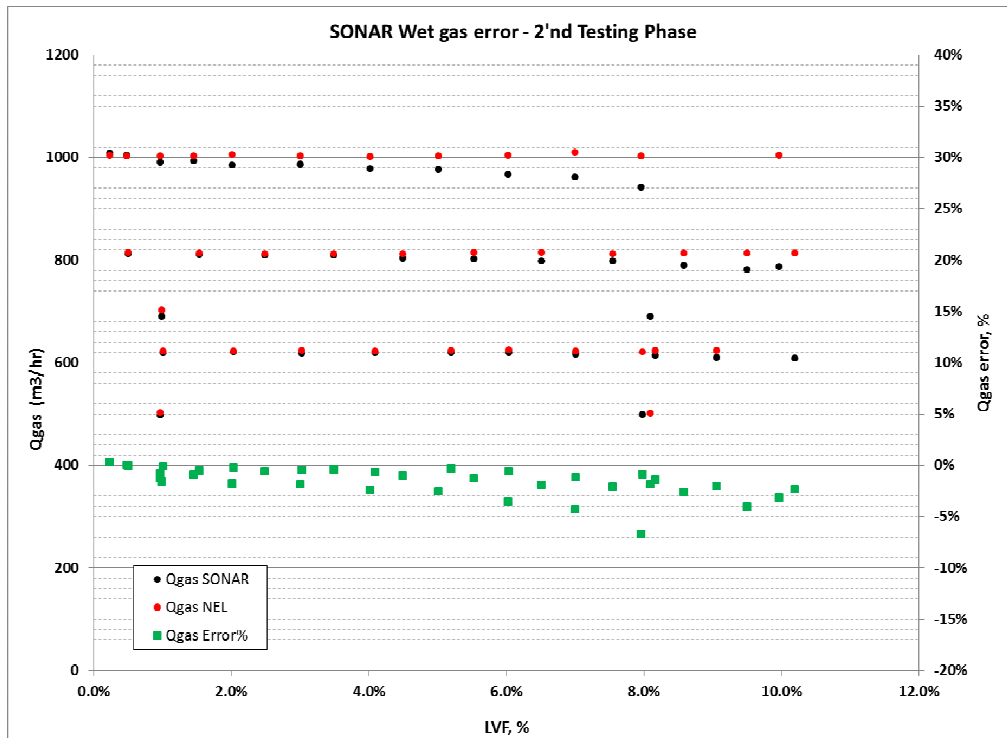


Fig. 8 -  $Q_{gas}$  error versus LVF (2<sup>nd</sup> Testing Phase)

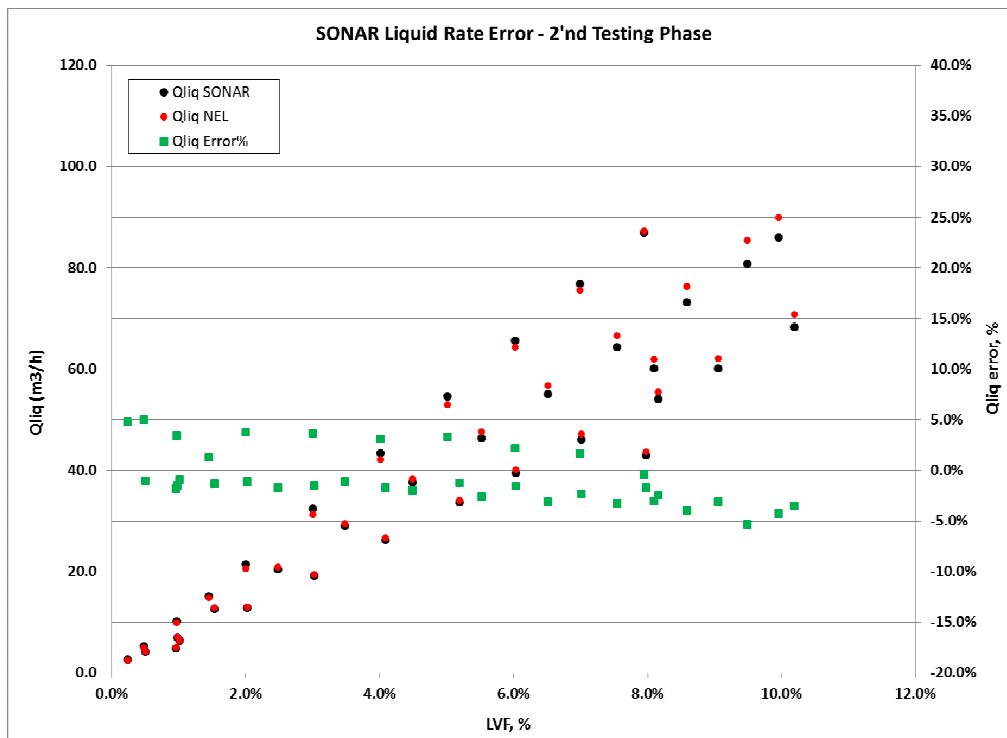


Fig. 9 -  $Q_{liq}$  error versus LVF (2<sup>nd</sup> Testing Phase)

# 34<sup>th</sup> International North Sea Flow Measurement Workshop 25-28 October 2016

## Technical Paper

### 6 CONCLUSIONS

The meter qualification testing performed in the 1<sup>st</sup> phase (Oct-2014) led to the development of a modified over-reading correlation for the 12-inSONAR meter in wet-gas flow. This correlation was also validated in the NEL test loop by additional testing in the 2<sup>nd</sup> Phase (March-2015). It is evident from the testing at NEL (and previous flow loop testing) that the SONAR meter over-reading characteristic for wet gas flows is pipe size dependent. The over-reading also seems to decrease with increasing pipe size. It is recommended to perform testing at intermediate pipe sizes (6" and 8") and at higher Froude numbers to characterize the meter over-reading and subsequently implement it for future field applications.

### 7 NOTATIONS

$\beta$	Beta (Calibration Coefficient)	C-Fit	Curve-Fit
$\phi$	Phi (Calibration Coefficient)	CGR	Condensate-Gas Ratio
LVF	Liquid Volumetric Fraction	Fr	Froude Number
OR	Overreading		

### 8 REFERENCES

- [1] Shoham, O., Mechanistic Modeling of Gas-liquid Two-Phase Flow in Pipes, Society of Petroleum Engineers, 2006, ISBN 978-1-55563-107-9
- [2] Murdock, J. W., "Two Phase Flow Measurement with Orifices", Journal of Basic Engineering, Vol.84, pp.419-433, 1962
- [3] Konopczynski, M.R., Large-Scale Application of Wet-Gas Metering at the Oman Upstream LNG Project, SPE 63119, presented at the 2000 Annual Technical Conference in Dallas, TX, USA, October, 2000
- [4] Gysling, D. and Morlino, N., "Pulsed-Array, Sonar-based Flow Measurement Technology for Clamp-on Wet Gas Metering, Presented at the 2009 Americas Flow Measurement Workshop, Houston, TX, USA February, 2009
- [5] Danesh, A., PVT and Phase Behaviour of Petroleum Reservoir Fluids, Developments in Petroleum Science, Vol. 47, Elsevier Science B.V., ISBN: 0-444-82196-1, 1998
- [6] Gysling D., Lu M. and Wen T., Clamp-on Two Phase Measurement of Gas Condensate Wells Using Integrated Equation of State Compositional Models, 28<sup>th</sup> International North Sea Flow Measurement Workshop, October, 2010

**Technical Paper****Wet Gas Flow Facility Inter-Comparison****D van Putten, DNV GL, The Netherlands  
R Steven and J Kinney, CEESI, USA**

---

**1 INTRODUCTION**

Multiphase wet natural gas flow metering is required throughout the natural gas production industry. However, there are only a few industrial grade multiphase wet gas flow test facilities worldwide. Industry practice tends to be to test and / or characterise multiphase wet gas meters at one of these test facilities. The inherent assumption is that all multiphase wet gas test facilities give the same result and the same result as the meter's subsequent performance in the field.

However, there has been no concerted attempt to prove the reproducibility of results for any one meter between different multiphase wet gas flow facilities. There is some anecdotal evidence that a DP meters response is reproducible amongst the multiphase wet gas test facilities, but there has never been a dedicated attempt to prove the assumption.

In this paper anecdotal evidence known to the authors is discussed. Then a basic wet gas test facility inter-comparison between CEESI and DNV GL is discussed. An ISO 5167-4 compliant 6", 0.6 $\beta$  Venturi meter was wet gas flow tested by CEESI and DNV GL. This particular meter was chosen for two reasons. The first was it is a typical size and design for what is used by industry for wet gas flow metering. The second was that ISO TR 11583 has adopted and published a TUV NEL Venturi meter wet gas correlation that covers this meter size. As a correlation is a fit to the source data, this ISO correlation is effectively a mathematical expression of the NEL data sets. Hence, the CEESI and DNV GL data can not only be directly compared, but indirectly compared to the equivalent NEL results, meaning an effective three laboratory check for reproducibility was achieved.

**2 WET GAS METER TECHNOLOGY**

A wet gas flow is defined by ISO [1, 2] & ASME [3] as any two-phase (liquid and gas) flow where the Lockhart-Martinelli parameter ( $X_{LM}$ ) is less or equal to 0.3, i.e.  $X_{LM} \leq 0.3$ . Note that this definition covers any combination of gaseous and liquid components. The term 'liquid loading' is widely used as a qualitative term to describe the amount of liquid with a gas flow.

The Lockhart-Martinelli parameter is defined as

$$X_{LM} = \sqrt{\frac{\rho_l u_{sl}}{\rho_g u_{sg}}} \quad (1)$$

where  $\rho_l$  and  $\rho_g$  are the liquid and gas density, respectively. The superficial velocities of the liquid and and gas are given by

# 34<sup>th</sup> International North Sea Flow Measurement Workshop 25-28 October 2016

## Technical Paper

$$\begin{aligned} u_{sl} &= \frac{\dot{Q}_l}{A} \\ u_{sg} &= \frac{\dot{Q}_g}{A} \end{aligned} \quad (2)$$

where  $A$  is the cross-sectional area of the meter inlet and  $\dot{Q}_l$  and  $\dot{Q}_g$  are the liquid and gas volumetric flow rate at line conditions. For multiphase wet gas flows, the liquid consists of a water and oil/condensate phase, denoted by subscript  $w$  and  $o$  respectively. For these liquid mixtures the total volumetric flow rate of the liquids need to be considered, i.e.  $\dot{Q}_l = \dot{Q}_w + \dot{Q}_o$ , and the density is assumed homogeneous

$$\rho_l = WLR \cdot \rho_w + (1 - WLR) \cdot \rho_o, \quad (3)$$

where  $WLR \equiv \dot{Q}_w / \dot{Q}_l$  is the Water Liquid Ratio at line conditions.

In wet gas flow metering two important dimensionless parameters need to be defined. The gas to liquid density ratio ( $DR = \rho_g / \rho_l$ ) is a non-dimensional expression of pressure. The gas densimetric Froude number ( $Fr_g$ ), shown as equation 4, is non-dimensional expressions of the gas flow rate, where  $g$  is the gravitational constant,  $D$  is the meter inlet diameter

$$Fr_g = \frac{u_{sg}}{\sqrt{\tilde{g}D}}, \quad \tilde{g} \equiv g \frac{\rho_l - \rho_g}{\rho_g} \quad (4)$$

### 2.1 Wet Gas DP Meters

Equation 5 shows the generic DP meter gas mass flow equation, where  $E$  is the velocity of approach (i.e. a geometric constant),  $A_t$  is the minimum cross sectional area,  $C_d$  is the discharge coefficient,  $\varepsilon$  is the expansibility factor and  $\Delta P_g$  is the differential pressure (DP). Wet gas flow conditions tend to cause a DP meter to have a positive bias in the gas flow rate prediction. This is often called an "over-reading" and denoted as "OR". The DP created by a wet gas ( $\Delta P_{tp}$ ) is different to when that gas flows alone ( $\Delta P_g$ ). The result is an erroneous, or "apparent", gas mass flow rate prediction,  $\dot{m}_{g,Apparent}$  (see equation 6). The over-reading is expressed either as a ratio (equation 7) or percentage (equation 7a) comparison of the apparent to actual gas mass flow rate.

$$\dot{m}_g = EA_t C_d \varepsilon \sqrt{2\rho_g \Delta P_g} \quad (5)$$

$$\dot{m}_{g,Apparent} = EA_t C_{d,tp} \varepsilon_{tp} \sqrt{2\rho_g \Delta P_{tp}} \quad (6)$$

# 34<sup>th</sup> International North Sea Flow Measurement Workshop 25-28 October 2016

## Technical Paper

$$OR = \frac{\dot{m}_{g,Apparent}}{\dot{m}_g} = \frac{\varepsilon_{tp} C_{d,tp}}{\varepsilon C_d} \sqrt{\frac{\Delta P_{tp}}{\Delta P_g}} \cong \sqrt{\frac{\Delta P_{tp}}{\Delta P_g}} \quad (7)$$

$$OR\% = \left( \frac{\dot{m}_{g,Apparent}}{\dot{m}_g} - 1 \right) \cdot 100\% \quad (7a)$$

### 3 WET GAS INTER-COMPARISON SETUP

For a wet gas inter-comparison to be successful, several conditions need to be satisfied. The chosen flow meter should reproduce within certain limits, the facilities need to have a statement about the uncertainties of the provided flow rates and the test matrices should have sufficient overlap in the dominant physical parameters, i.e. dimensionless numbers.

#### 3.1 Existing Evidence of Reproducibility

There are a few published data sets that imply that multiphase wet gas meters give reproducible meter results. ISO TR 12748 gives an orifice meter multiphase wet gas flow correction factor for horizontally installed meters (adopted from Steven et al [4]). This correlation was formed with a large data set consisting of tests at two test facilities (CEESI & NEL) over two decades. Figure 1 shows sample photographs of such orifice meter test at the CEESI & NEL wet gas test facilities.

These tests were largely uncoordinated, carried out by two Joint Industry Projects (JIPs), various meter end users and meter manufacturers. The orifice meters tested were from various manufacturers and consisted of paddle plate and chambered orifice meter designs. All data agreed to a remarkable extent. As the data from the different orifice meters at the different test facilities were found to be very reproducible, it was possible to create a mathematical expression of the response, i.e. a orifice meter wet gas correction factor. Figure 2 shows the ISO traceable data and the effect of applying the associated correction factor for a known liquid loading.



Fig. 1 - Orifice meter installed in CEESI Wet Gas Facility (left) and in NEL Wet Gas Facility (right).

Technical Paper

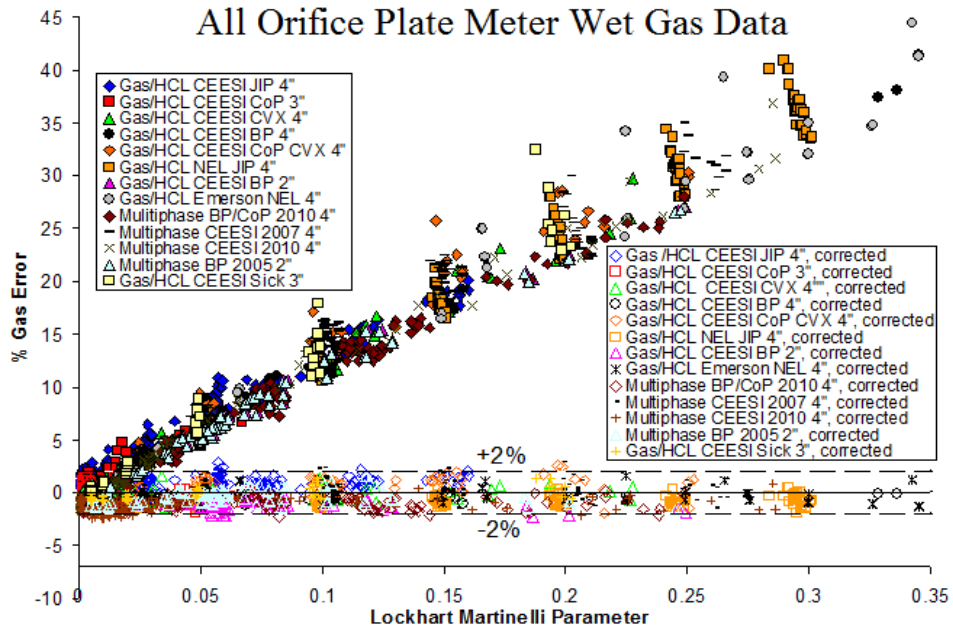


Fig. 2 - ISO TR 12748 orifice meter reproducible data set.

Figure 2 shows the remarkable reproducibility of the orifice meter performance at the different test facilities tested over a long period of time. This of course is a testament to both the reproducibility of the orifice meter in wet gas applications, as well as the ability of the different test facilities to create reproducible results. This orifice meter wet gas research produced in effect an inter-lab comparison between CEESI & NEL and, for the orifice meter at least, the result is that both facilities give the same results.

In 2006 CEESI (Steven [5]) released a 4", 0.4 $\beta$  Venturi meter wet gas data set tested at CEESI as part one of these JIPs. Figure 4 shows the meter installed at CEESI. This meter was donated to this JIP by Shell after they had previously tested it with wet gas flow at the Trondheim wet gas flow facility. De Leeuw [6] of Shell had published this Tondheim data set with an associated correlation. As a correlation is a fit to the source data, this Shell correlation is effectively a mathematical expression of the Trondheim data sets.



Fig. 3 - Shell's 4", 0.4 $\beta$  Venturi Meter at CEESI.

# 34<sup>th</sup> International North Sea Flow Measurement Workshop 25-28 October 2016

## Technical Paper

Figure 4 shows the CEESI JIP wet gas data and the effect of correcting the data for a known quantity of liquid using de Leeuw's correlation. The dotted lines represent the uncertainty claim of de Leeuw. Clearly the correlation works within the stated uncertainty, showing that the performance of the meter at Trondheim was essentially reproduced at CEESI.

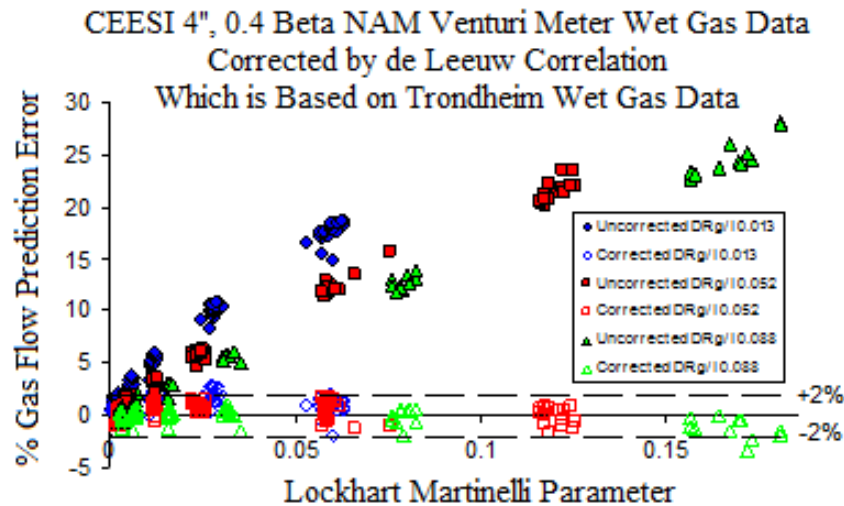


Fig. 4 - CEESI Wet Gas Data From Shell 4", 0.4 $\beta$  Venturi Meter Previously Tested at Trondheim.

### 3.2 Uncertainty of the Wet Gas Test Facilities

The reference gas volumetric flow rate at the CEESI wet gas test facility is measured by an ultrasonic flow meter and a turbine meter. The liquid flows are measured by means of a Coriolis mass flow meter. The DNV GL facility uses an ultrasonic flow meter as gas flow reference meter and also a Coriolis mass flow meter for the liquids. Both facilities are operated in a closed loop configuration. The claimed relative expanded uncertainties ( $k=2$ ) of the CEESI and DNV GL facility are given in Table 1.

**Table 1 – Claimed reference uncertainties of CEESI and DNV GL wet gas test facilities**

	CEESI	DNV GL
$U_{lab}^*(\dot{Q}_g)$	<0.7%	<0.7%
$U_{lab}^*(\dot{Q}_l)$	<0.5%	<0.5%

In 2009 Reader-Harris et al [7] released a Venturi meter wet gas correction factor applicable over a wide range of meter geometries and a wide range of wet gas flow conditions. The correction factor is shown in the box below. This correlation was subsequently adopted by ISO TC30 in the TR 11583.

**34<sup>th</sup> International North Sea Flow Measurement Workshop  
25-28 October 2016**

**Technical Paper**

$$\dot{m}_g = \frac{EA_t \epsilon C_d^* \sqrt{2\rho_g \Delta P_{tp}}}{\sqrt{1 + CX_{LM} + X_{LM}^2}} \quad (1)$$

$$C = \left(\frac{\rho_g}{\rho_l}\right)^n + \left(\frac{\rho_l}{\rho_g}\right)^n \quad (2)$$

$$C_d^* = 1 - 0.0463 \exp(-0.05 \cdot Fr_{g,th}) \min\left(1, \sqrt{\frac{X_{LM}}{0.016}}\right) \quad (3)$$

$$Fr_{g,th} = \frac{Fr_g}{\beta^{2.5}} \quad (4)$$

$$n = \max\left[0.583 - 0.18\beta^2 - 0.578 \exp\left(\frac{-0.8Fr_g}{H}\right), 0.392 - 0.18\beta^2\right] \quad (5)$$

The  $Fr_{g,th}$  is the throath Froude number and the parameter  $H$  is chosen as follows

$$\begin{aligned} H &= 1, & \text{for light hydrocarbon liquid} \\ H &= 1.35, & \text{for water at ambient temperature} \\ H &= 0.79, & \text{for water at elevated temperature} \end{aligned} \quad (8)$$

The correlation has the following stated limits of use:

$$\begin{aligned} 0.4 &\leq \beta \leq 0.75 \\ 0 &\leq X_{LM} \leq 0.3 \\ Fr_{g,th} &> 3, \\ DR &> 0.02 \end{aligned} \quad (9)$$

and gas flow rate uncertainty claims of:

$$\begin{aligned} U_{ISO}^*(\dot{m}_g) &< 3\%, \quad \text{for } X_{LM} \leq 0.15 \\ U_{ISO}^*(\dot{m}_g) &< 2.5\%, \quad \text{for } X_{LM} > 0.15 \end{aligned} \quad (10)$$

This correction factor was created from an extensive wet gas Venturi meter data set from NEL, a single data set from CEESI, and some older untraceable data from larger Venturi meters. Hence, it is heavily based on NEL data. This fact is useful when it comes to a wet gas flow facility inter-comparison. As a correlation is a fit to the source data, this ISO / NEL correlation is effectively a mathematical expression of the NEL data sets. Hence, in effect, any 3<sup>rd</sup> party wet gas facility Venturi meter data set can be compared to this ISO / NEL correlation to create a facility inter-comparison.

The adoption of this NEL wet gas Venturi meter correlation was at the time controversial. There were two main issues. The first issue was that some in

# 34<sup>th</sup> International North Sea Flow Measurement Workshop 25-28 October 2016

## Technical Paper

industry believed it was premature for ISO to adopt this correlation before significant 3<sup>rd</sup> party independent data was available to confirm its accuracy. Although it was probable the correlation would be proven sound, it was seen by some as good practice (and the scientific method) to have independent verifications. The second issue was that the correlation was restricted to gas with water or gas with oil. There was no allowance for the most common natural gas field flow conditions of gas with water & oil. The effect of the technically straight forward application of a fluid property extrapolation to account for these common field fluid compositions was unknown.

In response to the need for more wet gas flow facility inter-comparisons, and the controversy over ISO TR 11583 correlation not having enough independent checks, CEESI and DNV GL agreed to both wet gas test the same ISO compliant 6", 0.6 $\beta$  Venturi meter. Figure 5 shows the same meter installed at the CEESI (left) and DNV GL (right) wet gas test facilities, respectively. Both test facilities tested this meter by installing it in the respective facilities during a 3<sup>rd</sup> party commercial test of unrelated equipment. Therefore the data sets were restricted to both the range of the facilities, and the test matrix set by the 3<sup>rd</sup> party equipment tests.



Fig. 5 - 6", 0.6 $\beta$  Venturi meter at the CEESI (left) and DNV GL(right) wet gas test facility

The CEESI data set had the range:

$$\begin{aligned}0 &\leq X_{LM} \leq 0.16 \\0.015 &\leq DR \leq 0.085 \\0.7 &\leq Fr_{g,th} \leq 25.5 \\0 &\leq WLR \leq 1\end{aligned}$$

The DNV data set had the range:

# 34<sup>th</sup> International North Sea Flow Measurement Workshop 25-28 October 2016

## Technical Paper

$$0 \leq X_{LM} \leq 0.35$$

$$0.0125 \leq DR \leq 0.065$$

$$1.3 \leq Fr_{g,th} \leq 10.5$$

$$0 \leq WLR \leq 1$$

As observed the data set ranges have sufficient overlap between the facilities and the NEL correlation. It is important to notice that the test data was not shared between the facilities until after the execution of the tests.

The fluids used during the tests are given in Table 2. Both CEESI and DNV GL operate with natural gas, refined oil and (salt) water. A small part of the tests at DNV GL has been run with argon to attain higher  $DR$  and  $Fr_g$ . The differences between the pure oil properties at atmospheric pressure, i.e. not in equilibrium with natural gas at elevated pressure, are:

- Exxsol D80:  $\rho_o = 806 \text{ kg/m}^3$ ,  $\nu_o = 2.2 \text{ mm}^2/\text{s}$  and  $\sigma_o = 26.3 \text{ mN/m}$
- Exxsol D120:  $\rho_o = 831 \text{ kg/m}^3$ ,  $\nu_o = 4.85 \text{ mm}^2/\text{s}$  and  $\sigma_o = 28.1 \text{ mN/m}$

where the density is evaluated at 15°C and the kinematic viscosity and surface tension at 25°C. The effect of the oil density is taken into account in the ISO 11583 correlation. Although the factor  $H$  in the correlation is often associated with a surface tension effect, the effect of liquid viscosity and surface tension is still not fully understood.

**Table 2 – Used fluids at CEESI and DNV GL wet gas test facility during inter-comparison tests**

	CEESI	DNV GL
Gas	Natural gas	Natural gas, Argon
Oil	Exxsol D80	Exxsol D120
Water	Water	Salt water (38 g/kg)

## 4 WET GAS INTER-COMPARISON RESULTS

Figure 8 shows the combined data from CEESI and DNV GL where the data was within the ISO TR 11583 correlations range (inclusive of gas with oil or gas with water data only). Also shown is the result of applying the ISO TR 11583 correlation for a known quantity of liquid. The dashed lines represent the ISO stated uncertainty values. The CEESI & DNV GL data agree with each other and the combined data corrected by the NEL / ISO TR 11583 correction falls within the stated uncertainty bands.

**34<sup>th</sup> International North Sea Flow Measurement Workshop  
25-28 October 2016**

**Technical Paper**

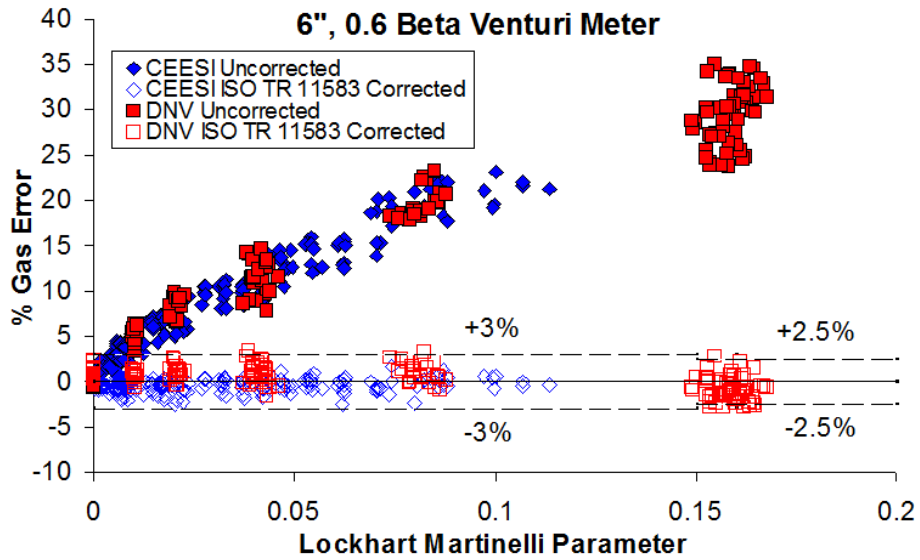


Fig.6 - CEESI & DNV GL 6", 0.6 $\beta$  Venturi meter wet gas data within ISO TR range

Figures 7 & 8 show the CEESI & DNV GL individual data sets, respectively, split into gas with oil and gas with water. (The DNV GL data shows a token multiphase wet gas data set, i.e. gas with water & oil.)

In effect this results show that NEL, DNV GL, & CEESI produce the same Venturi meter wet gas flow performance.

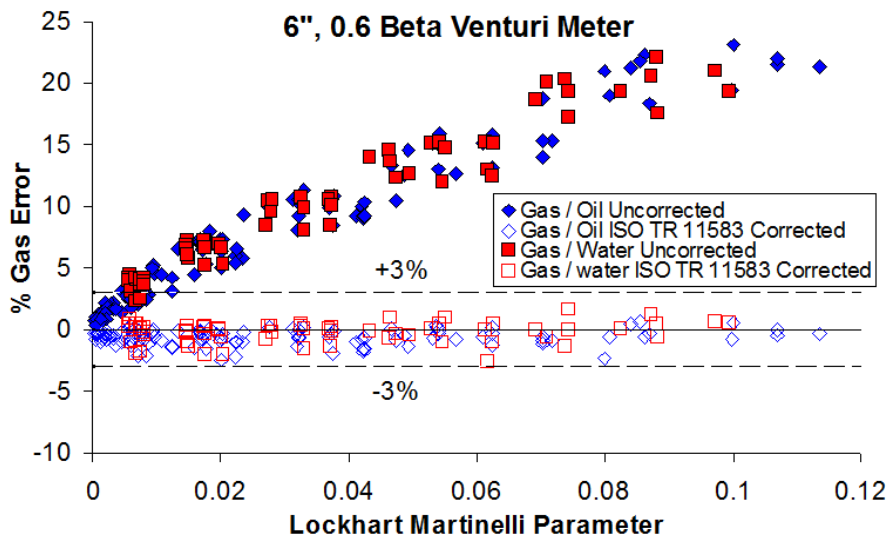


Fig. 7 - CEESI wet gas data within range of ISO TR 11583

Technical Paper

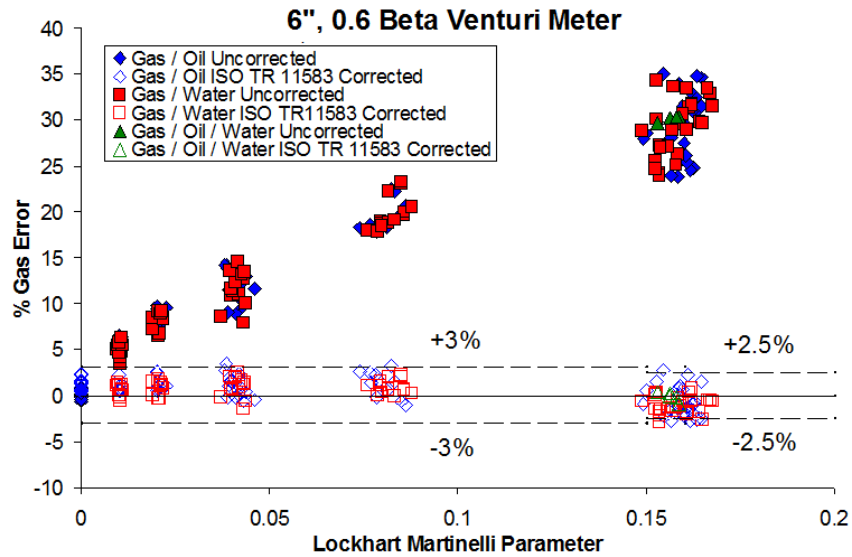


Fig. 8 - DNV GL wet gas data within range of ISO TR 11583 (plus a small multiphase wet gas data set)

A parameter to evaluate the success of the inter-comparison is given by the ISO 17043 [8] in terms of the  $E_n$ -numbers when using the Venturi combined with the ISO 11583 correlation as the travel standard

$$E_n = \frac{\varepsilon_{OR\%}}{\sqrt{(U_{ISO}^*)^2 + (U_{lab}^*)^2}} \quad (11)$$

where  $\varepsilon_{OR\%}$  is the remaining error in the over-reading after correction with the ISO 11583 correlation. In the case  $E_n \leq 1$  the inter-comparison can be qualified as satisfactory, which is the case for all test points in the range specified in equation (9).

## 5 EXTRAPOLATION OF ISO TR 11583's CORRELATION

It is useful to know the effects of extrapolating a correlation. Figure 9 shows the effect of using the ISO TR 11583 with the multiphase wet gas (i.e. gas with oil and water) CEESI data where all other parameters are within the correlations stated flow condition range. The correlation corrects the gas flow rate prediction to within the correlations stated uncertainty, however, this data set is only for  $X_{LM} < 0.12$ . For the value of  $H$  a linear interpolation is used.

**34<sup>th</sup> International North Sea Flow Measurement Workshop  
25-28 October 2016**

**Technical Paper**

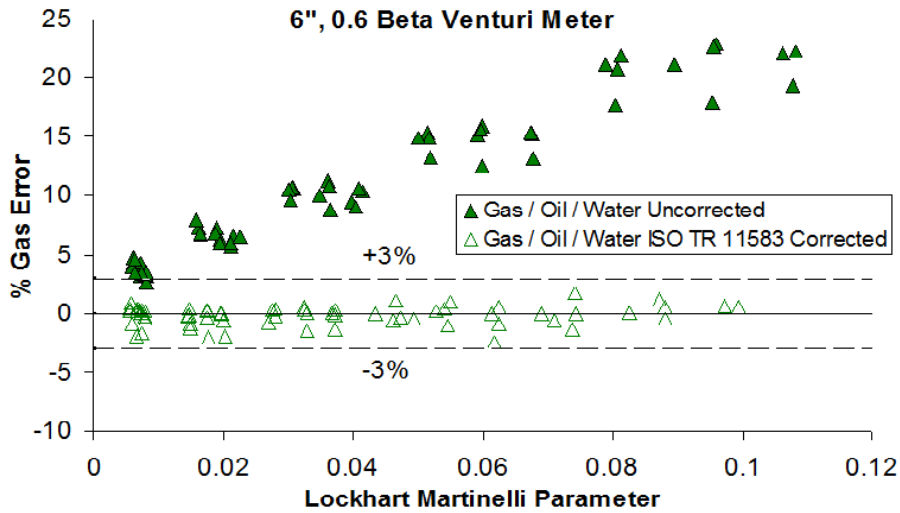


Fig. 9 - CEESI multiphase wet gas data

Figure 10 shows gas with oil CEESI data where the density ratio and / or the throat gas densimetric Froude number were marginally outside the correlation range. The CEESI data shown in Figure 10 has the ranges  $0.7 < Fr_{g,th} < 3$  and  $0.016 < DR < 0.02$ . The ISO TR 11583 correlation performs well.

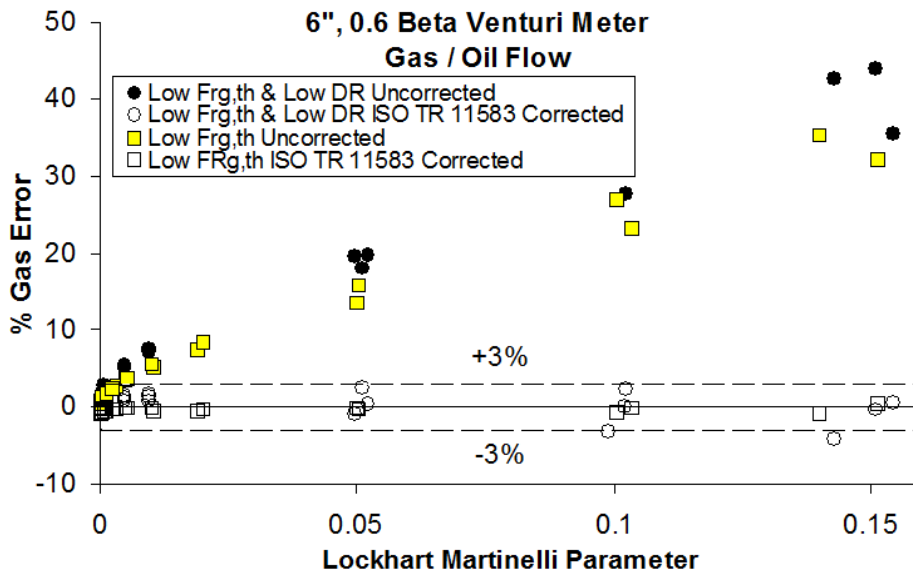


Fig. 10 - CEESI gas with oil wet gas data with  $DR$  and / or  $Fr_{g,th}$  outside ISO TR 11583 range

# 34<sup>th</sup> International North Sea Flow Measurement Workshop 25-28 October 2016

## Technical Paper

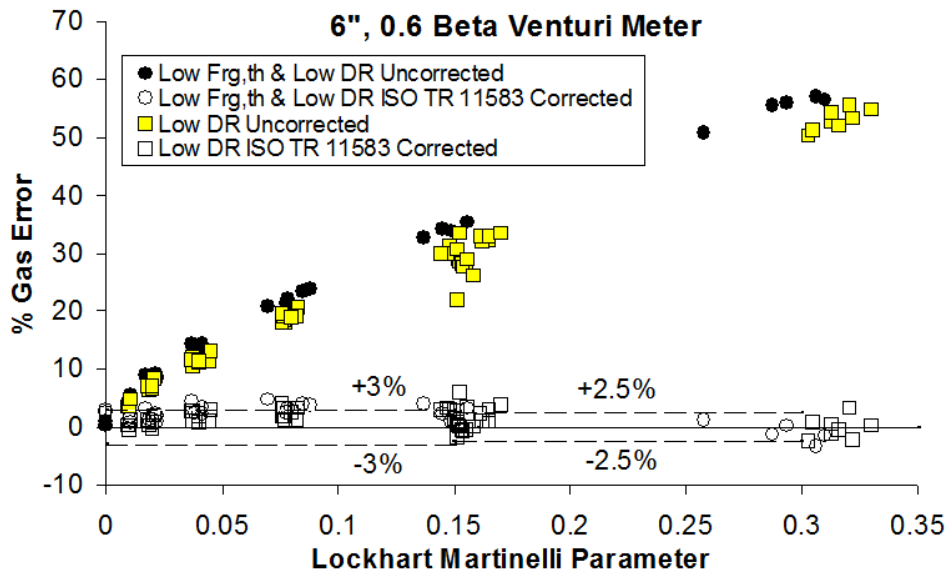


Fig. 11 - DNV GL gas with oil or water wet gas data with  $DR$  and / or  $Fr_{g,th}$  outside ISO TR 11583 range

Figure 11 shows gas with oil or water DNV data where the density ratio and / or the throat gas densimetric Froude number were marginally outside the correlation range. The DNV data shown in Figure 11 has the ranges  $1.3 < Fr_{g,th} < 3$  and  $0.012 < DR < 0.02$ . In this case the ISO TR 11583 correlation performs well.

However, it is a limited data set and it was noted that there was no multiphase wet gas flow data for the higher liquid loadings. Further data sets show the effect of such an extrapolation of the ISO TR 11583 correlation.

## 6 INDEPENDENT CHECKS ON ISO TR 11583 VENTURI METER WET GAS CORRELATION

CEESI has two independent sets of multiphase wet gas Venturi meter data. One data set consists of multiphase wet gas ISO compliant 2", 4", 6", & 8" 0.6 $\beta$  Venturi meters. Figures 12 and 13 show these meters under test at CEESI. Table 3 shows the test range compared to the TR 11583 range of applicability.

Although the ISO TR 11583 correlation is published as only applicable to gas with oil **or** water it is a simple procedure to interpolate the factor 'H' (relative to the water cut) to produce a correlation for use with gas with oil **&** water. Such a procedure is of course out with the scope of ISO TR 11583 and is not guaranteed to work within the correlations stated uncertainty. Figure 14 shows the results. For a known liquid flow rate, **within** the specified range of the ISO correlation, i.e. for gas with oil **or** water, all four Venturi meter gas flow rate predictions predicted the gas flow to within the stated uncertainty of the correlation. However, for the higher Lockhart-Martinelli parameter values ( $X_{LM} > 0.15$ ) the ISO TR 11583 correlation slightly over-corrects the multiphase wet gas flow data. This result has been repeatedly found.

**34<sup>th</sup> International North Sea Flow Measurement Workshop  
25-28 October 2016**

**Technical Paper**



Fig. 12 - 2" (left) and 4"(right), 0.6β Venturi meter at CEESI



Fig. 13 - 6" (left) and 8"(right), 0.6β Venturi Meter at CEESI

**Table 3 – CEESI 2" to 8" Venturi meter wet gas test data shown in Figure 14 & the ISO TR 11583 Venturi meter wet gas flow correlation ranges.**

Parameter	CEESI test range	ISO TR 11583 stated limits
Pressure	$14.8 \leq p < 77$ bara	N/A
Gas to Liquid $DR$	$0.016 < DR < 0.085$	$DR > 0.02$
$Fr_g$ range	$0.25 < Fr_g < 7.13$	$Fr_g > 3\beta^{2.5}$
$X_{LM}$	$0 \leq X_{LM} \leq 0.28$	$X_{LM} < 0.3$
Inlet Diameter	$1.939" \leq D \leq 7.981"$	$D \geq 2"$
Beta	$\beta = 0.6$	$0.4 \leq \beta < 0.75$
Gas / Liquid phase	Gas /Oil/ Water	Gas / Oil or Gas / Water

Technical Paper

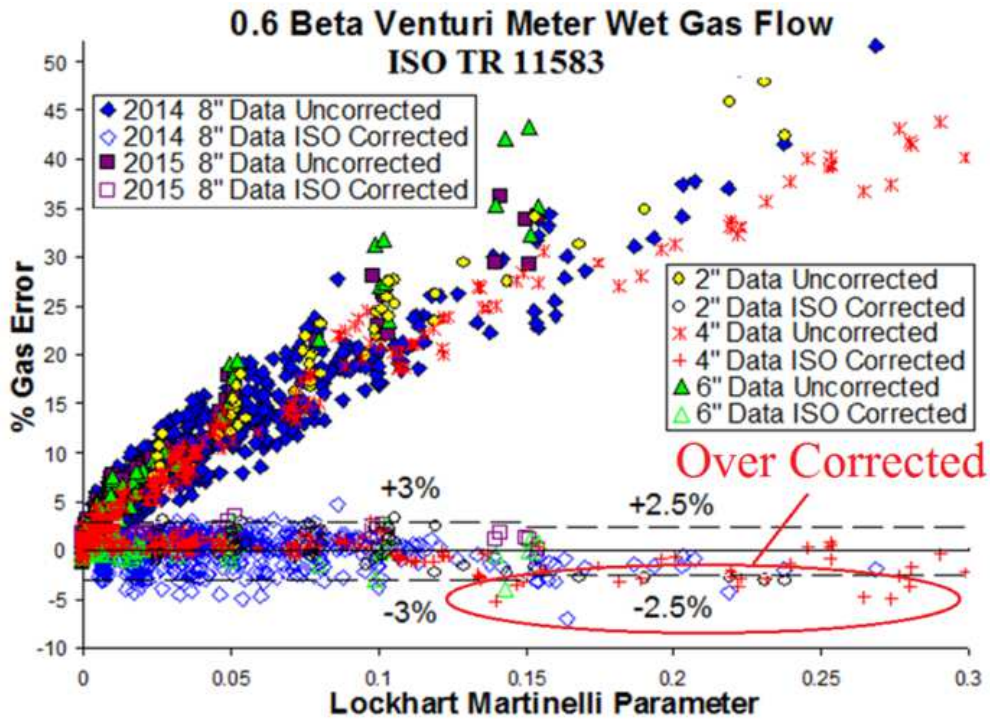


Fig. 14 - 2", 4", 6", & 8" ISO compliant Venturi meter wet gas data from CEESI, corrected by ISO TR 11583.

In a separate project CEESI multiphase wet gas tested seven nominally identical 6", 0.6 $\beta$  Venturi meters. Figure 15 shows four of these meters under test at the CEESI wet gas flow facility. Figure 16 shows the combined data set from these seven meters. Figure 17 shows the corrected data only. Again, as with the data shown in Figure 14, at higher Lockhart-Martinelli parameter values ( $X_{LM} > 0.15$ ) the ISO TR 11583 correlation slightly over-corrects the multiphase wet gas flow data.



Fig. 15 - Four Out of Seven 6", 0.6 $\beta$  Venturi Meters at CEESI

Technical Paper

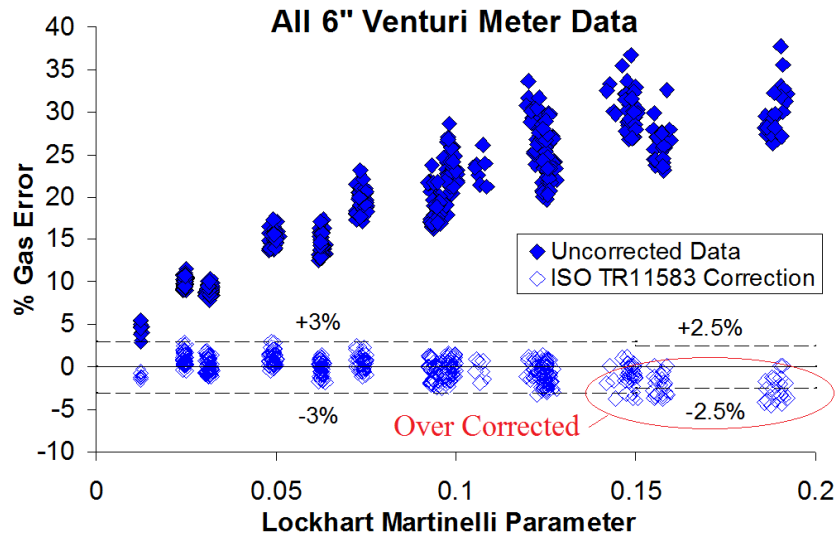


Fig. 16 - CEESI massed 6\" Venturi meter multiphase wet gas uncorrected & TR 11583 corrected data

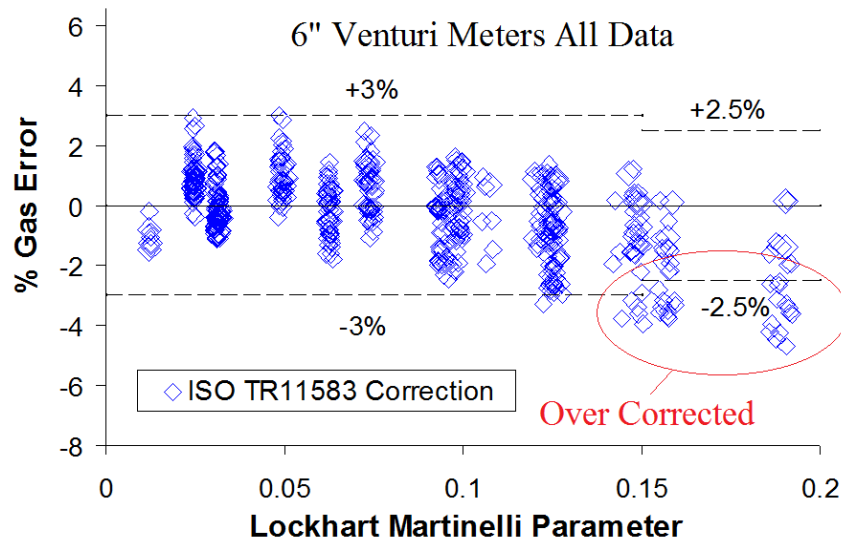


Fig. 17 - CEESI massed 6\" Venturi meter multiphase wet gas TR 11583 corrected data

TUV NEL, which created the correlation adopted by ISO using gas with oil or water data, have also now produced multiphase wet gas Venturi meter data that again shows this issue. NEL published (Graham et al [9]) 4\" Venturi meter data that shows for gas with oil or water the ISO TR 11583 correlation worked within its stated uncertainty, but for gas with oil and water at  $X_{LM} > 0.15$  the TR 11583 correlation slightly over-corrects the data. Figure 18 shows this. This is essentially the same result as independently found by CEESI on two different projects.

Technical Paper

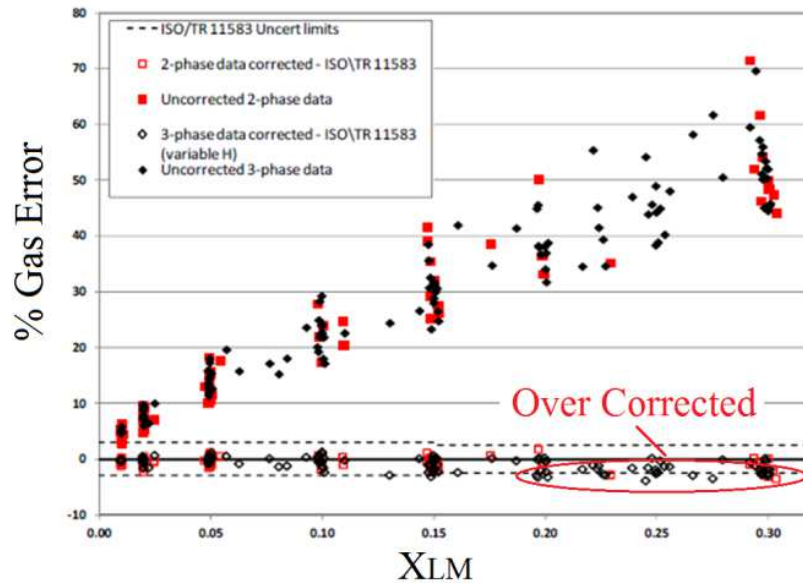


Fig. 18 - NEL 4" Venturi meter wet gas uncorrected & TR 11583 corrected data.

This result has been reproduced in different facilities, using different equipment and different times. This is another indicator that the different industrial grade wet gas test facilities do produce the same results.

## 7 CONCLUSIONS

The available evidence backs the assumption that a Venturi meter (and therefore by extension a generic DP meter) has a reproducible wet gas performance at different wet gas flow test facilities. As Venturi (& DP) meters are the most popular choice for economic wet gas metering this fact is important to industry. It means that DP meters tested in one wet gas test facility have a known wet gas performance in other test facilities with similar fluid properties, and far more importantly by extension, for the case of similar fluid properties a known performance in the field. The precise effects of extrapolating fluid properties are as yet uncertain. Also by extension, a DP meter wet gas correlation (such as the Venturi meter wet gas correlation TR 11583) created with data from one facility should be applicable within the stated meter geometry and wet gas flow condition range in the field.

However, this examination of the available multiphase wet gas Venturi meter data clearly shows that the old adage "...you extrapolate a correlation at your own risk" holds. The ISO TR 11583 correlation is not developed for multiphase (gas, oil, & water) wet gas flow, only gas with oil or water wet gas flow. Subsequently, use of this correlation with multiphase wet gas flow at higher liquid loadings (i.e.  $X_{LM} > 0.15$ ) will lead to a slight negative bias in the gas flow rate prediction.

ISO Venturi meter correlation applicable over a wide range of Venturi meter sizes is very useful to industry. It would be to industries benefit for a multiphase wet gas Venturi meter correlation to be created. However, although one test facility should produce data that is reproducible in other test facilities and in the field, it is still best practice that such a correlation should either be formed with data from multiple test facilities (ideally more than two), or the correlation formed with data from one test facility should be independently checked by 3<sup>rd</sup> parties at other multiphase wet gas flow test facilities.

# 34<sup>th</sup> International North Sea Flow Measurement Workshop 25-28 October 2016

## Technical Paper

### 8 NOTATION

$A_t$	Throath area of Venturi
$C_d$	Discharge coefficient
$DR$	Density ratio (gas/liquid)
$E$	Velocity of approach
$E_n$	Performance number
$Fr_g$	Gas densiometric Froude number
$Fr_{g,th}$	Gas densiometric Froude number evaluated at throath conditions
$H$	Parameter ISO 11583 correlation
$\dot{m}_g$	Mass flow rate of the gas
$OR$	Over-reading
$\Delta P_g$	Venturi differential pressure at single phase gas flow
$\Delta P_{tp}$	Venturi differential pressure at two-phase gas-liquid flow
$\dot{Q}_k$	Volume flow rate of phase $k$
$u_{sk}$	Superficial velocity of phase $k$
$U^*$	Relative expanded uncertainty
$WLR$	Water Liquid Ratio at line conditions
$X_{LM}$	Lockhart-Martinelli parameter
$\beta$	Venturi beta ratio
$\varepsilon$	Gas expansibility factor
$\rho_k$	Mass density of phase $k$

### 9 REFERENCES

- [1] ISO TC193 TR 12748, "Natural Gas – Wet Gas Flow Measurement in Natural Gas Operations".
- [2] ISO TC30 Technical Report 11583; "Measurement of wet gas flow by means of pressure differential devices inserted in circular cross-section conduits running full – Part 1: General principles and requirements".
- [3] American Society of Mechanical Engineering MFC, Report 19G "Wet Gas Metering", 2008.
- [4] Steven R., Stobie G., Hall A. & Priddy R., "Horizontally Installed Orifice Plate Meter Response to Wet Gas Flows" North Sea Flow Measurement Workshop Oct. 2011, Tonsberg, Norway.
- [5] Steven R., "Horizontally Installed Differential Pressure Meter Wet Gas Flow Performance Review", North Sea Flow Measurement Workshop, St Andrews, Scotland, 2006.
- [6] De Leeuw R, "Liquid Correction of Venturi Meter Readings in Wet Gas Flow", North Sea Workshop 1997.
- [7] M. Reader Harris & E. Graham, "An Improved Model for Venturi-Tube Over-Reading in Wet Gas", North Sea Flow Measurement Workshop, 2009.
- [8] ISO 17043, "Conformity assessment: General requirements for proficiency testing", (2010).

**34<sup>th</sup> International North Sea Flow Measurement Workshop  
25-28 October 2016**

**Technical Paper**

- [9] M. Reader Harris & E. Graham, "Impact of Using ISO/TR 11583 for Venturi Tube in 3-Phase Wet Gas Conditions", North Sea Flow Measurement Workshop, Tonsberg, Norway 2015.

**Extended Abstract**

**ISO/AWI 21354 Measurement of Multiphase Fluid  
Flow**

**Michael Reader-Harris, NEL**

---

**1 INTRODUCTION**

It has been recognized for some time that standards are an important enabler of innovation and international technology transfer. They have an important role in national and international trade and in wealth creation. Standards contributed to about 13 per cent of the growth in labour productivity in the UK over the period 1948-2002 [1], and contribute £2.5 billion annually to the UK economy. Many other national economies have benefited similarly.

By developing and adopting standards, barriers to trade are lowered, transaction costs are reduced and the operation of markets is improved through the smooth flow of goods and services. Standards enable compliance to be demonstrated, provide confidence in product performance, and help to eliminate or reduce disputes between companies and across borders. They help smaller firms by transferring technology from larger ones. Poorer countries may benefit similarly.

Flow measurement is an important area of standardization. For example UK natural gas demand is around £5 billion annually, and most of this is measured (generally more than once) using the ISO standard for flow measurement using differential-pressure meters, ISO 5167. Avoidance of both inaccuracy through inadequate specification and excessive cost through over-specification is absolutely vital. Standards give consistency. Accuracy in taxation is of great importance to Government.

Standardization is not only important for economic reasons. Accurate measurement of discharges, of produced water, for instance, is important to ensure a cleaner environment.

**2 ISO STANDARDS**

ISO standards are produced by more than 200 technical committees (TCs) and their subcommittees (SCs). The voting members (i.e. P-members) of these committees are the national standards bodies, e.g. BSI (the British Standards Institution). A TC covers a specific technical area, and its SCs are appointed to concentrate on specific areas within the remit of the TC. Under an SC (or under the TC directly) Working Groups (WGs) draft the text of the standards. The members of a WG are individual experts nominated by the national standards bodies. Participation in standards-making is an opportunity not only to share knowledge but also to gain it. The national standards bodies vote on the standards.

From a search of the ISO website it appears that about 160 standards from about 40 technical committees have reference to fluid flow measurement. Two thirds of the ISO standards that include reference to fluid flow measurement are produced by four technical committees: TC 28 Petroleum products and lubricants, TC 30 Measurement of fluid flow in closed conduits, TC 113 Hydrometry, and TC 131

# **34<sup>th</sup> International North Sea Flow Measurement Workshop 25-28 October 2016**

## **Extended Abstract**

Fluid power systems. Many standards on natural gas properties are produced by TC 193 Natural gas.

ISO/TC 30's remit is to produce standards on flow measurement in pipes for general use: TC 30/SC 2 covers differential-pressure meters (and sonic nozzles); TC 30/SC 5 covers velocity and mass methods (e.g tracer and velocity-area methods and electromagnetic, Coriolis, thermal mass and ultrasonic meters). As a result standards produced by ISO/TC 30 are referred to by many other technical committees.

In order to produce an ISO standard a country puts forward a New Work Item Proposal and nominates a project leader: for the project to be approved not only must a majority of those voting support the proposal but at least five countries (if there are at least 17 P-members) must agree to work on the project and nominate an expert. The Working Group consisting of these experts then produces a series of Working Drafts. When they are happy with a Working Draft it is sent to the SC (or if no SC the TC) as a CD (Committee Draft). The SC seeks comments on the CD, and considers them. Once the SC is happy with the CD it is sent to ISO CS (Central Secretariat) and becomes a DIS (Draft International Standard). It is sent out for ballot by ISO CS. Comments on the CD are considered by the SC, and an FDIS (Final Draft International Standard) is produced. The FDIS is balloted: no technical changes can be made after the FDIS ballot, but it is possible for the voters to check that all the changes agreed at the DIS stage have been correctly included. Then the new standard is published. Under certain circumstances the FDIS stage may be omitted. The procedure is described in much more detail in [2].

The procedure to publish a Technical Report is much simpler: once a committee draft is available a single ballot by the SC is sufficient.

### **3 MULTIPHASE FLOW MEASUREMENT**

An SC within TC 28, TC 30 or TC 193 could have produced a multiphase flow measurement standard, but the honour has fallen to TC 28/SC 2, responsible for oil flow measurement.

A New Work Item Proposal was made by BSI with Michael Reader-Harris as Project Leader and sent out in October 2015. The outline section titles were:

1. Scope
  2. Normative references
  3. Terms and definitions
  4. Symbols and subscripts
  5. Multiphase flow
  6. Multiphase meter technologies
  7. Aims of multiphase flow measurement
  8. Production envelope
  9. Performance specification
  10. Testing
  11. Field installation and commissioning
  12. Verification during operation
- Annex A Intercomparison between laboratories

# **34<sup>th</sup> International North Sea Flow Measurement Workshop 25-28 October 2016**

## **Extended Abstract**

The NWIP passed by 10 votes (China, France, Iran, Japan, Malaysia, Netherlands, Norway, Singapore, Sweden, UK) to 1 (USA). Five countries agreed to nominate members of the Working Group. There were 13 abstentions. In January 2016 work commenced. The first activity was for the Project Leader to convert the NFOGM (Norwegian Society for Oil and Gas Measurement) Handbook of Multiphase Flow Metering [3] into the format of an ISO Technical Report: NFOGM had very kindly given their document to form the basis of the TR. It took time for countries to nominate the WG members.

In May 2016 the first draft of the TR was sent to the WG members and they were asked to volunteer to review sections: the WG members are:

- China
  - Chen Liang, Petrochina
  - Gao Jun, Petrochina
- France
  - Jean-Paul Couput, Total
- Netherlands
  - Rick de Leeuw, Shell
  - Jankees Hogendoorn, Krohne
- UK
  - Wes Maru, Oil & Gas Measurement Limited
  - Bill Priddy (then BP)
  - Rogerio Ramos, Coventry University
- USA
  - Phil Lawrence, Enable Midstream
  - Richard Steven, CEESI

In June those who had volunteered were given their tasks. The volunteers revised their sections in July and early August. In mid-August the Project Leader sent out the 2<sup>nd</sup> draft to WG members for comment.

Comments were submitted in September. They were collated and circulated with non-controversial comments marked in October. A meeting to go through the comments has been planned for the day before the North Sea Flow Measurement Workshop. Following the meeting a 3<sup>rd</sup> draft will be sent to WG members.

In 2017 the results of the EMRP Multiphase Flow Metrology project will be available. They should provide material on how to test multiphase flow meters and on how well test laboratories agree. In 2018 the TR will be balloted.

# **34<sup>th</sup> International North Sea Flow Measurement Workshop 25-28 October 2016**

## **Extended Abstract**

### **4 ACKNOWLEDGMENTS**

This paper is published by permission of the Managing Director, NEL.

### **5 REFERENCES**

- 1 DEPARTMENT OF TRADE AND INDUSTRY The Empirical Economics of Standards. DTI Economics Paper No 12, 2005. Available as [www.berr.gov.uk/files/file9655.pdf](http://www.berr.gov.uk/files/file9655.pdf) London: DTI
- 2 INTERNATIONAL ORGANIZATION FOR STANDARDIZATION. ISO/IEC Directives, Part 1 — Consolidated ISO Supplement — Procedures specific to ISO (7<sup>th</sup> edition). Geneva: ISO/IEC, 2016.
- 3 NORWEGIAN SOCIETY FOR OIL AND GAS MEASUREMENT. Handbook of multiphase flow metering. NFOGM:2005

## **Extended Abstract**

### **Investigation of Multiphase Flow-Regimes After a Blind-T Mixer and at the Throat of the Venturi – Using Gamma-Ray Tomography and CFD Modelling**

**Stein-Arild Tjugum and Teerachai Leeungculsatien, Roxar - Emerson  
Process Management**

**Bjørn Tore Hjertaker and Rachid Maad, University of Bergen – Dept. of  
Physics and Tech.**

**Anders Hallanger, Cristian Michelsen Research AS**

---

#### **1 INTRODUCTION**

Multiphase flow meters (MPFMs) are often installed in a vertical section at a given distance downstream of a blind-T to provide a more predictable flow regime. Placing the measurement section at the throat of a venturi or downstream of a venturi is another method used in some MPFM designs to condition the flow regime. In this work the multiphase flow has been studied at different distances from the blind-T, at the throat and downstream of the venturi using gamma-ray tomography. The objective was to investigate the flow-regime and flow mixing quality at different locations required to optimize MPFM performance. This was done using high-speed gamma-ray tomography and CFD flow simulations. This work was a collaboration between the University of Bergen, CMR and Roxar - Emerson Process Management.

#### **2 DESCRIPTION OF THE TEST SETUP**

The tests were done in the CMR flow loop [1] using the measurement setup shown in figure 1. It was of interest to investigate how the flow regime develops after the blind-T and how the venturi influences the flow regime. Thus, the gamma-ray tomograph was installed in a number of positions along the vertical pipe at different distance downstream the blind-T, and close upstream, downstream and in the throat of the venturi. The measurement-positions are shown in figure 1. Positions 1, 2 and 5 were tested with no venturi, and positions 1, 3, 4 and 5 were tested with the venturi installed.

A drawing of the gamma-ray tomograph is shown in figure 2. This instrument enables tomographic images of the flow cross-section with a 10ms time resolution [2]. The time-average tomograph measurements are used to find a gas fraction profile of the multiphase flow at each measurement position.

Extended Abstract

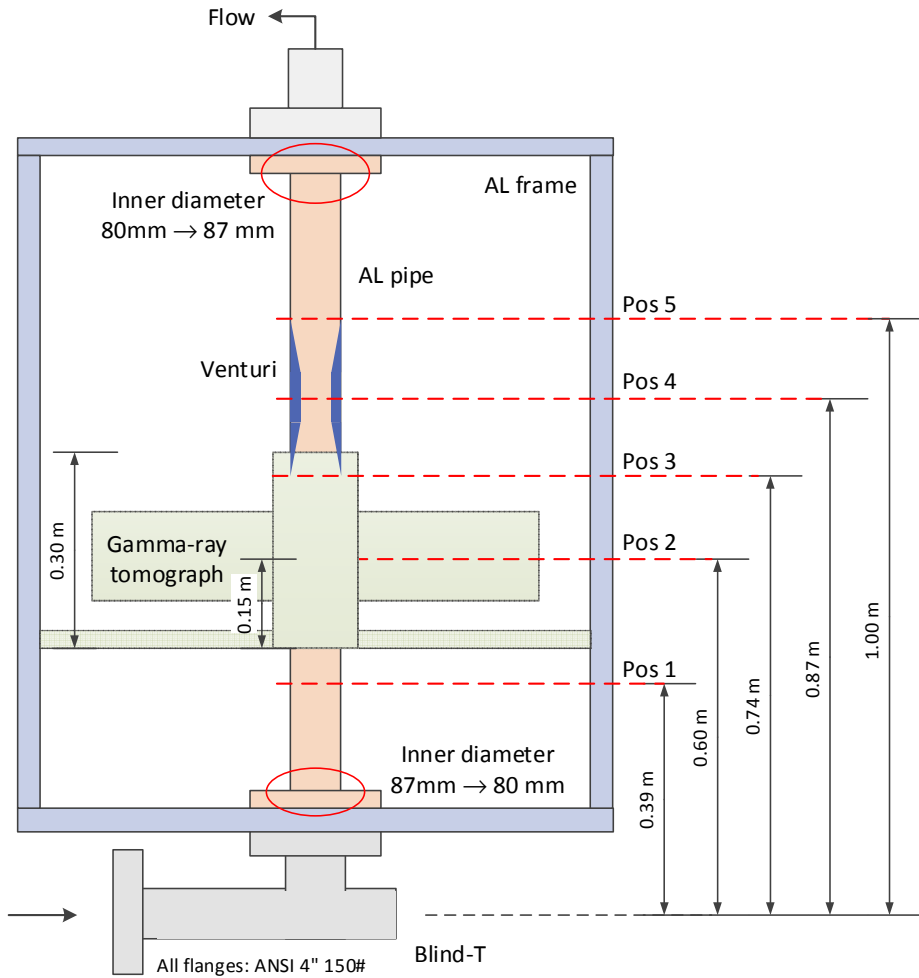


Figure 1 - The measurement section.

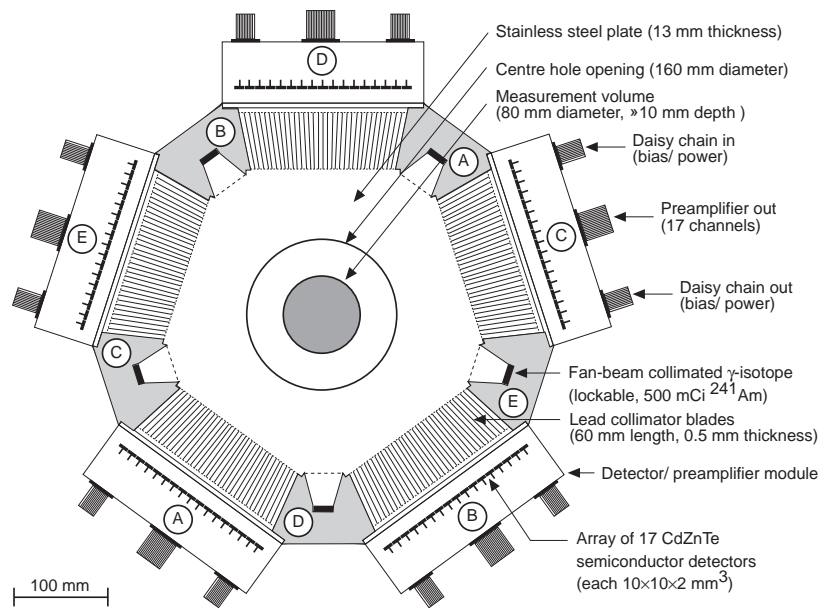


Figure 2 - The geometrical design of the high speed gamma-ray tomograph.

**Extended Abstract**

**3 RESULTS**

In full developed vertical multiphase flow, there is often an axis-symmetric time averaged gas fraction profile with more gas in the center of the flow. This is not always the circumstance closely downstream to the blind-T, where it is expected to have some deviation from axis-symmetry due to the fluid mechanics of the multiphase flow. This distribution of the gas fraction profile and deviation from axis-symmetric flow has been investigated. Figure 3 show gas fraction profiles and time-series plots of gas fraction obtained with the gamma-ray tomograph. The profile plots show that there is larger deviation from axis-symmetry close to the blind-T, and increasing symmetry with increasing distance downstream from the blind-T. The time average gas profile is close to symmetric at the position about a meter or 10 pipe diameters downstream from the Blind-T.

Measurements inside the venturi throat (pos. 4) also show a higher gas fraction in the center of the flow and some deviation from axis-symmetry. Measurements downstream of the venturi (pos. 5) show a more homogenous flow caused by the mixing effect of the venturi geometry. However, this venturi mixing effect is dependent on the flow velocity and the fluid properties and is therefore difficult to predict.

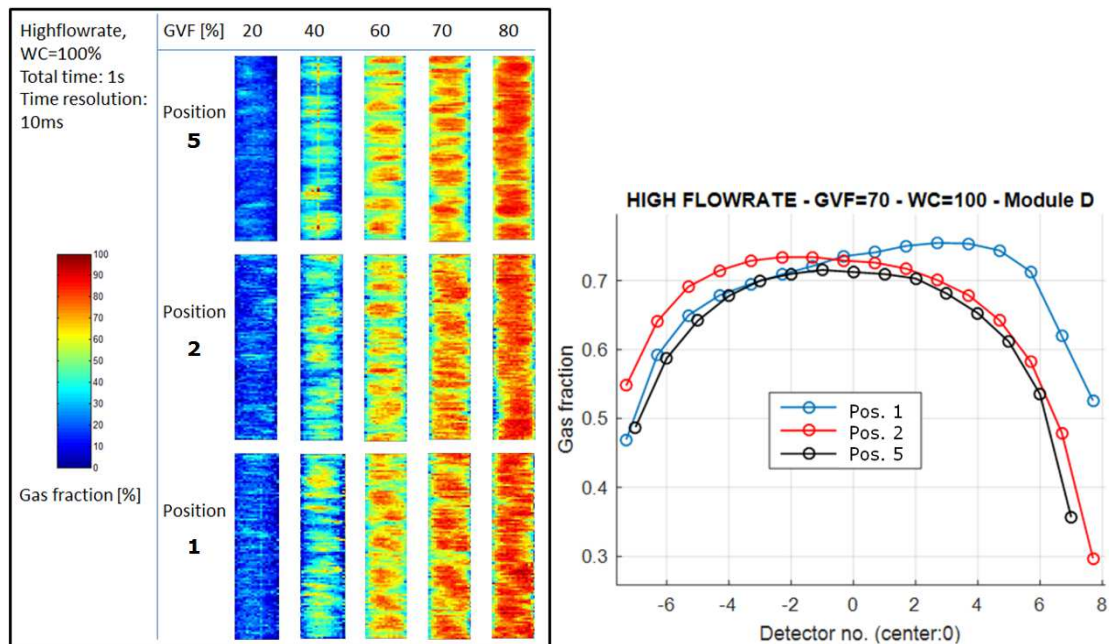


Figure 3 - Left: time-series plots of liquid/gas distribution, Right: Gas fraction plots from the gamma-ray tomograph.

The theoretical gas fraction profiles from the CFD simulations [3] show a more axis-symmetric flow with increasing distance from the blind-T in agreement with the measurements. The CFD simulations also provide a more detailed picture of the liquid gas distribution in the measurement-section as shown in figure 4.

**Extended Abstract**

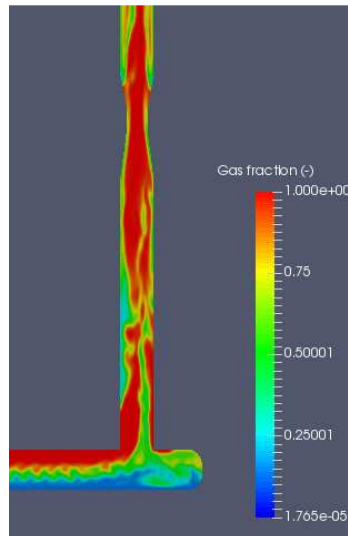


Figure 1 - Gas/liquid distribution found from CFD simulations

**4 STRATEGIES FOR OBTAINING FLOW REGIME INDEPENDENT MEASUREMENTS**

Multiphase flow meters are normally installed in the vertical section downstream of the blind-T, the possible positions for the fraction measurements are upstream, at the throat or downstream of the venturi [4]. It is preferable to do the measurements where the flow-regime is predictable and where the time-average of the gas fraction profile is axis-symmetric.

The Roxar measurement strategy is to do the fraction measurements on a well developed vertical flow downstream of the blind-T and before the venturi. By the use of six-electrode tomometric impedance measurements flow-regime effects are captured and compensated for, this technique can also handle deviation from axis symmetric flow.

**5 REFERENCES**

- [1] CMR (2014), Web page [online], Available: [www.cmr.no](http://www.cmr.no) (visited on 06/06/2016).
- [2] G.A. JOHANSEN, T. FRØYSTEIN, B.T. HJERTAKER, Ø. OLSEN (1996), A dual sensor flow imaging tomographic system. *Measurement Science and Technology*, Vol 7, pp. 297-307.
- [3] OpenFoam (2016), Web page [online], Available: <http://www.openfoam.com/> (visited 06/06/2016).
- [4] R. THORN, G.A. JOHANSEN, B.T. HJERTAKER (2013), Three-phase flow measurement in the petroleum industry, *Measurement Science and Technology*, Vol 24 (17 pp).

## **Technical Paper**

# **Compressible Fluid Calibration of Coriolis Meters**

**Thomas Kegel, Colorado Engineering  
Experiment Station, Inc.(CEESI)**

---

## **1 INTRODUCTION**

This paper presents and discusses new research results that represent an update of data and analysis as part of an ongoing program. The objective of the program is to gain a better understanding of Coriolis meter operation in compressible fluid flow measurement. Two types of data are available from a commercial calibration laboratory. First, numerous calibrations provides limited data on a relatively large number of meters. As part of the analysis the massed calibration data are classified into groups depending on the calibration curve shape. The second data category arises from more extensive testing of a smaller number of meters that allow for the variation of both mass flowrate and pressure. The results indicate dependence on one or more variables in addition to mass flowrate. The relevant secondary parameter appears to be either pressure or velocity. Test design and some results are discussed in detail in [1] and [2], this paper presents new data.

Historically Coriolis meters were restricted to liquid measurement applications, in recent years they have been widely used to measure natural gas. Some operators obtain calibration data using compressed air as a surrogate fluid; others select a water based calibration. While both fluids provide traceability, an air calibration includes compressibility that is similar to natural gas. As calibration experience has developed, compressibility effects seem to be observed with some meters but not with others.

Traditional meters exhibit a variety of second order effects which must be accounted for to maintain low uncertainty. Differential pressure meters require a gas expansion factor correction. The low flow K-factor of a gas turbine meter depends on flowing density and most liquid meters are affected by viscosity. An uncorrected compressibility effect when measuring gas with a Coriolis meter represents a potential similar measurement uncertainty source.

## **2 DATA SCOPE**

As noted the analysis is proceeding in two parts. The first database consists of 62 calibrations distribution by line size and flowing pressure as summarized in Table 1. The data are reasonably well distributed over the 1–4.5 MPa pressure range while being slightly skewed to the higher range. Most of the data came from three meter sizes, exceptions include three smaller (quarter inch) and one larger (three inch) meter. All the meters are calibrated using compressed air except the three inch which was calibrated in natural gas. The second database consists of three meters; the current paper presents recent diagnostic data from one of the meters.

# 34<sup>th</sup> International North Sea Flow Measurement Workshop 25-28 October 2016

## Technical Paper

### 3 INVESTIGATING CALIBRATION RESULTS

This paper represents the third publication of data and analysis of Coriolis meter calibrations. The first paper [1] divided calibrations into four categories and identified potential trending with tube velocity. The second paper [2] included additional calibrations and added several additional categories. A larger percentage of meters indicated consistent trending with tube velocity.

In the current paper more calibrations have been added. A more quantitative classification methodology has been adopted and the categories have been consolidated. The trend with velocity is apparent in a larger proportion of the calibrations.

For each calibration, data are collected of the deviation ( $\Delta_1$ ) between the meter reading and the laboratory value of mass flowrate. The high flowrate data (above 2% full scale) are fitted to a third order polynomial, a typical graph is shown in Figure 1. The low flowrate data are fitted to a second order polynomial. The polynomials represent the average calibration values as they vary with mass flowrate. The curve shapes associated with the individual meter calibrations were observed to exhibit some consistent shapes.

The previous analyses classified the calibration curves based on visual judgement. The current analysis represents an attempt to quantify the classification. The process begins with a linear fit of meter deviation ( $\Delta_2$ ) against mass flowrate; the coefficients from the previous analysis are used. For each calibration, an average difference ( $\Delta_3$ ) and standard deviation ( $s$ ) are calculated based on comparing the calibration data to fitted  $\Delta_2$  values. A figure of merit is defined as:

$$\text{FOM} = |\Delta_3| + 2s \quad (1)$$

where  $\pm\text{FOM}$  represents the 95% confidence interval of how closely a calibration matches the  $\Delta_2$  values. The calibrations are ranked based on FOM and divided into four groups identified numerically as Groups 1-4. The first three contain 15 calibrations, with 17 in the last group. The current analysis redefines the grouping of data; numerical group identification is intended to avoid confusion with the previous alphabetical group identification.

The calibration curve fits are shown in Figures 2-5. The ordinate in each represents  $\Delta_1$ , the abscissa represents tube velocity. The distributions of meter diameter and calibration pressure values are given in Tables 2 and 3. Qualitatively, Groups 1 and 2 both fit the clear trend, Group 1 better than Group 2. Quantitatively the 95% confidence intervals widths are  $\pm 0.121\%$  and  $\pm 0.175\%$ . The confidence interval contains 95% of the data, the interval width is an indicator of how well data fit a curve.

The 95% confidence interval width for Group 3 is  $\pm 0.260\%$ , the data don't fit as well as the first two groups. While most of the data fit the general curve shapes of Groups 1 and 2, two calibrations are observed to follow different trends. The first, indicated in green, is well centered about  $\Delta_1=0$ . The second curve, in red, is concave down while most of the rest are concave up. It is noted that a few of the Group 1 and 2 curves are also concave down.

The 95% confidence interval width for Group 4 is  $\pm 0.559\%$  indicating a rather poor fit. Group 4 contains ten calibrations that are well centered about zero

# 34<sup>th</sup> International North Sea Flow Measurement Workshop 25-28 October 2016

## Technical Paper

which indicate no velocity effects. These have been classified visually and identified in green; the distribution of diameters is given in the final column of Table 2. Qualitatively, the mean value is -0.110% and the 95% confidence interval width is  $\pm 0.230\%$ . The curves in green do not indicate the presence of a velocity effects, in fact they represent meters that work quite well.

Referring to Table 2 it seems as if the diameters become distributed towards larger values when moving from Group 1 to Group 4. That trend plus the observations regarding the green Group 4 data tend to indicate that the velocity effect becomes weaker as the meter size increases.

Prior work included extensive analysis of a one inch meter that was calibrated over a broad range of pressures. For the present discussion it will be identified as COR01. The data correlated well with volume flowrate and therefore would be expected to also correlate well with velocity. The results are shown in Figure 6. The yellow symbols represent most of the pressure values, these data collapse quite well into a single line. Interestingly, the lowest pressure data, in blue, don't fit the same trend.

The solid lines represent a 95% confidence interval with width of  $\pm 0.175\%$  about the curve fit of Groups 1 and 2. On average the solid lines agree with the COR01 data reasonably well. The slopes do not match as well; the COR01 data indicate a larger magnitude velocity effect. Also, the lower velocity data do not follow the same trend. Finally, the data at 7.5 m/s indicate a local "hump" in the curve. Comparable velocity data from multiple calibrations velocities have not been included in the current analysis. No explanation of the COR01 curve shape is currently proposed, it is hoped that additional data will help in understanding these behaviors.

## 4 INVESTIGATING DIAGNOSTIC PARAMETERS

The application of ultrasonic meter diagnostics has progressed over the past 10 years. A typical scenario has been described in numerous publications; an example is contained in [3]. In the typical case one or more diagnostic parameters indicates a potential measurement problem. The problem is identified during a field visit, often a foreign object or damaged component is found. The problem is resolved and the diagnostics return to normal. Laboratory testing identifies the potential range of measurement errors as a result. The industry is thus prepared for future occurrences if similar problems.

Coriolis diagnostics are in an earlier stage of development, few published examples are available. The discussion in [4] is used as a model for the current work. That example related changes in drive gain and pickoff amplitudes to a gradual increase in free liquids within flowing gas. The present analysis begins with the COR01 meter. The drive gain is plotted against pressure in Figure 7; it is expressed as a percentage of the maximum gain. Constant volume flowrates are identified by the different symbol colors. Two observed trends are easily understood: First, as the pressure increases the stiffness of the vibrating structure increases and more power (higher gain) is required to maintain resonance. Second, as the volume flowrate increases with constant pressure, the mass flowrate also increases. Once again more power is required.

Figure 8 shows the variation in drive gain expressed as a standard deviation of values obtained during one data point. The 3.5 MPa data represent the minimum

# 34<sup>th</sup> International North Sea Flow Measurement Workshop 25-28 October 2016

## Technical Paper

variation with volume flowrate, clearly this pressure has significance. The lower flowrate curves indicate a sharp peak at 3.5 MPa, the peak diminishes with increasing flowrate. No current explanation is proposed, it is hoped that additional data will help to gain a better understanding.

Many of the calibrations in the current analysis included a record of diagnostic parameters. In some cases "as found" and "as left" values were recorded; only the as found data are currently considered. The investigation begins by calculating mean and standard deviation for constant flowrate values of each diagnostic. Data were obtained approximately once every 1.5 seconds; multiple readings were made per data point and multiple data points were obtained at a fixed flowrate. Typically 200-500 readings were used to determine mean and standard deviation.

The first step to investigate recent calibrations of one inch meters, as the analysis proceeds additional meter sizes as well as older data will be added. The more recent data is more likely to include diagnostic data; it also represents the newest meters which are more likely to benefit from any technical developments.

The drive gains from the massed calibrations are plotted against mass flowrate in Figure 9. Each line represents a second order polynomial fit to data from a single calibration. Recalling the discussion of Figure 2-5, the calibration data are obtained over a nominally consistent velocity range. The variability in the calibration mass flowrate range Figure 9 is the result of the consistent velocity range subjected to variable pressure. In general the data are quite consistent, the magnitude of drive gain agrees with the COR01 results. Slight variation between the curve fits do not appear to correlate with pressure. It is concluded that the observed variation represents random variations between similar meters.

The drive gain standard deviation ( $s_G$ ) from the massed calibrations plotted against mass flowrate in Figure 10. Each line represents a second order polynomial fit to data from a single calibration. The black lines correspond to 13 calibrations of one inch meters; the red and green lines represent data from half inch and two inch size meters. Clearly there are differences between the multiple one inch meter calibrations; the  $s_G$  values vary by as much as 25%. The plot of Figure 11 shows a strong relationship between  $s_G$  and calibration pressure at a single value of mass flowrate [1.54 kg/s]. With the exception of one data point the  $s_G$  values are seen to increase with increasing pressure. It is concluded that the observed variation in Figure 10 is a result of pressure.

The drive gain values vary with nominal meter size. A half inch meter drive gain is approximately 8-12% while a two inch drive gain is approximately 1.5-2.0%. Data from multiple calibrations have not yet been collected; this step is planned for the future.

As previously noted, comparison with COR01 data provides a valuable link between the two data sets. Clear differences are noted in the magnitude of standard deviation values; values a bit larger than 1% compared to other values approaching 50%. The differences are due to sample rates and averaging because the values arise through to different routes. The larger standard deviation values are based on 200-500 readings produced directly by the meter; these are considered to be raw data. The smaller standard deviation values are based on gain values recorded by the calibration data acquisition system which calculates standard deviations based on averages rather than raw data. An

# **34<sup>th</sup> International North Sea Flow Measurement Workshop 25-28 October 2016**

## **Technical Paper**

averaging process will always reduce the standard deviation. Unfortunately the raw data were not saved so that comparable  $s_G$  values cannot be re-calculated.

While absolute  $s_G$  values are not comparable, general trends can be compared. Inspection of Figure 8 reveals that  $s_G$  values increase with volume flowrate at constant pressure and therefore also increase with mass flowrate. In general the trending agrees with the data of Figure 10. Further, the it is likely that the shape of the curve will change with pressure. Re-arranging the data will reveal the specific curve shape; this step has not yet been completed.

## **5 SUMMARY**

An ongoing Coriolis meter investigation has the objective of providing better understanding by CEESI as well as industry in general. This is the third paper to be published. It documents the steady increase in quantity of meters and parameters under investigation. The massed calibration database now contains 62 meters, clearly the meter output often depends on velocity. Also presented is the first investigation of diagnostic parameter. It appears as if the drive gain variations (standard deviation) are dependent on pressure for one inch meter.

## **6 REFERENCES**

- [1] Kegel, T. and Baldwin, S., "Compressible Flow Effects in Coriolis Meters," North Sea Flow Measurement Workshop, 21-24 October 2014.
- [2] Kegel, T., "Compressible Flow Effects in Coriolis Meters: A Continuing Study," Gas Mexico Congress, 2015.
- [3] Lansing, J. "Ultrasonic Meter Condition Based Monitoring – A New And Simplified Solution," AGA Operations Conference, American Gas Association, 2007.
- [4] Stobie, G. et al, "Blind Testing of a Micro Motion® Gas Coriolis Meter in Wet Gas Flows at the CEESI Wet Gas Facility." Americas Flow Measurement Conference, 2012.

**34<sup>th</sup> International North Sea Flow Measurement Workshop  
25-28 October 2016**

**Technical Paper**

**Table 1 – Summary of Calibration Data**

Pressure Range [MPa]	Quantity	Nominal Size [in]	Quantity
1.0 – 1.5	7	0.25	3
1.5 – 2.0	7	0.5	20
2.0 – 2.5	3	1.0	26
2.5 – 3.0	7	2.0	12
3.0 – 3.5	9	3.0	1
3.5 – 4.0	6		
4.0 – 4.5	19		
4.5 – 5.0	1		
5.0 – 5.5	3		

**Table 2 – Distribution of Meters Based on Nominal Diameter**

Nominal Size [inch]	Quantity Group 1	Quantity Group 2	Quantity Group 3	Quantity Group 4	Quantity Group 4 (green)
0.25	0	1	0	2	0
0.50	7	7	4	2	0
1.0	8	6	10	2	2
2.0	0	1	1	10	7
3.0	0	0	0	1	1

**Table 3 – Distribution of Meters Based on Calibration Pressure**

Pressure Range [MPa]	Quantity Group 1	Quantity Group 2	Quantity Group 3	Quantity Group 4
1.0 – 1.5	1	1	3	2
1.5 – 2.0	2	3	1	1
2.0 – 2.5	0	2	0	1
2.5 – 3.0	2	0	1	4
3.0 – 3.5	1	2	4	2
3.5 – 4.0	3	1	2	0
4.0 – 4.5	5	5	2	6
4.5 – 5.0	1	0	0	1
5.0 – 5.5	0	1	2	0

Technical Paper

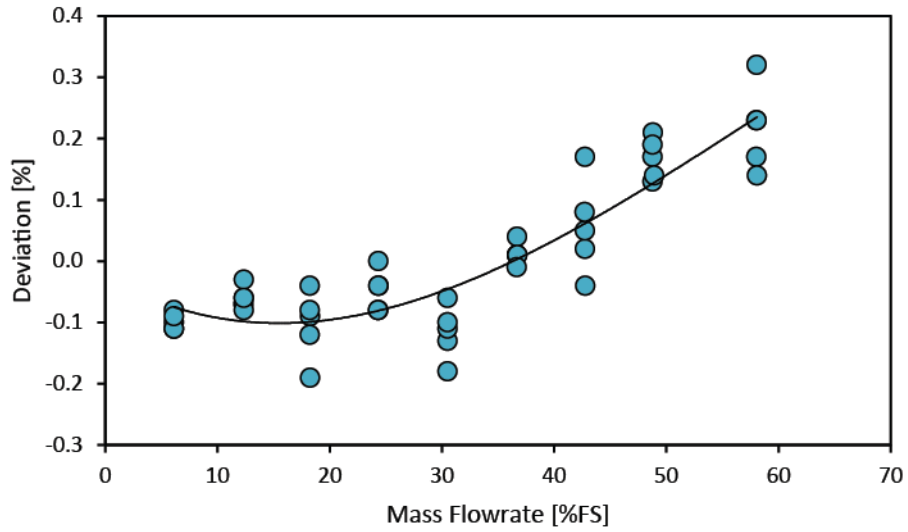


Fig. 1 – Typical Calibration Data With Polynomial Curve Fit

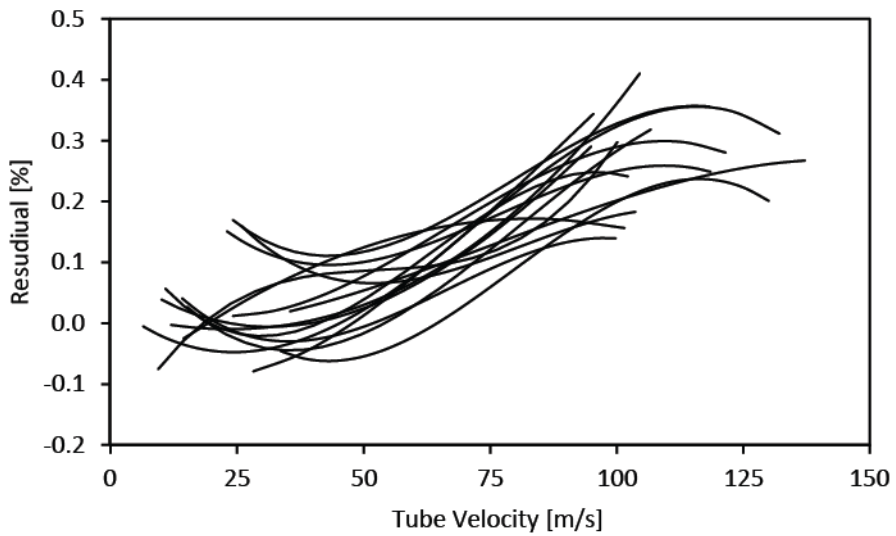


Fig. 2 – Group 1, Fifteen Calibrations

Technical Paper

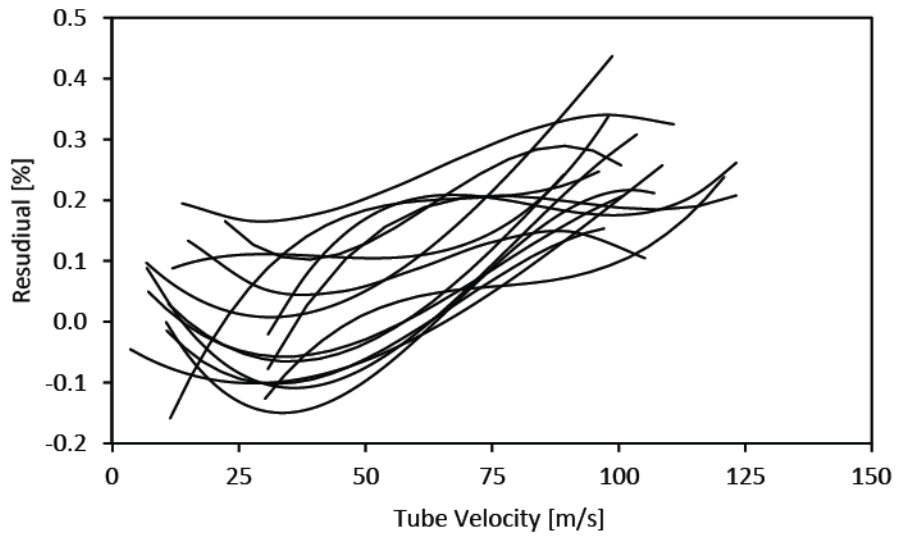


Fig. 3 – Group 2, 15 Calibrations

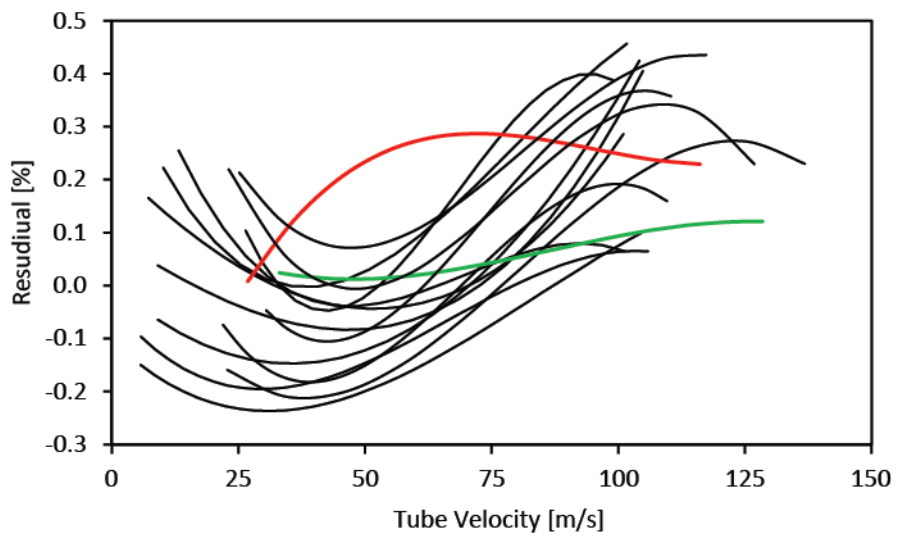


Fig. 4 – Group 3, Fifteen Calibrations

Technical Paper

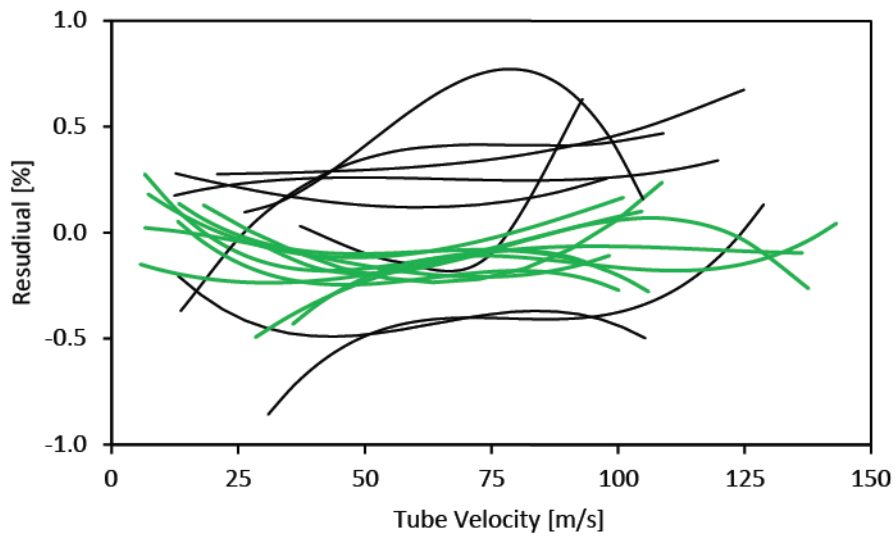


Fig. 5 – Group 4, Seventeen Calibrations

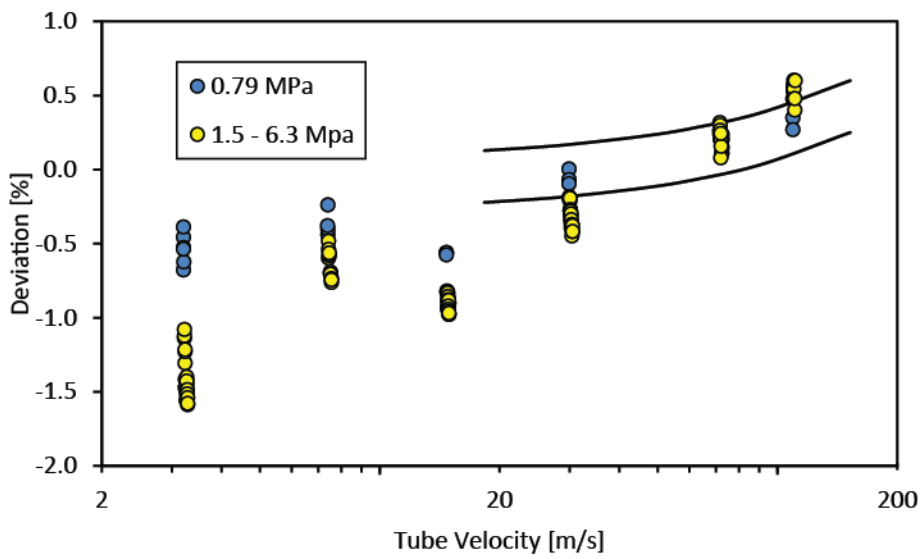


Fig. 6 – COR01 Meter Calibration Data

Technical Paper

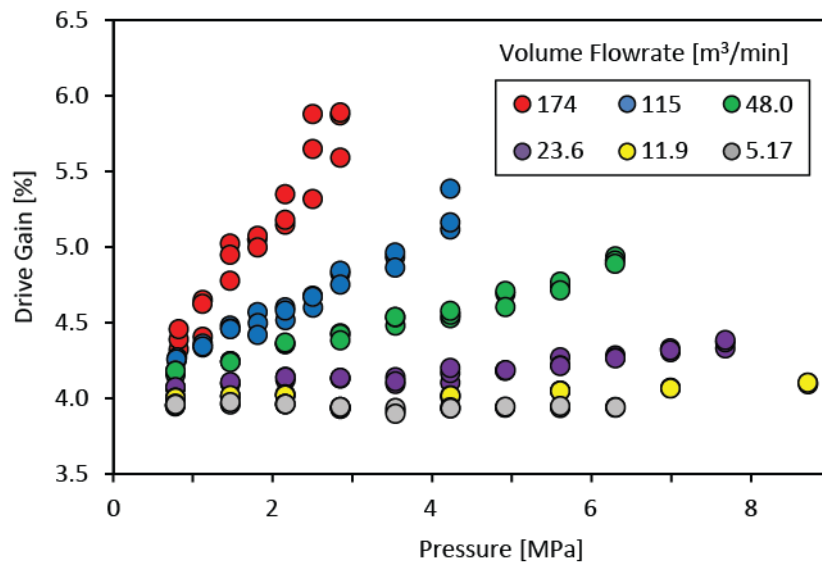


Fig. 7 – COR01 Meter Drive Gain

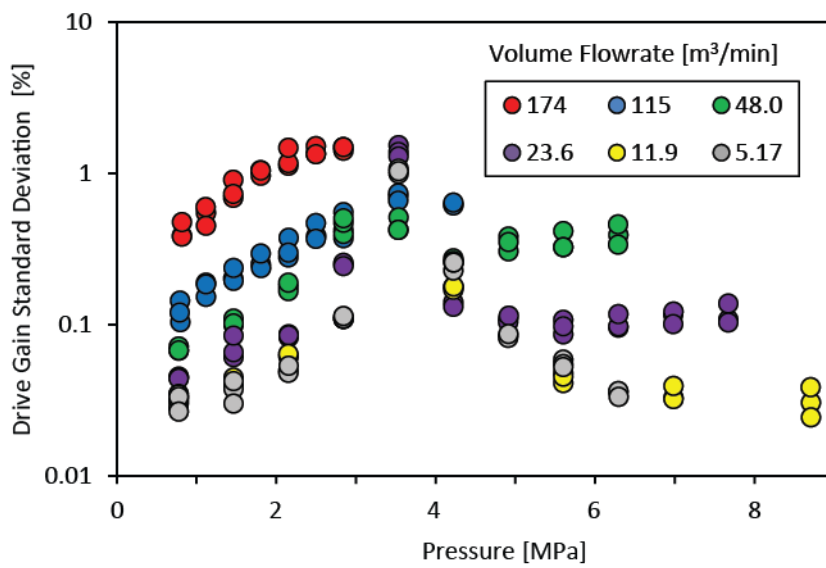


Fig. 8 – COR01 Meter Drive Gain Variation

Technical Paper

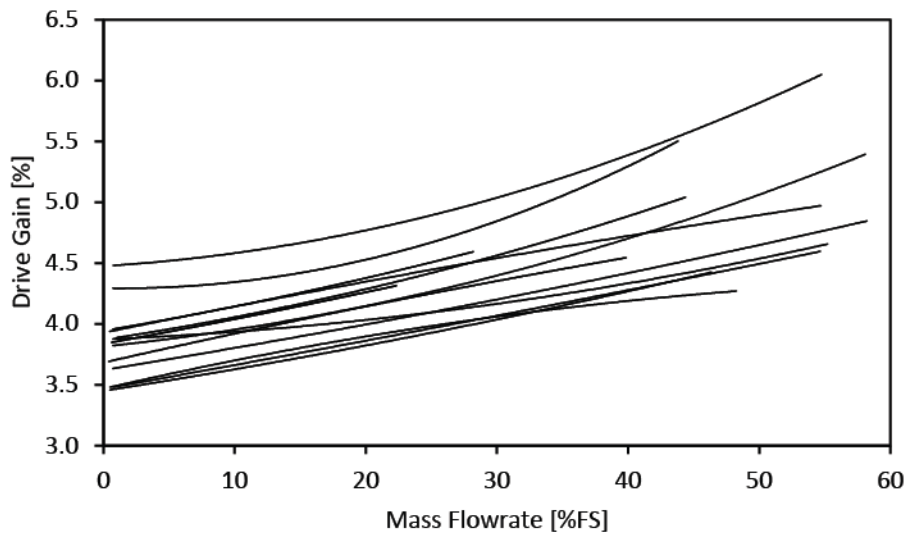


Fig. 9 - Drive Gains From Multiple Calibrations

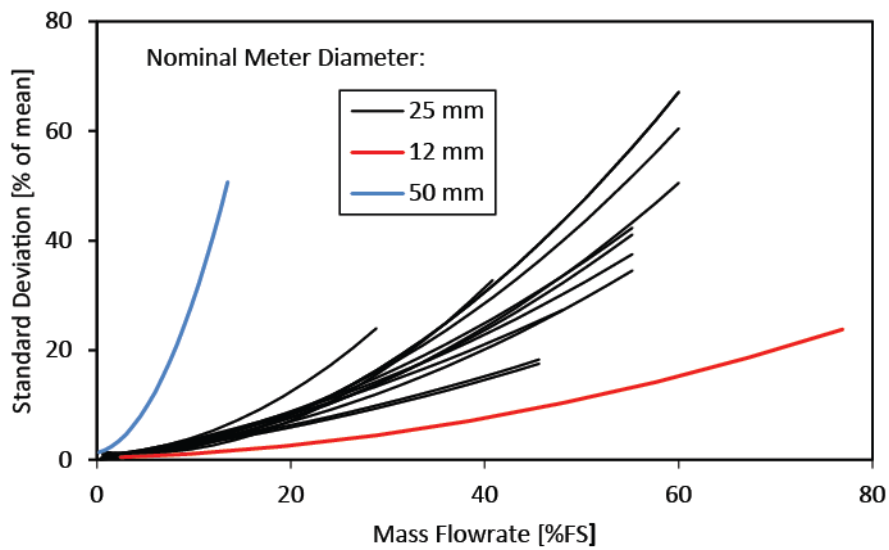


Fig. 10 - Drive Gain Variations From Multiple Calibrations

Technical Paper

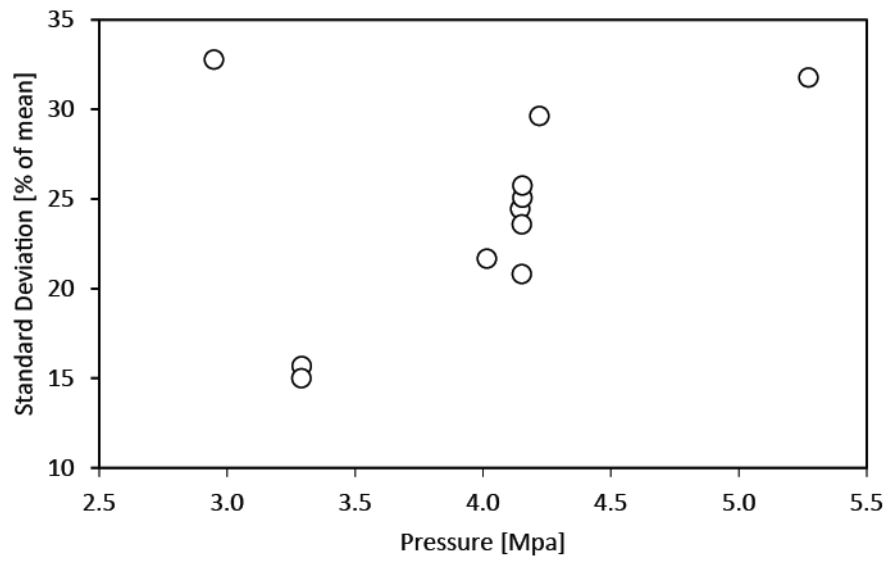


Fig. 11 - Drive Gain Variations From Multiple Calibrations, Data at Constant Mass Flowrate = 1.54 kg/s

## Technical Paper

# Are We Barking Up the Wrong Tree? Uncertainty vs Error and the Role of CBM to Measure Both

Anwar Sutan, i-Vigilant Technologies

---

## 1 INTRODUCTION

What is the best way to maintain a GC? Should we ensure that we have the best calibration gas? Should we measure calibration gas as unknown and compare the GC result against calibration gas certificate? Should we be worried about the non-linear effect of the detector, should we compare spot sample result against GC result?

Various different operators have different maintenance regime to ensure that their GC is maintained in the best way. As there are many ways of maintaining the GC, different operators perform their maintenance to comply with certain regulations or agreement. However, many times the type of maintenance adopted by operators may not be the one best suited for their pipeline conditions. Very often operators barking up the wrong tree trying to comply with certain regulations while completely overlooking the issue in hand which results in significant errors without operators even knowing or noticing that.

As an example, calibration gas is specified to be of highest accuracy with less than 1% uncertainty on each component. And operators have that. Surprisingly, quite often during the process of changing calibration gas, the new composition value is not updated in the GC. In one of the case study such error reached monetary value of more than £400,000 /month.

There are few other examples that will be shown throughout this paper. In many occasions, the fact that an operator wants to be in compliance with a certain method causes them to completely miss a bigger issue in their hands, and as a result their quest for higher accuracy will lead them to the wrong direction.

The aim of the paper is to firstly show that currently there exist no single method that can handle all possible issues with the GC, and secondly, how any chosen method when not combined with the other method can cause operators to overlook unpremeditatedly important things that may have big impact on the GC measurement accuracy.

The issues are that may bring bigger impact on the GC if the other issues are overlooked are currently known as follows:

1. Calibration gas quality
2. GC Calibration results
3. GC non-linearity
4. GC reproducibility
5. Sample let down system

# 34<sup>th</sup> International North Sea Flow Measurement Workshop 25-28 October 2016

## Technical Paper

This paper also offers a solution in a form of conditional based monitoring software tool for GC that takes into consideration all those methods within one program.

### 2 ARE WE BARKING UP THE WRONG TREE?

Selecting a certain maintenance method while overlooking some other methods can cause operators to, non-technically speaking, bark up the wrong tree. The following are a few possibilities of those wrong trees and recommendation on how to fix them.

#### 2.1 Calibration Gas Quality

2015/2016 has been a tough year for oil and gas industry. Most operators are looking to cut cost in all possible avenues. One of the cost saving avenue is by ordering calibration gas of lower quality. From buyer point of view, this might be a good way to cut cost, however, from the measurement point of view the impact can be quite significant.

The following is an example of the impact of calibration gas quality in terms of CV. Table 1 shows calibration gas composition with low composition uncertainty.

Component	Mole percentage	±	Absolute uncertainty	Relative uncertainty
Methane	84.994	±	0.03	0.0352966
Nitrogen	5.522	±	0.018	0.3259689
Carbon dioxide	1.995	±	0.005	0.2506266
Ethane	4.283	±	0.012	0.2801774
Propane	1.803	±	0.006	0.3327787
i-Butane	0.2496	±	0.0008	0.3205128
n-Butane	0.3474	±	0.0013	0.3742084
Neopentane	0.1	±	0.001	1
i-Pentane	0.3006	±	0.002	0.665336
n-Pentane	0.1995	±	0.0011	0.5513784
Hexane	0.1007	±	0.0021	2.0854022
Heptane	0.1008	±	0.0027	2.6785714
Total	99.995600			

Table 1. Calibration gas with low composition uncertainty

On GC measurement, each individual component impacts measurement of other components as the result will be normalised. Therefore error in one component measurement will impact all components. The low uncertainty of calibration gas means low CV uncertainty. The impact of the above calibration gas uncertainty on the CV calculation uncertainty is shown in Table 2. It is to be noted that the value shown herein ignores the 0.1% additional uncertainty from the calculation standard.

# 34<sup>th</sup> International North Sea Flow Measurement Workshop 25-28 October 2016

## Technical Paper

Component	Normalised mole fraction	U(cal gas)	S(cal gas) S(repro)	Standard uncertainty
Methane	0.849940	0.017648	-0.0197	0.000348
Nitrogen	0.055220	0.162984	-0.0554	0.009030
Carbon dioxide	0.019950	0.125313	-0.0199	0.002494
Ethane	0.042830	0.140089	0.0307	0.004300
Propane	0.018030	0.166389	0.0260	0.004330
i-Butane	0.002496	0.160256	0.0054	0.000864
n-Butane	0.003474	0.187104	0.0075	0.001411
Neopentane	0.001000	0.500000	0.0029	0.001436
i-Pentane	0.003006	0.332668	0.0087	0.002889
n-Pentane	0.001995	0.275689	0.0058	0.001595
Hexane	0.001007	1.042701	0.0037	0.003808
Heptane	0.001008	1.339286	0.0044	0.005881
	Combined standard uncertainty			0.013780
	Coverage factor (k)			2
	Combined expanded uncertainty			0.027561
	CV absolute uncertainty (MJ/m <sup>3</sup> )			<b>0.010660</b>

Table 2. CV uncertainty of gas with low composition uncertainty

From Table 2, it is demonstrated that the impact of uncertainty on CV is quite minimum. On the contrary, when calibration gas selected is of a lower quality, for example with compositional uncertainty of  $\pm 2\%$ , then the impact on CV uncertainty can become quite significant. Table 3 shows the same gas as above, only it has 2% measurement uncertainty.

Component	Mole percentage	$\pm$	Absolute uncertainty	Relative uncertainty
Methane	84.995481	$\pm$	0.3	0.3529599
Nitrogen	5.521183	$\pm$	0.11042366	2
Carbon dioxide	1.996865	$\pm$	0.0399373	2
Ethane	4.283801	$\pm$	0.08567602	2
Propane	1.803683	$\pm$	0.03607366	2
i-Butane	0.249655	$\pm$	0.0049931	2
n-Butane	0.347397	$\pm$	0.00694794	2
Neopentane	0.100055	$\pm$	0.0020011	2
i-Pentane	0.300574	$\pm$	0.00601148	2
n-Pentane	0.199614	$\pm$	0.00399228	2
Hexane	0.20169	$\pm$	0.0040338	2
Total	99.999998			

Table 3. Calibration gas with high composition uncertainty

# 34<sup>th</sup> International North Sea Flow Measurement Workshop 25-28 October 2016

## Technical Paper

The impact of the high composition uncertainty in CV can become quite significant. Table 4 shows the impact on CV uncertainty.

Component	Normalised mole fraction	U(cal gas)	S(cal gas) S(repro)	Standard uncertainty
Methane	0.849955	0.176480	-0.0191	0.003377
Nitrogen	0.055212	1.000000	-0.0554	0.055392
Carbon dioxide	0.019969	1.000000	-0.0199	0.019919
Ethane	0.042838	1.000000	0.0308	0.030755
Propane	0.018037	1.000000	0.0261	0.026063
i-Butane	0.002497	1.000000	0.0054	0.005397
n-Butane	0.003474	1.000000	0.0075	0.007548
Neopentane	0.001001	1.000000	0.0029	0.002876
i-Pentane	0.003006	1.000000	0.0087	0.008692
n-Pentane	0.001996	1.000000	0.0058	0.005793
Hexane	0.002017	1.000000	0.0073	0.007321
Combined standard uncertainty				0.073203
Coverage factor (k)				2
Combined expanded uncertainty				0.146406
CV absolute uncertainty (MJ/m <sup>3</sup> )				<b>0.056586</b>

Table 4. Calibration gas with high composition uncertainty

Assumption is made on pipeline that is flowing gas with monetary value worth £30 million /month. 0.146% uncertainty means an uncertainty of £43,921 /month in comparison to uncertainty of 0.027% which only means an uncertainty of £8,268 /month. it is obvious to use calibration gas with lower uncertainty that may be more expensive than the alternative, however from operation point of view it might potentially save much more money through more accurate measurement.

## 2.2 Calibration Gas Storage and Dew Point Temperature

Ordering calibration gas that is of high quality is the first step. However, many operators make mistake by filling as much pressure as possible into the calibration gas. Considerations need to be made in term of storing the calibration gas. This is crucial for the areas where ambient temperature can become quite cold. If the calibration gas is stored lower than its dew point temperature, it can have condensation on its heavier end and the impact will be a faulty calibration result. An example of the calibration result from non-homogenous gas can be seen in Figure 1.

# 34<sup>th</sup> International North Sea Flow Measurement Workshop 25-28 October 2016

## Technical Paper

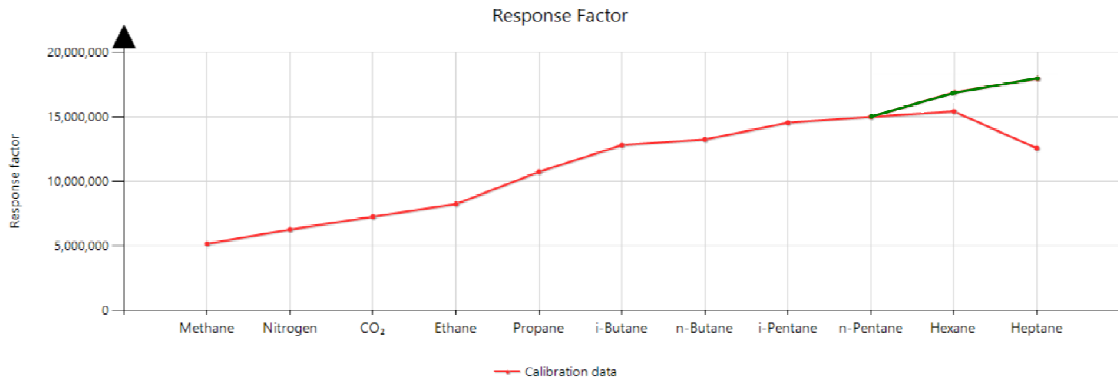


Figure 1. Non homogenous calibration gas

Because the calibration gas certificate is always used as the basis for the calibration gas bottle concentration, when the gas is not homogeneous it will lead to a measurement error.

From the Figure 1, it can be seen that hexane and heptane response factor is lower than expected (green line is the expected RF for hexane and heptane). This is due to the gas being stored in the cold weather, lower than its dew point temperature. This issue if goes undetected can lead to quite significant mis-measurement.

However, this can be avoided by observing the response factor trend as well as the correlation chart.

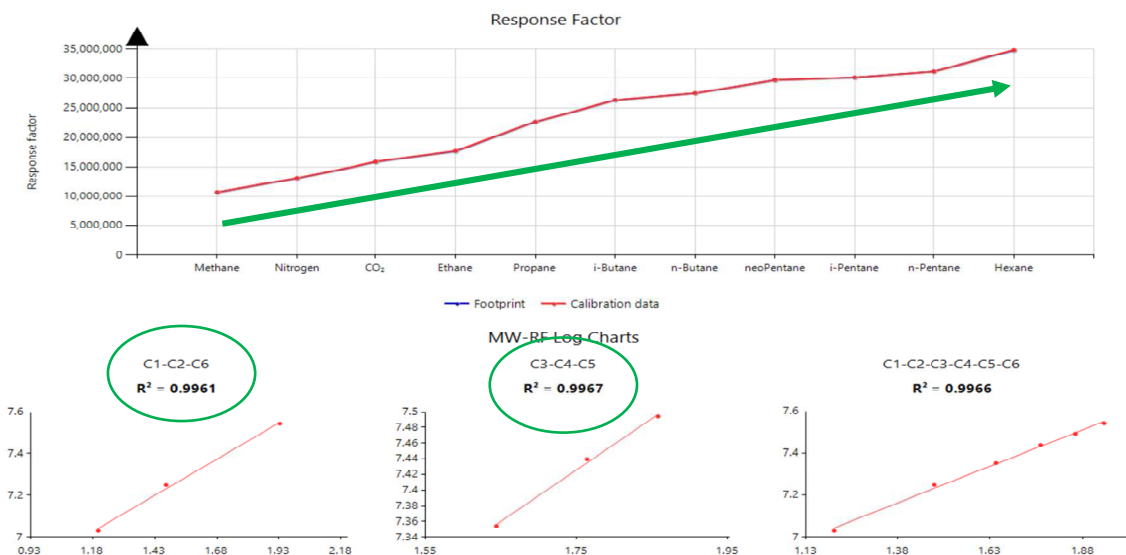


Figure 2. RF trend and correlation chart of healthy GC

A healthy GC will have an ascending response factor trend and high correlation between the Response Factor and Molecular Weight as shown in Figure 2. The case where the heavy end sits at the bottom of the bottle can be overcome by re-heating the gas to a homogenous state and running the GC using calibration gas for several cycles. Test performed has shown that the detected gas return into its normal homogeneous state after 10 runs as shown in Figure 3.

Technical Paper

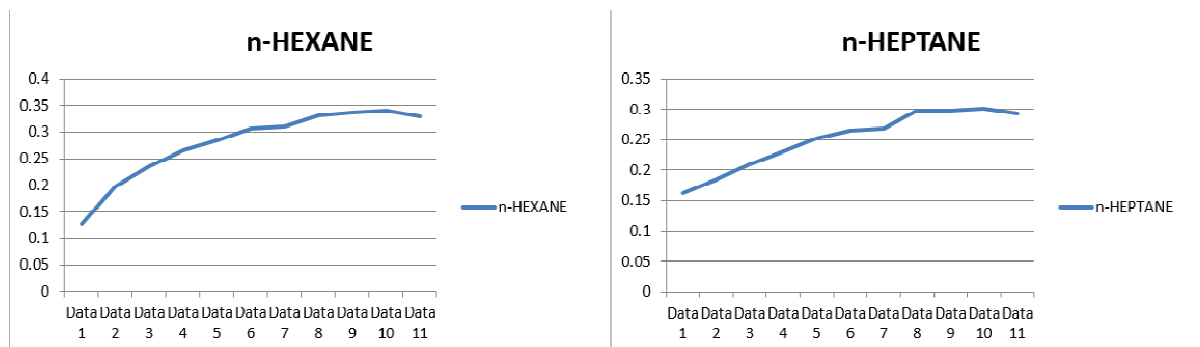


Figure 3. Runs of calibration gas prior to returning to homogenous state

Arguably after this process the composition within the bottle has been altered, however it can also be argued that normally the heavy end has low concentration with low sensitivity towards CV and density measurement and therefore the calibration gas will still be fit for purpose. Also the acceptability of calibration gas can be determined by the gas thermal conductivity property. Gas that flows through thermal conductivity detectors will follow consistent characteristic as shown in Figure 2 earlier. As long as the RF trend is ascending in the order of Methane – Nitrogen – CO<sub>2</sub> – Ethane – Propane – iButane – nButane – neoPentane – iPentane – nPentane – Hexane – Heptane, and the correlation between RF and MW is high, it can be concluded that calibration gas is healthy as well as the valve and other time events in the GC are healthy too.

This principle can also be used to determine if a calibration gas is as per what stated in its calibration certificate. There are some occasions where errors occur in the making of calibration gas which results in the bottle composition not as per the bottle's certificate. This can be determined by checking the calibration result.

When goes undetected, this issue can cause systematic error despite the low uncertainty of the calibration gas composition.

### 2.3 Calibration Issue

Having good calibration gas is a good first step. However, in many occasion it has been seen that operators perform calibration with the wrong calibration gas composition entered into the GC. This can have a significant error on measurement. The following is an example that has been used in previous paper, however, it is a very useful example to show few things that can go wrong from a single calibration and how the calibration data information can become a very useful diagnostic tool to ensure GC correct measurement.

The GC in this case study had been offline for a while, and it was time to bring it back online again. A new calibration gas was installed and a calibration was done. Instead of checking the trend and the result of the calibration, a forced calibration was performed and GC was assumed to run correctly as it did not produce any alarm. However, because it was a new calibration gas, the composition of the new calibration gas and the composition of the old calibration gas that still existed in the GC were not the same. The initial calibration RF trend on this GC is as the following:

# 34<sup>th</sup> International North Sea Flow Measurement Workshop 25-28 October 2016

## Technical Paper

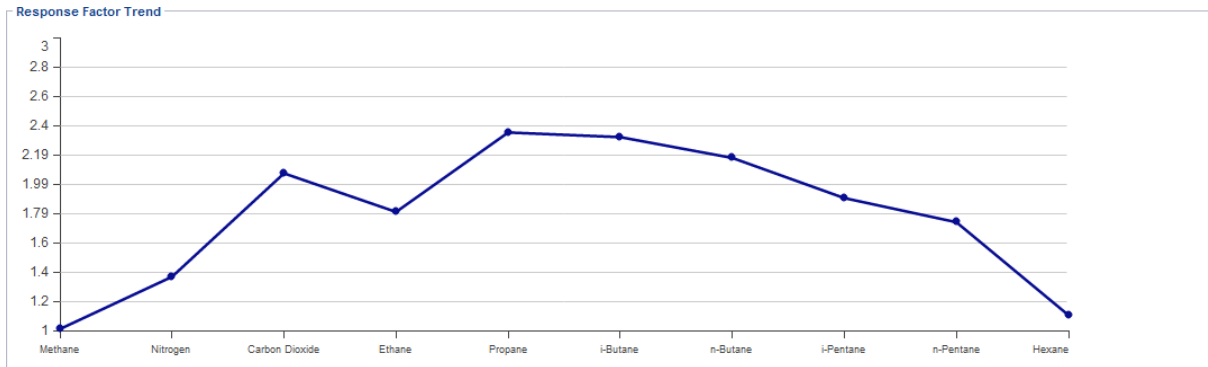


Figure 4. RF trend due to wrong component concentration entered in GC data table

Following this, component data table within the GC was changed to match the calibration gas certificate and further calibration was performed. The result was a better response factor, with several minor issues as shown in Figure 5.

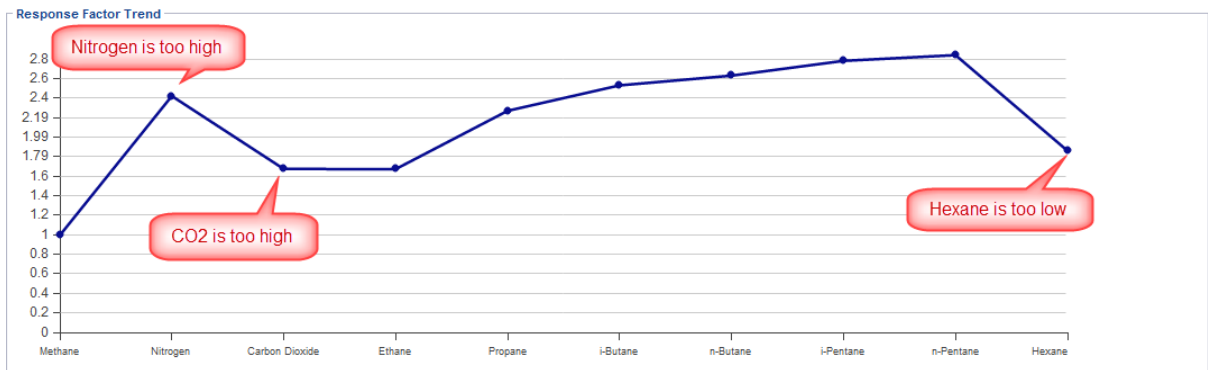


Figure 5. RF trend after component data table in GC was adjusted

From Figure 5, the trend shows that N<sub>2</sub> level was too high and hexane level was too low. The N<sub>2</sub> levels can be high after changing the calibration gas as the sample line can fill with air. To rectify this issue, the calibration sample line was purged with calibration gas. After clearing the air, the RF trend was significantly better as shown in Figure 6.

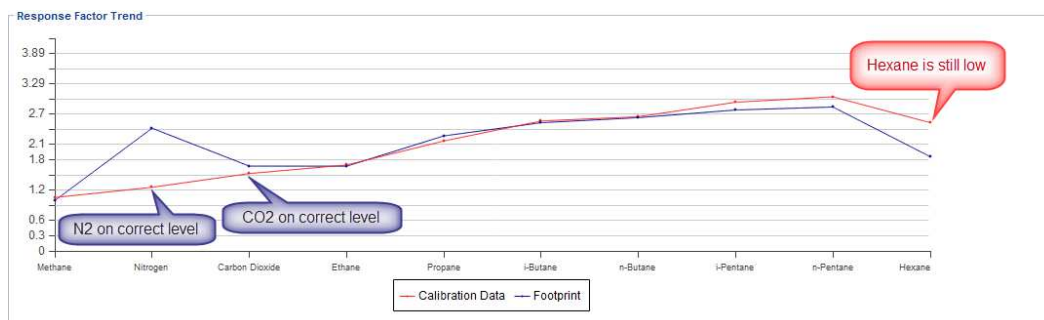


Figure 6. RF trend after calibration sample line has been purged

The blue line above shows the trend prior to purging, and the red line shows the trend after purging. The N<sub>2</sub> is now at its expected level; however hexane RF was still lower than expected. Inspection of the correlation between MW and RF is then used to help determine the cause of the low Hexane RF as shown in Figure 7.

# 34<sup>th</sup> International North Sea Flow Measurement Workshop 25-28 October 2016

## Technical Paper

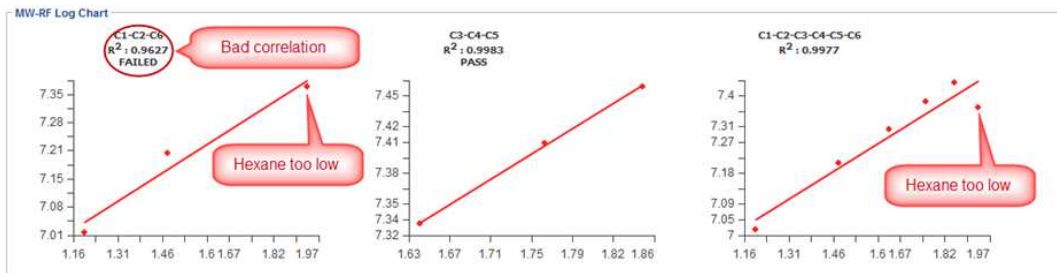


Figure 7. MW-RF Log chart of calibration data

It was determined from the plot that based on the poor correlation of C1-C2-C6; the problem was caused by some of the heavy component (hexane) leaving column 1 to flow through column 2 instead of all of it being back-flushed due to incorrect valve timing. The result was not all hexane component being detected by the GC and the RF was low.

Adjustment was performed to the valve timing to prevent C6+ from entering column 2. This resulted in the change of the response factor chart as depicted in Figure 12.

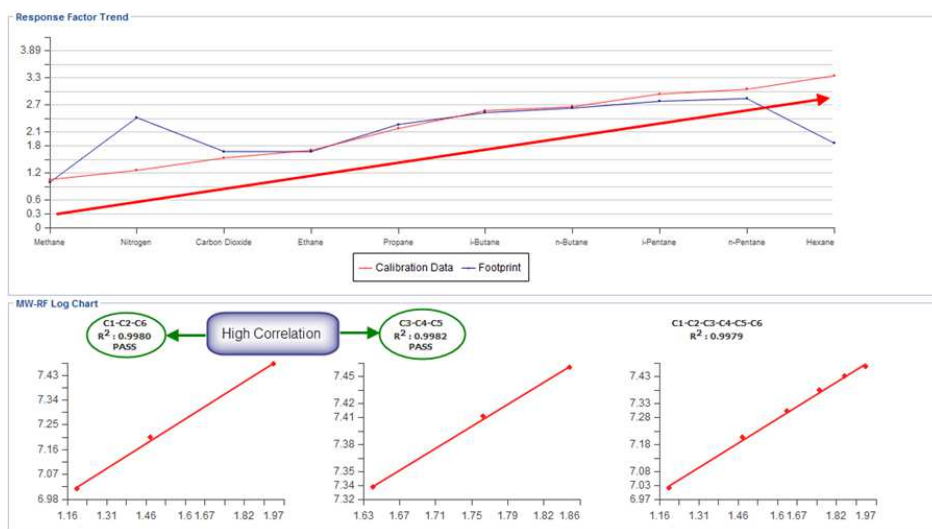


Figure 8. RF trend and MW-RF log chart of healthy GC

The charts now clearly indicate that the problem with the GC has been rectified and the trends are all as expected. The error introduced by this problem may not be apparent at the individual component level, however analysis of the resultant calculated calorific values of the two calibrations clearly show the difference to be significant. The potential difference in the final output result is given in Table 5.

# 34<sup>th</sup> International North Sea Flow Measurement Workshop 25-28 October 2016

## Technical Paper

Description	Wrong RF	Correct RF	Difference
CV	45.07	44.44	1.41%
Volume	100	100	
Volume	2,831,684	2,831,684	
Energy (MJ)	127,624	125,840	1,784
Energy (KWh)	35,451,330	34,958,311	493,019
Value per KWh	£0.02418	£0.02418	
Value /day	£857,213	£845,292	<b>£11,921</b>
Value /month	£25,716,394	£25,358,758	<b>£357,636</b>

Table 5. Unhealthy vs healthy result comparison, Value per KWh data is taken from Quarterly Energy Prices, June 2016

### 2.4 Dual Level Calibration to Reduce Non-Linear Bias

Calibration can be proven to be correct, calibration gas can be selected of the highest quality, however when the GC operates in the non-linear range, it will introduce bias that can also be quite significant. ISO 10723:2012 [3] specify how to perform GC performance evaluation test to understand the extent of non-linearity and how much impact the non-linearity has on overall measurement. This method requires 7 sets of different gas composition that covers the operational range of the GC. There are a lot of preparation prior to the performance evaluation test that can be quite impractical in case the test needed to be performed urgently.

Looking at the impracticality of performing ISO 10723, a new method was recently introduced in the UK and has received a letter of no objection from OGA (Oil and Gas Authority) as shown in 0. Dual Level Calibration is a middle ground between single point calibration using single set of gas compositions and multilevel calibration using 7 sets of gas compositions. The idea is to reduce the bias associated with single point calibration without exerting big efforts associated with performing evaluation test according to ISO 10723.

Single Point Calibration uses one set of calibration gas as compositions to get the GC response towards a certain component. Calibration result is calculated as a function of peak area generated by a certain mole%. This is illustrated in Figure 9.

# 34<sup>th</sup> International North Sea Flow Measurement Workshop 25-28 October 2016

## Technical Paper

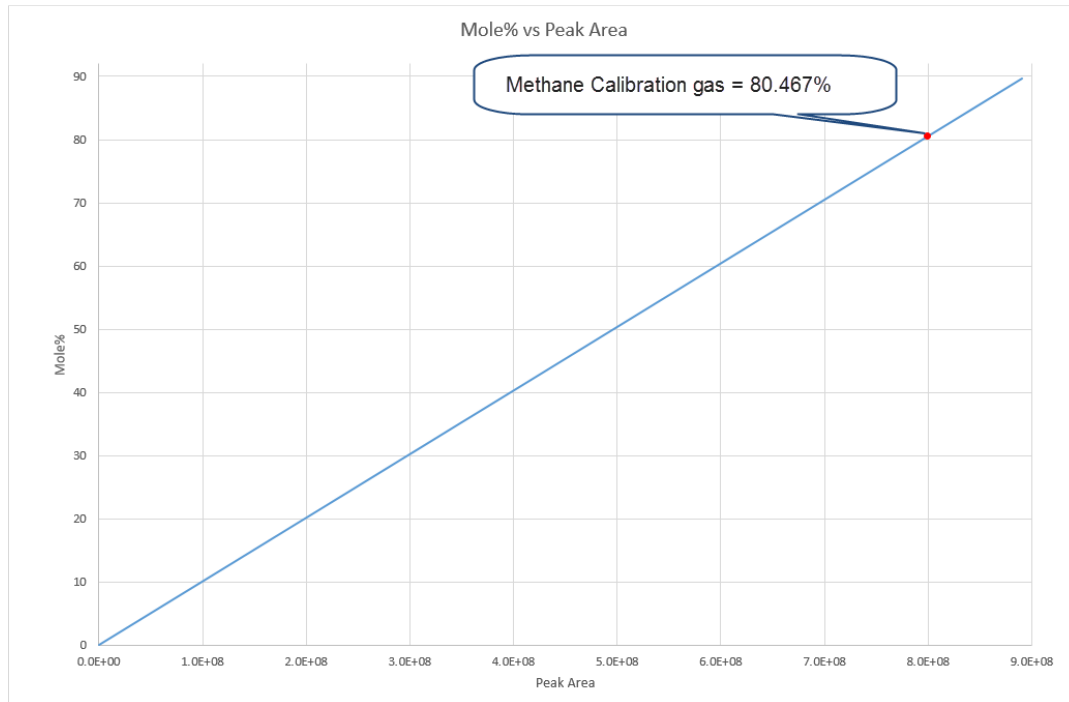


Figure 9. Single point calibration

As shown in Figure 9 above, the mole composition measurement is proportional to the changes in peak area as shown in Figure 12 below.

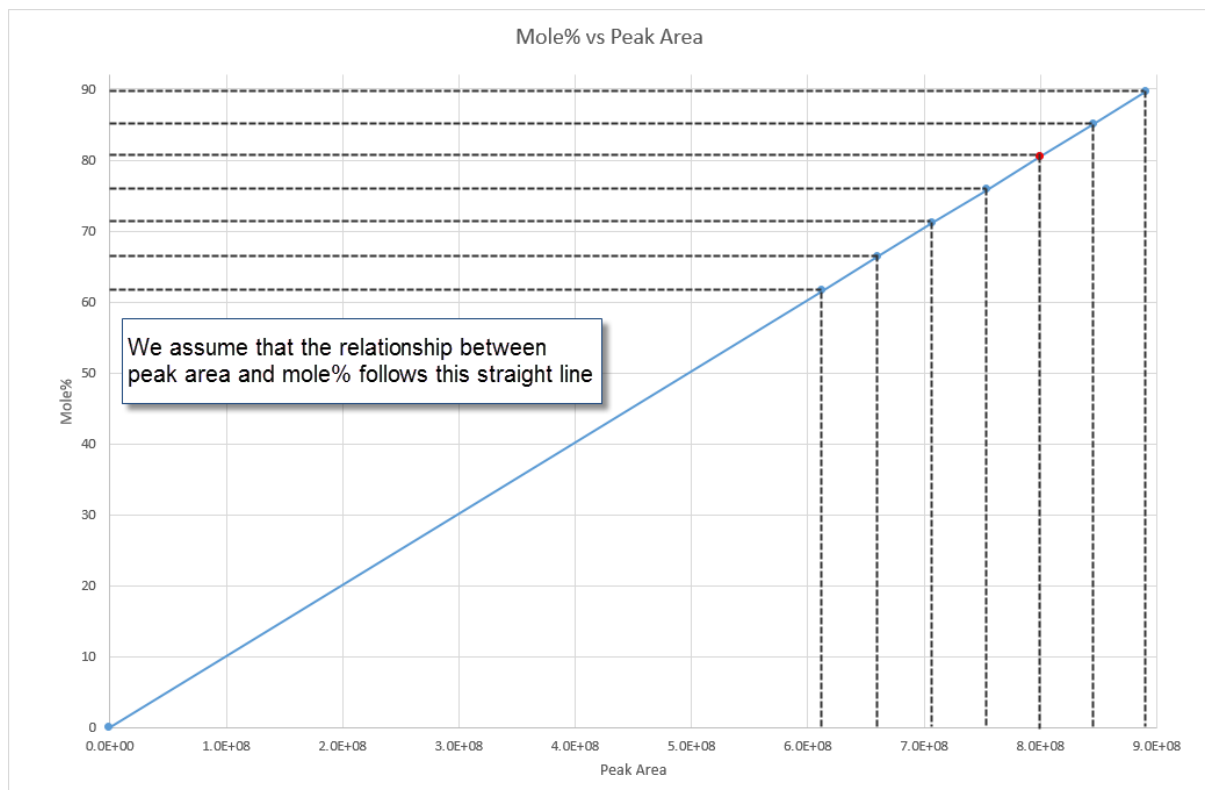


Figure 10. Peak Area – mole% relationship on a single point calibration

# 34<sup>th</sup> International North Sea Flow Measurement Workshop 25-28 October 2016

## Technical Paper

By performing single point calibration, the GC is assumed to be linear. However, the true response function of the GC does not follow linear line as shown in a single point calibration. Figure 13 illustrate a real response function in comparison to single point calibration function on methane calibration results. The function on orange line (true function) is generated using 7 sets of gases with different composition.

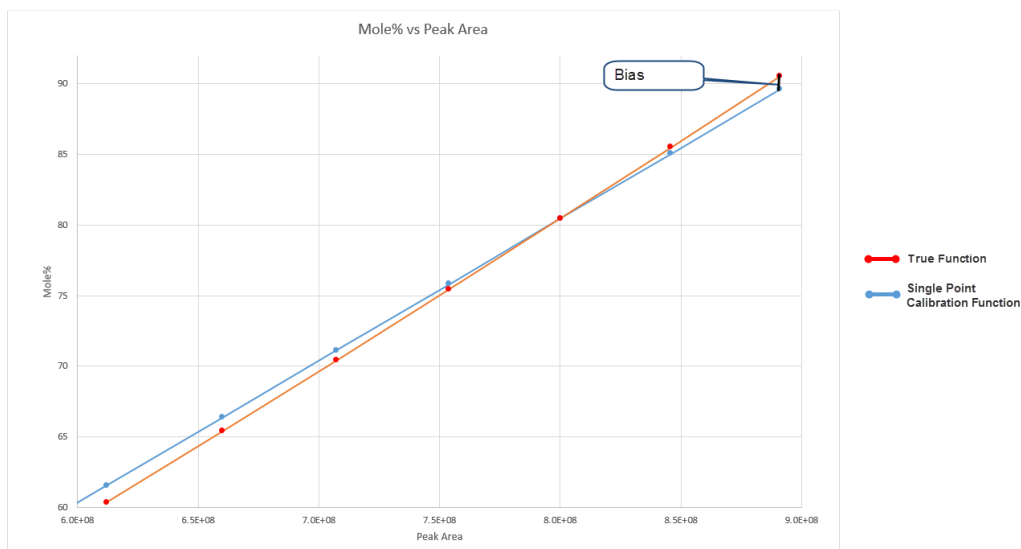


Figure 11. True function in comparison to single point calibration function

The impact of running single point calibration is bias where the measurement is not performed in the linear range of the gas. Figure 14 illustrates the bias of methane across range of measurement when calibrated using single point calibration in comparison to the true function.

# 34<sup>th</sup> International North Sea Flow Measurement Workshop 25-28 October 2016

## Technical Paper

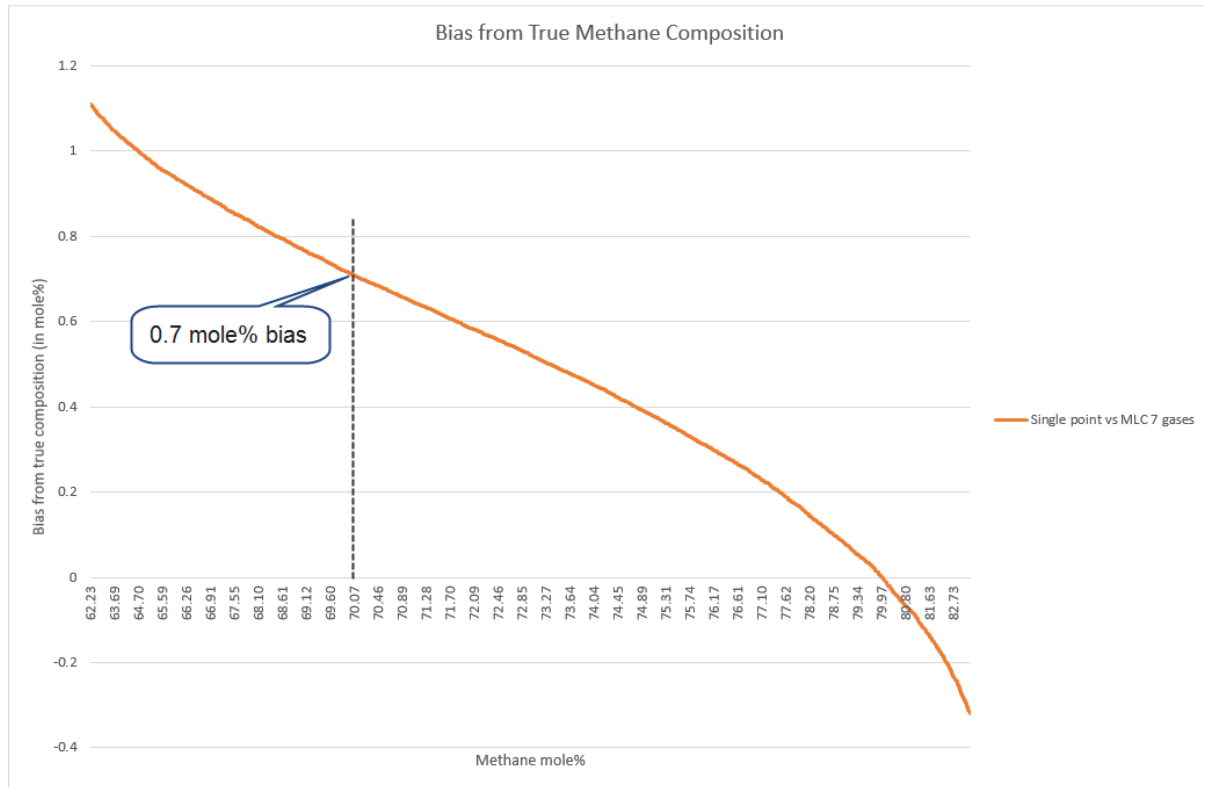


Figure 12. Single point calibration bias when compared against true function

The above illustration is the reason why when measuring a stable gas composition, for instance stable gas that comes from a single well, it is recommended to design calibration gas composition as close to the process gas composition as possible. Doing so will minimise the measurement bias from detector non-linearity. Table 6 shows measurement from GC that has calibration gas that is non-representative of the process gas.

Description	Calibration Gas (mole%)	Actual value	GC measurement	Difference
Methane	69.5	84.9948	84.7366	-0.2582
Nitrogen	10	5.5195	5.6051	0.0856
CO <sub>2</sub>	8	1.9973	2.0269	0.0296
Ethane	9	4.2856	4.3836	0.098
Propane	2	1.8035	1.829	0.0255
i-Butane	0.5	0.2497	0.2524	0.0027
n-Butane	0.5	0.3476	0.3527	0.0051
Neopentane	0.2	0.0999	0.1008	0.0009
i-Pentane	0.1	0.3007	0.3063	0.0056
n-Pentane	0.1	0.1996	0.2027	0.0031
Hexane	0.1	0.2017	0.2037	0.002
CV (MJ/m <sup>3</sup> )		38.6512	38.6704	0.0192
Difference (%)				0.0496%

Table 6. Big bias when calibration gas is non representative of process gas

# 34<sup>th</sup> International North Sea Flow Measurement Workshop 25-28 October 2016

## Technical Paper

This bias can easily be reduced to a negligible level when calibration gas is designed to be similar to the process gas composition. Table 7 shows the result between actual value and GC measurement when calibration gas is similar to the gas being measured.

Description	Calibration Gas (mole%)	Actual value	GC measurement	Difference
Methane	84.9955	84.9948	84.9944	-0.0004
Nitrogen	5.5212	5.5195	5.5197	0.0002
CO <sub>2</sub>	1.9969	1.9973	1.9974	1E-04
Ethane	4.2838	4.2856	4.2857	0.0001
Propane	1.8037	1.8035	1.8035	0
i-Butane	0.2497	0.2497	0.2497	0
n-Butane	0.3474	0.3476	0.3476	0
Neopentane	0.1001	0.0999	0.0999	0
i-Pentane	0.3006	0.3007	0.3007	0
n-Pentane	0.1996	0.1996	0.1996	0
Hexane	0.2017	0.2017	0.2018	0.0001
CV (MJ/m <sup>3</sup> )		100	100	0
Difference (%)		38.65125	38.65127	0.00002
				0.00005

Table 7. Negligible bias when calibration gas is similar to process gas

This is however only useful when the process gas is stable with low variation over time. When the process gas variation is high, GC may be impacted by non-linearity. How big of a bias a GC has from non-linearity can be tested. This is specified in the ISO 10723:2012 standard [3].

In many occasions, selecting the correct calibration gas can ensure that the bias will be acceptable across a defined range of measurement. For example, if the range of measurement is between 70 to 75% on methane, running ISO 10723 will give us information what composition will be the best to use.

Figure 13 shows Monte Carlo simulation of methane bias between 60% to 90% measurement where calibration gas sits at 84%. From Figure 13 it is visible that bias is expected to increase as methane concentration reduces.

Technical Paper

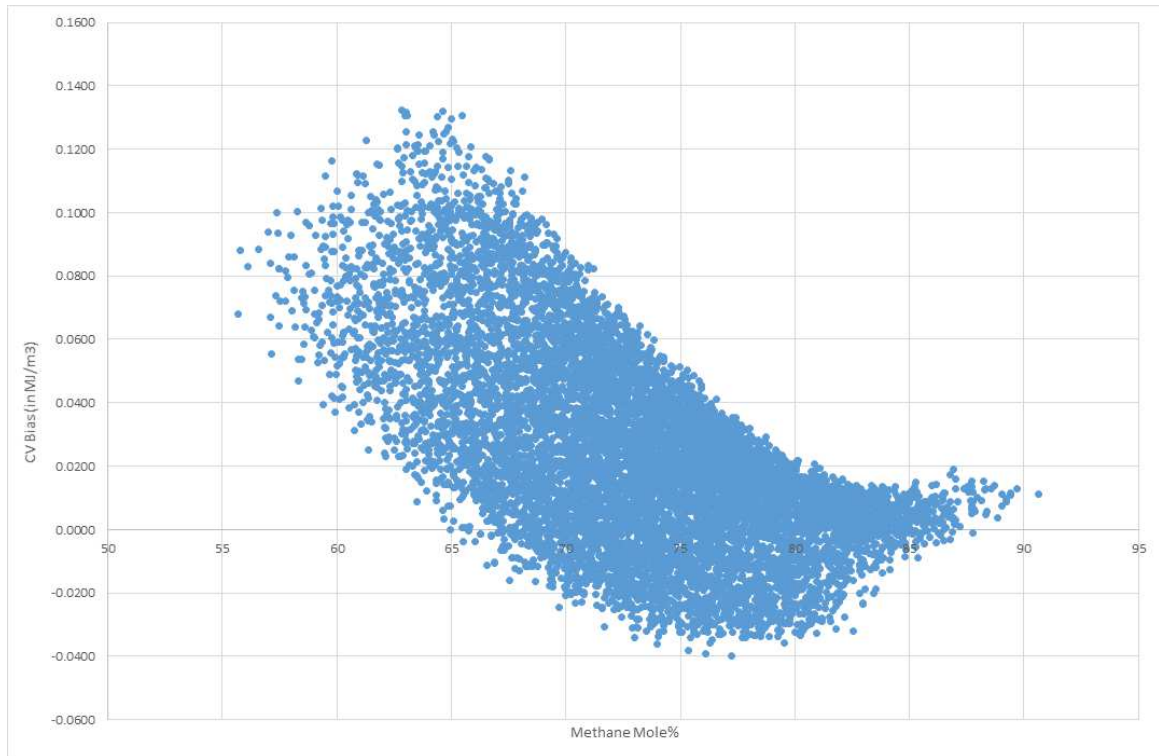


Figure 13. Methane bias distribution when using 84% methane as calibration gas

The same simulation is done using calibration gas where methane sits at 70%. Figure 14 shows the result.

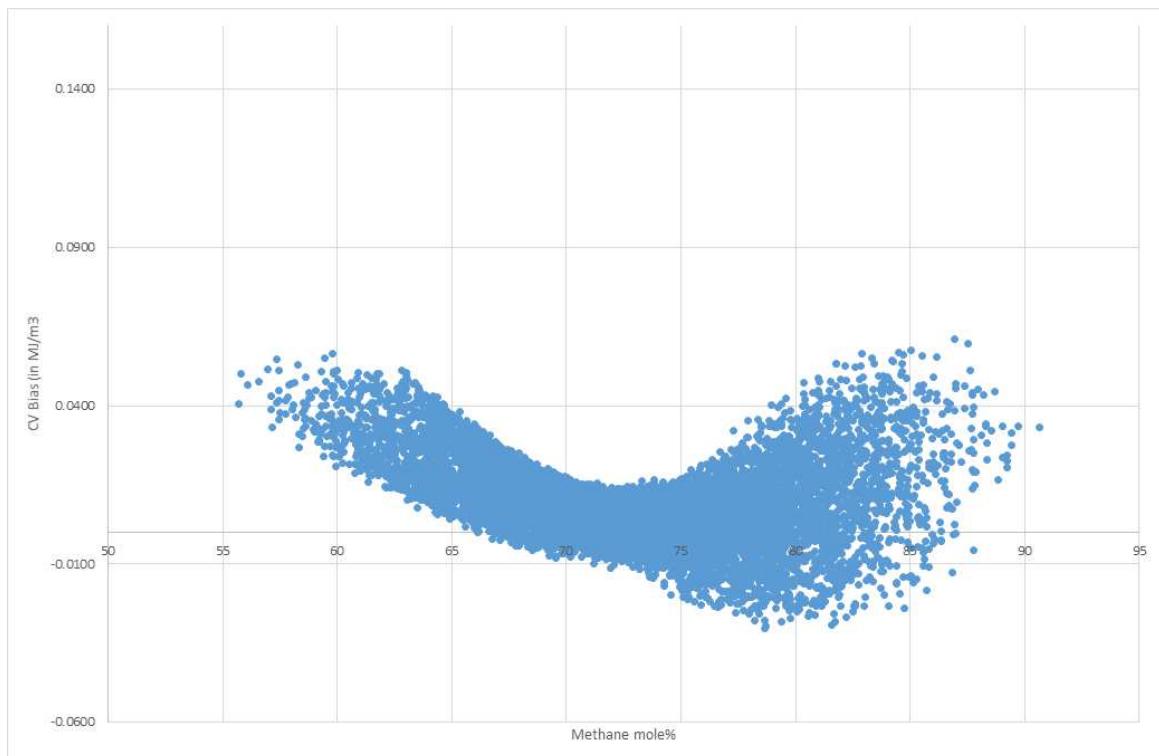


Figure 14. Methane bias distribution when using 70% methane as calibration gas

# 34<sup>th</sup> International North Sea Flow Measurement Workshop 25-28 October 2016

## Technical Paper

It can be seen that selecting more suitable calibration gas reduces the bias significantly.

Although performing ISO 10723 performance evaluation test can be very useful, it is not very practical as it involves quite a significant preparation with the logistic to order and deliver 7 set of calibration gases. The following are some of the practical issues associated with preparation for and implementation of ISO 10723 performance evaluation test.

1. Logistic to deliver the 7 sets of gases
2. It can be costly. Cost – benefit analysis needs to be done. If process gas is stable, the cost may exceed the benefit.
3. When performed on a faulty GC, actual fault may be masked as non-linearity
4. Drifts may invalidate the constant generated during calibration
5. When constants are implemented in GC, RF will be close to 1. Log-log plot cannot be used when all RF is close to 1 and therefore checks to ensure if GC is healthy is not possible
6. If tested in the wrong range, failed result may give impression of faulty GC when if tested in the correct range the result may pass

Because of the logistical issue, test is normally done once a year, and it can become impractical when GC experience some issue and need to perform another performance evaluation test.

Dual Level Calibration eliminates the impracticality of ISO 10723 and reduces the bias of single point calibration to negligible level. Instead of using seven sets of gases, DLC uses 2 sets of gases of which both calibration gas can be stored on site. Where storage space permits, it is recommended to have two big bottles where both of them can be used as daily use calibration gas. However where storage space is limited, it is recommended to have one big bottle as daily calibration usage, and a small bottle for the use of performing DLC and monthly reproducibility check.

To perform DLC, the range of gas that is going to be measured need to be understood. The calibration gas is then designed to cover the range of the gas, one on the upper range, and the other one on the lower range as illustrated in Figure 15 below. On the below example, the methane measurement range will be between 70% - 80%.

# 34<sup>th</sup> International North Sea Flow Measurement Workshop 25-28 October 2016

## Technical Paper

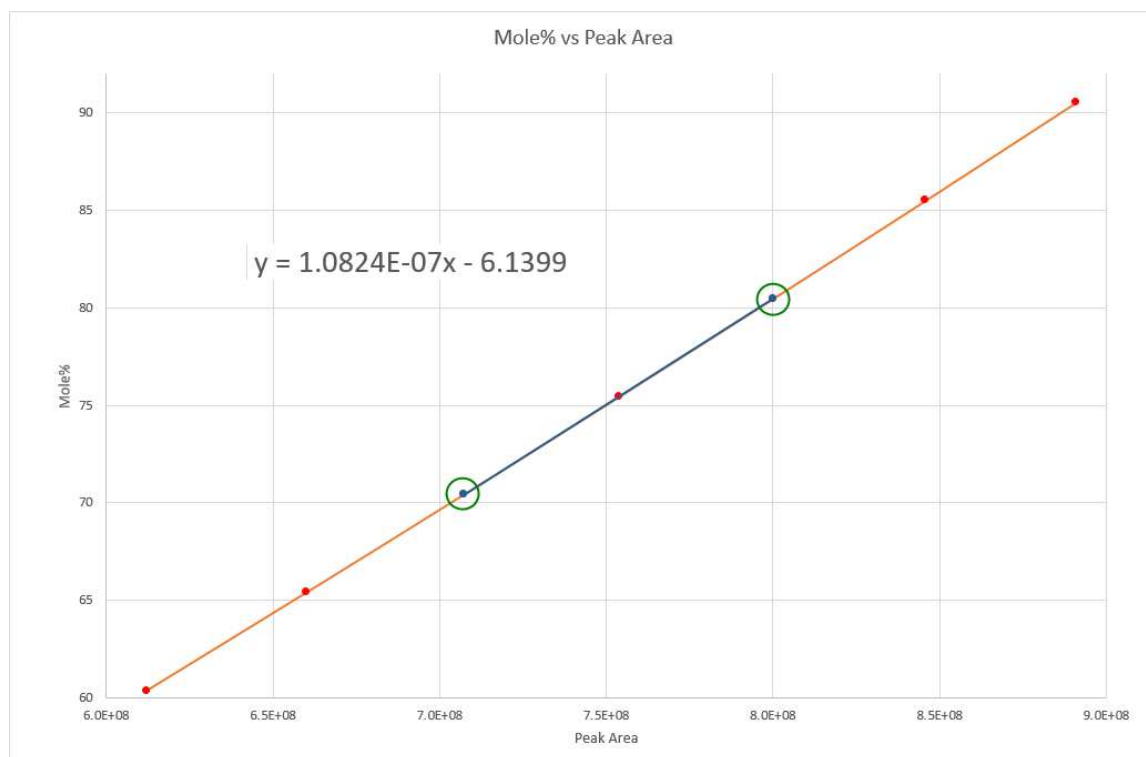


Figure 15. Dual Level Calibration Function

When this function is implemented on the GC, the bias on methane measurement on the range between 70%-80% is reduced to a negligible level as shown in Figure 16.

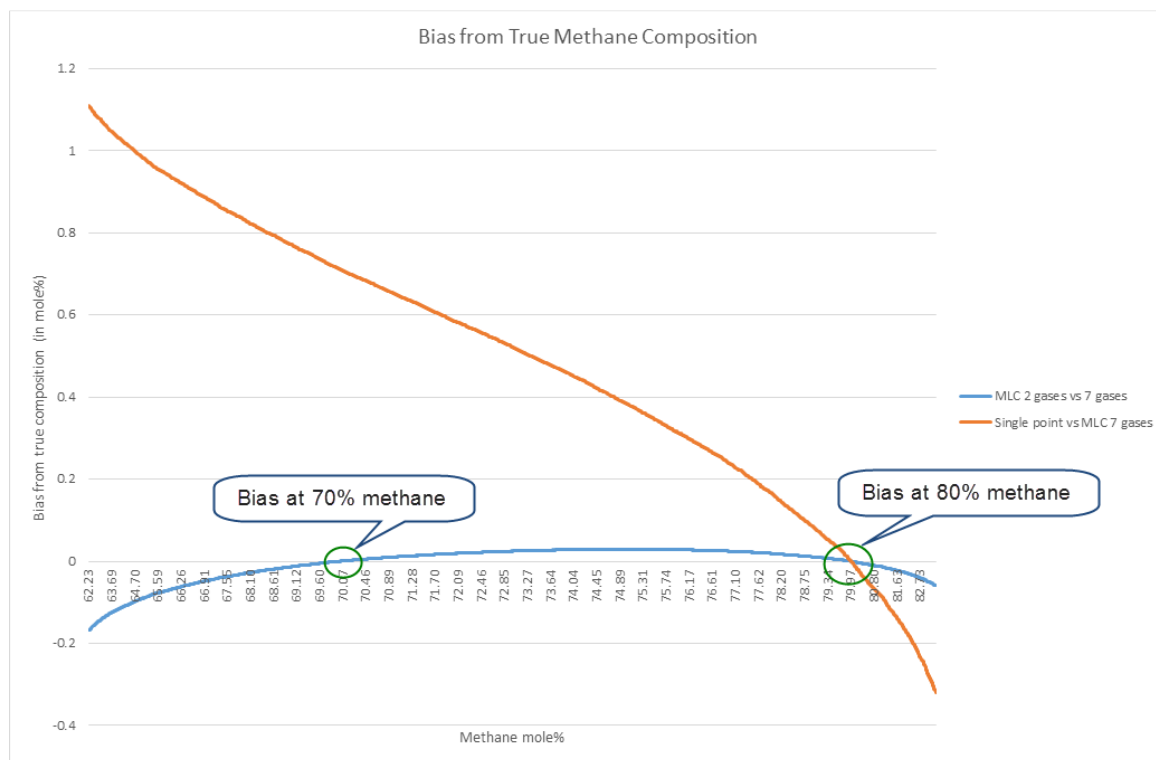


Figure 16. Bias reduced to negligible level

# 34<sup>th</sup> International North Sea Flow Measurement Workshop 25-28 October 2016

## Technical Paper

The impact on the CV and line density bias is also reduced to significantly. Figure 17 and Figure 18 shows the bias on CV and density respectively from one of the case.

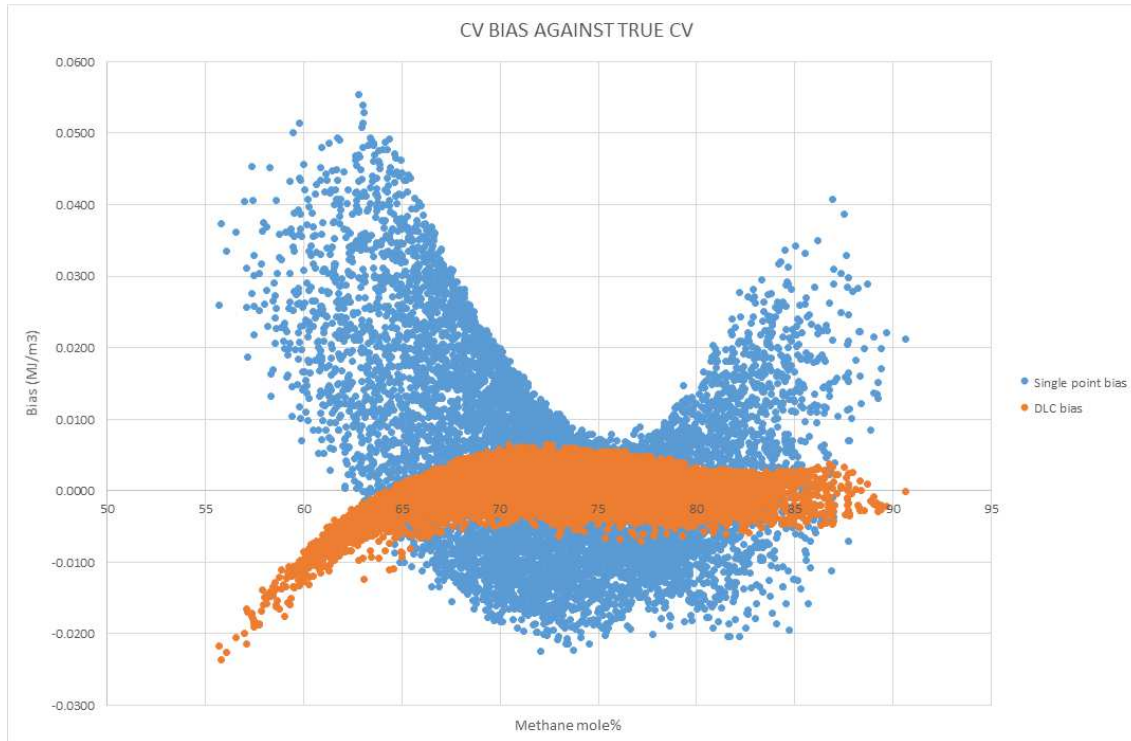


Figure 17. CV bias against true CV

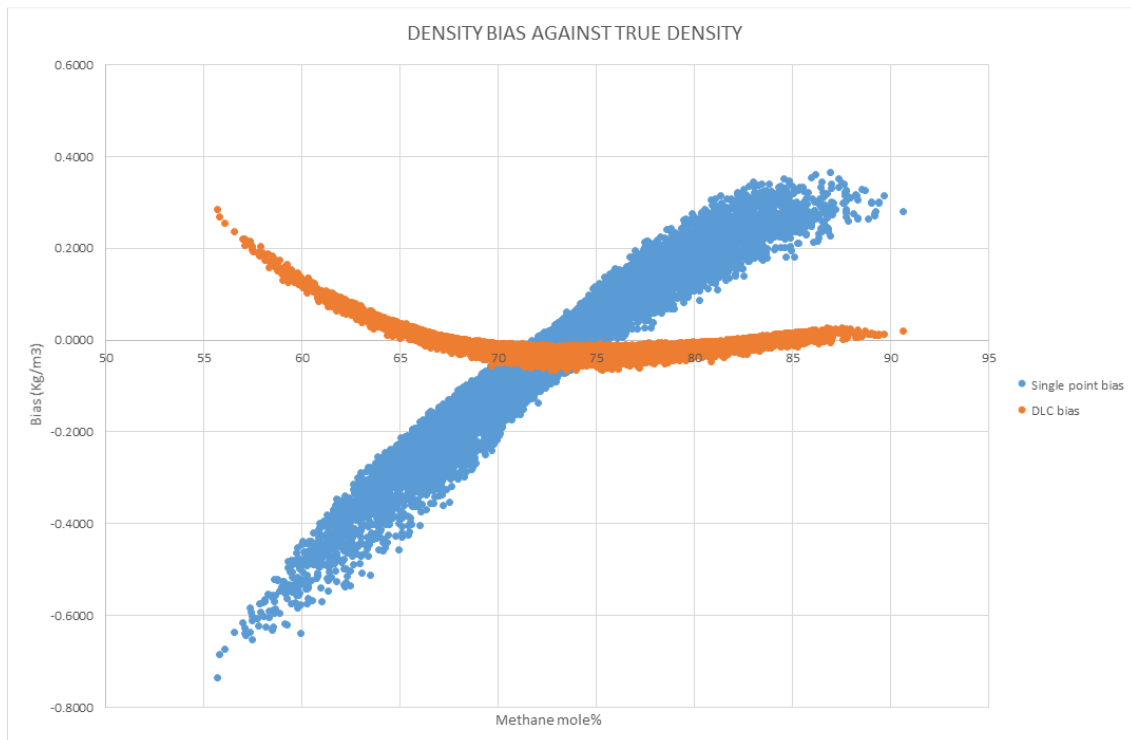


Figure 18. Density bias against true density

# **34<sup>th</sup> International North Sea Flow Measurement Workshop**

## **25-28 October 2016**

### **Technical Paper**

From the Figure 17 and Figure 18 above it is clear that implementing dual level calibration constant can reduce the bias to a negligible level. Few other examples along with the procedure on how the DLC bias are calculated is included in 0.

#### **2.4.1 DLC practicality**

From the practicality point of view DLC can be performed without adding any significant cost to the operator. The only thing operators need is two sets of calibration gas that would cover the whole operational range. Both calibration gas can be used as daily calibration. Therefore when one bottle is depleted, the other composition can be used as calibration gas.

The spare calibration gas can then be used as reproducibility check. Rather than checking repeatability of GC using the same gas the GC was calibrated on, it is a very useful exercise to perform reproducibility test using another bottle that has completely different composition. In effect, this test performs a linearity test. Rather than performing the ISO 10723 test on yearly basis, this test can be done on monthly basis with no extra cost.

In the events where linearity test fails, one of the following can be checked and done:

1. If linearity check fails due to some failure on the GC, further troubleshooting can be done immediately and fault can be identified and rectified.
2. If there are drifts that causes bias, new constant can be generated using available calibration gas on site.

Tolerance for reproducibility limits can be taken for instance from ASTM D1945:2001 [1] or ISO 6974-5:2001 [2]. ISO 6974-5:2001 [2] shows a more stringent tolerance in comparison to ASTM D1945:2001 [1] and maybe more suitable to be used as tolerance.

#### **2.4.2 Case study**

The following case study is performed on two GC that measures export gas in one of the North Sea platform. The initial issue was identified where both GC shows low unnormalised total, however both GC shows good consistent calibration result. This indicates that both GC are affected by non-linearity.

Later it was found that the calibration gas composition is significantly different from process gas composition which were being measured. The comparison between calibration gas composition and process gas average is shown in Table 8.

# 34<sup>th</sup> International North Sea Flow Measurement Workshop 25-28 October 2016

## Technical Paper

Description	Calibration Gas	Process Gas Average
Methane	69.476	82.196578
Nitrogen	2.65	1.259492
Carbon dioxide	5.634	1.68137
Ethane	12.941	8.397309
Propane	7.2172	4.082673
i-Butane	0.5234	0.499166
n-Butane	1.2489	1.134631
i-Pentane	0.1307	0.230733
n-Pentane	0.1366	0.280748
Hexane	0.0396	0.2373

Table 8. Calibration gas vs process gas average

Second calibration gas was then ordered to have quite a similar composition to the process gas.

Description	Calibration Gas	Process Gas Average
Methane	83.125	82.196578
Nitrogen	1.2085	1.259492
Carbon dioxide	1.2755	1.68137
Ethane	8.054	8.397309
Propane	3.864	4.082673
i-Butane	0.483	0.499166
n-Butane	1.087	1.134631
i-Pentane	0.231	0.230733
n-Pentane	0.3093	0.280748
Hexane	0.3578	0.2373

Table 9. Second calibration gas vs process gas average

Now that two calibration gases are available, a reproducibility test can be performed. Initial test was performed by having the GC single point calibrated using the first calibration gas, then the second calibration gas is measured as unknown. GC reading was then compared against calibration gas certificate. Result can be seen in Table 10.

Description	Calibration Gas	Repeatability test	Bias
Methane	83.12907332	82.935008	-0.194065
Nitrogen	1.208559219	1.22676	0.018201
Carbon dioxide	1.275562503	1.293297	0.017734
Ethane	8.054394665	8.071723	0.017328
Propane	3.864189345	3.950325	0.086136
i-Butane	0.483023668	0.489072	0.006048
n-Butane	1.087053266	1.099363	0.01231
i-Pentane	0.23101132	0.234153	0.003142
n-Pentane	0.309315156	0.314529	0.005214
Hexane	0.357817533	0.38577	0.027952
CV (% bias)	43.7879625	43.89291958	0.239694

# 34<sup>th</sup> International North Sea Flow Measurement Workshop 25-28 October 2016

## Technical Paper

Table 10. Bias from reproducibility test of second calibration gas

As shown in Table 10, the bias from reproducibility test is very significant. This bias can amount to more than £50,000 per month on production of 100 mmscf/d.

After the reproducibility test, dual level calibration constant was generated and implemented in the GC. Then GC was calibrated again still using the same first calibration gas, but now with DLC constants implemented in the GC. Reproducibility test on second calibration gas was performed with result shown in Table 11.

Description	Calibration Gas	Repeatability test	Bias
Methane	83.12907332	83.145382	0.016309
Nitrogen	1.208559219	1.208111	-0.00045
Carbon dioxide	1.275562503	1.276249	0.000686
Ethane	8.054394665	8.035965	-0.01843
Propane	3.864189345	3.865698	0.001509
i-Butane	0.483023668	0.483918	0.000894
n-Butane	1.087053266	1.087583	0.00053
i-Pentane	0.23101132	0.230822	-0.00019
n-Pentane	0.309315156	0.30945	0.000135
Hexane	0.357817533	0.356823	-0.00099
CV (% bias)	43.7879625	43.78318356	-0.01091

Table 11. Bias from reproducibility test of second calibration gas using DLC constant

From Table 11, it is shown that implementing DLC constant reduces the bias from non-linearity to an acceptable level.

When DLC constants are not implemented, measurement using single point calibration can show result that can be seen as acceptable. On this particular case, both of the GC shows very similar result which gives the impression that the GC measures correctly. Figure 19 shows comparison between GC A and GC B when measurement was done using single point calibration.

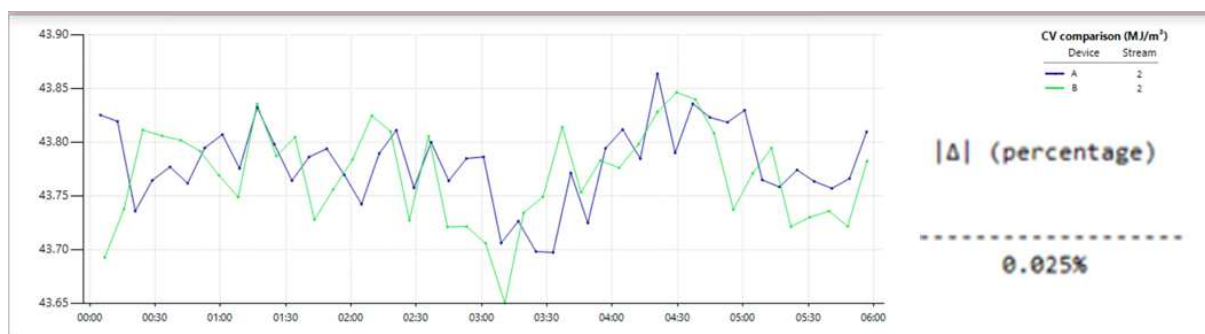


Figure 19. GC A vs GC B CV difference when measured using single point calibration

However, when DLC constants are implemented in the GC, it shows 0.2% of bias on both GC. Figure 20 shows the bias on GC A.

# 34<sup>th</sup> International North Sea Flow Measurement Workshop 25-28 October 2016

## Technical Paper

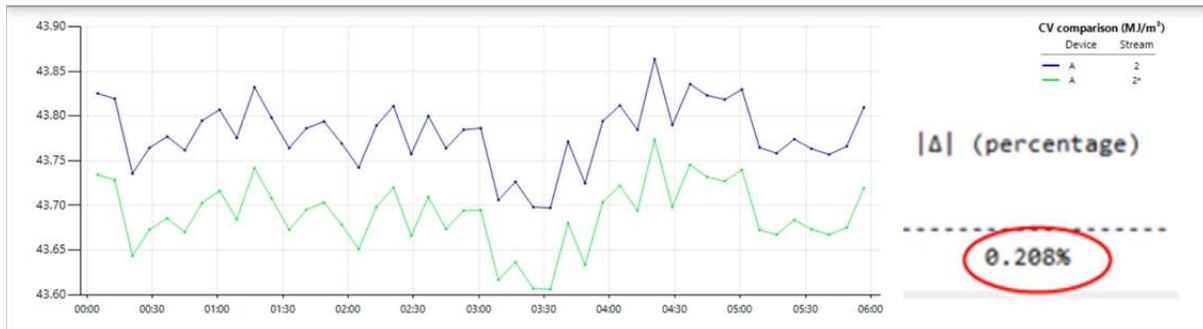


Figure 20. GC A CV comparison between single point vs DLC measurement

### 2.5 GC “Live” Uncertainty

GC Live uncertainty is associated with the reproducibility of the GC from its daily / periodic calibration result. This should be performed after all methods above are utilised and GC health status is confirmed to be good. Failing to perform one or more methods described above may result in consistent systematic errors. While the methods above will ensure that GC works correctly on an instantaneous basis, the live uncertainty method will ensure that the GC works in reproducible manner over a long period of time. It may also predict future failure that may not be identified by methods described earlier on this paper.

Uncertainty of GC parameter quantifies GC performance derived from response factor control charts. The monitoring of the GC response factor not only ensures the health of the GC throughout the year, but also provides early indication of deterioration of GC performance as it will be revealed by increment of the GC uncertainty value.

Figure 21 shows response factor trends of a healthy GC. Visually from the trend, many stories can be told. From Figure 21 it can be seen that there was a shutdown between August 2013 and October 2013. There was also change in calibration gas in April 2015 and some parameter changes were done on GC in June 2014. Also it can be seen visually that all response factor trends were up and down in harmonious way.

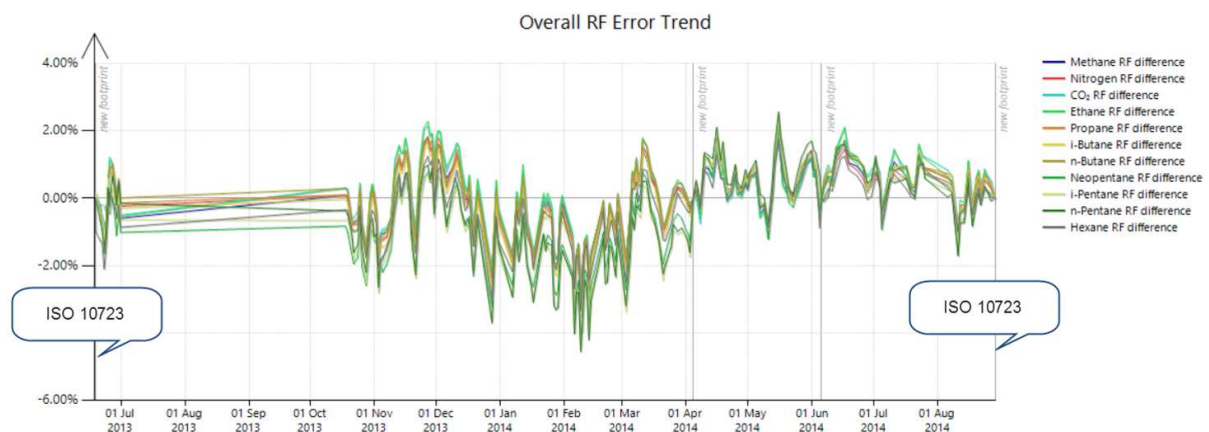


Figure 21. 1 year RF trend of healthy GC

# 34<sup>th</sup> International North Sea Flow Measurement Workshop 25-28 October 2016

## Technical Paper

Uncertainty trend is one way to quantify these parameters. Uncertainty trend of the GC associated with Figure 21 is shown in Figure 22 below.

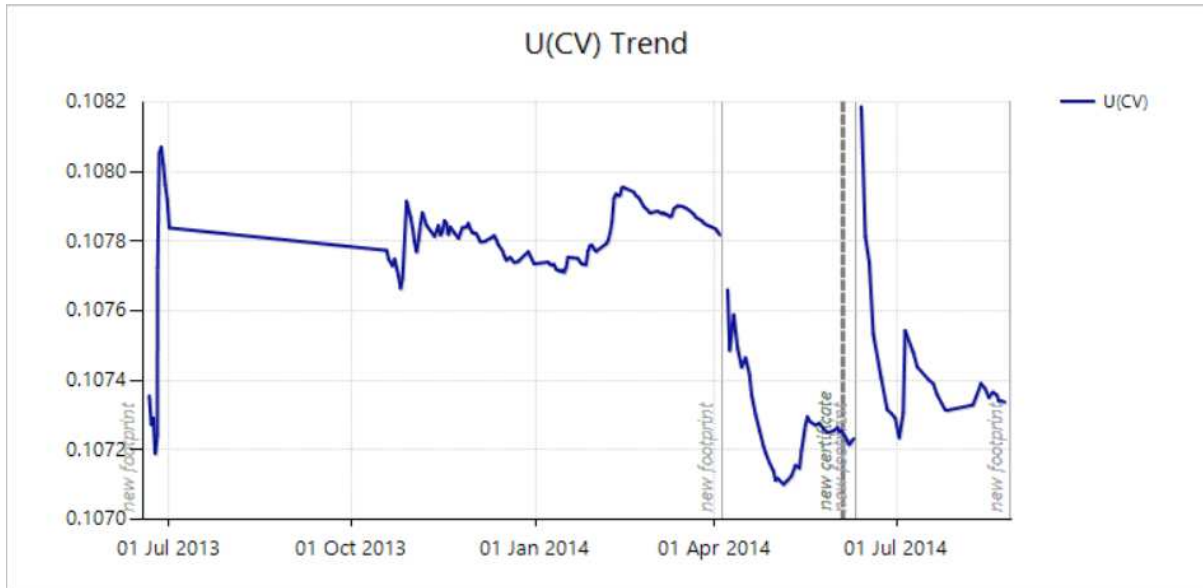


Figure 22. Uncertainty of CV associated with Figure 21

From here uncertainty limits can be set and alarm flagged at any time the uncertainty value exceeds the limit. Figure 23 shows an example where uncertainty limit is set at 0.12%. This limit is very useful to catch issues with GC before the issue becomes significant.

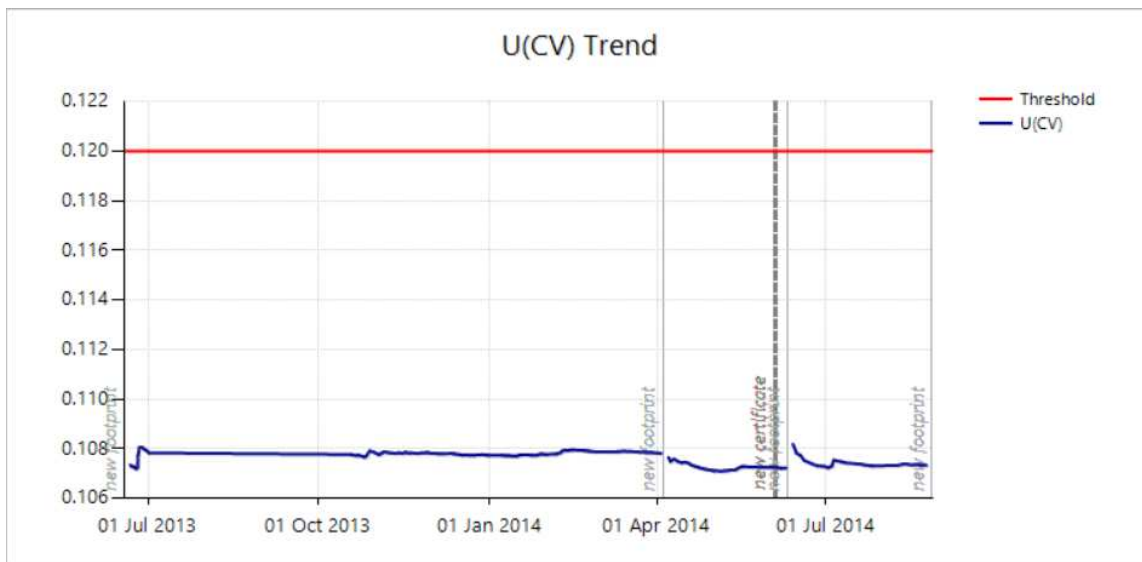


Figure 23. Uncertainty with set limit of 0.12%

The uncertainty method can also predict future failure that may otherwise be undetected using any other method. Figure 24 shows uncertainty trend that predicted GC failure two months prior to actual failure. This gives opportunity for the operator to order the required spare parts before the actual failure happens in the GC without losing much of down time.

**Technical Paper**

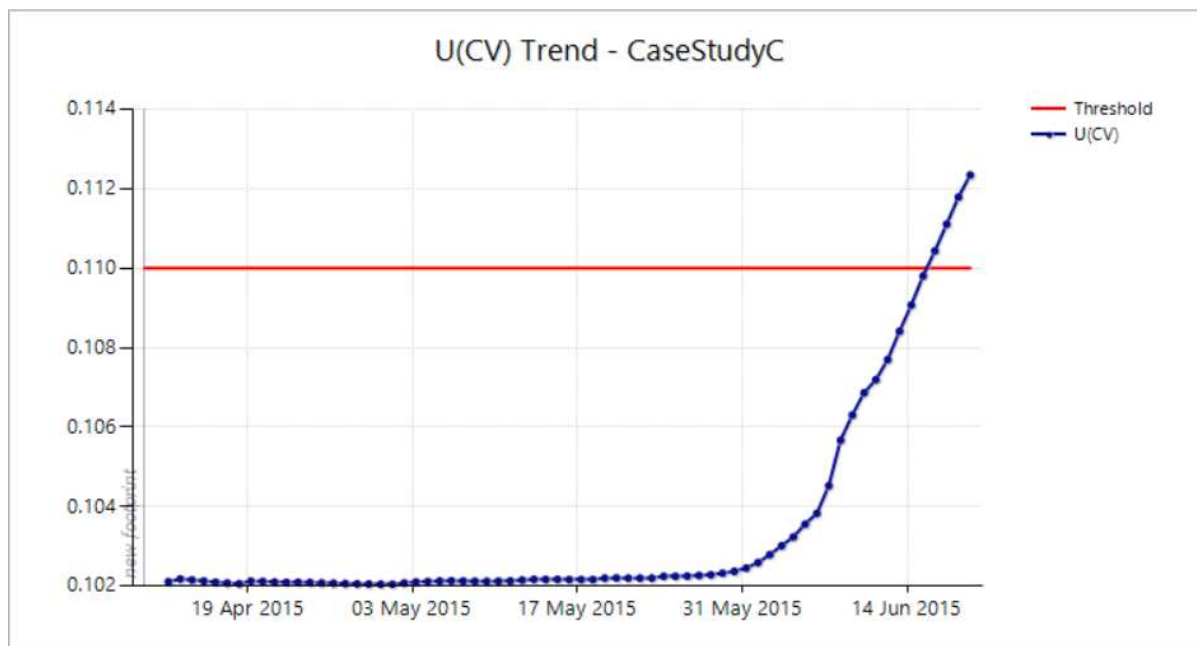


Figure 24. Increment in uncertainty predicted future failure

Ultimately when the GC is configured correctly and calibrated with high quality of calibration gas, the live uncertainty method can ensure that the GC provides accurate measurement at all time. Should error arises on the GC, the live uncertainty method will highlight the errors before the error become significant. Tools on the conditional based monitoring tool can be used to ensure correct operation during and after troubleshooting.

### **3 CONCLUSION AND RECOMMENDATION**

There are many ways to perform GC maintenance. Current maintenance regime splits the maintenance into two categories, yearly health check and daily / periodic calibration. When a certain maintenance method is employed and some others are overlooked it may cause the operator to oversee some of the issue in hand which may result in significant systematic error.

This paper has discussed some of the available methods to ensure accurate GC measurement which involves the selection of good calibration gas quality with the correct range, procedure of performing calibration and the checking of the calibration result parameters, the handling of non-linear property of the GC, and finally the monitoring of historical performance of calibration result.

This can be quite a significant task to perform all this activities. However, considering the potential errors a GC can contribute to measurement, it is worthwhile to ensure correct measurement of a GC. It is recommended to use GC conditional monitoring tool that covers all these with minimum effort.

GCAS is designed to capture all the necessary data automatically from GC and provide all the analysis automatically. It removes the need for data entry as data is gathered automatically from the GC. This will then be presented in a dashboard showing alarm in

# 34<sup>th</sup> International North Sea Flow Measurement Workshop

## 25-28 October 2016

### Technical Paper

case any failure or potential failure is detected. In essence it will ensure that the GC provides accurate measurement at all time.

#### 4 REFERENCES

[1] ASTM D1945. Standard test method for analysis of natural gas by gas chromatography. *ASTM*, 2001.

[2] BS EN ISO 6974-5. Natural gas - Determination of composition with defined uncertainty by gas chromatography - Part 5: Determination of nitrogen, carbon dioxide and C1 to C5 and C6+ hydrocarbons for a laboratory and on-line process application using three columns. *BS EN ISO*, 2001.

[3] ISO 10723. Natural Gas – Performance evaluation for Analytical Systems. *ISO*, 2012.

# 34<sup>th</sup> International North Sea Flow Measurement Workshop 25-28 October 2016

## Technical Paper

### Appendix 1. OGA Letter of No Objection

**From:** Arnould Patrick (Oil and Gas Authority)  
<patrick.arnould@oga.gsi.gov.uk>  
**Sent:** 29 June 2016 11:48  
**To:** Anwar Sutan  
**Cc:** Griffin Douglas (Oil and Gas Authority); Mankin Alan (Oil and Gas Authority); OGA Petroleum Measurement and Allocation Team  
**Subject:** RE: Dual Level Calibration

Hi Anwar,

Thank you for your email, I confirm OGA are content with the summary below with the following proviso:

In the case where either:

The simulations using the ISO-10723 results show the bias to be excessive and the associated non-linearity cannot be removed by changes to the GC configuration

*or*

The reproducibility test on the 3<sup>rd</sup> gas continually fails indicating non-linearity and this non-linearity cannot be removed by changes to the GC configuration

*then*

OGA may still require the ISO-10723 evaluation to be performed.

Please do not hesitate to contact me if you wish to discuss further.

Best regards,  
Patrick



Patrick Arnould  
Snr. Petroleum Measurement & Allocation Inspector  
Oil & Gas Authority  
AB1, 48 Huntly Street, Aberdeen AB10 1SH:  
[patrick.arnould@oga.gsi.gov.uk](mailto:patrick.arnould@oga.gsi.gov.uk) T: 0300 020 1011

**From:** Anwar Sutan [<mailto:anwar.sutan@i-Vigilant.com>]  
**Sent:** 28 June 2016 21:05  
**To:** Arnould Patrick (Oil and Gas Authority)  
**Cc:** Griffin Douglas (Oil and Gas Authority); Mankin Alan (Oil and Gas Authority); OGA Petroleum Measurement and Allocation Team  
**Subject:** RE: Dual Level Calibration

Hi Patrick,

Thank you very much for your email. I would like to summarise the effect of your email below in terms of the practicality of the method in the industry. I really appreciate if you can confirm the following summary:

# 34<sup>th</sup> International North Sea Flow Measurement Workshop 25-28 October 2016

## Technical Paper

### 1. OGA Guideline:

#### 7.5.8 Evaluation of Linearity and Repeatability– ISO 10723

A procedure for determining the linearity and repeatability of gas chromatograph response on 7 different test gases is set out in an International Standard [ISO 10723: 2012].

OGA may require operators of relevant systems to quantify at regular intervals the linearity and repeatability of fiscal gas chromatographs

Effect of the no objection to the use of Dual Level Calibration for GC's:

OGA has no objection to operators using a Dual Level Calibration. Using 7 gases is not necessary where operators can define two calibration gas compositions to cover the process conditions. The Dual Level Calibration will suffice and by implementing the dual level calibration function in the GC this will (as has been proven in several test cases) significantly reduce the associated bias.

### 2. Practicality of the method

To make the method practical the following will be recommended to operators planning to implement the method:

- 2 gases covering the operation range to be made available as calibration gas
- Based on the actual range of the gas composition and potential of the bias the following monthly test will be recommended:
  - Reproducibility test of the cal gas that is not being used for calibration → This is to be done if the actual range is narrow enough. Examples:
    - A site has export gas composition that has 69% methane, but when it takes import gas methane will go to 82%. The gas will be operating at  $69\% \pm 2$  mole% or  $82\% \pm 2$  mole%. In this particular case, it will not be necessary to run reproducibility test using test gas of 75% as the actual gas does not go to that range. In this case we can do reproducibility test using the second calibration gas.
    - A site has process gas range between 88 – 92%. If Tests against true function of ISO 10723 shows negligible bias then reproducibility test can be done using the second calibration gas.
  - Reproducibility test using test gas that sits in middle of operation range → this is to be done if the actual range is quite wide. Here are two examples of wide range:
    - A site has gas that have high variation (let's say 70% to 85%). The two cal gas will have 70% methane and 85% methane. It will be recommended to have the third cal gas that has around 77% methane so that reproducibility test can be done using this test gas to see if we have significant bias.
  - When reproducibility test fails:
    - Check if there is any issue with the GC. If there is issue with the GC, actions to be taken to fix the GC, then if need be new dual level calibration constant to be generated.
    - If there is no issue on the GC, and it is a natural drift, a new constant can then be generated.
- We will make procedure available on how to generate the constants. Based on this, it will also be recommended that operators have auditable trail of the constant generation on the GC and reproducibility tests being done.

# 34<sup>th</sup> International North Sea Flow Measurement Workshop 25-28 October 2016

## Technical Paper

Based on our discussion, I have come to the above conclusion. Can you confirm that you are in agreement with the above and please add any comments if you think I have missed something from our initial discussion. Thanks again for your time in reviewing the method and I look forward to be promoting and implementing the method in various operators that operates under OGA measurement guidelines.

Thanks and regards,  
Anwar

**Anwar Sutan CEng MInstMC** | Director  
T: +44 1224 820030 | M: +44 7812 141355  
[Anwar.Sutan@i-Vigilant.com](mailto:Anwar.Sutan@i-Vigilant.com) | [www.i-Vigilant.co.uk](http://www.i-Vigilant.co.uk)  
**GCAS** – Gas Chromatograph Condition Based Monitoring

**From:** Arnould Patrick (Oil and Gas Authority) [<mailto:patrick.arnould@oga.gsi.gov.uk>]

**Sent:** 27 June 2016 12:13

**To:** Anwar Sutan <[anwar.sutan@i-Vigilant.com](mailto:anwar.sutan@i-Vigilant.com)>

**Cc:** Griffin Douglas (Oil and Gas Authority) <[Douglas.Griffin@oga.gsi.gov.uk](mailto:Douglas.Griffin@oga.gsi.gov.uk)>; Mankin Alan (Oil and Gas Authority) <[alan.mankin@oga.gsi.gov.uk](mailto:alan.mankin@oga.gsi.gov.uk)>; OGA Petroleum Measurement and Allocation Team <[metering@oga.gsi.gov.uk](mailto:metering@oga.gsi.gov.uk)>

**Subject:** Dual Level Calibration

Anwar,

Thank you for explaining the new Dual Level Calibration method for use with GCs.

I have completed a technical review of the method itself and the method used for comparing it against conventional single point calibration and multi-level calibration. I have seen the evidence from numerous tests using the above methodology including one example of implementation in the field and agree the results show an improvement over single point calibration and can, depending on the operational range and the extent of non-linearity present in the GC, offer similar performance to a multi-level calibration.

Based on the above I confirm that OGA have no objection to the use of Dual Level Calibration for GCs used in measurement systems which are operating under our Measurement Guidelines.

Best regards,  
Patrick



Patrick Arnould  
Snr. Petroleum Measurement & Allocation Inspector  
Oil & Gas Authority  
AB1, 48 Huntly Street, Aberdeen AB10 1SH:  
[patrick.arnould@oga.gsi.gov.uk](mailto:patrick.arnould@oga.gsi.gov.uk) T: 0300 020 1011

# 34<sup>th</sup> International North Sea Flow Measurement Workshop 25-28 October 2016

## Technical Paper

### Appendix 2. DLC Results

Below are 5 case studies showing the comparison on bias when using 2 sets of gases (Dual Level Calibration) and single gas (Single Point Calibration) in comparison to 7 sets of gases Multilevel Calibration (MLC).

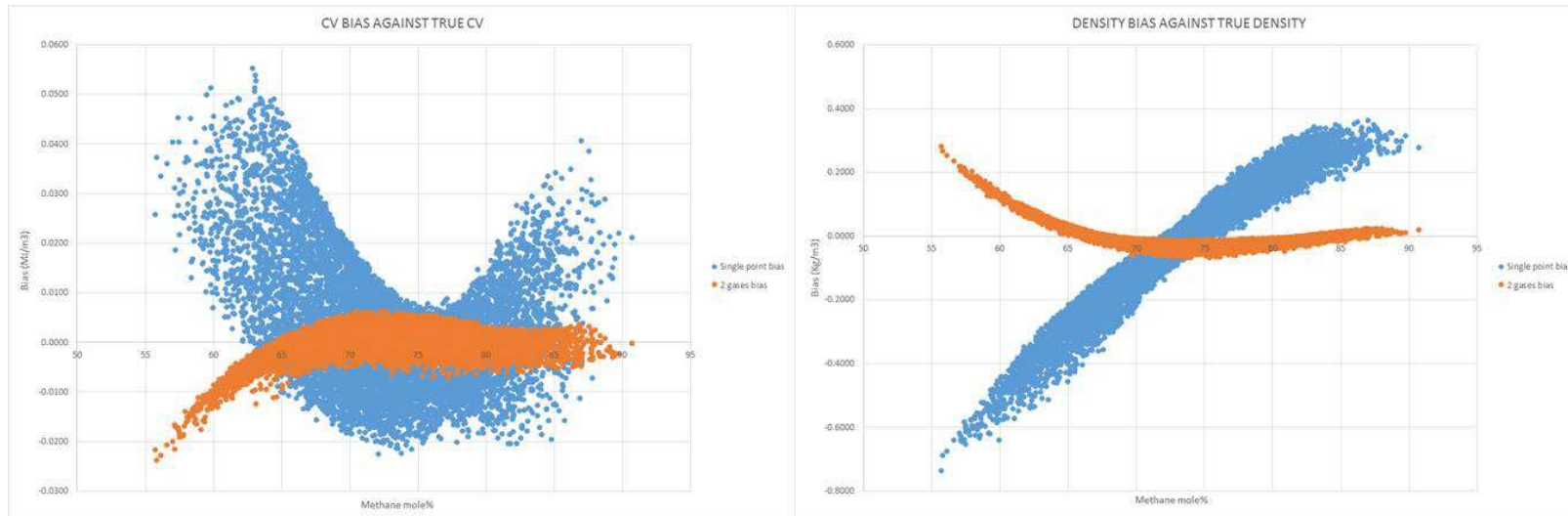
The data is generated as follows:

1. Generate 10,000 data points of MLC mole composition over a defined range.
2. Convert the data to the corresponding 'Single Point' data using the MLC functions for that GC (use calibration gas composition of either the high range or the low range of the range of interest and assume MLC RF of 1).
3. Generate the DLC linear curve for each component as follows:
  - a. Get the peak area of low range mole% of calibration gas used for 2 gases linearization using 7 gases MLC functions
  - b. Get the peak area of high range mole% of calibration gas used for 2 gases linearization using 7 gases MLC functions
  - c. Generate a linear function based on these two peak areas and mole%
  - d. Do this for every component
4. Convert the single point mole composition using the DLC functions to get the mole composition if we were to use the DLC linear functions
5. Convert the 7 gases MLC mole composition to single point mole composition, but this time using calibration gas that is used on the ISO 10723 performance report
6. Calculate the bias as follows:
  - a. Single point CV bias = Single point CV - 7 gases MLC CV
  - b. DLC CV bias = 2 gases DLC CV - 7 gases MLC CV
  - c. Single point density bias = Single point density - 7 gases MLC density
  - d. DLC density bias = 2 gases DLC density - 7 gases MLC density

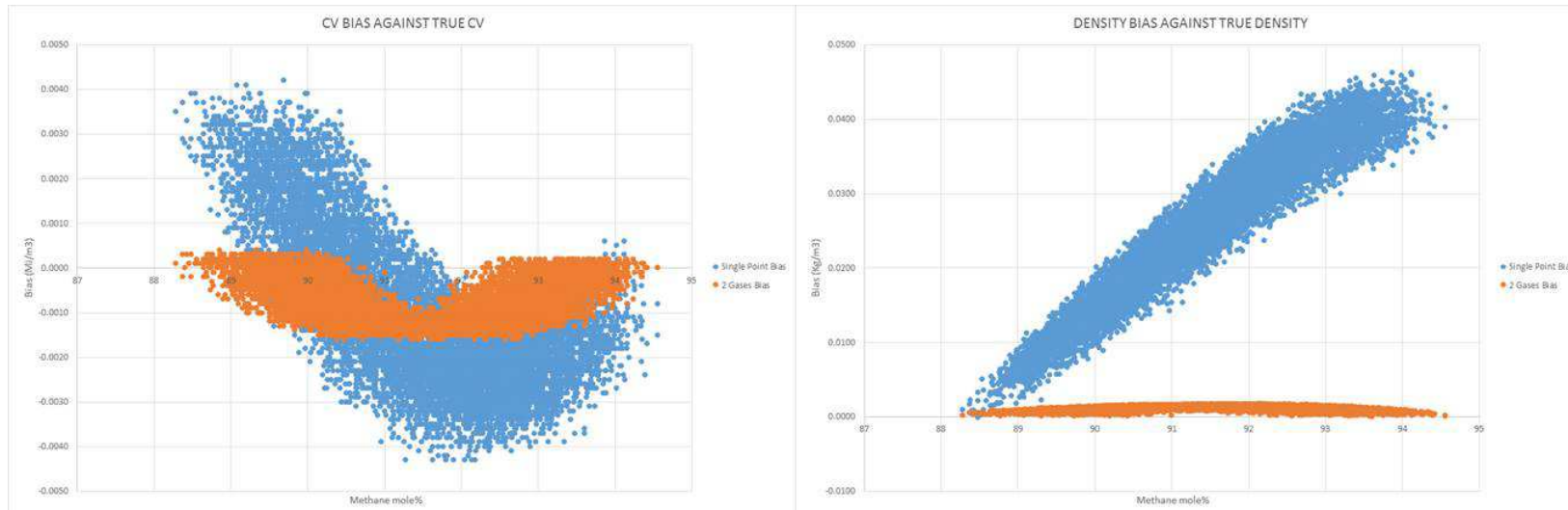
Below is the resulting bias in both CV and density for 5 different GCs and composition ranges.

34<sup>th</sup> International North Sea Flow Measurement Workshop  
25 – 28 October 2016

1. Case study 1 (area of interest between 70%-80% methane):

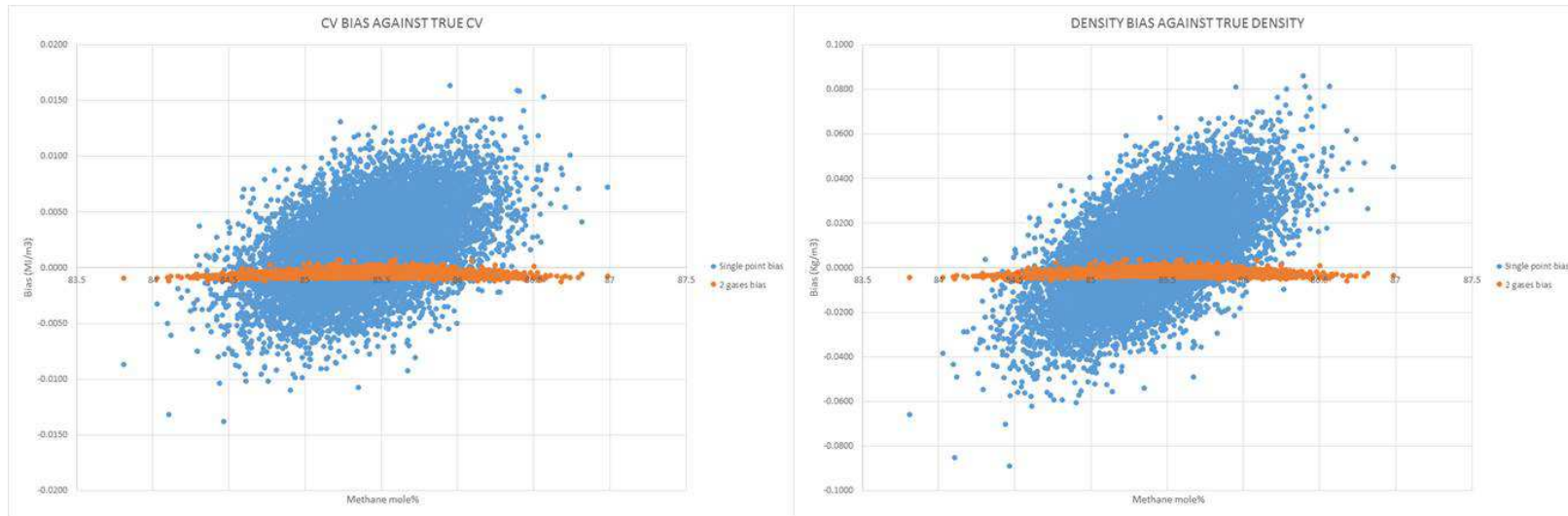


2. Case study 2 (area of interest between 89%-94% methane)

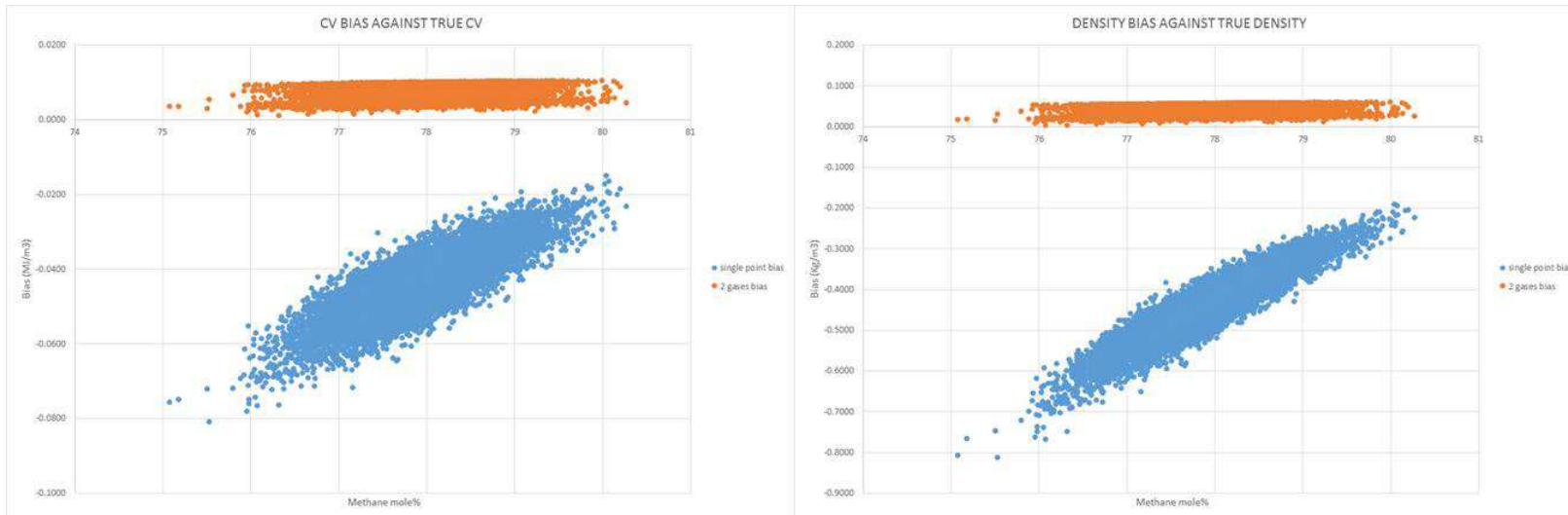


34<sup>th</sup> International North Sea Flow Measurement Workshop  
25 – 28 October 2016

3. Case study 3 (area of interest between 84%-86% methane):



4. Case study 4 (area of interest between 76%-80% methane):



5. Case study 5 (area of interest between 76%-84% methane):

